The Development of Microelectrochemical Choline and Acetylcholine Biosensors for Real-Time Neurochemical Monitoring

A thesis submitted by

Keeley L. Baker B.Sc. (Hons.)

to the

National University of Ireland, Maynooth

For the degree of Doctor of Philosophy

Volume 1 of 1

Based on the research carried out in the

Department of Chemistry, Faculty of Science and Engineering,

National University of Ireland, Maynooth

under the supervision and direction of

Prof. John P. Lowry and Dr. Fiachra B. Bolger

June 2013

Contents

Declaration

This thesis has not been submitted before, in whole or in part, to this or any other University for any degree, and except where otherwise stated, is the original work of the author.

Signed: ______________________________

Keeley Baker

Acknowledgements

First and foremost, I would like to thank my supervisors, Prof. John Lowry and Dr. Fiachra Bolger. John, thank you for the wonderful opportunity you have given me by allowing me to be a part of your research group. I am grateful of the support, guidance and encouragement you have given me during my research but especially your patience during the final months while correcting and proof reading of my thesis. Fi, I thank you for all your help over the last four years, you always answered any question I asked (and I asked alot!). I truly believe that your guidance and direction have made the writing of this thesis possible.

Thank you to every member of the J.Lo lab. Firstly to Dr. Niall Finnerty, thank you for always taking an interest and helping in any way you could. Also, for your enthusiasm for the work (which is contagious) and your general enthusiasm for all things. To the girls, Andy, Saidhbhe and Michelle, thank you for all the tea breaks, walks, fries and crepes which have kept me sane these last few months. I truly appreciate all the help and support you have given me over the years, and especially throughout the thesis writing, where and gossip and chats was welcomed. Keep herding cats. Also to Ken, I thank you for some of the funniest, and at the same time, scariest moments of the last few years. Finally, to the rest of the lab Emer, John and Rachel, thank you.

I would like to thank the staff, post grads and postdocs of the chemistry department. Thank you to Niamh and Trish for the 12 o'Clock lunches and all the chats in between. Niamh, the best excuse to avoid writing a thesis will always be to chase trains. Also Sam and Wayne, thank you for the write up room chatting when a break was needed. To the postgrads who I was lucky enough to start with in my year, Lorna, Rob, Emear, Orla, Gamma, Laura and Niall I wish you all the best with everything you do. To all the post grads in the department, thank you for the great nights out, lunch time banter and many other things that have made the department a great place to be in the last few years.

Thank you to my family, for all the love and support over the last four years without which none of this would have been possible. Thank you dad for always listening to what I'm doing at work and helping me to achieve this goal. To Ella thank you for your support and advice and your constant baby making for the great distraction they have provided. To Maggie and Graham who are a great excuse to visit and not do work. To Kim who also has supported me over the years along with Ewan, Devon and Luca who are three amazing nephews that provide a great source of distraction. To Andrina, thank you for supporting and encouraging me, for all the little pressies and really girly Sundays, that were great to keep me going. To Alexander, thanks for your support and insightful conversations about neurochemical analysis. Also to Rebecca, (and Michael and Leah), thanks for the girly chats, nights out and never getting mad when I'm late for everything. You're an amazing friend and I'm lucky I've had your support during this process.

Finally, a special thank you to Ruaidhrí, whose unwavering love, support and encouragement has made writing this thesis possible. I will forever be grateful for everything he does for me and helps me to do, he has played a major part in me achieving my goals.

There are a lot of people who have helped me along the way, thank you, and if I haven't mentioned you here I will thank you in person.

Abbreviations

5-HIAA	5-Hydroindoleacetic Acid
5-HT	5-Hydroxytyramine
AA	Ascorbic Acid
Ach	Acetylcholine
AchCl	Acetylcholine Chloride
AchE	Acetylcholine Esterase
aCSF	Artificial Cerebrospinal Fluid
BSA	Bovine Serum Albumin
CelAce	Cellulose Acetate
ChCl	Choline Cloride
ChOx	Choline Oxidase
CNS	Central Nervous System
CPA	Constant Potential Amperometry
DA	Dopamine
DHAA	Dehydroascorbic Acid
DMSO	Dimethylsulfoxide
DOPAC	3,4-Dihydroxyphenylacetic acid
ECF	Extracellular Fluid
GA	Glutaraldehyde
H_2O_2	Hydrogen Peroxide
HACU	High Affinity Choline Uptake
HC-3	Hemicholinium-3
HVA	Homovanillic Acid
i.p	Intraperitoneal Injection
LACU	Low Affinity Choline Uptake
LIVE	Long term *in-vivo* electrochemistry
L-Name	N (G)-nitro-L-arginine methyl ester
LOD	Limit of Detection
MD	Microdialysis
MMA	MethylMethacrylate
***o*-PD**	*Ortho*-Phenylenediamine
PBS	Phosphate Buffered Saline
PEA	3-sn-phosphatidylethanolimine
PEI	Polyethylenimine
PPD	Poly-*o*-Phenylenediamine
Pt	Platinum
Sty	Styrene
UA	Uric Acid
ZNF	Zero Net Flux

Abstract

The aim of this thesis was the development of a choline biosensor for the electrochemical detection of choline in the brain, which could subsequently be modified for acetylcholine detection. The choline biosensor was characterised *in-vitro* to optimise sensitivity towards choline which resulted in two biosensor designs (Chapter 4); Sty-(ChOx)(BSA)(GA)(PEI) and MMA-(ChOx)(BSA)(GA)(PEI) which suitably detected choline with sensitivities of 0.03 ± 0.0003 nA/µM, n=3 and 0.03 ± 0.001 nA/µM, n=4 respectively, and were subsequently progressed for further characterisation. Sensitivity to O_2 was also investigated as the biosensor was developed using an oxidase enzyme which utilises O_2 as a co-substrate (Chapter 5). In the *in-vivo* environment O_2 fluctuations can cause interference in the sensors response to substrate. The styrene design demonstrated high levels of O_2 interference which could not be improved upon. The MMA design was modified with cellulose acetate to (MMA)(CelAce)(MMA)-(ChOx)(BSA)(GA)(PEI) with a sensitivity of 0.58 nA/µM and experienced O_2 interference of 3 % at 20 µM choline. Further *in-vitro* characterisation was performed (Chapter 6) which demonstrated that the shelf life of the sensor for 14 days was subject to a decrease in sensitivity of 10 %. Upon exposure to brain tissue for 14 days the sensor experienced a decrease in sensitivity of 26 %. The effect of a variety of interferent species on the selectivity of the sensor was examined. The total average response attributed to 12 interferents was 0.182 ± 0.019 nA, (n = 4). The limit of detection of the sensor was determined to be 0.11 ± 0.02 µM, (n = 8) with subsecond recording.Chapter 7 utilises the choline biosensor in the *in-vivo* environment. Using microdialysis, the ability of the sensor to detect exogenous choline is examined with the perfusion of concentrations of choline between 20 and 1000 µM. As this was successful, pharmacological manipulations were utilised to determine the O_2 dependence of the sensor using chloral hydrate, Diamox and L-Name. Also, the sensors ability to detect changes in choline, as a result of manipulations of aspects of the cholinergic system were undertaken using HC-3, neostigmine and atropine. The choline biosensor was characterised in both the *in-vitro* and the *in-vivo* environment and demonstrated detection of choline in the striatum of a freely moving rat. This sensor was then further modified for the detection of Acetylcholine. A preliminary investigation into the modification of the choline biosensor with Acetylcholinesterase to detect acetylcholine is presented in chapter 8. It was demonstrated that the sensor can successfully detect acetylcholine in the *in-vitro* environment with a sensitivity of 0.26 ± 0.01 nA/µM.

1. Introduction

1.1. Introduction

This thesis focuses on the design and *in-vitro* and *in-vivo* characterisation of a sensor, for the real-time monitoring of choline in the brain, which can be subsequently modified for the detection of acetylcholine.

The mammalian brain is one of the most complex structures in the universe. The functional units are neurons (10^{11}) and glial cells (10^{12}). Neurons receive, process and transmit messages along a complex neuronal network where each neuron makes, on average (10^4) contacts with other neurons. Therefore, there are approximately 10^{15} neuronal connections in the human brain. Figure 1.1 illustrates the neuronal network. Each neuron consists of a cell body from which extend cytoplasmic projections. One of these projections is the axon, this usually projects further than the others and may bifurcate several times. The remaining extensions are dendrites. Glial cells provide physical and functional support in the central nervous system in the form of oligodendrocytes, that form myelin sheaths to increase the speed and efficacy of axonal conduction and astrocytes which connect the blood vessels in the brain with neuron cell bodies.

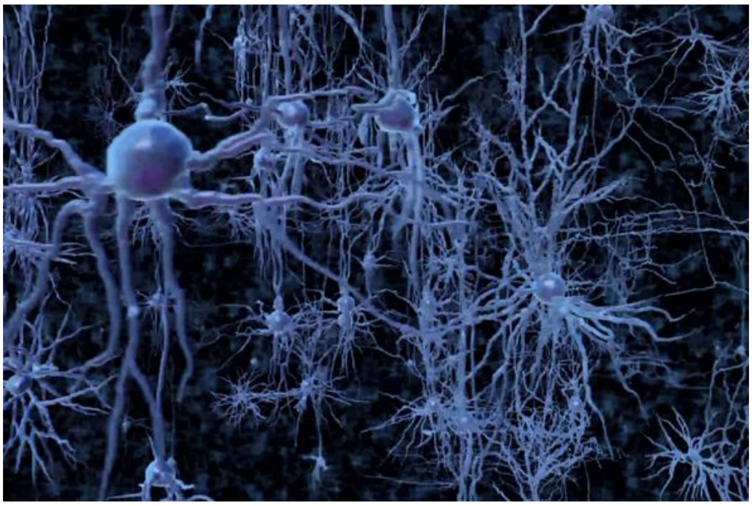

Figure 1.1: Neuronal connections.

http://www.learner.org/courses/neuroscience/text/text.html?dis=U&num=03&sec=01

The ends of axons are termed nerve terminals and contain specialised organelles called vesicles which contain neurotransmitters. Most neurons form networks, which facilitate communication among neurons through defined aqueous gaps known as synapses. Neurotransmitters are released from nerve terminals across these synapses. The resting potential of a neuron is about -70mV. The ions sodium (Na^+), potassium (K^+), chloride (Cl^-) and variously charged protein ions contribute to the resting potential of a neuron. The concentration of both Na^+ and Cl^- are both greater outside the neuron and K^+ is more concentrated inside the neuron. When a neuron is at rest synaptic vesicles containing neurotransmitters congregate next to the presynaptic membrane. During an action potential voltage-sensitive Na^+ ion channels open, causing depolarisation of the presynaptic membrane. Voltage-sensitive calcium channels open causing an influx of calcium which causes the vesicle to fuse with the synaptic membrane and empty the contents into the cleft. After a few milliseconds voltage sensitive K^+ channels open until the neuron is repolarised. These neurotransmitters produce signals in the post synaptic neuron by binding to post synaptic receptors. They then can either be degraded or re-taken up into the pre-synaptic neuron. Neurotransmitters and their metabolites can also flow into the extracellular fluid of the brain where their concentration is tightly regulated by their excretion into the cerebrospinal fluid or across the blood brain barrier.

1.2. Neurochemical analysis

Due to the complexity of the human brain, understanding the mechanisms underlying its function remains a challenge. Its electrical and chemical pathways are reflected in behaviour, feelings, thoughts and consciousness. However, it is the success of the clinical intervention in neurological disorders which target neuromediator related sites (The term neuromediator used to include classical neurotransmitters, neuromodulators and neurohormones) which suggest that intercellular chemical signalling plays a role in determining the properties of neural networks.

Although there was a time whereby studies were only possible *post mortem,* in recent years a variety of techniques have been developed for the analysis of brain function in the living brain. The non-invasive functional imaging techniques include positron emission tomography (PET) (Weaver *et al.*, 2007) and functional magnetic resonance imaging (Austin *et al.*, 2003). Alternatively, invasive techniques are available for the direct sampling of the extracellular environment in brain regions of freely moving animals. These techniques include *in-vivo* microdialysis (Lönnroth *et al.*, 1987) (Miele & Fillenz, 1996) which is discussed in detail in Section 2.5 and long term *in-vivo* electrochemistry (LIVE) (O'Neill *et al.*, 1998) (O'Neill & Lowry, 2006).

The first microdialysis probe was developed in 1972 (Delgado *et al.*, 1972). However it was Prof. Urban Ungerstedt at the Karolinska Institut in Sweden who greatly improved the design of the microdialysis probe by enlarging the surface area of the dialysis membrane, increasing the efficiency of the probe in collecting analyte (Ungerstedt & Pycock, 1974). This membrane demonstrates one key advantage of microdialysis over other *in-vivo* perfusion techniques for example, push-pull perfusions, as it provides a physical barrier between the perfusate and tissue limiting tissue exposure to turbulent flow of the perfusate. The perfusion of liquids through the microdialysis probe allows the free diffusion of analytes in the perfusion medium across the membrane as a result of a concentration gradient without the exchange of liquids. Another advantage of microdialysis, is that this technique is not restricted in its analyte sampling it is highly selective and can detect analytes in very low concentrations. The microdialysis technique is also subject to drawbacks. It is limited by its poor temporal resolution and the variable *in-vivo* recovery rate (see Section 2.5). The dialysis procedure can also create depletion around the probe area of solutes that can cross the membrane. Its large size also limits the technique to areas that are large enough to surround the probe.

The first reports of voltammetry in the living brain go back as far as 1958 when Leland C. Clark used voltammetry *in-vivo* for the detection of oxygen and ascorbic acid (Clark *et al.*, 1958) (Clark & Lyons, 1965). However, applying voltametric techniques to monitor neuromediators is generally attributed to Ralph. N. Adams *et al* in 1973 (Kissinger *et al.*, 1973). Voltammetry involves the application of a potential across an electrode-solution interface to oxidise or reduce species close to the electrode surface to generate a faradaic current. Some voltammetric techniques include fast cyclic voltametry (FCV), differential pulse amperometry (DPA) and constant potential amperometry (CPA). The advantages of voltammetry include real-time resolution, small size which reduces invasiveness and minimal extracellular fluid (ECF) chemical depletion. However, unlike microdialyisis, voltammetry is generally limited to the detection of a single anaylte. Additionally, endogenous electroactive species can pose a problem with respect to selectivity.

1.3. Biosensors

As mentioned above, Leland C. Clark used voltammetry for the detection of oxygen and ascorbic acid (AA) *in-vivo* (Clark *et al.*, 1958) (Clark & Lyons, 1965). Since then a range of electroactive species have been monitored *in-vivo* using unmodified electrodes such as uric acid (O'Neill, 1990), homovanillic acid (HVA) (O'Neill & Fillenz, 1985b), nitric oxide (Brown *et al.*, 2009) alongside AA (O'Neill & Fillenz, 1985a) and oxygen (Bolger & Lowry, 2005; Bolger *et al.*, 2011). However, in order to extend its application to the detection of important non-electroactive species (e.g. glucose, glutamate etc.) biosensors were developed.

A biosensor is a device that involves the immobilisation of a sensitive and selective biological element on, or in close proximity of an analytical detector. The type of analytical detector can vary – typical examples include electrodes, optical fibres and crystals, while the biological element can be enzymes, plant and animal tissue, microbes and antibodies (Cass, 1990).

Enzyme biosensors are the most thoroughly investigated sensors in the biosensor field. In 1962 Clark and Lyons developed the first reported biosensor for monitoring glucose (Clark & Lyons, 1962). This can be achieved with the immobilisation of the enzyme component onto the electrode surface by various strategies. They include physical adsorption by covalent bonding and/or cross-linking, entrapment behind a pre-cast or cast membrane or alternatively entrapment within a polymer matrix (Wilson & Thévenot, 1990).

Amperometric enzyme electrodes can be divided into first, second and third generation devices. A first generation biosensor monitors either the consumption of oxygen (Updike & Hicks, 1967) or the production of hydrogen peroxide (Lowry & O'Neill, 1994). These devices suffer from drawbacks due to fluctuations in response to oxygen, and interference from electroactive species at the necessary large overpotential applied for the oxidation of hydrogen peroxide. Second generation devices use a low overpotential and replace the oxygen required in the enzymatic reaction with a mediator (El Atrash & O'Neill, 1995). These devices are subject to drawbacks that include leaching of the mediator causing toxicity in the biological system and electrochemical interference (Wang, 2001). As this is the case third generation biosensors were developed. These are mediatorless electrodes made from conducting organic salts (Bartlett, 1990). However, there is some controversy as to whether they are actually mediatorless or not.

Biosensors used for neurochemical analysis, have the benefit of high temporal resolution and small size relative to microdialysis. These platinum electrodes are typically 125 µm in diameter, which is less than the threshold value for cellular damage. This was measured by uric acid release as a result of glial reaction to the perturbation of the tissue (Duff & O'Neill, 1994). The use of biosensors is also subject to problems, such as oxygen interference since fluctuating levels of co-substrate is a common problem for oxidase enzyme-based biosensors and will be referred to later in this thesis (Chapter 5). In addition, the interference of endogenous electroactive species can also pose a problem. The electropolymerisation of the monomer *o*-phenylenediamine (*o*-PD) to produce a polymer layer (PPD) facilitates the elimination of the detection of interferents while retaining the high permeability to hydrogen peroxide. PPD is used in this thesis to address the problem of electroactive interference and a detailed description of the process is given in Section 2.8.

1.4. The cholinergic system

Acetylcholine (Ach) was discovered in 1920 and was the first known neurotransmitter (Brown, 2006). Acetylcholine plays a role in movement, learning, memory and higher consciousness (Woolf & Butcher, 2011) (Blokland, 1995). Hence, the dysregulation of the cholinergic system has been linked to Alzheimer's disease (Muir, 1997), vascular dementia (Lojkowska *et al.*, 2003), schizophrenia (Hyde & Crook, 2001) and movement disorders such as Parkinson's and Huntington's disease (Pisani *et al.*, 2007). Acetylcholine and choline have been almost extensively monitored in the rat brain by means of microdialysis (Ikarashi *et al.*, 1997; Koppen *et al.*, 1997; Kehr *et al.*, 1998; Nakamura *et al.*, 2001) however detection by biosensors benefits from their real-time resolution and small size. Therefore, the real-time detection of these analytes can be useful with respect to gaining detailed information on the cholinergic system which is an important factor in these diseases.

The synthesis of Ach requires its precursor and metabolite; choline. The brain has little ability to synthesise choline de novo, therefore is dependent on the uptake of choline into the neurons from the blood mainly through dietary sources (Tuček, 1993) (Babb *et al.*, 2004). Neurons have the ability to transport choline into the neurons via the low or high affinity choline uptake systems (Hartmann *et al.*, 2008). The low affinity choline uptake (LACU) process guarantees choline availability for phospholipid synthesis (Hartmann *et al.*, 2008). After cellular uptake the choline is phosphorylated and incorporated into phospholipids (Zeisel *et al.*, 1991). This bound choline can be released by phospholipases in times of low choline availability for Ach synthesis (Löffelholz, 1998). Cholinergic neurons are also equipped with a high affinity choline uptake (HACU) system. The HACU is regarded as the regulatory step in the synthesis of acetylcholine (Kuhar & Murrin, 1978). Once choline is transported into the neuron by the HACU, Ach is synthesised using choline and acetyl-coenzyme A (acetyl-coA) by choline acetyltransferase (ChAT). The acetylcholine is then transported into the pre-synaptic vesicles by the vesicular Ach transporter (VAChT) (Mullen *et al.*, 2007). It exchanges two protons, generated by a proton ATPase with one Ach molecule via an electrochemical gradient (Nguyen *et al.*, 1998). Figure 1.2 illustrates the process involved in acetylcholine synthesis release and degredation.

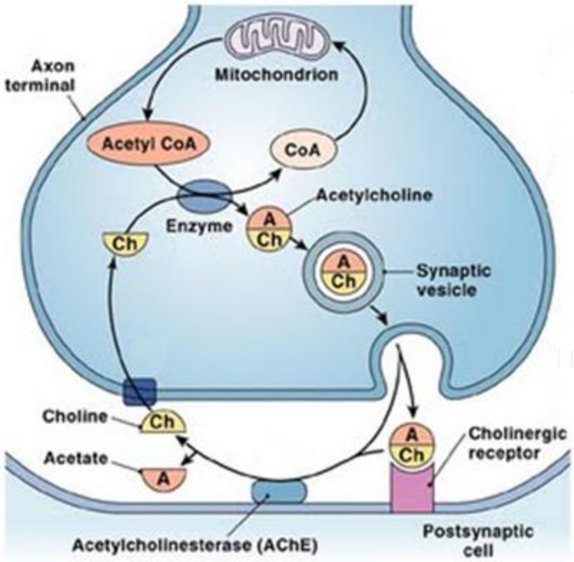

Figure 1.2 : Cholinergic neuron.

http://chekhovsgun.blogspot.ie/2009/12/cholinergic-hypothesis-of-depression.html

Acetylcholine has two receptor subtypes the muscarinic and nicotinic receptors. These are named because for the muscarinic receptor, muscarine is the agonist and for the nicotinic receptor, nicotine is the agonist (Itier & Bertrand, 2001). The muscarinic receptor has five subtypes M1-M5. These receptors belong to a superfamily of G-protein coupled receptors (Bonner, 1989) (Eglen, 2006). Each receptor has seven transmembrane domains connected by three intracellular and three extracellular loops. The seven transmembrane domains are thought to form a ring like structure where Ach binds extracellularly (Goyal, 1989). The M1, M3 an M4 subtypes are expressed mainly in the neocortex and hippocampus. The hippocampus also has the M5 subtype which is also expressed in the sustantia nigra. The striatum expresses the M1 and M4 subtypes and the M2 receptors are in the basal forebrain, thalamus and brainstem (Levey *et al.*, 1991). The nicotinic receptor was discovered a decade before any other receptor. Nicotinic receptors are ligand-gated ion channels assembled from five subunits into a pentemer with the stoichiometry $\alpha 2$, β, γ and δ. (Itier & Bertrand, 2001). The subunits are arranged around a central cavity that leads to the ion channel (Brady *et al.*, 2005).

Cholinergic activity is terminated by the hydrolysis of Ach in the synapse by acetylcholinesterase (AchE) (Abreu-Villaça *et al.*, 2011). The hydrolysis of Ach by AchE is a rapid and efficient process whereby one molecule of AchE can hydrolyse 5000 molecules of Ach per second (Lawler, 1961). This process is a major source of free choline for the uptake by the HACU for the synthesis of Ach. As already outlined, the brain is also dependent on the uptake of choline from the blood through dietary sources (Tuček, 1993; Babb *et al.*, 2004). However, choline is also the precursor to phosphotidylcholine, a major phospholipid component, and constitutes a reservoir of choline that can be used for Ach synthesis (Farber *et al.*, 1996). After cellular uptake the choline is phosphorylated and incorporated into phospholipids (Zeisel *et al.*, 1991). This bound choline can be released by phospholipases in times of low choline availability (Löffelholz, 1998). These three sources of choline are all taken up into the pre-synaptic terminal for the synthesis of Ach.

1.5. Overview of Research

This thesis describes the *in-vitro* development and *in-vitro* and *in-vivo* characterisation of a choline biosensor.

Although both choline and acetylcholine can be detected using microdialysis, the high temporal resolution of biosensors, makes this method of detection more desirable for the detection of these analytes. The theoretical aspects associated with the experimental studies is outlined in chapter two and chapter three details the materials and methods utilised in this.

The results chapters begin with the development of the choline biosensor (Chapter 4). This chapter outlines the steps taken in the optimisation of the design with respect to choline sensitivity. Chapter five details the modifications made to the sensor design to decrease the O_2 interference, as this co-factor for oxidase enzymes presents a problem in the *in-vivo* brain environment due to low O_2 concentrations compared to the *in-vitro* environment. Further characterisation of the sensor is presented in Chapter six, including studies of the stability of the sensor after contact with physiologically relevant components (e.g. lipids and proteins) and the rejection of known potential interferents.

Additionally, physiological ranges for temperature and pH are also presented. Chapter seven details the *in-vivo* characterisation of the sensor to determine if the sensor can detect choline in the brain. Chapter eight looks at the modification of the choline biosensor for the detection of acetylcholine. Finally, Chapter nine concludes the thesis and discusses the main experimental outcomes.

Abreu-Villaça Y, Filgueiras CC & Manhães AC. (2011). Developmental aspects of the cholinergic system. *Behavioural Brain Research* **221,** 367-378.

Austin VC, Blamire AM, Grieve SM, O'Neill MJ, Styles P, Matthews PM & Sibson NR. (2003). Differences in the BOLD fMRI response to direct and indirect cortical stimulation in the rat. *Magnetic Resonance in Medicine* **49,** 838-847.

Babb SM, Ke Y, Lange N, Kaufman MJ, Renshaw PF & Cohen BM. (2004). Oral choline increases choline metabolites in human brain. *Psychiatry Research: Neuroimaging* **130,** 1-9.

Bartlett PN. (1990). Conducting organic salt electrodes. pp. 47-95. IRL Press at Oxford University Press, New York, United States of America.

Blokland A. (1995). Acetylcholine: a neurotransmitter for learning and memory? *Brain Research Reviews* **21,** 285-300.

Bolger FB, Bennett R & Lowry JP. (2011). An *In-Vitro* characterisation comparing carbon paste and Pt microelectrodes for real-time detection of brain tissue oxygen. *Analyst* **136,** 4028-4035.

Bolger FB & Lowry JP. (2005). Brain tissue oxygen: *In-Vivo* monitoring with carbon paste electrodes. *Sensors* **5,** 473-487.

Bonner TI. (1989). The molecular basis of muscarinic receptor diversity. *Trends in Neurosciences* **12,** 148-151.

Brady S, Siegel G, Albers RW & Price D. (2005). *Basic Neurochemistry: Molecular, Cellular and Medical Aspects*. Lippencott-Raven, Philidelphia, United States of America

Brown DA. (2006). Acetylcholine. *British Journal of Pharmacology* **147,** S120-S126.

Brown FO, Finnerty NJ & Lowry JP. (2009). Nitric oxide monitoring in brain extracellular fluid: characterisation of Nafion-modified Pt electrodes *In-Vitro* and *In-Vivo*. *Analyst* **134,** 2012-2020.

Cass AEG. (1990). *Biosensors: A Practical Approach*. IRL Press at Oxford University Press, New York, United States of America.

Clark LC, Jr. & Lyons C. (1965). Studies of a glassy carbon electrode for brain polarography with observations on the effect of carbonic anhydrase inhibition. *Alabama Journal Medical Sciences* **2,** 353-359.

Clark LC & Lyons C. (1962). Electrode systems for continuous monitoring in cardiovascular surgery. *Annals of the New York Academy of Sciences* **102,** 29-45.

Clark LC, Misrahy G & Fox RP. (1958). Chronically Implanted Polarographic Electrodes. *Journal of Applied Physiology* **13,** 85-91.

Delgado JM, DeFeudis FV, Roth RH, Ryugo DK & Mitruka BM. (1972). Dialytrode for long term intracerebral perfusion in awake monkeys. *Archives Internationales de Pharmacodynamie* **198,** 9-21.

Duff A & O'Neill RD. (1994). Effect of probe size on the concentration of brain extracellular uric acid monitored with carbon paste electrodes. *Journal of Neurochemistry* **62,** 1496-1502.

Eglen RM. (2006). Muscarinic receptor subtypes in neuronal and non-neuronal cholinergic function. *Autonomic and Autacoid Pharmacology* **26,** 219-233.

El Atrash SS & O'Neill RD. (1995). Characterisation in vitro of a naphthoquinone-mediated glucose oxidase-modified carbon paste electrode designed for neurochemical analysis in vivo. *Electrochimica Acta* **40,** 2791-2797.

Farber SA, Savci V, Wei A, Slack BE & Wurtman RJ. (1996). Choline's phosphorylation in rat striatal slices is regulated by the activity of cholinergic neurons. *Brain Research* **723,** 90-99.

Goyal RK. (1989). Muscarinic Receptor Subtypes. *New England Journal of Medicine* **321,** 1022-1029.

Hartmann J, Kiewert C, Duysen EG, Lockridge O & Klein J. (2008). Choline availability and acetylcholine synthesis in the hippocampus of acetylcholinesterase-deficient mice. *Neurochemistry International* **52,** 972-978.

Hyde TM & Crook JM. (2001). Cholinergic systems and schizophrenia: primary pathology or epiphenomena? *Journal of Chemical Neuroanatomy* **22,** 53-63.

Ikarashi Y, Takahashi A, Ishimaru H, Arai T & Maruyama Y. (1997). Relations between the extracellular concentrations of choline and acetylcholine in rat striatum. *Journal of Neurochemistry* **69,** 1246-1251.

Itier V & Bertrand D. (2001). Neuronal nicotinic receptors: from protein structure to function. *FEBS Letters* **504,** 118-125.

Kehr J, Dechent P, Kato T & Ögren SO. (1998). Simultaneous determination of acetylcholine, choline and physostigmine in microdialysis samples from rat hippocampus by microbore liquid chromatography/electrochemistry on peroxidase redox polymer coated electrodes. *Journal of Neuroscience Methods* **83,** 143-150.

Kissinger PT, Hart JB & Adams RN. (1973). Voltammetry in brain tissue — a new neurophysiological measurement. *Brain Research* **55,** 209-213.

Koppen A, Klein J, Erb C & Loffelholz K. (1997). Acetylcholine release and choline availability in rat hippocampus: effects of exogenous choline and nicotinamide. *Journal of Pharmacology and Experimental Therapeutics* **282,** 1139-1145.

Kuhar MJ & Murrin LC. (1978). Sodium-Dependent, High Affinity Choline Uptake. *Journal of neurochemistry* **30,** 15-21.

Lawler HC. (1961). Turnover time of acetylcholinesterase. *Journal of Biological Chemistry* **236,** 2296-2301.

Levey AI, Kitt CA, Simonds WF, Price DL & Brann MR. (1991). Identification and localization of muscarinic acetylcholine receptor proteins in brain with subtype-specific antibodies. *Journal of Neuroscience* **11,** 3218-3226.

Löffelholz K. (1998). Brain choline has a typical precursor profile. *Journal of Physiology-Paris* **92,** 235-239.

Lojkowska W, Ryglewicz D, Jedrzejczak T, Minc S, Jakubowska T, Jarosz H & Bochynska A. (2003). The effect of cholinesterase inhibitors on the regional blood flow in patients with Alzheimer's disease and vascular dementia. *Journal of the Neurological Sciences* **216,** 119-126.

Lönnroth P, Jansson PA & Smith U. (1987). A microdialysis method allowing characterization of intercellular water space in humans. *American Journal of Physiology* **253,** E228-E231.

Lowry JP & O'Neill RD. (1994). Partial Characterization *In-Vitro* of Glucose Oxidase-Modified Poly(phenylenediamine)-coated electrodes for neurochemical analysis *In-Vivo*. *Electroanalysis* **6,** 369-379.

Miele M & Fillenz M. (1996). *In-Vivo* determination of extracellular brain ascorbate. *Journal of Neuroscience Methods* **70,** 15-19.

Muir JL. (1997). Acetylcholine, Aging, and Alzheimer's Disease. *Pharmacology Biochemistry and Behavior* **56,** 687-696.

Mullen GP, Mathews EA, Vu MH, Hunter JW, Frisby DL, Duke A, Grundahl K, Osborne JD, Crowell JA & Rand JB. (2007). Choline transport and de novo choline synthesis support acetylcholine biosynthesis in Caenorhabditis elegans cholinergic neurons. *Genetics* **177,** 195-204.

Nakamura A, Suzuki Y, Umegaki H, Ikari H, Tajima T, Endo H & Iguchi A. (2001). Dietary restriction of choline reduces hippocampal acetylcholine release in rats: *In-Vivo* microdialysis study. *Brain Research Bulletin* **56,** 593-597.

Nguyen ML, Cox GD & Parsons SM. (1998). Kinetic parameters for the vesicular acetylcholine transporter: two protons are exchanged for one acetylcholine. *Biochemistry* **37,** 13400-13410.

O'Neill RD. (1990). Uric acid levels and dopamine transmission in rat striatum: diurnal changes and effects of drugs. *Brain Research* **507,** 267-272.

O'Neill RD & Fillenz M. (1985a). Circadian changes in extracellular ascorbate in rat cortex, accumbens, striatum and hippocampus: correlations with motor activity. *Neuroscience Letters* **60,** 331-336.

O'Neill RD & Fillenz M. (1985b). Detection of homovanillic acid *In-Vivo* using microcomputer-controlled voltammetry: simultaneous monitoring of rat motor activity and striatal dopamine release. *Neuroscience* **14,** 753-763.

O'Neill RD & Lowry JP. (2006). Voltammetry *In-Vivo* for Chemical Analysis of the Living Brain. In *Encyclopedia of Analytical Chemistry*. John Wiley & Sons, Ltd.

O'Neill RD, Lowry JP & Mas M. (1998). Monitoring brain chemistry *In-Vivo*: voltammetric techniques, sensors, and behavioral applications. *Critical Reviews in Neurobiology* **12,** 69-127.

Pisani A, Bernardi G, Ding J & Surmeier DJ. (2007). Re-emergence of striatal cholinergic interneurons in movement disorders. *Trends in Neuroscience* **30,** 545-553.

Tuček S. (1993). Short-term control of the synthesis of acetylcholine. *Progress in Biophysics and Molecular Biology* **60,** 59-69.

Ungerstedt U & Pycock C. (1974). Functional correlates of dopamine neurotransmission. *Bulletin der Schweizerischen Akademie der Medizinischen Wissenschaften* **30,** 44-55.

Updike SJ & Hicks GP. (1967). The Enzyme Electrode. *Nature* **214,** 986-988.

Wang J. (2001). Glucose Biosensors: 40 Years of Advances and Challenges. *Electroanalysis* **13,** 983-988.

Weaver JD, Espinoza R & Weintraub NT. (2007). The Utility of PET Brain Imaging in the Initial Evaluation of Dementia. *Journal of the American Medical Directors Association* **8,** 150-157.

Wilson GS & Thévenot DR. (1990). *Unmediated Amperometric Enzyme Electrodes*. IRL Press at Oxford University Press, United States.

Woolf NJ & Butcher LL. (2011). Cholinergic systems mediate action from movement to higher consciousness. *Behavioural Brain Research* **221,** 488-498.

Zeisel SH, Da Costa KA, Franklin PD, Alexander EA, Lamont JT, Sheard NF & Beiser A. (1991). Choline, an essential nutrient for humans. *Federation of American Societies for Experimental Biology Journal* **5,** 2093-2098.

2. Theory

2.1. Introduction

As neither choline nor acetylcholine is electroactive, the direct measurement of these compounds is not possible. Therefore, in the case of the choline biosensor the incorporation of choline oxidase has been utilised to produce electrochemically detectable H_2O_2. For the detection of acetylcholine a two step process is utilised. Firstly, acetylcholine esterase is incorporated onto the sensor in order to liberate choline from acetylcholine. Then choline oxidase is incorporated in the sensor design in order to produce H_2O_2 from the choline liberated.

A description of the *in-vitro* electrochemical cell setup is described in full in Section 3.5.1.1 In addition; the *in-vivo* set-up for analyte detection is described in Section 3.5.2. The electrochemical cell set-up utilises a three electrode system. This consists of a working electrode where the electrochemical changes of interest take place, a reference electrode which has a known fixed potential, against which the potential of the working electrode can be measured. Also, an auxiliary or counter electrode is used which functions as a source or sink of electrons and completes the electrical circuit.

The primary work undertaken involved the development and characterisation of both a choline and acetylcholine biosensor. These biosensors were characterised in terms of their response to the target substrate, Michaelis-Menten kinetic parameters (V_{MAX}, K_M and α) and the rejection of potential interferents.

2.2. Oxidation and reduction

The H_2O_2 produced by the interaction between choline and choline oxidase is oxidised at the working electrode surface upon application of a potential giving a proportional Faradaic current. The reaction for the oxidisation and reduction of a species occurring at the active surface of an electrode is described in Equation 2.1, where *O* and *R* are the oxidised and reduced species and *n* is the number of electrons involved in the reaction.

$$O + ne^{-} \rightleftharpoons R \qquad \textbf{(2.1)}$$

The two main processes which contribute to this reaction are mass transport of the reactant to the active surface of the electrode and electron transfer.

Upon application of a potential in the absence of the target analyte, a capacitance current (background current) arises due to the opposing charges between the electrode and the aqueous media. This background current is subtracted from all experimental data in this thesis

2.3. Mass Transport

Mass transport of the analyte from the bulk solution to the electrode and the rate of electron transfer at the electrode surface, determine how the electrochemical reaction occurs. The experimentally measured current (I) is a direct indication of the rate of the electrochemical reaction and is given by Faraday's law.

$$I = nFAJ \qquad \textbf{(2.2)}$$

Where (*I*) indicates the current, *n* refers to the number of moles, F is the Faraday constant, A is the area of the electrode (m^2) and J is the flux of ions (mol m^{-2} s^{-1}).

Mass transport involves the following processes; migration, convection and diffusion. Migration is the movement of a charged species under the influence of an electric field.

Migration can be reduced to negligible levels by the inert electrolyte i.e. phosphate buffered saline (PBS) (see Section 3.3.2.1) at a concentration far greater than the electroactive species. Convection is the movement of species as a result of external, mechanical forces such as stirring. *In-vitro* experiments introduce forced convection into the electrochemical cell via a magnetic stirrer alongside aliquots of substrate. The convection contribution, however, can be neglected as the analysis of all calibration data was taken from the steady state currents in a quiescent solution.

The mass transport of the electroactive species has therefore been restricted to diffusion by the use of the inert electrolyte and operating in a quiescent solution. Diffusion is the movement of species under the influence of a concentration gradient. Diffusion is described by Fick's first law (see Equation 2.3), which states that the flux is proportional to the concentration gradient.

$$J = -D\frac{\partial c}{\partial x} \qquad \textbf{(2.3)}$$

Where J is the flux, $\frac{\partial c}{\partial x}$ is the concentration gradient in direction x, and D is the diffusion coefficient.

Fick's second law (Equation 2.4) describes the variation in concentration of the electroactive species with time due to movement described in Figure 2.1.

$$\frac{\partial c}{\partial t} = D\frac{\partial^2 c}{\partial x^2} \qquad \textbf{(2.4)}$$

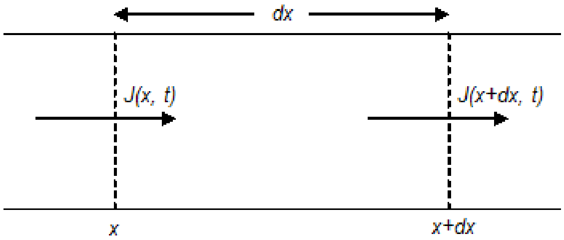

Figure 2.1: Diffusion in one dimension, in the direction opposing the concentration gradient.

The progress of the reaction may result in a concentration gradient being created due to the species being consumed. However, due to the small dimensions of microelectrodes, where the currents are small and minimal substrate is consumed, a steady-state current response is obtained (i.e. $\left(\frac{\partial c}{\partial t}\right) = 0$, no change in c with t).

For planar electrodes, which are uniformly accessible to species from the bulk solution, the variation of current with time calculated from Fick's second law results in the Cottrell equation (Equation 2.5):

$$I = nFAJ = \frac{nFAD^{1/2}c_{\infty}}{(\pi t)^{1/2}} \qquad \textbf{(2.5)}$$

with I the current measured at time t at the electrodes active surface of area A, being directly proportional to c_{∞}, the bulk concentration of the electroactive species. J is the flux, n the number of electrons, D the diffusion coefficient and F the Faraday constant.

A Laplace operator, ∇, is substituted into Equation 2.3 to determine the flux for any co-ordinate system (i.e. electrode geometry) giving:

$$J = -D\nabla^2 c \qquad \textbf{(2.6)}$$

and as a result, Fick's second law of diffusion for any geometry, becomes:

$$\frac{\partial c}{\partial t} = D\nabla^2 c \qquad \textbf{(2.7)}$$

The laplacian operator for cylinder electrodes is:

$$\frac{\partial^2}{\partial r^2} + \left(\frac{1}{r}\right)\left(\frac{\partial}{\partial r}\right) \qquad \textbf{(2.8)}$$

The solution to all the above diffusion equations requires that initial conditions (values at t = 0) and two boundary conditions (conditions associated with certain values of the spatial coordinates) be obeyed.

Fick's first law of diffusion shows that the flux of species R at the electrode, $J_R(0,t)$, is proportional to the current density, $\frac{i}{A}$.

$$-J_R(0,t) = \frac{i}{nFA} = D_R\left[\frac{\partial c_R(x,t)}{\partial x}\right]_{x=0} \qquad \textbf{(2.9)}$$

where i is the current, n the number of electrons transferred, F is the Faraday constant and A is the area of the active surface of the electrode. The sum of the electrons transferred at the electrode per unit time must be proportional to the concentration of R reaching the electrode surface over that time period.

2.4. Constant Potential Amperometry

All data presented in this thesis was recorded using constant potential amperometry (CPA). In CPA the current is recorded with the application of a fixed potential that oxidises or reduces the analyte being investigated. Diffusion is assumed to be the only form of mass transport which limits the consumption of the analyte resulting in a steady-state diffusion limited current (i_{ss}):

$$i_{ss} = \frac{nFACD}{r} \qquad \textbf{(2.10)}$$

where i_{ss} is the steady-state current, n is the number of electrons, A is the electrode area, D is the diffusion coefficient, F is the Faraday constant, C is the concentration and r is the radius.

Additional factors such as the geometry or the insulation thickness (Dayton *et al.*, 1980) of the electrode have an effect on the steady-state current and as a result a geometric factor, G, is incorporated into Equation 2.10:

$$i_{ss} = \frac{GnFACD}{r} \qquad \textbf{(2.11)}$$

The resulting current is directly proportional to the diffusion coefficient and the substrate concentration.

2.5. Microdialysis

Microdialysis (MD) is a technique which is utilised for the sampling of various neurotransmitters and metabolites in the living brain. MD involves the implantation of a small probe into the brain which consists of a hollow tube and a semi-permeable membrane. This membrane allows the passage of water and small solutes (10 – 30 kD molecular weight cut-off). The probe is perfused with artificial cerebrospinal fluid (aCSF) which mimics the ionic concentration of the brain. The perfusate equilibrates with the extracellular fluid (ECF) by diffusion of a higher concentration of analyte in the surrounding tissue across a concentration gradient towards the lower concentration present in the probe. The dialysate is then collected and analysed by high performance liquid chromatography (HPLC) (Perry *et al.*, 2009).

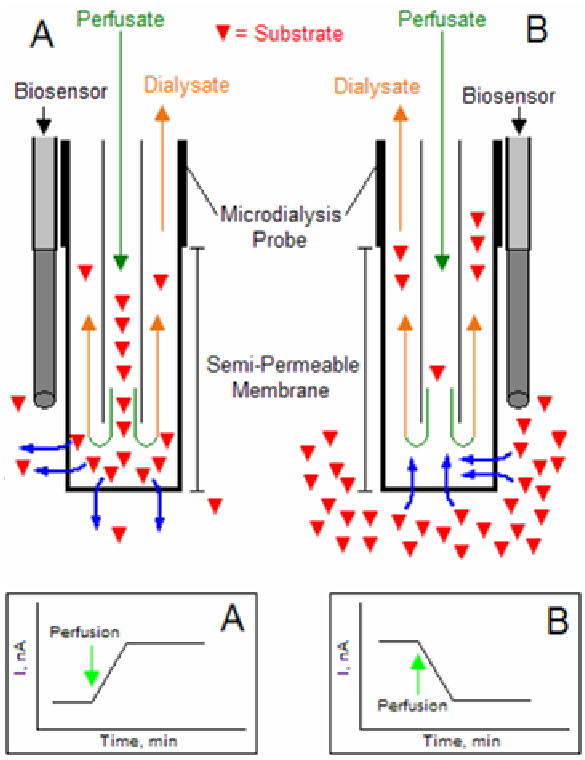

Figure 2.2: Schematic of the principles of (Top) *in-vivo* microdialysis coupled with (Bottom) *in-vivo* voltammetry.

(A): Perfusion of a substrate that is higher in concentration than the ECF substrate concentration.

(B): Perfusion of a substrate that is lower in concentration than the ECF substrate concentration.

In this thesis, the dialysate was not collected for analysis. The MD was coupled with a biosensor and co-implanted ensuring close proximity *ca.* 1mm (see Figure 2.2). This facilitates the real-time monitoring of perfused substances by the biosensor. The local administration of substances to the brain in this manner is termed retrodialysis (Huynh *et al.*, 2007). The perfusion of substances higher in concentration than the ECF concentration results in an increase in the observed current from the biosensor. The perfusion of a substrate that is a lower concentration than the ECF concentration results in a decrease in current from the biosensor. A modified Lönnroth zero-net flux (ZNF) method carried out by perfusing various substrate concentrations, results in a value for the extracellular concentration of the substrate (Lönnroth *et al.*, 1987).

The microdialysis method of substrate delivery to the sensor has been shown previously to be subject to limitations by recovery. Recovery is defined as the percentage of the concentration of analyte in the dialysate with respect to the concentration in the interstitial fluid. Recovery can be ideally close to 100 %, however, the conditions during use of microdialysis in the brain using long dialysis membranes and a low perfusion flow mean that recovery is estimated at approximately 70 % (Ungerstedt & Rostami, 2004). In addition to low recovery rates, microdialysis can be invasive, resulting in traumatic injury to the surrounding tissue. This can lead to alterations in the tissue adjacent to the probe compared to that undisturbed by the probe implantation (Khan & Michael, 2003).

2.6. Enzymes

2.6.1. Introduction

A biosensor can be defined as a device that involves the incorporation of a sensitive and selective biological element on, or within close proximity of, an analytical detector. The biological element used during the course of this project was enzymes. The use of enzymes in the development of biosensors has been instrumental in enabling the detection of non-electroactive or poorly electroactive compounds. Enzymes accelerate reactions in biological systems and can catalyse various biological reactions without themselves undergoing any chemical change and not altering the equilibrium of the reaction. In addition, enzymes are highly specific in their actions and only act upon one substrate. Therefore, the use of enzymes is highly desirable for the fabrication of biosensors. The incorporation of enzymes into biosensors allows the indirect measurement of the non-electroactive substrates by electrochemical means.

The entire enzyme molecule is not directly involved in the catalysis. The substrate interacts with a small portion known as the active site. The active site contains both binding and catalytic groups which bind the substrate on the enzyme then the catalytic groups promote the conversion to products.

2.6.2. Enzyme Kinetics

Enzymatic reactions are characterised by having fast complex mechanisms, the numerous active sites of the enzyme can interact in multiple ways with substrate molecules. A single substrate enzyme-catalysed reaction where one substrate-binding site is present results in the following general enzyme kinetic equation:

$$E + S \underset{k_{-1}}{\overset{k_1}{\rightleftharpoons}} ES \underset{k_{-2}}{\overset{k_2}{\rightleftharpoons}} E + P \qquad \textbf{(2.12)}$$

where E is the enzyme molecule, S is the substrate and P is the resulting product of the reaction. k_x refers to the rate constants for each specific reaction (x = 1, -1, 2, -2).

When experiments are limited to the initial period of the reaction, the product concentration is negligible and the formation of ES from product by pathway k_2 can be ignored. As a result Equation 2.12 becomes:

$$E + S \underset{k_{-1}}{\overset{k_1}{\rightleftharpoons}} ES \xrightarrow{k_2} E + P \qquad \textbf{(2.13)}$$

Michaelis and Menten derived the rate equation for enzyme catalysis. The steady-state approximation can be applied to the formation and destruction of the enzyme-substrate complex, ES (Michaelis & Menten, 1913). As a result the rate of change of $[ES]$ with time is shown in the following equation:

$$\frac{d[ES]}{dt} = k_1[E][S] - k_{-1}[ES] - k_2[ES] \qquad \textbf{(2.14)}$$

where $[E]$ is the concentration of unbound enzyme and $[ES]$ the concentration of the bound enzyme. Hence, the total enzyme concentration $[E]_0$, can be substituted by

$$[E] = [E]_0 - [ES] \quad \textbf{(2.15)}$$

Therefore,

$$\frac{d[ES]}{dt} = k_1[E]_0[S] - k_1[ES][S] - k_{-1}[ES] - k_2[ES] \quad \textbf{(2.16)}$$

Applying the steady state gives:

$$k_1[E]_0[S] - k_1[ES][S] - k_{-1}[ES] - k_2[ES] = 0 \quad \textbf{(2.17)}$$

So,

$$[ES] = \frac{k_1[E]_0[S]}{k_1[S] + k_{-1} + k_2} \quad \textbf{(2.18)}$$

$$[ES] = \frac{[E]_0[S]}{[S] + \dfrac{k_{-1} + k_2}{k_1}} \quad \textbf{(2.19)}$$

Allowing K_M, the Michaelis constant, to equate to the constants $\dfrac{k_{-1} + k_2}{k_1}$

As a result,

$$[ES] = \frac{[E]_0[S]}{[S] + K_M} \quad \textbf{(2.20)}$$

$[ES]$ has been isolated as it governs the rate of formation of products (overall rate of reaction) according to the relationship:

$$\nu = k_2[ES] \quad \textbf{(2.21)}$$

where ν is the overall rate of reaction.

Substituting gives:

$$v = \frac{k_2[E]_0[S]}{[S]+K_M} \qquad \textbf{(2.22)}$$

When substrate concentration is very high all the enzyme exists only as enzyme substrate complex and the limiting initial velocity (rate), $V_{\max}$, is reached.

Hence, $[S]$>>K_M and:

$$V_{\max} = k_2[E]_0 \qquad \textbf{(2.23)}$$

and so,

$$v = \frac{V_{\max}[S]}{[S]+K_M} \qquad \textbf{(2.24)}$$

Michaelis and Menten further assumed that the substrate was usually present in much greater concentration than the enzyme. Taking this into account, if the initial substrate concentration $[S]_0$ is much greater than the initial enzyme concentration $[E]_0$ then $[S] \cong [S]_0$ and as a result Equation 2.24 becomes:

$$v = \frac{V_{\max}[S]_0}{[S]_0+K_M} \qquad \textbf{(2.25)}$$

A rectangular hyperbola is observed when v is plotted against $[S]_0$ as displayed in Figure 2.3.

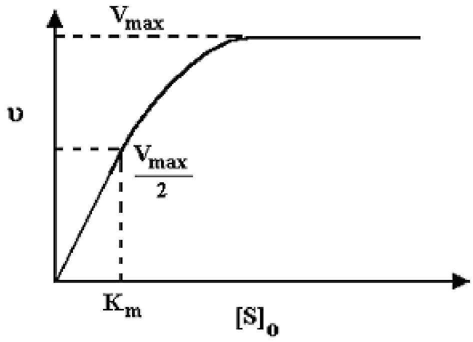

Figure 2.3: Graph of reaction rate *v* against substrate concentration $[S]_0$ for a given enzyme concentration $[E]_0$ for a single substrate enzyme catalysed reaction from the Michaelis-Menten equation. (see Equation 2.25)

V_{max}, the maximal initial velocity, at a particular $[E]_0$, can be obtained from the graph as indicated. K_M can also be obtained from the graph, when $v = \frac{V_{max}}{2}$.

With enzymes that exhibit sigmoidal kinetics rather than the hyperbolic response seen in Figure 2.3, a derivation of the Michaelis-Menten equation is required. This type of kinetics is apparent for example when more than one molecule of substrate binds to a single molecule of enzyme. If each binding site on the enzyme is similar and independent the response observed will still be hyperbolic. If there is an increase in affinity to a binding site a sigmoidal response is observed, known as the co-operative effect. In this body of work, deviations from ideal Michaelis-Menten kinetics and the constants, V_{max} and K_M, were determined using Equation 2.26, which is known as the Hill-type equation which was developed by Lowry *et al.* (Lowry & O'Neill, 1992) (Lowry et al., 1994)

$$i = \frac{V_{max}}{1 + \left(\frac{K_M}{[S]}\right)^{\alpha}} \qquad \textbf{(2.26)}$$

where i is the current observed due to electro-oxidation of H_2O_2 (see Equation 2.29) and is used to measure the rate of reaction, and α is used as a measure of deviation from the ideal Michaelis-Menten behaviour, where with ideal behaviour $\alpha = 1$. An α value of 2 is indicative of sigmoidal kinetics.

2.6.3. Choline Oxidase

In 1977 choline oxidase (ChOx) was purified from the soil bacterium *Arthrobacter globiformis* (Ikuta et al., 1977). Subsequently, the enzyme was also purified from *Alcaligenes* species (Ohta *et al.*, 1983) which is the enzyme used in this thesis. The molecular weight of the enzyme is estimated at 66 kDa for a monomer (Ohta-Fukuyama *et al.*, 1980) however, the 3D structure has not been determined.

ChOx, is a FAD- containing enzyme, which catalyses the oxidation of choline to glycine-betaine with betaine aldehyde as an intermediate and molecular oxygen is the primary electron acceptor (Gadda, 2003) (Tavakoli *et al.*, 2006). The role of FAD in the kinetic mechanism of choline oxidase has been determined demonstrating its role in the formation of the glycine-betaine by ChOx. After the formation of the E-FAD$_{ox}$-C complex, choline is oxidised to form betaine-aldehyde bound to the reduced enzyme. The E-FAD$_{red}$-BA complex reacts with oxygen, yielding the E-FAD$_{ox}$-BA species, in which the enzyme bound betaine-aldehyde then partitions to form glycine-betaine bound to the reduced enzyme and dissociation from the enzyme active site to form the E-FAD$_{ox}$ species. The E-FAD$_{red}$-B species then reacts with oxygen before the release of glycine-betaine (Gadda, 2003).

The mechanism of H_2O_2 liberation from ChOx is presented in the following Equation:

$$\begin{aligned} &(CH_3)_3 N^+ - (CH_2)_2 - OH + 2O_2 + H_2O \xrightarrow{ChOx} \\ &(CH_3)_3 N - CH_2 - COOH + 2H_2O_2 \end{aligned} \qquad \textbf{(2.27)}$$

2.6.4. Acetylcholinesterase

Acetylcholinesterases' (AchE) physiological task is the hydrolytic destruction of the neurotransmitter Acetylcholine (Ach). The hydrolysis of Ach by AchE is a rapid and efficient process whereby one molecule of AchE can hydrolyse 5000 molecules of Ach per second (Lawler, 1961). This is surprising as the catalytic site is found at the bottom of a deep narrow gorge. One theory suggest that the electric field of AchE assists catalysis by attracting the cationic species and expelling the anionic acetate product (Soreq & Seidman, 2001).

As Ach is neither electroactive nor does it produce H_2O_2 upon hydrolysis by AchE, this enzyme cannot be used solely for the amperometric detection of acetylcholine. AchE hydrolyses Ach by forming an acetyl-AchE intermediate with the release of choline and subsequent hydrolysis of the intermediate to release acetate shown in Equation 2.28.

$$\begin{aligned} &H_3C-COO-(CH_2)_2N^+(CH_3)_3+H_2O \xrightarrow{AchE} \\ &OH-(CH_2)_2-N^+(CH_3)_3+CH_3-COOH \end{aligned} \quad \textbf{(2.28)}$$

Subsequently H_2O_2 can be liberated as shown in Equation 2.27.

2.7. Hydrogen Peroxide

Platinum (Pt) electrodes have been reported for use in the oxidation of hydrogen peroxide (H_2O_2) which is produced from the enzymatic reactions in first generation biosensors (O'Neill *et al.*, 2004) (O'Neill & Lowry, 2006). At +700 mV *vs.* SCE, H_2O_2 is oxidised at a diffusion-controlled rate, resulting in a current response that is linear and can be used as a direct measure of analyte concentration (Lowry & O'Neill, 1994) (O'Brien *et al.*, 2007). The reaction for the oxidation of H_2O_2 is known to be a two-electron process (see Equation 2.32) and is similar in mechanism to the oxidation at palladium electrodes, where the formation of an oxide film on the metal surface is a necessary requirement to facilitate the oxidation of H_2O_2 (Hall *et al.*, 1997).

$$H_2O_2 \rightarrow O_2 + 2H^+ + 2e^- \qquad \textbf{(2.29)}$$

$$Pt(OH)_2 + H_2O_2 \rightarrow Pt + 2H_2O + O_2 \qquad \textbf{(2.30)}$$

$$Pt + 2H_2O \rightarrow Pt(OH)_2 + 2H^+ + 2e^- \qquad \textbf{(2.31)}$$

At the potential of +700 mV at which all enzymatic-based calibrations were performed, the platinum was in an oxidised state.

2.8. Electropolymerisation of *o*-Phenylenediamine

o-Phenylenediamine (*o*-PD) may be electropolymerised onto the surface of a Pt electrode to form an insulating poly-*o*-Phenylenediamine (PPD) layer. The use of PPD in sensor design has previously been demonstrated for the development of glucose and glutamate (Lowry & O'Neill, 1994) (McMahon & O'Neill, 2005). The purpose of PPD is to prevent access of larger interferent molecules such ascorbic acid while allowing access of smaller molecules such as H_2O_2 (Lowry *et al.*, 1994). The structure of the insulating form of PPD has not been determined, however two different structures of PPD have been proposed: a “ladder” like structure (see Figure 2.4 top) where the amino groups (NH_2) are condensed within the benzene ring adjacent to each other along the polymer chain. Alternatively, an “open” 1,4-substituted benzenoid-quinoid structure (Yano, 1995) (see Figure 2.4 bottom) has been proposed. Recent reports state increased NH_2 content is found when PPD is formed in neutral pH (Losito *et al.*, 2003). This suggests that the PPD formed in the experiments in this thesis are the ‘open’ structure.

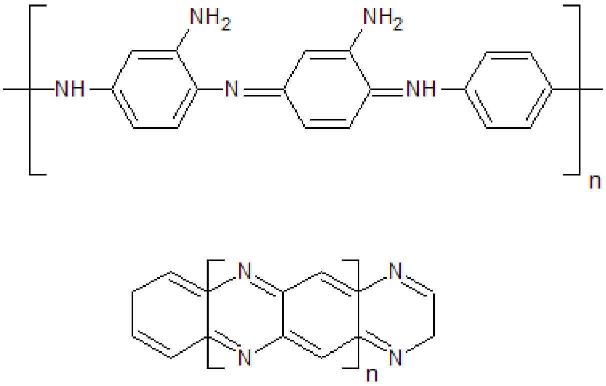

Figure 2.4: Possible structures for the polymeric form of *o*-phenylenediamine.

2.9. Ascorbic acid

Ascorbic acid is an electroactive compound which is readily oxidised at metal electrodes with an $E_{1/2}$ between the range -100 to +400 mV *vs.* SCE (O'Neill *et al.*, 1998). The mechanism for this reaction is a $2e^-$ process that results in the production of L-dehydroascorbic acid. This hydrolyses forming an electro-inactive open chain product, L-2,3-diketgulonic acid. The mechanism is shown in Figure 2.5:

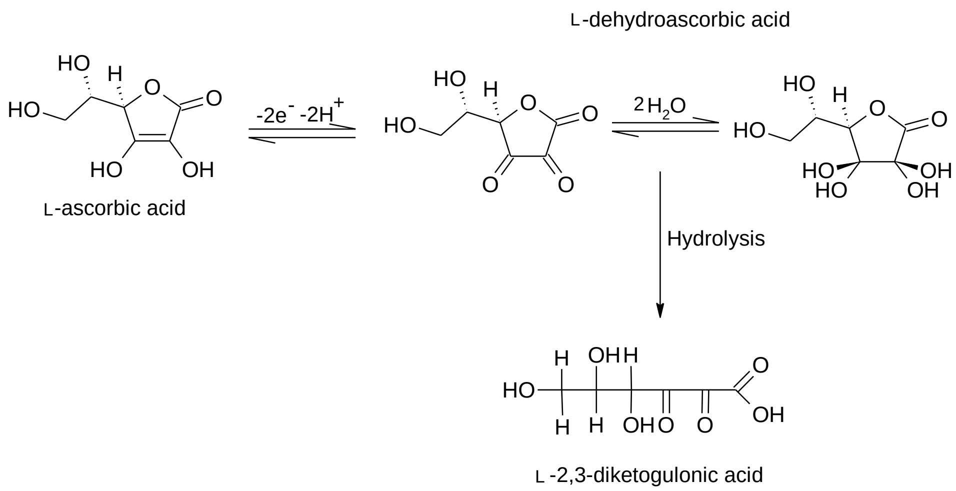

Figure 2.5: Reaction scheme for the oxidation of ascorbic acid.

2.10. Data Analysis

All experiments were analysed using either linear or non-linear regression. The regression was applied after the average steady-state current value was obtained and plotted in a graph of current response against substrate concentration.

2.10.1. Statistical analysis

In order to test whether two results are statistically different, *t*-tests were used as the method of analysis. Two forms of *t*-tests were employed; paired t-tests and unpaired *t*-tests. Paired tests were used for comparing signals recorded at the same electrodes, unpaired tests were used for comparing data from different electrodes. These tests were performed using Graphpad Prism and yielding a *P*-value.

The *P* value is a probability, where $0<P<1$. Small *P* values indicate that the results are significantly different. The standard 95% confidence interval was used for these tests, so a *P*-value less than 0.05 would indicate that there was a significant difference between the two sets of data analysed, whereas a *P*-value higher than 0.05 would indicate no significant difference.

The R^2 value is a measure of the goodness of fit of the data points to a line. It is a unitless fraction, where $0<R^2<1$. An R^2 value of 0 indicates that there is no linear (non-linear) relationship between the X and Y data values in the graph. An R^2 value of 1 indicates that all points lie on the line with no scatter, obeying the relationship perfectly.

2.10.2. Current Densities

In order to compare data from electrodes with different physical dimensions, transforming the current values into current densities was required. The formula for current density is shown in Equation 2.32.

$$J = \frac{I}{A} \qquad \textbf{(2.32)}$$

where J is the current density, I is the current and A is the area of the active surface of the electrode.

Dayton MA, Brown JC, Stutts KJ & Wightman RM. (1980). Faradaic electrochemistry at microvoltammetric electrodes. *Analytical Chemistry* **52,** 946-950.

Gadda G. (2003). pH and deuterium kinetic isotope effects studies on the oxidation of choline to betaine-aldehyde catalyzed by choline oxidase. *Biochimica et Biophysica Acta* **21,** 1-2.

Hall SB, Khudaish EA & Hart AL. (1997). Electrochemical oxidation of hydrogen peroxide at platinum electrodes. Part 1. An adsorption-controlled mechanism. *Electrochimica Acta* **43,** 579-588.

Huynh GH, Ozawa T, Deen DF, Tihan T & Szoka Jr FC. (2007). Retro-convection enhanced delivery to increase blood to brain transfer of macromolecules. *Brain Research* **1128,** 181-190.

Ikuta S, Imamura S, Misaki H & Horiuti Y. (1977). Purification and characterization of choline oxidase from Arthrobacter globiformis. *Journal of Biochemistry* **82,** 1741-1749.

Khan AS & Michael AC. (2003). Invasive consequences of using micro-electrodes and microdialysis probes in the brain. *TrAC Trends in Analytical Chemistry* **22,** 503-508.

Lawler HC. (1961). Turnover time of acetylcholinesterase. *Journal of Biological Chemistry* **236,** 2296-2301.

Lönnroth P, Jansson PA & Smith U. (1987). A microdialysis method allowing characterization of intercellular water space in humans. *American Journal of Physiology* **253,** E228-E231.

Losito I, Palmisano F & Zambonin PG. (2003). *o*-Phenylenediamine Electropolymerization by Cyclic Voltammetry Combined with Electrospray Ionization-Ion Trap Mass Spectrometry. *Analytical Chemistry* **75,** 4988-4995.

Lowry JP, McAteer K, El Atrash SS, Duff A & O'Neill RD. (1994). Characterization of Glucose Oxidase-Modified Poly(phenylenediamine)-Coated Electrodes *In-Vitro* and *In-Vivo*: Homogeneous Interference by Ascorbic Acid in Hydrogen Peroxide Detection. *Analytical Chemistry* **66,** 1754-1761.

Lowry JP & O'Neill RD. (1992). Homogeneous mechanism of ascorbic acid interference in hydrogen peroxide detection at enzyme-modified electrodes. *Analytical Chemistry* **64,** 453-456.

Lowry JP & O'Neill RD. (1994). Partial Characterization *In-Vitro* of Glucose Oxidase-Modified Poly(phenylenediamine)-coated electrodes for neurochemical analysis *In-Vivo*. *Electroanalysis* **6,** 369-379.

McMahon CP & O'Neill RD. (2005). Polymer−Enzyme Composite Biosensor with High Glutamate Sensitivity and Low Oxygen Dependence. *Analytical Chemistry* **77,** 1196-1199.

Michaelis L & Menten ML. (1913). Die kinetik der invertinwirkung. *Biochemistry* **49,** 352.

O'Brien KB, Killoran SJ, O'Neill RD & Lowry JP. (2007). Development and characterization *In-Vitro* of a catalase-based biosensor for hydrogen peroxide monitoring. *Biosensors and Bioelectronics* **22,** 2994-3000.

O'Neill RD, Chang SC, Lowry JP & McNeil CJ. (2004). Comparisons of platinum, gold, palladium and glassy carbon as electrode materials in the design of biosensors for glutamate. *Biosensors and Bioelectronics* **19,** 1521-1528.

O'Neill RD & Lowry JP. (2006). Voltammetry *In-Vivo* for Chemical Analysis of the Living Brain. In *Encyclopedia of Analytical Chemistry*. John Wiley & Sons, Ltd.

O'Neill RD, Lowry JP & Mas M. (1998). Monitoring brain chemistry *In-Vivo*: voltammetric techniques, sensors, and behavioral applications. *Critical Reviews in Neurobiology* **12,** 69-127.

Ohta-Fukuyama M, Miyake Y, Emi S & Yamano T. (1980). Identification and properties of the prosthetic group of choline oxidase from Alcaligenes sp. *Journal of Biochemistry* **88,** 197-203.

Ohta M, Miura R, Yamano T & Miyake Y. (1983). Spectroscopic studies on the photoreaction of choline oxidase, a flavoprotein, with covalently bound flavin. *Journal of Biochemistry* **94,** 879-892.

Perry M, Li Q & Kennedy RT. (2009). Review of recent advances in analytical techniques for the determination of neurotransmitters. *Analytica Chimica Acta* **653,** 1-22.

Soreq H & Seidman S. (2001). Acetylcholinesterase--new roles for an old actor. *Nature Reviews in Neuroscience* **2,** 294-302.

Tavakoli H, Ghourchian H, Moosavi-Movahedi AA & Saboury AA. (2006). Histidine and serine roles in catalytic activity of choline oxidase from Alcaligenes species studied by chemical modifications. *Process Biochemistry* **41,** 477-482.

Ungerstedt U & Rostami E. (2004). Microdialysis in neurointensive care. *Current Pharmaceutical Design* **10,** 2145-2152.

Yano J. (1995). Electrochemical and structural studies on soluble and conducting polymer from o-phenylenediamine. *Journal of Polymer Science A1* **33,** 2435-2441.

3. Experimental

3.1. Introduction

This chapter outlines the materials and methods used in the development and characterisation of choline and acetylcholine sensors both *in-vitro* and *in-vivo*. The fabrication of this sensor is based upon the foundation of previously designed platinum based biosensors (Lowry & O'Neill, 1994) (Ryan *et al.*, 1997). In addition, the use of styrene as an immobilisation matrix has been used previously for the development of a lactate biosensor within our research group, alongside the dip adsorption method (Bolger, 2007). The oxygen dependence considerations of the choline biosensor are based on previous work by Wang *et al.* (Wang & Lu, 1998) and Bolger *et al.* (Bolger, 2007). The rejection of potential endogenous electroactive interferents by the application of an *o*-PD layer is based on previously designed sensors (Malitesta *et al.*, 1990) (Lowry & O'Neill, 1994).

The instrumentation and chemicals used throughout this project are described in Sections 3.2 and 3.3. The modifications to the sensor throughout the project to obtain sensitive choline and acetylcholine sensors are outlined in Section 3.4. The modifications made to the sensor to combat oxygen dependence issues are outlined in Section 3.4. The further *in-vitro* characterisation techniques described in this thesis are outlined in Section 3.4.3 The electrochemical experiments used to characterise the electrodes *in-vivo* are described in Section 3.5.2. The electrodes were modified to give the maximum response to choline and acetylcholine *in-vitro*. Subsequently, the most suitable design for each analyte was chosen for characterisation *in-vivo*.

3.2. Computer-Based Instrumentation and Equipment

Throughout these experiments, the use of computer based instrumentation consisting of a computer, PowerLab® and potentiostat was used, incorporating the latest software packages for data acquisition and analysis.

3.2.1. Potentiostat, CPU and Data Acquisition

The potentiostat used for this project was a four channel biostat from ACM instruments. This was used in conjunction with a four channel PowerLab®/400 and a Dell Inspiron laptop displayed in the image in Figure 3.1.

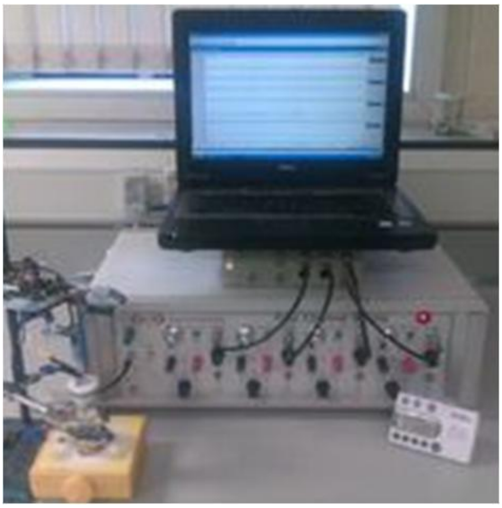

Figure 3.1: The *in-vitro* experimental set-up

3.2.2. Computer Programs

Constant potential amperometry (CPA) was carried out and analysed using chart 4 and LabChart 6 (AD Instruments, Oxford, UK) . The graphical analysis of data was performed in Graphpad Prism (Graphpad Softwear Inc. CA USA). This analysis included linear regression, non-linear regression (i.e. fitting Michaelis-Menten enzymatic curves to the Hill-type equation) and statistical analysis including paired and unpaired *t*-tests. Prism was also used in preparing graphs of the raw data from *in-vitro* and *in-vivo* experiments.

3.2.3. Movement Meter

The movement meter (Figure 3.2) consisted of a PIR detector (Elite Security Products, Unit 7, Leviss Trading Estate, Station Road, Stechford, Birmingham B33 9AE, UK) modified in-house with a micro-processor to enable enhancement of the resolution of the sensor thereby registering more movement. This is achieved by reducing the recovery time that is required after movement to *ca*. 5 ms. The digital output from the microcontroller is directly connected to the logic gate of the microprocessor from which the signal is generated.

The exact coupling of the movement data and the *in-vivo* electrochemical data is extremely important for correlating periods of movement with increases and decreases in substrate concentrations.

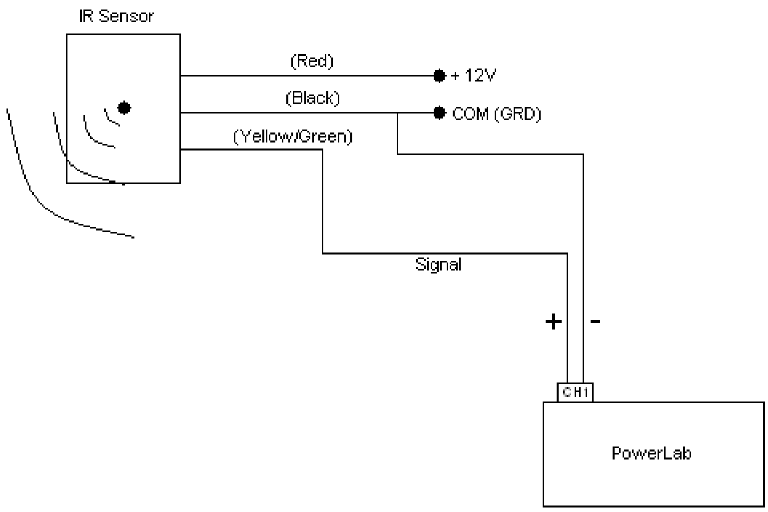

Figure 3.2 : Schematic of the IR movement sensor.

3.2.4. Supplementary equipment

3.2.4.1. *In-Vitro* equipment

Air-pump: The air pump used was a Rena Air 200 from RENA®, France

Electronic Balance: Two electronic balances were used in this project; a three decimal place BP 310P and a four decimal place LA 230S, both from Sartorius®, AG Gottingen, Germany.

Microscope: The microscopes used were the stereo microscope SZ51 from olympus America Inc. and the SM 33-745-F from Hund® WETZLER, Germany. *In-Vivo* surgeries utilised an SZ61 microscope from Olympus.

pH meter: The pH meter used was the S20 Seveneasy™ from Mettler-Toledo, Switzerland.

Sonicator: The sonicator was a Fisherbrand FB 11002, Leicestershire, UK.

Vortex: The vortex was Reax control from Heidolph.

Electrode wire: All platinum and silver wire was sourced from Advent Research Materials, Oxford, UK.

3.2.4.2. *In-Vivo* equipment

Anaesthetic setup: The set-up consisted of a vapouriser for induction and a Univentor 400 anaethesia unit. The air pump in the system was a stellar S30 and the induction chamber was a 1.4 L perspex box which were all obtained from Agnthos, Sweden. The entire system was contained within a laminar flow unit supplied by Air Science™.

Incubator: Following surgery the animals were placed in a Thermacage MKII heated incubator from from Datesand Ltd, UK.

Microdialysis Probes: All probes were BR4 brain microdialysis probes from BAS Inc.

Microdialysis Pump: A univentor 801 syringe pump was used for microdialysis.

Stereotaxic Frame: The stereotaxic frame was sourced from Kopf.

Uniswitch connector: Used during microdialysis from Bioanalytical Systems Inc. 2701 Kent Ave. W Lafayette, IN, USA

3.3. Chemicals and solutions

All chemicals were used as supplied unless stated otherwise. All solutions were prepared from doubly distilled deionised water unless stated otherwise.

3.3.1. Chemicals

The following is a list of all the chemicals used throughout the course of the project, categorised into enzymes, enzyme substrates and general *in-vitro* and *in-vivo* chemicals.

3.3.1.1. Enzymes

Choline oxidase (Alcaligenes sp.)	Sigma Aldrich
Acetylcholinesterase (Electric eel.)	Sigma Aldrich

3.3.1.2. Enzyme Substrates

Choline chloride	Sigma Aldrich
Acetylcholine chloride	Sigma Aldrich

3.3.1.3. *In-Vitro* Chemicals

3,4-Dihydroxyphenylacetic acid	Sigma Aldrich
3-sn-Phosphatidylethanolamine (PEA)	Sigma Aldrich
5-Hydroxyindoleacetic acid	Sigma Aldrich
5-Hydroxytryptomine	Sigma Aldrich

Acetone	Sigma Aldrich
Ascorbic Acid	Sigma Aldrich
Bovine Serum Albumin (Fraction V) (BSA)	Sigma Aldrich
Cellulose Acetate (CelAce)	Sigma Aldrich
Dehydroascorbic acid	Sigma Aldrich
Dopamine	Sigma Aldrich
Ethanol	Sigma Aldrich
Glutaraldehyde (GA)	Sigma Aldrich
Homovanillic acid	Sigma Aldrich
L-Cysteine	Sigma Aldrich
L-Glutathione	Sigma Aldrich
L-Tryptophan	Sigma Aldrich
L-Tyrosine	Sigma Aldrich
Methyl Methacrylate (MMA)	Sigma Aldrich
N_2 Gas	BOC Gases
Nafion	Sigma Aldrich
O_2 Gas	BOC Gases
o-Phenylenediamine (*o*-PD)	Sigma Aldrich
Polyethyleneimine (PEI)	Sigma Aldrich
Sodium Chloride	Sigma Aldrich
Sodium Hydroxide	Sigma Aldrich
Sodium Phosphate Monobasic Monohydrate	Sigma Aldrich
Styrene	Sigma Aldrich
Uric Acid	Sigma Aldrich

3.3.1.4. *In-Vivo* Chemicals

Acetazolamide (Diamox)	Sigma Aldrich
Atropine	Sigma Aldrich
Buprenorphine hydrochloride (Tamgesic®)	Sigma Aldrich
Calcium Chloride	Sigma Aldrich
Chloral Hydrate	BDH Laboratory Supplies, UK
Dentalon®	Hereaus Kulzer Gmbh
Dimethylsulfoxide (DMSO)	Sigma Aldrich
Hemicholinium-3	Sigma Aldrich
Isofluorane	Abbott Laboratories, IRL
N (G)-nitro-L-arginine methyl ester (L-NAME)	Sigma Aldrich
Magnesium Chloride	Sigma Aldrich
Neostigmine	Sigma Aldrich
Potassium Chloride	Sigma Aldrich
Sodium Ascorbate	Sigma Aldrich

3.3.2. Solutions

All solutions were prepared on the day of the experiment unless stated otherwise. All solutions were prepared as stated below.

3.3.2.1. *In-Vitro* Solutions

Enzyme Solutions

Choline Oxidase (ChOx;13U/mg)

Five enzyme solutions were used in the development of this sensor. A 50 unit solution was prepared by dissolving 0.00125 g of ChOx into 300 µL of PBS. A ChOx:BSA1 % solution was prepared by dissolving 0.00125 g of ChOx into 300 µL of PBS, 0.016 g of BSA was then added to the solution. A 240 unit solution was prepared by dissolving 0.006 g of ChOx into 300 µL of PBS. A 500 unit solution was prepared by dissolving 0.01248 g of ChOx into 300 µL of PBS. A 500 unit solution was also prepared by dissolving 0.01248 g of ChOx into 300 µL of H_2O.

Acetylcholinesterase (AchE; 658U/mg)

One enzyme solution was used in the acetylcholine biosensor. A 842 unit solution was prepared by dissolving 0.0004 g of AchE in 200 uL of PBS.

Enzyme Substrates

Choline Chloride

A 0.1 M solution was prepared by dissolving 0.068 g of Choline Chloride into 5 mL of H_2O.

Acetylcholine Chloride

A 0.1 M solution was prepared by dissolving 0.09 g of Acetylcholine Chloride into 5 mL of H_2O.

General Solutions

3-sn-phosphatidylethanolamine

A 10 % solution was prepared by dissolving 0.1 g in 1 mL H_2O.

Bovine Serum Albumin

For sensor design a 0.1 % and 1 % solution of BSA was used. These were prepared by dissolving 0.001 g and 0.01 g of BSA in 1 mL of water respectively. For biocompatibility studies, a 10 % solution was used and prepared by dissolving 0.1 g of BSA into 1 mL of H_2O.

Cellulose Acetate

Five concentrations of cellulose acetate were investigated for O_2 dependence studies 0.5 %, 1 %, 2 %, 3 % and 5 %. These solutions were prepared by dissolving 0.005 g, 0.01 g, 0.02 g, 0.03 g and 0.05 g of cellulose acetate into a 1 mL solution of 2:1 acetone:ethanol respectively.

Glutaraldehyde

Four concentrations of glutaraldehyde were investigated during development of 0.1 %, 0.5 %, 1 % and 1.5 %. The 0.1 % glutaraldehyde solution was prepared by dissolving 1 mL of a 1 % glutaraldehyde solution made from a 25 % stock in 1 mL of H_2O. 1 % glutaraldehyde was prepared by dissolving 40 µL of 25 % stock into 1 mL of H_2O. 0.5 % was prepared by dissolving 20 µL of 25 % stock into 1 mL. 1.5 % was prepared by dissolving 60 µL of 25 % stock into 1 mL of H_2O.

Glutaraldehyde:BSA

This solution was prepared by dissolving 0.01 g of BSA in 0.5 mL H_2O. 0.1 mL of 1 % glutaraldehyde solution was added and this solution was made up to 1 mL with H_2O. This process is preferred as BSA added to glutaraldehyde results in immediate and irreversible cross-linking.

Nafion®

Twelve Nafion® solutions were used in Chapter 5. All solutions were used immediately unless otherwise stated.

A 0.5 and 1 % Nafion® solution was prepared in styrene by dissolving 100 and 200 µL of Nafion® respectively in 1 mL of styrene. The solution was used immediately as styrene and Nafion® are immiscible and the Nafion® settles to the bottom of the solution.

A 0.5, 1 and 1.5 % Nafion® solution was prepared in MMA by dissolving 100, 200 and 300 µL of Nafion® respectively in 1 mL of MMA.

A 1.5 % Nafion® (vortexed) solution was prepared in MMA by dissolving 300 µL of Nafion® in 1 mL of MMA. The solution was vortexed for 30 seconds.

A 5 % Nafion® solution was used as supplied.

A 1.25 % Nafion® solution was prepared by dissolving 250 µL of Nafion into 1 mL of ethanol.

A 2.5 % Nafion® solution was prepared by dissolving 500 µL of Nafion into 1 mL of ethanol.

Three oxygenated Nafion® solutions were used. Firstly a 30 second oxygenated solution was used whereby the Nafion® solution was bubbled with pure O_2 for 30 seconds. Secondly, the Nafion® solution was bubbled with O_2 for 1 minute (1 minute oxygenated Nafion®). Lastly, the Nafion® solution was bubble with O_2 for 2 minutes (2 minute oxygenated Nafion®).

Three deoxygenated Nafion® solutions were used. Firstly a 1 minute deoxygenated solution was used whereby the Nafion® solution was bubbled with pure N_2 for 1 minute. Secondly, the Nafion® solution was bubbled with N_2 for 2 minutes (2 minute deoxygenated Nafion®).

A 10 % Nafion® solution was prepared by dissolving 0.5 mL of 20 wt % solution of Nafion® in 0.5 mL of ethanol.

o-Phenylenediamine (o-PD)

A 300 mM solution of *o*-PD was prepared by dissolving 0.324 g in 10 mL of N_2 saturated PBS. Maximum dissolution required the use of a sonic bath and agitation for a minimum of 10 minutes.

Polyethyleneimine (PEI)

Three concentrations of PEI were used during the development of this sensor 0.75 %, 1 % and 2 %. These were prepared by dissolving 0.02343 g, 0.03125 g and 0.0625 g respectively of PEI (80 % ethoxylated 35-40 % solution in water) into H_2O.

Phosphate Buffered Saline (PBS)

PBS was prepared by dissolving 8.9 g NaCl (0.15 M), 1.76 g NaOH (0.044 M) and 6.06 g $NaH_2PO_4.H_2O$ (0.044 M) in 1 L of distilled H_2O. If necessary the pH was adjusted to 7.4 by further additions of either $NaH_2PO_4.H_2O$ or NaOH as required.

Ascorbic Acid (AA)

A 0.1 M stock solution of AA was prepared by dissolving 0.176 g in 10 mL of H_2O. The solution was always prepared immediately prior to use.

3.3.2.2. *In-Vivo* Solutions

Acetozolamide (Diamox)

A 50 mg/kg solution was prepared by dissolving acetozolamide in a solution of 1 mL saline and 0.5 mL DMSO.

Artificial Cerebrospinal Fluid (aCSF)

aCSF was prepared by dissolving 8.6 g NaCl (0.15 M), 0.298 g KCl (0.0004 M), 0.176 g $CaCl_2$ (0.0016 M) and 0.204 g $MgCl_2$ (0.021 M) in 1 L of H_2O.

Atropine

A 5 mg/kg solution was prepared by dissolving atropine in 1 mL saline. Dissolution required the use of a sonic bath.

Chloral Hydrate

A 350 mg/kg solution was prepared by dissolving Chloral Hydrate in 1 mL saline.

Hemicholinium-3

A 200 µM solution was prepared by dissolving 0.11 mg into 1 mL of aCSF.

L-NAME

A 30 mg/kg solution was prepared by dissolving L-NAME into 1 mL saline.

Neostigmine

A 100 mM solution was prepared by dissolving 0.2 mL of a 500 mM solution in aCSF to a 1mL volume.

Saline Solution

A 0.9 % solution was prepared by dissolving 0.9 g NaCl in 100 mL H_2O.

3.4. Electrode Preparation

3.4.1. Disk and Cylinder platinum working electrodes

The disk electrodes were manufactured using approximately 6 cm of Teflon® coated Pt/Ir (90 %/10 %) wire (125 µm bare diameter, 160 µm coated diameter (5T), Advent Research Materials, Suffolk, UK). A section of the Teflon® insulation was removed at one end of the wire and soldered into a gold clip which provided both electrical contact and rigidity. To create an active surface, the opposite end of the wire was cut with a scalpel blade to expose a fresh disk surface. A schematic of a disk electrode is illustrated in Figure 3.3:

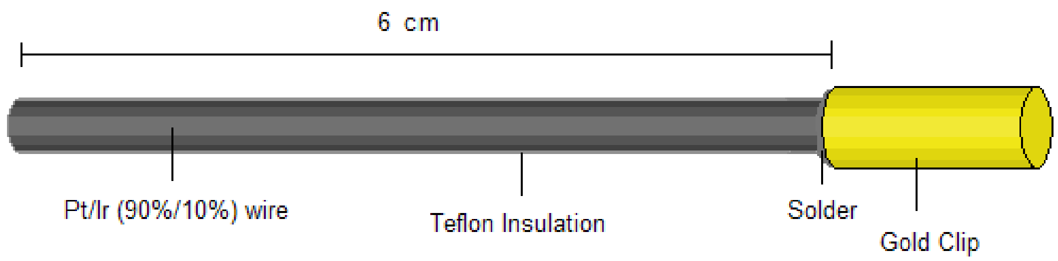

Figure 3.3 : Schematic representation of a Teflon® coated Platinum/Iridium disk working electrode.

For a cylinder electrode after the wire is soldered into the gold clip and a fresh disk surface was cut a 1 mm portion of the Teflon® coating was removed from the wire to expose a 1 mm active surface:

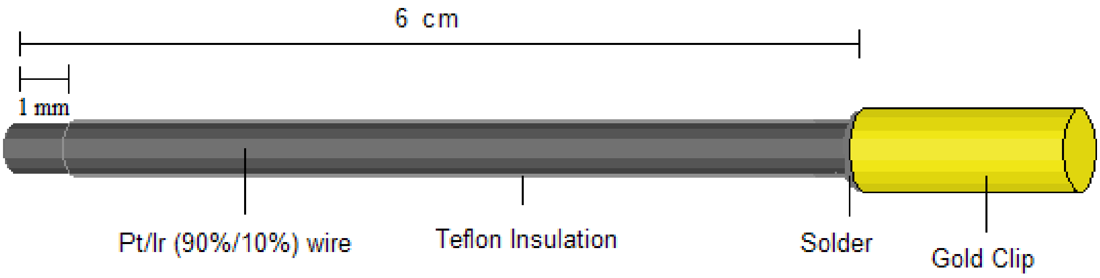

Figure 3.4 : Schematic representation of a Teflon® coated Platinum/Iridium 1mm cylinder working electrode.

3.4.2. Electrode Modifications

3.4.2.1. Choline Biosensor

During the development of the choline biosensor variations in the construction process were utilised. A list and description of each design is presented here. All modifications were allowed at least an hour to dry at 4°C unless otherwise stated.

Development

Sty-(ChOx)$_1$: A bare Pt electrode was dipped into a pure solution of styrene followed immediately by one dip into a solution of ChOx.

Sty-(ChOx)$_{10}$: A bare Pt electrode was dipped into a pure solution of styrene followed immediately by a dip into a solution of ChOx. This was allowed five minutes to dry. The electrode was then re-dipped into the enzyme solution a further nine times. Each dip had a five minute drying time.

Sty-(ChOx)$_{30min}$: A bare Pt electrode was dipped into a pure solution of styrene followed by the immediate submersion of the electrode within a solution of ChOx. This was left in the solution for thirty minutes. The electrode was removed after thirty minutes and allowed to dry.

Sty-(ChOx:BSA)$_{10}$: A bare Pt electrode was dipped into a pure solution of styrene followed by the immediate dip into a solution of ChOx and BSA. This was allowed five minutes to dry. The electrode was then re-dipped into the enzyme solution a further nine times. Each dip had a five minute drying time.

Sty-(ChOx)$_{10}$*-GA* : A bare Pt electrode was dipped into a pure solution of styrene followed immediately by a dip into a solution of ChOx. This was allowed five minutes to dry. The electrode was then re-dipped into the enzyme solution a further nine times. Each dip had a five minute drying time. Finally the sensor was dipped into a solution of GA.

Sty-(ChOx:BSA)$_{10}$*-GA* : A bare Pt electrode was dipped into a pure solution of styrene followed immediately by a dip into a solution of ChOx and BSA. This was allowed five minutes to dry. The electrode was then re-dipped into the enzyme solution a further nine times. Each dip had a five minute drying time. Finally the sensor was dipped into a solution of GA.

Sty-(ChOx:BSA)$_{10}$*-GA:BSA* : A bare Pt electrode was dipped into a pure solution of styrene followed immediately by a dip into a solution of ChOx and BSA. This was allowed five minutes to dry. The electrode was then re-dipped into the enzyme solution a further nine times. Each dip had a five minute drying time. Finally the sensor was dipped into a solution of GA:BSA.

Sty-((ChOx)-(PEI))$_{10}$*-GA* : A bare Pt electrode was dipped into a pure solution of styrene followed immediately by a dip into a solution of ChOx and a separate solution of PEI. This was allowed five minutes to dry. The electrode was then sequentially re-dipped into the enzyme and PEI solutions a further nine times. Each dip series had a five minute drying time. Finally the sensor was dipped into a solution of GA.

Sty-((ChOx:BSA)-(PEI))$_{10}$*-GA* : A bare Pt electrode was dipped into a pure solution of styrene followed immediately by a dip into a solution of ChOx and BSA and a separate solution of PEI. This was allowed five minutes to dry. The electrode was then sequentially re-dipped into the enzyme and PEI solutions a further nine times. Each dip series had a five minute drying time. Finally the sensor was dipped into a solution of GA.

(Sty-((ChOx:BSA)-(PEI))$_{10}$-GA)x2 : A bare Pt electrode was dipped into a pure solution of styrene followed immediately by a dip into a solution of ChOx and BSA and a separate solution of PEI. This was allowed five minutes to dry. The electrode was then sequentially re-dipped into the enzyme:BSA and PEI solutions a further nine times. Each dip series had a five minute drying time. Finally the sensor was dipped into a solution of GA. The final sensor was allowed to dry at 4°C for an hour. The procedure was then repeated. The sensor was allowed to dry at 4°C for at least three hours before calibrating.

Sty-(ChOx)(GA)$_{10}$: A bare Pt electrode was dipped into a pure solution of styrene followed immediately by a dip into a solution of ChOx and a separate solution of GA. This was allowed five minutes to dry. The electrode was then sequentially re-dipped into the enzyme and GA solutions a further nine times. Each dip series had a five minute drying time.

Sty-(ChOx)(BSA)(GA)$_{10}$: A bare Pt electrode was dipped into a pure solution of styrene followed immediately by a dip into a solution of ChOx, a separate solution of BSA and a separate solution of GA. This was allowed five minutes to dry. The electrode was then sequentially re-dipped into the enzyme, BSA and GA solutions a further nine times. Each dip series had a five minute drying time.

Sty-(ChOx)(PEI)(GA)$_{10}$: A bare Pt electrode was dipped into a pure solution of styrene followed immediately by a dip into a solution of ChOx, a separate solution of PEI and a separate solution of GA. This was allowed five minutes to dry. The electrode was then sequentially re-dipped into the enzyme, PEI and GA solutions a further nine times. Each dip series had a five minute drying time.

Sty-(ChOx)(GA)(PEI)$_{10}$: A bare Pt electrode was dipped into a pure solution of styrene followed immediately by a dip into a solution of ChOx, a separate solution of GA and a separate solution of PEI. This was allowed five minutes to dry. The electrode was then sequentially re-dipped into the enzyme, GA and PEI solutions a further nine times. Each dip series had a five minute drying time.

Sty-(ChOx)(BSA)(GA)(PEI)$_{10}$: A bare Pt electrode was dipped into a pure solution of styrene followed immediately by a dip into a solution of ChOx, a separate solution of BSA, a separate solution of GA and a separate solution of PEI. This was allowed five minutes to dry. The electrode was then sequentially re-dipped into the enzyme, BSA, GA and PEI solutions a further nine times. Each dip series had a five minute drying time. The final sensor was allowed to dry at 4°C for at least three hours before calibrating.

MMA-(ChOx)(BSA)(GA)(PEI)$_{10}$: A bare Pt electrode was dipped into a pure solution of MMA followed immediately by a dip into a solution of ChOx, a separate solution of BSA, a separate solution of GA and a separate solution of PEI. This was allowed five minutes to dry. The electrode was then sequentially re-dipped into the enzyme, BSA, GA and PEI solutions a further nine times. Each dip series had a five minute drying time. The final sensor was allowed to dry at 4°C for at least three hours before calibrating.

(Sty-(ChOx)(BSA)(GA)(PEI)$_{10}$)x2 : A bare Pt electrode was dipped into a pure solution of styrene followed immediately by a dip into a solution of ChOx, a separate solution of BSA, a separate solution of GA and a separate solution of PEI. This was allowed five minutes to dry. The electrode was then sequentially re-dipped into the enzyme, BSA, GA and PEI solutions a further nine times. Each dip series had a five minute drying time. The final sensor was allowed to dry at 4°C for an hour. The procedure was the repeated. The sensor was allowed to dry at 4°C for at least three hours before calibrating.

(MMA-(ChOx)(BSA)(GA)(PEI)$_{10}$)x2 : A bare Pt electrode was dipped into a pure solution of MMA followed immediately by a dip into a solution of ChOx, a separate solution of BSA, a separate solution of GA and a separate solution of PEI. This was allowed five minutes to dry. The electrode was then sequentially re-dipped into the enzyme, BSA, GA and PEI solutions a further nine times. Each dip series had a five minute drying time. The final sensor was allowed to dry at 4°C for an hour. The

procedure was then repeated. The sensor was allowed to dry at 4°C for at least three hours before calibrating.

<u>*Best Designs:*</u>

Sty-(ChOx 500U)(BSA1%)(GA0.5%)(PEI2%)$_{10}$: A bare Pt electrode was dipped into a pure solution of styrene followed immediately by a dip into a solution of ChOx, a separate solution of BSA, a separate solution of GA and a separate solution of PEI. This was allowed five minutes to dry. The electrode was then sequentially re-dipped into the enzyme, BSA, GA and PEI solutions a further nine times. Each dip series had a five minute drying time. The final sensor was allowed to dry at 4°C for at least three hours before calibrating.

MMA-(ChOx500U)(BSA1%)(GA0.5%)(PEI2%)$_{10}$: A bare Pt electrode was dipped into a pure solution of MMA followed immediately by a dip into a solution of ChOx, a separate solution of BSA, a separate solution of GA and a separate solution of PEI. This was allowed five minutes to dry. The electrode was then sequentially re-dipped into the enzyme, BSA, GA and PEI solutions a further nine times. Each dip series had a five minute drying time. The final sensor was allowed to dry at 4°C for at least three hours before calibrating.

Oxygen Dependence

During the O_2 dependence investigation of the choline biosensor variations in the construction process were introduced. A list and description of each design is described here. All modifications were allowed at least three hours to dry at 4°C unless otherwise stated.

Styrene:Nafion® : A solution of styrene:Nafion® was prepared as described in Section 3.3.2.1. The solution was used immediately. A bare Pt electrode was dipped into the styrene: Nafion® solution followed immediately by a dip into a solution of ChOx, a separate solution of BSA, a separate solution of GA and a separate solution of PEI. This was allowed five minutes to dry. The electrode was then sequentially re-dipped into the enzyme, BSA, GA and PEI solutions a further nine times. Each dip series had a five minute drying time.

MMA:Nafion® : A solution of MMA:Nafion® was prepared as described in Section 3.3.2.1. The solution was used immediately. A bare Pt electrode was dipped into the MMA: Nafion® solution followed immediately by a dip into a solution of ChOx, a separate solution of BSA, a separate solution of GA and a separate solution of PEI. This was allowed five minutes to dry. The electrode was then sequentially re-dipped into the enzyme, BSA, GA and PEI solutions a further nine times. Each dip series had a five minute drying time.

MMA:1.5%Nafion® (vortexed) : A solution of MMA:1.5 % Nafion® (vortexed) was prepared as described in Section 3.3.2.1. The solution was used immediately. A bare Pt electrode was dipped into the MMA: Nafion® solution followed immediately by a dip into a solution of ChOx, a separate solution of BSA, a separate solution of GA and a separate solution of PEI. This was allowed five minutes to dry. The electrode was then sequentially re-dipped into the enzyme, BSA, GA and PEI solutions a further nine times. Each dip series had a five minute drying time.

(MMA)(5%Nafion®): A bare Pt electrode was dipped into the MMA solution followed immediately by a dip into a solution of 5 % Nafion® followed by a dip into ChOx, a separate solution of BSA, a separate solution of GA and a separate solution of PEI. This was allowed five minutes to dry. The electrode was then sequentially re-dipped into the enzyme, BSA, GA and PEI solutions a further nine times. Each dip series had a five minute drying time.

(5%Nafion®)(MMA): A bare Pt electrode was dipped into the 5 % Nafion® solution followed immediately by a dip into a solution of MMA followed by a dip into ChOx, a separate solution of BSA, a separate solution of GA and a separate solution of PEI. This was allowed five minutes to dry. The electrode was then sequentially re-dipped into the enzyme, BSA, GA and PEI solutions a further nine times. Each dip series had a five minute drying time.

(MMA)(Nafion®5%)(MMA): A bare Pt electrode was dipped into MMA followed by the Nafion® solution as prepared in Section 3.3.2.1 followed immediately by a dip into a

solution of MMA. This is immediately followed by a dip into ChOx, a separate solution of BSA, a separate solution of GA and a separate solution of PEI. This was allowed five minutes to dry. The electrode was then sequentially re-dipped into the enzyme, BSA, GA and PEI solutions a further nine times. Each dip series had a five minute drying time.

Oxygenated Nafion®: A bare Pt electrode was dipped into MMA followed by the 5 % Nafion® solution oxygenated as in Section 3.3.2.1 followed immediately by a dip into a solution of MMA. This is immediately followed by a dip into ChOx, a separate solution of BSA, a separate solution of GA and a separate solution of PEI. This was allowed five minutes to dry. The electrode was then sequentially re-dipped into the enzyme, BSA, GA and PEI solutions a further nine times. Each dip series had a five minute drying time.

Deoxygenated Nafion®: A bare Pt electrode was dipped into MMA followed by the 5 % Nafion® solution deoxygenated as in Section 3.3.2.1 followed immediately by a dip into a solution of MMA. This is immediately followed by a dip into ChOx, a separate solution of BSA, a separate solution of GA and a separate solution of PEI. This was allowed five minutes to dry. The electrode was then sequentially re-dipped into the enzyme, BSA, GA and PEI solutions a further nine times. Each dip series had a five minute drying time.

(MMA)(CelAce)(MMA): A bare Pt electrode was dipped into MMA followed by the Cellulose Acetate solution prepared as in Section 3.3.2.1 followed immediately by a dip into a solution of MMA. This is immediately followed by a dip into ChOx, a separate solution of BSA, a separate solution of GA and a separate solution of PEI. This was allowed five minutes to dry. The electrode was then sequentially re-dipped into the enzyme, BSA, GA and PEI solutions a further nine times. Each dip series had a five minute drying time.

(MMA)(CelAce)(MMA)-(ChOx)(BSA)(GA)(PEI)CelAce: A bare Pt electrode was dipped into MMA followed by the Cellulose Acetate solution prepared as in Section 3.3.2.1, followed immediately by a dip into a solution of MMA. This is immediately followed by a dip into ChOx, a separate solution of BSA, a separate solution of GA and a

separate solution of PEI. This was allowed five minutes to dry. The electrode was then sequentially re-dipped into the enzyme, BSA, GA and PEI solutions a further nine times. A final layer of cellulose acetate was applied by dip evaporation. Each dip series had a five minute drying time.

<u>*Best Design:*</u>

(MMA)(CelAce2%)(MMA)(ChOx500U)(BSA1%)(GA0.5%)(PEI2%): A bare Pt electrode was dipped into MMA followed by the Cellulose Acetate solution prepared as in Section 3.3.2.1 followed immediately by a dip into a solution of MMA. This is immediately followed by a dip into ChOx, a separate solution of BSA, a separate solution of GA and a separate solution of PEI. This was allowed five minutes to dry. The electrode was then sequentially re-dipped into the enzyme, BSA, GA and PEI solutions a further nine times. Each dip series had a five minute drying time.

In-Vitro Characterisation

<u>*Design:*</u>

(MMA)(CelAce2%)(MMA)(ChOx500U)(BSA1%)(GA0.5%)(PEI2%): A bare Pt electrode was dipped into MMA followed by the Cellulose Acetate solution prepared as in Section 3.3.2.1 followed immediately by a dip into a solution of MMA. This is immediately followed by a dip into ChOx, a separate solution of BSA, a separate solution of GA and a separate solution of PEI. This was allowed five minutes to dry. The electrode was then sequentially re-dipped into the enzyme, BSA, GA and PEI solutions a further nine times. Each dip series had a five minute drying time.

In-Vivo Characterisation

Design:

PPD-(MMA)(CelAce2%)(MMA)(ChOx500U)(BSA1%)(GA0.5%)(PEI2%): A bare Pt was coated with Poly-*o*-phenylenediamine as described in section 3.4.2.4. This was allowed at least an hour to dry. The electrode was dipped into MMA followed by the Cellulose Acetate solution prepared as in Section 3.3.2.1 followed immediately by a dip into a solution of MMA. This is immediately followed by a dip into ChOx, a separate solution of BSA, a separate solution of GA and a separate solution of PEI. This was allowed five minutes to dry. The electrode was then sequentially re-dipped into the enzyme, BSA, GA and PEI solutions a further nine times. Each dip series had a five minute drying time.

3.4.2.2. Acetylcholine Biosensor

(MMA)(CelAce)(MMA)-(ChOx)(BSA)(GA)(PEI)AchE: A bare Pt electrode was dipped into MMA followed by the Cellulose Acetate solution prepared as in Section 3.3.2.1 followed immediately by a dip into a solution of MMA. This process was immediately followed by a dip into ChOx, a separate solution of BSA, a separate solution of GA and a separate solution of PEI. This was allowed five minutes to dry. The electrode was then sequentially re-dipped into the enzyme, BSA, GA and PEI solutions a further nine times. A final layer of Acetylcholinesterase was applied by dip evaporation. Each dip series had a five minute drying time. The acetylcholine biosensors differed in the layers of AchE applied. If more than one layer was applied then the sensor was re-dipped into the enzyme with five minutes drying time. The final sensor was allowed to dry at 4°C for at least three hours before calibrating.

3.4.2.3. Oxygen Electrodes

O_2 electrodes used for *in-vivo* studies were a Pt disk electrode calibrated as in Section 3.5.1.7.

3.4.2.4. Poly-*o*-phenylenediamine modified electrodes

The polymerisation process took place in a three-electrode cell, which consisted of a silver wire as the auxiliary, an SCE reference electrode and four working electrodes. As *o*-PD is easily oxidised in air the cell was N_2 saturated and a N_2 atmosphere was maintained throughout the polymerisation process. A 300 mM solution of *o*-PD was prepared as described in Section 3.3.2.1. The solution was placed in the N_2 saturated cell and a potential of +700 mV *vs.* SCE was applied to the working electrodes for thirty minutes. Immediately after polymerisation the electrodes were removed and rinsed in distilled H_2O. The electrodes were allowed to dry for at least an hour before either calibration or modification.

3.4.3. Electrode Treatments

In the development of a new sensor it is vital that the electrode-environment interactions are fully investigated prior to use in biological systems (Lyne & O'Neill, 1990). This is due to the complex chemical environment within the brain which consists of surfactants (lipids) and electrode poisons (proteins) (O'Neill, 1993). Previous studies have utilised bovine serum albumin (BSA), 3-sn-Phosphatidylethanolamine (PEA) and *ex-vivo* samples of brain tissue for biocompatibility studies to monitor the effect of sensors in contact with protein, lipids and brain tissue (Brown *et al.*, 2009) (Bolger *et al.*, 2011).

3.4.3.1. BSA treated electrodes

All choline electrodes were made and calibrated on day 1. The electrodes were then immersed in a 10 % solution of BSA and calibrated two days later on day 3. After calibration the sensors were then placed back the solution of BSA. This was repeated on days 5, 7 and 14.

3.4.3.2. PEA treated electrodes

The choline electrodes were made and calibrated on day 1. The electrodes were then immersed in a 10 % solution of PEA and calibrated two days later on day 3. After calibration the sensors were then placed back the solution of PEA. This was repeated on day 5, 7 and 14.

3.4.3.3. Brain tissue electrodes

The choline electrodes were made and calibrated on day 1. The electrodes were then placed in a sample of brain tissue and calibrated two days later on day 3. After calibration the sensors were then placed back the brain tissue. This was repeated on day 5, 7 and 14.

3.5. Electrochemical Experiments

This section details the various equipment and experiments which were used during both the *in-vitro* and *in-vivo* sections.

3.5.1. In-Vitro Experiments

3.5.1.1. Electrochemical Cell

The electrochemical cell was of in house construction. It consisted of a 25 mL glass vial and a custom made Teflon® lid. The lid allowed for placement of the reference, auxiliary and working electrodes. In addition, there was an injection port for the addition of aliquots of analyte and a gas inlet for regulating the atmosphere when needed. Below is a schematic of the cell:

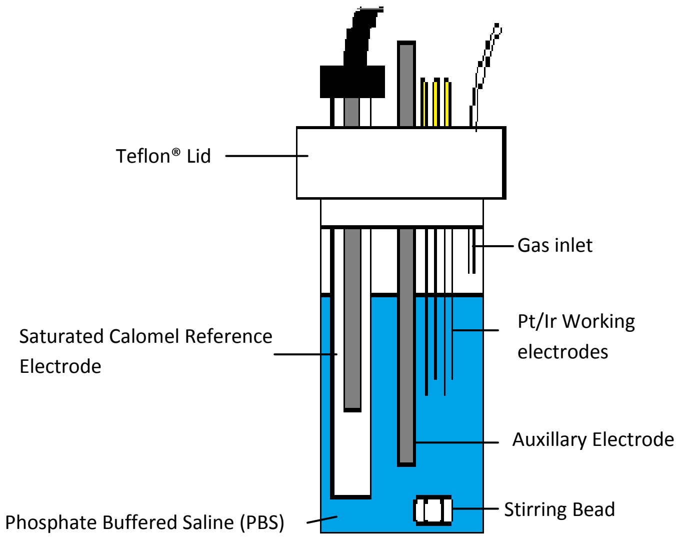

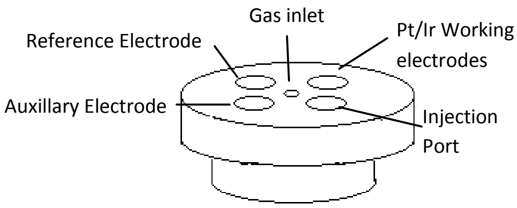

Figure 3.5 : Schematic of a typical three electrode cell set-up used in electrochemical experiments. Schematic of a Teflon® lid.

3.5.1.2. Constant Potential Amperometry (CPA)

Constant Potential Amperometry was utilised to calibrate all sensors in this thesis during the development of the choline and acetylcholine biosensors. All choline and acetylcholine experiments were performed at +700 mV. For the calibration of oxygen electrodes a potential of -650 mV was used. All experiments were performed in a three-electrode cell with a silver auxiliary and a Saturated Calomel reference electrode (SCE). The working electrodes were allowed time to settle under the influence of an applied potential until the non-faradaic current had reached a stable baseline. When the desired basal current level was achieved, calibrations consisting of injecting the analyte into the buffer solution through the injection port were performed. The solution was agitated using a magnetic stirring bead to aid mixing and the solution was then allowed to return to a steady-state before a subsequent injection.

3.5.1.3. Choline Calibrations

Choline electrodes were polarised at +700 mV *vs.* SCE and allowed to reach a steady state prior to calibration. A freshly prepared solution of 0.1 M choline chloride (see Section 3.3.2.1) was then used to inject aliquots into the buffer solution. This was then agitated using a magnetic stirring bead. The current was recorded continuously and the solution was allowed to return to a steady state before introducing the aliquots of choline. The complete range for the choline calibration was:

0, 5, 10, 20, 40, 60, 80, 100, 200, 400, 600, 800, 1000, 1500, 2000, 2500, 3000 µM

3.5.1.4. Acetylcholine Calibrations

Acetylcholine electrodes were polarised at +700 mV *vs.* SCE and allowed to reach a steady state prior to calibration. A freshly prepared solution of 0.1 M choline chloride (see Section 3.3.2.1) was then used to inject aliquots into the buffer solution. This was to determine the choline sensitivity of the electrode. This was then agitated using a magnetic stirring bead. The current was recorded continuously and the solution was allowed to return to a steady state before introducing the subsequent aliquot. The range for the choline calibration was:

0, 5, 10, 20, 40, 60, 80, 100 µM

After the initial choline injections of acetylcholine chloride were made from a 0.1 M acetylcholine chloride stock solution. The range of the choline calibration was:

0, 20, 40, 60, 80, 100, 200, 400, 600, 800, 1000, 1500, 2000, 2500, 3000 µM

3.5.1.5. Ascorbate Calibrations

For ascorbate tests on the choline and acetylcholine electrodes a potential of +700 mV *vs.* SCE was used and the electrodes were allowed to reach a steady state prior to calibration in N_2 saturated PBS with a N_2 atmosphere. A freshly prepared N_2 saturated solution of 0.1 M ascorbate stock solution (see Section 3.3.2.1) was then used to inject aliquots into the buffer solution. This was then agitated using a magnetic stirring bead. The current was recorded continuously and the solution was allowed to return to a steady state before introducing the subsequent aliquot. The range for the ascorbate calibration was:

0, 200, 400, 600, 800, 1000 µM

3.5.1.6. Oxygen dependence experiments.

Three types of oxygen calibrations were used in the determination of the choline sensors oxygen dependence. The first type of oxygen experiment was performed using three biosensors and a bare Pt oxygen electrode. The biosensors were polarised at +700 mV *vs.* SCE and the oxygen electrode was polarised at -650 mV *vs.* SCE. The electrodes were allowed to reach a steady state prior to calibration in a N_2 saturated PBS solution, under a N_2 atmosphere. An aliquot of 100 µM choline chloride, from a fresh stock solution of 0.1 M, was added to the PBS and time was allowed for the steady-state to return. The source of the N_2 atmosphere was removed and the PBS was allowed to slowly equilibrate with the air. As the concentration of O_2 increases over time, the ability of the sensor to turn-over substrate increases, corresponding to an increase in current. In addition, the O_2 electrode detects the changes in O_2 concentration which can directly extrapolate the choline current at individual O_2 concentrations.

The second type of oxygen calibration was performed using three biosensors and a bare Pt oxygen electrode. The biosensors were polarised at +700 mV *vs.* SCE and the oxygen electrode was polarised at -650 mV *vs.* SCE. The oxygen electrode was pre calibrated to determine 30, 50 and 80 µM O_2 concentrations. The PBS solution was then maintained at these O_2 concentrations and a brief choline calibration was performed. The range for this calibration was:

0, 20, 60, 100, 200 µM

The third type of oxygen calibration was performed using three biosensors and one bare Pt oxygen electrode. The biosensors were polarised at +700 mV *vs.* SCE and the oxygen electrode was polarised at -650 mV *vs.* SCE. The electrodes were allowed to settle to a steady state prior to calibration. Prior to the first injection air was bubbled into the PBS to introduce forced convection. The solution did not return to a quiescent solution during the experiments. The first aliquot of choline chloride was added to the PBS and allowed to plateau. The air was removed and replaced immediately with N_2 bubbling until the O_2 electrode displayed a plateau at 0 µM. This was reversed and the solution was allowed to return to an air saturated solution through constant bubbling. When the O_2 electrode again displayed a plateau of 240 µM, the next aliquot of choline was introduced. This was continued for a range of choline concentrations. The range for this calibration was:

0, 20, 40, 100 μM

3.5.1.7. Oxygen Experiments

Oxygen electrodes were polarised at -650 mV *vs.* SCE, and allowed to reach a steady state and calibrated over three O_2 concentrations. Firstly, the PBS solution was purged of O_2 by introducing N_2 into the cell. This was used as the zero point of the calibration. Secondly, air was introduced into the solution to achieve 240 μM O_2. Lastly, O_2 was introduced into the solution to achieve a concentration of 1200 μM O_2. All recordings were taken from a quiescent solution.

0, 240, 1200 μM

3.5.2. *In-Vivo* Experiments

This section describes the various details of the *in-vivo* work carried out. All animal experiments performed during the course of this work were conducted under licence B100/2205. All procedures were approved by the NUI Maynooth Ethics Committee (Animal Experimentation) in accordance with the Council of the European Parliament Directive 2010/ 63/ EU and Irish Statutory Instrument SI 543/2012. All *in-vivo* experiments were recorded continuously over a 24 hour period with animals assessed for good health according to published guidelines (*The Guide for the Care and Use of Laboratory Animals*, NIH Publication No. 85-23; and *The Handbook of Laboratory Animal Management and Welfare*, ISBN 1-4051-1159-3) immediately after recovery from anesthesia and at the beginning of each day. All efforts were made to minimise animal suffering and the number of animals used for the study.

3.5.2.1. Subjects

The Wistar strain of rat (*rattus norvegicus*) was used for all *in-vivo* experiments. Male rats were used and obtained from Charles River (UK Ltd., Manstin Rd., Margate, Kent CT9 4LT, UK). Rats were typically in the 200-250 g weight category at the time of delivery. The rats were subject to regular handling and were group housed prior to surgery (max = 4 per cage). Rats were kept in a windowless temperature controlled room (22° C) under a 12 hour light and dark cycle (lights on 7:00, lights off 19:00). Each rat was housed individually after surgery to protect the electrode-containing headpiece in a large plastic bowl mounted on a Raturn (Bioanalytical Systems Inc. 2701 Kent Ave. W Lafayette, IN, USA). All experiments were carried out during the light phase. The implanted electrodes were connected to a potentiostat through a six-pin Teflon® socket, and a flexible screened six core cable. All rats had free access to water. Food was available *ad libitum*.

3.5.2.2. Surgery

Rats were anaesthetised with Isoflurane, a volatile anaesthetic, using a vaporiser (Univentor). Once the animal was fully anaesthetised, it was placed in a stereotaxic frame (Kopf) on a heat controlled pad for maintenance of 37°C (PanLab, Barcelona), and the head was levelled between bregma and lambda. Prior to the incision the head was prepared using an iodine solution to protect from possible infection. An incision was made along the anterior-posterior plane. The scalp was pulled to each side. Clamps were used to secure the periosteum exposing the skull beneath. In addition, as the scalp is free from the cement layers the scalp can be drawn together and sutured around the cement layers to minimise infection and protect the skull piece from scratching. The lipid layer on the skull was removed as this is detrimental for the dental cement adhesion.

The stereotaxic co-ordinates are referenced from the rat atlas of Paxinos and Watson (Paxinos & Watson, 2006). Both the anterior-posterior (A-P) and medial-lateral (M-L) stereotaxic co-ordinates are referenced with respect to a zero point, bregma, with positive A-P representing anterior to bregma and positive M-L represents the right hemisphere. Dorsal ventral (D-V) stereotaxic co-ordinates are referenced with respect to the dura, with greater negative values indicating depth into the brain. All experiments were carried out in the striatum and the co-ordinates used are presented below:

Brain Region	A-P	M-L	D-V
Striatum	+1.0	± 2.5	-6.0

Table 3.1 : Stereotaxic co-ordinates for electrode implantation in the striatum

Bregma is the point on the skull where the sagittal (A-P) and coronal (M-L) sutures intersect and can be confirmed by applying pressure to the individual skull plates and observing the junction. With bregma used as the zero reference point the skull was drilled to allow for implantation of the electrodes and MD probe. Four additional holes were drilled for three support screws and the auxiliary screw (see Figure 3.7). A hole was also drilled for the reference electrode (see Figure 3.7) as seen in Figure 3.6.

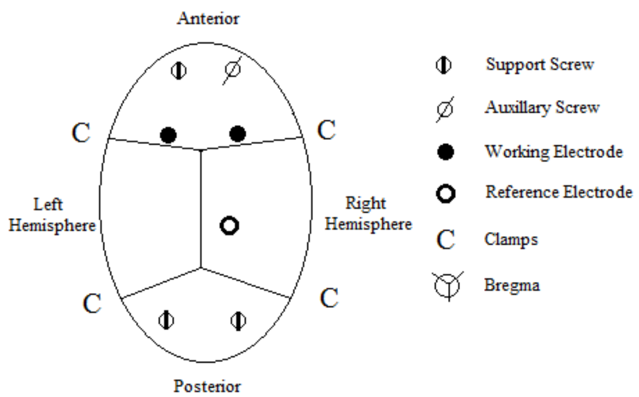

Figure 3.6 : Schematic of a typical orientation of drill holes for placement of scull screws, auxiliary screw and electrodes. Figure also shows the positioning of clamps to maximise skull suface area.

The reference potential provided by the Ag wire in brain tissue is similar to that of an SCE (O'Neill 1993). The screws and auxiliary screws were put in place to allow subsequent fixation of cement. The dura was pierced with a needle for *ca*. 10 seconds to provide a clear path for the electrodes to be implanted. The electrodes were mounted onto the stereotaxic arms and manoeuvred into the correct co-ordinates. The reference electrode was also put in place. The reference and auxiliary electrodes are silver wire soldered into a gold clip as illustrated in Section 3.4.1. The electrodes are then modified at the tips. The auxiliary electrode required the addition of a screw and the reference electrode is bent with exposed wire at the tip. These modifications are displayed in the image below. Additional schematics are presented by O'Neill and Lowry (O'Neill & Lowry, 2006).

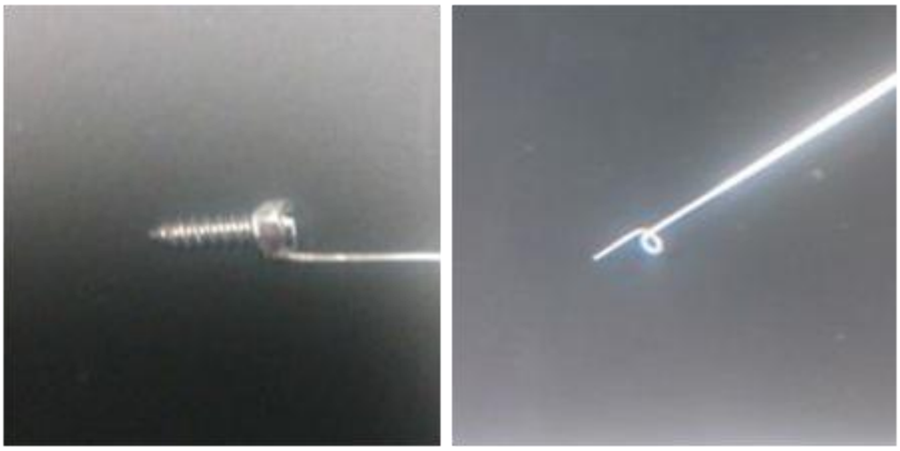

Figure 3.7 : The auxiliary electrode and the reference electrode

All electrodes were fully cemented in place before the gold clips were inserted into a Teflon® pedestal and cemented in place as shown in Figure 3.8. The pedestal and electrodes were then encased in cement to protect them from damage from the rat or any external influences.

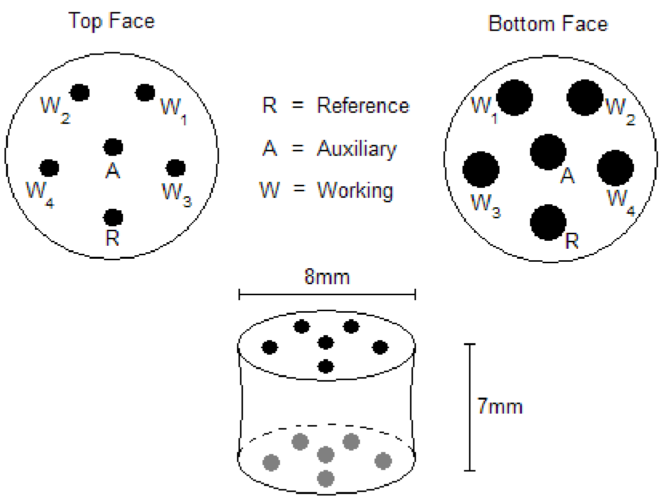

Figure 3.8 : Schematic of the Teflon® pedestal used for *in-vivo* experiments to connect electrodes with the recording equipment. Top panel: Schematic of respective faces of the pedestal detailing the various holes, highlighting the difference in size of the holes to accommodate the gold pins of the electrodes on the underside. Bottom panel: Dimensions of the pedestal.

The top of the pedestal remained cement-free to allow for the attachment of the cable connecting the electrodes to the potentiostat. Once all the cement was dry, the clamps were removed and the scalp was sutured together at the back of the head. The rat was removed from the stereotaxic frame and was placed in a heated incubation chamber until fully recovered. Post-operative analgesia was provided in the form of a single injection (0.1 mL) of buprenorphine which was administered before the removal from the stereotaxic. Animals were allowed to recover before they were connected to the potentiostat and were assessed for good health.

3.5.2.3. Continuous Monitoring

CPA was used to measure the response of the implanted electrodes during experiments. Initial connection to the potentiostat involved connection of the cable to the pedestal and then to the potentiostat. The potential was then applied to different electrodes with a short interval between each application to rule out cross-talk between each of the electrodes. Once the potential was applied the electrodes were allowed settling time typically 12 hrs.

3.5.2.4. Microdialysis

The surgical method described in Section 3.5.2.2 can be adapted for the implantation of a microdialysis probe. Microdialysis probes consist of two concentric hollow fibres that allow for uni-directional flow of the perfusion medium. There is a length of dialysis membrane exposed with a pore size that allows free diffusion of solute molecules but not proteins or other macromolecules in the extracellular fluid.

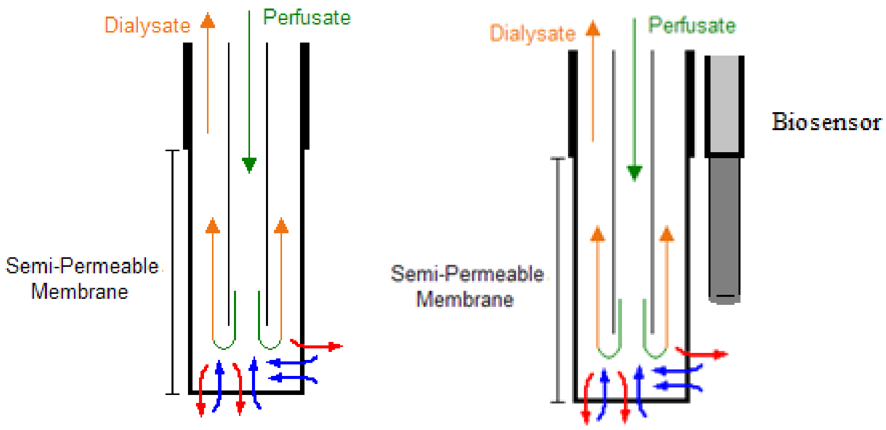

Figure 3.9 : Schematic of a microdialysis probe, highlighting unidirectional medium flow and bi directional passage of solutes. Schematic of a combined microdialysis probe and sensor.

The microdialysis probes themselves, can be adapted in-house for the combined implantation of a biosensor as in Figure 3.9, which is useful for the *in-vivo* characterisation of a biosensor. This adaptation involved gluing an *in-vitro* characterised biosensor to a microdialysis probe with epoxy *ca.* one hour prior to implantation.

The microdialysis experiments for this project were performed after a stable baseline was achieved with the biosensor. The microdialysis experiments utilised a microdialysis pump, a 1 mL gastight syringe, a microdialysis probe, tubing and silicon connectors. Various perfusions were undertaken and all were conducted at a perfusion flow rate of 2 μL/min.

3.5.2.5. Uniswitch Connector

A uniswitch connector was used during the microdialysis experiments to switch between solutions for perfusion into the probe. The uniswitch design means that the microdialysis tubing does not have to be disconnected and cleaned for a second solution to be perfused. Multiple pieces of tubing containing the desired solutions is connected to the uniswitch with only one outlet tube. The lever can be switched to change the source of the solution.

3.5.2.6. Intraperitoneal injection

Intraperitoneal (i.p) injection was performed at a 45° angle into the peritoneal cavity which is located in the lower quadrant of the abdomen.

3.5.2.7. Sub-Cutaneous Injection

The drug was administered into loose skin which is ‘scruffed’ on the back of the animal.

3.5.2.8. Termination

Euthanasia was facilitated by administration of 1 mL of Euthatal. The brains were removed following de-capitation and placed in a 10 % solution of formaldehyde for histology.

Bolger FB. (2007). The *In-Vitro* and *In-Vivo* Characterisation and Application of Real-Time Sensors and Biosensors for Neurochemical Studies of Brain Energy Metabolism. National University of Ireland, Maynooth, Maynooth.

Bolger FB, Bennett R & Lowry JP. (2011). An *In-Vitro* characterisation comparing carbon paste and Pt microelectrodes for real-time detection of brain tissue oxygen. *Analyst* **136,** 4028-4035.

Brown FO, Finnerty NJ & Lowry JP. (2009). Nitric oxide monitoring in brain extracellular fluid: characterisation of Nafion-modified Pt electrodes *In-Vitro* and *In-Vivo*. *Analyst* **134,** 2012-2020.

Lowry JP & O'Neill RD. (1994). Partial Characterization *In-Vitro* of Glucose Oxidase-Modified Poly(phenylenediamine)-coated electrodes for neurochemical analysis *In-Vivo*. *Electroanalysis* **6,** 369-379.

Lyne PD & O'Neill RD. (1990). Stearate-modified carbon paste electrodes for detecting dopamine *In-Vivo*: decrease in selectivity caused by lipids and other surface-active agents. *Analytical Chemistry* **62,** 2347-2351.

Malitesta C, Palmisano F, Torsi L & Zambonin PG. (1990). Glucose fast-response amperometric sensor based on glucose oxidase immobilized in an electropolymerized poly(*o*-phenylenediamine) film. *Analytical Chemistry* **62,** 2735-2740.

O'Neill RD. (1993). Sensor-tissue interactions in neurochemical analysis with carbon paste electrodes *In-Vivo*. *Analyst* **118,** 433-438.

O'Neill RD & Lowry JP. (2006). Voltammetry In Vivo for Chemical Analysis of the Living Brain. In *Encyclopedia of Analytical Chemistry*. John Wiley & Sons, Ltd.

Paxinos G & Watson C. (2006). *The Rat Brain in Stereotaxic Coordinates: Hard Cover Edition*. Elsevier Science, Academic Press.

Ryan M, Lowry J & O'Neill R. (1997). Biosensor for Neurotransmitter L-Glutamic Acid Designed for Efficient Use of L-Glutamate Oxidase and Effective Rejection of Interference. *Analyst* **122,** 1419-1424.

Wang J & Lu F. (1998). Oxygen-Rich Oxidase Enzyme Electrodes for Operation in Oxygen-Free Solutions. *Journal of the American Chemical Society* **120,** 1048-1050.

4. Development

4.1. Introduction

Acetylcholine (Ach) is a major excitatory neurotransmitter in the central nervous system which is hydrolysed by acetylcholinesterase (AchE) to choline. This is a rapid and efficient process whereby one molecule of AchE can hydrolyse 5000 molecules of Ach per second (Lawler, 1961). Due to this hydrolysis monitoring choline *in-vivo* may reflect the neuronal release of acetylcholine. Acetylcholine and choline have been extensively monitored in the rat brain by means of microdialysis (Ikarashi *et al.*, 1997) (Koppen *et al.*, 1997; Kehr *et al.*, 1998; Nakamura *et al.*, 2001), ceramic based multisite microelectrode arrays (Burmeister *et al.*, 2003) and amperometric microsensors (Garguilo & Michael, 1993). Although the microdialysis technique does present many advantages, it is limited by its poor temporal resolution, the variable *in-vivo* recovery and its large size. The development of biosensors for the detection of neuromediators benefits from their real-time resolution and small size. Sensors for the detection of choline have been successful previously by Garguilo *et al*. using carbon fibre microcylinder electrodes with a cross-linked redox-active gel containing horseradish peroxidase and choline oxidase (Garguilo & Michael, 1994). Burmeister *et al.* have also developed a ceramic based multisite microelectrode array for the detection of choline (Burmeister *et al.*, 2003). The aim of this thesis is the development and characterisation of a choline biosensor. This sensor will differ from previous sensor designs as the aim is to eliminate the use of a mediator, as used in the Garguilo design, as mediators are prone to leaching in tissue (Wang, 2001). In addition, the basis of this sensor will not be of microelectrode array design as they are prone to H_2O_2 cross-talk (Burmeister *et al.*, 2003).

This chapter outlines the developmental steps undertaken to optimise sensitivity of the choline biosensor. Discussed is the immobilisation method of choline oxidase onto the sensor surface. The use of stabilisers and cross-linkers is also discussed in sensor designs to determine their effect when used in conjunction with the enzyme. Enzymatic kinetic parameters were compared in order to determine the advantageous designs for optimal detection of choline. A summary of modifications is provided at the end of each section.

4.2. Experimental

All instrumentation and software used in this section are described in Section 3.2. All chemicals and solutions used are described in Section 3.3. The electrodes were constructed from a disk electrode as described in Section 3.4.1. The design and manufacture of designs is explained in detail in Section 3.4.2.1. All data was recorded using the cell setup described in Section 3.5.1.1. The calibrations were performed as described in Section 3.5.1.3.

The data is reported as mean ± SEM where n denotes the number of electrodes used. The significance of difference was estimated using two-tailed *t*-tests. Paired tests were used for comparing signals recorded at the same electrode, unpaired tests were used for comparing data from different electrodes.

4.3. Results and Discussion

This results section illustrates the preliminary work involved in the development of a choline biosensor. The main aim of this section is to identify how best to optimise sensitivity.

4.3.1. Immobilisation

There are various immobilisation strategies employed in the development of biosensors. The most common procedures are entrapment in gels or membranes, physical adsorption, covalence, cross-linking and affinity (Rothwell *et al.*, 2010) (Sassolas *et al.*, 2012) (Teles & Fonseca, 2008). Entrapment within both conducting and non-conducting polymers has commonly been utilised in biosensor design (Bayramoğlu *et al.*, 2010) (Tsai *et al.*, 2007) (Lowry & O'Neill, 1994). A poly *o*-(phenylenediamine) (PPD) solution containing oxidase enzymes has been reported for the development of glucose (Malitesta *et al.*, 1990) (Lowry & O'Neill, 1994) and glutamate biosensors (Berners *et al.*, 1994) by electropolymerisation. Although this method is convenient, it is not cost effective (Ryan *et al.*, 1997) and not suitable for all enzymes (Wilson & Thévenot, 1990). Thus, dip coating is a more advantageous approach to enzyme loading (Ryan *et al.*, 1997). Enzyme immobilisation strategies for dip coating glucose oxidase onto bare and polymer coated electrodes, cross-linked by glutaraldehyde demonstrates good active enzyme loading, an alternative when co-immobilisation is not suitable (Rothwell *et al.*, 2010).

Synthetic polymers have also been used for the entrapment of enzymes (Bernfeld & Wan, 1963). The synthetic polymer polystyrene has been utilised as a solid support for protein immobilisation in enzyme-linked immunosorbant assay (ELISA) (Kumada *et al.*, 2010). As monomeric styrene is liquid at room temperature, it is an ideal candidate for the entrapment of choline oxidase using the dip coating approach to enzyme loading, an approach previously demonstrated in this research group (Bolger, 2007) .

Initial experiments were carried out in order to investigate methods of dip coating choline oxidase (ChOx) onto the styrene monomer as an immobilisation strategy. One layer and ten layers of enzyme solution and alternately, a thirty minute immersion in the enzyme solution was performed.

A

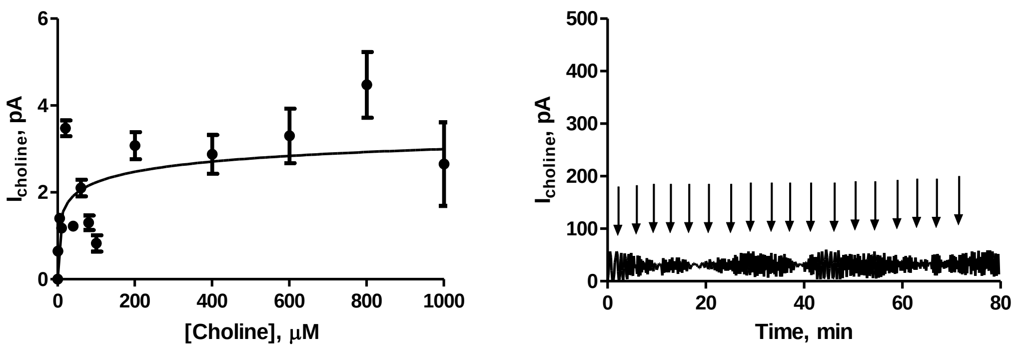

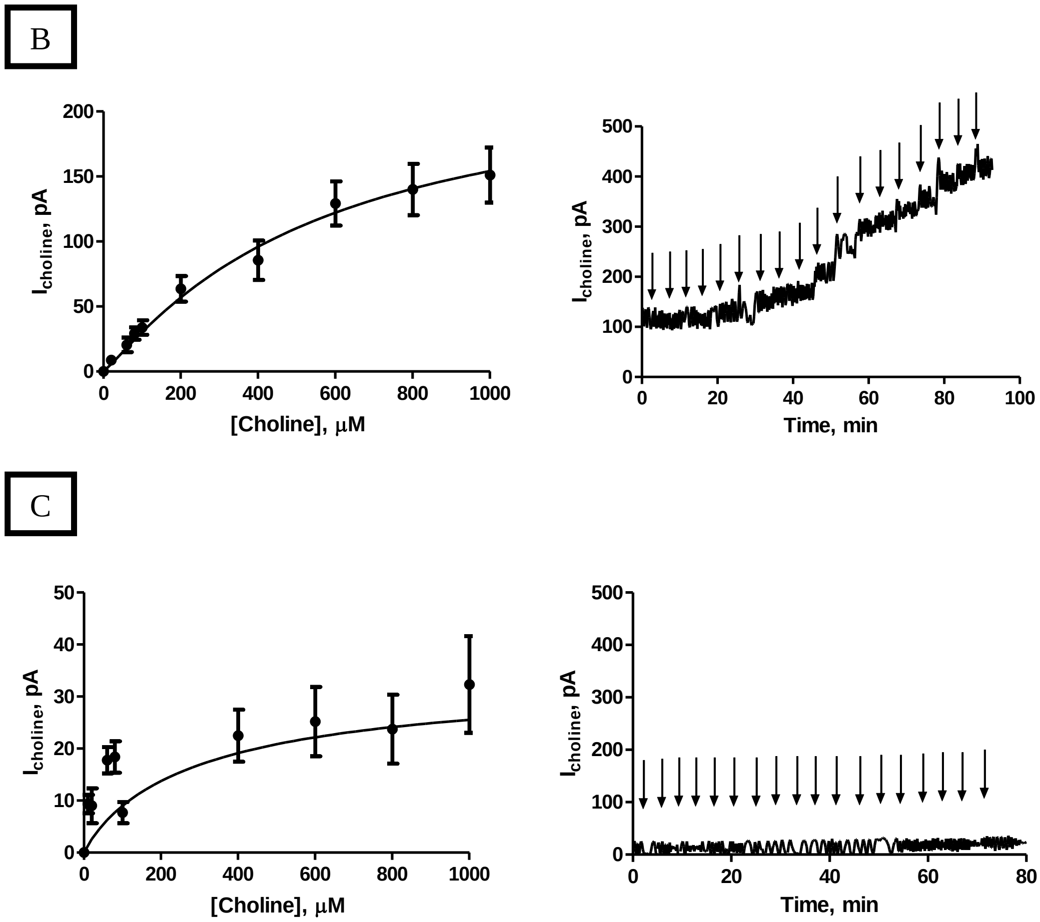

Figure 4.1 : The current-concentration profile for choline chloride calibrations in PBS (pH 7.4) buffer solution at 21°C using designs (A) Sty-(ChOx)$_1$, (B) Sty-(ChOx)$_{10}$ and (C) Sty-(ChOx)$_{30min.}$ CPA carried out at +700 mV *vs*. SCE. Sequential current steps for 5, 10, 20, 40, 60, 80, 100, 200, 400, 600, 800, 1000 μM choline chloride injections. A raw data trace for (A) Sty-(ChOx)$_1$, (B) Sty-(ChOx)$_{10}$ and (C) Sty-(ChOx)$_{30min}$ is presented. Arrows indicate sequential current steps.

	Sty-(ChOx)$_1$			Sty-(ChOx)$_{10}$			Sty-(ChOx)$_{30\ min}$		
Conc, µM	**Mean, pA**	**S.E.M, pA**	**n**	**Mean, pA**	**S.E.M, pA**	**n**	**Mean, pA**	**S.E.M, pA**	**n**
0	0.00	0.00	4	0.00	0.00	4	0.00	0.00	4
5	1.40	0.06	4	-16.83	0.01	4	-7.23	0.94	4
10	1.18	0.06	4	-3.18	4.13	4	9.35	1.77	4
20	3.48	0.18	4	8.80	3.55	4	9.00	3.36	4
40	1.23	0.09	4	-3.78	8.79	4	-9.08	2.23	4
60	2.10	0.19	4	20.48	5.61	4	17.75	2.53	4
80	1.30	0.17	4	29.20	4.70	4	18.38	3.01	4
100	0.83	0.19	4	33.80	5.55	4	7.70	2.04	4
200	3.08	0.32	4	63.65	9.83	4	-5.60	4.52	4
400	2.88	0.45	4	85.58	15.14	4	22.48	5.01	4
600	3.30	0.63	4	129.33	17.00	4	25.18	6.67	4
800	4.48	0.76	4	140.08	19.74	4	23.73	6.62	4
1000	2.65	0.96	4	151.08	21.15	4	32.30	9.29	4

Table 4.1 : Comparison table of mean current values for designs; (A) Sty-(ChOx)$_1$, (B) Sty-(ChOx)$_{10}$ and (C) Sty-(ChOx)$_{30min}$. Choline chloride calibrations carried out in PBS (pH 7.4) buffer solution at 21°C. CPA carried out at +700 mV *vs*. SCE. All currents are background subtracted.

The data presented in Figure 4.1 shows the effect of three dip coating strategies for the immobilisation of ChOx onto the sensor surface and its effect on sensitivity. One dip coat of enzyme did not immobilise a sufficient amount for adequate detection of the analyte. A thirty minute immersion in the enzyme solution immobilised more enzyme onto the sensor surface compared to one layer (quick removal from the solution) due to the increased length of exposure to the enzyme, therefore, sensitivity was increased. Ten layers of enzyme demonstrated the highest substrate detection of the three dip coating strategies which subsequently produced a Michaelis-Menten enzymatic curve. Ten individual layers with drying time between layers (5 minutes) allowed the enzyme to be ‘fixed’ in place prior to the subsequent dip coating layer. This layering process dramatically increased the amount of enzyme which was immobilised onto the sensor surface as illustrated by the higher analyte detection and the observed Michaelis Menten enzymatic curve.

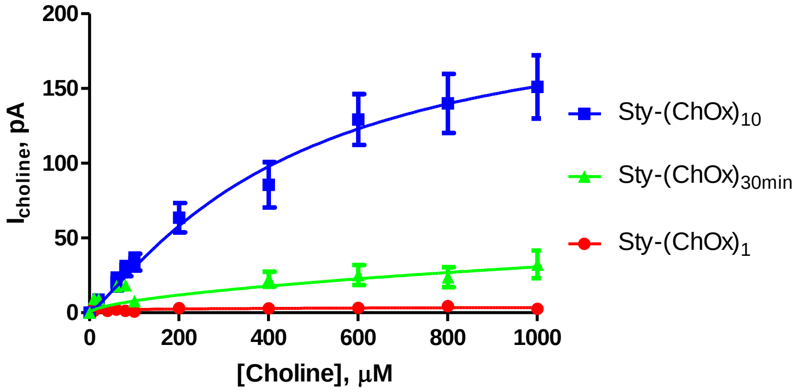

Kinetic Parameters	Sty-(ChOx)$_1$			Sty-(ChOx)$_{10}$			Sty-(ChOx)$_{30\,min}$		
	Mean	S.E.M	n	Mean	S.E.M	n	Mean	S.E.M	n
V_{MAX}, pA	4.32	3.18	4	234.10	29.50	4	34.19	11.85	4
Km, μM	81.09	406.00	4	554.80	171.50	4	308.20	336.80	4
α	0.33	0.28	4	1.11	0.22	4	0.92	0.53	4
$I_{100\mu M}$, pA	0.83	0.19	4	33.80	5.55	4	7.70	2.04	4
Sensitivity, pA/μM	0.002	0.010	4	0.44	0.08	4	0.16	0.09	4
R^2	0.01	0.02	4	0.11	0.06	4	0.05	0.02	4
Background, pA	29.25	0.94	4	82.95	14.84	4	17.68	1.69	4

Figure 4.2 : The current-concentration profile comparison and comparison tables for choline chloride calibrations in PBS (pH 7.4) buffer solution at 21°C for designs; (A) Sty-(ChOx)$_1$, (B) Sty-(ChOx)$_{10}$ and (C) Sty-(ChOx)$_{30min}$. CPA carried out at +700 mV *vs.* SCE. Sequential current steps for 5, 10, 20, 40, 60, 80, 100, 200, 400, 600, 800, 1000 μM choline chloride injections.

A comparison graph and data table of kinetic parameters are presented in Figure 4.2. The graph illustrates the comparison of the dip coat methods for the immobilisation of ChOx, the table presents the kinetic parameter comparisons for each design. The graph demonstrates the high level of analyte detection using the immobilisation of ten layers of enzyme. This dip coating process proved advantageous over the other design which incorporated one layer of enzyme. Despite the exposure of the sensor to the enzyme solution for 30 minutes, the sensitivity of this design compared to ten layers suggests that the layering process is required to increase the enzyme immobilisation.

The comparison of the $I_{100\mu M}$ choline currents of 1 layer to 10 layers demonstrates a significant increase (P = 0.0151) from 0.83 ± 0.19 pA, n = 4 (Sty-(ChOx)$_1$) to 33.80 ±

5.55 pA, n = 4 (Sty-$(ChOx)_{10}$). Thirty minute submersion in the enzyme solution increased enzyme loading onto the sensor surface compared to one layer as demonstrated by the $I_{100\mu M}$ current of 7.70 ± 2.04 pA, n = 4 (Sty-$(ChOx)_{30min}$), however, the ten layers produced highest currents overall.

The kinetic parameters in the table illustrate that with an α value of 1.11, ten layers of enzyme produces Michaelis-Menten behaviour. This is determined as the ideal Michaelis Menten kinetics will have an α value of 1 (see Section 2.6.2). Michaelis-Menten behaviour is also observed for a thirty minute submersion in the enzyme solution resulting in an α value of 0.92. However, one layer of enzyme resulted in insufficient enzyme loading to produce ideal Michaelis-Menten behaviour as the α value is 0.33. The V_{MAX} current produced by ten layers of enzyme (234.10 ± 29.50 nA) was significantly increased (P = 0.0239) compared to the thirty minute submersion in the enzyme solution (31.49 ± 11.85 nA), and increased (P = 0.0063) compared to one layer of enzyme (4.32 ± 3.18 pA). A comparison of the K_M concentrations shows that a thirty minute submersion in an enzyme solution (308.20 ± 336.30 µM) has lowered (P = 0.9226) the K_M concentration compared to ten enzyme layers (554.80 ± 171.50 µM). This reduction is potentially as a result of a low enzyme loading therefore a reduction in the diffusion constraints. One layer of enzyme produced the lowest K_M concentration (88.09 ± 4.06 µM).

The dip adsorption method using ten layers, produced the highest sensitivity and the most ideal Michaelis-Menten enzyme kinetics, therefore this immobilisation method was continued with for the rest of the experiments.

Summary

This section has determined that ten layers of enzyme are optimal for analyte detection. One layer of enzyme and a thirty minute suspension into solution were insufficient for adequate detection of choline.

4.3.2. BSA and GA Modifications

4.3.2.1. BSA

Bovine serum albumin (BSA) has been widely documented in the development of biosensors. BSA is an inert protein which has been employed in biosensor design for both enzyme protection and stabilisation (Wilson & Thévenot, 1990). Techniques utilised to immobilise an enzyme onto an electrode surface can have a detrimental effect on the activity (Costa *et al.*, 2002). Previously, the use of PPD to immobilise glutamate oxidase has shown that BSA protects the enzyme from potential inactivation from the polymerisation process (Ryan *et al.*, 1997). Glutaraldehyde; which cross-links enzymes to obtain higher enzyme loading, has also been used in conjunction with BSA. The glutaraldehyde cross-links the BSA in addition to the enzyme limiting the direct enzyme cross-linking, resulting in higher enzyme activity and stability (Wilson & Thévenot, 1990). The addition of various additives for enzymes has been widely studied for their beneficial effect on enzyme storage and stability. For example studies into the storage stability of the enzyme catalase showed that BSA can increase the half-life when compared to catalase alone even doubling the half-life when used in conjunction with glutaraldehyde (Costa *et al.*, 2002).

As determined in the previous section, the dip coating strategy using ten layers of enzyme was chosen as the immobilisation method for ChOx for use in subsequent investigations. This section determines if the inclusion of additives (BSA) within the sensor design could increase the stability and efficiency of the choline oxidase therefore, increasing sensitivity. BSA was added into the enzyme solution (ChOx:BSA) and the analyte detection was compared to the original choline oxidase solution (ChOx). BSA potentially could protect the enzyme coated on the sensor surface during the layering process or hinder access of the substrate to the active sites of the enzyme below, due to its comparatively larger size. The effect of BSA inclusion into the enzyme solution was investigated in this section to determine if the enzyme loading and thus sensitivity was affected.

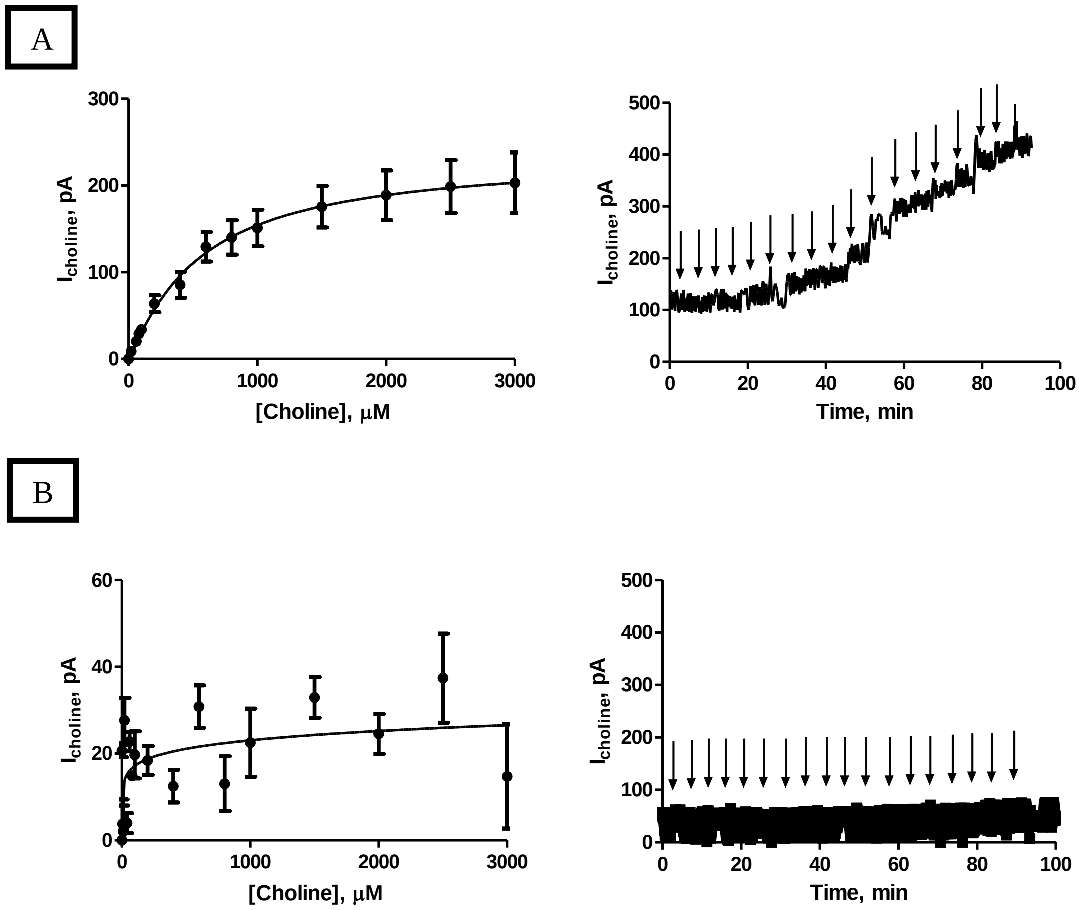

Figure 4.3 : The current-concentration profile for choline chloride calibrations in PBS (pH 7.4) buffer solution at 21°C using designs (A) Sty-$(ChOx)_{10}$ and (B) Sty-$(ChOx:BSA)_{10}$. CPA carried out at +700 mV *vs*. SCE. Sequential current steps for 5, 10, 20, 40, 60, 80, 100, 200, 400, 600, 800, 1000, 1500, 2000, 2500 and 3000 μM choline chloride injections. A raw data trace for (A) Sty-$(ChOx)_{10}$ and (B) Sty-$(ChOx:BSA)_{10}$ is presented. Arrows indicate sequential current steps.

	Sty-$(ChOx)_{10}$			Sty-$(ChOx:BSA)_{10}$		
Conc, µM	**Mean, pA**	**S.E.M, pA**	**n**	**Mean, pA**	**S.E.M, pA**	**n**
0	0.00	0.00	4	0.00	0.00	4
5	-16.825	0.002	4	3.75	5.70	4
10	-3.18	4.13	4	2.05	5.98	4
20	8.80	3.55	4	27.65	5.22	4
40	-3.78	8.79	4	3.98	2.28	4
60	20.48	5.61	4	22.75	2.24	4
80	29.20	4.70	4	14.85	1.08	4
100	33.80	5.55	4	19.70	5.43	4
200	63.65	9.83	4	18.43	3.31	4
400	85.58	15.14	4	12.50	3.79	4
600	129.33	17.00	4	30.83	4.89	4
800	140.08	19.74	4	13.05	6.33	4
1000	151.08	21.15	4	22.53	7.85	4
1500	175.60	0.02	4	32.95	4.66	4
2000	188.78	0.03	4	24.58	4.59	4
2500	198.80	0.03	4	37.40	10.27	4
3000	203.23	0.04	4	14.73	12.02	4

Table 4.2 : Comparison table of mean current values for designs; (A) Sty-$(ChOx)_{10}$ and (B) Sty-$(ChOx:BSA)_{10}$. Choline chloride calibrations carried out in PBS (pH 7.4) buffer solution at 21°C. CPA carried out at +700 mV *vs*. SCE. All currents are background subtracted.

The data presented in Figure 4.3 shows the addition of BSA to the enzyme solution. BSA has been previously utilised in biosensor construction to increase sensitivity. The results illustrate that BSA did not improve the sensitivity in this case and abolished enzyme kinetics. When compared to the sensor design which immobilised the ChOx solution, the reduction in sensitivity suggests that the addition of BSA blocks access of the substrate to the active site of the enzyme within the underlying layers, or alternatively, due to the comparatively larger size of the BSA may decrease the amount of enzyme immobilised on the sensor surface. As a result, the incorporation of BSA into the enzyme solution has both decreased sensitivity and abolished Michaelis-Menten kinetics. As BSA is traditionally used in conjunction with glutaraldehyde, it is possible that without additional means of securing the layers onto the electrode surface the protein loading is limited.

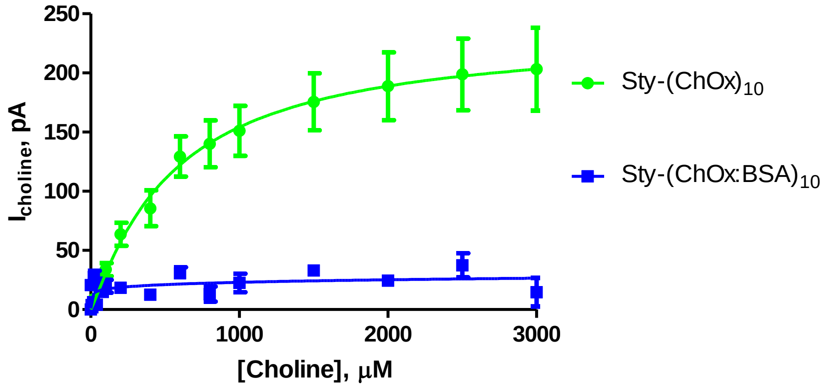

Kinetic Parameters	Sty-(ChOx)$_{10}$			Sty-(ChOx:BSA)$_{10}$		
	Mean	S.E.M	n	Mean	S.E.M	n
V_{MAX}, pA	234.10	29.50	4	-	-	
Km, μM	554.80	171.50	4	-	-	
α	1.11	0.22	4	-	-	
$I_{100μM}$, pA	33.80	5.55	4	19.70	5.43	4
Sensitivity, pA/μM	0.44	0.08	4	0.020	0.003	4
R^2	0.11	0.06	4	0.20	0.10	4
Background, pA	82.95	14.84	4	0.10	0.10	4

Figure 4.4 : The current-concentration profile comparison and comparison tables for choline chloride calibrations in PBS (pH 7.4) buffer solution at 21°C for designs; (A) Sty-(ChOx)$_{10}$ and (B) Sty-(ChOx:BSA)$_{10}$. CPA carried out at +700 mV *vs.* SCE. Sequential current steps for 5, 10, 20, 40, 60, 80, 100, 200, 400, 600, 800, 1000, 1500, 2000, 2500 and 3000 μM choline chloride injections.

A comparison graph and data table of kinetic parameters are presented in Figure 4.4. The graph illustrates the comparison of the addition of BSA into the enzyme solution, the table presents the parameter comparisons for each design, however, as the incorporation of BSA destroyed the kinetics, no values are given. The comparison data demonstrates that the addition of BSA into the enzyme solution decreases sensitivity potentially by limiting enzyme loading or blocking access to enzyme on underlying layers.

A comparison of the $I_{100\mu M}$ current demonstrates the detrimental effect of the BSA addition as the current was reduced from 33.80 ± 5.55 pA, n = 4 (Sty-$(ChOx)_{10}$) to 19.70 ± 5.43 pA, n = 4 (Sty$(ChOx{:}BSA)_{10}$).

Overall, the addition of BSA within the enzyme solution was not beneficial to the design.

Summary

This section has demonstrated that the incorporation of BSA into the enzyme medium is detrimental to sensitivity and the enzyme kinetics.

4.3.2.2. GA

Glutaraldehyde has been widely used for the immobilisation of enzymes in the construction of biosensors. Glutaraldehyde is a linear 5-carbon dialdehyde which can react with several functional groups of proteins such as amine, thiol, phenol and imidizole groups. Although this is the case, the cross-linking effect of glutaraldehyde is mainly with the ε-amino groups of lysine residues. Most proteins contain lysine residues usually located on the protein surface and are generally not involved in the catalytic site (Isabelle Migneault, 2004). This allows moderate cross-linking by intermolecular rather than intramolecular cross-bridges to preserve the conformation and biological activity of the protein (Payne, 1973). In an aqueous solution glutaraldehyde is not limited to the monomeric form, therefore, leading to debate on the mechanism of the cross-linking (Isabelle Migneault, 2004). The proposed mechanism for the monomeric form itself is that nucleophilic attack of the aldehyde groups by the ε-amino groups of the lysine residues on the protein yield a Schiff base (de Melo *et al.*, 1999) (Isabelle Migneault, 2004).

Glutaraldehyde is an effective cross-linking agent that has been used frequently in biosensor design. Although this is the case, it has been known to decrease the efficiency of enzymes, through the cross-linking process (Costa *et al.*, 2002). Therefore, BSA has previously been incorporated in conjunction with the cross-linking process to increase enzyme activity and stability (Wilson & Thévenot, 1990). In addition to this, the mechanism of glutaraldehyde is thought to involve the lysine amino group. Therefore it is used in conjunction with BSA; which is an inert lysine rich protein (Isabelle Migneault, 2004), to increase the amount on lysine residues with which glutaraldehyde can cross-link therefore, increasing immobilisation. Also, the addition of BSA can aid in protecting the enzyme, as the glutaraldehyde will preferentially cross-link with the BSA rather than the enzyme itself (Li *et al.*, 1999), potentially due to the increased lysine residues and its comparatively larger size.

The previous section illustrates the effect of BSA on enzyme activity. Although the BSA did not prove beneficial alone, the incorporation of BSA when investigating the inclusion of glutaraldehyde as a cross-linking layer was considered important for the reasons outlined above. This section looks at the introduction of glutaraldehyde for additional enzyme immobilisation due to enzyme cross-linking, and whether BSA could protect the enzyme from the harshness of this process.

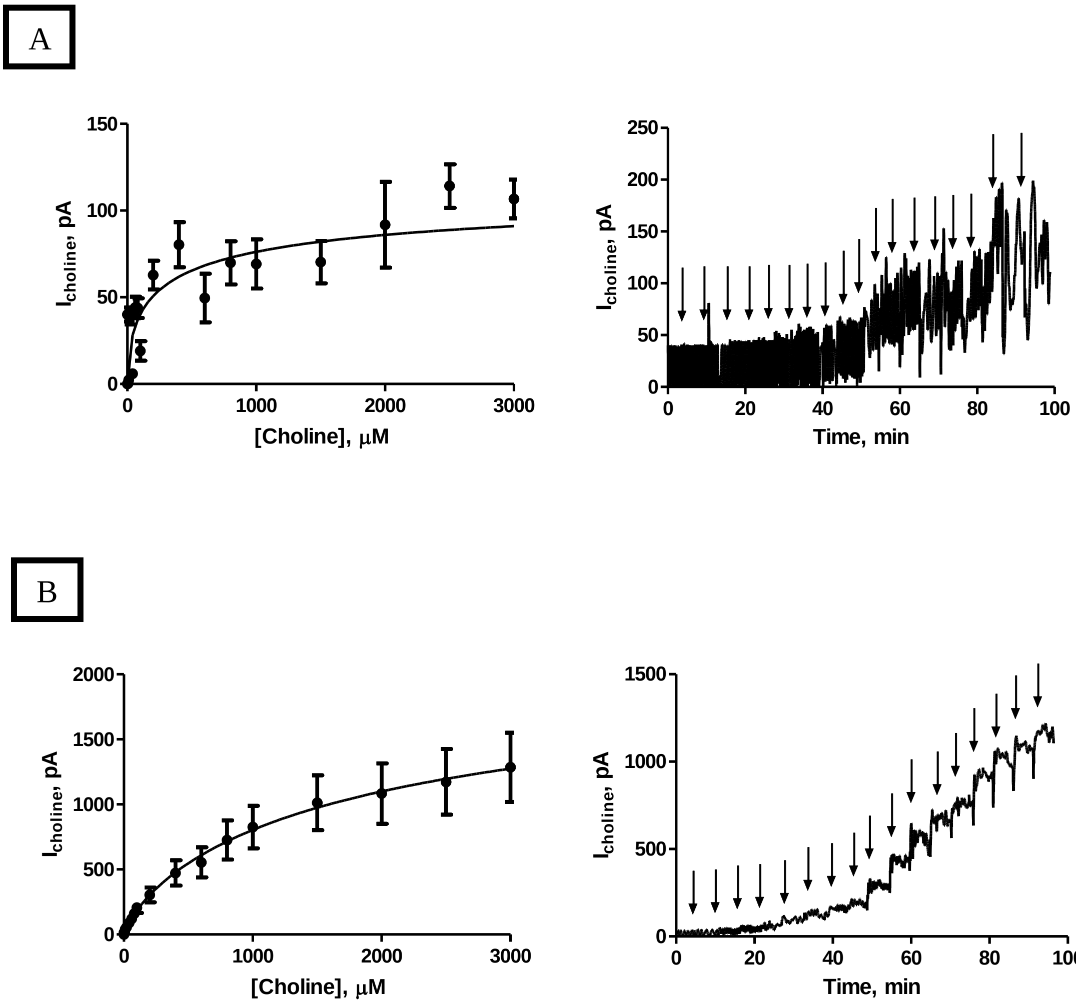

Figure 4.5 : The current-concentration profiles and raw data traces for choline chloride calibrations in PBS (pH 7.4) buffer solution at 21°C using designs (A) Sty-(ChOx)$_{10}$-GA1% and (B) Sty-(ChOx:BSA)$_{10}$-GA1%. CPA carried out at +700 mV *vs*. SCE. Sequential current steps for 5, 10, 20, 40, 60, 80, 100, 200, 400, 600, 800, 1000, 1500, 2000, 2500 and 3000 μM choline chloride injections.

	Sty-(ChOx)$_{10}$-GA1%			Sty-(ChOx:BSA)$_{10}$-GA1%		
Conc, µM	**Mean, pA**	**S.E.M, pA**	**n**	**Mean, pA**	**S.E.M, pA**	**n**
0	0.00	0.00	4	0.00	0.00	4
5	0.35	1.62	4	15.15	3.25	4
10	2.35	1.47	4	40.28	6.39	4
20	39.25	4.93	4	55.43	7.34	4
40	5.93	1.46	4	88.43	16.04	4
60	44.10	6.16	4	121.30	30.35	4
80	43.78	5.70	4	160.18	30.05	4
100	19.05	5.60	4	205.23	38.76	4
200	62.83	8.24	4	304.10	55.99	4
400	80.35	12.99	4	473.33	96.98	4
600	49.58	14.03	4	554.60	116.06	4
800	69.93	12.44	4	726.65	150.26	4
1000	69.23	14.18	4	825.80	163.93	4
1500	70.30	12.18	4	1013.03	210.36	4
2000	91.83	24.72	4	1083.58	232.44	4
2500	114.13	12.62	4	1173.13	252.50	4
3000	106.70	11.14	4	1285.20	265.36	4

Table 4.3 : Comparison table of mean current values for designs; (A) Sty-(ChOx)$_{10}$-GA1% and (B) Sty-(ChOx:BSA)$_{10}$-GA1%. Choline chloride calibrations carried out in PBS (pH 7.4) buffer solution at 21°C. CPA carried out at +700 mV *vs.* SCE. All currents are background subtracted.

The data presented in Figure 4.5 shows the effect of a glutaraldehyde layer on sensitivity. The glutaraldehyde solution was used to secure enzyme layers and enzyme layers which also incorporated BSA. The results indicate that glutaraldehyde was detrimental to sensitivity when used to cross-link the enzyme layers, however, the inclusion of BSA increased sensitivity when used in conjunction with this cross-linking process. The low sensitivity observed in the absence of BSA, may be due to glutaraldehyde cross-linking the enzyme, restricting access of the substrate to the active site. Alternatively, a lack of lysine residues within choline oxidase may mean that the glutaraldehyde is not cross-linking as expected, resulting in an additional layer that is blocking access of the substrate. The increase in sensitivity observed when glutaraldehyde is used in conjunction with BSA, may be due to the high level of lysine residues on BSA, which when incorporated into the enzyme layer the glutaraldehyde may preferentially cross-link with these, thus the BSA is a protective addition to the enzyme layers. This in turn, leaves the active sites unobstructed for efficient turnover of substrate, increasing sensitivity.

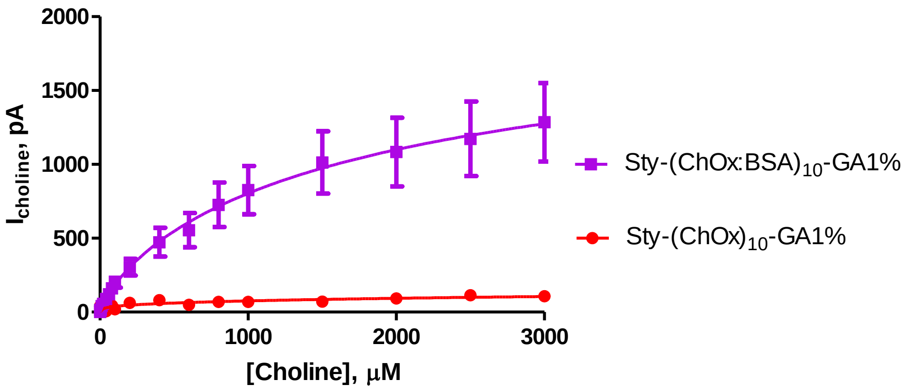

Kinetic Parameters	$Sty\text{-}(ChOx)_{10}\text{-}GA1\%$			$Sty\text{-}(ChOx{:}BSA)_{10}\text{-}GA1\%$		
	Mean	S.E.M	n	Mean	S.E.M	n
V_{MAX}, pA	119.90	32.63	4	2184.00	94.58	4
Km, μM	356.80	460.60	4	1966.00	214.70	4
α	0.54	0.21	4	0.80	0.02	4
$I_{100\mu M}$, pA	19.05	5.60	4	205.23	38.76	4
Sensitivity, pA/μM	0.21	0.19	4	1.92	0.07	4
R^2	0.16	0.07	4	0.980	0.001	4
Background, pA	-3.70	2.01	4	23.70	1.35	4

Figure 4.6 : The current-concentration profile comparison and comparison tables for choline chloride calibrations in PBS (pH 7.4) buffer solution at 21°C for designs; (A) Sty-$(ChOx)_{10}$-GA1% and (B) Sty-$(ChOx{:}BSA)_{10}$-GA1%. CPA carried out at +700 mV *vs.* SCE. Sequential current steps for 5, 10, 20, 40, 60, 80, 100, 200, 400, 600, 800, 1000, 1500, 2000, 2500 and 3000 μM choline chloride injections.

A comparison graph and data table of kinetic parameters are presented in Figure 4.6. The graph illustrates the comparison of glutaraldehyde incorporation and its interaction with BSA, the table presents the kinetic parameter comparisons for each design. Although the cross-linking process has a detrimental effect on the ChOx layers the introduction of BSA increases sensitivity dramatically.

A comparison of the $I_{100\mu M}$ values of the designs Sty-(ChOx)$_{10}$ (63.65 ± 9.83 pA, n = 4) (see Section 4.3.1) and Sty-(ChOx)$_{10}$-GA1% (19.05 ± 5.60 pA, n = 4) show a significant decrease in sensitivity (P = 0.0019) with the introduction of glutaraldehyde. In Section 4.3.2.1 the addition of BSA into the enzyme solution decreased sensitivity dramatically. However, it proved hugely beneficial when utilised in conjunction with glutaraldehyde. A comparison of the $I_{100\mu M}$ values shows that the combination of BSA and GA has decreased the detrimental cross-linking effect between GA and the enzyme increasing the currents from 19.05 ± 5.60 pA, n = 4 (Sty-(ChOx)$_{10}$-GA1%) to 205.23 ± 38.76 pA, n = 4 (Sty-(ChOx:BSA)$_{10}$-GA1%).

The introduction of BSA when used in conjunction with GA demonstrates Michaelis-Menten kinetics close to the ideal with an α value of 0.80. GA used in conjunction with enzyme layers destroys the enzyme kinetics reducing the α value to 0.54. The K_M concentration was reduced from 1966.00 ± 214.70 µM, n = 4 (Sty-(ChOx:BSA)$_{10}$-GA1%) to 356.80 ± 460.60 µM, n = 4 (Sty-(ChOx)$_{10}$-GA1%) in the absence of the protective BSA, potentially as the BSA increases the rate of diffusion. The V_{MAX} current was decreased from 2184.00 ± 94.58 pA, n = 4 (Sty-(ChOx:BSA)$_{10}$-GA1%) to 119.90 ± 32.63 pA, n = 4 (Sty-(ChOx)$_{10}$-GA1%) in the absence of BSA. Overall, this section illustrates that although BSA is detrimental when used in an enzyme solution without additional means of securing the enzyme to the sensor surface (see Section 4.3.2.1), when used in conjunction with GA it proves beneficial in increasing sensitivity which may be utilised in future designs.

Summary

This section has demonstrated that a GA solution used in conjunction with the enzyme is detrimental to sensitivity when compared to the design which does not use GA. However, the incorporation of the BSA and used in conjunction with GA increased the sensitivity of the sensor. The design Sty-(ChOx:BSA)$_{10}$-GA1% is determined as the optimal design for the incorporation of ChOx onto the sensor surface thus far.

4.3.2.3. GA Concentration

Incorporation of BSA within the enzyme solution used for dip coating was shown to be detrimental to sensitivity (Section 4.3.2.1), however, when this solution was used in conjunction with glutaraldehyde, it proved hugely beneficial, increasing the sensitivity of the sensor and proving to be the best method of enzyme incorporation (section 4.3.2.2). For this reason a solution of both ChOx and BSA was used in the following studies. The beneficial effect of glutaraldehyde has been demonstrated in Section 4.3.2.2. In order to fully investigate the effect that cross-linking with glutaraldehyde is having on sensitivity, the concentration of GA was decreased from 1% to 0.1%. In addition to this, BSA was added to a 0.1% solution of glutaraldehyde as this lysine rich protein may decrease the direct cross-linking of the enzyme, due to preferential cross-linking with BSA, prior to the dip coat process, further increasing sensitivity.

A

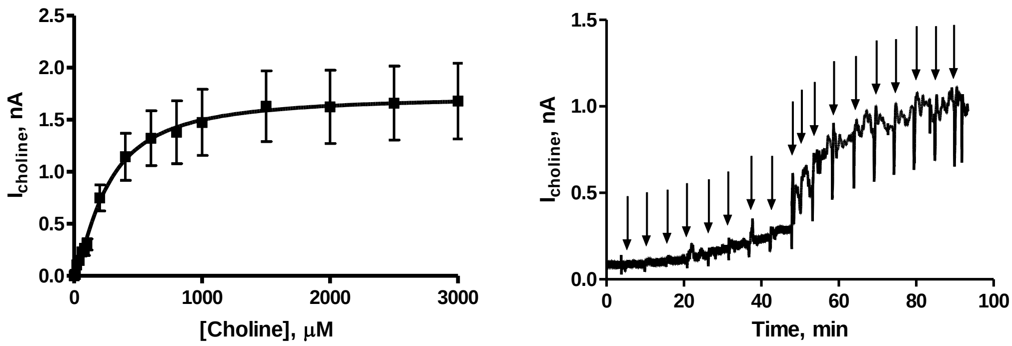

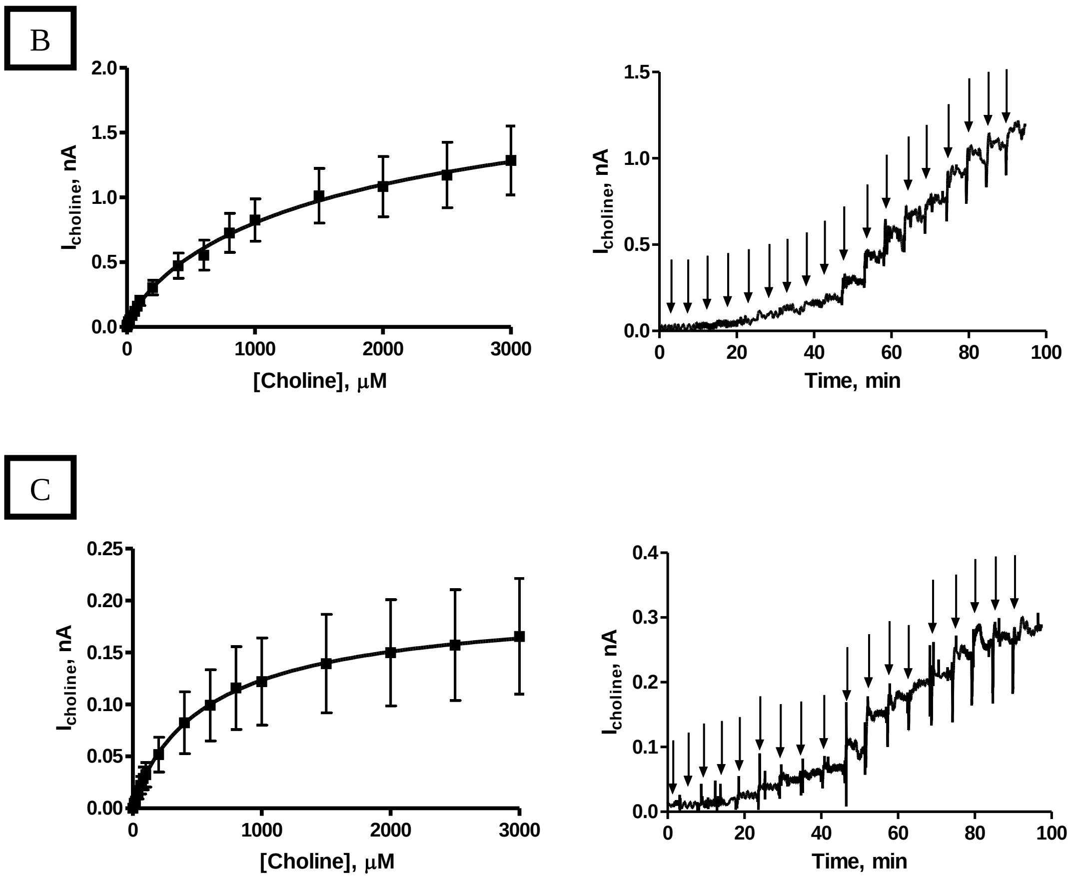

Figure 4.7 : The current-concentration profiles and raw data traces for choline chloride calibrations in PBS (pH 7.4) buffer solution at 21°C using designs (A) Sty-(ChOx:BSA)$_{10}$-GA0.1%, (B) Sty-(ChOx:BSA)$_{10}$-GA1% and (C) Sty-(ChOx:BSA)$_{10}$-GA1%:BSA. CPA carried out at +700 mV *vs*. SCE. Sequential current steps for 5, 10, 20, 40, 60, 80, 100, 200, 400, 600, 800, 1000, 1500, 2000, 2500 and 3000 μM choline chloride injection.

	Sty-(ChOx:BSA)$_{10}$-GA0.1%			Sty-(ChOx:BSA)$_{10}$-GA 1%			Sty-(ChOx:BSA)$_{10}$-GA:BSA		
Conc, µM	Mean, nA	S.E.M, nA	n	Mean, nA	S.E.M, nA	n	Mean, nA	S.E.M, nA	n
0	0.00	0.00	4	0.00	0.00	4	0.00	0.00	4
5	0.01	0.01	4	0.015	0.003	4	-0.001	0.001	3
10	0.01	0.01	4	0.04	0.01	4	0.010	0.002	3
20	0.11	0.04	4	0.06	0.01	4	0.007	0.003	3
40	0.15	0.04	4	0.09	0.01	4	0.02	0.01	3
60	0.23	0.05	4	0.12	0.03	4	0.02	0.01	3
80	0.25	0.05	4	0.16	0.03	4	0.03	0.01	3
100	0.30	0.05	4	0.21	0.04	4	0.03	0.01	3
200	0.75	0.13	4	0.30	0.10	4	0.05	0.02	3
400	1.14	0.23	4	0.47	0.01	4	0.08	0.03	3
600	1.32	0.26	4	0.60	0.10	4	0.10	0.01	3
800	1.38	0.30	4	0.70	0.20	4	0.11	0.04	3
1000	1.47	0.31	4	0.80	0.16	4	0.12	0.04	3
1500	1.63	0.34	4	1.01	0.21	4	0.14	0.04	3
2000	1.62	0.35	4	1.10	0.23	4	0.15	0.05	3
2500	1.65	0.36	4	1.17	0.25	4	0.16	0.05	3
3000	1.68	0.36	4	1.29	0.27	4	0.16	0.06	3

Table 4.4 : Comparison table of mean current values for designs; (A) Sty-(ChOx:BSA)$_{10}$-GA0.1%, (B) Sty-(ChOx:BSA)$_{10}$-GA1% and (C) Sty-(ChOx:BSA)$_{10}$-GA1%:BSA0.1%. Choline chloride calibrations carried out in PBS (pH 7.4) buffer solution at 21°C. CPA carried out at +700 mV *vs.* SCE. All currents are background subtracted.

Illustrated in Figure 4.7 is the effect of glutaraldehyde 0.1%, 1% and a GA0.1%:BSA1% solution on sensitivity. Decreasing the concentration from 1% to 0.1% had a beneficial effect, changing the kinetics of the enzymatic reaction and increasing sensitivity overall. The lower concentration of GA0.1% resulted in a less restricted diffusional barrier than the design using GA1%. The addition of BSA into the glutaraldehyde decreased the sensitivity of the electrode. This is possibly a result of the extra layer of BSA blocking access to the active sites of the enzyme and/or the BSA has decreased the amount of available GA for securing the enzyme layers to the surface of the electrode.

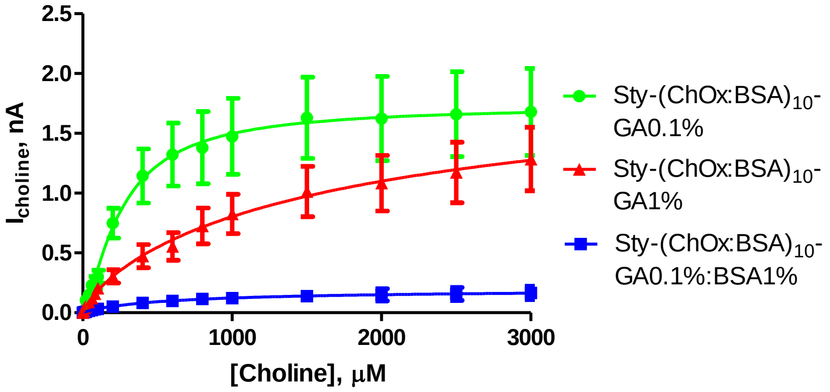

Kinetic Parameters	Sty-(ChOx:BSA)$_{10}$-GA0.1%			Sty-(ChOx:BSA)$_{10}$-GA1%			Sty-(ChOx:BSA)$_{10}$-GA0.1%:BSA1%		
	Mean	S.E.M	n	Mean	S.E.M	n	Mean	S.E.M	n
V_{MAX}, nA	1.73	0.16	4	1.63	0.33	4	0.20	0.07	3
Km, μM	260.10	69.10	4	979.80	543.10	4	608.20	570.10	3
α	1.38	0.35	4	0.94	0.26	4	0.92	0.38	3
$I_{100\mu M}$, nA	0.30	0.05	4	0.21	0.04	4	0.03	0.01	3
Sensitivity, nA/μM	0.0030	0.0002	4	0.002	0.002	4	0.0004	0.00002	3
R^2	0.948	0.021	4	0.979	0.008	4	0.975	0.008	3
Background, nA	0.14	0.02	4	0.023	0.001	4	0.013	0.001	3

Figure 4.8 : The current-concentration profile comparison and comparison tables for choline chloride calibrations in PBS (pH 7.4) buffer solution at 21°C for designs; (A) Sty-(ChOx:BSA)$_{10}$-GA0.1%, (B) Sty-(ChOx:BSA)$_{10}$-GA1% and (C) Sty-(ChOx:BSA)$_{10}$-GA1%:BSA0.1%. CPA carried out at +700 mV *vs.* SCE. Sequential current steps for 5, 10, 20, 40, 60, 80, 100, 200, 400, 600, 800, 1000, 1500, 2000, 2500 and 3000 μM choline chloride injections.

A comparison graph and data table of kinetic parameters are presented in Figure 4.8. The graph illustrates the comparison of glutaraldehyde concentrations, the table presents the kinetic parameter comparisons for each design. This section demonstrates the contribution of the GA to sensitivity, indicating that the cross-linking process can be detrimental to enzyme activity, as illustrated by the sensitivity and the enzyme kinetic changes to GA concentration changes.

Decreasing the concentration of glutaraldehyde increased (P = 0.1945) the $I_{100\mu M}$ current of the electrode from 0.21 ± 0.04 nA, n = 4 (Sty-(ChOx:BSA)$_{10}$-GA1%) to 0.30 ± 0.05

nA, n = 4 (Sty-(ChOx:BSA)$_{10}$-GA0.1%). The addition of BSA into the glutaraldehyde decreased the current further to 0.03 ± 0.01 nA, n = 3 (Sty-(ChOx:BSA)$_{10}$-GA:BSA).

The decrease in glutaraldehyde concentration also had a beneficial effect on the access of the substrate to the enzyme. This is illustrated by the reduction in the K_M concentrations from 979.80 ± 543.10 µM, n = 4 (Sty-(ChOx:BSA)$_{10}$-GA1%) to 260.1 ± 69.1 µM, n = 4 (Sty-(ChOx:BSA)$_{10}$-GA0.1%). The addition of BSA into the GA resulted in a K_M concentration of 608.20 ± 570.10 µM, n = 3. This is also reduced from the GA1%, however, higher than GA0.1%. The reduction in GA concentration from 1% to 0.1% increased the α value from 0.94, n = 4 (Sty-(ChOx:BSA)$_{10}$-GA1%) to 1.38, n = 4 (Sty-(ChOx:BSA)$_{10}$-GA0.1%). Reducing the GA concentration increased the α value above the ideal suggesting sigmoidal enzyme kinetics at low concentrations. The addition of BSA into the GA resulted in an α value of 0.92, n = 3. GA0.1% is the design with the α value closest to the ideal of 1. The reduction in GA concentration from 1% to 0.1% increased the V_{MAX} current from 1.63 ± 0.33 nA, n = 4 (Sty-(ChOx:BSA)$_{10}$-GA1%) to 1.73 ± 0.16 nA, n = 4 Sty-(ChOx:BSA)$_{10}$-GA0.1%). The addition of BSA into the GA demonstrated the lowest V_{MAX} current of 0.20 ± 0.07 nA, n = 4.

Clearly the GA concentration plays a vital role in sensitivity and enzyme kinetics. A low GA concentration has proved advantageous and will be considered for future experiments.

Summary

This section has determined that as the cross-linking process reduces sensitivity, the reduction in the GA concentration can increase sensitivity. The reduction in the GA concentration proved advantageous increasing the sensitivity of the sensor. The incorporation of additional BSA in the GA solution was detrimental to the sensitivity of the sensor. The sensitivity of the sensor was increased using the design Sty-(ChOx:BSA)(GA0.1%).

4.3.2.4. BSA / GA1%

In this section an investigation was undertaken in order to evaluate the contribution that the BSA1% solution is having on enzyme protection, when used in conjunction with glutaraldehyde cross-linking. As demonstrated in Section 4.3.2.3 a reduction in the GA concentration increased sensitivity by reducing the amount of enzyme subject to cross-linking which limits enzyme activity. Subsequent to this, the BSA concentration is investigated in this section as, although the necessity of its incorporation was demonstrated in Section 4.3.2.2, the size of the BSA when compared to the enzyme suggests that it may be blocking access to the enzyme. The concentration of BSA was decreased to 0.1% to show the effect the BSA was having on sensitivity.

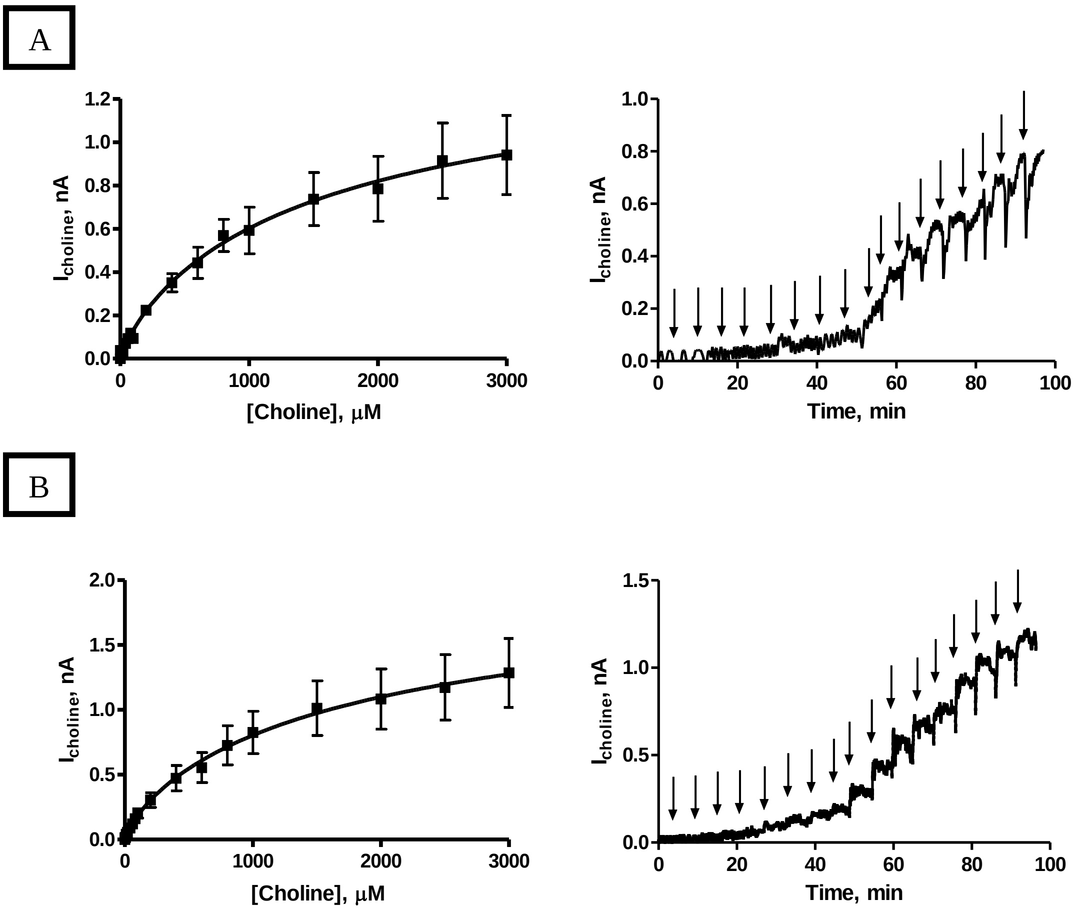

Figure 4.9 : The current-concentration profiles and raw data traces for choline chloride calibrations in PBS (pH 7.4) buffer solution at 21°C using designs (A) Sty-(ChOx:BSA0.1%)$_{10}$-GA1% and (B) Sty-(ChOx:BSA1%)$_{10}$-GA1%. CPA carried out at +700 mV *vs*. SCE. Sequential

current steps for 5, 10, 20, 40, 60, 80, 100, 200, 400, 600, 800, 1000, 1500, 2000, 2500 and 3000 µM choline chloride injections.

	Sty-(ChOx:BSA0.1%)$_{10}$-GA1%			Sty-(ChOx:BSA1%)$_{10}$-GA 1%		
Conc, µM	Mean, nA	S.E.M, nA	n	Mean, nA	S.E.M, nA	n
0	0.00	0.00	3	0.00	0.00	4
5	0.03	0.01	3	0.015	0.003	4
10	0.04	0.01	3	0.04	0.01	4
20	0.030	0.004	3	0.06	0.01	4
40	0.07	0.01	3	0.09	0.01	4
60	0.090	0.004	3	0.12	0.03	4
80	0.12	0.01	3	0.16	0.03	4
100	0.09	0.01	3	0.21	0.04	4
200	0.22	0.02	3	0.30	0.10	4
400	0.35	0.04	3	0.47	0.01	4
600	0.44	0.07	3	0.60	0.10	4
800	0.57	0.07	3	0.70	0.20	4
1000	0.59	0.11	3	0.80	0.16	4
1500	0.74	0.12	3	1.01	0.21	4
2000	0.78	0.14	3	1.10	0.23	4
2500	0.91	0.17	3	1.17	0.25	4
3000	0.94	0.18	3	1.29	0.27	4

Table 4.4 : Comparison table of mean current values for designs; (A) Sty-(ChOx:BSA0.1%)$_{10}$-GA1% and (B) Sty-(ChOx:BSA)$_{10}$-GA1%. Choline chloride calibrations carried out in PBS (pH 7.4) buffer solution at 21°C. CPA carried out at +700 mV *vs*. SCE. All currents are background subtracted.

The data presented in Figure 4.9 demonstrates that BSA has an influential effect on the immobilisation of the enzyme layers cross-linked by GA. These results illustrate that a BSA concentration of 1% is optimal for the protection of the enzyme and the effective cross-linking using GA1%. The use of 0.1% BSA did not prove to be beneficial to sensitivity. This illustrates the important effect of the BSA when used in conjunction with GA on sensitivity and the consideration of its concentration in proportion to the glutaraldehyde concentration.

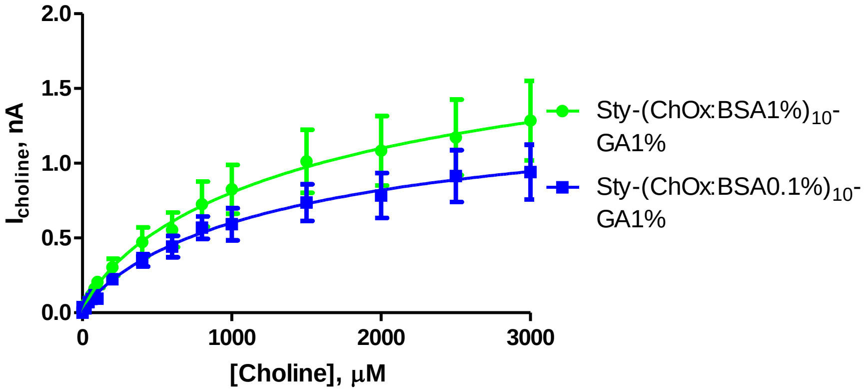

Kinetic Parameters	Sty-(ChOx:BSA0.1%)$_{10}$-GA1%			Sty-(ChOx:BSA1%)$_{10}$-GA1%		
	Mean	S.E.M	n	Mean	S.E.M	n
V_{MAX}, nA	1.50	0.54	3	2.18	1.12	4
Km, µM	1611	1432	3	1966	2544	4
α	0.85	0.20	3	0.80	0.23	4
$I_{100\mu M}$, nA	0.09	0.01	3	0.21	0.04	4
Sensitivity, nA/µM	0.0010	0.0002	3	0.0032	0.0002	4
R^2	0.79	0.07	3	0.98	0.01	4
Background, nA	0.001	0.007	3	0.024	0.001	4

Figure 4.10 : The current-concentration profile comparison and comparison tables for choline chloride calibrations in PBS (pH 7.4) buffer solution at 21°C for designs; (A) Sty-(ChOx:BSA0.1%)$_{10}$-GA1% and (B) Sty-(ChOx:BSA1%)$_{10}$-GA1%. CPA carried out at +700 mV *vs.* SCE. Sequential current steps for 5, 10, 20, 40, 60, 80, 100, 200, 400, 600, 800, 1000, 1500, 2000, 2500 and 3000 µM Choline chloride injections.

A comparison graph and data table of kinetic parameters are presented in Figure 4.10. The graph illustrates the comparison BSA concentrations when used in conjunction with GA1%, the table presents the kinetic parameter comparisons for each design. The comparison data above shows that decreasing the BSA concentration from 1% to 0.1% does not prove to have a beneficial effect on sensitivity.

A comparison of the $I_{100\mu M}$ currents illustrated a reduction in the current from 0.21 ± 0.04 nA, n = 4 (Sty-(ChOx:BSA1%)$_{10}$-GA1%) to 0.09 ± 0.01 nA, n = 3 (Sty-(ChOx:BSA0.1%)$_{10}$-GA1%).

The reduction in BSA concentration did however increase the rate of diffusion decreasing the K_M from 1966 ± 2544 nA, n = 4 (Sty-(ChOx:BSA1%)$_{10}$-GA1%) to 1611 ± 1432 nA, n = 3 (Sty-(ChOx:BSA0.1%)$_{10}$-GA1%). The reduction in the BSA concentration from 1% to 0.1% slightly increased the α value from 0.80 (Sty-(ChOx:BSA1%)$_{10}$-GA1%) to 0.85, n = 3 (Sty-(ChOx:BSA0.1%)$_{10}$-GA1%). In addition, it decreased the V_{MAX} current from 2.18 ± 1.12 nA, n = 4 (Sty-(ChOx:BSA1%)$_{10}$-GA1%) to 1.50 ± 0.54 nA, n = 3 (Sty-(ChOx:BSA0.1%)$_{10}$-GA1%).

This illustrates that BSA concentration is important for use with GA1%. A BSA1% solution is optimal for use with GA1%.

Summary

This section determined the contribution of the BSA in the enzyme solution in the protection of the enzyme from the harsh cross-linking process. When used in conjunction with a 1% GA solution the 1% BSA solution is essential as decreasing the BSA concentration decreases the sensitivity of the sensor.

4.3.2.5. BSA / GA0.1%

Section 4.3.2.4 demonstrated the beneficial contribution of BSA incorporation when used in conjunction with GA1%. This section demonstrated that the BSA1% is optimal for use with GA1%. Section 4.3.2.2 demonstrated that GA0.1% can be incorporated into the sensor design to increase sensitivity. This section investigates if the lower GA concentration of 0.1% can be used in conjunction with a lower BSA concentration. The reduction in the BSA concentration may prove beneficial as the lower GA concentration may not be as detrimental to sensitivity therefore, the BSA is merely surplus to requirement blocking access of the substrate.

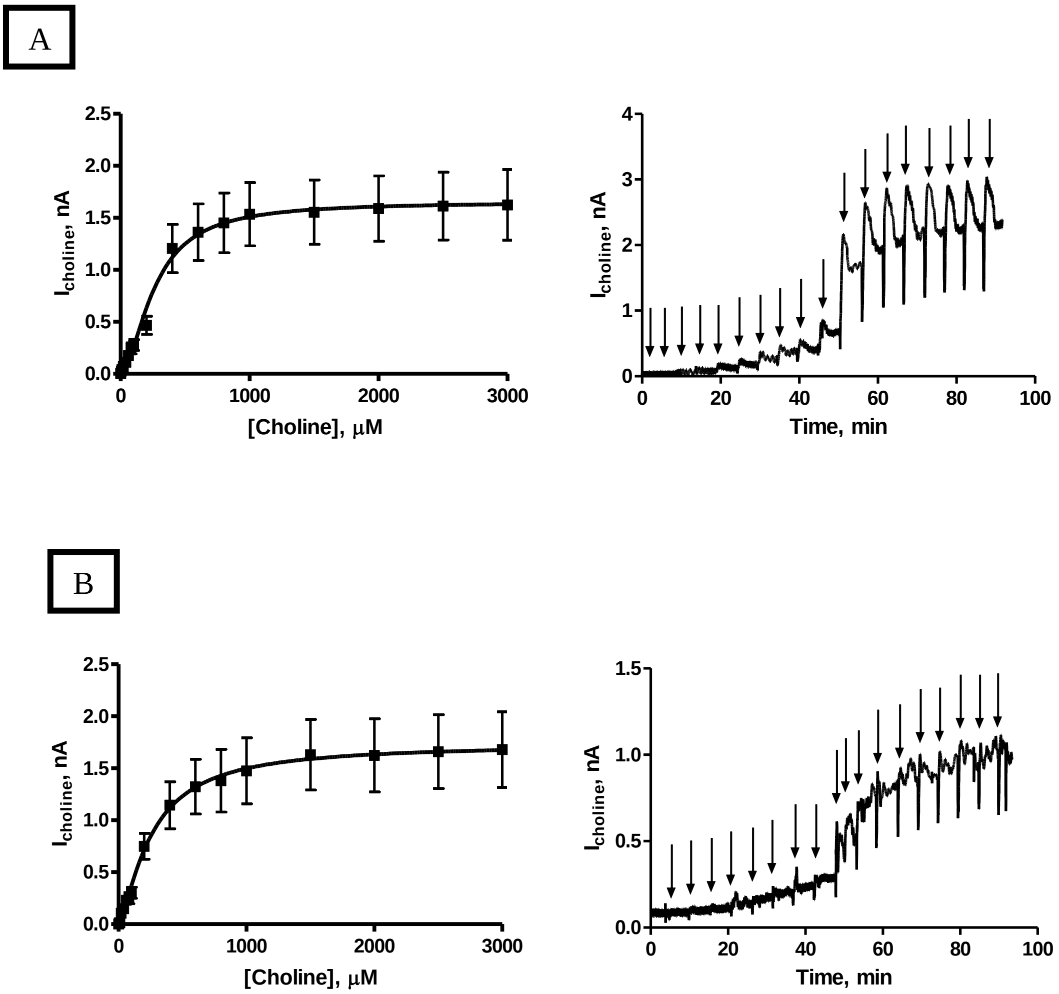

Figure 4.11 : The current-concentration profiles and raw data traces for choline chloride calibrations in PBS (pH 7.4) buffer solution at 21°C using designs (A) Sty-(ChOx:BSA0.1%)$_{10}$-GA0.1% and (B) Sty-(ChOx:BSA1%)$_{10}$-GA0.1%. CPA carried out at +700 mV *vs.* SCE. Sequential current steps for 5, 10, 20, 40, 60, 80, 100, 200, 400, 600, 800, 1000, 1500, 2000, 2500 and 3000 µM choline chloride injections.

	Sty-(ChOx:BSA1%)$_{10}$-GA0.1%			Sty-(ChOx:BSA0.1%)$_{10}$-GA0.1%		
Conc, µM	**Mean, nA**	**S.E.M, nA**	**n**	**Mean, nA**	**S.E.M, nA**	**n**
0	0.00	0.00	4	0.00	0.00	3
5	0.01	0.01	4	0.030	0.004	3
10	0.01	0.01	4	0.04	0.01	3
20	0.11	0.04	4	0.07	0.01	3
40	0.15	0.04	4	0.11	0.02	3
60	0.23	0.05	4	0.17	0.03	3
80	0.25	0.05	4	0.24	0.05	3
100	0.30	0.05	4	0.28	0.05	3
200	0.75	0.13	4	0.47	0.10	3
400	1.14	0.23	4	1.20	0.23	3
600	1.32	0.26	4	1.36	0.27	3
800	1.38	0.30	4	1.45	0.29	3
1000	1.47	0.31	4	1.53	0.31	3
1500	1.63	0.34	4	1.55	0.31	3
2000	1.62	0.35	4	1.59	0.31	3
2500	1.65	0.36	4	1.61	0.33	3
3000	1.68	0.36	4	1.62	0.34	3

Table 4.5 : Comparison table of mean current values for designs; (A) Sty-(ChOx:BSA)$_{10}$-GA0.1% and (B) Sty-(ChOx:BSA0.1%)$_{10}$-GA0.1%. Choline chloride calibrations carried out in PBS (pH 7.4) buffer solution at 21°C. CPA carried out at +700 mV *vs*. SCE. All currents are background subtracted.

The data in Figure 4.11 shows the effect of BSA when used in conjunction with the lower GA concentration of 0.1%. Very little difference is observed in the sensitivity and enzyme kinetics with the reduction of the BSA concentration from 1% to 0.1%. This illustrates that the BSA concentration does not greatly influence sensitivity when the low glutaraldehyde concentrations of 0.1% is used.

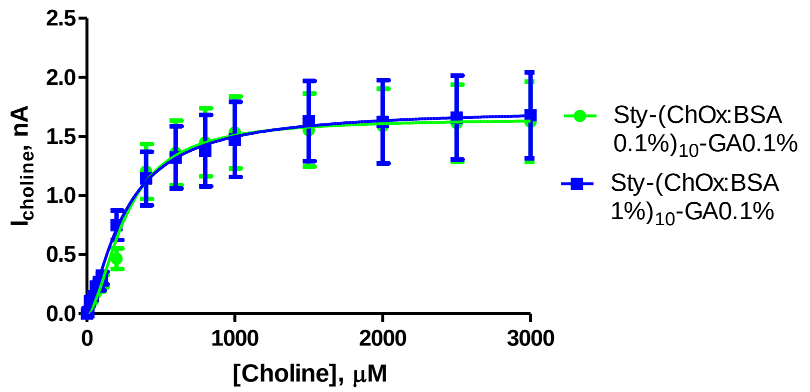

Kinetic Parameters	Sty-(ChOx:BSA0.1%)$_{10}$-GA0.1%			Sty-(ChOx:BSA1%)$_{10}$-GA0.1%		
	Mean	S.E.M	n	Mean	S.E.M	n
V_{MAX}, nA	1.65	0.11	3	1.73	0.16	4
Km, μM	263.70	49.94	3	260.10	69.10	4
α	1.76	0.42	3	1.38	0.35	4
$I_{100\mu M}$, nA	0.28	0.05	3	0.30	0.05	4
Sensitivity, nA/μM	0.0028	0.0001	3	0.00192	0.00006	4
R^2	0.994	0.002	3	0.95	0.02	4
Background, nA	0.03	0.004	3	0.14	0.02	4

Figure 4.12 : The current-concentration profile comparison and comparison tables for choline chloride calibrations in PBS (pH 7.4) buffer solution at 21°C for designs; (A) Sty-(ChOx:BSA)$_{10}$-GA0.1% and (B) Sty-(ChOx:BSA0.1%)$_{10}$-GA0.1%. CPA carried out at +700 mV *vs.* SCE. Sequential current steps for 5, 10, 20, 40, 60, 80, 100, 200, 400, 600, 800, 1000, 1500, 2000, 2500 and 3000 μM choline chloride injections.

A comparison graph and data table of kinetic parameters are presented in Figure 4.12. The graph illustrates the comparison BSA concentrations when used in conjunction with GA0.1%, the table presents the kinetic parameter comparisons for each design. Little difference was observed in sensitivity between the two designs.

A comparison of the $I_{100\mu M}$ currents illustrated that the reduction in BSA concentration used in conjunction with GA0.1% only reduced the $I_{100\mu M}$ current from 0.30 ± 0.05 nA, n = 4 (Sty-(ChOx:BSA1%)$_{10}$-GA0.1%) to 0.28 ± 0.05 nA, n = 3 (Sty-(ChOx:BSA0.1%)$_{10}$-GA0.1%). A much larger decrease is observed when used in conjunction with GA1% demonstrating the protective role BSA is playing on sensitivity.

The K_M only increased from 260.10 ± 69.10 µM, n = 4 (Sty-(ChOx:BSA1%)$_{10}$-GA0.1%) to 263.70 ± 49.94 µM, n = 3 (Sty-(ChOx:BSA0.1%)$_{10}$-GA0.1%). The V_{MAX} was reduced from 1.73 ± 0.16 nA, n = 4 (Sty-(ChOx:BSA1%)$_{10}$-GA0.1%) to 1.65 ± 0.11 nA, n = 3 (Sty-(ChOx:BSA0.1%)$_{10}$-GA0.1%). The α value was increased from 1.38, n = 4 (Sty-(ChOx:BSA1%)$_{10}$-GA0.1%) to 1.65, n = 3 (Sty-(ChOx:BSA0.1%)$_{10}$-GA0.1%) demonstrating more sigmoidal enzyme kinetics.

This has demonstrated that the concentration of BSA is not as crucial when used in conjunction with GA0.1% as previously seen with GA1%. The lower concentration of GA is not as harsh on the enzyme therefore requires less protection.

Summary

This section determined the contribution of the BSA in the protection of the enzyme during the cross-linking process when used in conjunction with GA0.1%. Decreasing the BSA concentration has little effect on the sensitivity of the sensor when used with the low GA concentration.

4.3.3. PEI

Polyethyleneimine (PEI) has been previously used in the fabrication of biosensors for immobilisation (Hart & Collier, 1998) (Reybier *et al.*, 2002) (McMahon *et al.*, 2006) and stabilisation (Andersson & Hatti-Kaul, 1999). In addition to this, the most noteworthy effect of PEI on biosensor design is the ability to increase sensitivity (Jezkova *et al.*, 1997) (McMahon *et al.*, 2006), reduce the Michaelis constant K_M and increase the linear region slope (McMahon *et al.*, 2007). Proteins are polyampholytic molecules which can interact with polyelectrolytes via long range coulomb forces (Andersson & Hatti-Kaul, 1999). PEI is a polybasic positively charged aliphatic amine with the highest concentration of amino groups per unit of all synthetic polymers (Jezkova *et al.*, 1997). It is believed that the beneficial effect which PEI has on biosensor performance is attributed to the formation of polyanionic/polycationic complexes and by decreasing the electrostatic repulsion between the enzyme substrate and biosensor components (McMahon *et al.*, 2007). Also, this interaction of the negative charges on the enzyme and the positive charges on the polycation result in a stable configuration for long term stability (Belay *et al.*, 1999).

Experiments were undertaken to investigate the effect of the introduction of PEI1% into the dip coating process. The addition of a PEI layer should affect the enzyme subsequently dipped. The use of both pure enzyme solutions and enzyme:BSA solutions were used to look at the effect of BSA during the interaction of PEI and enzyme. In addition to this, the concentration of glutaraldehyde was considered as extra layers of PEI may require a higher glutaraldehyde concentration to secure the design.

A

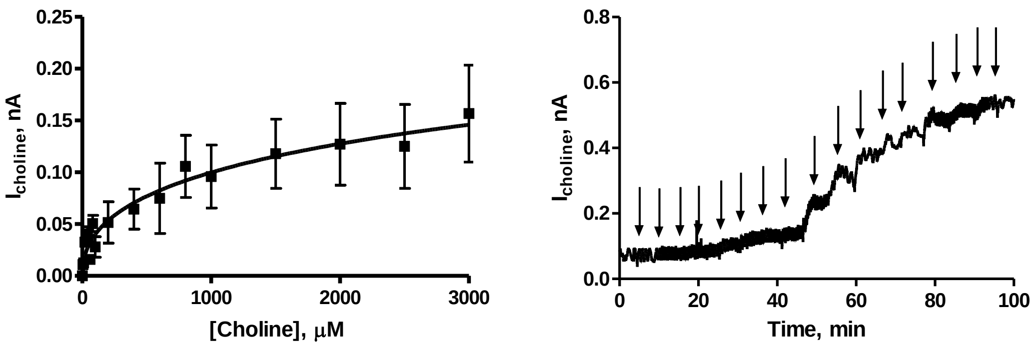

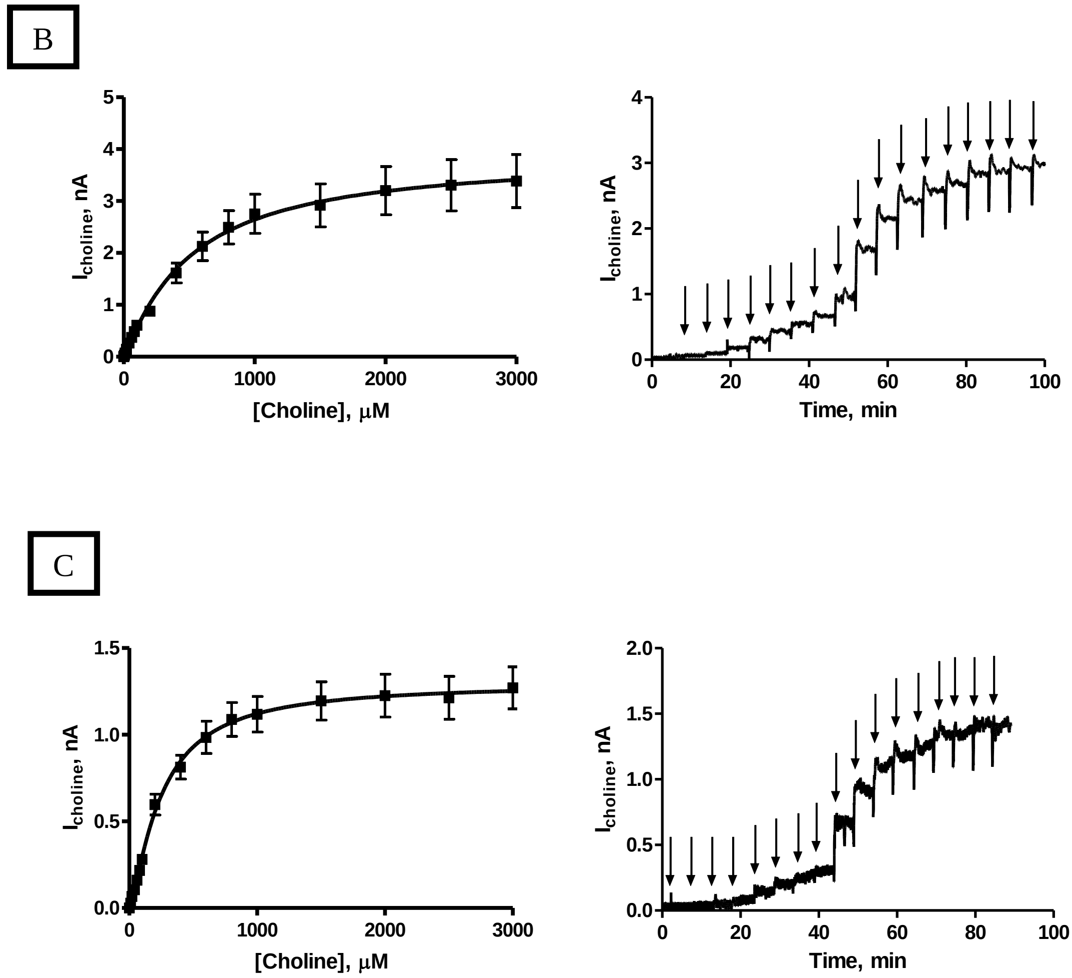

Figure 4.13 : The current-concentration profiles and raw data traces for choline chloride calibrations in PBS (pH 7.4) buffer solution at 21°C using designs (A) Sty-((ChOx)-(PEI))$_{10}$-GA1% (B) Sty-((ChOx:BSA)-(PEI))$_{10}$-GA1%, and (C) Sty-((ChOx:BSA)-(PEI))$_{10}$-GA0.1%. CPA carried out at +700 mV *vs*. SCE. Sequential current steps for 5, 10, 20, 40, 60, 80, 100, 200, 400, 600, 800, 1000, 1500, 2000, 2500 and 3000 μM choline chloride injections.

	Sty-((ChOx)-(PEI))$_{10}$-GA1%			Sty-((ChOx:BSA)-(PEI))$_{10}$-GA 1%			Sty-((ChOx:BSA)-(PEI))$_{10}$-GA0.1%		
Conc, µM	Mean, nA	S.E.M, nA	n	Mean, nA	S.E.M, nA	n	Mean, nA	S.E.M, nA	n
0	0.00	0.00	3	0.00	0.00	4	0.00	0.00	4
5	0.010	0.003	3	0.033	0.004	4	-0.01	0.002	4
10	0.010	0.004	3	0.07	0.01	4	0.03	0.01	4
20	0.030	0.002	3	0.14	0.02	4	0.07	0.01	4
40	0.04	0.01	3	0.27	0.03	4	0.11	0.01	4
60	0.016	0.004	3	0.37	0.04	4	0.16	0.02	4
80	0.05	0.01	3	0.49	0.06	4	0.22	0.02	4
100	0.03	0.01	3	0.61	0.07	4	0.28	0.02	4
200	0.05	0.02	3	0.88	0.09	4	0.60	0.10	4
400	0.07	0.02	3	1.61	0.19	4	0.81	0.07	4
600	0.08	0.03	3	2.13	0.27	4	0.98	0.09	4
800	0.11	0.03	3	2.49	0.32	4	1.10	0.10	4
1000	0.10	0.03	3	2.75	0.38	4	1.12	0.10	4
1500	0.12	0.03	3	2.92	0.42	4	1.20	0.11	4
2000	0.13	0.04	3	3.20	0.47	4	1.23	0.12	4
2500	0.13	0.04	3	3.31	0.49	4	1.21	0.12	4
3000	0.16	0.05	3	3.39	0.51	4	1.27	0.12	4

Table 4.6 : Comparison table of mean current values for designs; (A) Sty-((ChOx)-(PEI))$_{10}$-GA1%, (B) Sty-((ChOx:BSA)-(PEI))$_{10}$-GA1% and (C) Sty-((ChOx:BSA)-(PEI))$_{10}$-GA0.1%. Choline chloride calibrations carried out in PBS (pH 7.4) buffer solution at 21°C. CPA carried out at +700 mV *vs.* SCE. All currents are background subtracted.

The results in Figures 4.13 show the effect of the incorporation of PEI on sensitivity. The PEI was sequentially dipped directly after the dip of enzyme resulting in ten layers of both enzyme and PEI which was secured with a final layer of GA. This layering process was considered, as the incorporation of PEI required the interaction with each layer of enzyme and would not have sufficient interaction as a final layer like GA. Initially, the PEI was used in conjunction with enzyme for direct interaction in the absence of BSA. This showed a marginal improvement over the same design without the PEI (see Section 4.3.2.2). However, the sensitivity is improved when BSA in incorporated, suggesting that the PEI is 'smothering' the enzyme. The introduction of BSA appears to protect the enzyme similar to that seen in conjunction with glutaraldehyde (see Section 4.3.2.2). In order to see the effect of reducing the glutaraldehyde concentration, which had previously proved beneficial (see Section 4.3.2.3), a 0.1% glutaraldehyde solution was used. The low GA concentration demonstrated a reduction in the sensitivity in conjunction with the additional layers of PEI. This suggests that the additional layers may require a higher glutaraldehyde concentration for immobilisation.

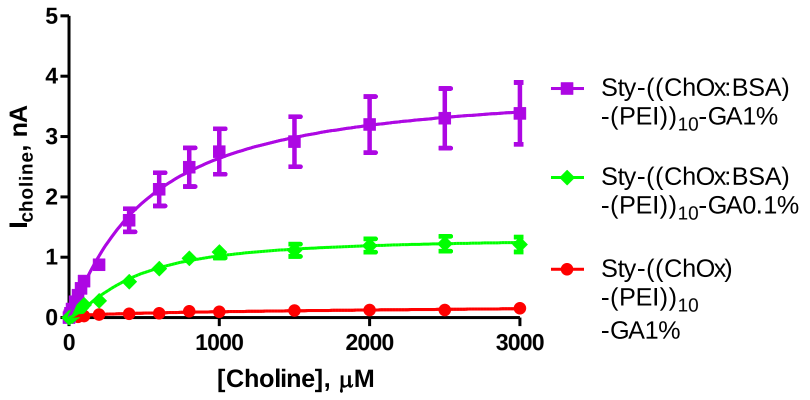

Kinetic Parameters	Sty-((ChOx:BSA)-(PEI))$_{10}$-GA1%			Sty-((ChOx)-(PEI))$_{10}$-GA1%			Sty-((ChOx:BSA)-PEI))$_{10}$-GA0.1%		
	Mean	S.E.M	n	Mean	S.E.M	n	Mean	S.E.M	n
V_{MAX}, nA	3.88	0.42	4	0.50	1.39	3	1.30	0.06	4
Km, µM	506.80	137.80	4	20974	197303	3	250.30	31.33	4
α	1.11	0.19	4	0.46	0.26	3	1.34	0.15	4
$I_{100µM}$, nA	0.61	0.07	4	0.03	0.01	3	0.28	0.02	4
Sensitivity, nA/µM	0.0100	0.0001	4	0.0003	0.0002	3	0.0030	0.0001	4
R^2	0.998	0.0001	4	0.34	0.12	3	0.98	0.01	4
Background, nA	0.030	0.002	4	0.02	0.01	3	0.04	0.01	4

Figure 4.14 : The current-concentration profile comparison and comparison tables for choline chloride calibrations in PBS (pH 7.4) buffer solution at 21°C for designs; (A) Sty-((ChOx:BSA)-(PEI))$_{10}$-GA1%, (B) Sty-((ChOx)-(PEI))$_{10}$-GA1% and (C) Sty-((ChOx:BSA)-(PEI))$_{10}$-GA0.1%. CPA carried out at +700 mV *vs*. SCE. Sequential current steps for 5, 10, 20, 40, 60, 80, 100, 200, 400, 600, 800, 1000, 1500, 2000, 2500 and 3000 µM choline chloride injections.

A comparison graph and data table of kinetic parameters are presented in Figure 4.14. The graph illustrates the comparison of PEI incorporation, the table presents the kinetic parameter comparisons for each design. The comparison illustrates the beneficial effect of PEI incorporation, increasing sensitivity. The PEI however requires the additional use of BSA to increase sensitivity.

Comparison of the $I_{100\mu M}$ values of the designs Sty-((ChOx)-(PEI))$_{10}$-GA1% (0.03 ± 0.01 nA, n = 3) and Sty-((ChOx:BSA)-(PEI))$_{10}$-GA1% (0.61 ± 0.07 nA, n = 4) show a significant increase in sensitivity (P = 0.0010) with the introduction of BSA. A reduction in the glutaraldehyde concentration reduced the $I_{100\mu M}$ value from 0.61 ± 0.07 nA (Sty-((ChOx:BSA)-(PEI))$_{10}$- GA1%) to 0.28 ± 0.02 nA (Sty-((ChOx:BSA)-(PEI))$_{10}$-GA0.1%). This illustrates that the higher glutaraldehyde concentration is needed to secure the twenty total layers of enzyme and PEI to the surface.

The reduction in glutaraldehyde concentration did however affect the K_M. Reducing the glutaraldehyde concentration reduced the K_M from 506.80 ± 137.80 µM, n = 4 (Sty-((ChOx:BSA)-(PEI))$_{10}$-GA1%) to 250.30 ± 31.33 µM, n = 4 (Sty-((ChOx:BSA)-(PEI))$_{10}$-GA0.1%). The diffusional constraints were greatly reduced with a lower glutaraldehyde concentration. This however, is more likely to be as a result of a decrease in the number of layers obstructing the enzyme, as the glutaraldehyde was unable to secure them, rather than an effect of the glutaraldehyde itself, as the sensitivity was severely affected. In the absence of BSA within the enzyme solution, the K_M increased from 506.80 ± 137.80 µM, n = 4 (Sty-((ChOx:BSA)-(PEI))$_{10}$-GA1%) to 20974 ± 197303 µM, n = 3 (Sty-((ChOx)-(PEI))$_{10}$-GA1%) as a result of poor enzyme kinetics. A reduction in the GA concentration from 1% to 0.1% decreased the V_{MAX} current from 3.88 ± 0.42 nA, n = 4 (Sty-((ChOx:BSA)-(PEI))$_{10}$-GA 1%) to 1.30 ± 0.06 nA, n = 4 Sty-((ChOx:BSA)-(PEI))$_{10}$-GA0.1%). The absence of BSA in the enzyme solution decreased the V_{MAX} current to 0.50 ± 1.39 nA, n = 3 (Sty-((ChOx)-(PEI))$_{10}$-GA1%). The introduction of PEI resulted in an α value of 1.11, n = 4 (Sty-((ChOx:BSA)-(PEI))$_{10}$-GA1%). This value is closer to the ideal value of 1. The reduction of GA to 0.1% increased the α value to 1.34 illustrating sigmoidal enzyme kinetics. The removal of BSA from the enzyme solution reduced the α value to 0.46.

This section has illustrated the effect of adding PEI into the dipping series. As both GA1% and GA0.1% have both proved advantageous previously, both were compared. GA1% appears to be a better concentration for securing the additional layers. The removal of the BSA from the enzyme was also investigated, as the enzyme will be directly interacting with the PEI and not the GA. However, the PEI was detrimental to sensitivity as the BSA was required to protect the enzyme from the PEI. The use of GA1% proved the most advantageous and was continued with for further experiments.

Summary

This section determined that PEI used in conjunction with BSA and GA1% could be used in the sensor design to increase sensitivity.

4.3.4. Double Layering

In an attempt to increase enzyme loading a second full layer consisting of ten layers of enzyme was added. This resulted in the incorporation of twenty enzymatic layers. The increase in enzyme layers was investigated in an attempt to further increase sensitivity.

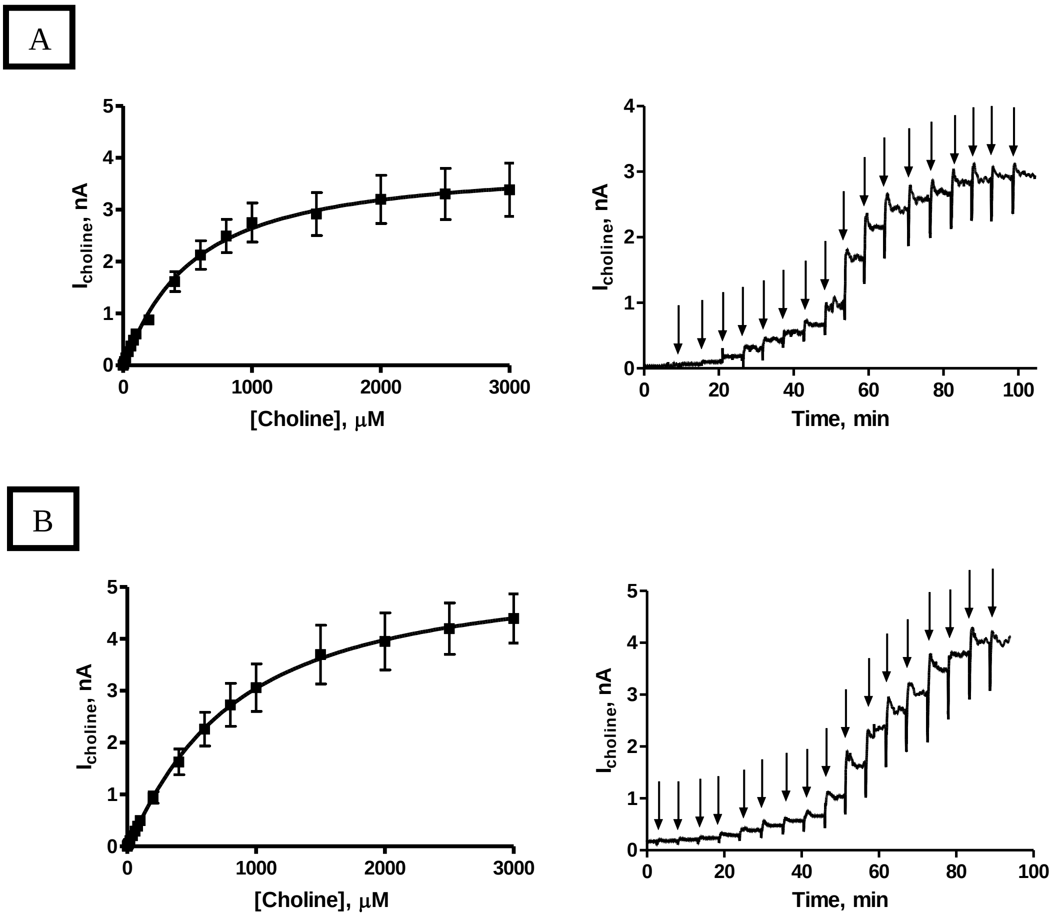

Figure 4.15 : The current-concentration profiles and raw data traces for choline chloride calibrations in PBS (pH 7.4) buffer solution at 21°C using designs (A) Sty-((ChOx:BSA)-(PEI)$_{10}$-GA1%, (B) ((Sty-((ChOx:BSA)-(PEI))$_{10}$-GA1%)x2). CPA carried out at +700 mV *vs*. SCE. Sequential current steps for 5, 10, 20, 40, 60, 80, 100, 200, 400, 600, 800, 1000, 1500, 2000, 2500 and 3000 µM Choline chloride injections.

	Sty-((ChOx:BSA)-(PEI))$_{10}$ GA1%			(Sty((ChOx:BSA)-(PEI))$_{10}$ GA1%)x2		
Conc, µM	Mean, nA	S.E.M, nA	n	Mean, nA	S.E.M, nA	n
0	0.00	0.00	4	0.00	0.00	4
5	0.033	0.004	4	0.04	0.01	4
10	0.07	0.01	4	0.06	0.01	4
20	0.14	0.02	4	0.11	0.01	4
40	0.27	0.03	4	0.21	0.02	4
60	0.37	0.04	4	0.29	0.02	4
80	0.49	0.06	4	0.39	0.03	4
100	0.61	0.07	4	0.50	0.04	4
200	0.88	0.09	4	0.94	0.11	4
400	1.61	0.19	4	1.63	0.25	4
600	2.13	0.27	4	2.26	0.33	4
800	2.49	0.32	4	2.72	0.42	4
1000	2.75	0.38	4	3.06	0.46	4
1500	2.92	0.42	4	3.70	0.57	4
2000	3.20	0.47	4	3.95	0.55	4
2500	3.31	0.49	4	4.20	0.50	4
3000	3.39	0.51	4	4.39	0.48	4

Table 4.7 : Comparison table of mean current values for designs; (A) Sty-((ChOx:BSA)-(PEI))$_{10}$-GA1%, (B) ((Sty-((ChOx:BSA)-(PEI))$_{10}$-GA1%)x2). Choline chloride calibrations carried out in PBS (pH 7.4) buffer solution at 21°C. CPA carried out at +700 mV *vs.* SCE. All currents are background subtracted.

The results in Figure 4.15 show the effect of an extra layer of the dipping series on sensitivity. It can be seen that this did not increase sensitivity. It is possible that the second layer has no effect as it negated the sensitivity of the original layer due to an inability to access the enzymes on the underlying layers.

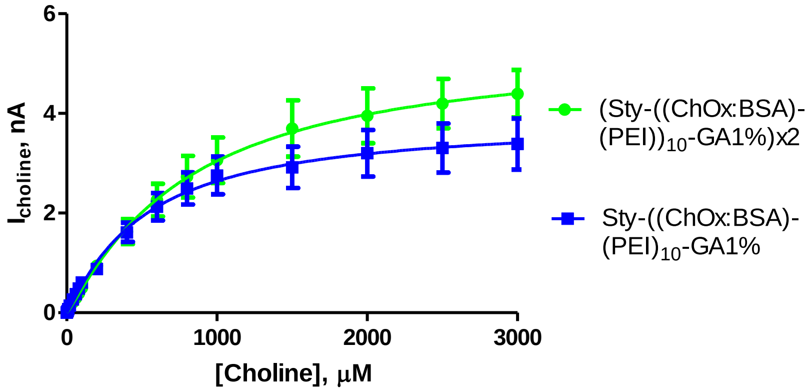

Kinetic Parameters	Sty-((ChOx:BSA)-(PEI))$_{10}$-GA1%			(Sty-((ChOx:BSA)-(PEI))$_{10}$-GA1%)x2		
	Mean	S.E.M	n	Mean	S.E.M	n
V_{MAX}, nA	3.88	0.42	4	5.37	0.72	4
Km, μM	506.80	137.80	4	786.80	235.40	4
α	1.11	0.19	4	1.13	0.20	4
$I_{100μM}$, nA	0.61	0.07	4	0.50	0.04	4
Sensitivity, nA/μM	0.0060	0.0001	4	0.0048	0.0001	4
R^2	0.9981	0.0001	4	0.998	0.001	4
Background, nA	0.026	0.002	4	0.168	0.001	4

Figure 4.16 : The current-concentration profile comparison and comparison tables for choline chloride calibrations in PBS (pH 7.4) buffer solution at 21°C for designs; (A) Sty-((ChOx:BSA)-(PEI)$_{10}$-GA1%, (B) ((Sty-((ChOx:BSA)-(PEI))$_{10}$-GA1%)x2). CPA carried out at +700 mV *vs.* SCE. Sequential current steps for 5, 10, 20, 40, 60, 80, 100, 200, 400, 600, 800, 1000, 1500, 2000, 2500 and 3000 μM choline chloride injections.

A comparison graph and data table of kinetic parameters are presented in Figure 4.16. The graph illustrates the comparison of an extra layer, the table presents the kinetic parameter comparisons for each design. The extra enzyme layers did not increase the sensitivity of the design further.

The extra layer has increased the diffusion constraint to the surface increasing the K_M from 506.8 ± 137.8 μM, n = 4 (Sty-((ChOx:BSA)-(PEI))$_{10}$-GA1%) to 786.8 ± 235.4 μM, n = 4 ((Sty-((ChOx:BSA)-(PEI))$_{10}$-GA1%)x2). The slower diffusion has resulted in an increase in the V_{MAX} current from 3.88 ± 0.42 nA, n = 4 (Sty-((ChOx:BSA)-(PEI))$_{10}$-GA1%) to 5.37 ± 0.72, n = 4 ((Sty-((ChOx:BSA)-(PEI))$_{10}$-GA1%)x2). The additional layer had little effect on the α value increasing it from 1.11, n = 4 (Sty-((ChOx:BSA)-(PEI))$_{10}$-GA1%) to 1.13, n = 4 ((Sty-((ChOx:BSA)-(PEI))$_{10}$-GA1%)x2).

A comparison of the $I_{100\mu M}$ values also shows a significant decrease (P = 0.0049) in sensitivity with the additional layer as the current is reduced from 0.61 ± 0.07 nA, n = 4 (Sty-((ChOx:BSA)-(PEI))$_{10}$-GA1%) 0.50 ± 0.04 nA, n = 4 ((Sty-((ChOx:BSA)-(PEI))$_{10}$-GA1%)x2).

The double layer did not have any beneficial effect and is not a viable option for the sensor design.

Summary

This section determined that a double layer of the design is not beneficial to the sensitivity.

4.3.5. Units Increase

The previous section has outlined preliminary studies into the effect of various immobilisation methods, stabilisers and cross-linking methods, utilised in an attempt to design a choline biosensor, with suitable sensitivity to detect choline. These sections demonstrate that the dip adsorption method using ten layers of enzyme is optimum for enzyme immobilisation. The inclusion of BSA was demonstrated as essential when GA was used for cross-linking and during the incorporation of PEI. GA was proved beneficial for securing the enzyme and BSA layers increasing sensitivity. The addition of PEI proved the most successful, with BSA and GA resulting in a design with the highest sensitivity. The previous experiments have been used to determine if each of these components can be used with ChOx to optimise sensitivity. The use of BSA, GA and PEI will be continued with for further experiments to determine if the sensitivity can be optimised further. Although the previous experiments have demonstrated that the development of a sensor for the detection of choline is viable, further experiments were performed in order to optimise sensitivity. The detection of choline must be suitably high to differentiate the choline response from endogenous interference once implanted in the *in-vivo* environment, which can be minimised but not eliminated. The choline sensor must be sensitive enough to detect minor fluctuations in the extracellular fluid concentration, which the current sensor design is not suitable for. Therefore, an investigation into the effect of increasing the concentration of enzyme from 50 units to 500 units was undertaken. The increase in enzyme units has required the removal of the BSA from the enzyme solution. Therefore, the initial experiments were undertaken using the immobilisation of 10 layers of ChOx and cross-linked with a GA1% layer. Although this design did not present the highest sensitivity during the preliminary studies, the interaction between additional components will be investigated during this chapter in full detail and this will determine if increasing the enzyme units will increase sensitivity or similar to the double layer seen in Section 4.3.4 decrease the sensitivity by limiting access to lower layers. All individual graphs, raw data traces and data tables shall be presented in Appendix 1 for the remainder of the experiments in this chapter.

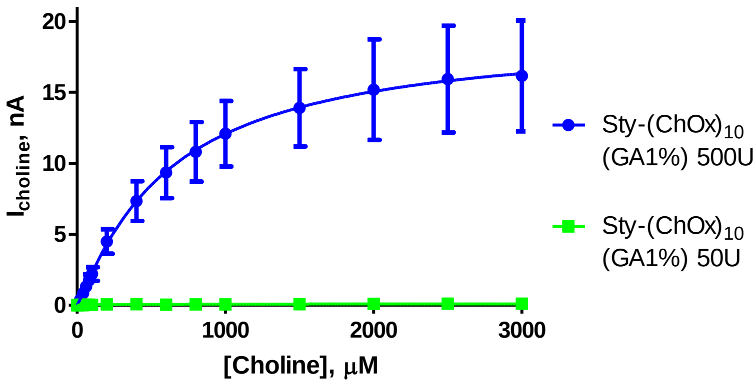

Kinetic Parameters	Sty-$(ChOx)_{10}$-GA1% 50U			Sty-$(ChOx)_{10}$-GA1% 500U		
	Mean	S.E.M	n	Mean	S.E.M	n
V_{MAX}, nA	0.12	0.03	4	19.21	3.74	4
Km, µM	358.10	464.40	4	621.50	290.80	4
α	0.54	0.17	4	1.10	0.31	4
$I_{100\mu M}$, nA	0.02	0.01	4	2.21	0.48	4
Sensitivity, nA/µM	0.0002	0.0002	4	0.0225	0.0003	4
R^2	0.75	0.04	4	0.98	0.02	4
Background, nA	-0.004	0.002	4	0.60	0.10	4

Figure 4.17 : The current-concentration profile comparison and comparison tables for choline chloride calibrations in PBS (pH 7.4) buffer solution at 21°C for designs; (A) Sty-$(ChOx)_{10}$-GA1% 50U and (B) Sty-$(ChOx)_{10}$-GA1% 500U. CPA carried out at +700 mV *vs.* SCE. Sequential current steps for 5, 10, 20, 40, 60, 80, 100, 200, 400, 600, 800, 1000, 1500, 2000, 2500 and 3000 µM choline chloride injections.

A comparison graph and data table of kinetic parameters are presented in Figure 4.17. The graph illustrates the comparison of enzyme concentrations, the table presents the kinetic parameter comparisons for each design. This section demonstrates the effect of increasing the concentration of enzyme. A clear improvement in sensitivity can be seen when increasing the enzyme concentration from a 50 unit to 500 unit enzyme solution. In addition, improved enzyme kinetics can be seen as the enzyme loading has increased substantially.

When comparing the $I_{100\mu M}$ values the current was significantly increased (P = 0.0006) from 0.02 ± 0.01 nA, n = 4 (Sty-$(ChOx)_{10}$-GA1% 50U) to 2.21 ± 0.48 nA, n = 4 (Sty-$(ChOx)_{10}$-GA1% 500U). The sensitivity was also increased compared to best design obtained thus far illustrated in Section 4.3.3.

The V_{MAX} currents were significantly increased (P = 0.0039) from 0.12 ± 0.03 nA, n = 4 (Sty-$(ChOx)_{10}$-GA1% 50U) to 19.21 ± 3.74 nA, n = 4 (Sty-$(ChOx)_{10}$-GA1% 500U). In addition to this, the K_M was increased from 358.10 ± 464.40 µM, n = 4 (Sty-$(ChOx)_{10}$-GA1% 50U) to 621.50 ± 290.80 µM, n = 4 (Sty-$(ChOx)_{10}$-GA1% 500U). Ideal Michaelis-Menten kinetics were also demonstrated as the α values was increased from 0.54 ± 0.17, n = 4 (Sty-$(ChOx)_{10}$-GA1% 50U) to 1.10 ± 0.48, n = 4 (Sty-$(ChOx)_{10}$-GA1% 500U).

These experiments have clearly outlined that increasing the enzyme concentration from 50U to 500U increased sensitivity. As this is the case 500U was chosen for use in future designs.

Summary

This section used the basic sensor design to demonstrate that increasing the units of enzyme in the solution used for dipping to 500 U, could increase the sensitivity of the sensor. BSA was therefore removed from the solution to increase the enzyme units.

4.3.6. GA Layering

The previous section illustrated the effect of increasing the concentration of the enzyme solution. The results showed that increasing the concentration from 50 units to 500 units increased the sensitivity substantially. As the quantity of enzyme and hence enzyme loading onto the electrode surface was increased, the next set of experiments were undertaken in order to investigate, if a layer of enzyme immediately followed by a layer of glutaraldehyde, could potentially decrease the amount of enzyme loss during the ten layer application of enzyme, securing each layer immediately after dipping. Section 4.3.3 demonstrated that the addition of GA increased sensitivity by securing the layers in place by the cross-linking process. In addition Section 4.3.3 demonstrated that when incorporating additional layers a higher concentration of GA is required. Therefore, the additional layers of GA may provide additional security for the higher unit enzyme layers increasing sensitivity.

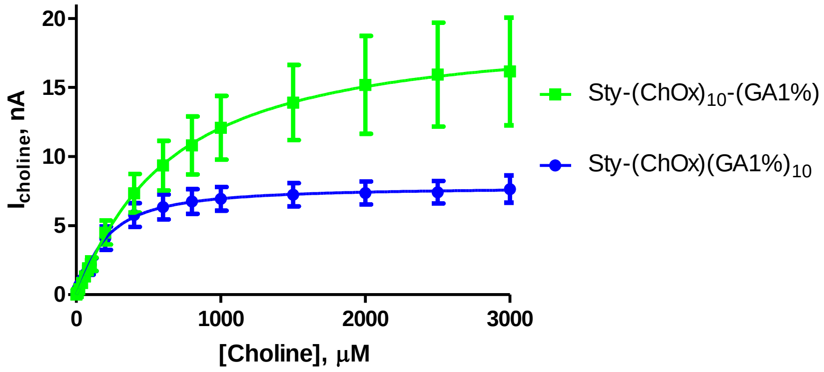

Kinetic Parameters	Sty-(ChOx)$_{10}$-GA			Sty-(ChOx)(GA)$_{10}$		
	Mean	S.E.M	n	Mean	S.E.M	n
V_{MAX}, nA	19.21	3.74	4	7.80	0.46	4
Km, μM	621.50	290.80	4	188.80	35.96	4
α	1.10	0.31	4	1.26	0.22	4
I_{100}, nA	2.21	0.48	4	2.17	0.47	4
Sensitivity, nA/μM	0.0225	0.0003	4	0.019	0.001	4
R^2	0.98	0.02	4	0.984	0.001	4
Background, nA	0.60	0.10	4	0.44	0.05	4

Figure 4.18 : The current-concentration profile comparison and comparison tables for choline chloride calibrations in PBS (pH 7.4) buffer solution at 21°C for designs; (A) Sty-(ChOx)$_{10}$-GA and (B) Sty-(ChOx)(GA)$_{10}$. CPA carried out at +700 mV *vs.* SCE. Sequential current steps for 5, 10, 20, 40, 60, 80, 100, 200, 400, 600, 800, 1000, 1500, 2000, 2500 and 3000 μM choline chloride injections.

A comparison graph and data table of kinetic parameters are presented in Figure 4.18. The graph illustrates the comparison between glutaraldehyde layering, the table presents the kinetic parameter comparisons for each design. This section demonstrates that the introduction of glutaraldehyde into each layer did not affect sensitivity but decreased the K_M concentration demonstrating the reduction in the diffusional constraints of the sensor. Cross-linking the enzyme layers directly appears to secure the layers without detrimentally affecting the access to the enzyme.

The glutaraldehyde did not significantly change (P = 0.9520) the $I_{100μM}$ current from 2.21 ± 0.48 nA, n = 4 (Sty-(ChOx)$_{10}$-GA) to 2.17 ± 0.47 nA, n = 4 (Sty-(ChOx)(GA)$_{10}$). Although the $I_{100μM}$ does not illustrate an improvement in sensitivity, comparatively the current at lower concentrations were improved using glutaraldehyde in every layer (see Appendix 1).

The V_{MAX} was reduced from 19.21 ± 0.48 nA, n = 4 (Sty-$(ChOx)_{10}$-GA) to 7.80 ± 0.46 nA, n = 4 (Sty-(ChOx)$(GA)_{10}$) indicating a change in the enzyme kinetics. This is also illustrated in the reduction of the K_M concentration from 621.5 ± 290.80 µM, n = 4 (Sty-$(ChOx)_{10}$-GA) to 188.80 ± 35.96 µM, n = 4 (Sty-(ChOx)$(GA)_{10}$). The α value was increased from 1.10, n = 4 (Sty-$(ChOx)_{10}$-GA) to 1.26, n = 4 (Sty-(ChOx)$(GA)_{10}$).

This shows beneficial characteristics for further studies with the potential to secure more enzyme and additional components onto the electrode surface. Also, the reduction in the K_M concentration demonstrates advantageous enzyme kinetics for the currents at low concentrations which are closer to the physiological range. The increase in enzyme units on the sensor may not be as affected by the harsh cross-linking effects of GA as the lower enzyme unit designs. As this is the case, this layering process was further investigated.

Summary

This section determined the effect on sensitivity of a GA layer directly after the enzyme layer. This process would secure each layer which may prove advantageous when other components are considered for use in conjunction with the enzyme. GA layering did not prove detrimental to sensitivity when used on each layer. The GA layers also improved the diffusional constraints of 10 layers of enzyme together. This process of enzyme incorporation was continued with.

4.3.7. BSA Layering

As shown in Section 4.3.2.2 BSA can increase sensitivity when used in conjunction with glutaraldehyde. BSA can be used to protect the enzyme layers from the detrimental effect of the cross-linking by glutaraldehyde; as this is a harsh process. As the new process incorporates GA layers directly after the enzyme layers BSA was incorporated into the dipping procedure to investigate if the glutaraldehyde layer directly after the enzyme layer was too harsh, and if the BSA could aid in protecting the enzyme increasing sensitivity further. Although the results obtained in Section 4.3.5 suggest that the interaction of the enzyme, with higher unit activity with GA may not be as affected by the cross-linking process as the designs which used the lower enzyme concentrations, the BSA may also aid in the cross-linking process as suggested in Section 4.3.2.2. Therefore, the incorporation of BSA was investigated in this section.

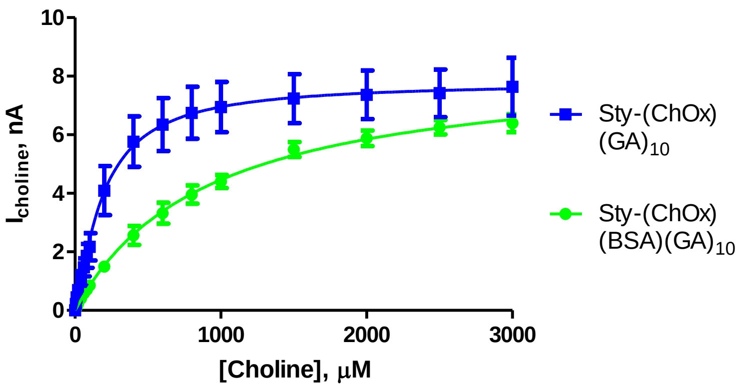

Kinetic Parameters	Sty-(ChOx)(GA)$_{10}$			Sty-(ChOx)(BSA)(GA)$_{10}$		
	Mean	S.E.M	n	Mean	S.E.M	n
V_{MAX}, nA	7.80	0.46	4	8.46	0.61	3
Km, μM	188.80	35.96	4	899.80	154.80	3
α	1.26	0.22	4	1.01	0.08	3
$I_{100\mu M}$, nA	2.17	0.47	4	0.86	0.10	3
Sensitivity, nA/μM	0.019	0.001	4	0.0086	0.0002	3
R^2	0.984	0.001	4	0.990	0.003	3
Background, nA	0.44	0.05	4	0.04	0.001	3

Figure 4.19 : The current-concentration profile comparison and comparison tables for choline chloride calibrations in PBS (pH 7.4) buffer solution at 21°C for designs; (A) Sty-(ChOx)(GA)$_{10}$ and (B) Sty-(ChOx)(BSA)(GA)$_{10}$. CPA carried out at +700 mV *vs.* SCE. Sequential current steps for 5, 10, 20, 40, 60, 80, 100, 200, 400, 600, 800, 1000, 1500, 2000, 2500 and 3000 μM choline chloride injections.

A comparison graph and data table of kinetic parameters are presented in Figure 4.19. The graph illustrates the comparison of BSA incorporation, the table presents the kinetic parameter comparisons for each design. This section demonstrates that the BSA layer between the enzyme layer and the glutaraldehyde layer has a detrimental effect on sensitivity and has created an additional barrier limiting access to the enzyme as demonstrated by the increase in the linear region.

A comparison of the $I_{100\mu M}$ values shows a significant decrease (P = 0.0288) from 2.17 ± 0.47 nA, n = 4 (Sty-(ChOx)$(GA)_{10}$) to 0.86 ± 0.10 nA, n = 3 (Sty-(ChOx)(BSA)$(GA)_{10}$).

The BSA has also increased the rate of diffusion of the substrate, significantly increasing (P = 0.0215) the K_M from 188.80 ± 35.96 µM, n = 4 (Sty-(ChOx)$(GA)_{10}$) to 899.80 ± 154.80 µM, n = 3 (Sty-(ChOx)(BSA)$(GA)_{10}$). Alongside the increase in K_M, the introduction of BSA increased the V_{MAX} current from 7.70 ± 0.46 nA, n = 4 (Sty-(ChOx)$(GA)_{10}$) to 8.46 ± 0.61 nA, n = 3 (Sty-(ChOx)(BSA)$(GA)_{10}$). The α value was also decreased from 1.26, n = 4 (Sty-(ChOx)$(GA)_{10}$) to 1.01, n = 3 (Sty-(ChOx)(BSA)$(GA)_{10}$), a value in line with the ideal α value for Michaelis-Menten kinetics.

Although BSA has previously shown to be beneficial, as this design requires a BSA layer on top of each enzyme layer, any beneficial effect of the BSA is negated by the blocking effect of the BSA which has reduced sensitivity and increased the rate of diffusion at the sensor. This decrease in sensitivity and increase in K_M concentration illustrates that this design is not viable.

Summary

This section determined the effect of BSA on each layer in order to protect from the GA layers. This however proved detrimental to the sensitivity. The incorporation of the BSA both decreased the sensitivity and increased the rate of diffusion.

4.3.8. PEI Layering

The incorporation of PEI has been shown to increase sensitivity in Section 4.3.3. The PEI was incorporated into the design directly after the layers of enzyme and cross-linked with a layer of GA. This study demonstrated that the increased layering required additional GA to secure them. Therefore, the incorporation of the PEI was investigated in this design as the interaction of the enzyme and PEI may increase sensitivity and the additional layering of GA may prove successful in increasing sensitivity further.

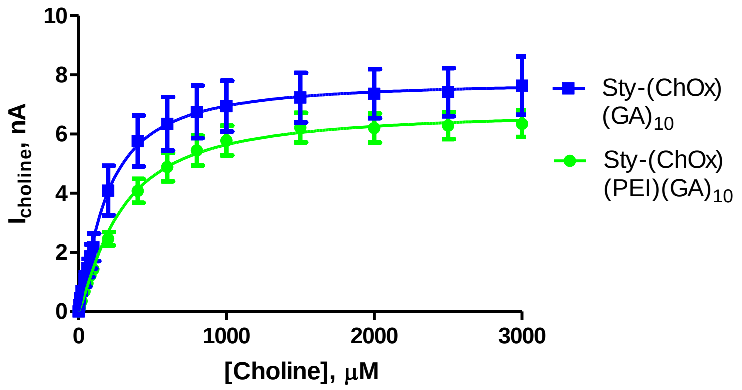

Kinetic Parameters	Sty-(ChOx)(GA)$_{10}$			Sty-(ChOx)(PEI)(GA)$_{10}$		
	Mean	S.E.M	n	MEAN	S.E.M	n
V_{MAX}, nA	7.80	0.46	4	6.81	0.28	3
Km, μM	188.80	35.96	4	283.4	33.06	3
α	1.26	0.22	4	1.24	0.12	3
$I_{100\mu M}$, nA	2.17	0.47	4	1.43	0.14	3
Sensitivity, nA/μM	0.019	0.001	4	0.015	0.001	3
R^2	0.984	0.001	4	0.990	0.001	3
Background, nA	0.44	0.049	4	0.030	0.002	3

Figure 4.20 : The current-concentration profile comparison and comparison tables for choline chloride calibrations in PBS (pH 7.4) buffer solution at 21°C for designs; (A) Sty-(ChOx)(GA)$_{10}$ and (B) Sty-(ChOx)(PEI)(GA)$_{10}$. CPA carried out at +700 mV *vs.* SCE. Sequential current steps for 5, 10, 20, 40, 60, 80, 100, 200, 400, 600, 800, 1000, 1500, 2000, 2500 and 3000 μM choline chloride injections.

A comparison graph and data table of kinetic parameters are presented in Figure 4.20. The graph illustrates the comparison of PEI incorporation, the table presents the kinetic parameter comparisons for each design. This section demonstrates that the PEI did not improve sensitivity as seen previously. The sensitivity of the design is decreased with the incorporation of PEI. Potentially, the decrease in sensitivity is as a result of the glutaraldehyde that directly follows the PEI layer. This glutaraldehyde layer will minimise the interaction of the PEI with the subsequent enzyme layer. In addition to this it is possible that the glutaraldehyde layer may have a detrimental effect on the PEI itself as PEI is an aliphatic amine and glutaraldehyde cross-links with amine groups.

The PEI layer did not significantly decrease (P = 0.2434) the $I_{100\mu M}$ values although a decrease was observed from 2.17 ± 0.47 nA, n = 4 Sty-(ChOx)$(GA)_{10}$ to 1.43 ± 0.14 nA, n = 3 Sty-(ChOx)(PEI)$(GA)_{10}$.

The K_M was increased from 188.80 ± 35.96 µM, n = 4 Sty-(ChOx)$(GA)_{10}$ to 283.4 ± 33.06 µM, n = 3 Sty-(ChOx)(PEI)$(GA)_{10.}$ The increase in K_M was not significant (P = 0.1193) although indicating that the PEI has some effect on the rate of diffusion. The V_{MAX} current was decreased from 7.80 ± 0.46 nA, n = 4 (Sty-(ChOx)$(GA)_{10}$) to 6.81 ± 0.28 nA, n = 3 (Sty-(ChOx)(PEI)$(GA)_{10}$). The α value was slightly effected decreasing it from 1.26, n = 4 (Sty-(ChOx)$(GA)_{10}$) to 1.24, n = 3 (Sty-(ChOx)(PEI)$(GA)_{10}$).

Illustrated here is the effect of PEI on sensitivity. These results illustrate that PEI had a detrimental effect on sensitivity, this may however, be as a result of the direct PEI-GA contact or the layer of GA which is limiting the PEI interaction with the following enzyme layer.

Summary

This section demonstrated that the incorporation of PEI on each layer was not beneficial to sensitivity as had been seen previously in Section 4.3.3. Similar to the effect of the BSA incorporation the PEI decreased sensitivity and increased the rate of diffusion.

4.3.8.1. PEI Layering Position

In Section 4.3.3 the addition of PEI into the dipping series increased sensitivity. The position of the PEI was advantageous as the PEI was positioned directly before the incoming layer of enzyme. Therefore, these experiments were undertaken in order to investigate the effect of a PEI layer at the end of the dipping series that will be in direct contact with the following enzyme layer as in the study in section 4.3.3.

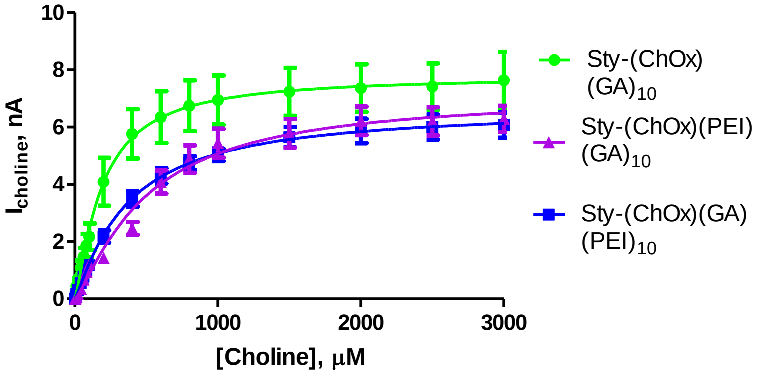

Kinetic Parameters	Sty-(ChOx)(GA)$_{10}$			Sty-(ChOx)(PEI)(GA)$_{10}$			Sty-(ChOx)(GA)(PEI)$_{10}$		
	Mean	S.E.M	n	Mean	S.E.M	n	Mean	S.E.M	n
V_{MAX}, nA	7.80	0.46	4	6.81	0.28	3	6.69	0.28	3
Km, µM	188.80	35.96	4	283.40	33.06	3	367.70	41.43	3
α	1.26	0.22	4	1.24	0.12	3	1.14	0.09	3
$I_{100\mu M}$, nA	2.17	0.47	4	1.43	0.14	3	1.18	0.14	3
Sensitivity, nA/µM	0.019	0.001	4	0.015	0.001	3	0.012	0.00033	3
R^2	0.984	0.001	4	0.993	0.001	3	0.995	0.001	3
Background, nA	0.44	0.049	4	0.03	0.002	3	0.11	0.004	3

Figure 4.21 : The current-concentration profile comparison and comparison tables for choline chloride calibrations in PBS (pH 7.4) buffer solution at 21°C for designs; (A) Sty-(ChOx)(GA)$_{10}$ and (B) Sty-(ChOx)(PEI)(GA)$_{10}$ and (C) Sty-(ChOx)(GA)(PEI)$_{10}$. CPA carried out at +700 mV *vs.* SCE. Sequential current steps for 5, 10, 20, 40, 60, 80, 100, 200, 400, 600, 800, 1000, 1500, 2000, 2500 and 3000 µM choline chloride injections.

A comparison graph and data table of kinetic parameters are presented in Figure 4.21. The graph illustrates the comparison of the PEI position; the table presents the kinetic parameter comparisons for each design. This section demonstrates that the position of the PEI layer directly after the GA layer and preceding the subsequent enzyme layer did not prove beneficial. The PEI layer in addition to the GA layer potentially envelops the enzyme reducing access of the substrate to the enzyme. The interaction of the PEI layer with the layer of enzyme that follows has potentially been negated because of this.

The position of the PEI at the end of the dipping series directly before the enzyme layer was not beneficial to sensitivity. This decreased the $I_{100\mu M}$ value from 1.43 ± 0.14 nA, n = 3 (Sty-(ChOx)(PEI)$(GA)_{10}$) to 1.18 ± 0.14 nA, n = 3 (Sty-(ChOx)(GA)$(PEI)_{10}$). This decrease was not a significant decrease (P = 0.2767). A further decrease from the design which did not include PEI from 2.17 ± 0.47 nA, n = 4 (Sty-(ChOx)$(GA)_{10}$) to 1.18 ± 0.14 nA, n = 3 (Sty-(ChOx)(GA)$(PEI)_{10}$) which was also not significant (P = 0.1384).

The position of the PEI also decreased the rate of diffusion as illustrated by the increase in the K_M concentration from 283.40 ± 33.06 nA, n = 3 (Sty-(ChOx)(PEI)$(GA)_{10}$) to 367.70 ± 41.43 nA, n = 3 (Sty-(ChOx)(GA)$(PEI)_{10}$). The design that did not contain PEI remained the design with the lowest K_M of 188.80 ± 35.96 µM, n = 4. The V_{MAX} was slightly decreased from 6.81 ± 0.28 nA, n = 3 (Sty-(ChOx)(PEI)$(GA)_{10}$) to 6.69 ± 0.28 nA, n = 3 (Sty-(ChOx)(GA)$(PEI)_{10}$) by the altered position of the PEI. In addition, the α value was reduced from 1.24, n = 3 (Sty-(ChOx)(PEI)$(GA)_{10}$) to 1.14, n = 3 (Sty-(ChOx)(GA)$(PEI)_{10}$).

These results illustrate the effect of a PEI layer after the GA layer and directly before the enzyme layer. The direct interaction of PEI and enzyme in this order has not demonstrated any difference in sensitivity.

Summary

This section looked at the incorporation of PEI at the end of the dipping series to have direct contact with the subsequent enzyme layer. This did not increase the sensitivity observed.

4.3.8.2. BSA Layering

In the previous section, moving the position of PEI did not increase sensitivity. This however, was potentially as a result of the extra PEI layer in addition to the GA layer covering the enzyme underneath, which resulted in a reduction in sensitivity. A BSA layer added in between the enzyme and the following GA layer proved successful in increasing sensitivity in when used in conjunction with GA in Section 4.3.2.2. BSA has the potential to protect the enzyme from the harsh cross-linking of the GA and increase sensitivity. BSA was incorporated into this design to determine if the enzyme GA interaction was hampering the increase in sensitivity that can be achieved using PEI.

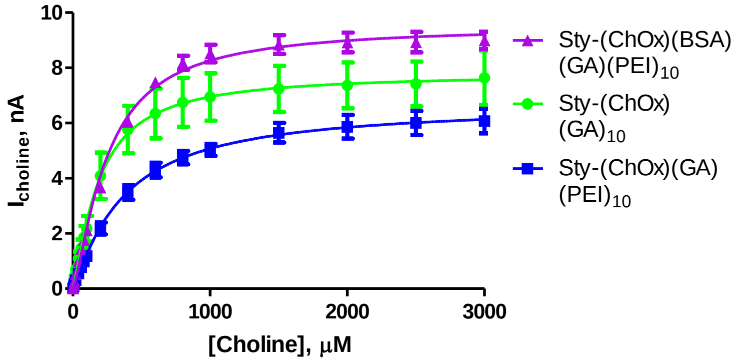

Kinetic Parameters	Sty-(ChOx)(GA)$_{10}$			Sty-(ChOx)(GA)(PEI)$_{10}$			Sty-(ChOx)(BSA)(GA)(PEI)$_{10}$		
	Mean	S.E.M	n	Mean	S.E.M	n	Mean	S.E.M	n
V_{MAX}, nA	7.80	0.46	4	6.69	0.28	3	9.53	0.17	4
Km, µM	188.80	35.96	4	367.70	41.43	3	249.00	12.92	4
α	1.26	0.22	4	1.14	0.09	3	1.34	0.06	4
$I_{100\mu M}$, nA	2.17	0.47	4	1.18	0.14	3	2.11	0.04	4
Sensitivity, nA/µM	0.019	0.001	4	0.012	0.00033	3	0.022	0.001	4
R^2	0.984	0.001	4	0.995	0.001	3	0.993	0.001	4
Background, nA	0.44	0.049	4	0.11	0.004	3	0.03	0.01	4

Figure 4.22 : The current-concentration profile and comparison tables for choline chloride calibrations in PBS (pH 7.4) buffer solution at 21°C for designs; (A) Sty-(ChOx)(GA)$_{10}$, (B) Sty-(ChOx)(GA)(PEI)$_{10}$ and (C) Sty-(ChOx)(BSA)(GA)(PEI)$_{10}$. CPA carried out at +700 mV *vs.* SCE. Sequential current steps for 5, 10, 20, 40, 60, 80, 100, 200, 400, 600, 800, 1000, 1500, 2000, 2500 and 3000 µM choline chloride injections.

A comparison graph and data table of kinetic parameters are presented in Figure 4.22. The graph illustrates the comparison of the BSA addition in conjunction with PEI and GA, the table presents the kinetic parameter comparisons for each design. This section demonstrates the effect of the addition of a BSA layer to protect the enzyme layer from the subsequent GA and PEI layers. The BSA was successful in protecting the enzyme from the GA and PEI layers which resulted in an increase in sensitivity. The effect of the PEI is also demonstrated as the sensitivity is increased from the same design without the additional PEI layer (see Section 4.3.6).

The BSA layer significantly increased (P = 0.0006) the $I_{100\mu M}$ values from 1.18 ± 0.14 nA, n = 3 (Sty-(ChOx)(GA)$(PEI)_{10}$) to 2.11 ± 0.04 nA, n = 4 (Sty-(ChOx)(BSA)(GA)$(PEI)_{10}$). There was no significant difference (P = 0.9088) between the $I_{100\mu M}$ values of Sty-(ChOx)$(GA)_{10}$ (2.17 ± 0.47 nA, n = 4) and Sty-(ChOx)(BSA)(GA)$(PEI)_{10}$ (2.11 ± 0.04 nA, n = 4).

The K_M concentration was reduced from 367.70 ± 41.43 nA, n = 3 (Sty-(ChOx)(GA)$(PEI)_{10}$) to 249.00 ± 12.92 nA, n = 4 (Sty-(ChOx)(BSA)(GA)$(PEI)_{10}$) with the addition of BSA. The addition of the BSA and PEI layers increased the K_M from 188.80 ± 35.96 nA, n = 4 (Sty-(ChOx)$(GA)_{10}$) to 249.00 ± 12.92 nA, n = 4 (Sty-(ChOx)(BSA)(GA)$(PEI)_{10}$) as to be expected with the additional layers. The addition of the BSA increased the V_{MAX} from 6.69 ± 0.28 nA, n = 3 (Sty-(ChOx)(GA)$(PEI)_{10}$) to 9.53 ± 0.17 nA, n = 4 (Sty-(ChOx)(BSA)(GA)$(PEI)_{10}$). The α value however, was increased from 1.14, n = 3 (Sty-(ChOx)(GA)$(PEI)_{10}$) and 1.34, n = 4 (Sty-(ChOx)(BSA)(GA)$(PEI)_{10}$).

These results have demonstrated both the effect of PEI as a layer prior to the enzyme, and the effect of the BSA layer for enzyme protection. The results of Sty-(ChOx)(BSA)(GA)$(PEI)_{10}$ show little difference from the design of Sty-(ChOx)(GA). This design shows promise for further investigations.

Summary

This section determined the effect of the incorporation of BSA after the enzyme layer in conjunction with PEI as the final layer. This proved beneficial to sensitivity. The sensitivity was comparable to the design Sty-(ChOx)(GA)$_{10}$.

4.3.9. Concentration Studies

4.3.9.1. PEI Concentration

The design Sty-(ChOx)(BSA)(GA)(PEI) shown in Section 4.3.8.2 showed potential for improvement of sensitivity. Different concentrations of PEI could potentially increase the sensitivity further. This design was continued with into a PEI concentration investigation. This section investigates the effect of three PEI concentrations 0.75%, 1% (seen previously in Section 4.3.8.2) and 2%. This study was undertaken to evaluate the effect of PEI concentration on sensitivity.

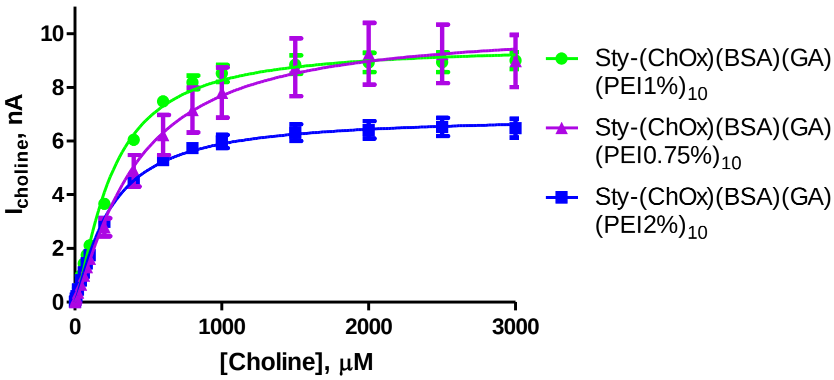

Kinetic Parameters	Sty-(ChOx)(BSA)(GA)(PEI1%)$_{10}$			Sty-(ChOx)(BSA)(GA)(PEI0.75%)$_{10}$			Sty-(ChOx)(BSA)(GA)(PEI2%)$_{10}$		
	Mean	S.E.M	n	Mean	S.E.M	n	Mean	S.E.M	n
V_{MAX}, nA	9.53	0.17	4	10.23	0.73	4	6.92	0.15	3
Km, µM	249.00	12.92	4	408.80	73.73	4	237.70	15.18	3
α	1.34	0.065	4	1.24	0.18	4	1.21	0.06	3
$I_{100µM}$, nA	2.11	0.04	4	1.62	0.19	4	1.75	0.04	3
Sensitivity, nA/µM	0.022	0.001	4	0.0161	0.00014	4	0.017	0.001	3
R^2	0.993	0.001	4	0.9992	0.0001	4	0.995	0.0004	3
Background, nA	0.03	0.01	4	0.20	0.10	4	0.1125	0.003	3

Figure 4.23 : The current-concentration profile comparison and comparison tables for choline chloride calibrations in PBS (pH 7.4) buffer solution at 21°C for designs; (A) Sty-(ChOx)(BSA)(GA)(PEI 1%)$_{10}$ and (B) Sty-(ChOx)(BSA)(GA)(PEI0.75%)$_{10}$ and (C) Sty-(ChOx)(BSA)(GA)(PEI2%)$_{10}$. CPA carried out at +700 mV *vs.* SCE. Sequential current steps for 5, 10, 20, 40, 60, 80, 100, 200, 400, 600, 800, 1000, 1500, 2000, 2500 and 3000 µM choline chloride injections.

A comparison graph and data table of kinetic parameters are presented in Figure 4.23. The graph illustrates the comparison of PEI concentration, the table presents the kinetic parameter comparisons for each design. This section demonstrates changing the PEI concentration did not prove beneficial for sensitivity although demonstrated an effect on enzyme kinetics.

Decreasing the PEI concentration increased the K_M from 249.00 ± 12.92 nA, n = 4 Sty-(ChOx)(BSA)(GA)(PEI1%)$_{10}$ to 408.80 ± 73.73 nA, n = 4 Sty-(ChOx)(BSA)(GA)(PEI0.75%)$_{10}$. This increase in K_M concentration illustrates the effect PEI has on the efficiency of the substrate to access the enzyme and be turned-over. This increase in K_M concentration cannot be as a result of a diffusion constraint as increasing the PEI concentration from 1% to 2% decreased (P = 0.5942) the K_M concentration from 249.00 ± 12.92 nA, n = 4 (Sty-(ChOx)(BSA)(GA)(PEI 1%)$_{10}$) to 237.70 ± 15.18 nA n = 3 (Sty-(ChOx)(BSA)(GA)(PEI 2%)$_{10}$). In addition to increasing the K_M, decreasing the PEI concentration increased the V_{MAX} current (P = 0.3870) from 9.53 ± 0.17 nA, n = 4 (Sty-(ChOx)(BSA)(GA)(PEI 1%)$_{10}$) to 10.23 ± 0.73 nA, n = 4 (Sty-(ChOx)(BSA)(GA)(PEI 0.75%)$_{10}$). Increasing the PEI concentration from 1% to 2% decreased the V_{MAX} current from 9.53 ± 0.17 nA, n = 4 (Sty-(ChOx)(BSA)(GA)(PEI 1%)$_{10}$) to 6.92 ± 0.15 nA, n = 4

(Sty-(ChOx)(BSA)(GA)(PEI 2%)$_{10}$). Altering the PEI concentration had little effect on the α value increasing the PEI concentration decreased the α value from 1.34, n = 4 (Sty-(ChOx)(BSA)(GA)(PEI1%)$_{10}$) to 1.21, n = 3 (Sty-(ChOx)(BSA)(GA)(PEI2%)$_{10}$). Decreasing the PEI concentration from 1% to 0.75% decreased the α value from 1.34, n = 4 (Sty-(ChOx)(BSA)(GA)(PEI1%)$_{10}$) to 1.24, n = 3 (Sty(ChOx)(BSA)(GA)(PEI0.75%)$_{10}$).

The concentration of PEI also affected the sensitivity. A comparison of the $I_{100\mu M}$ values illustrate that the decrease in PEI concentration decreases the current from 2.11 ± 0.04 nA, n = 4 (Sty-(ChOx)(BSA)(GA)(PEI1%)$_{10}$) to 1.62 ± 0.19 nA, n = 4 (Sty-(ChOx)(BSA)(GA)(PEI0.75%)$_{10}$). Increasing the PEI concentration from 1% to 2% also decreased the $I_{100\mu M}$ value from 2.11 ± 0.04 nA, n = 4 (Sty-(ChOx)(BSA)(GA)(PEI 1%)$_{10}$) to 1.75 ± 0.04 nA, n = 4 (Sty-(ChOx)(BSA)(GA)(PEI2%)$_{10}$), this was increased from the current using 0.75% PEI (1.62 ± 0.19 nA, n = 4).

This section illustrates that although increasing the PEI concentration can have a beneficial effect on enzyme kinetics, the sensitivity is not increased as a result. PEI1% is optimal for this design.

Summary

This section determined using PEI and BSA; which has shown promise in section 4.3.8.2 if changing the concentration of PEI could increase sensitivity. Changing the PEI concentration did not have a beneficial effect on sensitivity.

4.3.9.2. GA Concentration

The previous section illustrated the effect of PEI concentration on sensitivity. Glutaraldehyde has also been shown to have an effect on sensitivity (see Section 4.3.2.3). As this is the case the GA concentrations 0.5%, 1% (used previously) and 1.5% were used to investigate the effect of glutaraldehyde concentration on the design Sty-

(ChOx)(BSA)(GA)(PEI). 0.5% was chosen as 0.1% proved detrimental for securing additional layers (see Section 4.3.3).

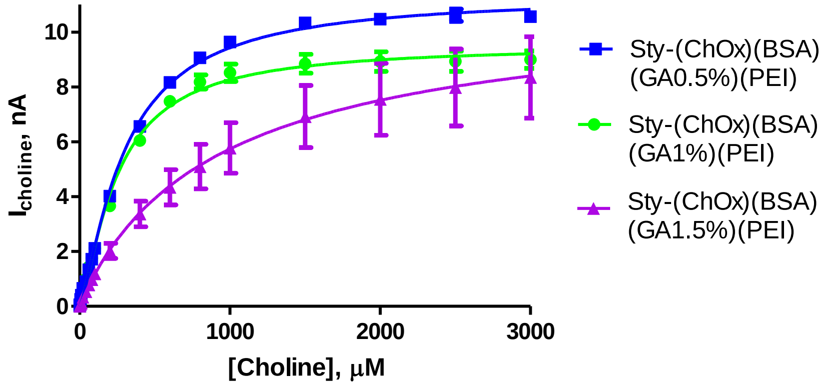

Kinetic Parameters	Sty-(ChOx)(BSA)(GA1%)$(PEI)_{10}$			Sty-(ChOx)(BSA)(GA0.5%)$(PEI)_{10}$			Sty-(ChOx)(BSA)(GA1.5%)$(PEI)_{10}$		
	Mean	S.E.M	n	Mean	S.E.M	n	Mean	S.E.M	n
V_{MAX}, nA	9.53	0.17	4	11.35	0.12	4	11.17	2.69	11
Km, µM	249.00	12.92	4	298.60	8.59	4	944.80	557.50	11
α	1.34	0.065	4	1.32	0.03	4	0.96	0.23	11
$I_{100\mu M}$, nA	2.11	0.04	4	2.12	0.05	4	1.18	0.15	11
Sensitivity, nA/µM	0.022	0.001	4	0.020	0.001	4	0.0119	0.0004	11
R^2	0.993	0.001	4	0.9895	0.0003	4	0.986	0.002	11
Background, nA	0.03	0.01	4	0.13	0.01	4	0.26	0.07	11

Figure 4.24 : The current-concentration profile comparison and comparison tables for choline chloride calibrations in PBS (pH 7.4) buffer solution at 21°C for designs; (A) Sty-(ChOx)(BSA)(GA 1%)$(PEI)_{10}$, (B) Sty-(ChOx)(BSA)(GA 0.5%)$(PEI)_{10}$ and (C) Sty-(ChOx)(BSA)(GA 1.5%)$(PEI)_{10}$. CPA carried out at +700 mV *vs*. SCE. Sequential current steps for 5, 10, 20, 40, 60, 80, 100, 200, 400, 600, 800, 1000, 1500, 2000, 2500 and 3000 µM choline chloride injections.

A comparison graph and data table of kinetic parameters are presented in Figure 4.24. The graph illustrates the comparison of GA concentrations, the table presents the kinetic parameter comparisons for each design. This section demonstrates the increase in GA concentration from 1% to 1.5% led to a decrease in sensitivity. This concentration is potentially too high to allow efficient access for the substrate to the enzyme (see K_M concentration). Increasing the GA concentration affected the rate of diffusion leading to a change in enzyme kinetics. Decreasing the GA concentration did not affect the enzyme kinetics or improve sensitivity.

The comparison data above illustrates the effect of three GA concentrations 0.5%, 1% and 1.5%. Increasing the GA concentration from 1% to 1.5% significantly decreased (*P* = 0.0034) the $I_{100\mu M}$ value from 2.11 ± 0.04 nA, n = 4 Sty-(ChOx)(BSA)(GA1%)$(PEI)_{10}$ to 1.18 ± 0.15 nA, n = 11 Sty-(ChOx)(BSA)(GA1.5%)$(PEI)_{10}$. These results show that GA1.5% is too high for use in this design. When the GA concentration was decreased from 1% to 0.5% the $I_{100\mu M}$ value was not significantly different (*P* = 0.9642) from 2.11 ± 0.04 nA, n = 4 (Sty-(ChOx)(BSA)(GA1%)$(PEI)_{10}$) to 2.12 ± 0.05 nA, n = 4 (Sty-(ChOx)(BSA)(GA0.5%)$(PEI)_{10}$).

The increase in GA concentration from 1% to 1.5% also significantly increased (*P* = 0.0328) the K_M from 249.00 ± 12.92 µM, n = 4 Sty-(ChOx)(BSA)(GA1%)$(PEI)_{10}$ to 944.80 ± 557.50 µM, n = 11 Sty-(ChOx)(BSA)(GA1.5%)$(PEI)_{10}$. The V_{MAX} current was not significantly different (*P* = 0.6584) when increasing the GA from 1% (9.53 ± 0.17 nA, n = 4) to 1.5% (11.17 ± 2.69 nA, n = 11). The α value was decreased from 1.34, n = 4 (Sty-(ChOx)(BSA)(GA1%)$(PEI)_{10}$) to 0.96, n = 11 (Sty-(ChOx)(BSA)(GA1.5%)$(PEI)_{10}$). The K_M was not significantly different (*P* = 0.0872) from 1% (249.00 ± 12.92 µM, n = 4) to 0.5% (298.60 ± 8.59 µM, n = 4). The V_{MAX} current was significantly different (*P* = 0.0112) from 9.53 ± 0.17 nA, n = 4 (Sty-(ChOx)(BSA) (GA1%)$(PEI)_{10}$) to 11.35 ± 0.12 nA, n = 4 (Sty-(ChOx)(BSA)(GA0.5%)$(PEI)_{10}$). The α value was reduced from 1.34, n = 4 (Sty-(ChOx)(BSA)(GA1%)$(PEI)_{10}$) to 1.32, n=4 (Sty-(ChOx)(BSA)(GA0.5%)$(PEI)_{10}$).

This section illustrates that the GA concentration can affect sensitivity and enzyme kinetics. The reduction in GA concentration 1% to 0.5% shows promise as potentially the reduction in GA concentration may affect the PEI interaction when used in conjunction with varying PEI concentrations.

Summary

This section determined the effect of altering the GA concentration on sensitivity. Increasing the GA concentration was detrimental to sensitivity however decreasing the GA concentration increased the V_{MAX} observed.

4.3.9.3. 0.5% GA / PEI

The previous section illustrates the effect of GA concentration on sensitivity. In addition, Section 4.3.9.1 illustrated that varying PEI concentrations can affect sensitivity. As there may need to be a balance between the GA and PEI concentrations, so as not to decrease sensitivity, or increase the rate of diffusion because of increased layers of high concentrations, this section investigates the effect of varying PEI concentrations (seen in Section 4.3.9.1) used in conjunction with a lower GA concentration of 0.5%. Previously shown (see Section 4.3.9.1), increasing the PEI concentration decreased sensitivity, potentially as a result of high concentrations of both PEI and GA as the subsequent layers to the enzyme. This study was undertaken to evaluate if the concentration of GA in conjunction with PEI concentration plays an important role.

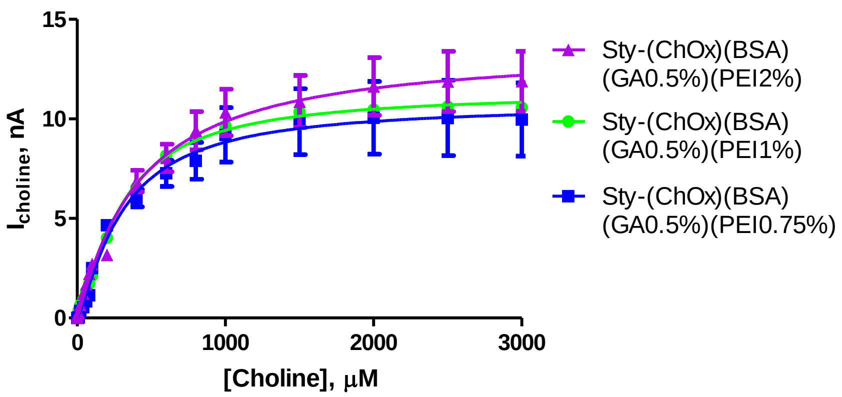

Kinetic Parameters	Sty-(ChOx)(BSA)(GA 0.5%)(PEI 1%)$_{10}$			Sty-(ChOx)(BSA)(GA 0.5%)(PEI 0.75%)$_{10}$			Sty-(ChOx)(BSA)(GA 0.5%)(PEI 2%)$_{10}$		
	Mean	S.E.M	n	Mean	S.E.M	n	Mean	S.E.M	n
V_{MAX}, nA	11.35	0.12	4	11.31	1.16	4	12.69	0.65	3
Km, µM	298.60	8.59	4	495.10	121.50	4	269.10	38.47	3
α	1.32	0.03	4	1.24	0.27	4	1.29	0.16	3
$I_{100\mu M}$, nA	2.12	0.05	4	1.44	0.07	4	2.71	0.16	3
Sensitivity, nA/µM	0.020	0.001	4	0.015	0.001	4	0.027	0.001	3
R^2	0.9895	0.0003	4	0.992	0.002	4	0.996	0.001	3
Background, nA	0.13	0.01	4	0.12	0.01	4	0.27	0.02	3

Figure 4.25 : The current-concentration profile concentration and comparison tables for choline chloride calibrations in PBS (pH 7.4) buffer solution at 21°C for designs (A) Sty-(ChOx)(BSA)(GA 0.5%)(PEI 1%)$_{10}$ (B) Sty-(ChOx)(BSA)(GA 0.5%)(PEI 0.75%)$_{10}$ and (C) Sty-(ChOx)(BSA)(GA 0.5%)(PEI 2%)$_{10}$. CPA carried out at +700 mV *vs.* SCE. Sequential current steps for 5, 10, 20, 40, 60, 80, 100, 200, 400, 600, 800, 1000, 1500, 2000, 2500 and 3000 µM choline chloride injections.

A comparison graph and data table of kinetic parameters are presented in Figure 4.25. The graph illustrates the comparison of PEI concentrations with GA0.5%, the table presents the kinetic parameter comparisons for each design. This section demonstrates a reduction in the PEI concentration has had an effect on sensitivity decreasing the current at the low and high choline concentrations. This has also affected the enzymatic curve reducing the efficiency of the enzyme–substrate turn-over. The higher PEI concentration of 2% increased the sensitivity increasing the efficiency of the enzyme – substrate turn-over.

The decrease in PEI concentration from 1% to 0.75% resulted in a decrease in sensitivity. A comparison of the $I_{100\mu M}$ values shows that the current was significantly reduced (*P* = 0.0003) from 2.12 ± 0.05 nA, n = 4 (Sty-(ChOx)(BSA)(GA0.5%)(PEI1%)$_{10}$) to 1.44 ± 0.07 nA, n = 4 (Sty-(ChOx)(BSA)(GA0.5%)(PEI0.75%)$_{10}$).

In addition, the K_M was increased from 298.60 ± 8.59 µM, n = 4 (Sty-(ChOx)(BSA)(GA0.5%)(PEI1%)$_{10}$) to 495.10 ± 121.50 µM, n=4 (Sty-(ChOx)(BSA)(GA0.5%)(PEI 0.75%)$_{10}$). The V_{MAX} remained relatively unchanged from 11.35 ± 0.12 nA, n = 4 (Sty-(ChOx)(BSA)(GA0.5%)(PEI1%)$_{10}$) to 11.31 ± 1.16 nA, n = 4 (Sty-(ChOx)(BSA)(GA0.5%)(PEI0.75%)$_{10}$). The α value was also only decreased from 1.32, n = 4 (Sty-(ChOx)(BSA)(GA0.5%)(PEI1%)$_{10}$) to 1.24, n = 4 (Sty-(ChOx)(BSA)(GA 0.5%)(PEI 0.75%)$_{10}$.

Increasing the PEI concentration from 1% to 2% increased the sensitivity. A comparison of the $I_{100\mu M}$ values show that the change in concentration significantly increased (P = 0.0097) the current from 2.12 ± 0.05 nA, n = 4 (Sty-(ChOx)(BSA)(GA0.5%)(PEI1%)$_{10}$) to 2.71 ± 0.16 nA, n = 3 (Sty-(ChOx)(BSA)(GA0.5%)(PEI 2%)$_{10}$).

The increase in PEI concentration also decreased the K_M concentration from 298.60 ± 8.59 µM, n = 4 (Sty-(ChOx)(BSA)(GA0.5%)(PEI1%)$_{10}$) to 269.10 ± 38.47 nA, n = 3 (Sty-(ChOx)(BSA)(GA0.5%)(PEI2%)$_{10}$).The V_{MAX} current was increased from 11.35 ± 0.12 nA, n = 4 (Sty-(ChOx)(BSA)(GA0.5%)(PEI1%)$_{10}$) to 12.69 ± 0.65 nA, n = 3 (Sty-(ChOx)(BSA)(GA0.5%)(PEI2%)$_{10}$). The α value remained relatively unchanged from 1.32, n = 4 (Sty-(ChOx)(BSA)(GA0.5%)(PEI1%)$_{10}$) to 1.29, n = 3 (Sty-(ChOx)(BSA)(GA0.5%)(PEI2%)$_{10}$). However is slightly closer to the ideal value of 1.

This section has demonstrated the effect of changing the PEI concentration when used in conjunction with GA0.5%. The results illustrate the delicate balance between a lower GA concentration, in addition to a higher PEI concentration. This combination has the ability to increase sensitivity as the combination of both using a high concentrations may potentially “drown” the enzyme.

Summary

This section determined the effect of different PEI concentrations in conjunction with the GA concentration of 0.5%. The use of PEI2% in conjunction with this GA concentration increased the choline current at 100 µM choline. This design has the highest $I_{100\ \mu M}$ value of the designs seen in this chapter.

4.3.9.4. 1.5% GA / PEI

The previous section illustrated GA0.5% used in conjunction with PEI concentration variations. The combination of GA0.5% and PEI2% proved successful in increasing the sensitivity towards choline. Although Section 4.3.9.2 demonstrated that GA1.5% did not improve sensitivity, this concentration was used in conjunction with varying PEI concentration as this may increase the sensitivity further.

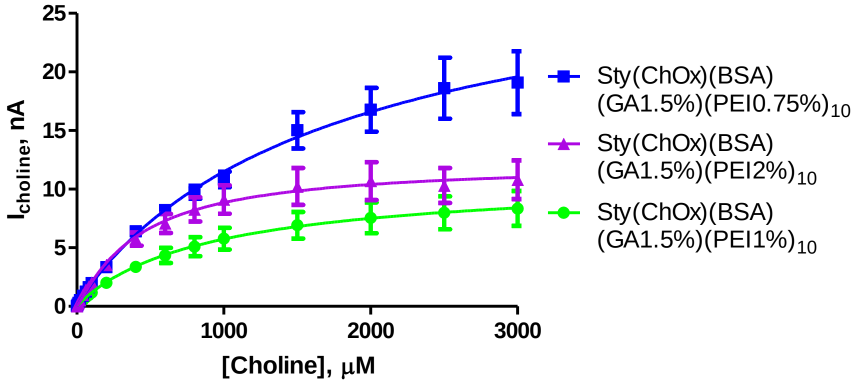

Kinetic Parameters	Sty-(ChOx)(BSA)(GA 1.5%)(PEI 1%)$_{10}$			Sty-(ChOx)(BSA)(GA 1.5%)(PEI 0.75%)$_{10}$			Sty-(ChOx)(BSA)(GA 1.5%)(PEI 2%)$_{10}$		
	Mean, nA	S.E.M, nA	n	Mean, nA	S.E.M, nA	n	Mean, nA	S.E.M, nA	n
V_{MAX}, nA	11.17	2.69	11	31.98	7.95	3	12.23	1.12	3
Km, µM	944.80	557.50	11	1847.00	1008.00	3	422.50	102.20	3
α	0.96	0.23	11	0.94	0.15	3	1.12	0.18	3
$I_{100\mu M}$, nA	1.18	0.15	11	1.99	0.03	3	2.03	0.14	3
Sensitivity, nA/µM	0.0119	0.0004	11	0.019	0.001	3	0.021	0.001	3
R^2	0.986	0.002	11	0.996	0.575	3	0.988	0.57	3
Background, nA	0.26	0.07	11	0.09	0.05	3	0.7	0.4	3

Figure 4.26 : The current-concentration profile and comparison tables for choline chloride calibrations in PBS (pH 7.4) buffer solution at 21°C for designs; (A) Sty-(ChOx)(BSA)(GA1.5%)(PEI1%)$_{10}$, (B) Sty-(ChOx)(BSA)(GA1.5%)(PEI0.75%)$_{10}$ and (C) Sty-(ChOx)(BSA)(GA1.5%)(PEI2%)$_{10}$. CPA carried out at +700 mV *vs*. SCE. Sequential current steps for 5, 10, 20, 40, 60, 80, 100, 200, 400, 600, 800, 1000, 1500, 2000, 2500 and 3000 µM choline chloride injections.

A comparison graph and data table of kinetic parameters are presented in Figure 4.26. The graph illustrates the comparison of PEI concentrations with GA1.5%, the table presents the kinetic parameter comparisons for each design. This section demonstrates that changing the PEI concentration affects the enzyme kinetics of the design. These results also illustrate the effect of a combination of GA and PEI concentration on sensitivity and that 1.5% may be too harsh for the enzyme.

Both the reduction and increase in PEI concentration increased sensitivity. The reduction in PEI concentration from 1% to 0.75% significantly increased (P = 0.0198) the $I_{100\mu M}$ value from 1.18 ± 0.15 nA, n = 11 Sty-(ChOx)(BSA)(GA1.5%)(PEI1%)$_{10}$) to 1.99 ± 0.03 nA, n = 3 (Sty-(ChOx)(BSA)(GA1.5%)(PEI0.75%)$_{10}$). Similarly, the increase in PEI concentration from 1% to 2% significantly increased (P = 0.0181) the $I_{100\mu M}$ value from 1.18 ± 0.15 nA, n = 11 Sty-(ChOx)(BSA)(GA1.5%)(PEI 1%)$_{10}$) to 2.03 ± 0.14 nA, n = 3 (Sty-(ChOx)(BSA)(GA1.5%)(PEI 2%)$_{10}$).

The decrease in PEI concentration from 1% to 0.75% significantly increased (P = 0.0348) the K_M concentration from 944.80 ± 557.50 µM, n = 11 (Sty-(ChOx)(BSA)(GA 1.5%)(PEI1%)$_{10}$) to 1847.00 ± 1008.00 µM, n = 3 (Sty-(ChOx)(BSA)(GA1.5%)(PEI 0.75%)$_{10}$). Increasing the PEI concentration from 1% to 2% decreased the K_M concentration from 944.80 ± 557.50 µM, n = 11 Sty-(ChOx)(BSA)(GA1.5%)(PEI1%)$_{10}$) to 422.50 ± 102.20 µM, n = 3 (Sty-(ChOx)(BSA)(GA1.5%)(PEI2%)$_{10}$) although this was not significant (P = 0.1619). Decreasing the PEI concentration from 1% to 0.75% significantly increased (P = 0.0053) the V_{MAX} current from 11.17 ± 2.69 nA, n = 11 Sty-(ChOx)(BSA)(GA1.5%)(PEI1%)$_{10}$) to 31.98 ± 7.95 nA, n = 3 (Sty-(ChOx)(BSA)(GA1.5%)(PEI0.75%)$_{10}$). Increasing the PEI concentration from 1% to 2% increased the V_{MAX} current from 11.17 ± 2.69 nA, n = 11 (Sty-(ChOx)(BSA)(GA1.5%)(PEI1%)$_{10}$) to 12.23 ± 1.12 nA, n = 3 (Sty-(ChOx)(BSA)(GA1.5%)(PEI2%)$_{10}$) although this was not significant (P = 0.8591).The α value was decreased with the reduction of PEI concentration from 1% to 0.75% from 0.96, n = 11 (Sty-(ChOx)(BSA)(GA1.5%)(PEI1%)$_{10}$) to 0.94, n = 3 (Sty-(ChOx)(BSA)(GA1.5%)(PEI0.75%)$_{10}$). Increasing the PEI concentration from 1% to 2% increased the α value from Sty-(ChOx)(BSA)(GA1.5%)(PEI 1%)$_{10}$) to 1.12, n = 3 (Sty-(ChOx)(BSA)(GA1.5%)(PEI 2%)$_{10}$).

These experiments did illustrate the effect of PEI concentrations when used in conjunction with GA1.5%. The same balance of constituents was illustrated here as in Section 4.3.9.3. The use of GA1.5% was too high for further experiments.

Summary

This section has determined that the use of GA1.5% is too high and is not a viable choice of sensor development in conjunction with any PEI concentration.

4.3.10. Enzyme Medium

Every enzyme has a specific range of pH which is characteristic for the particular enzyme to give optimum reactivity. An immobilised enzyme can have a different pH range to an enzyme in solution (Tripathi, 2009). The optimum pH value for an enzyme may change after immobilisation (Brady & Jordaan, 2009). In addition, pH plays an important role in the enzyme maintaining its proper conformation (Bankar *et al.*, 2009). Studies into the parameters which influence the immobilisation of oxidase enzymes, illustrate that the pH of the immobilisation medium influenced the amount of enzyme immobilised onto the polymer. In addition pH values close to the isoelectric points of the enzyme increased the immobilisation efficiency (Hall *et al.*, 1996). The following experiments were undertaken in order to investigate if using an enzyme medium of deionised water of pH 5.5, would alter the immobilisation efficiency as the isoelectric point of choline oxidase is 4.1 when compared to PBS of pH 7.4.

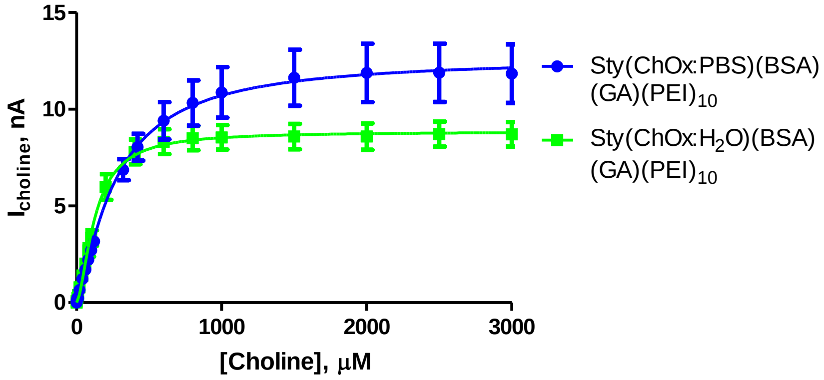

Kinetic Parameters	Sty-(ChOx:PBS)(BSA)(GA)(PEI)$_{10}$			Sty-(ChOx:H_2O)(BSA)(GA)(PEI)$_{10}$		
	Mean, nA	S.E.M, nA	n	Mean, nA	S.E.M, nA	n
V_{MAX}, nA	12.69	0.65	3	8.84	0.21	3
Km, μM	269.10	38.47	3	127.6	10.5	3
α	1.29	0.16	3	1.60	0.18	3
$I_{100\mu M}$, nA	2.71	0.16	3	3.34	0.41	3
Sensitivity, nA/μM	0.03	0.001	3	0.03	0.0003	3
R^2	0.996	0.001	3	0.999	0.0001	3
Background, nA	0.27	0.02	3	0.15	0.01	3

Figure 4.27 : The current-concentration profile and comparison tables for choline chloride calibrations in PBS (pH 7.4) buffer solution at 21°C for designs; (A) Sty-(ChOx:PBS)(BSA)(GA)(PEI)$_{10}$ and (B) Sty-(ChOx:H_20)(BSA)(GA)(PEI)$_{10}$. CPA carried out at +700 mV *vs.* SCE. Sequential current steps for 5, 10, 20, 40, 60, 80, 100, 200, 400, 600, 800, 1000, 1500, 2000, 2500 and 3000 μM choline chloride injections.

A comparison graph and data table of kinetic parameters are presented in Figure 4.27. The graph illustrates the comparison of enzyme medium, the table presents the kinetic parameter comparisons for each design. This section demonstrates the effect of changing the pH of the enzyme medium from 7.4 to 5.5 a value closer to the isoelectric point of 4.1 for choline oxidase. This change of pH has had a positive effect on both sensitivity and enzyme kinetics.

Changing the enzyme medium from PBS to H_2O increased (P = 0.2235) the I_{100}µM current from 2.71 ± 0.16 nA, n = 3 (Sty-(ChOx:PBS) (BSA)(GA)$(PEI)_{10}$) to 3.34 ± 0.41 nA, n = 3 (Sty-(ChOx:H_2O)(BSA)(GA)$(PEI)_{10}$) an increase of 23.24 %.

Changing the enzyme medium to H_2O also had a beneficial effect on the enzyme kinetics significantly decreasing (P = 0.0159) the K_M from 269.10 ± 38.47 µM, n = 3 (Sty-(ChOx:PBS)(BSA)(GA)$(PEI)_{10}$) to 127.60 ± 10.50 µM, n = 3 (Sty-(ChOx:H_2O)(BSA)(GA)$(PEI)_{10}$). In addition, the V_{MAX} current was decreased (P = 0.1045) from 12.69 ± 0.65 nA, n = 3 (Sty-(ChOx:PBS)(BSA)(GA)$(PEI)_{10}$) to 8.84 ± 0.21 nA, n = 3 (Sty-(ChOx:H_2O)(BSA)(GA)$(PEI)_{10}$). The α value was increased from 1.29, n = 3 (Sty-(ChOx:PBS)(BSA)(GA)$(PEI)_{10}$) to 1.60, n = 3 (Sty-(ChOx:H_2O)(BSA)(GA) $(PEI)_{10}$).

This section has illustrated the effect of changing the enzyme medium on immobilisation. It is unclear whether the increase in sensitivity and improvement in enzyme kinetics is as a result of better immobilisation or a stabilising effect of the water on the enzyme prior to immobilisation.

Summary

This section determined the effect of the use of H_2O as the enzyme medium and if this could increase the sensitivity of the sensor. It is demonstrated that the H_2O medium increased the sensitivity of the sensor resulting in the highest $I_{100\ \mu M}$ observed of any sensor design thus far.

4.3.11. Styrene Double Layer

Section 4.3.4 demonstrated the effect loading a second full layer consisting of ten layers of enzyme. This design was found to be detrimental to sensitivity. This design however utilised a 50 U enzyme solution. Potentially, the enzyme concentration was too low to demonstrate a beneficial effect, as the enzyme from the bottom layers was being negated. The following experiments investigate the effect of additional layering using the optimal design which utilises an enzyme concentration of 500U.

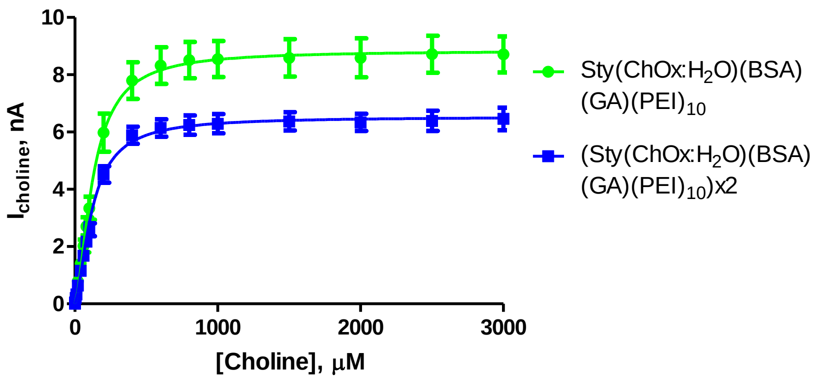

Kinetic Parameters	Sty-($ChOx.H_2O$)(BSA)(GA)$(PEI)_{10}$			Sty-($ChOx.H_2O$)(BSA)(GA)$(PEI)_{10}$)X2		
	Mean	S.E.M	n	Mean	S.E.M	n
V_{MAX}, nA	8.84	0.21	3	6.53	0.12	3
Km, µM	127.60	10.50	3	120.00	7.15	3
α	1.60	0.18	3	1.55	0.13	3
$I_{100\mu M}$, nA	3.34	0.41	3	2.59	0.22	3
Sensitivity, nA/µM	0.03	0.0003	3	0.026	0.001	3
R^2	0.999	0.0001	3	0.996	0.002	3
Background, nA	0.15	0.01	3	2.16	1.88	3

Figure 4.31 : The current-concentration profile and comparison tables for choline chloride calibrations in PBS (pH 7.4) buffer solution at 21°C for designs; (A) Sty-($ChOx:H_2O$)(BSA)(GA)$(PEI)_{10}$ and (B) (Sty-($ChOx:H_2O$)(BSA)(GA)$(PEI)_{10}$)x2. CPA carried out at +700 mV *vs.* SCE. Sequential current steps for 5, 10, 20, 40, 60, 80, 100, 200, 400, 600, 800, 1000, 1500, 2000, 2500 and 3000 µM choline chloride injections.

A comparison graph and data table of kinetic parameters are presented in Figure 4.31. The graph illustrates the comparison of the double layer, the table presents the kinetic parameter comparisons for each design. This section demonstrates the addition of ten extra layers of enzyme decreased sensitivity. The additional layering has negated the analyte detection of the lower layers similar to the design seen in Section 4.3.4.

The additional layering was detrimental to sensitivity. The $I_{100\mu M}$ current was decreased (P = 0.1789) from 3.34 ± 0.41 nA, n = 3 (Sty-(ChOx:H_2O)(BSA)(GA)$(PEI)_{10}$) to 2.59 ± 0.22 nA, n = 3 ((Sty-(ChOx:H_2O)(BSA)(GA)$(PEI)_{10}$)x2).

The V_{MAX} was significantly reduced (P = 0.0337) from 8.84 ± 0.21 nA, n = 3 (Sty-(ChOx:H_2O)(BSA)(GA)$(PEI)_{10}$) to 6.53 ± 0.12 nA, n = 3 ((Sty-(ChOx:H_2O)(BSA)(GA)$(PEI)_{10}$) x2). The double layer decreased (P = 0.5219) the K_M concentration from 127.60 ± 10.50 nA, n = 3 (Sty-(ChOx:H_2O)(BSA)(GA)$(PEI)_{10}$) to 120.00 ± 7.15 nA, n = 3 ((Sty-(ChOx:H_2O)(BSA)(GA)$(PEI)_{10}$)x2). The α value was decreased from 1.60, n = 3 (Sty-(ChOx:H_2O)(BSA)(GA)$(PEI)_{10}$) to 1.55, n = 3 (Sty-(ChOx:H_2O)(BSA)(GA)$(PEI)_{10}$). These experiments illustrate that the ten extra layers of enzyme has no positive effect on the design and is not viable for future use.

Summary

This section determined that a double layer of the design has no beneficial effect on sensitivity.

4.3.12. MMA Modifications

There have been reports of enzyme immobilisation based on methacrylate derivatives (Pérez *et al.*, 2006). Choline oxidase and glucose oxidase have been covalently immobilised on the surface of 2-hydroxythyl and glycidyl methacrylate copolymer membranes (Doretti *et al.*, 1996). Also, glucose oxidase was immobilised using poly(hydroxyethyl methacrylate) (Schulz *et al.*, 1999). The polymerised form of methyl methacrylate has also been used in sensor design. PMMA has been used for the design of an imunosensor (Holt *et al.*, 2002) and an odour sensor (Doleman & Lewis, 2001). MMA is an inexpensive commodity plastic similar to that of polystyrene (Holt *et al.*, 2002). For this reason the effect of changing the immobilisation polymer was investigated in order to evaluate if the polymer had any effect on the enzyme, perhaps changing the kinetics or changing the sensitivity.

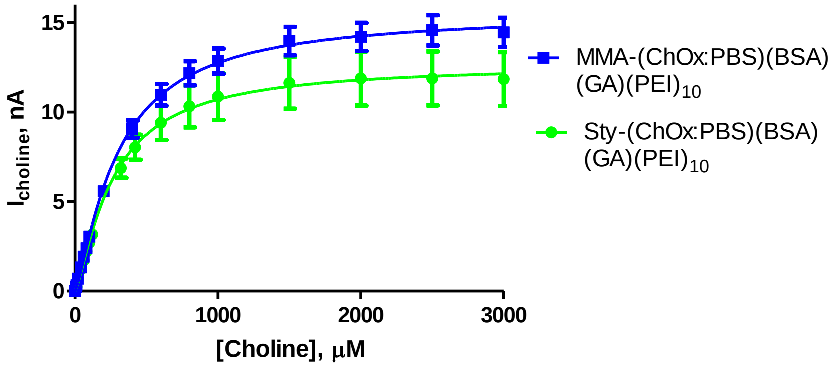

Kinetic Parameters	Sty-(ChOx)(BSA)(GA)(PEI)$_{10}$			MMA-(ChOx)(BSA)(GA)(PEI)$_{10}$		
	Mean, nA	S.E.M, nA	n	Mean, nA	S.E.M, nA	n
V_{MAX}, nA	12.69	0.65	3	15.56	0.44	4
Km, μM	269.10	38.47	3	302.30	24.09	4
α	1.29	0.16	3	1.26	0.08	4
$I_{100\mu M}$, nA	2.71	0.16	3	3.04	0.14	4
Sensitivity, nA/μM	0.03	0.001	3	0.03	0.001	4
R^2	0.996	0.001	3	0.997	0.0004	4
Background, nA	0.27	0.02	3	0.13	0.01	4

Figure 4.28 : The current-concentration profile and comparison tables for choline chloride calibrations in PBS (pH 7.4) buffer solution at 21°C for designs; (A) Sty-(ChOx)(BSA)(GA)(PEI)$_{10}$ and (B) MMA-(ChOx)(BSA)(GA)(PEI)$_{10}$. CPA carried out at +700 mV *vs.* SCE. Sequential current steps for 5, 10, 20, 40, 60, 80, 100, 200, 400, 600, 800, 1000, 1500, 2000, 2500 and 3000 μM choline chloride injections.

A comparison graph and data table of kinetic parameters are presented in Figure 4.28. The graph illustrates the comparison of immobilisation matrix, the table presents the kinetic parameter comparisons for each design. This section demonstrates that changing the polymer has a positive effect on sensitivity. The polymer has altered the immobilisation of the enzyme, therefore, altered the effectiveness of the enzyme to interact with the substrate.

Changing the immobilisation polymer from Styrene to MMA has proved successful in increasing (P = 0.1900) the $I_{100\mu M}$ current from 2.71 ± 0.16 nA, n = 3 (Sty-(ChOx)(BSA)(GA)(PEI)$_{10}$) to 3.04 ± 0.14 nA, n = 4 (MMA-(ChOx)(BSA)(GA)(PEI)$_{10}$).

The V_{MAX} has also been increased (P = 0.1697) from 12.69 ± 0.65 nA, n = 3 (Sty-(ChOx)(BSA)(GA)(PEI)$_{10}$) to 15.56 ± 0.44 nA, n = 4 (MMA-(ChOx)(BSA)(GA)(PEI)$_{10}$). This suggests that MMA is a more efficient immobilisation matrix. The K_M was increased (P = 0.3521) from 269.10 ± 38.47 µM, n = 3 (Sty-(ChOx)(BSA)(GA)(PEI)$_{10}$) to 302.30 ± 24.09 nA, n = 4 (MMA-(ChOx)(BSA)(GA)(PEI)$_{10}$). This suggests an increase in the rate of diffusion potentially as a result of higher enzyme loading. The α value remained similar decreasing slightly from 1.29, n = 3 (Sty-(ChOx)(BSA)(GA)(PEI)$_{10}$) to 1.26, n=4 (MMA-(ChOx)(BSA)(GA)(PEI)$_{10}$).

This section has concluded that changing the immobilisation polymer can be advantageous for sensitivity. It is undetermined if the use of polymer will have an effect for future characterisation studies. As such the use of both styrene and MMA will be considered in future experiments.

Summary

This section determined the effect of an alternative polymer for the immobilisation of the enzyme; MMA. The polymer increased the sensitivity observed when compared to the styrene design.

4.3.12.1. Enzyme medium

Section 4.3.10 investigated the effect of changing the enzyme medium from PBS to H_2O. With this the pH of the enzyme medium was changed from 7.4 to 5.5 as reports suggest that pH can influence enzyme immobilisation. In conjunction with the styrene polymer, both sensitivity was increased and the enzyme kinetics were improved with H_2O as the enzyme medium. The following investigation was undertaken to investigate the effect of the H_2O when used in conjunction with the MMA polymer.

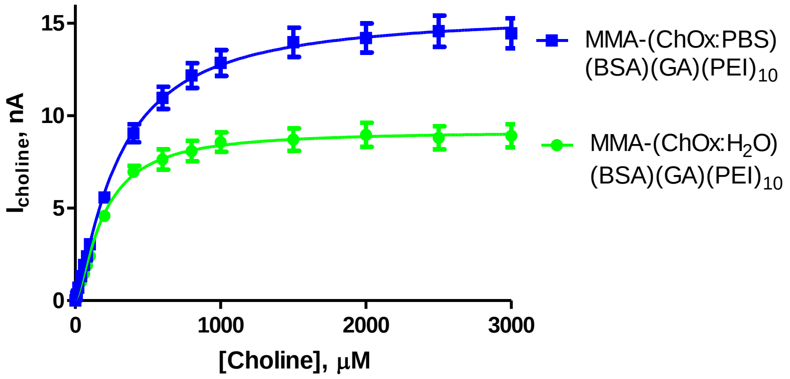

Kinetic Parameters	MMA-(ChOx.PBS)(BSA)(GA)(PEI)$_{10}$			MMA-(ChOx.H_2O)(BSA)(GA)(PEI)$_{10}$		
	Mean	S.E.M	n	Mean	S.E.M	n
V_{MAX}, nA	15.56	0.44	4	9.18	0.23	4
Km, µM	302.30	24.09	4	194.00	15.63	4
α	1.26	0.08	4	1.45	0.12	4
$I_{100µM}$, nA	3.04	0.14	4	2.41	0.12	4
Sensitivity, nA/µM	0.03	0.001	4	0.02	0.0004	4
R^2	0.997	0.0004	4	0.997	0.001	4
Background, nA	0.13	0.01	4	0.12	0.02	4

Figure 4.29 : The current-concentration profile and comparison tables for choline chloride calibrations in PBS (pH 7.4) buffer solution at 21°C for designs; (A) MMA-(ChOx:PBS)(BSA)(GA)(PEI)$_{10}$ and (B) MMA-(ChOx:H_2O)(BSA)(GA)(PEI)$_{10}$. CPA carried out at +700 mV *vs.* SCE. Sequential current steps for 5, 10, 20, 40, 60, 80, 100, 200, 400, 600, 800, 1000, 1500, 2000, 2500 and 3000 µM choline chloride injections.

A comparison graph and data table of kinetic parameters are presented in Figure 4.29. The graph illustrates the comparison of enzyme medium, the table presents the kinetic parameter comparisons for each design. This section demonstrates that the H_2O medium in conjunction with the MMA polymer, similar to the styrene, had an effect. The sensitivity was however, not improved. The current at the low choline concentrations were not dramatically altered (see Appendix 1), however as the H_2O had affected the enzyme kinetics, the current at the V_{MAX} plateaux was changed dramatically.

The use of the H_2O did not prove beneficial to the design. A comparison of the $I_{100\mu M}$ currents shows that the current was significantly decreased (P = 0.0146) from 3.04 ±

0.14 nA, n = 4 (MMA-(ChOx:PBS)(BSA)(GA)$(PEI)_{10}$) to 2.41 ± 0.12 nA, n = 4 (MMA-(ChOx:H_2O)(BSA)(GA)$(PEI)_{10}$).

The V_{MAX} current was significantly decreased (P = 0.0016) from 15.56 ± 0.44 nA, n = 4 (MMA-(ChOx:PBS)(BSA)(GA)$(PEI)_{10}$) to 9.18 ± 0.23 nA, n = 4 (MMA-(ChOx:PBS)(BSA)(GA)$(PEI)_{10}$). However, the K_M was significantly decreased (P = 0.0188) from 302.30 ± 24.09 µM, n = 4 (MMA-(ChOx:PBS)(BSA)(GA)$(PEI)_{10}$) to 194.00 ± 15.63 nA, n = 4 (MMA-(ChOx:H_2O)(BSA)(GA)$(PEI)_{10}$). The α value was increased from 1.26, n = 4 (MMA-(ChOx:PBS)(BSA)(GA)$(PEI)_{10}$) to 1.45, n = 4 (MMA-(ChOx:H_2O)(BSA)(GA)$(PEI)_{10}$).

This section illustrated the effect of changing the enzyme medium from PBS to H_2O in conjunction with the MMA immobilisation polymer. The results indicate that the effect of the enzyme medium is different for styrene and MMA. The results used with styrene show that H_2O increased sensitivity. In conjunction with MMA the H_2O had a detrimental effect on sensitivity; and PBS was the preferred enzyme medium.

Summary

This section determined the effect of the H_2O medium when used in conjunction with the MMA polymer. The H_2O did not increase the sensitivity of the sensor.

4.3.12.2. MMA Double Layer

Similar to Sections 4.3.4 and 4.3.11 a second full layer consisting of ten layers of enzyme was added to the dipping series to investigate if it would increase sensitivity.

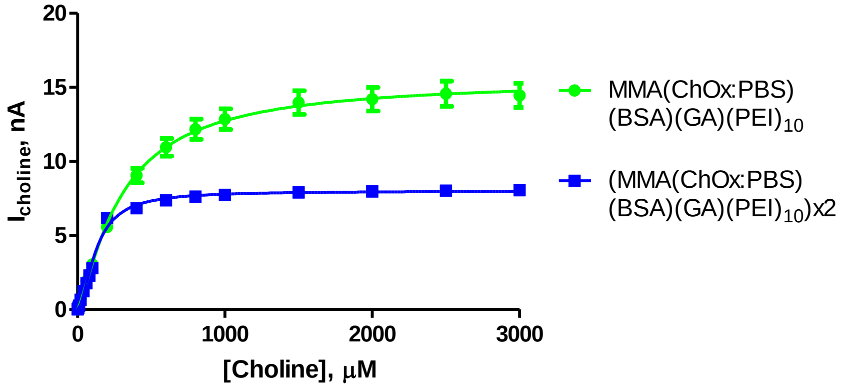

Kinetic Parameters	MMA-(ChOx.PBS)(BSA)(GA)(PEI)$_{10}$			MMA-(ChOx.PBS)(BSA)(GA)(PEI)$_{10}$)x2		
	MEAN	S.E.M	n	MEAN	S.E.M	n
V_{MAX}, nA	15.56	0.44	4	8.83	0.22	4
Km, µM	302.30	24.09	4	143.60	12.22	4
α	1.26	0.09	4	1.55	0.16	4
$I_{100\mu M}$, nA	3.04	0.14	4	2.78	0.10	4
Sensitivity, nA/µM	0.03	0.001	4	0.0284	0.0004	4
R^2	0.997	0.0004	4	0.997	0.001	4
Background, nA	0.13	0.01	4	0.12	0.02	4

Figure 4.32 : The current-concentration profile and comparison tables for choline chloride calibrations in PBS (pH 7.4) buffer solution at 21°C for designs; (A) MMA-(ChOx:H_2O)(BSA)(GA)(PEI)$_{10}$ and (B) (MMA-(ChOx:H_2O)(BSA)(GA)(PEI)$_{10}$)x2. CPA carried out at +700 mV *vs*. SCE. Sequential current steps for 5, 10, 20, 40, 60, 80, 100, 200, 400, 600, 800, 1000, 1500, 2000, 2500 and 3000 µM choline chloride injections.

A comparison graph and data table of kinetic parameters are presented in Figure 4.32. The graph illustrates the comparison of the double layer, the table presents the kinetic parameter comparisons for each design. This section demonstrates the additional layering has negated the analyte detection of the lower layers similar to the design seen in sections 4.3.7 and 4.3.22.

The $I_{100\mu M}$ current was decreased (P = 0.2071) from 3.04 ± 0.14 nA, n = 4 (MMA-(ChOx:PBS)(BSA)(GA)(PEI)$_{10}$) to 2.78 ± 0.10 nA, n = 4 ((MMA-(ChOx:PBS)(BSA)(GA)(PEI)$_{10}$)x2).

The V_{MAX} was significantly reduced (P = 0.0021) from 15.56 ± 0.44 nA, n=4 (MMA-(ChOx:PBS)(BSA)(GA)(PEI)$_{10}$) to 8.83 ± 0.22 nA, n=4 ((MMA-(ChOx:PBS)(BSA)(GA)(PEI)$_{10}$)x2). The double layer significantly decreased (P = 0.0032) the K_M concentration from 302.30 ± 24.09 nA, n=4 (MMA-(ChOx:PBS)(BSA)(GA)(PEI)$_{10}$) to 143.60 ± 12.22 nA, n=4 ((MMA-(ChOx:PBS) (BSA)(GA)(PEI)$_{10}$)x2). The α value was increased from 1.26, n=4 (MMA-(ChOx:PBS)(BSA)(GA)(PEI)$_{10}$) to 1.55, n=4 (MMA-(ChOx:PBS)(BSA)(GA)(PEI)$_{10}$).

These experiments illustrate that the ten extra layers of enzyme has no positive effect on the design and is not viable for future use.

Summary

This section demonstrated that a double layer of the design does not have a beneficial effect on sensitivity.

4.3.13. Best design

Throughout the previous experiments the effect of immobilisation polymer, unit activity, enzyme medium, BSA, GA and PEI were all investigated for use with the enzyme choline oxidase with the aim of obtaining high sensitivity and a low K_M concentration representative of good Michaelis-Menten kinetics. Two designs were chosen as the optimal designs for future work. Firstly, the optimal design for use with the styrene polymer is Sty-(ChOx:H_2O)(BSA1%)(GA0.5%)(PEI2%). Secondly, the optimal design for use with the MMA polymer is MMA-(ChOx:PBS)(BSA1%)(GA0.5%)(PEI2%). Both designs were chosen for future work.

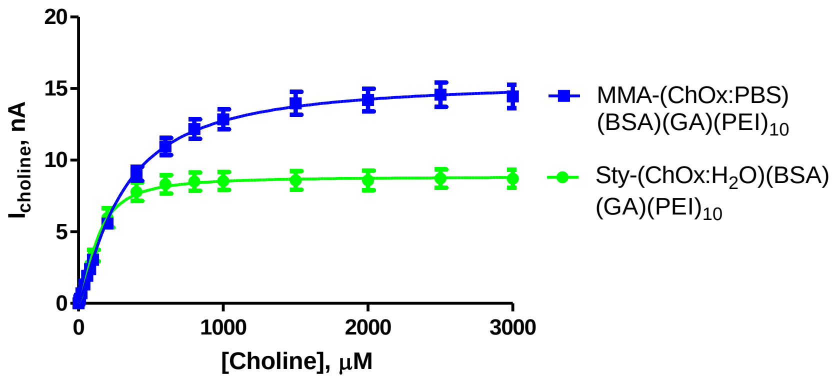

Kinetic Parameters	Sty-(ChOx.H_2O)(BSA)(GA)(PEI)$_{10}$			MMA-(ChOx.PBS)(BSA)(GA)(PEI)$_{10}$		
	Mean	S.E.M	n	Mean	S.E.M	n
V_{MAX}, nA	8.84	0.21	3	15.56	0.44	4
Km, μM	127.60	10.50	3	302.30	24.09	4
α	1.60	0.18	3	1.26	0.08	4
$I_{100\mu M}$, nA	3.34	0.41	3	3.04	0.14	4
Sensitivity, nA/μM	0.03	0.0003	3	0.03	0.001	4
R^2	0.999	0.0001	3	0.997	0.0004	4
Background, nA	0.15	0.01	3	0.13	0.01	4

Figure 4.30 : The current-concentration profile and comparison tables for choline chloride calibrations in PBS (pH 7.4) buffer solution at 21°C for designs; (A) Sty-(ChOx:H_2O)(BSA)(GA)(PEI)$_{10}$ and (B) MMA-(ChOx:PBS)(BSA)(GA)(PEI)$_{10}$. CPA carried out at +700 mV *vs.* SCE. Sequential current steps for 5, 10, 20, 40, 60, 80, 100, 200, 400, 600, 800, 1000, 1500, 2000, 2500 and 3000 μM choline chloride injections.

A comparison graph and data table of kinetic parameters are presented in Figure 4.30. The graph illustrates the comparison of the sensor designs using Styrene and MMA, the table presents the kinetic parameter comparisons for each design. This section represents the best combination of kinetic parameters for the detection of choline using different immobilisation matrixes.

The designs illustrate differences for each of the kinetic parameters. The styrene design presents a lower V_{MAX} current (8.84 ± 0.21 nA, n = 3) than that of the MMA design (15.56 ± 0.44, n = 4).The styrene design also has a lower K_M concentration of 127.60 ±

10.50 µM, n = 3 compared with 302.30 ± 24.09 µM, n = 4 for MMA. Also the α value was reduced from 1.60 (styrene) to 1.26 (MMA).

The $I_{100\mu M}$ current is higher in the styrene design (3.34 ± 0.41 nA, n = 3) compared to the MMA design (3.04 ± 0.14 nA, n = 4). These designs will be continued with for future work.

Summary

This section demonstrates the two designs which have produced the highest sensitivities using the Styrene and MMA polymers.

4.4. Conclusion

This chapter detailed the modifications undertaken in the development of the choline biosensor. The immobilisation matrixes used were both styrene and MMA polymers. It was also determined that ten layers of enzyme immobilised within these polymers was optimal for the design. The optimal enzyme unit activity was determined as a 500 U solution. The incorporation of the stabiliser BSA proved advantageous in the design alongside PEI and the cross-linker GA. These three components were added and extensively characterised in terms of their effect on the immobilisation of ChOx until the optimal arrangement was determined for the choline detection. The use of enzyme medium was determined in conjunction with the two polymers. Styrene is used in conjunction with water medium and MMA is used with a PBS medium. Two choline biosensor designs were developed and described in this chapter using Styrene and MMA polymers. The styrene design obtained a sensitivity of 0.03 ± 0.0003 nA/µM, n=3 and the MMA design obtained a sensitivity of 0.03 ± 0.001 nA/µM, n=4. These designs will be continued with, in the next chapter.

Andersson MM & Hatti-Kaul R. (1999). Protein stabilising effect of polyethyleneimine. *Journal of Biotechnology* **72,** 21-31.

Bankar SB, Bule MV, Singhal RS & Ananthanarayan L. (2009). Glucose oxidase — An overview. *Biotechnology Advances* **27,** 489-501.

Bayramoğlu G, Metin AÜ, Altıntas B & Arıca MY. (2010). Reversible immobilization of glucose oxidase on polyaniline grafted polyacrylonitrile conductive composite membrane. *Bioresource Technology* **101,** 6881-6887.

Belay A, Collins A, Ruzgas T, T. Kissinger P, Gorton L & Csöregi E. (1999). Redox hydrogel based bienzyme electrode for l-glutamate monitoring. *Journal of Pharmaceutical and Biomedical Analysis* **19,** 93-105.

Berners MOM, Boutelle MG & Fillenz M. (1994). Online Measurement of Brain Glutamate with an Enzyme/Polymer-Coated Tubular Electrode. *Analytical Chemistry* **66,** 2017-2021.

Bernfeld P & Wan J. (1963). Antigens and Enzymes Made Insoluble by Entrapping Them into Lattices of Synthetic Polymers. *Science* **142,** 678-679.

Bolger FB. (2007). The *In-Vitro* and *In-Vivo* Characterisation and Application of Real-Time Sensors and Biosensors for Neurochemical Studies of Brain Energy Metabolism. National University of Ireland, Maynooth, Maynooth.

Brady D & Jordaan J. (2009). Advances in enzyme immobilisation. *Biotechnology Letters* **31,** 1639-1650.

Burmeister JJ, Palmer M & Gerhardt GA. (2003). Ceramic-based multisite microelectrode array for rapid choline measures in brain tissue. *Analytica Chimica Acta* **481,** 65-74.

Costa SA, Tzanov T, Filipa Carneiro A, Paar A, Gübitz GM & Cavaco-Paulo A. (2002). Studies of stabilization of native catalase using additives. *Enzyme and Microbial Technology* **30,** 387-391.

de Melo JV, Bello ME, de Azevêdo WM, de Souza JM & Diniz FB. (1999). The effect of glutaraldehyde on the electrochemical behavior of polyaniline. *Electrochimica Acta* **44,** 2405-2412.

Doleman BJ & Lewis NS. (2001). Comparison of odor detection thresholds and odor discriminablities of a conducting polymer composite electronic nose versus mammalian olfaction. *Sensors and Actuators B: Chemical* **72,** 41-50.

Doretti L, Ferrara D, Gattolin P & Lora S. (1996). Covalently immobilized enzymes on biocompatible polymers for amperometric sensor applications. *Biosensors and Bioelectronics* **11,** 365-373.

Garguilo MG & Michael AC. (1993). An enzyme-modified microelectrode that detects choline injected locally into brain tissue. *Journal of the American Chemical Society* **115,** 12218-12219.

Garguilo MG & Michael AC. (1994). Quantitation of Choline in the Extracellular Fluid of Brain Tissue with Amperometric Microsensors. *Analytical Chemistry* **66,** 2621-2629.

Hall CE, Datta D & Hall EAH. (1996). Parameters which influence the optimal immobilisation of oxidase type enzymes on methacrylate copolymers as demonstrated for amperometric biosensors. *Analytica Chimica Acta* **323,** 87-96.

Hart AL & Collier WA. (1998). Stability and function of screen printed electrodes, based on cholinesterase, stabilised by a co-polymer/ sugar alcohol mixture. *Sensors and Actuators B: Chemical* **53,** 111-115.

Holt DB, Gauger PR, Kusterbeck AW & Ligler FS. (2002). Fabrication of a capillary immunosensor in polymethyl methacrylate. *Biosensors and Bioelectronics* **17,** 95-103.

Ikarashi Y, Takahashi A, Ishimaru H, Arai T & Maruyama Y. (1997). Relations between the extracellular concentrations of choline and acetylcholine in rat striatum. *Journal of Neurochemistry* **69,** 1246-1251.

Isabelle Migneault CD, Michel J. Bertrand, and Karen C. Waldron. (2004). Glutaraldehyde behavior in aqueous solution, reaction with proteins, and application to enzyme crosslinking. *BioTechniques* **37,** 790-802.

Jezkova J, Iwuoha EI, Smyth MR & Vytras K. (1997). Stabilization of an osmium bis-bipyridyl polymer-modified carbon paste amperometric glucose biosensor using polyethyleneimine. *Electroanalysis* **9,** 978-984.

Kehr J, Dechent P, Kato T & Ögren SO. (1998). Simultaneous determination of acetylcholine, choline and physostigmine in microdialysis samples from rat hippocampus by microbore liquid chromatography/electrochemistry on peroxidase redox polymer coated electrodes. *Journal of Neuroscience Methods* **83,** 143-150.

Koppen A, Klein J, Erb C & Loffelholz K. (1997). Acetylcholine release and choline availability in rat hippocampus: effects of exogenous choline and nicotinamide. *Journal of Pharmacology and Experimental Therapeutics* **282,** 1139-1145.

Kumada Y, Kuroki D, Yasui H, Ohse T & Kishimoto M. (2010). Characterization of polystyrene-binding peptides (PS-tags) for site-specific immobilization of proteins. *Journal of Bioscience and Bioengineering* **109,** 583-587.

Lawler HC. (1961). Turnover time of acetylcholinesterase. *Journal of Biological Chemistry* **236,** 2296-2301.

Li Y-G, Zhou Y-X, Feng J-L, Jiang Z-H & Ma L-R. (1999). Immobilization of enzyme on screen-printed electrode by exposure to glutaraldehyde vapour for the construction of amperometric acetylcholinesterase electrodes. *Analytica Chimica Acta* **382,** 277-282.

Lowry JP & O'Neill RD. (1994). Partial Characterization *In-Vitro* of Glucose Oxidase-Modified Poly(phenylenediamine)-coated electrodes for neurochemical analysis *In-Vivo*. *Electroanalysis* **6,** 369-379.

Malitesta C, Palmisano F, Torsi L & Zambonin PG. (1990). Glucose fast-response amperometric sensor based on glucose oxidase immobilized in an electropolymerized poly(*o*-phenylenediamine) film. *Analytical Chemistry* **62,** 2735-2740.

McMahon CP, Rocchitta G, Kirwan SM, Killoran SJ, Serra PA, Lowry JP & O'Neill RD. (2007). Oxygen tolerance of an implantable polymer/enzyme composite glutamate biosensor displaying polycation-enhanced substrate sensitivity. *Biosensors and Bioelectronics* **22,** 1466-1473.

McMahon CP, Rocchitta G, Serra PA, Kirwan SM, Lowry JP & O'Neill RD. (2006). The efficiency of immobilised glutamate oxidase decreases with surface enzyme loading: an electrostatic effect, and reversal by a polycation significantly enhances biosensor sensitivity. *Analyst* **131,** 68-72.

Nakamura A, Suzuki Y, Umegaki H, Ikari H, Tajima T, Endo H & Iguchi A. (2001). Dietary restriction of choline reduces hippocampal acetylcholine release in rats: *In-Vivo* microdialysis study. *Brain Research Bulletin* **56,** 593-597.

Payne JW. (1973). Polymerization of Proteins with Glutaraldehyde. *Journal of Biochemistry* **135,** 867-873.

Pérez JPH, López-Cabarcos E & López-Ruiz B. (2006). The application of methacrylate-based polymers to enzyme biosensors. *Biomolecular Engineering* **23,** 233-245.

Reybier K, Zairi S, Jaffrezic-Renault N & Fahys B. (2002). The use of polyethyleneimine for fabrication of potentiometric cholinesterase biosensors. *Talanta* **56,** 1015-1020.

Rothwell SA, Killoran SJ & O'Neill RD. (2010). Enzyme Immobilization Strategies and Electropolymerization Conditions to Control Sensitivity and Selectivity Parameters of a Polymer-Enzyme Composite Glucose Biosensor. *Sensors* **10,** 6439-6462.

Ryan M, Lowry J & O'Neill R. (1997). Biosensor for Neurotransmitter L-Glutamic Acid Designed for Efficient Use of L-Glutamate Oxidase and Effective Rejection of Interference. *Analyst* **122,** 1419-1424.

Sassolas A, Blum LJ & Leca-Bouvier BD. (2012). Immobilization strategies to develop enzymatic biosensors. *Biotechnology Advances* **30,** 489-511.

Schulz B, Riedel A & Abel PU. (1999). Influence of polymerization parameters and entrapment in poly(hydroxyethyl methacrylate) on activity and stability of GOD. *Journal of Molecular Catalysis B: Enzymatic* **7,** 85-91.

Teles FRR & Fonseca LP. (2008). Applications of polymers for biomolecule immobilization in electrochemical biosensors. *Materials Science and Engineering: C* **28,** 1530-1543.

Tripathi G. (2009). *Enzyme Biotechnology*. ABD Publishers, Jaipur, India

Tsai Y-C, Chen S-Y & Liaw H-W. (2007). Immobilization of lactate dehydrogenase within multiwalled carbon nanotube-chitosan nanocomposite for application to lactate biosensors. *Sensors and Actuators B: Chemical* **125,** 474-481.

Wang J. (2001). Glucose Biosensors: 40 Years of Advances and Challenges. *Electroanalysis* **13,** 983-988.

Wilson GS & Thévenot DR. (1990). *Unmediated Amperometric Enzyme Electrodes*. IRL Press at Oxford University Press, United States.

5. Oxygen Dependence

5.1. Introduction

As a 'first generation biosensor', this sensor relies on the enzymatic process which involves the catalysis of the oxidation of choline to glycine betaine with betaine aldehyde as an intermediate and molecular oxygen as the primary electron acceptor (Hekmat *et al.*, 2008).

$$\begin{aligned}&(CH_3)_3N^+-(CH_2)_2-OH+2O_2+H_2O\xrightarrow{ChOx}\\&(CH_3)_3N-CH_2-COOH+2H_2O_2\end{aligned}$$

A limitation of first generation biosensors, is that changes in O_2 concentration may cause interference in the choline response (Dixon *et al.*, 2002). Therefore, one criteria to which a biosensor must adhere, is a low sensitivity to changes in oxygen over the range of substrate and oxygen concentrations relevant to the intended application (McMahon *et al.*, 2006). The application of *in-vivo* monitoring where pO_2 can fluctuate, highlights the relevance of oxygen interference studies for biosensor functionality (McMahon *et al.*, 2007a) (Bolger & Lowry, 2005) as the reported normal oxygen concentrations throughout the brain vary between 30 and 80 µM (Bolger & Lowry, 2005). One approach to overcome this is the development of 'second generation biosensors' which replaces oxygen with an artificial mediator (Di Gleria *et al.*, 1986). The mediator acts as an artificial electron acceptor (Chaubey & Malhotra, 2002). The development of a choline biosensor using a different type of mediated system by Garguilo *et al*. has been reported which incorporates the immobilisation of choline oxidase and horseradish peroxidise by a cross-linkable redox polymer (Gregg & Heller, 1991) which mediates electron transfer between horse radish peroxidise and the electrode (Garguilo & Michael, 1993). Although the use of mediators may aid in oxygen dependence of biosensors they suffer from leaching of the untethered mediator from the enzyme layer (McMahon *et al.*, 2007a), toxicity in biological tissues (Beh *et al.*, 1991) and the insensitivity to oxygen interference has been questioned for certain mediators (Martens & Hall, 1994). An alternative to the second generation biosensor is the use of fluorochemical pasting liquids, with high O_2 solubility, within carbon paste electrodes. Studies by Wang *et al.* have demonstrated the advantage of a poly(chlorotrifluorethylene) (Kel-F) based carbon paste glucose biosensor compared to both conventional and mediator based carbon paste glucose biosensors, on oxygen demand to successfully eliminate the effect of O_2 dependence of the glucose biosensor (Wang & Lu, 1998). Further work by this group, has highlighted the use of a variety of fluorocarbon oils for their internal oxygen supply in carbon paste glucose biosensors (Wang *et al.*, 2000).

5.2. Experimental

All instrumentation and software used in this section are described in Section 3.2. All chemicals and solutions used are described in Section 3.3. The electrodes were constructed from disk and 1 mm cylinder electrodes as described in Section 3.4.1. The design and manufacture of these designs are explained in detail in Section 3.4.2.1.

All data was recorded using the cell setup described in Section 3.5.1.1. The calibrations were performed as described in Section 3.5.1.6. The data is reported as mean ± SEM where n denotes the number of electrodes used. Normalised data is presented as a percentage of the I_{MAX}.

5.3. Results and Discussion

This section demonstrates the investigation into the design modification of the choline biosensor in order to decrease the level of O_2 dependence of the sensor. This section also investigates experimental designs in order to accurately determine the level of O_2 dependence of the biosensor.

5.3.1. Oxygen Dependence

This section will aim to determine the level of oxygen dependence of the biosensors described in Chapter 4; Sty-(ChOx)(BSA)(GA)(PEI) and MMA-(ChOx)(BSA)(GA)(PEI). The physiologically relevant concentration range of choline has been reported to be between 0 and 100 µM (Garguilo & Michael, 1995). As previous oxygen dependence studies on a glucose biosensor has illustrated that the level of O_2 dependence increases with increasing substrate concentration (Dixon *et al.*, 2002) 100 µM choline concentration was chosen for these experiments to accommodate fluctuations in choline concentration *in-vivo*. The O_2 dependence experimental design is similar to that utilised by McMahon *et al* (McMahon *et al.*, 2007b) (McMahon & O'Neill, 2005). Oxygen sensor and biosensor data were recorded simultaneously. The electrochemical cell was filled with N_2 and the electrodes allowed to settle to a steady background. After adding an aliquot of 100 µM choline under a N_2 cloud, the N_2 source was removed and air was slowly introduced into the system (see Section 3.5.1.6). All individual calibrations and raw data is presented in Appendix 2.

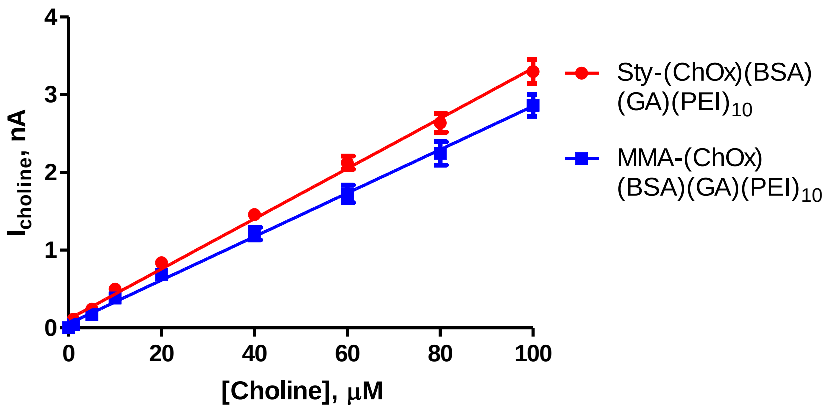

	Sty-(ChOx)(BSA)(GA)(PEI)$_{10}$			MMA-(ChOx)(BSA)(GA)(PEI)$_{10}$		
Choline Conc, µM	**Mean, nA**	**S.E.M, nA**	**n**	**Mean, nA**	**S.E.M, nA**	**n**
0	0.00	0.00	11	0.00	0.00	8
5	0.24	0.02	11	0.17	0.03	8
10	0.50	0.03	11	0.38	0.04	8
20	0.84	0.04	11	0.69	0.05	8
40	1.46	0.07	11	1.21	0.08	8
60	2.13	0.08	11	1.72	0.11	8
80	2.64	0.12	11	2.25	0.15	8
100	3.30	0.15	11	2.87	0.14	8

Figure 5.1 : The current-concentration profile comparison and comparison table for choline chloride calibration in PBS (pH 7.4) buffer solution at 21°C using design (A) Sty-(ChOx)(BSA)(GA)(PEI)$_{10}$ and (B) MMA-(ChOx)(BSA)(GA)(PEI)$_{10}$. CPA carried out at +700 mV *vs*. SCE. Sequential current steps for 5, 10, 20, 40, 60, 80, 100 µM choline chloride injections.

A comparison graph and comparison data table for the choline sensitivity of the designs Sty-(ChOx)(BSA)(GA)(PEI)$_{10}$ and MMA-(ChOx)(BSA)(GA)(PEI)$_{10}$ are presented in Figure 5.1. A comparison of the $I_{100\ \mu M}$ values show that the styrene design has obtained the higher sensitivity with a current of 3.30 ± 0.15 nA, n = 11 and the MMA design has a slightly reduced current of 2.87 ± 0.14 nA, n = 8. Current plays an important role in O_2 dependence as the more O_2 required by the sensor to generate the enzymatic reaction, the more O_2 dependent the sensor. As this is the case, the difference in sensitivity may be an important factor for the O_2 dependence studies.

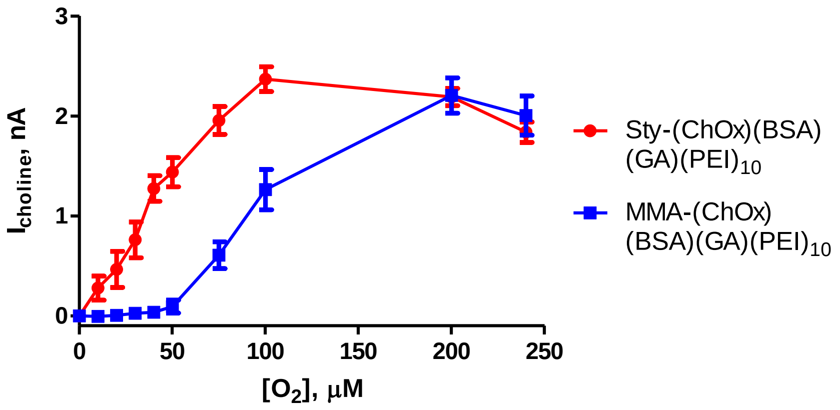

	Sty-(ChOx)(BSA)(GA)(PEI)$_{10}$			MMA-(ChOx)(BSA)(GA)(PEI)$_{10}$		
O_2 Conc, µM	Mean, nA	S.E.M, nA	n	Mean, nA	S.E.M, nA	n
0	0.00	0.00	11	0.00	0.00	8
10	0.27	0.12	11	-0.01	0.01	8
20	0.46	0.18	11	0.004	0.018	8
30	0.76	0.18	11	0.03	0.03	8
40	1.27	0.13	11	0.04	0.04	7
50	1.44	0.15	11	0.09	0.07	8
75	1.96	0.14	11	0.61	0.13	8
100	2.37	0.12	11	1.26	0.20	8
200	2.19	0.09	11	2.20	0.18	8
240	1.84	0.10	11	2.00	0.20	8

Figure 5.2 : The choline current-oxygen concentration profile comparison and comparison table for calibration in PBS (pH 7.4) buffer solution at 21°C using designs (A) Sty-(ChOx)(BSA)(GA)(PEI)$_{10}$ and (B) MMA-(ChOx)(BSA)(GA)(PEI)$_{10}$. CPA carried out at +700 mV *vs*. SCE for choline electrodes and -650 mV *vs*. SCE. Current values for 100 µM choline chloride injection at 10, 20, 30, 40, 50, 75, 100, 200, 240 µM O_2 concentrations.

A comparison graph and comparison data table for the designs Sty-(ChOx)(BSA)(GA)(PEI)$_{10}$ and MMA-(ChOx)(BSA)(GA)(PEI)$_{10}$ is presented in Figure 5.2. The data presented shows the effect of changing the dissolved O_2 concentration in the PBS on the current response of the electrode in the presence of 100 µM choline. The data above illustrates the vast difference in the O_2 dependence of the two designs. A comparison of the choline current at three physiologically relevant O_2 concentrations of 30, 50 and 75 µM O_2 demonstrates the fluctuation in choline detection in the *in-vivo* environment. The O_2 dependence graph for the styrene design shows a linear relationship between the choline current and the O_2 concentration until the graph plateau's at 100 µM O_2. In contrast, the O_2 dependence graph for the MMA design illustrates the inability for the enzyme to turn over the substrate at O_2 concentrations below 50 µM. The substrate turnover then increases linearly until the plateau at 200 µM O_2. For the styrene design, the choline current obtained at 30 µM O_2 is 0.76 ± 0.18 nA, n = 11, this choline current increases to 1.44 ± 0.15 nA, n = 11 with an increase in O_2 concentration to 50 µM. At 75µM O_2 the choline current is further increased to 1.96 ± 0.14 nA, n = 11. An I_{MAX} of

2.37 ± 0.12 nA, n = 11 is reached at 100 µM O_2. The choline current at 30 µM O_2 represents 30.19 ± 6.79 % of the I_{MAX} current, meanwhile 50 µM is 57.90 ± 5.01 % and 75 µM is 78.61 ± 3.86 %. The potential fluctuation in choline current as a result of the fluctuation in O_2 concentration between 30 and 75 µM in the *in-vivo* environment, suggest that the sensor would be subject to oxygen interference of 48 % once implanted. The MMA based choline sensor obtained a choline current of 0.03 ± 0.03 nA, n = 8 for 30 µM O_2, 0.09 ± 0.07 nA, n = 8 for 50 µM O_2 and 1.26 ± 0.20 nA, n = 8 for 75 µM O_2. The I_{MAX} of 2.20 ± 0.19 nA, n = 8 was obtained at 200 µM O_2. The choline current at 30 µM choline represents 0.83 ± 0.93 % of the I_{MAX} current, in addition 50 µM represents 3.10 ± 2.20 % and 75 µM is 28.98 ± 7.82 %. This data illustrates that the enzymatic reaction at this sensor would be severely hindered at these physiological concentrations, and may be unable to function entirely in the presence of the lower O_2 concentrations.

Both the styrene and MMA based sensor designs have illustrated varying degrees of oxygen dependence. As this is the case neither sensor can be utilised in the *in-vivo* environment. The following studies were undertaken in order to reduce the oxygen interference of these sensors within the physiological O_2 concentration range.

5.3.2. Nafion® incorporation

Clark and Gollen first demonstrated the ability of liquid perfluorocarbons (PFC's) to support animal life by the submersion of mice that continued to live by breathing the liquid (Clark & Gollan, 1966). Perfluorocarbons have high degrees of oxygen solubility (Wang & Lu, 1998), with gas solubility in PFC's being increased by a factor of at least 20 when compared to water (Riess & Le Blanc, 1982). As a result of this, perfluorocarbons have been utilised in many fields. For example, perfluorocarbons have been utilised for aerobic fermentation in antibiotic production where oxygen is the limiting factor. The cells are immobilised onto perfluorocarbons in order to increase the available oxygen to increase antibiotic concentration (Elibol & Mavituna, 1996). Perfluorocarbons have also been utilised to increase the larval growth of the nematode *C. elegans*, as overcrowding in the standard growth medium, depletes the available oxygen and the worm's growth is slowed. The use of the oxygenated perfluorocarbon therefore promotes the nematode growth (Jewitt *et al.*, 1999). The use of perfluorocarbons has also demonstrated potential for heart preservation when removed from a non-heart-beating donor for the purpose of thoracic transplantation. The PFC has the potential to protect the hypoxic donor heart, this would allow for expansion of the donor pool to non-heart-beating donors at a time where there is high demand for organs (Scheule *et al.*, 2000). As previously discussed in Section 5.1, the availability of oxygen at the biosensor surface is crucial for the enzymatic process to occur. As the oxygen concentration of the brain is approximately 5 times lower than that of the *in-vitro* environment, work has been done to use fluorocarbons to aid in biosensor operation. Fluorocarbon pasting liquids have been incorporated into carbon paste to overcome the oxygen dependence of a glucose biosensor (Wang & Lu, 1998). Nafion® is a perfluorinated polymer (Brown & Lowry, 2003) generated from the copolymerisation of a perfluorinated vinyl ether comonomer with tetrafluoroethylene (Mauritz & Moore, 2004). The use of Nafion® within a styrene matrix has been successfully utilised in a lactate biosensor design to overcome O_2 dependence (Bolger, 2007). This chapter will attempt to use Nafion® in the choline biosensor design and determine if Nafion® can be used to alleviate O_2 dependence and if it is due to the O_2 solubility of the polymer. Here, Nafion® was added into the styrene monomer in concentrations of 0.5% and 1%. This was undertaken as potentially the Nafion® would have a high level of solubilised oxygen which will be available to the enzyme which is immobilised on the styrene layer.

5.3.2.1. Styrene

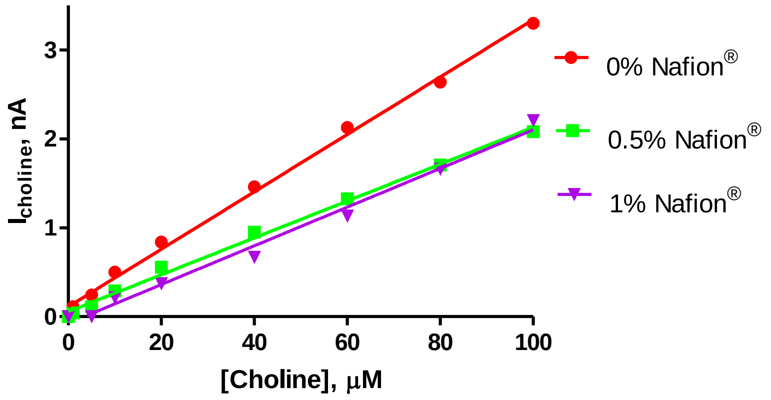

	0% Nafion®			0.5% Nafion®			1% Nafion®		
Choline Conc, μM	**Mean, nA**	**S.E.M, nA**	**n**	**Mean, nA**	**S.E.M, nA**	**n**	**Mean, nA**	**S.E.M, nA**	**n**
0	0.00	0.00	11	0.00	0.00	9	0.00	0.00	3
5	0.24	0.02	11	0.11	0.01	9	0.002	0.002	3
10	0.50	0.03	11	0.29	0.02	9	0.22	0.030	3
20	0.84	0.04	11	0.54	0.05	9	0.37	0.05	3
40	1.46	0.07	11	0.94	0.09	9	0.67	0.09	3
60	2.13	0.08	11	1.31	0.13	9	1.14	0.12	3
80	2.64	0.12	11	1.69	0.18	9	1.66	0.13	3
100	3.30	0.15	11	2.07	0.20	9	2.21	0.16	3

Figure 5.3 : The current-concentration profile comparison and comparison table for choline chloride calibration in PBS (pH 7.4) buffer solution at 21°C using designs (A) 0% Nafion®, (B) 0.5% Nafion® and (C) 1% Nafion®. CPA carried out at +700 mV *vs*. SCE. Sequential current steps for 5, 10, 20, 40, 60, 80, 100 μM choline chloride injections.

A comparison graph and comparison data table for the choline sensitivity of the designs 0%, 0.5% and 1% Nafion® are presented in Figure 5.3. The addition of Nafion® has decreased the choline sensitivity in both concentrations of 0.5% and 1%. A comparison of the $I_{100\ \mu M}$ values show that the incorporation of Nafion® had a detrimental effect on the choline current. The addition of 0.5% Nafion® reduced the current from 3.30 ± 0.15 nA, n = 11 (0% Nafion®) to 2.07 ± 0.20 nA, n = 9 (0.5% Nafion®). Increasing the Nafion® concentration to 1% also decreased the concentration from 3.30 ± 0.15 nA, n =

11 (0% Nafion®) to 2.21 ± 0.16 nA, n = 3 (1% Nafion®). As stated previously, the current plays a role in oxygen dependence of biosensors as they will require the availability of less oxygen. Therefore, the reduction in current observed may serve to alleviate O_2 dependence.

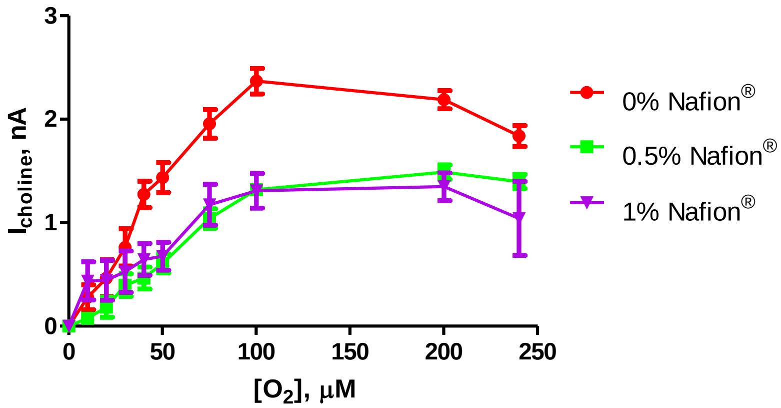

	0% Nafion®			0.5% Nafion®			1% Nafion®		
O_2 Conc, μM	**Mean, nA**	**S.E.M, nA**	**n**	**Mean, nA**	**S.E.M, nA**	**n**	**Mean, nA**	**S.E.M, nA**	**n**
0	0.00	0.00	11	0.00	0.00	9	0.00	0.00	3
10	0.27	0.12	11	0.08	0.05	9	0.44	0.18	3
20	0.46	0.18	11	0.18	0.10	9	0.44	0.19	3
30	0.76	0.18	11	0.40	0.11	9	0.53	0.20	3
40	1.27	0.13	11	0.46	0.11	9	0.64	0.15	3
50	1.44	0.15	11	0.61	0.09	9	0.68	0.14	3
75	1.96	0.14	11	1.04	0.09	9	1.17	0.20	3
100	2.37	0.12	11	1.32	0.06	9	1.31	0.17	3
200	2.19	0.09	11	1.55	0.08	9	1.35	0.13	3
240	1.84	0.10	11	1.40	0.07	9	1.04	0.36	2

Figure 5.4 : The choline current-oxygen concentration profile comparison and comparison table for calibration in PBS (pH 7.4) buffer solution at 21°C using designs (A) 0% Nafion®, (B) 0.5% Nafion® and (C) 1% Nafion®. CPA carried out at +700 mV *vs.* SCE for choline electrodes and -650 mV *vs.* SCE. Current values for 100 μM choline chloride injection at 10, 20, 30, 40, 50, 75, 100, 200, 240 μM O_2 concentrations.

A comparison graph and comparison data table for the designs 0%, 0.5% and 1% Nafion® for the choline current at varying O_2 concentrations is presented in Figure 5.4.

The data above illustrates the effect of the addition of Nafion® within the styrene monomer on O_2 dependence. The data presented also shows the effect of changing the dissolved O_2 concentration in the PBS on the current response of the electrode in the presence of 100 µM choline. The reduction in sensitivity of the design results in a reduced current at the plateau compared to the 0% Nafion® design. The O_2 dependence trace for the 0% Nafion® and the 0.5% Nafion® designs show a linear relationship between the choline response and the O_2 concentration. The 0% Nafion® design plateaus at 100 µM O_2 and the 0.5% Nafion® design plateaus at 200 µM O_2 concentration. The incorporation of the 1% Nafion® demonstrates an increase in the substrate turnover at the lower O_2 concentrations. A high choline current is observed at 5 µM O_2 with a linear relationship between choline current and O_2 concentration observed thereafter and a plateau in the current at 100 µM O_2. A comparison of the choline current at three physiological concentrations 30, 50 and 75 µM O_2 demonstrates the fluctuation in choline detection in the *in-vivo* environment.

For the 0% Nafion® design, the choline current obtained at 30 µM O_2 is 0.76 ± 0.18 nA, n = 11, this choline current increases to 1.44 ± 0.15 nA, n = 11 with an increase in O_2 concentration to 50 µM. At 75µM O_2 the choline current is further increased to 1.96 ± 0.14 nA, n = 11. An I_{MAX} of 2.37 ± 0.12 nA, n = 11 is reached at 100 µM O_2. The choline current at 30 µM O_2 represents 30.19 ± 6.79 % of the I_{MAX} current, meanwhile 50 µM is 57.90 ± 5.01 % and 75 µM is 78.61 ± 3.86 %. The potential fluctuation in choline current as a result in the fluctuation of O_2 concentration between 30 and 75 µM in the *in-vivo* environment, suggests that the sensor would be subject to oxygen interference once implanted. The 0.5% Nafion® design obtained a choline current of 0.40 ± 0.11 nA, n = 9 for 30 µM O_2, 0.61 ± 0.09 nA, n = 9 for 50 µM O_2 and 1.04 ± 0.09 nA, n = 9 for 75 µM O_2. The I_{MAX} of 1.55 ± 0.08 nA, n = 9 was obtained at 200 µM O_2. The choline current at 30 µM choline represents 26.33 ± 7.47 % of the I_{MAX} current, in addition 50 µM represents 40.65 ± 6.93 % and 75 µM is 68.67 ± 7.43 %. This data illustrates that the enzymatic reaction at this sensor would be hindered at these physiological O_2 concentrations. A comparison of the addition of 0.5% Nafion®, illustrates that in addition to lowering the current response obtained, the percentage values representing the choline current at the physiological O_2 concentrations is also reduced. This demonstrates that the reduced current does not decrease O_2 independence.

At 30 µM O_2 the percentage choline current of the I_{MAX} is reduced from 30.19 ± 6.79 % (0% Nafion®) to 26.33 ± 7.47 % (0.5% Nafion®). At 50 µM the percentage is reduced from 57.90 ± 5.01 % (0% Nafion®) to 40.65 ± 6.93 % (0.5% Nafion®) and at 75µM the percentage is reduced from 78.61 ± 3.86 % (0% Nafion®) to 68.67 ± 7.43 % (0.5% Nafion®). This comparison illustrates that the addition of 0.5% Nafion® has reduced the O_2 dependence of the sensor despite the reduction in sensitivity. The 1% Nafion® design obtained a choline current of 0.53 ± 0.20 nA, n = 3 for 30 µM O_2, 0.68 ± 0.14 nA, n = 3 for 50 µM O_2 and 1.17 ± 0.20 nA, n = 3 for 75 µM O_2. The I_{MAX} of 1.35 ± 0.13 nA, n = 3 was obtained at 200 µM O_2. The choline current at 30 µM choline represents 35.51 ± 11.31 % of the I_{MAX} current, in addition 50 µM represents 47.04 ± 9.25 % and 75 µM is 80.79 ± 10.88 %. These percentage values are comparable with the values obtained in the 0% Nafion® design. At 30 µM O_2 the percentage choline current of the I_{MAX} is increased from 30.19 ± 6.79 % (0% Nafion®) to 35.51 ±11.31 % (1% Nafion®). At 50 µM the percentage is reduced from 57.90 ± 5.01 % (0% Nafion®) to 47.04 ± 9.25 % (1% Nafion®) and at 75µM the percentage is reduced from 78.61 ± 3.86 % (0% Nafion®) to 80.79 ± 10.88 % (1% Nafion®). Although these values illustrate that increasing the Nafion® concentration to 1% Nafion® can have a positive effect on the oxygen dependence when compared to 0.5%, the values are not as high as the original design which did not incorporate Nafion®. In addition, the choline current was reduced with the incorporation of 1% Nafion® which did not aid the O_2 dependence. As this is the case the incorporation of Nafion® has not proved advantageous for the styrene based choline biosensor with respect to oxygen dependence.

5.3.2.2. MMA

The following experiments were carried out in order to investigate if the addition of Nafion® within the MMA polymer would aid the oxygen dependence of the sensor. In addition, it was also considered if the use of an alternate polymer would present different results due to a different interaction with the Nafion®. The incorporation of 0%, 0.5%, 1% and 1.5% Nafion® was investigated.

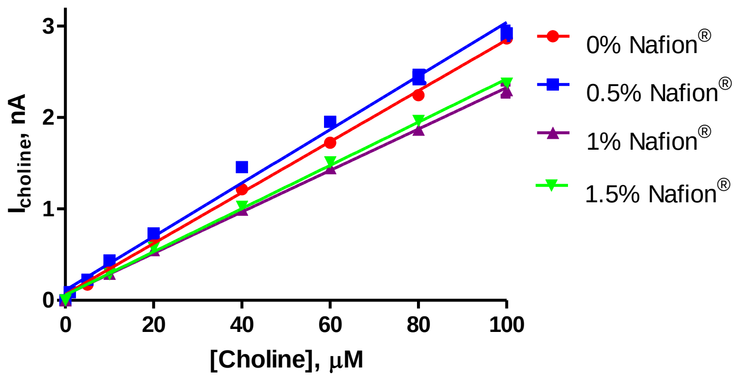

	0% Nafion®			0.5% Nafion®			1% Nafion®			1.5% Nafion®		
Choline Conc, µM	**Mean, nA**	**S.E.M, nA**	**n**	**Mean, nA**	**S.E.M, nA**	**n**	**Mean, nA**	**S.E.M, nA**	**n**	**Mean, nA**	**S.E.M, nA**	**n**
0	0.00	0.00	8	0.00	0.00	9	0.00	0.00	9	0.00	0.00	9
10	0.38	0.04	8	0.44	0.03	9	0.28	0.03	9	0.29	0.01	9
20	0.69	0.05	8	0.73	0.05	9	0.53	0.05	9	0.57	0.03	9
40	1.21	0.08	8	1.46	0.16	9	0.95	0.09	9	1.03	0.05	9
60	1.72	0.11	8	1.95	0.18	9	1.39	0.14	9	1.51	0.08	9
80	2.25	0.15	8	2.44	0.19	9	1.79	0.17	9	1.97	0.11	9
100	2.87	0.14	8	2.92	0.21	9	2.20	0.20	9	2.37	0.13	9

Figure 5.5 : The current-concentration profile comparison and comparison table for choline chloride calibration in PBS (pH 7.4) buffer solution at 21°C using designs (A) 0% Nafion®, (B) 0.5% Nafion®, (C) 1% Nafion® and (D) 1.5% Nafion®. CPA carried out at +700 mV *vs.* SCE. Sequential current steps for 10, 20, 40, 60, 80, 100 µM choline chloride injections.

A comparison graph and comparison data table for the choline sensitivity of the designs 0%, 0.5%, 1% and 1.5% Nafion® are presented in Figure 5.5. Initially, the effect of the incorporation of Nafion® within the polymer was determined with respect to sensitivity. Low concentrations of Nafion® did not have a detrimental effect on sensitivity, however as the concentration of the Nafion® was increased, the sensitivity was reduced. A comparison of the $I_{100\ \mu M}$ current values show that the incorporation of 0.5% Nafion® does not have a detrimental effect on the choline current as seen previously with the styrene based design. The addition of Nafion® 0.5% increased the current from 2.87 ± 0.14 nA, n = 8 (0% Nafion®) to 2.92 ± 0.21 nA, n = 9 (0.5% Nafion®). Increasing the

Nafion® concentration to 1% however did decrease the concentration from 2.87 ± 0.14 nA, n = 8 (0% Nafion®) to 2.20 ± 0.20 nA, n = 9 (1% Nafion®). However the incorporation of 1.5% Nafion® only decreased the current from 2.87 ± 0.14 nA, n = 8 (0% Nafion®) to 2.37 ± 0.13 nA, n = 9 (1.5% Nafion®). The minimal decrease in current with the addition of 0.5% Nafion® using the MMA polymer may prove advantageous for future oxygen dependence studies and illustrates the benefit of the comparison of designs with different polymer bases.

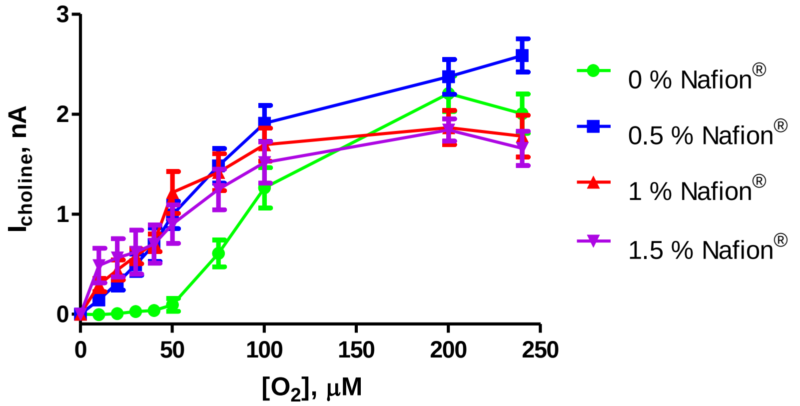

	0% Nafion®			0.5% Nafion®			1% Nafion®			1.5% Nafion®		
O_2 Conc, µM	Mean, nA	S.E.M, nA	n	Mean, nA	S.E.M, nA	n	Mean, nA	S.E.M, nA	n	Mean, nA	S.E.M, nA	n
0	0.00	0.00	8	0.00	0.00	9	0.00	0.00	9	0.00	0.00	9
10	-0.01	0.01	8	0.14	0.06	9	0.29	0.07	9	0.49	0.17	9
20	0.004	0.018	8	0.31	0.07	9	0.44	0.10	9	0.56	0.19	9
30	0.03	0.03	8	0.49	0.11	9	0.58	0.07	9	0.62	0.22	9
40	0.04	0.04	7	0.69	0.17	9	0.71	0.09	9	0.70	0.19	9
50	0.09	0.07	8	0.99	0.14	9	1.22	0.21	9	0.90	0.19	9
75	0.61	0.13	8	1.48	0.17	9	1.42	0.19	9	1.25	0.20	9
100	1.26	0.20	8	1.91	0.18	9	1.69	0.17	9	1.52	0.21	9
200	2.20	0.18	8	2.37	0.17	9	1.87	0.17	9	1.84	0.11	8
240	2.00	0.20	8	2.59	0.17	9	1.78	0.21	9	1.66	0.17	9

Figure 5.6 : The choline current-oxygen concentration profile comparison and comparison table for calibration in PBS (pH 7.4) buffer solution at 21°C using design (A) 0% Nafion®, (B) 0.5% Nafion® (C) 1% Nafion® and (D) 1.5% Nafion®. CPA carried out at +700 mV *vs.* SCE. Current values for 100 µM choline chloride injection at 10, 20, 30, 40, 50, 75, 100, 200, 240 µM O_2 concentrations.

The comparison in Figure 5.6 illustrates the difference in the level of O_2 dependence for the designs. The data presented shows the effect of changing the dissolved O_2 concentration in the PBS on the current response of the electrode in the presence of 100 µM choline. The addition of the Nafion® into the MMA has clearly decreased the level of O_2 dependence of the MMA sensor. In the absence of the Nafion® the sensor is unable to turn over the substrate in the presence of less than 50 µM O_2. The addition of 0.5% Nafion® introduced a linear relationship between the choline current and the O_2 concentration which reached a plateau at 240 µM O_2. Increasing the concentration of Nafion® from 0.5% to 1% increased the amount of substrate turnover at the equivalent O_2 concentrations, thus leading to an increase in choline current for each O_2 concentration which reached a plateau at 200 µM O_2. Increasing the Nafion® concentration further to 1.5% again increased the current values at each O_2 concentration however maintaining the plateau at 200 µM O_2.

A comparison of the choline current at three physiological concentrations 30, 50 and 75 µM O_2 demonstrates the fluctuation in choline detection in the *in-vivo* environment. For the 0% Nafion® design, the choline current obtained at 30 µM O_2 is 0.03 ± 0.03 nA, n = 8, this choline current increases to 0.09 ± 0.07 nA, n = 8 with an increase in O_2 concentration to 50 µM. At 75µM O_2 the choline current is further increased to 0.61 ± 0.13 nA, n = 8. An I_{MAX} of 2.20 ± 0.18 nA, n = 8 is reached at 200 µM O_2. The choline current at 30 µM choline represents 0.83 ± 0.93 % of the I_{MAX} current, in addition 50 µM represents 3.10 ± 2.20 % and 75 µM is 28.98 ± 7.82 %. The potential fluctuation in choline current as a result of the fluctuation in O_2 concentration between 30 and 75 µM in the *in-vivo* environment, suggest that the sensor would be subject to oxygen interference once implanted. The 0.5% Nafion® design obtained a choline current of 0.49 ± 0.11 nA, n = 9 for 30 µM O_2, 0.99 ± 0.14 nA, n = 9 for 50 µM O_2 and 1.48 ± 0.17 nA, n = 9 for 75 µM O_2. The I_{MAX} of 2.59 ± 0.17 nA, n = 9 was obtained at 240 µM O_2. The choline current at 30 µM choline represents 19.52 ± 4.60 % of the I_{MAX} current, in addition 50 µM represents 37.49 ± 4.77 % and 75 µM is 56.85 ± 6.88 %. This data illustrates that the enzymatic reaction at this sensor would be hindered at these physiological concentrations and subject to large fluctuations in current of 37 %. A comparison of the addition of 0.5% Nafion®, illustrates that the addition of 0.5% Nafion® has been hugely beneficial for the oxygen dependence of the sensor. At 30 µM

O_2 the percentage choline current of the I_{MAX} is increased from 0.83 ± 0.95 % (0% Nafion®) to 19.52 ± 4.60 % (0.5% Nafion®). At 50 µM the percentage is increased from 3.09 ± 2.20 % (0% Nafion®) to 37.49 ± 4.77 % (0.5% Nafion®) and at 75µM the percentage is increased from 28.98 ± 7.82 % (0% Nafion®) to 56.85 ± 6.88 % (0.5% Nafion®). This comparison illustrates that the addition of 0.5% Nafion® has been hugely beneficial to the O_2 dependence of the sensor in addition to increasing the choline current. The 1% Nafion® design obtained a choline current of 0.58 ± 0.07 nA, n = 9 for 30 µM O_2, 1.22 ± 0.21 nA, n = 9 for 50 µM O_2 and 1.69 ± 0.17 nA, n = 9 for 75 µM O_2. The I_{MAX} of 1.87 ± 0.17 nA, n = 8 was obtained at 200 µM O_2. The choline current at 30 µM choline represents 31.27 ± 3.25 % of the I_{MAX} current, in addition 50 µM represents 62.19 ± 6.25 % and 75 µM is 73.68 ± 4.00 %, this demonstrates a fluctuation of 42 %. These values are increased from the values obtained using 0.5% Nafion® and are hugely increased from the design without Nafion® however the potential fluctuations are similar. This illustrates that increasing the Nafion® concentration is maybe having a beneficial effect on oxygen dependence. It is noteworthy however, that the increase in Nafion® concentration has also decreased the choline current. The 1.5% Nafion® design obtained a choline current of 0.62 ± 0.22 nA, n = 9 for 30 µM O_2, 0.90 ± 0.19 nA, n = 9 for 50 µM O_2 and 1.25 ± 0.20 nA, n = 9 for 75 µM O_2. The I_{MAX} of 1.84 ± 0.11 nA, n = 8 was obtained at 200 µM O_2. The choline current at 30 µM choline represents 31.71 ± 10.67 % of the I_{MAX} current, in addition 50 µM represents 45.66 ± 9.34 % and 75 µM is 62.77 ± 8.96 %. These values are decreased from the values obtained using 1% Nafion®. However in the region of 10 to 40 µM O_2 the 1.5% Nafion® design obtains higher choline currents when compared with the 1% Nafion® design. This in turn may be reason for the lower current at later concentrations, due to less available choline substrate and the limitation of diffusion. As this design has higher choline currents at lower oxygen concentrations this design may prove advantageous for further oxygen dependence studies. The raw data containing an inset for the 1.5% Nafion® is presented in Appendix 2. The inset illustrates the oxygen dependence observed at the individual electrodes in which one electrode became O_2 independent almost instantaneously. It is possible that the Nafion® has provided an O_2 source for the electrode to turn over the substrate at the low O_2 concentrations. This however is not observed on all electrodes and may be as a result of the distribution of the Nafion® within the MMA polymer. Further investigation of this is undertaken in the next section.

5.3.2.3. 1.5% Nafion®

The previous section illustrated the beneficial effect the incorporation of Nafion®, within the MMA polymer, can have on the O_2 dependence of the sensor. The incorporation of 1.5% Nafion® demonstrated the potential to provide complete O_2 independence to the sensor. This however was not the case for all the electrodes of this design. This section investigates methods for incorporating Nafion® onto the electrode surface in order to provide a more uniform inclusion within the MMA polymer therefore providing a reproducible O_2 source with which the electrode can draw on in low O_2 concentrations.

This section investigates the effect of a vortexed MMA and 1.5% Nafion® solution in order to overcome any heterogeneity of the solution which may cause the non-reproducibility of the O_2 dependence.

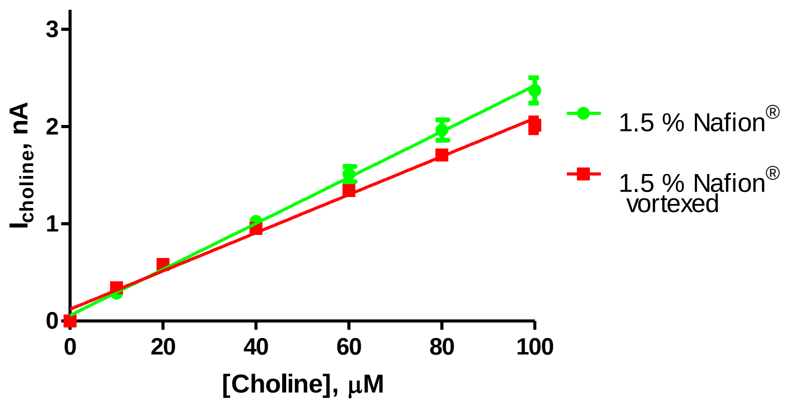

	1.5% Nafion®			1.5% Nafion® vortexed		
Choline Conc, µM	Mean, nA	S.E.M, nA	n	Mean, nA	S.E.M, nA	n
0	0.00	0.00	9	0.00	0.00	7
10	0.29	0.01	9	0.34	0.02	7
20	0.57	0.03	9	0.58	0.03	7
40	1.03	0.05	9	0.95	0.03	7
60	1.51	0.08	9	1.34	0.04	7
80	1.97	0.11	9	1.71	0.05	7
100	2.37	0.13	9	2.01	0.08	7

Figure 5.7: The current-concentration profile comparison and comparison table for choline chloride calibration in PBS (pH 7.4) buffer solution at 21°C using designs (A) 1.5% Nafion®and (B) 1.5% Nafion® vortexed. CPA carried out at +700 mV *vs*. SCE. Sequential current steps for 10, 20, 40, 60, 80, 100 µM choline chloride injections.

A comparison graph and comparison data table for the choline sensitivity of the designs 1.5% Nafion® and 1.5% Nafion® vortexed are presented in Figure 5.7. The effects of the vortexed MMA solution were determined with respect to sensitivity. Vortexing the MMA:Nafion® solution decreased sensitivity. A comparison of the $I_{100\ \mu M}$ current values show vortexing the solution of MMA and Nafion® in order to obtain a more uniform distribution of the Nafion® within the polymer decreased the current from 2.37 ± 0.13 nA, n = 9 (1.5% Nafion®) to 2.01 ± 0.08 nA, n = 7 (1.5% Nafion® vortexed) when compared with the non vortexed solution. It is possible that the distribution of the Nafion® has decreased the amount of MMA which is dip-coated onto the surface. This in turn would affect enzyme loading. Alternatively, the higher Nafion® content may denature the enzyme as it dissolved in ethanol.

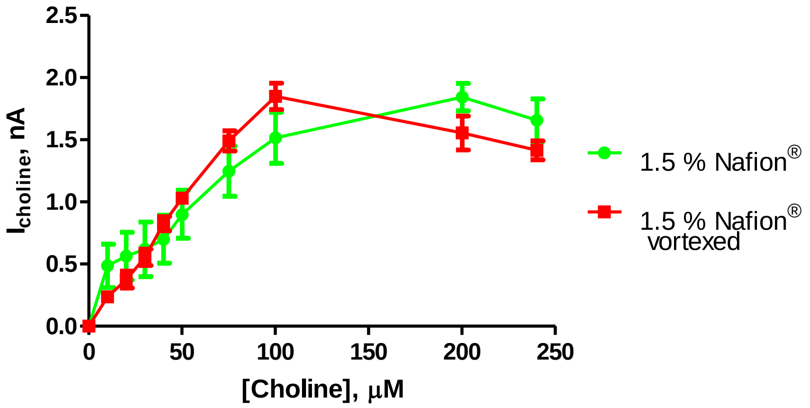

	1.5% Nafion®			1.5% Nafion® vortexed		
O_2 Conc, µM	Mean, nA	S.E.M, nA	n	Mean, nA	S.E.M, nA	n
0	0.00	0.00	9	0.00	0.00	7
10	0.49	0.17	9	0.24	0.04	7
20	0.56	0.19	9	0.38	0.07	7
30	0.62	0.22	9	0.55	0.07	7
40	0.70	0.19	9	0.83	0.06	7
50	0.90	0.19	9	1.03	0.05	7
75	1.25	0.20	9	1.49	0.08	7
100	1.52	0.21	9	1.85	0.11	7
200	1.84	0.11	8	1.55	0.14	7
240	1.66	0.17	9	1.42	0.08	7

Figure 5.8 : The choline current-oxygen concentration profile comparison and comparison table for calibration in PBS (pH 7.4) buffer solution at 21°C using design (A) 1.5% Nafion® and (B) 1.5% Nafion® vortexed. CPA carried out at +700 mV *vs.* SCE. Current values for 100 µM choline chloride injection at 10, 20, 30, 40, 50, 75, 100, 200, 240 µM O_2 concentrations.

A comparison graph and comparison data table for the designs 1.5% Nafion® and 1.5% Nafion® vortexed, demonstrating the choline current at varying O_2 concentrations is presented in Figure 5.8. The comparison above illustrates the difference in the level of O_2 dependence for the designs. The data presented shows the effect of changing the dissolved O_2 concentration in the PBS on sensitivity of the electrode in the presence of 100 µM choline. The data illustrates the effect of vortexing the MMA and Nafion® solution which produced a uniform and almost linear relationship between the dissolved O_2 concentration and the choline current observed.

A comparison of the choline current at three physiological concentrations 30, 50 and 75 µM O_2 demonstrates the fluctuation in choline detection in the *in-vivo* environment. For the 1.5% Nafion® design, the choline current obtained at 30 µM O_2 is 0.62 ± 0.22 nA, n = 9, this choline current increases to 0.90 ± 0.19 nA, n = 9 with an increase in O_2 concentration to 50 µM. At 75µM O_2 the choline current is further increased to 1.25 ± 0.13 nA, n = 9. An I_{MAX} of 1.84 ± 0.11 nA, n = 8 is reached at 200 µM O_2. The choline current at 30 µM O_2 represents 31.71 ± 10.67 % of the I_{MAX} current, in addition 50 µM represents 45.66 ± 9.34 % and 75 µM is 62.77 ± 8.96 %. For the 1.5% Nafion® vortexed design the choline current obtained at 30 µM O_2 is 0.55 ± 0.07 nA, n = 7 this increased to 1.03 ± 0.05 nA, n = 7 at 50 µM O_2 and 1.49 ± 0.08 nA, n = 7 at 75 µM O_2. The I_{MAX} is reached at 100 µM with a current of 1.85 ± 0.11 nA, n = 7. The choline current at 30 µM O_2 represents 28.26 ± 2.42 % of the I_{MAX} current, 50 µM is 53.50 ± 2.22 % and 75 µM is 76.93 ± 2.02 % of the I_{MAX} current. This demonstrates better O_2 independence at the higher O_2 concentrations compared to the non-vortexed design. At 30 µM O_2 the percentage choline current of the I_{MAX} remains the same between these designs. At 50 µM the percentage is increased from 45.66 ± 9.34 % (1.5% Nafion®) to 53.50 ± 2.22 % (1.5% Nafion® vortexed) and at 75µM the percentage is increased from 62.77 ± 8.96 % (1.5% Nafion®) to 76.93 ± 2.02 % (1.5% Nafion® vortexed). The vortexed solution has decreased the O_2 dependence at higher O_2 concentrations but remains similar at the lower O_2 concentrations. These results indicate that a uniform distribution of Nafion® within the MMA polymer is neither beneficial for sensitivity or O_2 dependence. To investigate this further the MMA and Nafion® solutions were separated to determine if Nafion® layers in addition to MMA may be beneficial.

5.3.2.4. Nafion® Position

The previous section illustrated that the heterogeneity of the MMA and Nafion® solution may have caused variable results. Therefore, this section investigates the use of undiluted 5% Nafion® to potentially provide a higher concentration of dissolved O_2 within the perfluorocarbon, in addition, the position of the Nafion® in relation to the MMA is investigated.

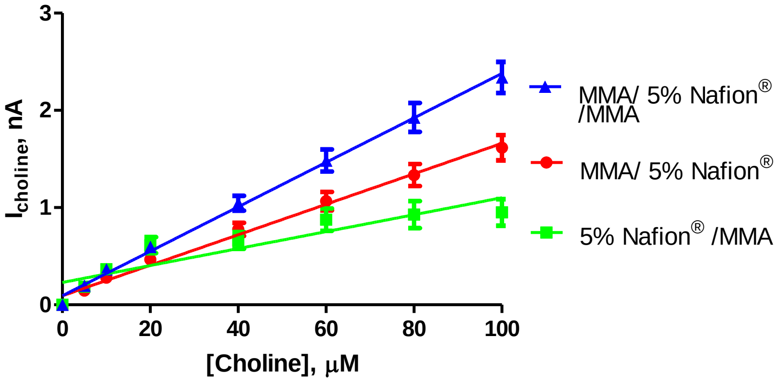

	(MMA)(5% Nafion®)			(5% Nafion®)(MMA)			(MMA)(5% Nafion®)(MMA)		
Choline Conc, µM	**Mean, nA**	**S.E.M, nA**	**n**	**Mean, nA**	**S.E.M, nA**	**n**	**Mean, nA**	**S.E.M, nA**	**n**
0	0.00	0.00	5	0.00	0.00	6	0.00	0.00	7
10	0.15	0.01	5	0.19	0.03	6	0.20	0.02	7
20	0.28	0.02	5	0.37	0.05	6	0.36	0.04	7
40	0.47	0.04	5	0.62	0.08	6	0.60	0.05	7
60	0.78	0.07	5	0.66	0.09	6	1.05	0.08	7
80	1.07	0.10	5	0.88	0.12	6	1.48	0.11	7
100	1.33	0.11	5	0.93	0.14	6	1.93	0.15	7

Figure 5.9 : The current-concentration profile comparison and comparison table for choline chloride calibration in PBS (pH 7.4) buffer solution at 21°C using designs (A) (MMA)(5% Nafion®), (B) (5% Nafion®)(MMA) and (C) (MMA)(5% Nafion®)(MMA). CPA carried out at +700 mV *vs.* SCE. Sequential current steps for 10, 20, 40, 60, 80, 100 µM choline chloride injections.

A comparison graph and comparison data table for the choline sensitivity of the designs (MMA)(Nafion®), (Nafion®)(MMA) and (MMA)(Nafion®)(MMA) are presented in Figure 5.9. Initially, the effects of the (Nafion®)(MMA), (MMA/Nafion®) and (MMA)(Nafion®)(MMA) solution were determined with respect to sensitivity. Each design had a noticeable effect on sensitivity. The use of Nafion® prior to the MMA affected the diffusion of the H_2O_2 to the metal surface producing a non linear response to choline (see Appendix 2 for individual calibration). A layer of Nafion® after the layer of MMA did not affect the linearity of the response however decreased the sensitivity of the sensor. The best choline response was obtained with the (MMA)(Nafion®)(MMA) design. The current responses were all decreased in comparison to the use of 1.5% in the MMA solution. This is possibly due to an increase in the Nafion® concentration to 5% and the positions of the Nafion® layers with respect to the enzyme layers causing lower enzyme loading or enzyme denaturation. This is potentially the reason that the design which encapsulated the Nafion® between two MMA layers produced the highest sensitivity. The $I_{100\ \mu M}$ current for the MMA/Nafion® design is 1.33 ± 0.11 nA, n = 5. This is reduced to 0.93 ± 0.14 nA, n = 6 when Nafion® is used prior to the MMA. The highest current was achieved with the (MMA)(Nafion®)(MMA) design increasing the current to 1.93 ± 0.15 nA, n = 7. This design has incorporated a high concentration of Nafion® within two MMA layers. This allows for enzyme immobilisation which is not in contact with the Nafion® directly, and the Nafion® is not affecting the diffusion of the H_2O_2 as the MMA prior to this layer prevents this.

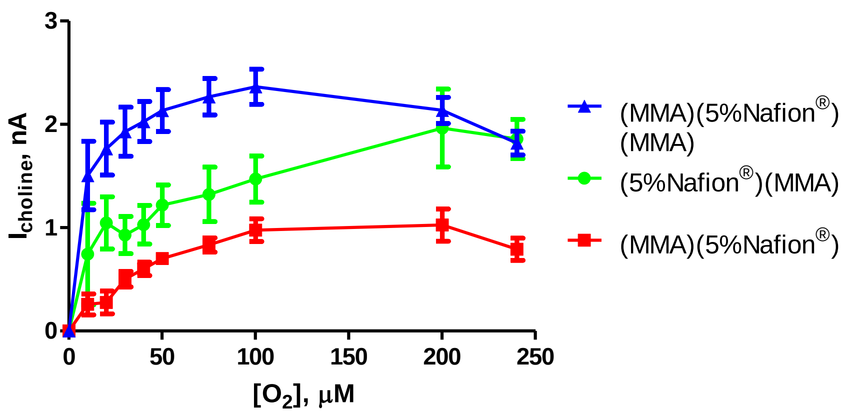

	(MMA)(5% Nafion®)			(5% Nafion®)(MMA)			(MMA)(5% Nafion®)(MMA)		
O_2 Conc, µM	Mean, nA	S.E.M, nA	n	Mean, nA	S.E.M, nA	n	Mean, nA	S.E.M, nA	n
0	0.00	0.00	5	0.00	0.00	6	0.00	0.00	7
10	0.26	0.10	5	0.76	0.49	3	1.50	0.33	7
20	0.28	0.11	5	1.05	0.25	6	1.76	0.26	7
30	0.50	0.08	5	0.93	0.18	6	1.93	0.24	7
40	0.60	0.08	5	1.03	0.19	6	2.03	0.19	7
50	0.70	0.06	5	1.22	0.20	6	2.13	0.20	7
75	0.83	0.07	5	1.32	0.26	6	2.27	0.18	7
100	0.98	0.11	5	1.47	0.22	6	2.36	0.17	7
200	1.03	0.16	5	1.97	0.38	5	2.14	0.13	7
240	0.79	0.11	5	1.86	0.19	5	1.82	0.12	7

Figure 5.10 : The choline current-oxygen concentration profile comparison and comparison table for calibration in PBS (pH 7.4) buffer solution at 21°C using design (A) (MMA)(5%Nafion®), (B) (5%Nafion®)(MMA) and (C) (MMA)(5%Nafion®)(MMA). CPA carried out at +700 mV *vs*. SCE. Current values for 100 µM choline chloride injection at 10, 20, 30, 40, 50, 75, 100, 200, 240 µM O_2 concentrations.

A comparison graph and comparison data table for the designs (MMA)(Nafion®), (Nafion®)(MMA) and (MMA)(Nafion®)(MMA) demonstrating the choline current at varying O_2 concentrations is presented in Figure 5.10. The comparison above illustrates the difference in the level of O_2 dependence for the designs. In addition to obtaining the best sensitivity, (MMA)(Nafion®)(MMA) achieved the best level of O_2 independence. The effect on diffusion caused by the different positions of the Nafion®, illustrates a potential correlation between obtaining O_2 independence and an increase in the diffusion barrier. A Nafion® layer prior to the MMA layer has clearly affected the rate of diffusion as illustrated by the non-linearity of the choline calibration (see Appendix 2). This in turn has potentially decreased the level of O_2 dependence of the sensor. In addition to this however a large decrease in sensitivity was observed, this may be as a result of lower enzyme loading which would require less oxygen for substrate turnover. The incorporation of the Nafion® after the MMA has potentially denatured the enzyme due to the ethanol content in the Nafion® leading to a decrease in current. This however, did not aid O_2 independence as, if the enzyme is denatured, it would block access to the active sites to the surrounding enzyme negating any positive effect the Nafion® may be having.

A comparison of the choline current at three physiological concentrations 30, 50 and 75 µM O_2 demonstrates the fluctuation in choline detection in the *in-vivo* environment. For the (MMA)(Nafion®) design, the choline current obtained at 30 µM O_2 is 0.50 ± 0.08 nA, n = 5 this increased to 0.70 ± 0.06, n = 5 at 50 µM O_2. At 75 µM O_2 a current of 0.83 ± 0.07 nA, n = 5 was obtained. The I_{MAX} was reached at 200 µM O_2 with a current of 1.03 ± 0.16 nA, n = 5. The current observed at 30 µM represents 49.14 ± 7.24 % of the I_{MAX} current. 50 µM O_2 represents 70.22 ± 7.55 % and 75 µM is 82.19 ± 5.90 % of the I_{MAX} current. When the Nafion® is coated before the MMA, the current obtained at 30 µM is increased from 0.50 ± 0.08 nA, n = 5 ((MMA)(Nafion®)) to 0.93 ± 0.18 nA, n = 6 ((Nafion®)(MMA)). At 50 µM the current is increased from 0.50 ± 0.08 nA, n = 5 ((MMA)(Nafion®)) to 0.93 ± 0.18 nA, n = 6 ((Nafion®)(MMA)), 75µM O_2 also demonstrated an increase from 0.83 ± 0.07 nA, n = 5 ((MMA)(Nafion®)) to 1.32 ± 0.26 nA, n = 6 ((Nafion®)(MMA)) this potentially demonstrates the effect of both the diffusion and the enzyme denaturing. The I_{MAX} was reached at 200 µM O_2 with a current of 1.97 ± 0.38 nA, n = 5. 30 µM represents 51.60 ± 8.86 % of the I_{MAX} current, 50 µM is 64.72 ± 8.96 % and 75 µM is 72.52 ± 3.25 % of the I_{MAX} current which are similar values to those obtained from (MMA)(Nafion®). The choline current obtained at 30 µM from the design (MMA)(Nafion®)(MMA) was 1.93 ± 0.24 nA, n = 7. The current at 50 µM was increased to 2.13 ± 0.20 nA, n = 7 and at 75 µM is 2.27 ± 0.18 nA, n = 7. The I_{MAX} was reached at 100 µM O_2 with a current of 2.36 ± 0.17 nA, n = 7. The current observed at 30 µM O_2 represents 78.90 ± 6.19 % of the I_{MAX} current. The current at 50 µM represents 88.50 ± 3.59 % of the I_{MAX} current and at 75 µM is 94.67 ± 1.31 % of the I_{MAX} current. This represents the highest level of O_2 independence achieved so far with a potential fluctuation of 26 %. The next section was undertaken in order to determine the effect the concentration of Nafion® had on the level of O_2 dependence.

5.3.2.5. Nafion® Concentration Comparison

The previous section determined that the most effective incorporation of Nafion® was between two layers of MMA. This section was undertaken to investigate the effect the Nafion® layer was having on the level of O_2 dependence. Three concentrations of Nafion® 1.25, 2.5 and 5% were used to determine the effect of the Nafion® on the O_2 dependence of the sensor.

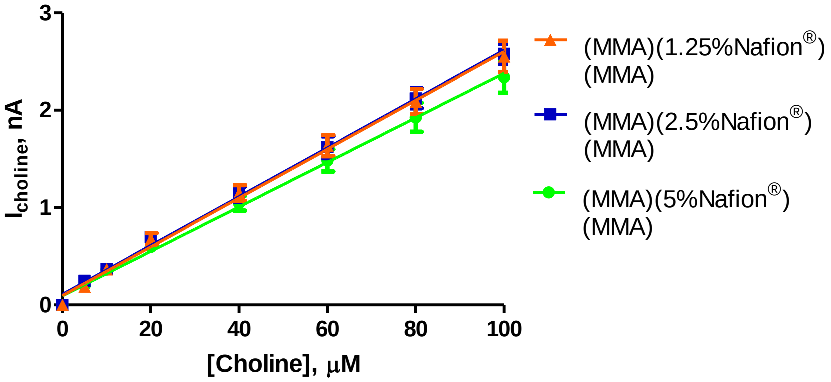

	(MMA)(5% Nafion®)(MMA)			(MMA)(2.5% Nafion®)(MMA)			(MMA)(1.25% Nafion®)(MMA)		
Choline Conc, µM	Mean, nA	S.E.M, nA	n	Mean, nA	S.E.M, nA	n	Mean, nA	S.E.M, nA	n
0	0.00	0.00	7	0.00	0.00	6	0.00	0.00	5
10	0.20	0.02	7	0.25	0.03	6	0.19	0.02	5
20	0.36	0.04	7	0.37	0.03	6	0.37	0.03	5
40	0.60	0.05	7	0.70	0.04	6	0.68	0.06	5
60	1.05	0.08	7	1.14	0.08	6	1.15	0.08	5
80	1.48	0.11	7	1.62	0.11	6	1.64	0.11	5
100	1.93	0.15	7	2.12	0.10	6	2.09	0.13	5

Figure 5.11 : The current-concentration profile comparison and comparison table for choline chloride calibration in PBS (pH 7.4) buffer solution at 21°C using designs (A) (MMA)(5%Nafion®)(MMA), (B) (MMA)(2.5%Nafion®)(MMA) and (C) (MMA)(1.25%Nafion®)(MMA). CPA carried out at +700 mV *vs.* SCE. Sequential current steps for 10, 20, 40, 60, 80, 100 µM choline chloride injections.

A comparison graph and comparison data table for the choline sensitivity of the designs (MMA)(5%Nafion®)(MMA), (MMA)(2.5%Nafion®)(MMA) and (MMA)(1.25% Nafion®)(MMA) are presented in Figure 5.11. Changing the concentration of the Nafion® had little effect on sensitivity. The $I_{100\ \mu M}$ current for the (MMA)(5%Nafion®)(MMA) design is 1.93 ± 0.15 nA, n = 7. The reduction of Nafion® concentration to 2.5% marginally increased the $I_{100\ \mu M}$ current from 1.93 ± 0.15 nA, n = 7 ((MMA)(5%Nafion®)(MMA)) to 2.21 ± 0.10 nA, n = 6 ((MMA)(2.5%Nafion®)(MMA)). Decreasing the Nafion® concentration to 1.25% produced a current of 2.09 ± 0.13 nA, n = 5. Decreasing the Nafion® concentration did not have a dramatic effect on the sensitivity of the design.

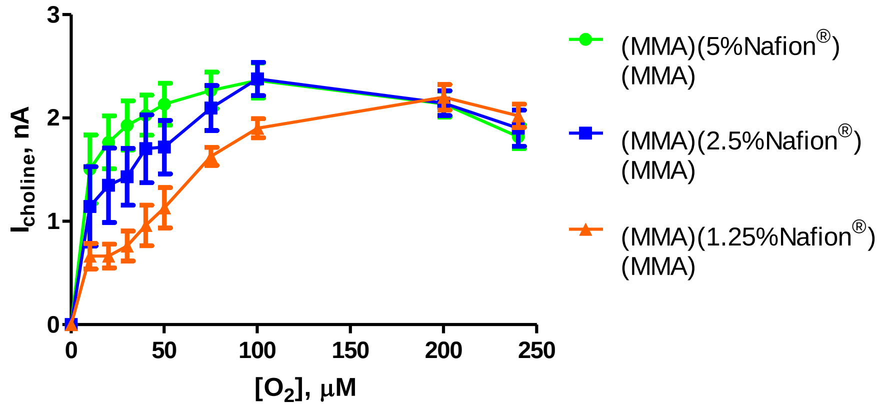

	(MMA)(5% Nafion®)(MMA)			(MMA)(2.5% Nafion®)(MMA)			(MMA)(1.25% Nafion®)(MMA)		
O_2 Conc, µM	Mean, nA	S.E.M, nA	n	Mean, nA	S.E.M, nA	n	Mean, nA	S.E.M, nA	n
0	0.00	0.00	7	0.00	0.00	6	0.00	0.00	6
10	1.50	0.33	7	1.15	0.38	6	0.66	0.12	6
20	1.76	0.26	7	1.35	0.36	6	0.66	0.12	6
30	1.93	0.24	7	1.43	0.28	6	0.76	0.15	6
40	2.03	0.19	7	1.70	0.33	6	0.96	0.20	6
50	2.13	0.20	7	1.72	0.26	6	1.13	0.20	6
75	2.27	0.18	7	2.10	0.22	6	1.63	0.09	6
100	2.36	0.17	7	2.38	0.16	6	1.90	0.09	6
200	2.14	0.13	7	2.14	0.12	6	2.20	0.12	6
240	1.82	0.12	7	1.90	0.18	6	2.02	0.11	6

Figure 5.12 : The choline current-oxygen concentration profile comparison and comparison table for calibration in PBS (pH 7.4) buffer solution at 21°C using design (A) (MMA)(5%Nafion®)(MMA), (B) (MMA)(2.5%Nafion®)(MMA) and (C) (MMA)(1.25%Nafion®)(MMA). CPA carried out at +700 mV *vs.* SCE. Current values for 100 µM choline chloride injection at 10, 20, 30, 40, 50, 75, 100, 200, 240 µM O_2 concentrations.

A comparison graph and comparison data table for the designs (MMA)(5%Nafion®)(MMA), (MMA)(2.5%Nafion®)(MMA) and (MMA)(1.25% Nafion®)(MMA) demonstrating the choline current at varying O_2 concentrations is presented in Figure 5.12. The comparison above illustrates the difference in the level of O_2 dependence for the designs. Decreasing the Nafion® concentration increased the level of O_2 dependence of the sensor. A comparison of the choline current at three physiological concentrations 30, 50 and 75 µM O_2 demonstrates the fluctuation in choline detection in the *in-vivo* environment. For the (MMA)(5%Nafion®)(MMA) design, the choline current obtained at 30 µM was 1.93 ± 0.24 nA, n = 7. The current at 50 µM was increased to 2.13 ± 0.20 nA, n = 7 and at 75 µM is 2.27 ± 0.18 nA, n = 7. The I_{MAX} was reached at 100 µM O_2 with a current of 2.36 ± 0.17 nA, n = 7. The current observed at 30 µM O_2 represents 78.90 ± 6.19 % of the I_{MAX} current. The current at 50 µM represents 88.50 ± 3.59 % of the I_{MAX} current and at 75 µM is 94.67 ± 1.31 % of the I_{MAX} current. Decreasing the Nafion® concentration to 2.5% decreased the level of O_2 independence. At 30 µM O_2 the choline current observed was decreased from 1.93 ± 0.24 nA, n = 7 ((MMA)(5%Nafion®)(MMA)) to 1.43 ± 0.28 nA, n = 6 ((MMA)(2.5%Nafion®)(MMA)). At 50 µM the current was reduced from 2.13 ± 0.20 nA, n = 7 ((MMA)(5%Nafion®)(MMA)) to 1.72 ± 0.26 nA, n = 6 ((MMA)(2.5% Nafion®)(MMA)) and at 75 µM the current was reduced from 2.27 ± 0.18 nA, n = 7 ((MMA)(5%Nafion®)(MMA)) to 2.10 ± 0.22 nA, n = 6 ((MMA)(2.5% Nafion®)(MMA)). The I_{MAX} was reached at 100 µM O_2 with a current of 2.38 ± 0.16 nA, n = 6. The current observed at 30 µM represents 57.46 ± 7.64 % of the I_{MAX} current. The current observed at 50 µM and 80 µM represent 69.75 ± 6.21 % and 86.20 ± 3.99 % respectively. At 30 µM O_2 the percentage choline current of the I_{MAX} is decreased from 78.90 ± 6.19 % (5% Nafion®) to 57.46 ± 7.64 % (2.5% Nafion®). At 50 µM the percentage is decreased from 88.50 ± 3.59 % (5% Nafion®) to 69.75 ± 6.21 % (2.5% Nafion®) and at 75µM the percentage is decreased from 94.67 ± 1.31 % (5% Nafion®) to 86.20 ± 3.99 % (0.5% Nafion®). Reducing the Nafion® concentration to 1.25% reduced the level of O_2 independence further. The current obtained at 30 µM was 0.76 ± 0.15 nA, n = 6. The current at 50 µM was increased to 1.13 ± 0.20 nA, n = 6 and at 75 µM is 1.63 ± 0.09 nA, n = 6. The I_{MAX} was reached at 200 µM O_2 with a current of 2.20 ± 0.12 nA, n = 7. The current observed at 30 µM O_2 represents 34.59 ± 6.57 % of the I_{MAX} current, a further reduction in the O_2 independence previously observed. The current at 50 µM represents 51.36 ± 8.84 % of the I_{MAX} current and at 75 µM is 74.00 ± 3.94 % of the I_{MAX} current a reduction from the values observed with 2.5% Nafion®. This section has illustrated the effect of the Nafion® on the level of O_2 dependence of the sensor and demonstrated 5% Nafion® is the optimum concentration. A direct correlation is observed between the Nafion® concentration and the level of O_2 dependence of the design which is not as a result of the sensitivity. Although an optimum concentration of Nafion® has been determined, reproducible O_2 independence has not been achieved. This potentially, is as a result of the experimental design, as the experiments were undertaken from a N_2 saturated solution which may be purging the O_2 reservoirs. This will be investigated further in the next section.

5.3.3. Fixed Oxygen Calibration Protocol

Nafion® was incorporated into the sensor design as perfluorocarbons have demonstrated high degrees of oxygen solubility (Wang & Lu, 1998), and have been utilised previously to overcome O_2 dependence of biosensors. Fluorocarbon pasting liquids have been incorporated into carbon paste to overcome the oxygen dependence of a glucose biosensor (Wang & Lu, 1998). The incorporation of Nafion® using the design (MMA)(5%Nafion®)(MMA)-(ChOx)(BSA)(GA)(PEI) has shown remarkable O_2 independence. This level of O_2 independence however, is variable for sensors of the same design. As this is the case an alternative experimental procedure was investigated. The experimental design used in the previous sections, requires that the level of oxygen in the PBS at the beginning of the experiment is brought to 0 µM (see Section 3.5.1.6). Potentially, this may create an O_2 gradient which draws the dissolved O_2 within the perfluorocarbon out into the bulk solution of PBS. As the reported oxygen concentrations throughout the brain vary between 30 and 80 µM (Bolger & Lowry, 2005), four O_2 concentrations were chosen to perform a choline calibration. A choline calibration of 20, 60, 100 and 200 µM was performed in O_2 concentrations of 30, 50, 80 and 240 µM (see Section 3.5.1.6). These calibrations therefore, do not subject the sensor to low O_2 concentrations that are not physiologically relevant. The choline calibration was performed on the sensors in order to determine the effect of choline concentration on the O_2 dependence of the sensor. The biosensor and O_2 currents were recorded simultaneously. The biosensor data was normalised relative to the I_{MAX} value and plotted against the measured concentration of O_2.

This section investigates the O_2 dependence of the design (MMA)(5% Nafion®)(MMA)-(ChOx)(BSA)(GA)(PEI) using the new experimental protocol.

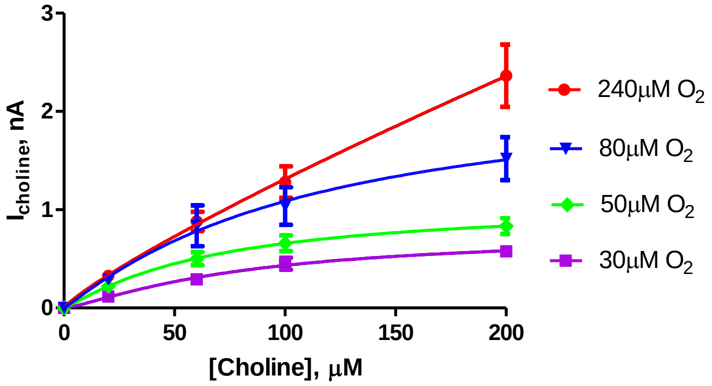

	30 µM O_2			50 µM O_2			80 µM O_2			240 µM O_2		
Choline Conc, µM	Mean, nA	S.E.M, nA	n	Mean, nA	S.E.M, nA	n	Mean, nA	S.E.M, nA	n	Mean, nA	S.E.M, nA	n
0	0.00	0.00	3	0.00	0.00	3	0.00	0.00	3	0.00	0.00	3
20	0.12	0.03	3	0.22	0.04	3	0.29	0.06	3	0.33	0.03	3
60	0.29	0.04	3	0.50	0.07	3	0.84	0.21	3	0.88	0.10	3
100	0.45	0.06	3	0.66	0.08	3	1.04	0.19	3	1.28	0.16	3
200	0.58	0.05	3	0.83	0.08	3	1.52	0.22	3	2.37	0.32	3

Figure 5.13 : The choline current-oxygen concentration profile comparison and comparison table for calibration in PBS (pH 7.4) buffer solution at 21°C using design (A) (MMA)(5%Nafion®)(MMA)-(ChOx)(BSA)(GA)(PEI) CPA carried out at +700 mV *vs.* SCE. Sequential current steps for 20, 60, 100 and 200 µM choline chloride injection at 30, 50 and 80 µM O_2 concentrations.

The results obtained from the investigation into the new experimental procedure on the sensor design (MMA)(5%Nafion®)(MMA)-(ChOx)(BSA)(GA)(PEI) are presented in Figure 5.13. The data illustrates the effect of four O_2 concentrations 240, 80, 50 and 30 µM on the choline calibration curve. The data also illustrates the effect of decreasing the O_2 concentration on the choline calibration of 20, 60, 100 and 200 µM choline. Oxygen dependence is clearly observed as an O_2 independent graph would demonstrate similar current values at each O_2 concentration. In the initial experiments using the 240 µM O_2, the graph presents a linear response to choline. This is the case as neither the availability of the choline or the O_2 are a limiting factor in the efficiency of the enzyme to turn over the substrate and produce H_2O_2. However, the reduction in the O_2 concentration from 240 µM to 80 µM, has both reduced the availability of enough O_2 with which to allow for efficient substrate turnover to produce the same quantities of H_2O_2 and has eliminated the linearity of the calibration plot. The lack of linearity in the plot is as a result of different required O_2 concentrations for different choline concentrations as a higher choline concentration will require more O_2 for enzymatic turnover than a lower choline concentration. The current at 20 µM choline decreased from 0.33 ± 0.03 nA to 0.29 ± 0.06 nA, n = 3 with a decrease in O_2 concentration from 240 µM to 80 µM. The decrease to 50 µM O_2 decreased the current further to 0.22 ± 0.04 nA, n = 3 and at 30 µM the current was 0.12 ± 0.03 nA, n = 3. A similar level of O_2 dependence is observed using 60 µM choline. At 80 µM O_2 the current is reduced from 0.88 ± 0.10 nA to 0.84 ± 0.21 nA, n = 3. This was reduced to 0.50 ± 0.07 nA, n = 3 at 50 µM O_2 and 0.29 ± 0.04 nA, n = 3 at 30 µM. 100 µM choline demonstrated a decrease in current from 1.28 ± 0.16 nA to 1.04 ± 0.19 nA, n = 3 with a reduction in O_2 concentration from 240 to 80 µM. This was reduced to 0.66 ± 0.08 nA, n = 3 at 50 µM O_2 and 0.45 ± 0.06 nA, n = 3 at 30 µM O_2. 200 µM choline demonstrates a decrease from 2.37 ± 0.32 nA to 1.52 ± 0.22 nA, n = 3 from 240 µM to 80 µM O_2. This decreased to 0.83 ± 0.08 nA, n = 3 at 50 µM O_2 and 0.58 ± 0.05 nA, n = 3 at 30 µM O_2. The effect of the decrease in O_2 concentration is evident in Figure 5.13 demonstrated that this design suffers from O_2 dependence.

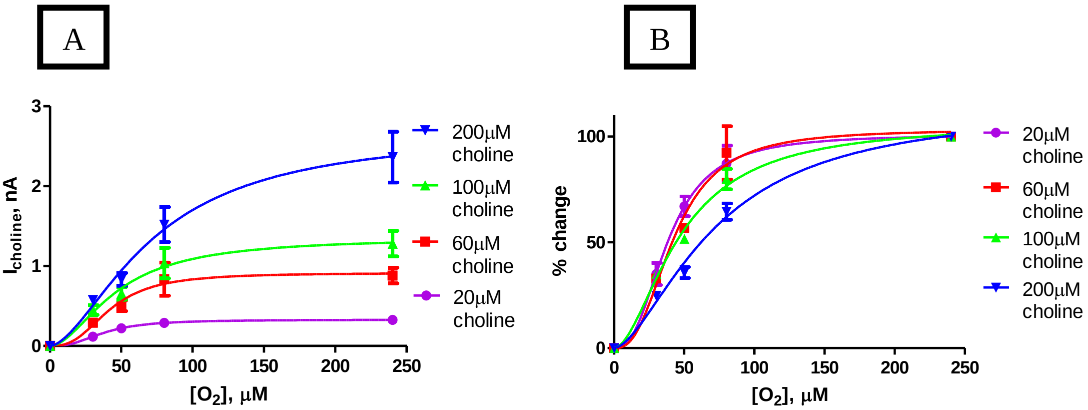

	20 µM			60 µM			100 µM			200 µM		
O_2 Conc, µM	Mean %	S.E.M	n	Mean %	S.E.M	n	Mean %	S.E.M	n	Mean %	S.E.M	n
0	0.00	0.00	3	0.00	0.00	3	0.00	0.00	3	0.00	0.00	3
30	35.06	5.22	3	32.84	1.94	3	35.01	0.36	3	24.77	1.69	3
50	66.97	4.64	3	56.81	1.22	3	51.54	1.10	3	35.76	2.64	3
80	87.13	8.51	3	92.23	12.59	3	79.84	4.81	3	64.47	3.88	3
240	100.00	0.00	3	100.00	0.00	3	100.00	0.00	3	100.00	0.00	3

Figure 5.14 A : The choline current-oxygen concentration profile comparison for calibration in PBS (pH 7.4) buffer solution at 21°C using design (MMA)(5%Nafion®)(MMA)-(ChOx)(BSA)(GA)(PEI) CPA carried out at +700 mV *vs.* SCE. Sequential current steps for 20, 60, 100 and 200 µM choline chloride injection at 30, 50 and 80 µM O_2 concentrations. Figure 5.14 B the normalised choline current-oxygen concentration profile comparison and comparison table for the design (MMA)(5%Nafion®)(MMA)-(ChOx)(BSA)(GA)(PEI).

In order to determine the effect that the individual O_2 concentrations have on the choline concentrations the data in Figure 5.14 A illustrates the effect choline concentration on the O_2 dependence of the sensor. The data is normalised in Figure 5.14 B to directly compare the level of O_2 dependence of the choline concentrations.

The level of O_2 dependence observed during this experiment using 100 µM choline can be compared with the level of O_2 dependence observed in Section 5.3.2.4 undertaken using the previous experimental design. In Section 5.3.2.4 the percentage value of the I_{MAX} current observed for 30, 50 and 75 µM O_2 was 84, 91 and 96 % respectively. The results obtained in Figure 5.14 B demonstrate that this is reduced to 35, 51 and 79 % for the O_2 concentrations 30, 50 and 80 µM respectively. The data in the table demonstrates the severity of the O_2 dependence of the design by comparing the rate of enzyme turnover of each choline concentration. The lowest of the choline concentrations, 20 µM at 30, 50 and 80 µM O_2 yielded percentage values of 35.06 ± 5.22, 66.97 ± 4.64 and 87.13 ± 8.51 % respectively. The higher level of O_2 independence observed using 20 µM choline however, is only observed at O_2 concentrations of 50 µM or higher. Therefore, this implies that the level of O_2 dependence of this design is such that 30 µM O_2 is an inadequate oxygen concentration for the substrate turn-over of even the low choline concentrations. 60 µM choline demonstrated percentage values of 32.84 ± 1.94, 56.81 ± 1.22 and 92.23 ± 12.59 % for the O_2 concentration 30, 50 and 80 µM. The highest level of O_2 dependence was demonstrated by the highest choline concentration with percentage values of 24.77 ± 1.69, 35.76 ± 2.64 and 64.47 ± 3.88 % for 30, 50 and 80 µM O_2. This experimental design has demonstrated very different results to that in Section 5.3.2.4. This experimental design was used in order to investigate the effect of the O_2 content of the perfluorcarbon on the level of O_2 dependence. The fully nitrogen saturated PBS solution does not appear to have an effect on the O_2 dependence of the sensor, as demonstrated by the results presented here (Figure 5.14 B) which did not utilise low O_2 concentrations.

5.3.3.1. Oxygenation -30 Seconds

The sensor design (MMA)(5%Nafion®)(MMA)-(ChOx)(BSA)(GA)(PEI) demonstrated excellent O_2 independence potential in Section 5.3.2.4. This design however did not produce consistent O_2 independent results. In order to examine the effect the N_2 saturation of the PBS on the O_2 content of the Nafion®, the experimental procedure was altered so the lowest O_2 concentration the sensor was exposed to during calibration was 30 µM. This however, did not improve the O_2 independence of the sensor, however demonstrated more O_2 dependent results. This section investigates the effect of increasing the O_2 content of the Nafion® by introducing O_2 into the solution for 30 seconds, 1 minute and 2 minutes and removing the O_2 in the Nafion® by introducing N_2 into the Nafion® for 1 minute and 2 minutes.

This section investigates the effect of oxygenating the Nafion® for 30 seconds using the design (MMA)(5%Nafion®)(MMA)-(ChOx)(BSA)(GA)(PEI)

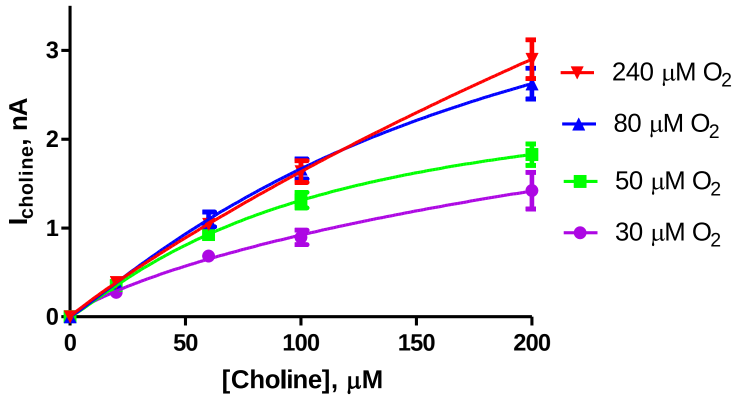

	30 µM O_2			50 µM O_2			80 µM O_2			240 µM O_2		
Choline Conc, µM	Mean, nA	S.E.M, nA	n	Mean, nA	S.E.M, nA	n	Mean, nA	S.E.M, nA	n	Mean, nA	S.E.M, nA	n
0	0.00	0.00	12	0.00	0.00	12	0.00	0.00	12	0.00	0.00	12
20	0.27	0.03	12	0.35	0.03	12	0.38	0.03	12	0.39	0.02	12
60	0.68	0.06	12	0.93	0.06	12	1.10	0.08	12	1.04	0.07	12
100	0.89	0.08	12	1.31	0.09	12	1.67	0.11	12	1.64	0.12	12
200	1.42	0.21	12	1.83	0.12	12	2.63	0.17	12	2.90	0.22	12

Figure 5.15 : The choline current-oxygen concentration profile comparison and comparison table for calibration in PBS (pH 7.4) buffer solution at 21°C using 30 second oxygenated Nafion®. CPA carried out at +700 mV *vs.* SCE. Sequential current steps for 20, 60, 100 and 200 µM choline chloride injection at 30, 50 and 80 µM O_2 concentrations.

The results obtained from the investigation into oxygenating the Nafion® for 30 seconds are presented in Figure 5.15. The data illustrates the effect of four O_2 concentrations 240, 80, 50 and 30 µM on the choline calibration curve. The data also illustrates the effect of decreasing the O_2 concentration on the choline calibration of 20, 60, 100 and 200 µM choline. The data shows that introducing the O_2 into the Nafion® alleviates the O_2 dependence constraints at 80 µM O_2. The current at 20 µM choline decreased from 0.39 ± 0.02 nA to 0.38 ± 0.03 nA, n = 12 with a decrease in O_2 concentration from 240 µM to 80 µM. Increasing the choline concentration to 60 µM also remained O_2 independent as the choline current increased from 1.04 ± 0.07 nA to 1.10 ± 0.08 nA, n = 12 decreasing the O_2 concentration from 240 to 80 µM O_2. 100 µM choline also demonstrated an increase in current from 1.64 ± 0.12 nA to 1.67 ± 0.11 nA with a decrease in O_2 concentration from 240 to 80 µM O_2. The increase in choline concentration to 200 µM demonstrated a decrease in current suggesting the introduction of O_2 dependence. The current was reduced from 2.90 ± 0.22 nA to 2.63 ± 0.17 nA, n = 12 from 240 to 80 µM O_2. This design has demonstrated O_2 independence at O_2 concentrations of 80 µM at 100 µM choline or less. 50 µM O_2 illustrates small fluctuations in current at 20 µM choline as the current is reduced from 0.39 ± 0.02 nA to 0.35 ± 0.03 nA, n = 12. 60 µM choline suffers from larger fluctuations in current from 1.04 ± 0.07 nA to 0.93 ± 0.06 nA, n = 12. 100 µM choline is reduced from 1.64 ± 0.12 nA to 1.31 ± 0.09 nA, n = 12. 200 µM demonstrates the highest level of O_2 dependence decreasing the current from 2.90 ± 0.22 nA to 1.83 ± 0.12 nA, n = 12. Reducing the O_2 concentration further to 30 µM demonstrates a large reduction in the current for each choline concentration. For 20 µM choline the current is reduced from 0.39 ± 0.02 nA to 0.27 ± 0.03 nA, n = 12. 60 µM choline demonstrated a reduction from 1.04 ± 0.07 nA to 0.68 ± 0.06 nA, n = 12. 100 µM choline exhibits a reduction from 1.64 ± 0.12 nA to 0.89 ± 0.08 nA, n = 12. 200 µM choline displays a reduction from 2.90 ± 0.22 nA to 1.42 ± 0.21 nA, n = 12. This data demonstrates O_2 independence at 80 µM O_2 for 100 µM choline and less. However, this design has not produced O_2 independence.

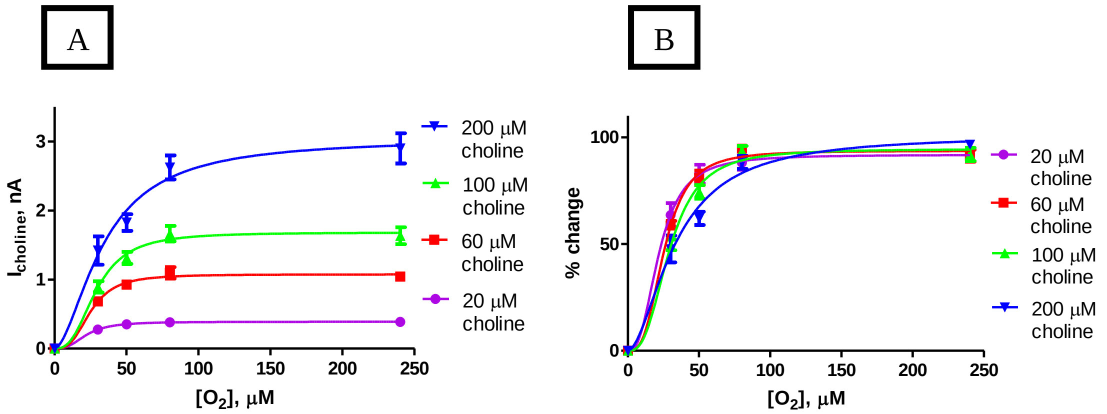

	20 µM			60 µM			100 µM			200 µM		
O_2 Conc, µM	**Mean %**	**S.E.M**	**n**	**Mean %**	**S.E.M**	**n**	**Mean %**	**S.E.M**	**n**	**Mean%**	**S.E.M**	**N**
0	0.00	0.00	12	0.00	0.00	12	0.00	0.00	12	0.00	0.00	12
30	63.54	5.59	12	58.65	2.13	12	49.58	2.48	12	47.64	6.27	12
50	82.81	4.31	12	80.98	3.43	12	74.38	3.17	12	62.02	3.14	12
80	88.04	3.29	12	94.69	2.03	12	93.53	2.43	12	88.26	3.05	12
240	92.02	3.13	12	91.33	2.80	12	91.98	3.07	12	96.61	1.81	12

Figure 5.16 A : The choline current-oxygen concentration profile comparison for calibration in PBS (pH 7.4) buffer solution at 21°C using design (MMA)(5%Nafion®)(MMA)-(ChOx)(BSA)(GA)(PEI). CPA carried out at +700 mV *vs*. SCE. Sequential current steps for 20, 60, 100 and 200 µM choline chloride injection at 30, 50 and 80 µM O_2 concentrations. Figure 5.16 B the normalised choline current-oxygen concentration profile comparison and comparison table for the design (MMA)(5%Nafion®)(MMA)-(ChOx)(BSA)(GA)(PEI).

The data in Figure 5.16 A illustrates the effect of four choline concentrations 20, 60, 100 and 200 µM on the O_2 dependence. The data in Figure 5.16 B also illustrates the normalised percentage values for each choline concentration at the O_2 concentrations 30, 50 and 80 µM. 20 µM choline demonstrates a low level of O_2 dependence. At 30 µM O_2 20 µM choline demonstrates 63.54 ± 5.59 % of the current observed at 240 µM O_2. At 50 µM O_2 the current is 82.81 ± 4.31 % and at 80 µM the current is 88.04 ± 3.29% of that observed at 240 µM O_2. Similar values are observed for 60 µM choline. At 30 µM O_2 the current is 58.65 ± 2.13 % , 50 µM the current is 80.98 ± 3.43 % and 80 µM is 94.69 ± 2.03 % of the current observed at 240 µM O_2. 100 µM choline demonstrates increased O_2 dependence at the lower O_2 concentrations, due to increased substrate requiring O_2 for turn-over. At 30 µM O_2 the current is 49.58 ± 2.48% , 50 µM the current is 74.38 ± 3.17 % and 80 µM is 93.53 ± 2.43 % of the current observed at 240 µM O_2. Increasing the choline concentration to 200 µM demonstrated increased O_2 dependence for O_2 concentrations at 50 µM and lower. At 30 µM O_2 the current is 47.64 ± 6.27 % , 50 µM the current is 62.02 ± 3.14 % and 80 µM is 88.26 ± 3.05 % of the current observed at 240 µM $O_{2.}$ Although 30 seconds of oxygenation of the Nafion® proved promising at high O_2 concentrations, O_2 independence was not achieved.

5.3.3.2. Oxygenation - 1 minute

As oxygenation of the Nafion® showed promise, although not full O_2 independence, the oxygenation time was increased to 1 minute.

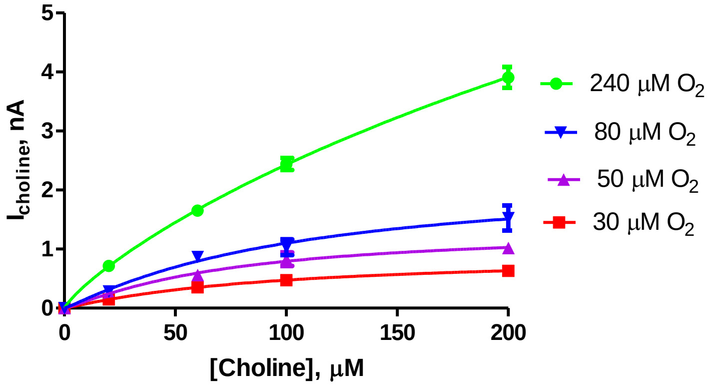

	30 µM O_2			50 µM O_2			80 µM O_2			240 µM O_2		
Choline Conc, µM	Mean, nA	S.E.M, nA	n	Mean, nA	S.E.M, nA	n	Mean, nA	S.E.M, nA	n	Mean, nA	S.E.M, nA	n
0	0.00	0.00	3	0.00	0.00	3	0.00	0.00	3	0.00	0.00	3
20	0.15	0.01	3	0.26	0.01	3	0.28	0.04	3	0.71	0.03	3
60	0.35	0.03	3	0.56	0.05	3	0.87	0.08	3	1.65	0.06	3
100	0.47	0.05	3	0.83	0.11	3	1.03	0.13	3	2.44	0.10	3
200	0.63	0.07	3	1.02	0.07	3	1.53	0.21	3	3.91	0.18	3

Figure 5.17 : The choline current-oxygen concentration profile comparison and comparison table for calibration in PBS (pH 7.4) buffer solution at 21°C using 30 second oxygenated Nafion®. CPA carried out at +700 mV *vs.* SCE. Sequential current steps for 20, 60, 100 and 200 µM choline chloride injection at 30, 50 and 80 µM O_2 concentrations.

The results obtained from the investigation into oxygenating the Nafion® for 1 minute are presented in Figure 5.17. The data illustrates the effect of four O_2 concentrations 240, 80, 50 and 30 µM on the choline calibration curve. The data also illustrates the effect of the decreasing the O_2 concentration on the choline calibration of 20, 60, 100 and 200 µM choline. An increased level of O_2 dependence is observed. The current at 20 µM choline decreased from 0.71 ± 0.03 nA to 0.28 ± 0.04 nA, n = 3 with a decrease in O_2 concentration from 240 µM to 80 µM. The decrease to 50 µM O_2 decreased the current further to 0.26 ± 0.01 nA, n = 3 and at 30 µM the current was 0.15 ± 0.01 nA, n = 3. A similar level of O_2 dependence is observed using 60 µM choline. At 80 µM O_2 the current is reduced from 1.65 ± 0.06 nA to 0.87 ± 0.08 nA, n = 3. This was reduced to 0.56 ± 0.05 nA, n = 3 at 50 µM O_2 and 0.35 ± 0.03 nA, n = 3 at 30 µM. 100 µM choline demonstrated a decrease in current from 2.44 ± 0.10 nA to 1.03 ± 0.13 nA, n = 3 with a reduction in O_2 concentration from 240 to 80 µM. This was reduced to 0.83 ± 0.11 nA, n = 3 at 50 µM O_2 and 0.47 ± 0.04 nA, n = 3 at 30 µM O_2. 200 µM choline demonstrates a decrease from 3.91 ± 0.18 nA to 1.53 ± 0.21 nA, n = 3 from 240 µM to 80 µM O_2. This decreased to 1.02 ± 0.07 nA, n = 3 at 50 µM O_2 and 0.63 ± 0.07 nA, n = 3 at 30 µM O_2. This data demonstrates that this design has a high degree of O_2 dependence.

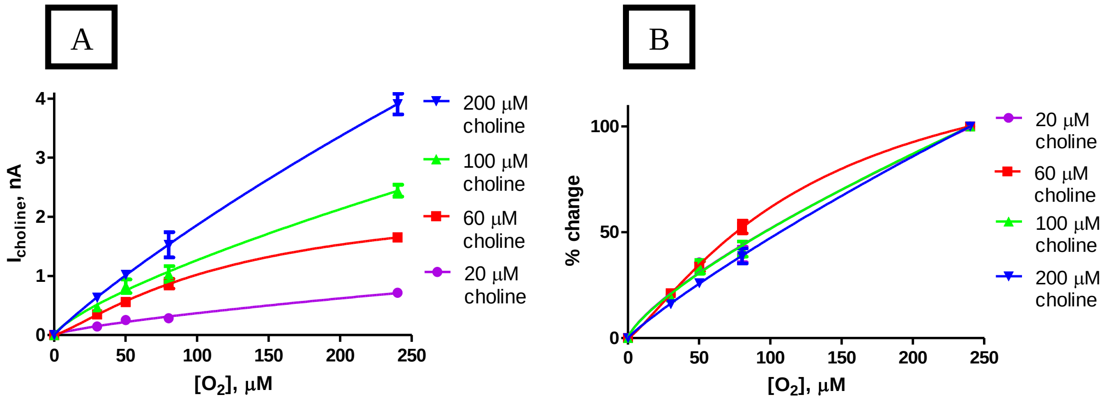

	20 µM			60 µM			100 µM			200 µM		
O_2 Conc, µM	Mean %	S.E.M	n	Mean %	S.E.M	n	Mean %	S.E.M	n	Mean %	S.E.M	n
0	0.00	0.00	3	0.00	0.00	3	0.00	0.00	3	0.00	0.00	3
30	20.39	0.94	3	21.18	1.07	3	19.31	1.23	3	16.08	1.08	3
50	35.82	0.93	3	33.82	2.35	3	33.64	3.23	3	26.03	1.07	3
80	39.43	3.67	3	52.49	3.00	3	42.00	3.59	3	38.76	3.55	3
240	100.00	0.00	3	100.00	0.00	3	100.00	0.00	3	100.00	0.00	3

Figure 5.18 A : The choline current-oxygen concentration profile comparison for calibration in PBS (pH 7.4) buffer solution at 21°C using design 1 minute oxygenation. CPA carried out at +700 mV *vs*. SCE. Sequential current steps for 20, 60, 100 and 200 µM choline chloride injection at 30, 50 and 80 µM O_2 concentrations. Figure 5.18 B the normalised choline current-oxygen concentration profile comparison and comparison table for the design 1 minute oxygenation.

The data in Figure 5.18 A illustrates the effect of four choline concentrations 20, 60, 100 and 200 µM on the O_2 dependence. The data in Figure 5.18 B also illustrates the normalised percentage values for each choline concentration at the O_2 concentrations 30, 50 and 80 µM. This data demonstrates a high degree of O_2 dependence. The normalised data demonstrates that the increased level of O_2 dependence observed due to increased choline concentration has been eliminated. Almost identical levels of O_2 dependence are observed for each choline concentration. For 20 µM choline the current is reduced to 39.43 ± 3.67 % at 80 µM O_2. This was decreased to 35.82 ± 0.93 % at 50 µM and 20.39 ± 0.94 % at 30 µM O_2. For 60 µM choline the current is reduced to 52.49 ± 3.00 % at 80 µM O_2. This was decreased to 33.82 ± 2.35 % at 50 µM and 21.18 ± 1.07 % at 30 µM O_2. Similarly, for 100 µM choline the current is reduced to 42.00 ± 3.59 % at 80 µM O_2. This was decreased to 33.64 ± 3.23 % at 50 µM and 19.31 ± 1.23 % at 30 µM O_2. Finally, for 200 µM choline the current is reduced to 38.76 ± 3.55 % at 80 µM O_2. This was decreased to 26.03 ± 1.07 % at 50 µM and 16.08 ± 1.08 % at 30 µM O_2. Oxygenation of Nafion® for 1 minute has resulted in a linear response in relation to O_2 concentration. In addition, the level of O_2 dependence for increased choline concentrations remained the same. This demonstrates that the level of O_2 dependence observed by the sensor is not as a result of choline concentration, however, the level of O_2 dependence observed is too severe for use in the *in-vivo* environment.

5.3.3.3. Oxygenation - 2 minutes

The oxygenation of the Nafion® was increased to 2 minutes to determine if an improvement on the O_2 dependence could be made when compared to the 1 minute of oxygenation.

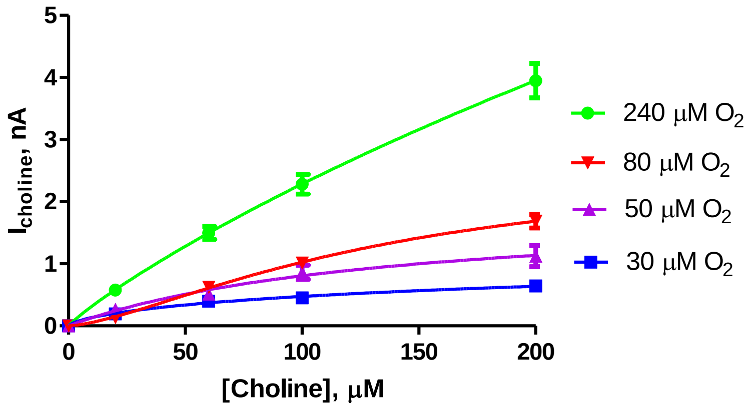

	30 µM O_2			50 µM O_2			80 µM O_2			240 µM O_2		
Choline Conc, µM	**Mean, nA**	**S.E.M, nA**	**n**	**Mean, nA**	**S.E.M, nA**	**n**	**Mean, nA**	**S.E.M, nA**	**n**	**Mean, nA**	**S.E.M, nA**	**n**
0	0.00	0.00	3	0.00	0.00	3	0.00	0.00	3	0.00	0.00	3
20	0.20	0.01	3	0.27	0.02	3	0.140	0.002	3	0.58	0.04	3
60	0.40	0.03	3	0.52	0.07	3	0.63	0.03	3	1.50	0.10	3
100	0.45	0.04	3	0.86	0.12	3	1.02	0.05	3	2.28	0.16	3
200	0.64	0.05	3	1.12	0.17	3	1.69	0.11	3	3.95	0.28	3

Figure 5.19 : The choline current-oxygen concentration profile comparison and comparison table for calibration in PBS (pH 7.4) buffer solution at 21°C using 30 second oxygenated Nafion® . CPA carried out at +700 mV *vs.* SCE. Sequential current steps for 20, 60, 100 and 200 µM choline chloride injection at 30, 50 and 80 µM O_2 concentrations.

The results obtained from the investigation into oxygenating the Nafion® for 2 minutes are presented in Figure 5.19. The data illustrates the effect of four O_2 concentrations 240, 80, 50 and 30 µM on the choline calibration curve. The data also illustrates the effect of the decreasing the O_2 concentration on the choline calibration of 20, 60, 100 and 200 µM choline. This design demonstrates O_2 dependence and no improvement from the 1 minute oxygenation in Section 5.3.3.3. The current at 20 µM choline decreased from 0.58 ± 0.04 nA to 0.14 ± 0.002 nA, n = 3 with a decrease in O_2 concentration from 240 µM to 80 µM. The decrease to 50 µM O_2 increased the current to 0.27 ± 0.02 nA, n = 3 and at 30 µM the current was reduced to 0.20 ± 0.01 nA, n = 3. O_2 dependence was observed using 60 µM choline. At 80 µM O_2 the current is reduced from 1.50 ± 0.10 nA to 0.63 ± 0.03 nA, n = 3. This was reduced to 0.52 ± 0.07 nA, n =

3 at 50 µM O_2 and 0.40 ± 0.03 nA, n = 3 at 30 µM. 100 µM choline demonstrated a decrease in current from 2.28 ± 0.16 nA to 1.02 ± 0.05 nA, n = 3 with a reduction in O_2 concentration from 240 to 80 µM. This was reduced to 0.86 ± 0.12 nA, n = 3 at 50 µM O_2 and 0.45 ± 0.04 nA, n = 3 at 30 µM O_2. 200 µM choline demonstrates a decrease from 3.95 ± 0.28 nA to 1.69 ± 0.11 nA, n = 3 from 240 µM to 80 µM O_2. This decreased to 1.12 ± 0.17 nA, n = 3 at 50 µM O_2 and 0.64 ± 0.05 nA, n = 3 at 30 µM O_2. This data demonstrates that this design has a high degree of O_2 dependence. These current values are comparable to those using 1 minute of oxygenation. No improvement has been made by increasing the oxygenation time.

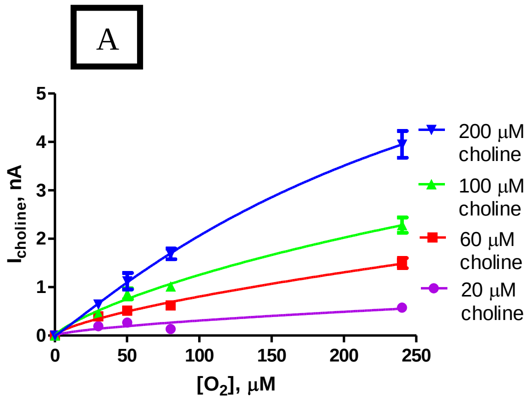

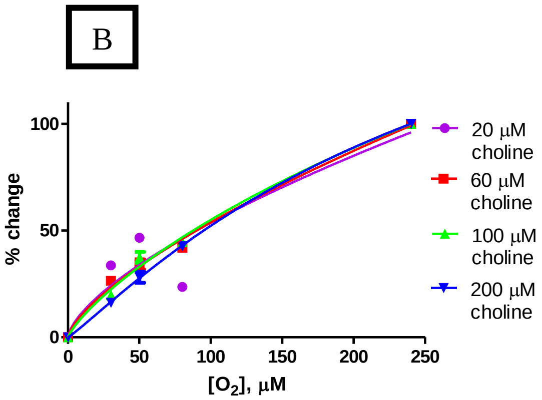

	20 µM			60 µM			100 µM			200 µM		
O_2 Conc, µM	**Mean %**	**S.E.M**	**n**	**Mean %**	**S.E.M**	**n**	**Mean %**	**S.E.M**	**n**	**Mean %**	**S.E.M**	**n**
0	0.00	0.00	3	0.00	0.00	3	0.00	0.00	3	0.00	0.00	3
30	33.71	1.66	3	26.48	0.42	3	19.75	0.14	3	16.26	0.14	3
50	46.59	0.52	3	34.22	2.33	3	37.47	2.58	3	28.16	2.61	3
80	23.61	1.13	3	41.89	1.66	3	44.67	1.13	3	42.75	0.30	3
240	100.00	0.00	3	100.00	0.00	3	100.00	0.00	3	100.00	0.00	3

Figure 5.20 : The choline current-oxygen concentration profile comparison for calibration in PBS (pH 7.4) buffer solution at 21°C using design (MMA)(5%Nafion®)(MMA)-(ChOx)(BSA)(GA)(PEI) CPA carried out at +700 mV *vs.* SCE. Sequential current steps for 20, 60, 100 and 200 µM choline chloride injection at 30, 50 and 80 µM O_2 concentrations. Figure B the normalised choline current-oxygen concentration profile comparison and comparison table for the design (MMA)(5%Nafion®)(MMA)-(ChOx)(BSA)(GA)(PEI)

The data illustrates the effect of four choline concentrations 20, 60, 100 and 200 µM on the O_2 dependence. The data also illustrates the normalised percentage values for each choline concentration at the O_2 concentrations 30, 50 and 80 µM. A high degree of O_2 dependence is observed similar to that of 1 minute of oxygenation of Nafion®. The normalised data demonstrates that the increased level of O_2 dependence observed due to increased choline concentration has been eliminated. Almost identical levels of O_2 dependence are observed for each choline concentration. For 20 µM choline the current is reduced to 23.61 ± 1.13 % at 80 µM O_2. This was increased to 46.59 ± 0.93 % at 50 µM and reduced to 20.39 ± 0.94 % at 30 µM O_2. For 60 µM choline the current is reduced to 41.89 ± 1.66 % at 80 µM O_2. This was decreased to 34.22 ± 2.33 % at 50 µM and 26.48 ± 0.42 % at 30 µM O_2. Similarly, for 100 µM choline the current is reduced to 44.67 ± 1.13 % at 80 µM O_2. This was decreased to 37.47 ± 2.58 % at 50 µM and 19.75 ± 0.14 % at 30 µM O_2. Finally, for 200 µM choline the current is reduced to 42.75 ± 3.55 % at 80 µM O_2. This was decreased to 28.16 ± 2.61 % at 50 µM and 16.26 ± 0.14 % at 30 µM O_2. Oxygenation of Nafion® for 2 minute has resulted in a linear response in relation to O_2 concentration. In addition, the level of O_2 dependence for increased choline concentration remained the same. These results are comparable to those observed with 1 minute of oxygenation of the Nafion® (Section 5.3.3.3). These results suggest that the oxygenation of the Nafion®, rather than increasing the oxygen content, has caused evaporation of the solvent. Potentially, the ethanol with which the Nafion® is dissolved in has evaporated increasing the Nafion® concentration. A higher Nafion® concentration would create a diffusion barrier which would produce a linear response to O_2 dependence as illustrated in Figure 5.20 B. Therefore it is more probable that the effect the Nafion® is displaying is due to an increased diffusion barrier at the electrode surface rather that the oxygen content of the Nafion®.

5.3.3.4. Deoxygenate – 1 minute

The previous section demonstrates that the oxygenation of the Nafion® does not aid O_2 independence of the sensor. In addition, the oxygenation of the Nafion® for both 1 minute and 2 minutes are comparable and produce a linear correlation between current an O_2 concentration. Therefore, an investigation was undertaken to determine if introducing N_2 into the Nafion® for 1 minute and 2 minutes would produce similar results to those observed with oxygenation of the Nafion®. This would potentially highlight the effect of diffusion on O_2 dependence as the O_2 will be purged from the reservoirs, therefore this cannot be the effect on O_2 dependence.

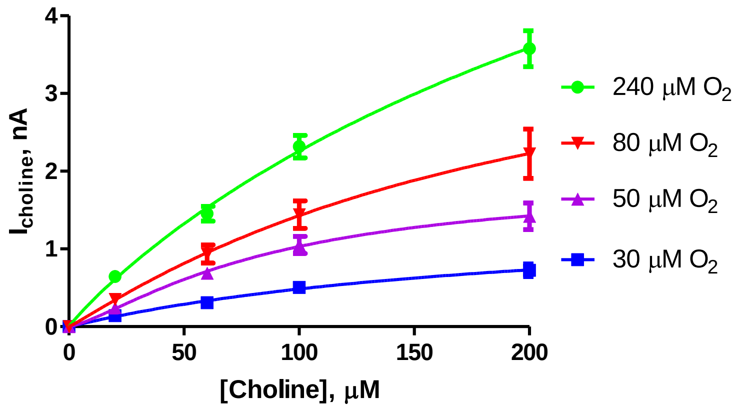

	30 μM O_2			50 μM O_2			80 μM O_2			240 μM O_2		
Choline Conc, μM	**Mean, nA**	**S.E.M, nA**	**n**	**Mean, nA**	**S.E.M, nA**	**n**	**Mean, nA**	**S.E.M, nA**	**n**	**Mean, nA**	**S.E.M, nA**	**n**
0	0.00	0.00	3	0.00	0.00	3	0.00	0.00	3	0.00	0.00	3
20	0.14	0.02	3	0.24	0.03	3	0.35	0.04	3	0.65	0.04	3
60	0.31	0.04	3	0.69	0.06	3	0.94	0.12	3	1.45	0.09	3
100	0.51	0.06	3	1.05	0.11	3	1.44	0.18	3	2.32	0.15	3
200	0.73	0.08	3	1.42	0.17	3	2.22	0.32	3	3.58	0.23	3

Figure 5.21 : The choline current-oxygen concentration profile comparison and comparison table for calibration in PBS (pH 7.4) buffer solution at 21°C using 1 minute deoxygenated Nafion®. CPA carried out at +700 mV *vs.* SCE. Sequential current steps for 20, 60, 100 and 200 μM choline chloride injection at 30, 50 and 80 μM O_2 concentrations.

The results obtained from the investigation into deoxygenating the Nafion® for 1 minute are presented in Figure 5.21. The data illustrates the effect of four O_2 concentrations 240, 80, 50 and 30 μM on the choline calibration curve. The data also illustrates the effect of the decreasing the O_2 concentration on the choline calibration of 20, 60, 100 and 200 μM choline. This design demonstrates a lower degree of O_2 dependence compared to the 1 minute of oxygenation (Section 5.3.3.3), however there is still a high degree of O_2 dependence with this design. This suggests however, that the O_2 content of the Nafion® does not play a large role in obtaining O_2 independence. The current at 20 μM choline decreased from 0.65 ± 0.04 nA to 0.35 ± 0.04 nA, n = 3 with a decrease in O_2 concentration from 240 μM to 80 μM. The decrease to 50 μM O_2 decreased the current to 0.24 ± 0.03 nA, n = 3 and at 30 μM the current was reduced to 0.14 ± 0.02 nA, n = 3. O_2 dependence was also observed using 60 μM choline. At 80 μM O_2 the current is reduced from 1.45 ± 0.09 nA to 0.94 ± 0.12 nA, n = 3. This was reduced to 0.69 ± 0.06 nA, n = 3 at 50 μM O_2 and 0.31 ± 0.04 nA, n = 3 at 30 μM. 100 μM choline demonstrated a decrease in current from 2.32 ± 0.15 nA to 1.44 ± 0.18 nA, n = 3 with a reduction in O_2 concentration from 240 to 80 μM. This was reduced to 1.05 ± 0.11 nA, n = 3 at 50 μM O_2 and 0.51 ± 0.06 nA, n = 3 at 30 μM O_2. 200 μM choline demonstrates a decrease from 3.58 ± 0.23 nA to 2.22 ± 0.32 nA, n = 3 from 240 μM to 80 μM O_2. This decreased to 1.42 ± 0.17 nA, n = 3 at 50 μM O_2 and 0.73 ± 0.08 nA, n = 3 at 30 μM O_2. This design does display a high level of O_2 dependence however is improved compared to the same design using oxygenation of the Nafion® for 1 minute.

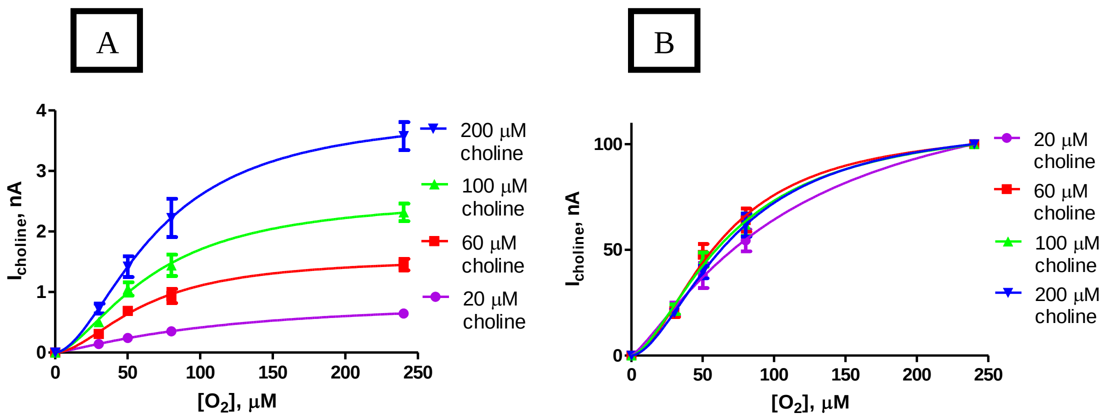

	20 µM			60 µM			100 µM			200 µM		
O_2 Conc, µM	Mean %	S.E.M	n	Mean %	S.E.M	n	Mean %	S.E.M	n	Mean %	S.E.M	n
0	0.00	0.00	3	0.00	0.00	3	0.00	0.00	3	0.00	0.00	3
30	21.95	3.09	3	21.12	2.92	3	21.86	2.33	3	20.24	1.51	3
50	37.86	5.91	3	47.60	5.12	3	45.31	3.37	3	39.51	2.99	3
80	54.44	5.20	3	64.01	5.49	3	61.94	5.29	3	61.70	5.47	3
240	100.00	0.00	3	100.00	0.00	3	100.00	0.00	3	100.00	0.00	3

Figure 5.22 A : The choline current-oxygen concentration profile comparison for calibration in PBS (pH 7.4) buffer solution at 21°C using design 1 minute deoxygenated Nafion®. CPA carried out at +700 mV *vs*. SCE. Sequential current steps for 20, 60, 100 and 200 µM choline chloride injection at 30, 50 and 80 µM O_2 concentrations. Figure 5.22 B the normalised choline current-oxygen concentration profile comparison and comparison table for the design 1 minute deoxygenated Nafion®.

The data in Figure 5.22 A illustrates the effect of four choline concentrations 20, 60, 100 and 200 µM on the O_2 dependence. The data in Figure 5.22 B also illustrates the normalised percentage values for each choline concentration at the O_2 concentrations 30, 50 and 80 µM. A high degree of O_2 dependence is observed similar to that for 1 minute of oxygenation of Nafion® (see Section 5.3.3.3). This demonstrates that the oxygenation of the Nafion® is not the primary cause of the change in the level of O_2 dependence, however is more potentially as a result of the evaporation of the Nafion® solvent due to the bubbling of gas through the Nafion®. The normalised data demonstrates that the increased level of O_2 dependence observed due to increased choline concentration has been eliminated. Almost identical levels of O_2 dependence are observed for each choline concentration. For 20 µM choline the current is reduced to 54.44 ± 5.20 % at 80 µM O_2. This was decreased to 37.86 ± 5.91 % at 50 µM and reduced to 21.95 ± 3.09 % at 30 µM O_2. For 60 µM choline the current is reduced to 64.01 ± 5.49 % at 80 µM O_2. This was decreased to 47.60 ± 5.12 % at 50 µM and 21.12 ± 2.92 % at 30 µM O_2. Similarly, for 100 µM choline the current is reduced to 61.94 ± 5.29 % at 80 µM O_2. This was decreased to 45.31 ± 3.37 % at 50 µM and 21.86 ± 2.33 % at 30 µM O_2. Finally, for 200 µM choline the current is reduced to 61.70 ± 5.47 % at 80 µM O_2. This was decreased to 39.51 ± 2.99 % at 50 µM and 20.24 ± 1.51 % at 30 µM O_2. This data demonstrates the beneficial effect deoxygenating has on O_2

dependence compared to the same design oxygenating the Nafion®. This suggests that the Nafion® introduces a diffusion constraint to aid O_2 dependence rather than the Nafion® containing high levels of O_2 for release in low levels of O_2.

5.3.3.5. Deoxygenate – 2 minutes

As 1 minute deoxygenation of the Nafion® proved to have similar effects to 1 minute oxygenation this section was undertaken to investigate the effect of deoxygenation of Nafion® for 2 minutes.

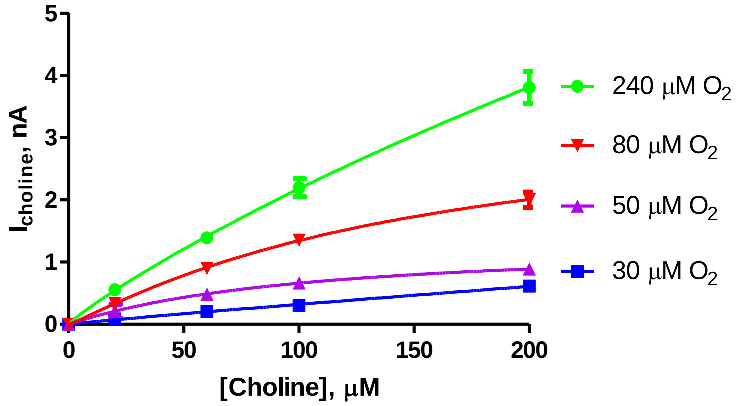

	30 µM O_2			50 µM O_2			80 µM O_2			240 µM O_2		
Choline Conc, µM	Mean, nA	S.E.M, nA	n	Mean, nA	S.E.M, nA	n	Mean, nA	S.E.M, nA	n	Mean, nA	S.E.M, nA	n
0	0.00	0.00	3	0.00	0.00	3	0.00	0.00	3	0.00	0.00	3
20	0.08	0.01	3	0.21	0.11	3	0.34	0.01	3	0.56	0.03	3
60	0.20	0.02	3	0.48	0.05	3	0.90	0.05	3	1.39	0.09	3
100	0.31	0.03	3	0.67	0.06	3	1.36	0.10	3	2.20	0.14	3
200	0.61	0.05	3	0.89	0.06	3	2.01	0.12	3	3.81	0.26	3

Figure 5.23 : The choline current-oxygen concentration profile comparison and comparison table for calibration in PBS (pH 7.4) buffer solution at 21°C using 2 minutes deoxygenated Nafion®. CPA carried out at +700 mV *vs.* SCE. Sequential current steps for 20, 60, 100 and 200 µM choline chloride injection at 30, 50 and 80 µM O_2 concentrations.

The results obtained from the investigation into deoxygenating the Nafion® for 2 minutes are presented in Figure 5.23. The data illustrates the effect of four O_2 concentrations 240, 80, 50 and 30 µM on the choline calibration curve. The data also illustrates the effect of the decreasing the O_2 concentration on the choline calibration of 20, 60, 100 and 200 µM choline. This design demonstrates a similar degree of O_2 dependence compared to the 1 minute of deoxygenation (Section 5.3.3.5), however there is still a high degree of O_2 dependence with this design. This is similar to the oxygenated Nafion® design see Section 5.3.3.4. The current at 20 µM choline decreased from 0.56 ± 0.03 nA to 0.34 ± 0.01 nA, n = 3 with a decrease in O_2 concentration from 240 µM to 80 µM. The decrease to 50 µM O_2 decreased the current to 0.21 ± 0.11 nA, n = 3 and at 30 µM the current was reduced to 0.08 ± 0.02 nA, n = 3. O_2 dependence was also observed using 60 µM choline. At 80 µM O_2 the current is reduced from 1.39 ± 0.09 nA to 0.90 ± 0.05 nA, n = 3. This was reduced to 0.48 ± 0.05 nA, n = 3 at 50 µM O_2 and 0.20 ± 0.02 nA, n = 3 at 30 µM. 100 µM choline demonstrated a decrease in current from 2.20 ± 0.14 nA to 1.36 ± 0.10 nA, n = 3 with a reduction in O_2 concentration from 240 to 80 µM. This was reduced to 0.67 ± 0.06 nA, n = 3 at 50 µM O_2 and 0.31 ± 0.03 nA, n = 3 at 30 µM O_2. 200 µM choline demonstrates a decrease from 3.81 ± 0.26 nA to 2.01 ± 0.12 nA, n = 3 from 240 µM to 80 µM O_2. This decreased to 0.89 ± 0.06 nA, n = 3 at 50 µM O_2 and 0.61 ± 0.05 nA, n = 3 at 30 µM O_2. Deoxygenating the Nafion® for 2 minutes has had little effect on both the current observed and the level of O_2 dependence observed when compared to both the 1 minute deoxygenated design and the 2 minute oxygenated design. This suggests that the oxygen content of the Nafion® is of little importance for O_2 dependence.

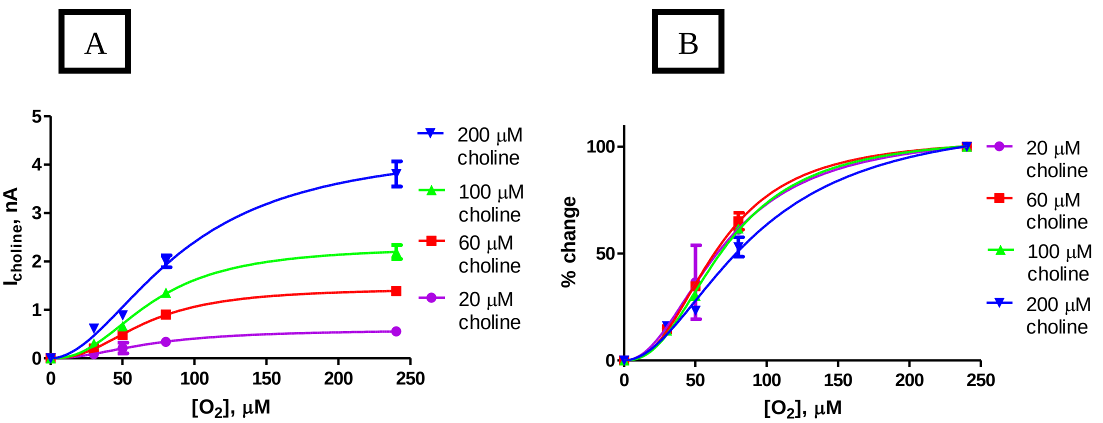

	20 µM			60 µM			100 µM			200 µM		
O_2 Conc, µM	Mean %	S.E.M	n	Mean %	S.E.M	n	Mean %	S.E. M	n	Mean %	S.E. M	n
0	0.00	0.00	3	0.00	0.00	3	0.00	0.00	3	0.00	0.00	3
30	15.01	0.33	3	14.59	0.30	3	14.01	0.28	3	16.08	0.27	3
50	36.60	17.26	3	34.70	2.10	3	30.22	0.80	3	23.36	0.43	3
80	61.06	1.75	3	65.13	3.95	3	61.71	0.28	3	53.07	4.55	3
240	100.00	0.00	3	100.00	0.00	3	100.00	0.00	3	100.00	0.00	3

Figure 5.24 A: The choline current-oxygen concentration profile comparison for calibration in PBS (pH 7.4) buffer solution at 21°C using 2 minutes deoxygenated Nafion®. CPA carried out at +700 mV *vs*. SCE. Sequential current steps for 20, 60, 100 and 200 µM choline chloride injection at 30, 50 and 80 µM O_2 concentrations. Figure 5.24 B the normalised choline current-oxygen concentration profile comparison and comparison table for the design 2 minutes deoxygenated Nafion®.

The data in Figure 5.24 A illustrates the effect of four choline concentrations 20, 60, 100 and 200 µM on the O_2 dependence. The data in Figure 5.24 B also illustrates the normalised percentage values for each choline concentration at the O_2 concentrations 30, 50 and 80 µM. A high degree of O_2 dependence is observed similar to that of 1 minute of deoxygenation of Nafion® (see Section 5.3.3.5). The normalised data demonstrates that the increased level of O_2 dependence observed due to increased choline concentration has been eliminated. Almost identical levels of O_2 dependence are observed for each choline concentration. For 20 µM choline the current is reduced to 61.06 ± 1.75 % at 80 µM O_2. This was decreased to 36.60 ± 17.26 % at 50 µM and reduced to 15.01 ± 0.33 % at 30 µM O_2. For 60 µM choline the current is reduced to 65.13 ± 3.95 % at 80 µM O_2. This was decreased to 34.70 ± 2.10 % at 50 µM and 14.59 ± 0.30 % at 30 µM O_2. Similarly, for 100 µM choline the current is reduced to 61.71 ± 0.28 % at 80 µM O_2. This was decreased to 30.22 ± 0.80 % at 50 µM and 14.01 ± 0.28 % at 30 µM O_2. Finally, for 200 µM choline the current is reduced to 53.07 ± 4.55 % at 80 µM O_2. This was decreased to 23.36 ± 0.43 % at 50 µM and 16.08 ± 0.27 % at 30 µM O_2. This section has illustrated that 2 minutes of oxygenation of Nafion® demonstrates comparable results to 1 minute of deoxygenation. In addition, these results have determined that purging the O_2 from the Nafion® has no detrimental effect to the O_2 dependence. As this is the case, this data has demonstrated that the effect that Nafion® has on O_2 dependence is more likely as a result of an additional diffusion barrier.

5.3.3.6. 10% Nafion®

The previous sections have illustrated that O_2 independence cannot be achieved by oxygenating the Nafion® solution. However, potentially the Nafion® has created a diffusion barrier with which to aid O_2 dependence. The addition of oxygen into the Nafion® for 30 seconds however did show promise. This may be as a result of an increase in Nafion® concentration through the evaporation of the ethanol which it is dissolved in. Therefore, this section investigates the effect of increasing the Nafion® concentration from 5% to 10%.

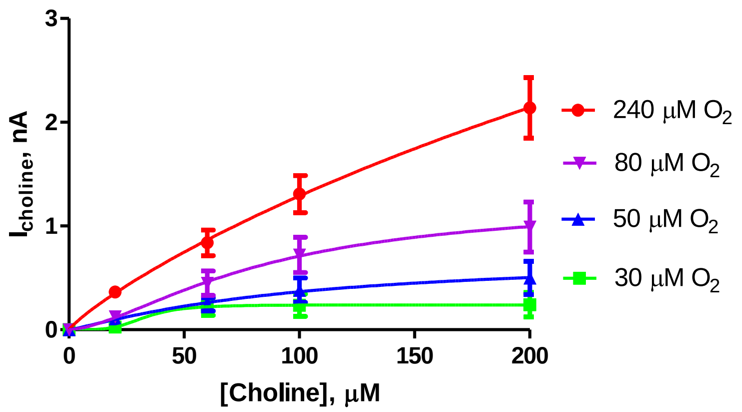

	30 µM O_2			50 µM O_2			80 µM O_2			240 µM O_2		
Choline Conc, µM	**Mean, nA**	**S.E.M, nA**	**n**	**Mean, nA**	**S.E.M, nA**	**n**	**Mean, nA**	**S.E.M, nA**	**n**	**Mean, nA**	**S.E.M, nA**	**n**
0	0.00	0.00	3	0.00	0.00	3	0.00	0.00	3	0.00	0.00	3
20	0.03	0.03	3	0.11	0.03	3	0.13	0.04	3	0.37	0.06	3
60	0.22	0.08	3	0.25	0.07	3	0.45	0.12	3	0.83	0.12	3
100	0.24	0.11	3	0.38	0.12	3	0.72	0.17	3	1.31	0.18	3
200	0.24	0.12	3	0.50	0.16	3	0.99	0.24	3	2.14	0.29	3

Figure 5.25 : The choline current-oxygen concentration profile comparison and comparison table for calibration in PBS (pH 7.4) buffer solution at 21°C using 10% Nafion® . CPA carried out at +700 mV *vs.* SCE. Sequential current steps for 20, 60, 100 and 200 µM choline chloride injection at 30, 50 and 80 µM O_2 concentrations.

The results obtained from the investigation into 10% Nafion® are presented in Figure 5.25. The data illustrates the effect of four O_2 concentrations 240, 80, 50 and 30 µM on the choline calibration curve. The data also illustrates the effect of the decreasing the O_2 concentration on the choline calibration of 20, 60, 100 and 200 µM choline. Increasing the Nafion® concentration to 10% did not have a beneficial effect on the O_2 dependence of the sensor. The current at 20 µM choline decreased from 0.37 ± 0.06 nA to 0.13 ± 0.04 nA, n = 3 with a decrease in O_2 concentration from 240 µM to 80 µM. The decrease to 50 µM O_2 decreased the current further to 0.11 ± 0.03 nA, n = 3 and at 30 µM the current was 0.03 ± 0.03 nA, n = 3. O_2 dependence is also observed using 60 µM choline. At 80 µM O_2 the current is reduced from 0.83 ± 0.12 nA to 0.45 ± 0.12 nA, n = 3. This was reduced to 0.25 ± 0.07 nA, n = 3 at 50 µM O_2 and 0.22 ± 0.08 nA, n = 3 at 30 µM. 100 µM choline demonstrated a decrease in current from 1.31 ± 0.18 nA to 0.72 ± 0.17 nA, n = 3 with a reduction in O_2 concentration from 240 to 80 µM. This was reduced to 0.38 ± 0.12 nA, n = 3 at 50 µM O_2 and 0.24 ± 0.11 nA, n = 3 at 30 µM O_2. 200 µM choline demonstrates a decrease from 2.14 ± 0.29 nA to 0.99 ± 0.24 nA, n = 3 from 240 µM to 80 µM O_2. This decreased to 0.50 ± 0.16 nA, n = 3 at 50 µM O_2 and 0.24 ± 0.12 nA, n = 3 at 30 µM O_2. These results demonstrate a high level of O_2 dependence.

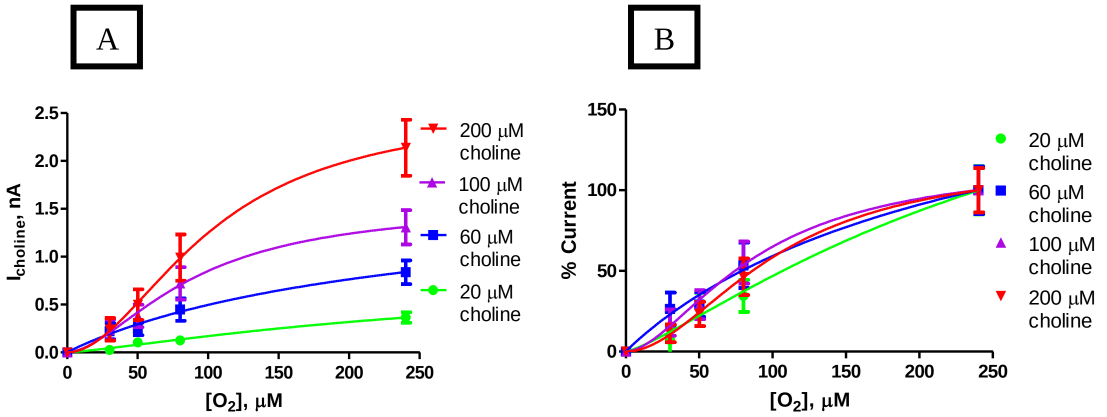

	20 μM			60 μM			100 μM			200 μM		
O_2 Conc, μM	Mean %	S.E.M	n	Mean %	S.E.M	n	Mean %	S.E.M	n	Mean %	S.E.M	n
0	0.00	0.00	3	0.00	0.00	3	0.00	0.00	3	0.00	0.00	3
30	7.14	7.37	3	26.48	10.04	3	18.00	8.19	3	11.30	5.51	3
50	29.04	7.37	3	29.22	7.75	3	29.11	9.01	3	23.36	7.50	3
80	34.50	9.91	3	53.48	14.04	3	55.13	13.00	3	46.34	11.30	3
240	100.00	14.96	3	100.00	14.79	3	100.00	13.70	3	100.00	13.69	3

Figure 5.26 A : The choline current-oxygen concentration profile comparison for calibration in PBS (pH 7.4) buffer solution at 21°C using 10% Nafion®. CPA carried out at +700 mV *vs.* SCE. Sequential current steps for 20, 60, 100 and 200 μM choline chloride injection at 30, 50 and 80 μM O_2 concentrations. Figure 5.26 B the normalised choline current-oxygen concentration profile comparison and comparison table for the design 10% Nafion®.

The data in Figure 5.26 A illustrates the effect of four choline concentrations 20, 60, 100 and 200 μM on the O_2 dependence. The data in Figure 5.26 B also illustrates the normalised percentage values for each choline concentration at the O_2 concentrations 30, 50 and 80 μM. A high degree of O_2 dependence is observed. For 20 μM choline the current is reduced to 34.50 ± 9.91 % at 80 μM O_2. This was decreased to 29.04 ± 7.37 % at 50 μM and reduced to 7.14 ± 7.37 % at 30 μM O_2. For 60 μM choline the current is reduced to 53.48 ± 14.04 % at 80 μM O_2. This was decreased to 29.22 ± 7.75 % at 50 μM and 26.48 ± 10.04 % at 30 μM O_2. Similarly, for 100 μM choline the current is reduced to 55.13 ± 13.00 % at 80 μM O_2. This was decreased to 29.11 ± 9.01 % at 50 µM and 18.00 ± 8.19 % at 30 µM O_2. Finally, for 200 µM choline the current is reduced to 46.34 ± 11.30 % at 80 µM O_2. This was decreased to 23.36 ± 7.50 % at 50 µM and 11.30 ± 5.51 % at 30 µM O_2. This data has demonstrated that increasing the Nafion® concentration to 10% does not have a beneficial effect on O_2 dependence. The normalised data demonstrates a similar linear response to O_2 dependence as seen oxygenating the Nafion®. This suggests that the introduction of O_2 into the Nafion® has evaporated the ethanol which the Nafion® is dissolved in concentrating the Nafion® solution.

5.3.4. Effect of Diffusion

The previous section investigated the O_2 content of the Nafion® and an alternative approach to the O_2 dependence experiments. These experiments were undertaken in order to determine the contribution of the high O_2 solubility characteristics of the Nafion® on the level of O_2 dependence. However the experiments potentially demonstrated that O_2 independence is not achieved as a result of the O_2 content of the Nafion® however rather as a result of an increase in the diffusion barrier. In order to examine this further, the Nafion® was removed from the sensor design and replaced with cellulose acetate (CelAce). Cellulose acetate will merely act as a diffusion barrier as it is not a perfluorcarbon. In order to determine the effect of diffusion on the level of O_2 dependence, the original O_2 dependence experimental design was utilised. In addition this will allow for easier comparison. In this section three concentrations of cellulose acetate were utilised 1, 2 and 3%.

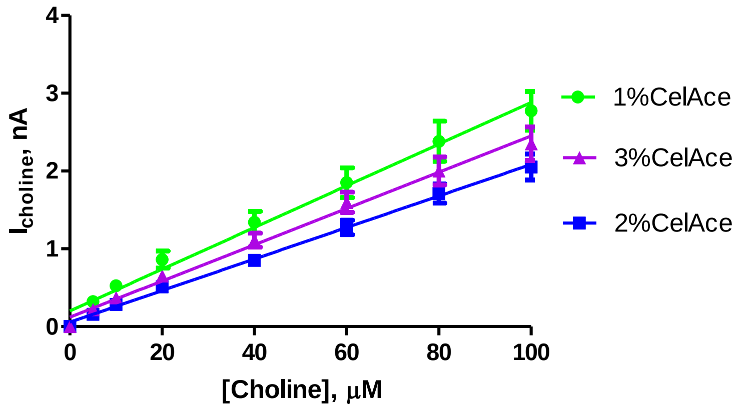

	1%CelAce			2%CelAce			3%CelAce		
Choline Conc, µM	Mean, nA	S.E.M, nA	n	Mean, nA	S.E.M, nA	n	Mean, nA	S.E.M, nA	n
0	0.00	0.00	3	0.00	0.00	7	0.00	0.00	3
5	0.32	0.03	3	0.16	0.01	7	0.22	0.02	3
10	0.53	0.05	3	0.28	0.02	7	0.37	0.03	3
20	0.86	0.11	3	0.51	0.03	7	0.65	0.05	3
40	1.34	0.14	3	0.85	0.07	7	1.11	0.09	3
60	1.85	0.19	3	1.28	0.09	7	1.60	0.13	3
80	2.38	0.26	3	1.71	0.12	7	2.00	0.18	3
100	2.77	0.25	3	2.05	0.17	7	2.35	0.22	3

Figure 5.27 : The current-concentration profile comparison and comparison table for choline chloride calibration in PBS (pH 7.4) buffer solution at 21°C using designs (A) 1%CelAce, (B) 2%CelAce and (C) 3%CelAce. CPA carried out at +700 mV *vs.* SCE. Sequential current steps for 10, 20, 40, 60, 80, 100 µM choline chloride injections.

Initially, the effect of the cellulose acetate was investigated with respect to sensitivity. The current values were reduced with increasing concentrations of cellulose acetate. However, the inclusion of cellulose acetate for the three concentrations had higher sensitivities than that displayed with the same design which incorporated Nafion®. A comparison graph and comparison data table for the choline sensitivity of the designs 1%CelAce, 2%CelAce and 3%CelAce are presented in Figure 5.27. The $I_{100\ \mu M}$ current for the CelAce1% is 2.77 ± 0.25 nA, n = 3. The increase in CelAce concentration to 2% decreased the $I_{100\ \mu M}$ current from 2.77 ± 0.25 nA, n = 3 (1%CelAce) to 2.05 ± 0.17 nA, n = 7 (2%CelAce). Increasing the CelAce concentration to 3% produced a current of 2.35 ± 0.22 nA, n = 3.

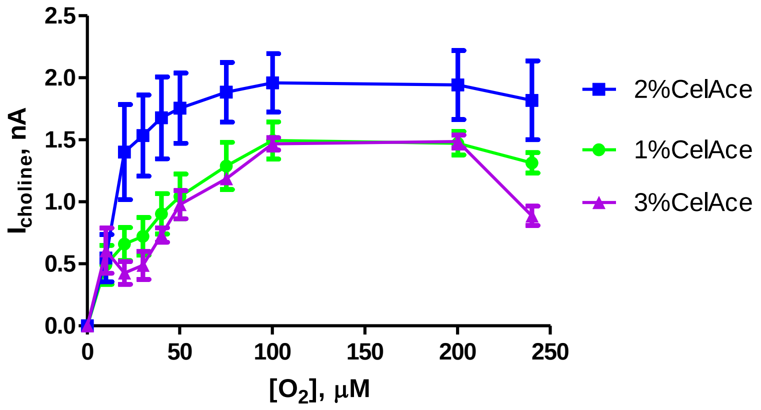

	1%CelAce			2%CelAce			3%CelAce		
O_2 Conc, μM	Mean, nA	S.E.M, nA	n	Mean, nA	S.E.M, nA	n	Mean, nA	S.E.M, nA	n
0	0.00	0.00	5	0.00	0.00	7	0.00	0.00	3
10	0.49	0.16	5	0.55	0.19	7	0.61	0.18	3
20	0.66	0.13	5	1.40	0.38	7	0.43	0.09	3
30	0.72	0.15	5	1.53	0.33	7	0.49	0.11	3
40	0.90	0.16	5	1.68	0.33	7	0.73	0.06	3
50	1.04	0.18	5	1.76	0.28	7	0.98	0.11	3
75	1.29	0.19	5	1.88	0.24	7	1.19	0.03	3
100	1.50	0.15	5	1.96	0.24	7	1.47	0.05	3
200	1.47	0.10	5	1.94	0.28	7	1.49	0.05	3
240	1.31	0.08	5	1.82	0.32	7	0.89	0.08	3

Figure 5.28 : The choline current-oxygen concentration profile comparison and comparison table for calibration in PBS (pH 7.4) buffer solution at 21°C using design (A) 1%CelAce, (B) 2%CelAce and (C) 3%CelAce. CPA carried out at +700 mV *vs.* SCE. Sequential current steps for 100 μM choline chloride injection at 10, 20, 30, 40, 50, 75, 100, 200, 240 μM O_2 concentrations.

Each design is also investigated with respect to their effect on O_2 dependence. It is evident from the traces in Figure 5.28 that the incorporation of 2%CelAce is the most O_2 independent design. The use of 1%CelAce demonstrates a similar O_2 dependence as that observed using 2.5%Nafion® (see Section 5.3.2.5). A linear response is observed until a plateau is reached at 100 μM. Increasing the concentration of CelAce to 2%

decreased the level of O_2 dependence of the sensor which is comparable to the (MMA)(5%Nafion®)(MMA) design. Increasing the concentration to 3% had no beneficial effect on the O_2 dependence. For the 1%CelAce design, the choline current obtained at 30 µM was 0.72 ± 0.15 nA, n = 5. The current at 50 µM was increased to 1.04 ± 0.18 nA, n = 5 and at 75 µM is 1.29 ± 0.19 nA, n = 7. The I_{MAX} was reached at 100 µM O_2 with a current of 1.50 ± 0.15 nA, n = 5. The current observed at 30 µM O_2 represents 43.96 ± 6.14 % of the I_{MAX} current. The current at 50 µM represents 64.60 ± 6.84 % of the I_{MAX} current and at 75 µM is 80.50 ± 6.61 % of the I_{MAX} current. Increasing the CelAce concentration to 2% decreased the level of O_2 dependence. At 30 µM O_2 the choline current observed was increased from 0.72 ± 0.15 nA, n = 5 (1%CelAce) to 1.53 ± 0.33 nA, n = 7 (2%CelAce). At 50 µM the current was increased from 1.04 ± 0.18 nA, n = 5 (1%CelAce) to 1.76 ± 0.28 nA, n = 7 (2%CelAce) and at 75 µM the current was from 1.29 ± 0.19 nA, n = 5 (1%CelAce) to 1.88 ± 0.24 nA, n = 7 (2%CelAce). The I_{MAX} was reached at 100 µM O_2 with a current of 1.96 ± 0.16 nA, n = 6. At 30 µM O_2 the percentage choline current of the I_{MAX} is increased from 43.96 ± 6.14 % (1%CelAce) to 69.37 ± 6.14 % (2%CelAce). At 50 µM the percentage is increased from 64.60 ± 6.84 % (1%CelAce) to 82.75 ± 2.83 % (2%CelAce) and at 75µM the percentage is increased from 80.50 ± 6.61 % (1%CelAce) to 91.34 ± 2.05 % (2%CelAce). Increasing the CelAce concentration further to 3% reduced the level of O_2 independence. The current obtained at 30 µM was 0.49 ± 0.11 nA, n = 3. The current at 50 µM was increased to 0.98 ± 0.11 nA, n = 3 and at 75 µM is 1.19 ± 0.03 nA, n = 3. The I_{MAX} was reached at 200 µM O_2 with a current of 1.49 ± 0.05 nA, n = 3. The current observed at 30 µM O_2 represents 32.50 ± 7.16 % of the I_{MAX} current, a further reduction in the O_2 independence previously observed. The current at 50 µM represents 65.89 ± 7.66 % of the I_{MAX} current and at 75 µM is 98.78 ± 0.14 % of the I_{MAX} current. The use of 2%CelAce is comparable to the use of 5% Nafion®. A comparison of the percentage current achieved compared to the I_{MAX} values shows that at 30 µM O_2 the percentage choline current of the I_{MAX} is decreased from 78.90 ± 6.19 % (5%Nafion®) to 69.37 ± 6.14 % (2%CelAce). At 50 µM the percentage is decreased from 88.50 ± 3.59 % (5%Nafion®) to 82.75 ± 2.83 % (2%CelAce) and at 75µM the percentage is decreased from 94.67 ± 1.31 % (5%Nafion®) to 91.34 ± 2.05 % (2%CelAce). These results verify that the benefit to O_2 dependence observed using Nafion® is not as a result of the O_2 content of the Nafion® however is a result of the additional diffusion barrier.

5.3.4.1. Cylinder

The previous section has illustrated the contribution of introducing additional diffusion layering to O_2 dependence. Increasing the diffusion layer has the potential to improve O_2 independence. This however is not possible for the current response observed with this sensor. Preliminary investigations were undertaken increasing the diffusional barrier on the sensor surface by a layer of glutaraldehyde as an additional layer on the sensor (data not shown). These investigations demonstrated potential for improving O_2 dependence however, the design was not viable on a disk electrode of this sensitivity, as the additional layer reduced the sensitivity of the design. In order to investigate the effect of additional diffusion layers, the sensitivity was increased by using a 1 mm cylinder design electrode. The increase in sensitivity would therefore allow for potential sacrifice of current during the investigation into additional diffusion layers.

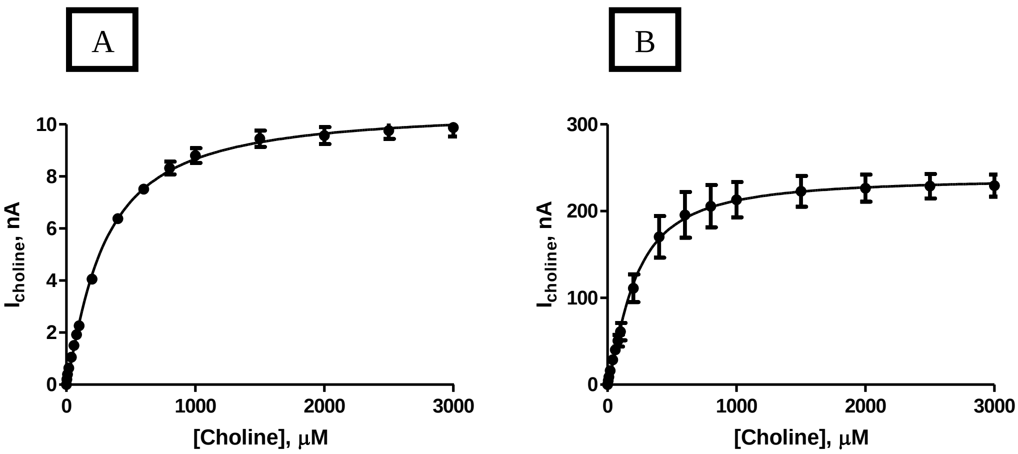

	Disk			Cylinder		
Choline Conc, μM	**Mean, nA**	**S.E.M, nA**	**n**	**Mean, nA**	**S.E.M, nA**	**n**
0	0.00	0.00	3	0.00	0.00	3
5	0.20	0.01	3	4.54	0.67	3
10	0.40	0.01	3	8.86	1.41	3
20	0.64	0.01	3	16.20	2.98	3
40	1.05	0.02	3	28.59	3.94	3
60	1.50	0.03	3	40.24	5.16	3
80	1.92	0.04	3	50.65	6.81	3
100	2.27	0.04	3	61.19	10.06	3
200	4.05	0.05	3	111.08	16.06	3
400	6.38	0.16	3	170.34	23.98	3
600	7.52	0.19	3	195.74	26.46	3
800	8.32	0.25	3	205.70	24.38	3
1000	8.81	0.28	3	213.15	20.38	3
1500	9.45	0.31	3	222.86	17.68	3
2000	9.57	0.33	3	226.50	15.62	3
2500	9.77	0.32	3	228.78	14.17	3
3000	9.88	0.34	3	229.42	12.82	3

Figure 5.29: The current-concentration profile for choline chloride in PBS (pH 7.4) buffer solution at 21°C using design (A) Pt(disk)(MMA)(CelAce)(MMA)-(ChOx)(BSA)(GA)(PEI) and (B) Pt(Cylinder)(MMA)(CelAce)(MMA)-(ChOx)(BSA)(GA)(PEI). CPA carried out at +700 mV *vs.* SCE for choline electrodes. Sequential current steps for 5, 10, 20, 40, 60, 80, 100, 200, 400, 600, 800, 1000, 1500, 2000, 2500, 3000 μM choline chloride injections.

The results presenting the current response obtained from the 1 mm cylinder electrode and disk electrode of design (MMA)(CelAce)(MMA)-(ChOx)(BSA)(GA)(PEI) are presented in Figure 5.29. The current response was increased dramatically by using a 1 mm cylinder electrode as expected. However, in order to accurately compare the sensitivity observed on the disk and cylinder electrode the currents were converted to current density which determines the current per unit area (O'Neill *et al.*, 2008) (see Section 3.2).

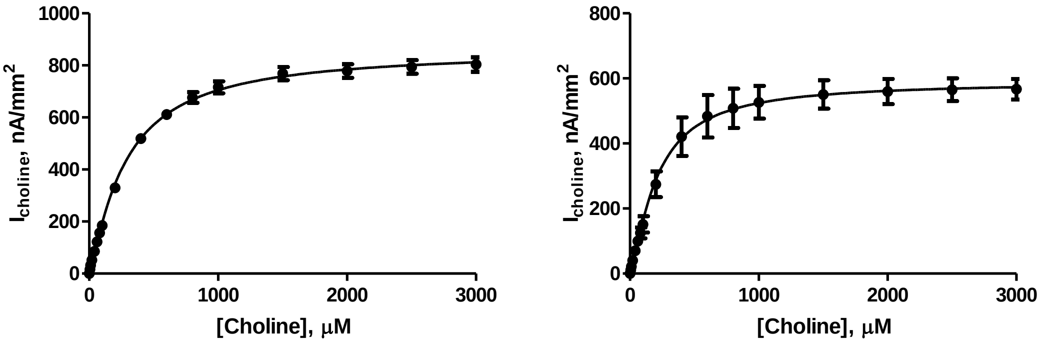

	Disk			Cylinder		
Choline Conc, μM	Mean, nA/mm^2	S.E.M, nA/mm^2	n	Mean, nA/mm^2	S.E.M, nA/mm^2	n
0	0.00	0.00	3	0.00	0.00	3
5	16.59	0.46	3	11.22	1.65	3
10	32.31	0.44	3	21.87	3.48	3
20	51.92	1.01	3	40.03	7.35	3
40	85.71	1.69	3	70.63	9.74	3
60	122.02	2.26	3	99.42	12.75	3
80	155.99	2.81	3	125.11	16.84	3
100	184.25	3.19	3	151.17	24.84	3
200	329.30	4.14	3	274.41	39.66	3
400	518.67	12.77	3	420.81	59.25	3
600	610.98	15.20	3	483.53	65.37	3
800	676.66	20.01	3	508.14	60.23	3
1000	715.94	22.87	3	526.55	50.34	3
1500	768.36	25.24	3	550.55	43.68	3
2000	778.37	26.42	3	559.53	38.58	3
2500	794.00	26.28	3	565.16	34.99	3
3000	803.44	27.77	3	566.75	31.66	3

Figure 5.30 : The current density-concentration profile for choline chloride in PBS (pH 7.4) buffer solution at 21°C using design (A) Pt(disk)(MMA)(CelAce)(MMA)-(ChOx)(BSA)(GA)(PEI) and (B) Pt(Cylinder)(MMA)(CelAce)(MMA)-(ChOx)(BSA)(GA)(PEI). CPA carried out at +700 mV *vs.* SCE for choline electrodes. Sequential current steps for 5, 10, 20, 40, 60, 80, 100, 200, 400, 600, 800, 1000, 1500, 2000, 2500, 3000 μM choline chloride injections.

The results presenting the current density response obtained from the 1 mm cylinder electrode and disk electrode of design (MMA)(CelAce)(MMA)-(ChOx)(BSA)(GA)(PEI) are presented in Figure 5.30. This presents the current obtained per unit area. The data demonstrates that although the current response has increased by using a 1 mm cylinder the current response with respect to the area of detection is decreased.

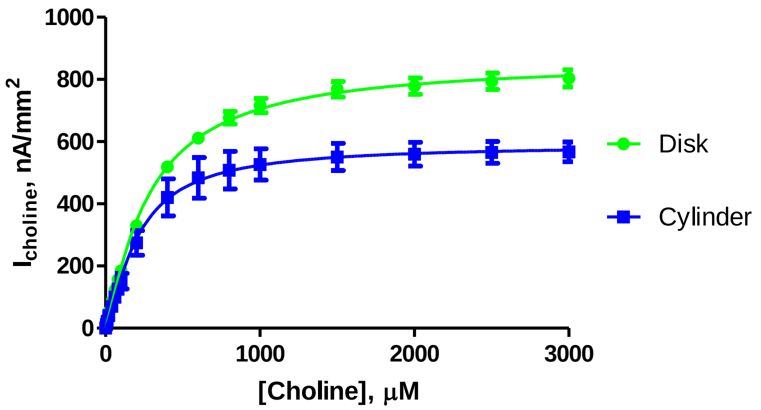

Kinetic Parameters	Disk			Cylinder		
	Mean	S.E.M	n	Mean	S.E.M	n
Vmax, nA/mm^2	859.60	14.96	3	589.50	23.93	3
Km, µM	281.30	14.21	3	208.50	26.34	3
α	1.20	0.05	3	1.33	0.16	3
$I_{100\ \mu M}$, nA/mm^2	184.25	3.19	3	151.17	24.84	3
Sensitivity, nA/ mm^2/µM	1.81	0.06	3	1.50	0.04	3
R^2	0.9929	0.0002	3	0.9921	0.0023	3
Background, nA/mm^2	21.12	2.77	3	3.62	0.25	3

Figure 5.31 : The current density-concentration profile comparison and comparison table for choline chloride calibration in PBS (pH 7.4) buffer solution at 21°C using designs (A) Pt(disk)(MMA)(CelAce)(MMA)-(ChOx)(BSA)(GA)(PEI) and (B) Pt(Cylinder)(MMA)(CelAce)(MMA)-(ChOx)(BSA)(GA)(PEI). CPA carried out at +700 mV *vs.* SCE. Sequential current steps for 5, 10, 20, 40, 60, 80, 100, 200, 400, 600, 800, 1000, 1500, 2000, 2500, 3000 µM choline chloride injections.

A comparison graph of current densities for the disk and cylinder electrodes is presented in Figure 5.31. The data demonstrates that the cylinder has a decrease in sensitivity per unit area when compared with the disk electrode. This has decreased the $I_{100\ \mu M}$ current density value from 184.25 ± 3.19 nA/mm^2, n = 3 (Disk) to 151.17 ± 24.84 nA/mm^2, n = 3 (Cylinder) despite the fact analysis of the current values illustrates that the $I_{100\ \mu M}$ current was increased from 2.27 ± 0.04 nA, n = 3 (Disk) to 61.19 ± 10.06 nA, n = 4 (Cylinder). In addition, the current density illustrates a decrease in the Vmax from 859.60 ± 14.96 nA/mm^2, n = 3 (Disk) to 589.50 ± 23.93 nA/mm^2, n = 3 (Cylinder) despite a current increase from 10.57 ± 0.18 nA, n = 3 (Disk) to 238.60 ± 9.69 nA, n = 4 (Cylinder). As current density demonstrates the current observed per unit area, the 1 mm cylinder design has a decreased current density compared to the disk electrode. This is potentially due to the retention of a dome of enzyme solution around the disk tip as it is removed from the solution; however the dome formed at the bottom of the cylinder electrode is negated by the total cylinder size which is 30 times bigger than a disk as the cylinder sides do not hold much solution (McMahon *et al.*, 2005). The current density is a consideration for the O_2 dependence of an electrode as an increase in the sensitivity of the electrode can have undesired effects on O_2 dependence (McMahon *et al.*, 2007b) however as the current per unit area is decreased this may prove beneficial for the use of a cylinder electrode.

5.3.5. Alternative Calibration Protocol

The experimental protocol utilised in Section 5.3.2 introduced air slowly after an aliquot of choline was added. This procedure did not yield consistent results. In Section 5.3.3 calibrations were performed in PBS of specific O_2 concentrations. This protocol was laborious and difficult to keep consistent. The protocol utilised in the following section requires the introduction of aliquots of choline in PBS which is bubbled with air. The air bubbling is replaced with N_2 bubbling until a plateau of N_2 saturation is reached. The N_2 bubbling is then replaced with air bubbling until a plateau of air saturation is reached (see Section 3.5.1.6). Both designs have been used previously by McMahon *et al.* for the O_2 dependence studies of both glucose and glutamate sensors (McMahon *et al.*, 2005; McMahon & O'Neill, 2005). The cell is constantly agitated by the gas bubbling. As with the previous designs the biosensor and O_2 currents were recorded simultaneously. The biosensor data was normalised relative to the I_{MAX} value and plotted against the measured concentration of O_2. The data from the calibrations performed from air saturated PBS to a N_2 saturated solution and the N_2 saturated PBS to and air saturated solution are presented. Firstly the effect of using a 1mm cylinder was determined with respect to sensitivity. Initial experiments were undertaken to investigate the O_2 dependence of the design (MMA)(CelAce)(MMA)-(ChOx)(BSA)(GA)(PEI) using a 1 mm cylinder Pt electrode.

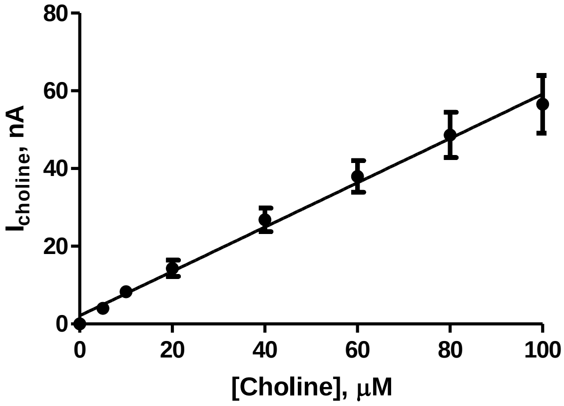

Choline Conc, µM	Mean, nA	S.E.M, nA	n
0	0.00	0.00	3
5	4.06	0.47	3
10	8.31	1.08	3
20	14.33	2.10	3
40	26.80	3.03	3
60	37.96	4.10	3
80	48.67	5.81	3
100	56.55	7.45	3

Figure 5.32 : The current-concentration profile for choline chloride in PBS (pH 7.4) buffer solution at 21°C using design Pt(cylinder)(MMA)(CelAce)(MMA)-(ChOx)(BSA)(GA)(PEI) CPA carried out at +700 mV *vs*. SCE for choline electrodes. Sequential current steps for 5, 10, 20, 40, 60, 80, 100 µM choline chloride injections.

The data in Figure 5.32 illustrates the current response observed for the Pt(cylinder)(MMA)(CelAce)(MMA)-(ChOx)(BSA)(GA)(PEI). The $I_{100\ \mu M}$ current observed was 56.55 ± 7.45 nA, n = 3.

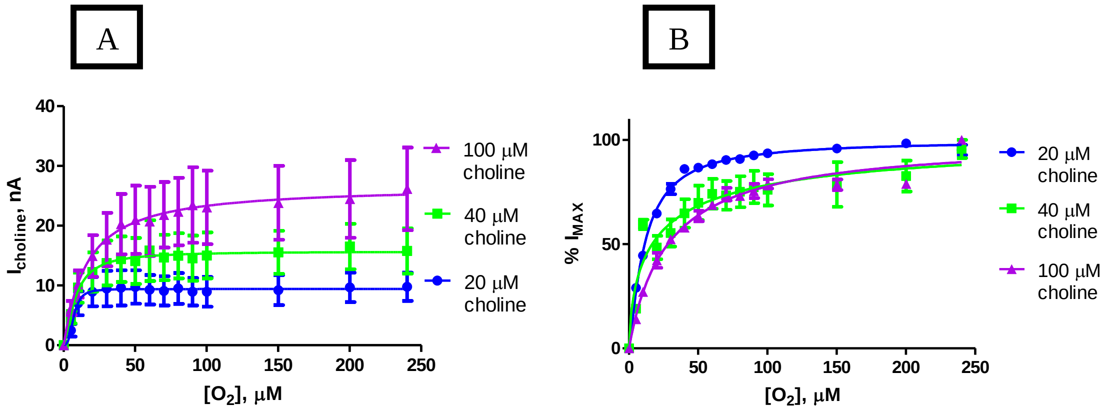

	20 µM Choline			40 µM Choline			100 µM Choline		
O_2 Conc, µM	Mean, nA	S.E.M, nA	n	Mean, nA	S.E.M, nA	n	Mean, nA	S.E.M, nA	n
0	0.00	0.00	3	0.00	0.00	3	0.00	0.00	3
10	3.18	0.94	3	4.97	1.52	3	6.82	1.37	3
20	4.62	1.32	3	7.01	2.25	3	10.66	2.27	3
30	5.53	1.68	3	7.99	2.54	3	13.49	3.30	3
40	6.15	1.77	3	9.29	2.81	3	15.13	4.07	3
50	6.20	1.76	3	10.12	3.25	3	16.68	4.83	3
60	6.33	1.83	3	10.60	3.11	3	18.03	4.95	3
70	6.55	2.04	3	10.58	3.17	3	19.24	5.16	3
80	6.53	1.94	3	10.78	3.22	3	19.25	5.49	3
90	6.57	1.79	3	11.17	3.41	3	19.77	5.58	3
100	6.66	1.86	3	10.96	3.32	3	20.50	5.38	3
150	6.82	1.91	3	11.52	3.94	3	20.86	6.28	3
200	7.10	2.15	3	11.85	3.47	3	20.83	5.99	3
240	6.75	1.86	3	13.12	2.26	3	26.15	7.01	3

Figure 5.33 A : The choline current-oxygen concentration profile comparison for calibration in PBS (pH 7.4) buffer solution at 21°C using design Pt(cylinder)(MMA)(CelAce)(MMA)-(ChOx)(BSA)(GA)(PEI) CPA carried out at +700 mV *vs.* SCE for choline electrodes and -650 mV *vs* SCE for the O_2 electrode. Current values for 20 µM, 40 µM and 100 µM choline chloride injections at 10, 20, 30, 40, 50, 60, 70, 80, 90, 100, 150, 200, 240 µM O_2 concentrations. Figure 5.33 B: The normalised choline current-oxygen concentration profile comparison. Table: Data table for choline current-oxygen concentration profile comparison.

The data illustrates the effect of three choline concentrations 20, 40 and 100 µM on O_2 dependence. Also presented is the graphically normalised data for the determination of the level of O_2 dependence of the sensors at the three choline concentrations. This experiment was performed from an air saturated cell and the air was purged by the introduction of N_2 until a plateau of N_2 saturation was reached. The current comparison above illustrates the difference in the level of O_2 dependence for the choline concentration 20 µM, 40 µM and 100 µM. A comparison of the choline current at three physiologically relevant O_2 concentrations of 30, 50 and 80 µM O_2 demonstrates the level of O_2 dependence that may be experienced in the *in-vivo* environment. Using 20 µM choline, the current observed at 30 µM O_2 is 5.53 ± 1.68 nA, n = 3 at 50 µM O_2 this is increased to 6.20 ± 1.76 nA, n = 3 and current observed at 80 µM is 6.53 ± 2.59 nA, n = 3. The low choline concentration displays minimal fluctuations in choline current at the physiological range of O_2 concentrations. An I_{MAX} of 7.10 ± 2.15 nA, n = 3 is reached at 200 µM O_2. The choline current at 30 µM O_2 represents 76.38 ± 2.46 % of the I_{MAX} current, meanwhile 50 µM is 86.70 ± 0.74 % and 80 µM is 90.77 ± 0.37 %. There is a potential 14 % fluctuation in the choline current over the physiological O_2 concentration range. This is comparable to the previous designs which incorporated Nafion® (see Section 5.3.2.4) and Cellulose Acetate (see Section 5.3.4). These designs however, were developed using a disk electrode. The O_2 dependence of these previous designs were investigated using 100 µM choline, however the dramatic increase in sensitivity of the electrode using a 1 mm cylinder will automatically increase the level of O_2 dependence of the sensor. The sensitivity of the current sensor at 20 µM is seven times higher than that of the current observed using 100 µM choline on the disk design. Therefore, the comparability of the levels of O_2 dependence of the disk and cylinder electrodes suggests that the cylinder electrode has decreased the O_2 dependence of the sensor. The current observed using 40 µM choline at 30 µM O_2 is 7.99 ± 2.54 nA, n = 3 at 50 µM O_2 this is increased to 10.12 ± 3.25 nA, n = 3 and the current observed at 80 µM is 10.78 ± 3.22 nA, n = 3. The increase in choline concentration from 20 µM to 40 µM increased the level of O_2 dependence increasing the current fluctuations observed between 30 µM and 50 µM O_2 when compared with 20 µM choline. An I_{MAX} of 13.12 ± 2.26 nA, n = 3 is reached at 200 µM O_2. The choline current at 30 µM O_2 represents 55.34 ± 6.48 % of the I_{MAX} current, meanwhile 50 µM is 69.79 ± 8.22 % and 80 µM is

75.13 ± 7.43 %. This demonstrates a potential fluctuation in the choline current of 20 % between the physiologically relevant O_2 concentrations. Increasing the choline concentration to 100 µM choline, the current observed at 30 µM O_2 is 13.49 ± 3.30 nA, n = 3 at 50 µM O_2 this is increased to 16.68 ± 4.83 nA, n = 3 and the current observed at 80 µM is 19.25 ± 5.49 nA, n = 3. The increase in choline concentration to 100 µM increased the level of O_2 dependence increasing the current fluctuations observed between 30 µM and 50 µM O_2. An I_{MAX} of 26.15 ± 7.01 nA, n = 3 is reached at 240 µM O_2. The choline current at 30 µM O_2 represents 52.31 ± 1.53 % of the I_{MAX} current, meanwhile 50 µM is 63.40 ± 2.52 % and 80 µM is 73.09 ± 1.48 % a potential fluctuation of 21 %. The level of O_2 dependence observed at 40 µM and 100 µM choline are similar as demonstrated by the normalised graph in Figure 5.33. However, both are reduced in comparison to the level of O_2 independence observed at 20 µM choline. The level of O_2 dependence of this design is suitable for low concentrations of choline. The level of choline has been reported to be as low as 6 µM (Garguilo & Michael, 1996) which this design could suitably detect without O_2 interference.

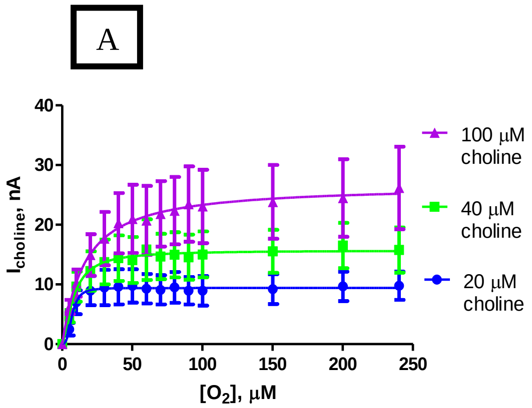

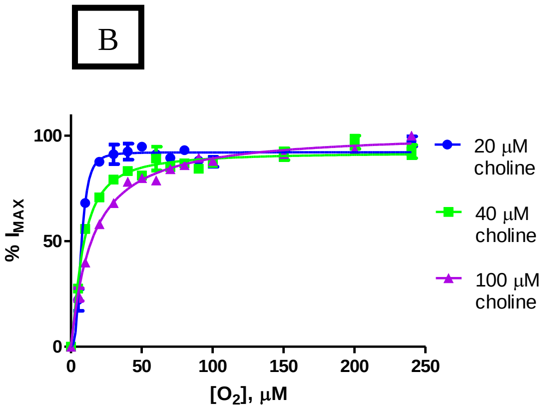

	20 µM Choline			40 µM Choline			100 µM Choline		
O_2 Conc, µM	Mean, nA	S.E.M, nA	n	Mean, nA	S.E.M, nA	n	Mean, nA	S.E.M, nA	N
0	0.00	0.00	3	0.00	0.00	3	0.00	0.00	3
10	7.02	2.00	3	9.64	2.52	3	10.23	2.29	3
20	8.96	2.46	3	12.26	3.31	3	14.94	3.48	3
30	9.48	2.96	3	13.75	3.75	3	17.70	4.47	3
40	9.61	2.95	3	14.40	3.81	3	20.27	5.05	3
50	9.76	2.80	3	14.09	3.85	3	21.00	5.73	3
60	9.28	2.47	3	15.84	5.08	3	20.73	5.79	3
70	9.10	2.45	3	14.69	3.79	3	21.83	5.49	3
80	9.50	2.59	3	14.97	3.79	3	22.37	5.64	3
90	8.95	2.31	3	14.56	3.79	3	23.47	6.31	3
100	8.94	2.48	3	15.03	3.85	3	23.08	6.15	3
150	9.23	2.50	3	15.55	3.59	3	23.82	6.19	3
200	9.68	2.46	3	16.51	3.80	3	24.48	6.50	3
240	9.79	2.37	3	15.78	3.78	3	26.18	6.92	3

Figure 5.34 A : The choline current-oxygen concentration profile comparison for calibration in PBS (pH 7.4) buffer solution at 21°C using design Pt(cylinder)(MMA)(CelAce)(MMA)-(ChOx)(BSA)(GA)(PEI). CPA carried out at +700 mV *vs.* SCE for choline electrodes and -650 mV *vs* SCE for the O_2 electrode. Current values for 20 µM, 40 µM and 100 µM choline chloride injections at 10, 20, 30, 40, 50, 60, 70, 80, 90, 100, 150, 200, 240 µM O_2 concentrations. Figure 5.34 B: The normalised choline current-oxygen concentration profile comparison. Table: Data table for choline current-oxygen concentration profile comparison.

The data in Figure 5.34 A illustrates the effect of three choline concentrations 20, 40 and 100 µM on O_2 dependence. Also presented is Figure 5.34 B is the graphically normalised data for the determination of the level of O_2 dependence of the sensors at the three choline concentrations. Alternatively to the approach taken in Figure 5.33 this experiment was performed from a N_2 saturated cell and the air was introduced until a plateau of air saturation was reached. The current comparison above illustrates the difference in the level of O_2 dependence for the choline concentration 20 µM, 40 µM and 100 µM. A comparison of the choline current at three physiologically relevant O_2 concentrations of 30, 50 and 80 µM O_2 demonstrates the level of O_2 dependence that may be experienced in the *in-vivo* environment. Using 20 µM choline, the current observed at 30 µM O_2 is 9.48 ± 2.96 nA, n = 3 at 50 µM O_2 this is increased to 9.76 ±

2.80 nA, n = 3 and current observed at 80 µM is 9.50 ± 2.59 nA, n = 3. An I_{MAX} of 9.79 ± 2.37 nA, n = 3 is reached at 240 µM O_2. The choline current at 30 µM O_2 represents 91.12 ± 4.62 % of the I_{MAX} current, meanwhile 50 µM is 94.78 ± 2.01 % and 80 µM is 93.08 ± 1.19 %. There is a potential 3 % fluctuation in the choline current at the physiological O_2 concentration range. This design demonstrates minimal fluctuations in the current between 30 µM and 80 µM O_2. This design demonstrates excellent levels of O_2 independence at 20 µM choline. The current observed using 40 µM choline at 30 µM O_2 is 13.75 ± 3.75 nA, n = 3 at 50 µM O_2 this is increased to 14.09 ± 3.84 nA, n = 3 and the current observed at 80 µM is 15.84 ± 5.08 nA, n = 3. The increase in choline concentration from 20 µM to 40 µM increased the level of O_2 dependence increasing the current fluctuations observed between 30 µM and 50 µM O_2 when compared with 20 µM choline. An I_{MAX} of 16.51 ± 3.80 nA, n = 3 is reached at 200 µM O_2. The choline current at 30 µM O_2 represents 79.20 ± 1.84 % of the I_{MAX} current, meanwhile 50 µM is 81.06 ± 1.35 % and 80 µM is 86.88 ± 1.04 % a potential fluctuation of 7 %. Increasing the choline concentration to 100 µM choline, the current observed at 30 µM O_2 is 17.70 ± 4.47 nA, n = 3 at 50 µM O_2 this is increased to 21.00 ± 5.73 nA, n = 3 and the current observed at 80 µM is 22.37 ± 5.68 nA, n = 3. The increase in choline concentration to 100 µM increased the level of O_2 dependence increasing the current fluctuations observed between 30 µM and 50 µM O_2. An I_{MAX} of 26.18 ± 6.92 nA, n = 3 is reached at 240 µM O_2. The choline current at 30 µM O_2 represents 68.06 ± 0.90 % of the I_{MAX} current, meanwhile 50 µM is 79.88 ± 0.88 % and 80 µM is 86.04 ± 1.23 %. For 100 µM choline the potential fluctuation in current between the physiological O_2 concentration range is 18 %. This is comparable to the fluctuation observed on the Nafion® disk design (see Section 5.3.2.4).

5.3.5.1. CelAce 0.5%

The motivation behind increasing the dimensions of the active surface to a 1 mm cylinder, thus increasing the current, was to determine the effect of additional layers which would increase the diffusion barrier and examine the effect on O_2 dependence. The high current was required as additional layers may decrease the sensitivity of the design, a sacrifice which could not be afforded on the disk design. In order to investigate additional diffusion barriers a layer of cellulose acetate was added to the end of the design (MMA)(CelAce)(MMA)-(ChOx)(BSA)(GA)(PEI). Initially the effect of 0.5% cellulose acetate was examined.

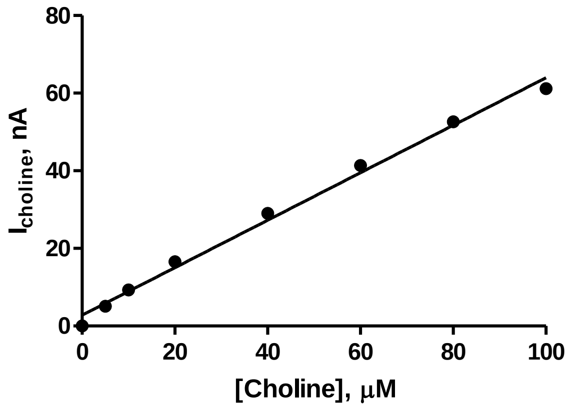

Choline Conc, μM	Mean, nA	S.E.M, nA	n
0	0.00	0.00	3
5	5.09	0.16	3
10	9.33	0.24	3
20	16.56	0.42	3
40	29.01	0.69	3
60	41.37	0.88	3
80	52.60	1.21	3
100	61.18	1.24	3

Figure 5.35 : The current-concentration profile for choline chloride in PBS (pH 7.4) buffer solution at 21°C using design (Pt(cylinder)(MMA)(CelAce)(MMA)-(ChOx)(BSA)(GA)(PEI))CelAce0.5%. CPA carried out at +700 mV *vs.* SCE for choline electrodes. Sequential current steps for 5, 10, 20, 40, 60, 80, 100 μM choline chloride injections.

The data in Figure 5.35 illustrates the current response observed for the (Pt(cylinder)(MMA)(CelAce)(MMA)-(ChOx)(BSA)(GA)(PEI))CelAce0.5%. The $I_{100\ \mu M}$ current observed was 61.18 ± 1.24 nA, n = 3.

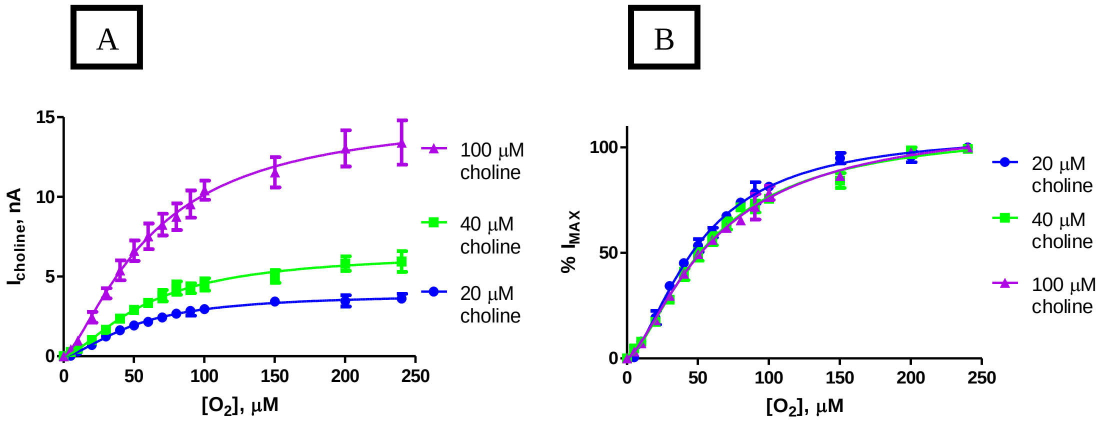

	20 µM Choline			40 µM Choline			100 µM Choline		
O_2 Conc, µM	Mean, nA	S.E.M, nA	n	Mean, nA	S.E.M, nA	n	Mean, nA	S.E.M, nA	n
0	0.00	0.00	3	0.00	0.00	3	0.00	0.00	3
10	0.30	0.08	3	0.47	0.02	3	0.98	0.26	3
20	0.70	0.14	3	1.02	0.03	3	2.44	0.34	3
30	1.25	0.13	3	1.65	0.12	3	3.95	0.32	3
40	1.63	0.14	3	2.35	0.11	3	5.39	0.63	3
50	1.93	0.18	3	2.90	0.16	3	6.62	0.64	3
60	2.16	0.18	3	3.34	0.17	3	7.53	0.80	3
70	2.43	0.13	3	3.80	0.36	3	8.26	0.68	3
80	2.67	0.18	3	4.28	0.42	3	8.76	0.84	3
90	2.84	0.29	3	4.27	0.31	3	9.55	0.85	3
100	2.95	0.25	3	4.50	0.39	3	10.44	0.60	3
150	3.43	0.27	3	5.01	0.40	3	11.54	0.95	3
200	3.47	0.36	3	5.81	0.46	3	13.04	1.14	3
240	3.62	0.29	3	5.94	0.65	3	13.41	1.39	3

Figure 5.36 A : The choline current-oxygen concentration profile comparison for calibration in PBS (pH 7.4) buffer solution at 21°C using design (Pt(cylinder)(MMA)(CelAce)(MMA)-(ChOx)(BSA)(GA)(PEI))CelAce0.5% . CPA carried out at +700 mV *vs.* SCE for choline electrodes and -650 mV *vs* SCE for the O_2 electrode. Current values for 20 µM, 40 µM and 100 µM choline chloride injections at 10, 20, 30, 40, 50, 60, 70, 80, 90, 100, 150, 200, 240 µM O_2 concentrations. Figure 5.36 B: The normalised choline current-oxygen concentration profile comparison. Table: Data table for choline current-oxygen concentration profile comparison.

The data in Figure 5.36 A illustrates the effect of three choline concentrations 20, 40 and 100 µM on O_2 dependence. Also presented in Figure 5.36 B is the graphically normalised data for the determination of the level of O_2 dependence of the sensors at the three choline concentrations. This experiment was performed from an air saturated cell and the air was purged by the introduction of N_2 until a plateau of N_2 saturation was reached. The current comparison above illustrates the difference in the level of O_2 dependence for the choline concentration 20 µM, 40 µM and 100 µM. A comparison of the choline current at three physiologically relevant O_2 concentrations of 30, 50 and 80 µM O_2 demonstrates the level of O_2 dependence that may be experienced in the *in-vivo* environment. Using 20 µM choline, the current observed at 30 µM O_2 is 1.25 ± 0.13 nA, n = 3 at 50 µM O_2 this is increased to 1.93 ± 0.18 nA, n = 3 and current observed at 80 µM is 2.67 ± 0.18 nA, n = 3. An I_{MAX} of 3.62 ± 0.29 nA, n = 3 is reached at 240 µM O_2. The choline current at 30 µM O_2 represents 34.29 ± 1.31 % of the I_{MAX} current, meanwhile 50 µM is 53.42 ± 3.06 % and 80 µM is 73.82 ± 1.03 %. There is a potential 39 % fluctuation in the choline current at the physiological O_2 concentration range. The addition of the cellulose acetate has decreased the level of O_2 independence of the sensor when compared with the design in Section 5.3.5 using the method of calibration which removes the air from the solution. The current observed using 40 µM choline at 30 µM O_2 is 1.65 ± 0.12 nA, n = 3 at 50 µM O_2 this is increased to 2.90 ± 0.16 nA, n = 3 and the current observed at 80 µM is 4.28 ± 0.42 nA, n = 3. The increase in choline concentration from 20 µM to 40 µM has dramatically increased the level of O_2 dependence increasing the current fluctuations observed between 30 µM and 50 µM O_2 when compared with 20 µM choline. An I_{MAX} of 5.91 ± 0.65 nA, n = 3 is reached at 240 µM O_2. The choline current at 30 µM O_2 represents 27.84 ± 1.71 % of the I_{MAX} current, meanwhile 50 µM is 49.06 ± 2.85 % and 80 µM is 71.56 ± 7.43 %. This is a potential 44 % fluctuation in current between 30 µM and 80 µM O_2. Increasing the choline concentration to 100 µM choline, the current observed at 30 µM O_2 is 3.95 ± 0.32 nA, n = 3 at 50 µM O_2 this is increased to 6.62 ± 0.64 nA, n = 3 and the current observed at 80 µM is 8.76 ± 0.84 nA, n = 3. An I_{MAX} of 13.41 ± 1.39 nA, n = 3 is reached at 240 µM O_2. The choline current at 30 µM O_2 represents 29.66 ± 1.55 % of the I_{MAX} current, meanwhile 50 µM is 49.49 ± 1.43 % and 80 µM is 65.39 ± 0.64 % a potential fluctuation of 36 %. The addition of the cellulose acetate layer has increased the level of O_2 dependence of the sensor when using this experimental design.

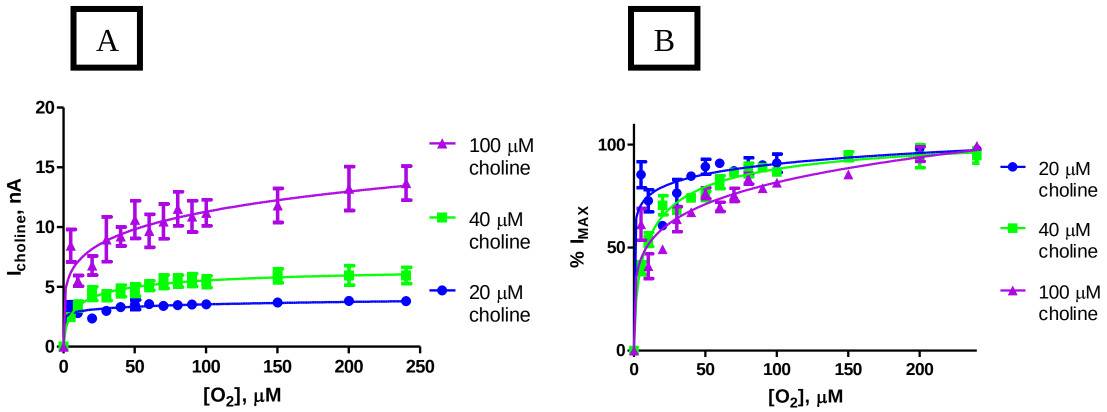

	20 µM Choline			40 µM Choline			100 µM Choline		
O_2 Conc, µM	Mean, nA	S.E.M, nA	n	Mean, nA	S.E.M, nA	n	Mean, nA	S.E.M, nA	n
0	0.00	0.00	3	0.00	0.00	3	0.00	0.00	3
10	2.81	0.10	3	3.39	0.42	3	5.50	0.45	3
20	2.36	0.12	3	4.44	0.57	3	6.79	0.80	3
30	2.99	0.38	3	4.27	0.41	3	8.98	1.88	3
40	3.31	0.24	3	4.66	0.49	3	9.22	0.80	3
50	3.50	0.40	3	4.72	0.52	3	10.63	1.58	3
60	3.55	0.31	3	5.11	0.40	3	9.69	1.39	3
70	3.41	0.30	3	5.43	0.55	3	10.48	1.46	3
80	3.48	0.21	3	5.49	0.51	3	11.54	1.42	3
90	3.52	0.30	3	5.57	0.53	3	10.90	1.31	3
100	3.54	0.29	3	5.44	0.49	3	11.20	1.09	3
150	3.69	0.30	3	5.92	0.59	3	11.82	1.42	3
200	3.83	0.31	3	5.96	0.82	3	13.23	1.84	3
240	3.81	0.30	3	5.96	0.69	3	13.69	1.42	3

Figure 5.37 A : The choline current-oxygen concentration profile comparison for calibration in PBS (pH 7.4) buffer solution at 21°C using design (Pt(cylinder)(MMA)(CelAce)(MMA)-(ChOx)(BSA)(GA)(PEI))CelAce0.5%. CPA carried out at +700 mV *vs*. SCE for choline electrodes and -650 mV *vs* SCE for the O_2 electrode. Current values for 20 µM, 40 µM and 100 µM choline chloride injections at 10, 20, 30, 40, 50, 60, 70, 80, 90, 100, 150, 200, 240 µM O_2 concentrations. Figure 5.37 B: The normalised choline current-oxygen concentration profile comparison. Table: Data table for choline current-oxygen concentration profile comparison.

The data in Figure 5.37 A illustrates the effect of three choline concentrations 20, 40 and 100 µM on O_2 dependence. Also presented in Figure 5.37 B is the graphically normalised data for the determination of the level of O_2 dependence of the sensors at the three choline concentrations. This experiment was performed from a N_2 saturated cell and the air was introduced until a plateau of N_2 saturation was reached. The current comparison above illustrates the difference in the level of O_2 dependence for the choline concentration 20 µM, 40 µM and 100 µM. A comparison of the choline current at three physiologically relevant O_2 concentrations of 30, 50 and 80 µM O_2 demonstrates the level of O_2 dependence that may be experienced in the *in-vivo* environment. Using 20 µM choline, the current observed at 30 µM O_2 is 2.99 ± 0.38 nA, n = 3 at 50 µM O_2 this is increased to 3.50 ± 0.40 nA, n = 3 and current observed at 80 µM is 3.48 ± 0.21 nA, n = 3. An I_{MAX} of 3.83 ± 0.31 nA, n = 3 is reached at 200 µM O_2. The choline current at 30 µM O_2 represents 76.42 ± 6.57 % of the I_{MAX} current, meanwhile 50 µM is 89.22 ± 3.62 % and 80 µM is 89.54 ± 3.96 %. There is a potential 13 % fluctuation in the choline current at the physiological O_2 concentration range. This level of O_2 independence is dramatically different to the levels observed with this sensor using the experimental design which removes the air rather than introduces it. This experimental design better illustrates the effect of diffusion on O_2 dependence. The current observed using 40 µM choline at 30 µM O_2 is 4.27 ± 0.41 nA, n = 3 at 50 µM O_2 this is increased to 4.72 ± 0.52 nA, n = 3 and the current observed at 80 µM is 5.49 ± 0.51 nA, n = 3. An I_{MAX} of 5.96 ± 0.82 nA, n = 3 is reached at 200 µM O_2. The choline current at 30 µM O_2 represents 68.05 ± 0.29 % of the I_{MAX} current, meanwhile 50 µM is 75.06 ± 2.27 % and 80 µM is 87.64 ± 3.32 %. This is a potential 19 % fluctuation in current between 30 µM and 80 µM O_2, a dramatic reduction to that experienced in the air removal protocol. Increasing the choline concentration to 100 µM choline, the current observed at 30 µM O_2 is 8.98 ± 1.88 nA, n = 3 at 50 µM O_2 this is increased to 10.63 ± 1.58 nA, n = 3 and the current observed at 80 µM is 11.54 ± 1.42 nA, n = 3. An I_{MAX} of 13.69 ± 1.43 nA, n = 3 is reached at 240 µM O_2. The choline current at 30 µM O_2 represents 63.76 ± 6.06 % of the I_{MAX} current, meanwhile 50 µM is 76.41 ± 2.62 % and 80 µM is 83.43 ± 2.62 % a potential fluctuation of 20 %. The addition of the cellulose acetate layer has decreased the level of O_2 dependence of the sensor when using this experimental design. A vast difference is observed using two different experimental protocols. The design which removes the air from the cell demonstrates a high level of O_2 dependence; however the reversal which introduces the air demonstrates a low level of O_2 dependence.

5.3.5.2. CelAce 1%

The effect of increasing the cellulose acetate concentration from 0.5% to 1% was investigated in this section.

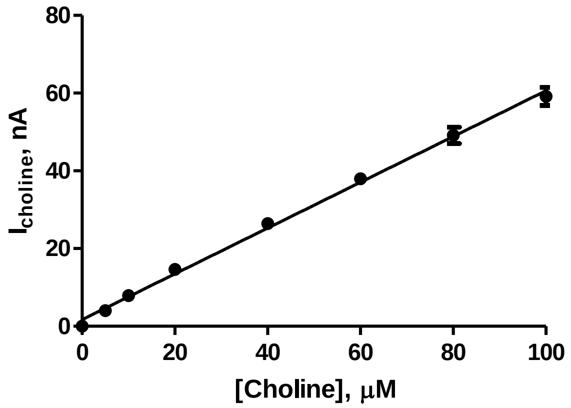

Choline Conc, µM	**Mean, nA**	**S.E.M, nA**	**n**
0	0.00	0.00	3
5	4.05	0.17	3
10	7.92	0.31	3
20	14.62	0.64	3
40	26.42	1.08	3
60	37.97	1.51	3
80	49.14	2.08	3
100	59.18	2.32	3

Figure 5.38 : The current-concentration profile for choline chloride in PBS (pH 7.4) buffer solution at 21°C using design (Pt(cylinder)(MMA)(CelAce)(MMA)-(ChOx)(BSA)(GA)(PEI))CelAce1%. CPA carried out at +700 mV *vs.* SCE for choline electrodes. Sequential current steps for 5, 10, 20, 40, 60, 80, 100 µM choline chloride injections.

The data in Figure 5.38 illustrates the current response observed for the (Pt(cylinder)(MMA)(CelAce)(MMA)-(ChOx)(BSA)(GA)(PEI))CelAce1%. The $I_{100\ \mu M}$ current observed was 59.18 ± 2.32 nA, n = 3. The increase in the concentration of CelAce has not affected the sensitivity of the electrode.

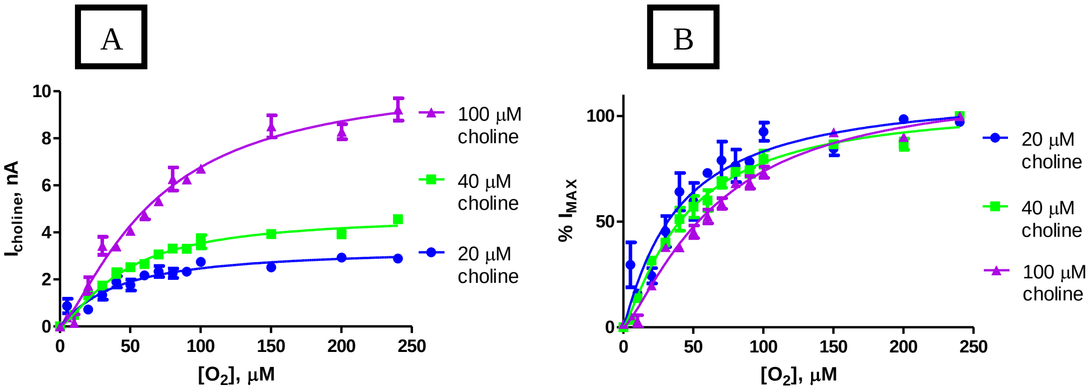

	20 µM Choline			40 µM Choline			100 µM Choline		
O_2 Conc, µM	Mean, nA	S.E.M, nA	n	Mean, nA	S.E.M, nA	n	Mean, nA	S.E.M, nA	n
0	0.00	0.00	3	0.00	0.00	3	0.00	0.00	3
10	0.48	0.02	3	0.49	0.06	3	0.15	0.36	3
20	0.72	0.10	3	1.33	0.12	3	1.74	0.36	3
30	1.34	0.20	3	1.74	0.12	3	3.43	0.38	3
40	1.90	0.24	3	2.24	0.20	3	3.40	0.18	3
50	1.76	0.24	3	2.52	0.17	3	4.07	0.14	3
60	2.17	0.05	3	2.66	0.15	3	4.75	0.19	3
70	2.34	0.23	3	3.06	0.02	3	5.33	0.18	3
80	2.26	0.20	3	3.32	0.16	3	6.27	0.49	3
90	2.33	0.03	3	3.30	0.09	3	6.26	0.14	3
100	2.75	0.08	3	3.61	0.28	3	6.72	0.18	3
150	2.51	0.05	3	3.93	0.14	3	8.51	0.47	3
200	2.93	0.08	3	3.92	0.02	3	8.28	0.32	3
240	2.89	0.09	3	4.56	0.14	3	9.23	0.47	3

Figure 5.39 A : The choline current-oxygen concentration profile comparison for calibration in PBS (pH 7.4) buffer solution at 21°C using design (Pt Pt(cylinder)(MMA)(CelAce)(MMA)-(ChOx)(BSA)(GA)(PEI))CelAce 1%. CPA carried out at +700 mV *vs.* SCE for choline electrodes and -650 mV *vs* SCE for the O_2 electrode. Current values for 20 µM, 40 µM and 100 µM choline chloride injections at 10, 20, 30, 40, 50, 60, 70, 80, 90, 100, 150, 200, 240 µM O_2 concentrations.

Figure 5.39 B: The normalised choline current-oxygen concentration profile comparison. Table: Data table for choline current-oxygen concentration profile comparison.

The data in Figure 5.39 A illustrates the effect of three choline concentrations 20, 40 and 100 µM on O_2 dependence. Also presented in Figure 5.39 B is the graphically normalised data for the determination of the level of O_2 dependence of the sensors at the three choline concentrations. This experiment was performed from an air saturated cell and the air was purged by the introduction of N_2 until a plateau of N_2 saturation was reached. The current comparison above illustrates the difference in the level of O_2 dependence for the choline concentration 20 µM, 40 µM and 100 µM. A comparison of the choline current at three physiologically relevant O_2 concentrations of 30, 50 and 80 µM O_2 demonstrates the level of O_2 dependence that may be experienced in the *in-vivo* environment. Using 20 µM choline, the current observed at 30 µM O_2 is 1.34 ± 0.20 nA, n = 3 at 50 µM O_2 this is increased to 1.76 ± 0.24 nA, n = 3 and current observed at 80 µM is 2.26 ± 0.20 nA, n = 3. An I_{MAX} of 2.93 ± 0.08 nA, n = 3 is reached at 200 µM O_2. The choline current at 30 µM O_2 represents 45.34 ± 7.34 % of the I_{MAX} current, meanwhile 50 µM is 59.59 ± 8.74 % and 80 µM is 76.39 ± 7.73 %. There is a potential 31 % fluctuation in the choline current at the physiological O_2 concentration range. The current observed using 40 µM choline at 30 µM O_2 is 1.74 ± 0.12 nA, n = 3 at 50 µM O_2 this is increased to 2.52 ± 0.17 nA, n = 3 and the current observed at 80 µM is 3.32 ± 0.16 nA, n = 3. An I_{MAX} of 4.56 ± 0.14 nA, n = 3 is reached at 240 µM O_2. The choline current at 30 µM O_2 represents 40.15 ± 1.43 % of the I_{MAX} current, meanwhile 50 µM is 57.07 ± 5.15 % and 80 µM is 73.59 ± 1.87 %. This is a potential 33 % fluctuation in current between 30 µM and 80 µM O_2. Increasing the choline concentration to 100 µM choline, the current observed at 30 µM O_2 is 3.43 ± 0.38 nA, n = 3 at 50 µM O_2 this is increased to 4.07 ± 0.14 nA, n = 3 and the current observed at 80 µM is 6.27 ± 0.49 nA, n = 3. An I_{MAX} of 9.23 ± 0.47 nA, n = 3 is reached at 240 µM O_2. The choline current at 30 µM O_2 represents 37.96 ± 1.64 % of the I_{MAX} current, meanwhile 50 µM is 45.20 ± 2.97 % and 80 µM is 68.27 ± 1.51 % a potential fluctuation of 31 %. There is little difference in the level of O_2 dependence of the sensor when increasing the choline concentration. Similar to the addition of the 0.5% cellulose acetate the 1% cellulose acetate layer has increased the level of O_2 dependence of the sensor compared to the same experimental design without additional layers. However, the increase in concentration of the cellulose acetate from 0.5% to 1% appears to decrease the level of O_2 dependence of the sensor. Overall however, this design does demonstrate a high level of O_2 dependence when using this experimental protocol.

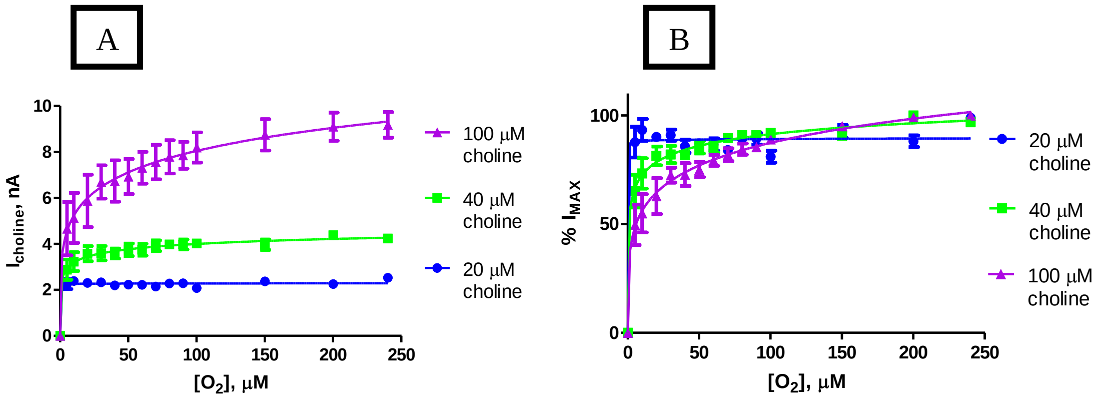

	20 µM Choline			40 µM Choline			100 µM Choline		
O_2 Conc, µM	Mean, nA	S.E.M, nA	n	Mean, nA	S.E.M, nA	n	Mean, nA	S.E.M, nA	n
0	0.00	0.00	3	0.00	0.00	3	0.00	0.00	3
10	2.39	0.17	3	3.23	0.41	3	5.13	1.08	3
20	2.31	0.09	3	3.57	0.33	3	5.87	1.14	3
30	2.33	0.09	3	3.60	0.32	3	6.70	0.73	3
40	2.20	0.12	3	3.58	0.22	3	6.74	0.90	3
50	2.23	0.08	3	3.75	0.27	3	6.93	0.76	3
60	2.22	0.12	3	3.75	0.26	3	7.31	0.69	3
70	2.15	0.06	3	3.92	0.23	3	7.56	0.75	3
80	2.28	0.07	3	3.98	0.19	3	7.79	0.73	3
90	2.28	0.08	3	3.98	0.22	3	7.86	0.58	3
100	2.08	0.12	3	4.02	0.19	3	8.20	0.66	3
150	2.37	0.13	3	3.97	0.23	3	8.75	0.68	3
200	2.26	0.12	3	4.38	0.17	3	9.10	0.61	3
240	2.53	0.03	3	4.24	0.15	3	9.18	0.56	3

Figure 5.40 A : The choline current-oxygen concentration profile comparison for calibration in PBS (pH 7.4) buffer solution at 21°C using design (Pt(cylinder)(MMA)(CelAce)(MMA)-(ChOx)(BSA)(GA)(PEI))CelAce1%. CPA carried out at +700 mV *vs.* SCE for choline electrodes and -650 mV *vs* SCE for the O_2 electrode. Current values for 20 µM, 40 µM and 100 µM choline chloride injections at 10, 20, 30, 40, 50, 60, 70, 80, 90, 100, 150, 200, 240 µM O_2 concentrations.

Figure 5.40 B: The normalised choline current-oxygen concentration profile comparison. Table: Data table for choline current-oxygen concentration profile comparison.

The data in Figure 5.40 A illustrates the effect of three choline concentrations 20, 40 and 100 µM on O_2 dependence. Also presented in Figure 5.40 B is the graphically normalised data for the determination of the level of O_2 dependence of the sensors at the three choline concentrations. This experiment was performed from a N_2 saturated cell and the air was introduced until plateau of N_2 saturation was reached. The current comparison above illustrates the difference in the level of O_2 dependence for the choline concentration 20 µM, 40 µM and 100 µM. A comparison of the choline current at three physiologically relevant O_2 concentrations of 30, 50 and 80 µM O_2 demonstrates the level of O_2 dependence that may be experienced in the *in-vivo* environment. Using 20 µM choline, the current observed at 30 µM O_2 is 2.33 ± 0.09 nA, n = 3 at 50 µM O_2 this is increased to 2.23 ± 0.08 nA, n = 3 and current observed at 80 µM is 2.28 ± 0.07 nA, n = 3. An I_{MAX} of 2.53 ± 0.03 nA, n = 3 is reached at 240 µM O_2. The choline current at 30 µM O_2 represents 90.86 ± 2.61 % of the I_{MAX} current, meanwhile 50 µM is 87.04 ± 1.38 % and 80 µM is 89.14 ± 1.65 %. There is a potentially no fluctuation in the choline current at the physiological O_2 concentration range. This level of O_2 independence is dramatically different to the levels observed with this sensor using the experimental design which removes the air rather than introduces it (see Figure 5.39). The O_2 dependence of this design is also improved in comparison to the addition of the 0.5% cellulose acetate layer. The detection of choline is almost instantaneous at as low as 10 µM O_2. The current observed using 40 µM choline at 30 µM O_2 is 3.60 ± 0.32 nA, n = 3 at 50 µM O_2 this is increased to 3.75 ± 0.27 nA, n = 3 and the current observed at 80 µM is 3.98 ± 0.19 nA, n = 3. An I_{MAX} of 4.38 ± 0.17 nA, n = 3 is reached at 200 µM O_2. The choline current at 30 µM O_2 represents 82.01 ± 3.93 % of the I_{MAX} current, meanwhile 50 µM is 85.36 ± 2.87 % and 80 µM is 90.86 ± 0.98 %. This is a potential 8 % fluctuation in current between 30 µM and 80 µM O_2, a dramatic reduction to that experienced in the air removal protocol. Increasing the choline concentration to 100 µM choline, the current observed at 30 µM O_2 is 6.70 ± 0.73 nA, n = 3 at 50 µM O_2 this is increased to 6.93 ± 0.76 nA, n = 3 and the current observed at 80 µM is 7.79 ± 0.73 nA, n = 3. An I_{MAX} of 9.18 ± 0.56 nA, n = 3 is reached at 240 µM O_2. The choline current at

30 µM O_2 represents 72.51 ± 3.48 % of the I_{MAX} current, meanwhile 50 µM is 75.02 ± 3.47 % and 80 µM is 84.44 ± 2.55 % a potential fluctuation of 12 %. The addition of the cellulose acetate layer has decreased the level of O_2 dependence of the sensor when using this experimental design. A vast difference is observed using two different experimental protocols. The design which removes the air from the cell demonstrates a high level of O_2 dependence; however the reversal which introduces the air demonstrates a low level of O_2 dependence. The increase in the concentration of the cellulose acetate has also improved the level of O_2 dependence observed.

5.3.5.3. CelAce 2%

The effect of increasing the cellulose acetate concentration from 1% to 2% was investigated in this section.

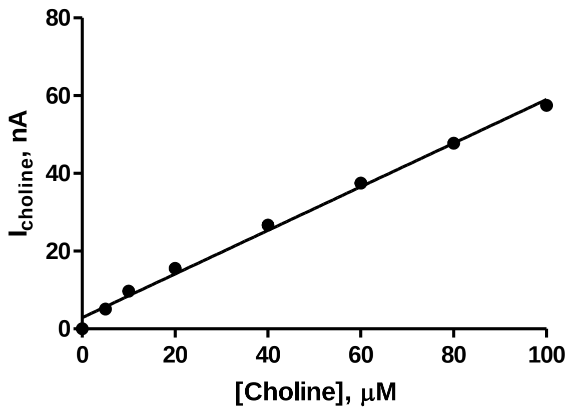

Choline Conc, µM	Mean, nA	S.E.M, nA	n
0	0.00	0.00	3
5	5.13	0.07	3
10	9.71	0.16	3
20	15.57	0.26	3
40	26.72	0.52	3
60	37.52	0.64	3
80	47.77	0.89	3
100	57.51	0.96	3

Figure 5.41 : The current-concentration profile for choline chloride in PBS (pH 7.4) buffer solution at 21°C using design (Pt(cylinder)(MMA)(CelAce)(MMA)-(ChOx)(BSA)(GA)(PEI))CelAce2%. CPA carried out at +700 mV vs. SCE for choline electrodes. Sequential current steps for 5, 10, 20, 40, 60, 80, 100 µM choline chloride injections.

The data in Figure 5.41 illustrates the current response observed for the (Pt(cylinder)(MMA)(CelAce)(MMA)-(ChOx)(BSA)(GA)(PEI))CelAce2%. The $I_{100\ \mu M}$ current observed was 57.51 ± 0.96 nA, n = 3.

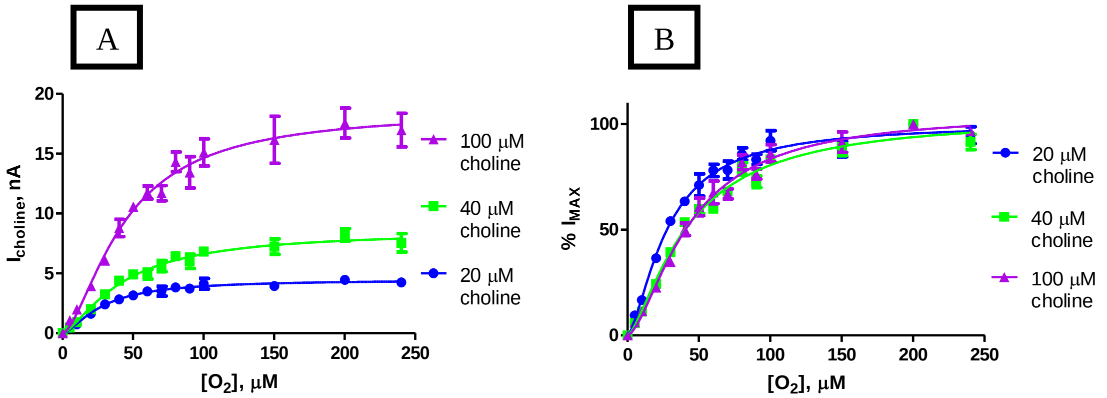

	20 µM Choline			40 µM Choline			100 µM Choline		
O_2 Conc, µM	Mean, nA	S.E.M, nA	n	Mean, nA	S.E.M, nA	n	Mean, nA	S.E.M, nA	n
0	0.00	0.00	3	0.00	0.00	3	0.00	0.00	3
10	0.74	0.04	3	0.93	0.10	3	2.00	0.08	3
20	1.63	0.07	3	2.00	0.14	3	3.95	0.23	3
30	2.41	0.14	3	3.25	0.25	3	6.08	0.31	3
40	2.83	0.16	3	4.39	0.19	3	8.79	0.72	3
50	3.17	0.23	3	4.90	0.15	3	10.57	0.37	3
60	3.49	0.28	3	4.94	0.40	3	11.76	0.55	3
70	3.51	0.40	3	5.61	0.46	3	11.71	0.63	3
80	3.83	0.27	3	6.45	0.20	3	14.32	0.81	3
90	3.73	0.31	3	6.00	0.60	3	13.44	1.32	3
100	4.13	0.45	3	6.83	0.33	3	15.10	1.14	3
150	3.94	0.30	3	7.24	0.65	3	16.16	1.97	3
200	4.46	0.26	3	8.22	0.52	3	17.56	1.25	3
240	4.24	0.38	3	7.56	0.77	3	16.98	1.41	3

Figure 5.42 A : The choline current-oxygen concentration profile comparison for calibration in PBS (pH 7.4) buffer solution at 21°C using design (Pt(cylinder)(MMA)(CelAce)(MMA)-(ChOx)(BSA)(GA)(PEI))CelAce1%. CPA carried out at +700 mV *vs.* SCE for choline electrodes and -650 mV *vs* SCE for the O_2 electrode. Current values for 20 µM, 40 µM and 100 µM choline chloride injections at 10, 20, 30, 40, 50, 60, 70, 80, 90, 100, 150, 200, 240 µM O_2 concentrations. Figure 5.42 B: The normalised choline current-oxygen concentration profile comparison. Table: Data table for choline current-oxygen concentration profile comparison.

The data in Figure 5.42 A illustrates the effect of three choline concentrations 20, 40 and 100 µM on O_2 dependence. Also presented in Figure 5.42 B is the graphically normalised data for the determination of the level of O_2 dependence of the sensors at the three choline concentrations. This experiment was performed from an air saturated cell and the air was purged by the introduction of N_2 until a plateau of N_2 saturation was reached. The current comparison above illustrates the difference in the level of O_2 dependence for the choline concentration 20 µM, 40 µM and 100 µM. A comparison of the choline current at three physiologically relevant O_2 concentrations of 30, 50 and 80 µM O_2 demonstrates the level of O_2 dependence that may be experienced in the *in-vivo* environment. Using 20 µM choline, the current observed at 30 µM O_2 is 2.41 ± 0.14 nA, n = 3 at 50 µM O_2 this is increased to 3.17 ± 0.23 nA, n = 3 and current observed at 80 µM is 3.83 ± 0.27 nA, n = 3. An I_{MAX} of 4.46 ± 0.26 nA, n = 3 is reached at 200 µM O_2. The choline current at 30 µM O_2 represents 54.01 ± 1.64 % of the I_{MAX} current, meanwhile 50 µM is 71.13 ± 5.25 % and 80 µM is 85.79 ± 2.85 %. There is a potential 31 % fluctuation in the choline current at the physiological O_2 concentration range. The current observed using 40 µM choline at 30 µM O_2 is 3.25 ± 0.25 nA, n = 3 at 50 µM O_2 this is increased to 4.90 ± 0.15 nA, n = 3 and the current observed at 80 µM is 6.45 ± 0.20 nA, n = 3. An I_{MAX} of 8.22 ± 0.52 nA, n = 3 is reached at 200 µM O_2. The choline current at 30 µM O_2 represents 39.41 ± 0.66 % of the I_{MAX} current, meanwhile 50 µM is 59.87 ± 5.15 % and 80 µM is 78.80 ± 2.96 %. This is a potential 39 % fluctuation in current between 30 µM and 80 µM O_2. Increasing the choline concentration to 100 µM choline, the current observed at 30 µM O_2 is 6.08 ± 0.31 nA, n = 3 at 50 µM O_2 this is increased to 10.57 ± 0.37 nA, n = 3 and the current observed at 80 µM is 14.32 ± 0.81 nA, n = 3. An I_{MAX} of 17.56 ± 1.25 nA, n = 3 is reached at 200 µM O_2. The choline current at 30 µM O_2 represents 34.73 ± 0.81 % of the I_{MAX} current, meanwhile 50 µM is

60.73 ± 4.17 % and 80 μM is 81.87 ± 3.47 % a potential fluctuation of 47 %. The addition of 2% cellulose acetate has decreased the level of O_2 dependence of the design at higher O_2 concentrations. This however has lead to higher potential fluctuations in the choline current in the physiological O_2 concentration range.

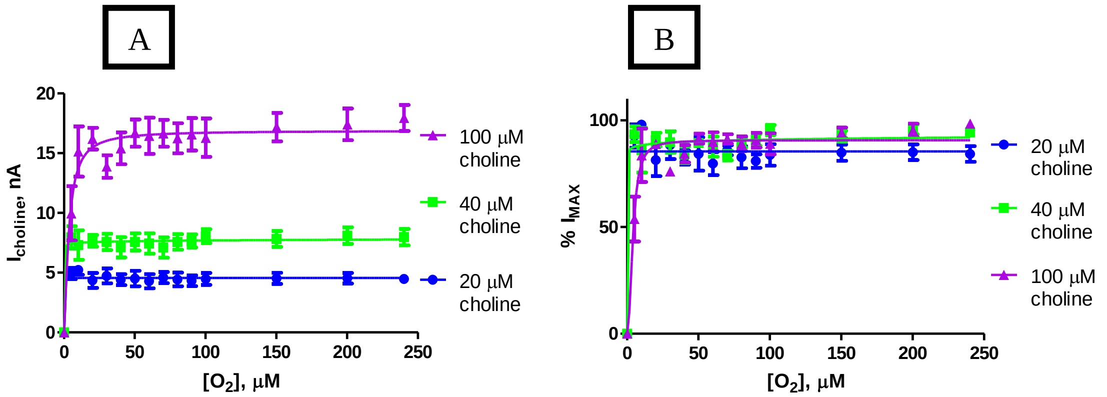

	20 μM Choline			40 μM Choline			100 μM Choline		
O_2 Conc, μM	Mean, nA	S.E.M, nA	n	Mean, nA	S.E.M, nA	n	Mean, nA	S.E.M, nA	n
0	0.00	0.00	3	0.00	0.00	3	0.00	0.00	3
10	5.22	0.39	3	7.31	1.24	3	15.14	2.11	3
20	4.36	0.62	3	7.67	0.50	3	16.21	0.90	3
30	4.73	0.62	3	7.58	0.68	3	13.89	0.94	3
40	4.41	0.46	3	7.13	0.85	3	15.41	1.33	3
50	4.51	0.65	3	7.58	0.72	3	16.69	1.14	3
60	4.28	0.60	3	7.43	0.85	3	16.45	1.52	3
70	4.60	0.47	3	7.11	0.85	3	16.66	1.13	3
80	4.43	0.57	3	7.57	0.65	3	16.25	1.25	3
90	4.33	0.45	3	7.67	0.55	3	16.58	1.36	3
100	4.47	0.50	3	8.06	0.58	3	16.30	1.61	3
150	4.53	0.47	3	7.83	0.67	3	17.19	1.19	3
200	4.54	0.44	3	8.10	0.69	3	17.42	1.33	3
240	4.48	0.37	3	7.98	0.68	3	17.95	1.08	3

Figure 5.43 A : The choline current-oxygen concentration profile comparison for calibration in PBS (pH 7.4) buffer solution at 21°C using design (Pt(cylinder)(MMA)(CelAce)(MMA)-(ChOx)(BSA)(GA)(PEI))CelAce1%. CPA carried out at +700 mV *vs.* SCE for choline electrodes and -650 mV *vs* SCE for the O_2 electrode. Current values for 20 μM, 40 μM and 100 μM choline chloride injections at 10, 20, 30, 40, 50, 60, 70, 80, 90, 100, 150, 200, 240 μM O_2 concentrations.

Figure 5.43 B: The normalised choline current-oxygen concentration profile comparison. Table: Data table for choline current-oxygen concentration profile comparison.

The data in Figure 5.43 A illustrates the effect of three choline concentrations 20, 40 and 100 µM on O_2 dependence. Also presented in Figure 5.43 B is the graphically normalised data for the determination of the level of O_2 dependence of the sensors at the three choline concentrations. This experiment was performed from a N_2 saturated cell and the air was introduced until plateau of N_2 saturation was reached. The current comparison above illustrates the difference in the level of O_2 dependence for the choline concentration 20 µM, 40 µM and 100 µM. A comparison of the choline current at three physiologically relevant O_2 concentrations of 30, 50 and 80 µM O_2 demonstrates the level of O_2 dependence that may be experienced in the *in-vivo* environment. Using 20 µM choline, the current observed at 30 µM O_2 is 4.73 ± 0.62 nA, n = 3 at 50 µM O_2 this is increased to 4.51 ± 0.65 nA, n = 3 and current observed at 80 µM is 4.43 ± 0.57 nA, n = 3. An I_{MAX} of 4.54 ± 0.44 nA, n = 3 is reached at 200 µM O_2. The choline current at 30 µM O_2 represents 88.31 ± 6.50 % of the I_{MAX} current, meanwhile 50 µM is 84.21 ± 7.77 % and 80 µM is 82.67 ± 5.16 %. There is potentially no fluctuation in the choline current at the physiological O_2 concentration range. The current observed using 40 µM choline at 30 µM O_2 is 7.58 ± 0.68 nA, n = 3 at 50 µM O_2 this is increased to 7.58 ± 0.72 nA, n = 3 and the current observed at 80 µM is 7.57 ± 0.65 nA, n = 3. An I_{MAX} of 8.10 ± 0.69 nA, n = 3 is reached at 200 µM O_2. The choline current at 30 µM O_2 represents 89.72 ± 5.01 % of the I_{MAX} current, meanwhile 50 µM is 89.35 ± 0.96 % and 80 µM is 89.48 ± 2.32 %. There is potentially no fluctuation in current between 30 µM and 80 µM O_2, a dramatic reduction to that experienced in the air removal protocol. Increasing the choline concentration to 100 µM choline, the current observed at 30 µM O_2 is 13.89 ± 0.94 nA, n = 3 at 50 µM O_2 this is increased to 16.69 ± 1.14 nA, n = 3 and the current observed at 80 µM is 16.25 ± 1.25 nA, n = 3. An I_{MAX} of 17.95 ± 1.08 nA, n = 3 is reached at 240 µM O_2. The choline current at 30 µM O_2 represents 76.06 ± 1.88 % of the I_{MAX} current, meanwhile 50 µM is 91.41 ± 2.35 % and 80 µM is 88.99 ± 3.42 % a potential fluctuation of 12 %. The increase in cellulose acetate concentration has decreased the level of O_2 dependence of the sensor at higher concentrations choline. In both the usage of cellulose acetate 1% and 2% the addition of 20 µM choline saw an almost instantaneous substrate turnover with the introduction of air. For 1% cellulose acetate the increase in choline concentration increased the level of O_2 dependence. However, the use of 2% cellulose acetate has resulted in even the higher concentrations of choline having very limited O_2 dependence. These results are in stark contrast to those observed using the experimental protocol which introduces N_2.

5.3.5.4. CelAce 5%

The effect of increasing the cellulose acetate concentration from 2% to 5% was investigated in this section.

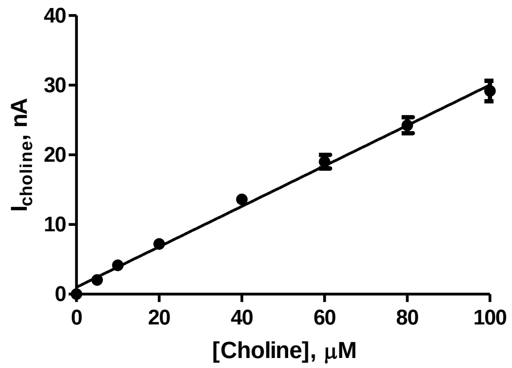

Choline Conc, μM	Mean, nA	S.E.M, nA	n
0	0.00	0.00	3
5	2.06	0.08	3
10	4.13	0.16	3
20	7.22	0.33	3
40	13.63	0.72	3
60	19.02	0.98	3
80	24.27	1.16	3
100	29.17	1.47	3

Figure 5.44 : The current-concentration profile for choline chloride in PBS (pH 7.4) buffer solution at 21°C using design (Pt(cylinder)(MMA)(CelAce)(MMA)-(ChOx)(BSA)(GA)(PEI))CelAce5%.

CPA carried out at +700 mV *vs.* SCE for choline electrodes. Sequential current steps for 5, 10, 20, 40, 60, 80, 100 μM choline chloride injections.

The data in Figure 5.44 illustrates the current response observed for the (Pt(cylinder)(MMA)(CelAce)(MMA)-(ChOx)(BSA)(GA)(PEI))CelAce5%. The $I_{100\ \mu M}$ current observed was 29.17 ± 1.47 nA, n = 3. Increasing the concentration of the cellulose layer from 2 to 5 % has almost halved the sensitivity of the design.

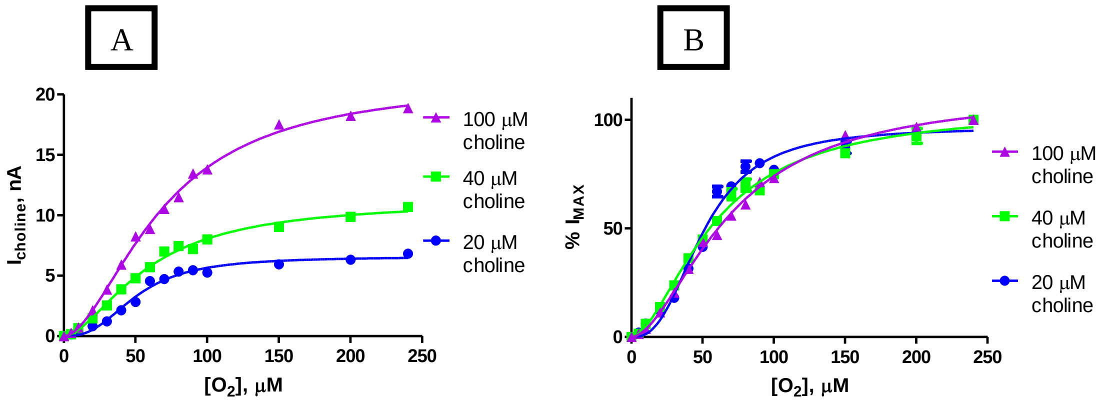

	20 μM Choline			40 μM Choline			100 μM Choline		
O_2 Conc, μM	Mean, nA	S.E.M, nA	n	Mean, nA	S.E.M, nA	n	Mean, nA	S.E.M, nA	n
0	0.00	0.00	3	0.00	0.00	3	0.00	0.00	3
10	0.42	0.01	3	0.65	0.03	3	0.72	0.03	3
20	0.83	0.01	3	1.48	0.05	3	2.14	0.07	3
30	1.23	0.03	3	2.55	0.05	3	3.86	0.11	3
40	2.15	0.01	3	3.87	0.06	3	5.93	0.15	3
50	2.84	0.02	3	4.80	0.13	3	8.26	0.12	3
60	4.56	0.11	3	5.70	0.08	3	8.87	0.10	3
70	4.73	0.001	3	7.01	0.12	3	10.53	0.03	3
80	5.34	0.09	3	7.46	0.14	3	11.50	0.08	3
90	5.45	0.06	3	7.22	0.09	3	13.46	0.30	3
100	5.25	0.12	3	8.01	0.10	3	13.81	0.33	3
150	5.94	0.16	3	9.04	0.33	3	17.53	0.34	3
200	6.32	0.14	3	9.88	0.18	3	18.25	0.38	3
240	6.82	0.14	3	10.69	0.21	3	18.87	0.34	3

Figure 5.45 A : The choline current-oxygen concentration profile comparison for calibration in PBS (pH 7.4) buffer solution at 21°C using design (Pt(cylinder)(MMA)(CelAce)(MMA)-

(ChOx)(BSA)(GA)(PEI))CelAce1%. CPA carried out at +700 mV *vs*. SCE for choline electrodes and -650 mV *vs* SCE for the O_2 electrode. Current values for 20 µM, 40 µM and 100 µM choline chloride injections at 10, 20, 30, 40, 50, 60, 70, 80, 90, 100, 150, 200, 240 µM O_2 concentrations. Figure 5.45 B: The normalised choline current-oxygen concentration profile comparison. Table: Data table for choline current-oxygen concentration profile comparison.

The data in Figure 5.45 A illustrates the effect of three choline concentrations 20, 40 and 100 µM on O_2 dependence. Also presented in Figure 5.45 is the graphically normalised data for the determination of the level of O_2 dependence of the sensors at the three choline concentrations. This experiment was performed from an air saturated cell and the air was purged by the introduction of N_2 until a plateau of N_2 saturation was reached. The current comparison above illustrates the difference in the level of O_2 dependence for the choline concentration 20 µM, 40 µM and 100 µM. A comparison of the choline current at three physiologically relevant O_2 concentrations of 30, 50 and 80 µM O_2 demonstrates the level of O_2 dependence that may be experienced in the *in-vivo* environment. Using 20 µM choline, the current observed at 30 µM O_2 is 1.23 ± 0.03 nA, n = 3 at 50 µM O_2 this is increased to 2.84 ± 0.02 nA, n = 3 and current observed at 80 µM is 5.34 ± 0.09 nA, n = 3. An I_{MAX} of 4.54 ± 0.44 nA, n = 3 is reached at 240 µM O_2. The choline current at 30 µM O_2 represents 17.98 ± 0.35 % of the I_{MAX} current, meanwhile 50 µM is 41.47 ± 0.98 % and 80 µM is 78.42 ± 2.48 %. There is a potential 61 % fluctuation in the choline current at the physiological O_2 concentration range. The use of 5% cellulose acetate demonstrates a significant level of O_2 dependence. The current observed using 40 µM choline at 30 µM O_2 is 2.55 ± 0.05 nA, n = 3 at 50 µM O_2 this is increased to 4.80 ± 0.13 nA, n = 3 and the current observed at 80 µM is 7.46 ± 0.14 nA, n = 3. An I_{MAX} of 8.10 ± 0.69 nA, n = 3 is reached at 240 µM O_2. The choline current at 30 µM O_2 represents 23.82 ± 0.37 % of the I_{MAX} current, meanwhile 50 µM is 44.87 ± 0.88 % and 80 µM is 69.91 ± 2.76 %. This is a potential 46 % fluctuation in current between 30 µM and 80 µM O_2. Increasing the choline concentration to 100 µM choline, the current observed at 30 µM O_2 is 3.86 ± 0.11 nA, n = 3 at 50 µM O_2 this is increased to 8.26 ± 0.12 nA, n = 3 and the current observed at 80 µM is 11.50 ± 0.08 nA, n = 3. An I_{MAX} of 17.95 ± 1.08 nA, n = 3 is reached at 240 µM O_2. The choline current at 30 µM O_2 represents 20.42 ± 0.20 % of the I_{MAX} current, meanwhile 50 µM is 43.81 ± 0.85 % and 80 µM is 61.00 ± 1.44 % a potential fluctuation of 41 %. The addition of 5% cellulose acetate has dramatically increased the level of O_2 dependence of the sensor.

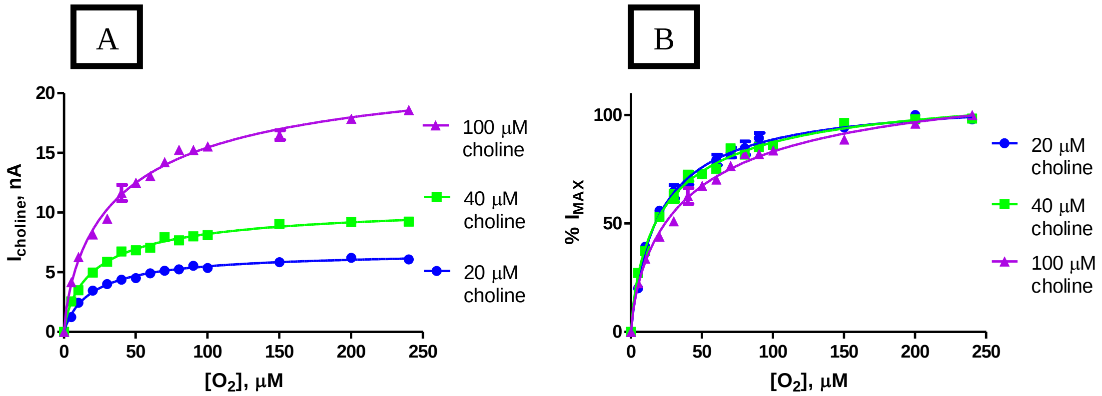

	20 μM Choline			40 μM Choline			100 μM Choline		
O_2 Conc, μM	Mean, nA	S.E.M, nA	n	Mean, nA	S.E.M, nA	n	Mean, nA	S.E.M, nA	n
0	0.00	0.00	3	0.00	0.00	3	0.00	0.00	3
10	2.44	0.09	3	3.50	0.11	3	6.28	0.11	3
20	3.46	0.05	3	4.97	0.08	3	8.18	0.09	3
30	4.00	0.11	3	5.87	0.21	3	9.49	0.12	3
40	4.37	0.09	3	6.74	0.18	3	11.65	0.67	3
50	4.51	0.01	3	6.85	0.11	3	12.51	0.08	3
60	4.92	0.08	3	7.06	0.01	3	13.06	0.09	3
80	5.12	0.04	3	7.95	0.11	3	14.22	0.35	3
90	5.25	0.10	3	7.68	0.15	3	15.26	0.08	3
100	5.54	0.04	3	8.00	0.14	3	15.24	0.16	3
150	5.36	0.04	3	8.10	0.16	3	15.55	0.24	3
200	5.84	0.12	3	9.05	0.13	3	16.49	0.40	3
240	6.21	0.12	3	9.21	0.07	3	17.86	0.06	3

Figure 5.46 A : The choline current-oxygen concentration profile comparison for calibration in PBS (pH 7.4) buffer solution at 21°C using design (Pt(cylinder)(MMA)(CelAce)(MMA)-(ChOx)(BSA)(GA)(PEI))CelAce1%. CPA carried out at +700 mV *vs.* SCE for choline electrodes and -650 mV *vs* SCE for the O_2 electrode. Current values for 20 μM, 40 μM and 100 μM choline chloride injections at 10, 20, 30, 40, 50, 60, 70, 80, 90, 100, 150, 200, 240 μM O_2 concentrations. Figure 5.46 B: The normalised choline current-oxygen concentration profile comparison. Table: Data table for choline current-oxygen concentration profile comparison.

The data in Figure 5.46 A illustrates the effect of three choline concentrations 20, 40 and 100 µM on O_2 dependence. Also presented in Figure 5.46 B is the graphically normalised data for the determination of the level of O_2 dependence of the sensors at the three choline concentrations. This experiment was performed from a N_2 saturated cell and the air was introduced until plateau of N_2 saturation was reached. The current comparison above illustrates the difference in the level of O_2 dependence for the choline concentration 20 µM, 40 µM and 100 µM. A comparison of the choline current at three physiologically relevant O_2 concentrations of 30, 50 and 80 µM O_2 demonstrates the level of O_2 dependence that may be experienced in the *in-vivo* environment. Using 20 µM choline, the current observed at 30 µM O_2 is 4.00 ± 0.11 nA, n = 3 at 50 µM O_2 this is increased to 4.51 ± 0.01 nA, n = 3 and current observed at 80 µM is 5.12 ± 0.04 nA, n = 3. An I_{MAX} of 6.21 ± 0.21 nA, n = 3 is reached at 240 µM O_2. The choline current at 30 µM O_2 represents 64.65 ± 3.00 % of the I_{MAX} current, meanwhile 50 µM is 72.74 ± 1.70 % and 80 µM is 84.69 ± 3.12 % a fluctuation of 20 %. These results are improved when compared to the air removal protocol however the O_2 dependence is greatly increased in comparison to the other cellulose acetate concentrations. The current observed using 40 µM choline at 30 µM O_2 is 5.87 ± 0.21 nA, n = 3 at 50 µM O_2 this is increased to 6.85 ± 0.11 nA, n = 3 and the current observed at 80 µM is 7.95 ± 0.11 nA, n = 3. An I_{MAX} of 9.21 ± 0.07 nA, n = 3 is reached at 240 µM O_2. The choline current at 30 µM O_2 represents 62.48 ± 2.55 % of the I_{MAX} current, meanwhile 50 µM is 72.87 ± 1.57 % and 80 µM is 81.75 ± 1.94 %. There is potentially a 19 % fluctuation in current between 30 µM and 80 µM O_2. Increasing the choline concentration to 100 µM choline, the current observed at 30 µM O_2 is 9.49 ± 0.12 nA, n = 3 at 50 µM O_2 this is increased to 12.51 ± 0.08 nA, n = 3 and the current observed at 80 µM is 14.22 ± 0.35 nA, n = 3. An I_{MAX} of 17.86 ± 0.06 nA, n = 3 is reached at 240 µM O_2. The choline current at 30 µM O_2 represents 51.04 ± 0.32 % of the I_{MAX} current, meanwhile 50 µM is 67.34 ± 1.36 % and 80 µM is 82.10 ± 0.87 % a potential fluctuation of 32 %. The increase in cellulose acetate concentration has increased the level of O_2 dependence of the sensor dramatically. This concentration has both been detrimental to sensitivity and O_2 dependence using both experimental protocols. It is possible that the high concentration of the cellulose acetate has limited the access of the required $O_{2.}$

5.4. Conclusion

This chapter outlines the modifications to the choline biosensor in order to decrease the level of O_2 dependence of the design. The initial section outlines the incorporation of Nafion® into the design. The use of Nafion® had successfully been used previously in the design of a Lactate biosensor to decrease the levels of O_2 dependence. This section further investigated if this was due to the high O_2 solubility of the polymer as suggested by reports of high O_2 solubility in other perfluorinated polymers. Although the incorporation of Nafion® did successfully reduce the level of O_2 dependence of the design as demonstrated in Section 5.3.2.4, it was further determined that this was primarily as a result of an increase in the diffusion barrier created by it incorporation. This was shown when the use of Nafion® was replaced with cellulose acetate which demonstrated the same level of O_2 dependence as the Nafion® design. In order to investigate the use of additional diffusion barriers, the sensor was modified to a cylinder design. This increased the sensitivity of the design which would allow for additional diffusion layers to be incorporated without detrimentally affecting the sensitivity of the sensor. The increase in the surface area of the sensor to a cylinder decreased the level of O_2 dependence of the sensor. The experimental protocol which was utilised in the determination of the O_2 dependence with additional diffusion barriers highlighted a difference in the levels of O_2 dependence depending if the protocol was carried out from an air saturated solution or a N_2 saturated solution. The design chosen for further characterisation is Pt(cylinder)(MMA)(CelAce2%)(MMA)-(ChOx)(BSA1%)(GA0.5%)(PEI2%). This design demonstrated high levels of O_2 independence in both O_2 calibration protocols.

Beh SK, Moody GJ & Thomas JDR. (1991). Studies on enzyme electrodes with ferrocene and carbon paste bound with cellulose triacetate. *Analyst* **116,** 459-462.

Bolger FB. (2007). The *In-Vitro* and *In-Vivo* Characterisation and Application of Real-Time Sensors and Biosensors for Neurochemical Studies of Brain Energy Metabolism. National University of Ireland, Maynooth, Maynooth.

Bolger FB & Lowry JP. (2005). Brain tissue oxygen: *In-Vivo* monitoring with carbon paste electrodes. *Sensors* **5,** 473-487.

Brown FO & Lowry JP. (2003). Microelectrochemical sensors for *In-Vivo* brain analysis: an investigation of procedures for modifying Pt electrodes using Nafion. *Analyst* **128,** 700-705.

Chaubey A & Malhotra BD. (2002). Mediated biosensors. *Biosensors and Bioelectronics* **17,** 441-456.

Clark LC & Gollan F. (1966). Survival of mammals breathing organic liquids equilibrated with oxygen at atmospheric pressure. *Science* **152,** 1755-1756.

Di Gleria K, Green MJ, Hill HAO & McNeil CJ. (1986). Homogeneous ferrocene-mediated amperometric immunoassay. *Analytical Chemistry* **58,** 1203-1205.

Dixon BM, Lowry JP & O'Neill RD. (2002). Characterization *In-Vitro* and *In-Vivo* of the oxygen dependence of an enzyme/polymer biosensor for monitoring brain glucose. *Journal of Neuroscience Methods* **119,** 135-142.

Elibol M & Mavituna F. (1996). Use of perfluorocarbon for oxygen supply to immobilised Streptomyces coelicolor A3(2). *Process Biochemistry* **31,** 507-512.

Garguilo MG & Michael AC. (1993). An enzyme-modified microelectrode that detects choline injected locally into brain tissue. *Journal of the American Chemical Society* **115,** 12218-12219.

Garguilo MG & Michael AC. (1995). Enzyme-modified electrodes for peroxide, choline, and acetylcholine. *TrAC Trends in Analytical Chemistry* **14,** 164-169.

Garguilo MG & Michael AC. (1996). Amperometric microsensors for monitoring choline in the extracellular fluid of brain. *Journal of Neuroscience Methods* **70,** 73-82.

Gregg BA & Heller A. (1991). Redox polymer films containing enzymes. 1. A redox-conducting epoxy cement: synthesis, characterization, and electrocatalytic oxidation of hydroquinone. *The Journal of Physical Chemistry* **95,** 5970-5975.

Hekmat A, Saboury AA, Moosavi-Movahedi AA, Ghourchian H & Ahmad F. (2008). Effects of pH on the activity and structure of choline oxidase from Alcaligenes species. *Acta Biochimica Polonica* **55,** 549-557.

Jewitt N, Anthony P, Lowe KC & de Pomerai DI. (1999). Oxygenated perfluorocarbon promotes nematode growth and stress-sensitivity in a two-phase liquid culture system. *Enzyme and Microbial Technology* **25,** 349-356.

Martens N & Hall EAH. (1994). Model for an Immobilized Oxidase Enzyme Electrode in the Presence of Two Oxidants. *Analytical Chemistry* **66,** 2763-2770.

Mauritz KA & Moore RB. (2004). State of Understanding of Nafion. *Chemical Reviews* **104** 4535–4586.

McMahon CP, Killoran SJ & O’Neill RD. (2005). Design variations of a polymer–enzyme composite biosensor for glucose: Enhanced analyte sensitivity without increased oxygen dependence. *Journal of Electroanalytical Chemistry* **580,** 193-202.

McMahon CP & O'Neill RD. (2005). Polymer−Enzyme Composite Biosensor with High Glutamate Sensitivity and Low Oxygen Dependence. *Analytical Chemistry* **77,** 1196-1199.

McMahon CP, Rocchitta G, Kirwan SM, Killoran SJ, Serra PA, Lowry JP & O'Neill RD. (2007a). Oxygen tolerance of an implantable polymer/enzyme composite glutamate biosensor displaying polycation-enhanced substrate sensitivity. *Biosensors & Bioelectronics* **22,** 1466-1473.

McMahon CP, Rocchitta G, Kirwan SM, Killoran SJ, Serra PA, Lowry JP & O’Neill RD. (2007b). Oxygen tolerance of an implantable polymer/enzyme composite glutamate biosensor displaying polycation-enhanced substrate sensitivity. *Biosensors and Bioelectronics* **22,** 1466-1473.

McMahon CP, Rocchitta G, Serra PA, Kirwan SM, Lowry JP & O'Neill RD. (2006). Control of the oxygen dependence of an implantable polymer/enzyme composite biosensor for glutamate. *Analytical Chemistry* **78,** 2352-2359.

O'Neill RD, Rocchitta G, McMahon CP, Serra PA & Lowry JP. (2008). Designing sensitive and selective polymer/enzyme composite biosensors for brain monitoring in vivo. *TrAC Trends in Analytical Chemistry* **27,** 78-88.

Riess JG & Le Blanc M. (1982). Solubility and transport phenomena in perfluorochemicals relevant to blood substitution and other biomedical applications. *Pure and Applied Chemistry* **54,** 2383-2406.

Scheule AM, Pappas I, Vogel U, Miller S, Roehlke W, Reuter P, Wendel HP & Ziemer G. (2000). Heart preservation of non–heart-beating donors by in situ perfusion: comparison of artificial oxygen carrier perfluorocarbons with University of Wisconsin solution in a big animal model. *Transplantation Proceedings* **32,** 192-195.

Wang J, Chen L & Chatrathi M-P. (2000). Evaluation of different fluorocarbon oils for their internal oxygen supply in glucose microsensors operated under oxygen-deficit conditions. *Analytica Chimica Acta* **411,** 187-192.

Wang J & Lu F. (1998). Oxygen-Rich Oxidase Enzyme Electrodes for Operation in Oxygen-Free Solutions. *Journal of the American Chemical Society* **120,** 1048-1050.

6. *In-Vitro* Characterisation

6.1. Introduction

In the development of a new sensor, it is vital that the electrode-environment interactions are fully investigated prior to use in biological systems (Lyne & O'Neill, 1990). This is due to the complex chemical environment within the brain which consists of surfactants (lipids), electrode poisons (proteins) and electro-catalysts such as ascorbic acid (O'Neill, 1993). Much work has been undertaken to illustrate the importance of these tests. Lipids have been shown previously to decrease the selectivity of a stearate modified carbon- Nujol paste electrode (SMEs) for the detection of dopamine. The basis of these sensors relies upon the presence of unprotonated carboxylic moieties which retard the electrooxidation of anionic species such as ascorbate and 3,4 – Dihydroxyphenylacetic acid (DOPAC) such that the dopamine can be detected in their presence. However, it has been shown that contact with brain tissue renders the surface stearate ineffective, therefore, reducing the selectivity of the sensor (Lyne & O'Neill, 1990). Carbon paste electrodes are known to be modified after their contact with brain tissue as the tissue removes the pasting oil, leaving behind a surface with similar properties to carbon powder which is responsible for their stability *in-vivo* over long periods for the detection of ascorbic acid and oxygen (Ormonde & O'Neill, 1990) (A. Kane & D. O'Neill, 1998) (Bolger *et al.*, 2011b). In addition, Nafion®-modified platinum electrodes for the detection of nitric oxide have illustrated a drop in sensitivity as a result of exposure to protein and lipids. This drop was observed in the first 24 hours of exposure with no further loss in sensitivity thereafter (Brown *et al.*, 2009). Shelf-life studies of a glucose oxidase based biosensor demonstrated a 50 % in sensitivity after forty days of storage in the refrigerator at 4 °C (Lowry & O'Neill, 1994). Previous work by Garguilo *et al.* during the development of a choline biosensor has demonstrated a 25 % decrease in sensitivity after the exposure to brain tissue for 0.5-5 hrs (Garguilo & Michael, 1994). The modifications to previous sensors during *in-vitro* characterisation, determining how the *in-vivo* environment can affect the performance of the sensor, have highlighted the importance of mimicking the exposure of the sensors to the brain. This chapter investigates the response of the choline biosensor to physiologically relevant testing to investigate how the sensor may be affected once in the *in-vivo* environment.

6.2. Experimental

All instrumentation and software used in this section are described in Section 3.2. All chemicals and solutions used are described in Section 3.3. The electrodes were constructed from 1 mm cylinder electrodes as described in Section 3.4.1. The design and manufacture of (MMA)(CelAce2%)(MMA)-(ChOx)(BSA1%)(GA0.5%)(PEI2%) is explained in detail in section 3.4.2.1. All data was recorded using the cell setup described in Section 3.5.1.1. The calibrations were performed as described in Section 3.5.1.6.

The data is reported as mean ± SEM where n denotes the number of electrodes used. The significance of difference was estimated using two-tailed *t*-tests. Paired tests were used for comparing signals recorded at the same electrode, unpaired tests were used for comparing data from different electrodes.

6.3. Results and Discussion

Many sensors have shown alterations to the sensors morphology and/or sensitivity during *in-vitro* studies, as a result of exposure to proteins, lipids and brain tissue. In order to determine the effect of these constituents, the choline biosensor was exposed to the protein bovine serum albumin (BSA), the lipid 3-sn-phosphatidylethanolamine (PEA), and intact brain tissue. As determined in Chapter 5 the choline biosensor design which is continued with for further characterisation is (MMA)(CelAce)(MMA)-(ChOx)(BSA)(GA)(PEI). The sensors were immersed in each component and stored in the refrigerator when not in use. They were removed and calibrated on days 1, 3, 5, 7 and 14. Initial tests were undertaken in order to determine the effect of these calibrations.

6.3.1. Calibration effect

The first investigation was to calibrate the sensor on days 1, 3, 5, 7, and 14 without exposure to any of the biological components. This will investigate the effect of both storage of the sensor and the effect of the repeated calibrations. This may need to be considered later in this section when the electrodes are both repeatedly calibrated and exposed to protein, lipids and brain tissue

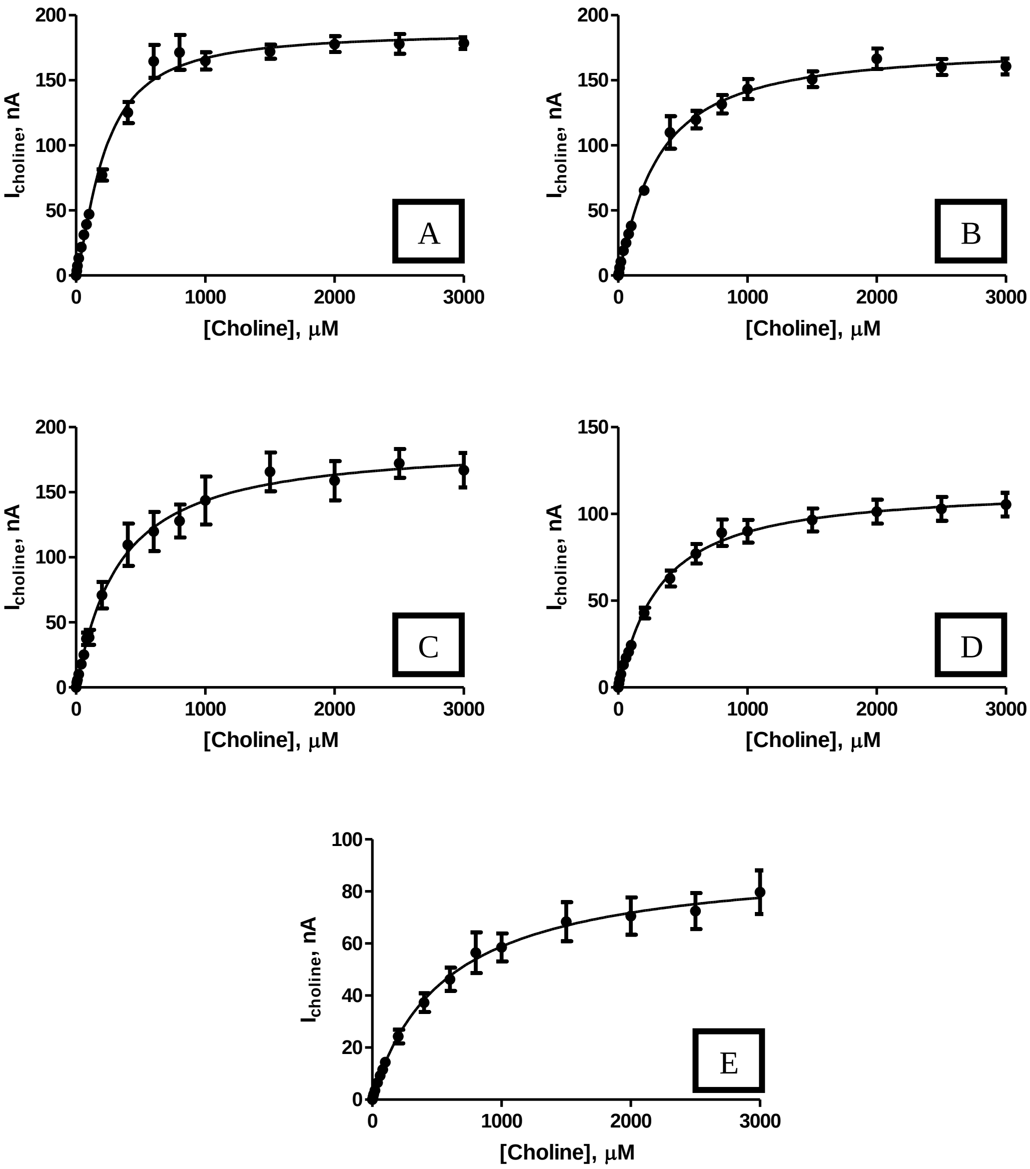

Figure 6.1 : The current-concentration profile and results table (below) for choline chloride calibrations in PBS (pH 7.4) buffer solution at 21°C using PPD-(MMA)(CelAce)(MMA)-

(ChOx)(BSA)(GA)(PEI) electrodes on days (A) 1, (B) 3, (C) 5, (D) 7 and (E) 14. CPA carried out at +700 mV *vs*. SCE. Sequential current steps for 5, 10, 20, 40, 60, 80, 100, 200, 400, 600, 800, 1000, 1500, 2000, 2500, 3000 μM choline chloride injections.

	Day 1			Day 3			Day 5		
Conc, μM	**Mean, nA**	**S.E.M, nA**	**n**	**Mean, nA**	**S.E.M, nA**	**n**	**Mean, nA**	**S.E.M, nA**	**n**
0	0.00	0.00	4	0.00	0.00	4	0.00	0.00	4
5	3.53	0.20	4	1.85	0.04	4	3.72	0.53	4
10	7.35	0.36	4	5.92	0.28	4	5.69	0.77	4
20	13.22	0.79	4	10.63	0.42	4	10.07	1.21	4
40	21.82	1.26	4	19.01	0.92	4	17.99	2.04	4
60	31.27	1.78	4	25.01	1.33	4	25.13	3.35	4
80	39.26	2.28	4	31.96	1.74	4	37.39	4.77	4
100	47.00	2.74	4	38.05	2.10	4	38.50	5.68	4
200	77.22	4.31	4	65.48	3.47	4	70.93	10.13	4
400	125.25	8.14	4	109.93	12.54	4	109.64	16.22	4
600	164.58	12.60	4	119.78	6.74	4	119.87	15.04	4
800	171.49	13.42	4	131.64	7.04	4	127.94	12.62	4
1000	164.88	6.65	4	143.21	7.65	4	143.68	18.44	4
1500	172.01	5.37	4	150.78	6.06	4	165.67	14.85	4
2000	177.80	6.10	4	166.60	7.83	4	158.90	15.10	4
2500	177.98	7.58	4	160.28	6.21	4	172.17	11.15	4
3000	178.60	4.49	4	160.70	6.08	4	166.97	13.27	4

	Day 7			Day 14		
Conc, µM	**Mean, nA**	**S.E.M, nA**	**n**	**Mean, nA**	**S.E.M, nA**	**n**
0	0.00	0.00	4	0.00	0.000	4
5	2.28	0.53	4	1.01	0.10	4
10	4.55	0.29	4	2.04	0.20	4
20	7.74	0.59	4	3.54	0.35	4
40	13.01	1.16	4	6.50	0.65	4
60	17.09	1.38	4	9.21	0.95	4
80	20.45	1.25	4	11.57	1.11	4
100	24.25	1.68	4	14.39	1.42	4
200	42.92	3.05	4	24.25	2.60	4
400	62.80	4.56	4	37.28	3.61	4
600	77.01	5.63	4	46.23	4.48	4
800	89.16	7.64	4	56.47	7.82	4
1000	90.03	6.56	4	58.54	5.37	4
1500	96.59	6.62	4	68.38	7.47	4
2000	101.34	6.90	4	70.51	7.18	4
2500	102.95	6.87	4	72.44	6.93	4
3000	105.41	6.82	4	79.72	8.40	4

The data in Figure 6.1 illustrates the effect of repeated calibrations over a period of 14 days. The sensor undergoes an initial drop in sensitivity which then remains stable until day 5. The sensitivity is dramatically reduced by day 7 and then further by day 14. This data illustrates the dramatic loss in sensitivity observed due to the repeated calibrations.

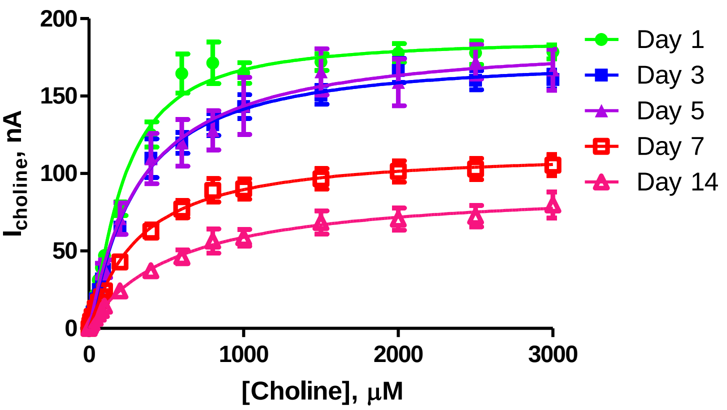

Kinetic Parameters	Day 1			Day 3			Day 5		
	Mean	S.E.M	n	Mean	S.E.M	n	Mean	S.E.M	n
V_{MAX}, nA	187.10	4.69	4	176.10	5.79	4	187.30	13.07	4
Km, µM	215.60	16.62	4	291.80	27.91	4	325.00	66.08	4
α	1.38	0.10	4	1.15	0.08	4	1.06	0.14	4
$I_{100\mu M}$, nA	47.00	2.74	4	38.05	2.10	4	38.50	5.68	4
Sensitivity, nA/µM	0.46	0.02	4	0.38	0.016	4	0.40	0.02	4
R^2	0.989	0.004	4	0.996	0.002	4	0.992	0.005	4
Background, nA	1.58	0.21	4	0.90	0.21	4	0.82	0.09	4

Kinetic Parameters	Day 7			Day 14		
	Mean	S.E.M	n	Mean	S.E.M	n
V_{MAX}, nA	115.00	5.29	4	92.74	9.51	4
Km, µM	313.00	41.88	4	571.90	155.80	4
α	1.09	0.10	4	0.98	0.13	4
$I_{100\mu M}$, nA	24.25	1.68	4	14.39	1.42	4
Sensitivity, nA/µM	0.24	0.01	4	0.140	0.003	4
R^2	0.998	0.001	4	0.997	0.002	4
Background, nA	7.37	0.53	4	0.52	0.14	4

Figure 6.2 : The current-concentration profile comparison and comparison table for choline chloride calibrations in PBS (pH 7.4) buffer solution at 21°C using PPD-(MMA)(CelAce)(MMA)-(ChOx)(BSA)(GA)(PEI) electrodes on days 1, 3, 5, 7 and 14. CPA carried out at +700 mV *vs.* SCE. Sequential current steps for 5, 10, 20, 40, 60, 80, 100, 200, 400, 600, 800, 1000, 1500, 2000, 2500, 3000 µM choline chloride injections.

A comparison graph and data table of the results for the repeated calibrations are presented in Figure 6.2. In addition, a graphical representation of the effect of repeated calibrations on the kinetic parameters V_{MAX}, K_M, α and the $I_{100\ \mu M}$ current is presented.

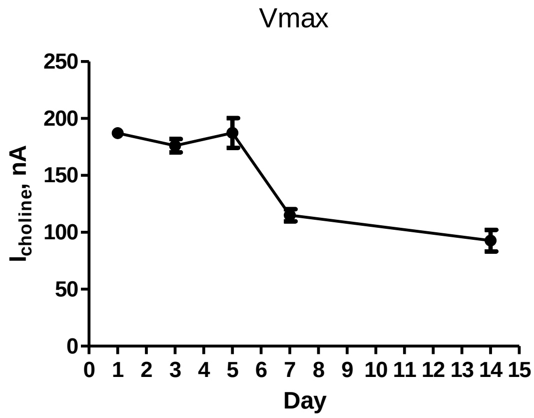

A comparison of the V_{MAX} current during the initial 5 days illustrates that it remains stable over time. A 5 % drop (*P* = 0.0137) in V_{MAX} current from day 1 to day 3 was observed reducing the current from 187.10 ± 4.69 nA, n = 4 (Day 1) to 176.10 ± 5.79 nA, n = 4 (Day 3). On day 5, the V_{MAX} current returned to a similar value of that seen on day 1. The values were not significantly different (*P* = 0.6277) from 187.10 ± 4.69 nA, n = 4 (Day 1) to 187.30 ± 13.07 nA, n = 4 (Day 5). On day 7, the V_{MAX} current was significantly reduced (*P* = 0.0009) by 39 % to 115.00 ± 5.29 nA, n = 4 (Day 7). By day 14, the V_{MAX} current had been significantly reduced (*P* = 0.0004) by 50 % from that on day 1 to 92.74 ± 9.51 nA, n = 4 (Day 14).

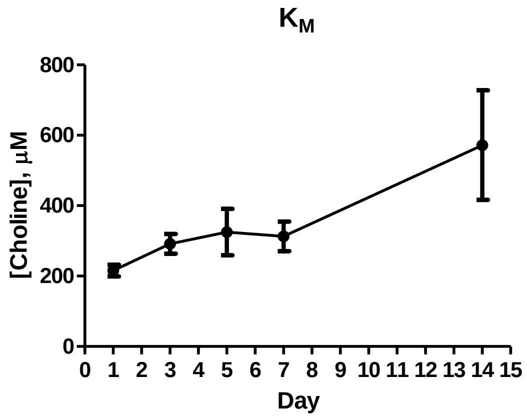

The K_M concentration was increased as a result of repeated calibrations. From day 1 to day 3 the K_M concentration was significantly increased (*P* = 0.0077) by 35 % increasing the concentration from 215.60 ± 16.62 µM, n = 4 (Day 1) to 291.80 ± 27.91 µM, n = 4 (Day 3). By day 5 the K_M concentration was increased from 215.60 ± 16.62 µM, n = 4 (Day 1) to 325.00 ± 66.08 µM, n = 4 (Day 5) an increase of 50 % this however, was not significant (P = 0.1069). After day 5 to day 7 the K_M concentration did not increase further. A decrease was observed from day 5 to day 7. However, in comparison to day 1 the K_M concentration was significantly increased (P = 0.0044) by 45 % from 215.60 ± 16.62 µM, n = 4 (Day 1) to 313.00 ± 41.88 µM, n = 4 (Day 7). A dramatic increase was observed by day 14 of 165 % significantly increasing (P = 0.0024) the concentration from 215.60 ± 16.62 µM, n = 4 (Day 1) to 571.90 ± 155.80 µM, n = 4 (Day 14).

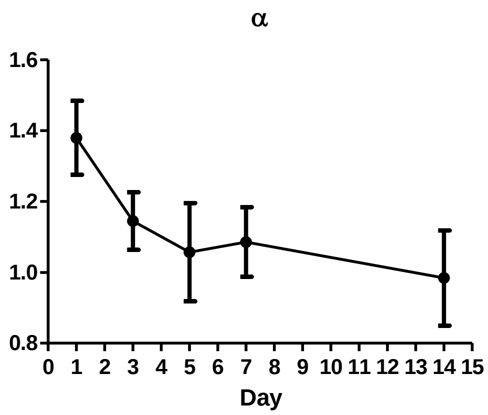

The α values illustrate a steady decrease over the 14 day period. Between day 1 and day 3 the α value significantly decreases (P = 0.0002) by 18 % from 1.38, n = 4 (Day 1) to 1.15, n = 4 (Day 3). A 24 % drop is observed by day 5 from 1.38, n = 4 (Day 1) to 1.06, n = 4 (Day 5) (P = 0.0074). From day 5 a 2 % increase is observed by day 7. A total drop of 24 % when compared to day 1 is observed significantly decreasing (P = 0.0166) the α value from 1.38, n = 4 (Day 1) to 1.09, n = 4 (Day 7). By day 14, the α value dropped from 1.38, n = 4 (Day 1) to 0.98, n = 4 (Day 14) a total decrease of 29 % (P = 0.0066).

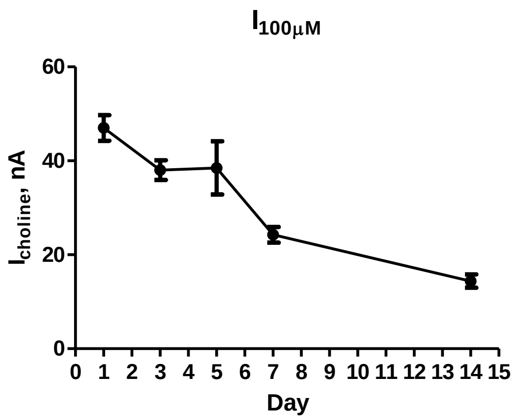

A comparison of the $I_{100\ \mu M}$ currents illustrates that by day 3, a significant decrease (P = 0.0008) of 20 % is observed decreasing the current from 47.00 ± 2.74 nA, n = 4 (Day 1) to 38.05 ± 2.10 nA, n = 4 (Day 3). This was stabilised until day 7 as the current did not significantly change (P = 0.0833) from 38.05 ± 2.10 nA, n = 4 (Day 3) to 38.50 ± 5.68 nA, n = 4 (Day 5). By day 7 the current was significantly reduced (P = 0.0004) to 24.25 ± 1.68 nA, n = 4 (Day 7) a decrease of 50 %. By day 14, the $I_{100\ \mu M}$ current was significantly decreased (P = 0.0001) by 70 % from 47.00 ± 2.74 nA, n = 4 (Day 1) to 14.39 ± 1.42 nA, n = 4 (Day 14).

It is illustrated that the 5 calibrations over the 14 days decreases the sensitivity of the sensor and alters the kinetic parameters. The V_{MAX} and $I_{100\ \mu M}$ currents steadily decreased over the 14 days, alongside an increase in the K_M concentration. It is possible that the enzyme is being denatured over time and is blocking access to the active enzyme on the lower layers. This is a factor which is important when determining the effect of proteins, lipids and brain tissue in future experiments.

6.3.2. Shelf-life

In the previous experiments, the effect of 5 calibrations on days 1, 3, 5, 7 and 14 were investigated. This illustrated the effect of both repeated calibrations on the sensor and the effect of 14 day storage on the stability of the sensor. In this section, the effect of storage of the sensor for 14 days undisturbed after fabrication was investigated to determine the true stability of the sensor over the 14 days.

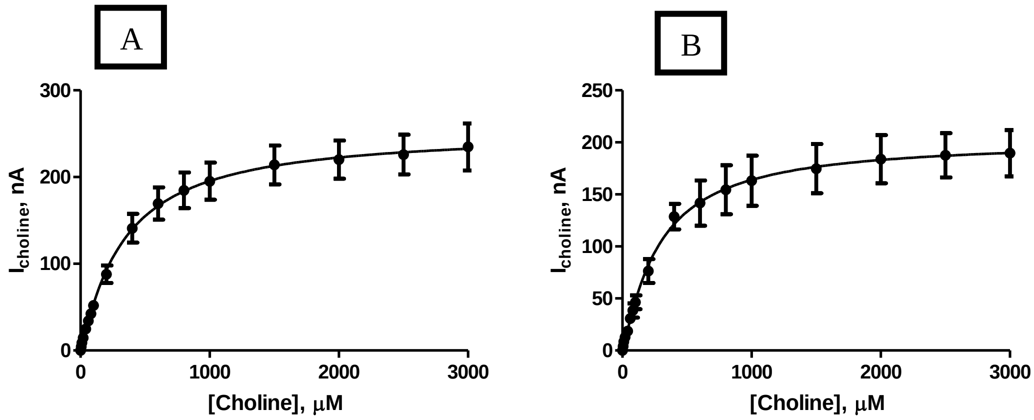

	Day 1			Day 14		
Conc, μM	**Mean, nA**	**S.E.M, nA**	**n**	**Mean, nA**	**S.E.M, nA**	**n**
0	0.00	0.00	4	0.00	0.00	4
5	4.35	0.42	4	3.97	0.59	4
10	8.89	0.86	4	8.43	1.41	4
20	14.72	1.39	4	12.72	1.96	4
40	24.76	2.12	4	18.63	1.67	4
60	34.14	3.50	4	30.74	4.19	4
80	42.39	4.20	4	38.49	6.87	4
100	51.83	5.57	4	46.43	6.68	4
200	87.98	10.14	4	76.29	11.42	4
400	140.91	16.62	4	128.65	12.30	4
600	169.48	18.72	4	141.69	21.79	4
800	184.69	20.58	4	154.58	23.54	4
1000	195.21	21.42	4	163.15	24.07	4
1500	214.01	22.33	4	174.79	23.55	4
2000	220.09	21.95	4	183.88	23.20	4
2500	225.94	22.91	4	187.66	21.29	4
3000	234.80	27.07	4	189.66	22.18	4

Figure 6.3 : The current-concentration profile and data table for choline chloride calibrations in PBS (pH 7.4) buffer solution at 21°C using PPD-(MMA)(CelAce)(MMA)-(ChOx)(BSA)(GA)(PEI) electrodes on days (A) 1 and (B) 14. CPA carried out at +700 mV *vs.* SCE. Sequential current steps for 5, 10, 20, 40, 60, 80, 100, 200, 400, 600, 800, 1000, 1500, 2000, 2500, 3000 μM choline chloride injections.

The data in Figure 6.3 illustrates the effect of shelf-life over a period of 14 days without intermittent calibrations. The data above shows that the storage stability of the sensor over 14 days is far better than previously observed by day 14 in Section 6.3.1. This illustrates the negative effect the repeated calibrations had on the sensor which will be accounted for in future studies.

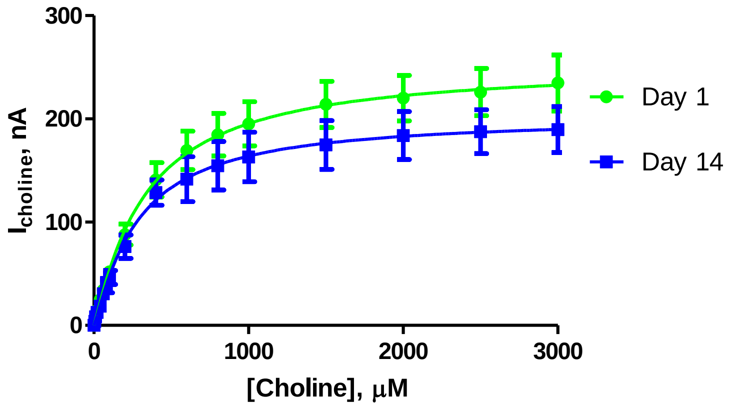

Kinetic Parameters	Day 1			Day 14		
	Mean	S.E.M	n	Mean	S.E.M	n
V_{MAX}, nA	253.10	17.47	4	202.60	15.32	4
Km, µM	331.00	65.03	4	282.00	62.64	4
α	1.10	0.15	4	1.14	0.19	4
$I_{100\mu M}$, nA	51.83	5.57	4	46.43	6.68	4
Sensitivity, nA/µM	0.50	0.02	4	0.45	0.02	4
R^2	0.991	0.002	4	0.987	0.004	4
Background, nA	0.26	0.04	4	0.22	0.04	4

Figure 6.4 : The current-concentration profile comparison and comparison table for choline chloride calibrations in PBS (pH 7.4) buffer solution at 21°C using PPD-(MMA)(CelAce)(MMA)-(ChOx)(BSA)(GA)(PEI) electrodes on days 1 and 14. CPA carried out at +700 mV *vs*. SCE. Sequential current steps for 5, 10, 20, 40, 60, 80, 100, 200, 400, 600, 800, 1000, 1500, 2000, 2500, 3000 µM choline chloride injections.

A comparison graph and data table for the shelf-life study are presented in Figure 6.4. This data illustrates the drop in sensitivity observed over a 14 day period without intermittent calibrations. The results show improvements to that observed in Section 6.3.1.

The V_{MAX} was not significantly reduced (*P* = 0.3518) by 20 % from 253.10 ± 17.47 nA, n = 4 (Day 1) to 202.60 ± 15.32 nA, n = 4 (Day 14). This can be compared to the 50 % drop observed in Section 6.3.1. The K_M is not significantly reduced (*P* = 0.0554) by 15 % from 331.00 ± 65.03 µM, n = 4 (Day 1) to 282.00 ± 62.64 µM, n = 4 (Day 14). This is vastly different from the previous section which illustrated an increase of 165 %. The α value did not significantly increase (*P* = 0.4067), only increasing from 1.10, n = 4 (Day 1) to 1.14, n = 4 (Day 14) a difference of 3 %.

In a comparison of the $I_{100\ \mu M}$ currents, a non significant decrease (*P* = 0.6451) of 10 % is observed from 51.83 ± 5.57 nA, n = 4 (Day 1) to 46.43 ± 6.68 nA, n = 4 (Day 14). This is a vastly different response to that observed in section which observed a drop of 70 %.

This section has illustrated that the sensor shelf-life over a 14 day period and observes a 10 % reduction in current at 100 µM choline. Section 6.3.1 investigated the effect over 14 days with the addition of calibrations on days 1, 5 and 7. These experiments observed a 70 % decrease in the current at 100 µM. This indicates that the repeated calibrations in the lipid, protein and brain tissue studies may also influence the sensitivity and kinetic parameters of the sensor.

6.3.3. BSA Study

One important component of the chemical environment of the brain which the sensor will be in contact with is proteins (O'Neill, 1993). Previous studies have utilised bovine serum albumin (BSA) for biocompatibility studies to monitor the effect of sensors in contact with protein (Brown *et al.*, 2009) (Bolger *et al.*, 2011a). This section will look at the effect of emersion of the sensors in a 10 % BSA solution for 14 days. The sensors were calibrated on days 1, 3, 5, 7 and 14.

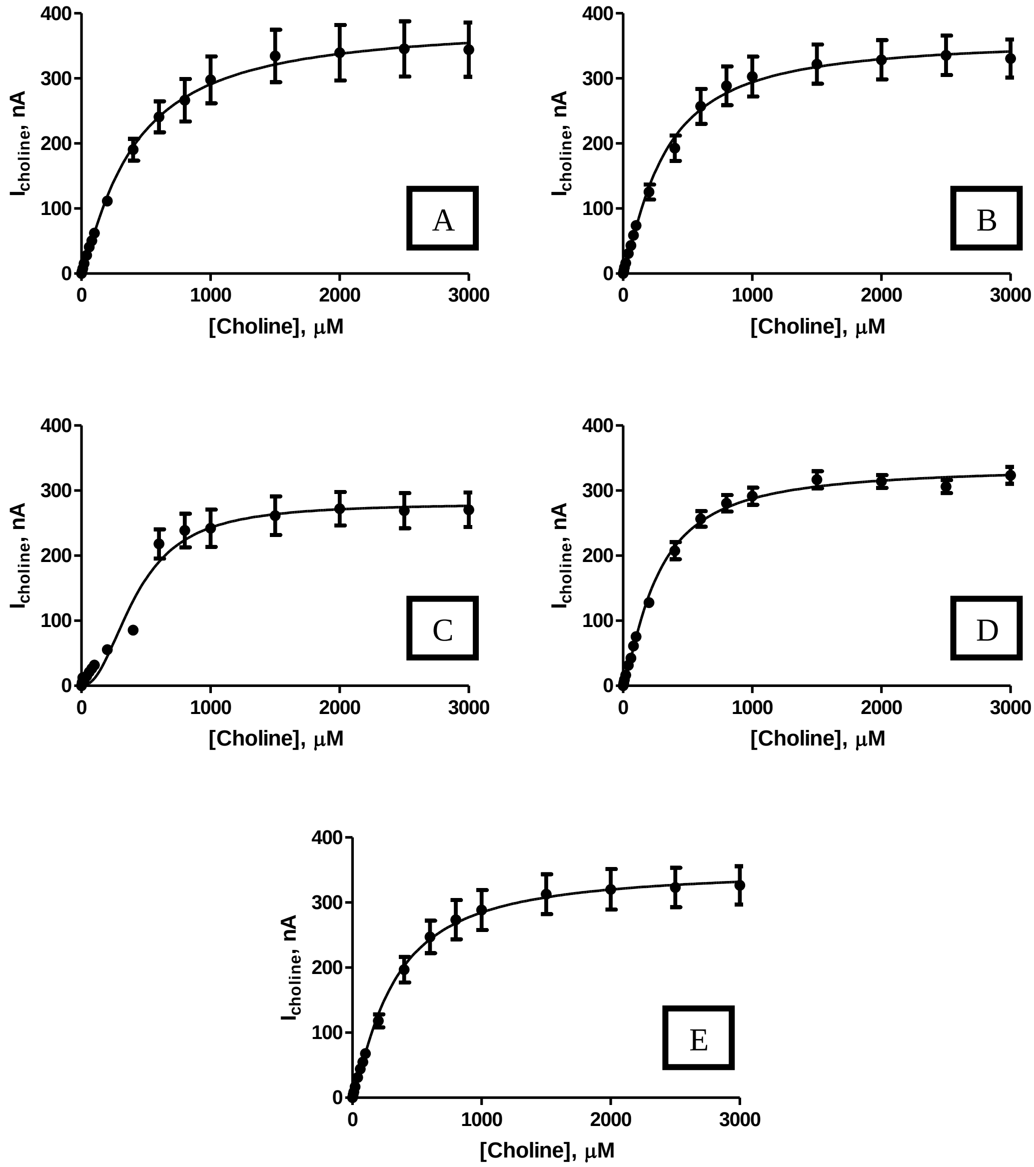

Figure 6.5 : The current-concentration profile and tables (below) for choline chloride calibrations in PBS (pH 7.4) buffer solution at 21°C using PPD-(MMA)(CelAce)(MMA)-(ChOx)(BSA)(GA)(PEI) electrodes exposed to 10 % BSA on days (A) 1, (B) 3, (C) 5, (D) 7 and (E) 14. CPA carried out at +700 mV *vs*. SCE. Sequential current steps for 5, 10, 20, 40, 60, 80, 100, 200, 400, 600, 800, 1000, 1500, 2000, 2500, 3000 μM choline chloride injections.

	Day 1			Day 3			Day 5		
Conc, µM	**Mean, nA**	**S.E.M, nA**	**n**	**Mean, nA**	**S.E.M, nA**	**n**	**Mean, nA**	**S.E.M, nA**	**n**
0	0.00	0.00	4	0.00	0.00	4	0.00	0.00	4
5	3.86	0.13	4	4.57	0.35	4	5.04	0.37	4
10	7.76	0.35	4	9.42	0.76	4	12.39	0.97	4
20	15.62	0.77	4	16.32	1.30	4	8.46	0.66	4
40	28.27	1.40	4	30.96	2.59	4	14.89	1.27	4
60	40.89	2.01	4	43.25	3.60	4	21.09	1.85	4
80	50.52	2.52	4	58.82	5.03	4	26.60	2.37	4
100	62.23	3.59	4	73.67	6.38	4	31.94	2.91	4
200	111.39	6.98	4	125.37	11.45	4	55.65	5.20	4
400	190.45	16.83	4	192.68	19.38	4	85.51	7.23	4
600	240.89	23.83	4	257.10	26.82	4	218.08	22.44	4
800	266.39	32.67	4	288.64	29.94	4	238.70	25.96	4
1000	297.74	35.94	4	302.82	30.53	4	242.22	28.57	4
1500	334.49	40.37	4	321.97	30.09	4	261.36	29.69	4
2000	339.59	42.60	4	328.51	30.16	4	272.28	25.70	4
2500	345.37	42.55	4	335.45	30.39	4	269.22	26.95	4
3000	344.18	41.77	4	330.60	29.29	4	270.59	26.54	4

	Day 7			Day 14		
Conc, µM	**Mean, nA**	**S.E.M, nA**	**n**	**Mean, nA**	**S.E.M, nA**	**n**
0	0.00	0.00	4	0.00	0.00	4
5	4.78	0.40	4	4.76	0.31	4
10	9.62	0.91	4	8.81	0.62	4
20	16.60	1.88	4	16.99	1.13	4
40	31.55	2.58	4	31.12	2.14	4
60	42.42	4.95	4	44.04	3.15	4
80	61.15	4.03	4	54.99	4.05	4
100	75.63	3.90	4	67.68	5.15	4
200	127.87	7.78	4	118.19	9.91	4
400	207.60	13.14	4	196.83	19.63	4
600	256.50	12.05	4	247.14	25.05	4
800	280.46	12.56	4	273.54	30.14	4
1000	291.37	13.06	4	288.44	30.72	4
1500	316.77	13.15	4	312.80	30.63	4
2000	314.09	9.87	4	320.19	31.19	4
2500	306.08	10.01	4	323.17	30.18	4
3000	323.60	13.01	4	326.39	29.53	4

The data in Figure 6.5 illustrates that BSA does not have a negative effect on the sensor. The storage of the sensor in the BSA solution presents a stabilising effect compared to the shelf-life experiments in Section 6.3.1.

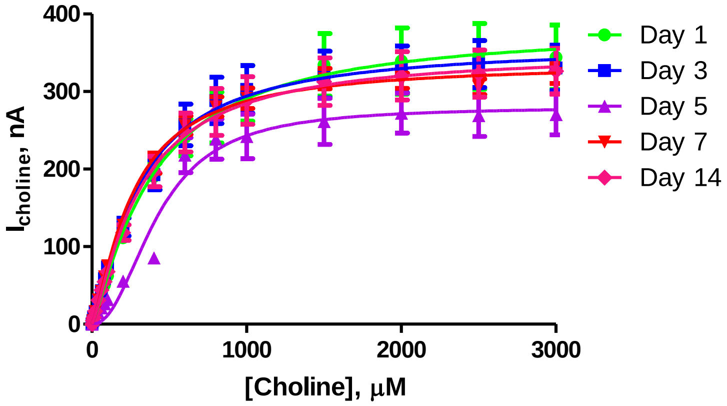

Kinetic Parameters	Day 1			Day 3			Day 5		
	Mean	S.E.M	n	Mean	S.E.M	n	Mean	S.E.M	n
V_{MAX}, nA	384.90	28.09	4	360.80	18.46	4	280.40	12.04	4
Km, µM	392.10	74.29	4	308.00	43.75	4	427.00	38.04	4
α	1.21	0.18	4	1.26	0.15	4	2.20	0.38	4
$I_{100\mu M}$, nA	62.23	3.59	4	73.67	6.38	4	31.94	2.91	4
Sensitivity, nA/µM	0.56	0.02	4	0.63	0.02	4	0.26	0.02	4
R^2	0.995	0.001	4	0.999	0.000	4	0.939	0.004	4
Background, nA	0.54	0.02	4	0.33	0.03	4	2.75	0.09	4

Kinetic Parameters	Day 7			Day 14		
	Mean	S.E.M	n	Mean	S.E.M	n
V_{MAX}, nA	337.10	7.43	4	351.70	18.68	4
Km, µM	263.30	16.85	4	313.90	46.13	4
α	1.32	0.08	4	1.25	0.15	4
$I_{100\mu M}$, nA	75.63	3.90	4	67.68	5.15	4
Sensitivity, nA/µM	0.65	0.02	4	0.59	0.02	4
R^2	0.994	0.003	4	0.996	0.001	4
Background, nA	0.43	0.07	4	0.23	0.02	4

Figure 6.6 : The current-concentration profile comparison and comparison table for choline chloride calibrations in PBS (pH 7.4) buffer solution at 21°C using design PPD-(MMA)(CelAce)(MMA)-(ChOx)(BSA)(GA)(PEI) exposed to BSA on days (A) 1, (B) 3, (C) 5, (D) 7 and (E) 14. CPA carried out at +700 mV *vs*. SCE. Sequential current steps for 5, 10, 20, 40, 60, 80, 100, 200, 400, 600, 800, 1000, 1500, 2000, 2500, 3000 µM choline chloride injections.

A comparison graph and data table for the BSA study are presented in Figure 6.6. In addition, a graphical representation of the kinetic parameters V_{MAX}, K_M, α and the $I_{100\ \mu M}$ current are presented illustrating the effect of BSA exposure on the sensor over a 14 day period.

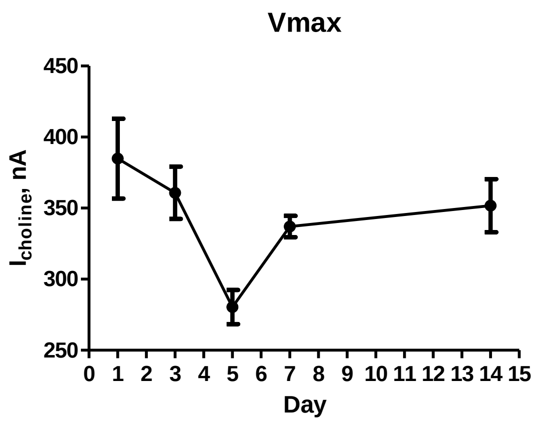

A comparison of the V_{MAX} currents, illustrates a decrease between the first three days of exposure. The current is not significantly reduced (*P* = 0.2656) by 7 % from 384.90 ± 28.09 nA, n = 4 (Day 1) to 351.70 ± 18.68 nA, n = 4 (Day 3). On day 5 the current is significantly reduced (*P* = 0.0418) by 19 % from day 1 reducing the current from 384.90 ± 28.09 nA, n = 4 (Day 1) to 280.40 ± 12.04 nA, n = 4 (Day 5). This however is possibly an outlier as the V_{MAX} then increases by day 7. The decrease observed on day 7 is a 13 % reduction (*P* = 0.3100) to 337.10 ± 7.43 nA, n = 4 (Day 7). This increases further on day 14 to 351.70 ± 18.68 nA, n = 4 (Day 14) decreasing the current by 9 % from day 1 (*P* = 0.2171).

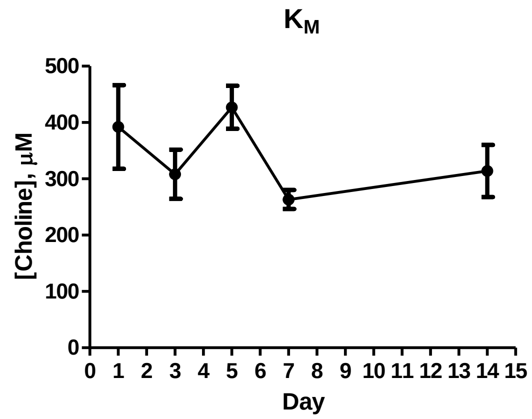

The K_M also decreased over the 14 days. By day 3 the K_M had decreased by 22 % (*P* = 0.0699) from 392.10 ± 74.29 µM, n = 4 (Day 1) to 308.40 ± 43.75 µM, n = 4 (Day 3). Day 5 remained an outlier for the K_M study increasing from 392.10 ± 74.29 µM, n = 4 (Day 1) to 427.00 ± 38.04 µM, n = 4 (Day 5) an increase of 8 % from day 1 (*P* = 0.0301). By day 7 the K_M was significantly reduced (*P* = 0.0335) by 33 % from day 1 reducing the concentration from 392.10 ± 74.29 μM, n = 4 (Day 1) to 263.30 ± 16.85 μM, n = 4 (Day 7). The K_M concentration on day 14 was significantly reduced (*P* = 0.0433) by 20 % from day 1. A reduction from 392.10 ± 74.29 μM, n = 4 (Day 1) to 313.90 ± 46.13 μM, n = 4 (Day 14). The reduction in K_M concentration over time illustrates that the BSA solution storage may decrease the diffusional constraints which may occur from over time.

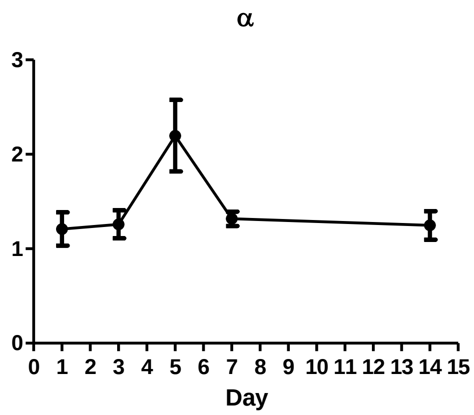

The α value remains stable over the 14 days. By day three the α value had only increased by 3 % from 1.21, n = 4 (Day 1) to 1.26, n = 4 (Day 1) however this was significant (*P* = 0.0233). Day 5 remains an outlier increasing the α value by 81 % from 1.21, n = 4 (Day 1) to 2.20, n = 4 (Day 5) (*P* = 0.0742). By day 7, the α value returned to 1.32, n = 4 (Day 7) a non significant increase (P = 0.0757) of 9 % from day 1. By day 14 the α value increased by 3 % from 1.21, n = 4 (Day 1) to 1.25, n = 4 (Day 14) however was significantly different (*P* = 0.6584).

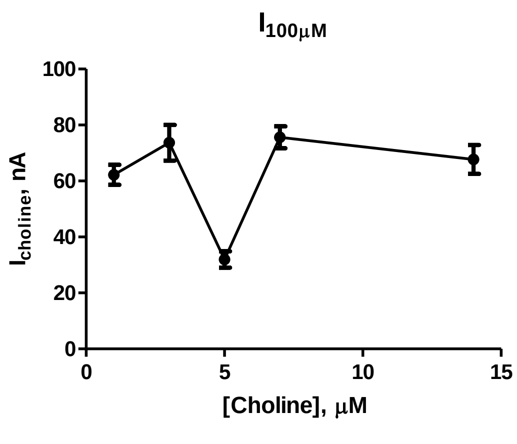

A comparison of the $I_{100\ \mu M}$ currents illustrates that by day 3 the current had increased by 18 % however not significantly (*P* = 0.0754) from 62.23 ± 3.59 nA, n = 4 (Day 1) to 73.67 ± 6.38 nA, n = 4 (Day 3). On day 5 the current was significantly reduced (*P* = 0.0017) to 31.94 ± 2.91 nA, n = 4 (Day 5). Day 5 remains an outlier as the current significantly increased (*P* = 0.0128) by day 7 to 75.63 ± 3.90 nA, n = 4 (Day 7) an increase of 20 % from day 1. On day 14 the current was increased by 8 % however not significantly (*P* = 0.1123) from 62.23 ± 3.59 nA, n = 4 (Day 1) to 67.68 ± 5.15 nA, n = 4 (Day 14).

This section has illustrated that exposure to BSA benefits the sensor stability over the 14 days. The current obtained at 100 µM choline increased by day 14. In addition, the K_M was reduced over time suggesting that the BSA solution storage is beneficial for diffusion. Day 5 was an outlier throughout this set of experiments, this is possibly due to a build up of BSA on the sensor surface between day 3 and 5 which is later removed by day 7, potentially as a result of the calibration on day 5.

6.3.4. PEA study

Another important component of the chemical environment of the brain which the sensor will be in contact with and may have an effect on the sensor performance is lipids (O'Neill, 1993). Previous studies have utilised 3-sn-phosphatidylethanolamine (PEA) for biocompatibility studies to monitor the effect of sensors in contact with lipid (Brown *et al.*, 2009) (Bolger *et al.*, 2011a). This section will look at the effect of immersion of the sensors in a 10 % PEA solution for 14 days when not in use. The sensors were calibrated on days 1, 3, 5, 7 and 14.

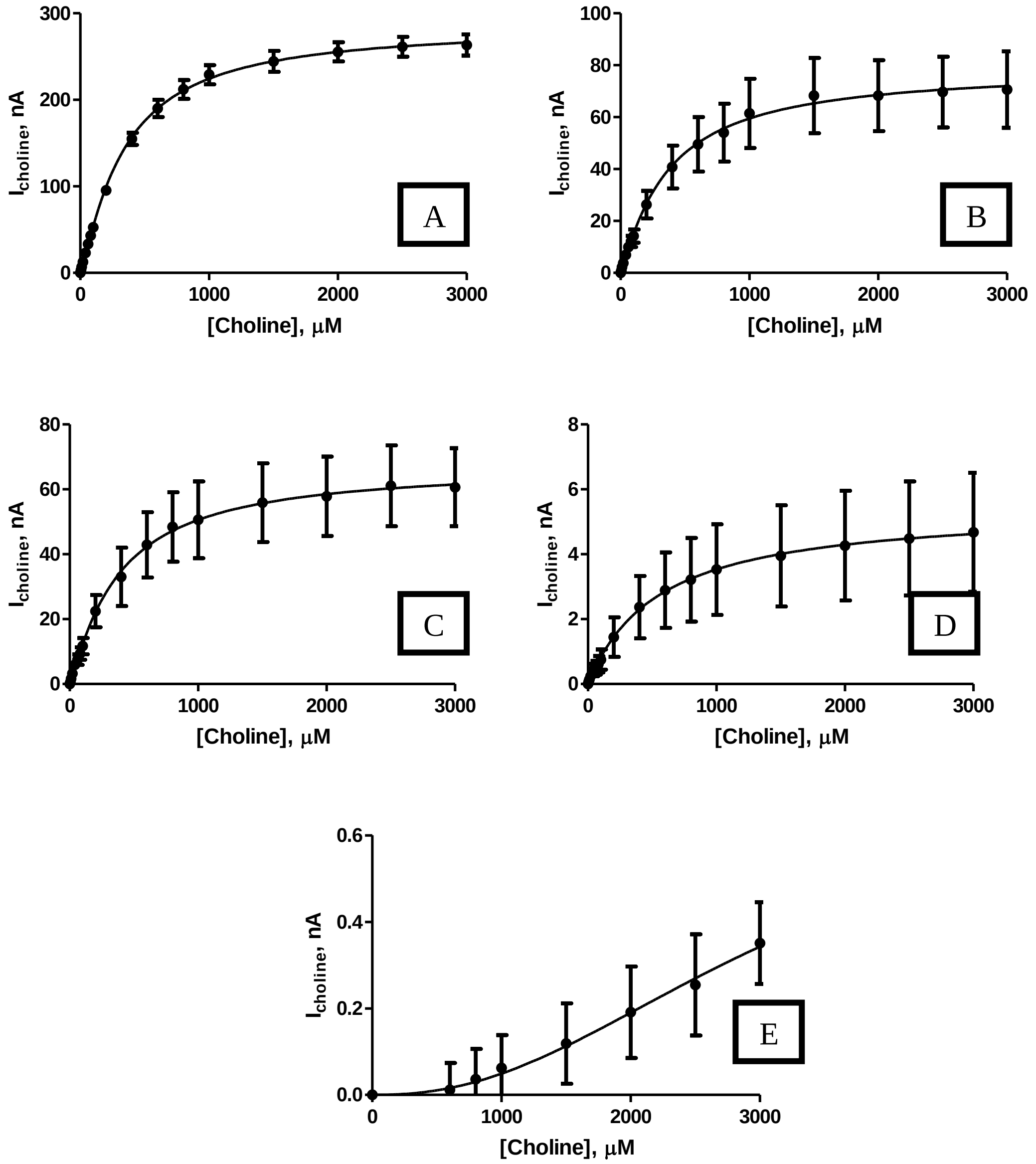

Figure 6.7 : The current-concentration profile and table (below) for choline chloride calibrations in PBS (pH 7.4) buffer solution at 21°C using design PPD-(MMA)(CelAce)(MMA)-(ChOx)(BSA)(GA)(PEI) exposed to PEA on days (A) 1, (B) 3, (C) 5, (D) 7 and (E) 14. CPA carried out at +700 mV *vs*. SCE. Sequential current steps for 5, 10, 20, 40, 60, 80, 100, 200, 400, 600, 800, 1000, 1500, 2000, 2500, 3000 µM choline chloride injections.

	Day 1			Day 3			Day 5		
Conc, µM	**Mean, nA**	**S.E.M, nA**	**n**	**Mean, nA**	**S.E.M, nA**	**n**	**Mean, nA**	**S.E.M, nA**	**n**
0	0.00	0.00	4	0.00	0.00	4	0.00	0.00	4
5	3.36	0.08	4	0.87	0.17	4	0.62	0.12	4
10	6.88	0.21	4	2.23	0.52	4	1.63	0.33	4
20	12.65	0.40	4	3.81	0.80	4	3.21	0.69	4
40	23.18	0.81	4	6.93	1.32	4	5.99	1.20	4
60	33.27	1.11	4	9.94	1.91	4	7.51	1.59	4
80	43.08	1.41	4	12.14	2.17	4	9.39	1.90	4
100	52.63	1.94	4	14.17	2.54	4	11.68	2.51	4
200	95.39	3.33	4	26.31	5.32	4	22.46	4.95	4
400	154.88	6.96	4	40.79	8.28	4	33.04	9.01	4
600	190.15	10.02	4	49.56	10.49	4	42.90	10.09	4
800	212.01	10.93	4	54.02	11.16	4	48.41	10.71	4
1000	229.03	11.17	4	61.48	13.32	4	50.62	11.84	4
1500	244.50	12.10	4	68.28	14.52	4	55.90	12.14	4
2000	255.46	11.08	4	68.28	13.64	4	57.86	12.25	4
2500	261.33	11.48	4	69.68	13.63	4	61.09	12.47	4
3000	263.45	12.23	4	70.64	14.73	4	60.66	12.01	4

	Day 7			Day 14		
Conc, µM	Mean, nA	S.E.M, nA	n	Mean, nA	S.E.M, nA	n
0	0.00	0.00	4	0.00	0.00	4
5	0.07	0.04	4	-0.04	0.02	4
10	0.13	0.06	4	-0.05	0.03	4
20	0.24	0.11	4	-0.03	0.01	4
40	0.43	0.19	4	-0.05	0.03	4
60	0.50	0.21	4	-0.04	0.01	4
80	0.61	0.25	4	-0.07	0.04	4
100	0.75	0.31	4	-0.09	0.05	4
200	1.45	0.61	4	-0.06	0.050	4
400	2.37	0.96	4	-0.03	0.07	4
600	2.89	1.16	4	0.01	0.06	4
800	3.21	1.29	4	0.04	0.07	4
1000	3.53	1.39	4	0.06	0.08	4
1500	3.95	1.56	4	0.12	0.09	4
2000	4.26	1.69	4	0.19	0.11	4
2500	4.49	1.76	4	0.25	0.12	4
3000	4.68	1.84	4	0.35	0.09	4

The data in Figure 6.7 illustrates the negative effect that the PEA has on sensitivity. The PEA solution is a harsh treatment on the sensor. The negative effect is clearly illustrated by the gradual decrease in sensitivity. The concentration of the PEA used in this study is high compared to the free lipid expected in the brain. It is not an accurate representation of the effect of lipids on the sensor as the solution is of a thick viscous consistency not similar to brain tissue, however is an important test to conduct as part of the investigation into the effect of the brain tissue constituent parts have on the sensor.

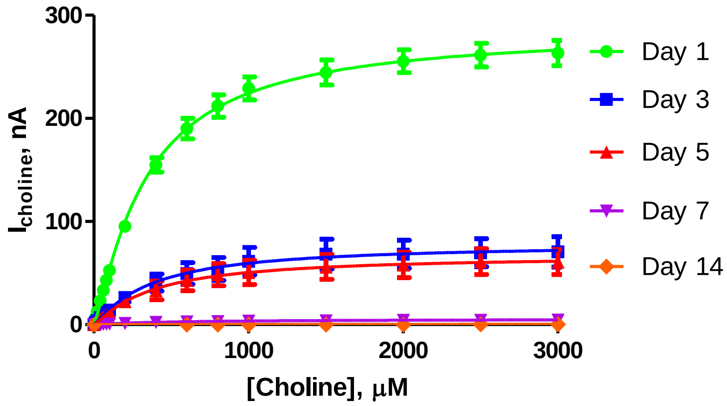

Kinetic Parameters	Day 1			Day 3			Day 5		
	Mean	S.E.M	n	Mean	S.E.M	n	Mean	S.E.M	n
V_{MAX}, nA	285.60	7.88	4	78.82	10.67	4	67.38	9.61	4
Km, μM	339.20	25.55	4	366.30	136.30	4	378.10	146.00	4
α	1.20	0.07	4	1.12	0.29	4	1.13	0.31	4
$I_{100\mu M}$, nA	52.63	1.94	4	14.17	2.54	4	11.68	2.51	4
Sensitivity, nA/μM	0.52	0.01	4	0.14	0.01	4	0.12	0.01	4
R^2	0.9980	0.0001	4	0.987	0.005	4	0.986	0.001	4
Background, nA	2.43	0.17	4	4.03	0.69	4	0.55	0.13	4

Kinetic Parameters	Day 7			Day 14		
	Mean	S.E.M	n	Mean	S.E.M	n
V_{MAX}, nA	5.45	1.97	4	0.72	1.41	4
Km, μM	548.30	520.50	4	3122	4975	4
α	1.01	0.51	4	2.29	1.87	4
$I_{100\mu M}$, nA	0.75	0.31	4	-0.09	0.05	4
Sensitivity, nA/μM	0.007	0.001	4	-0.0005	0.0002	4
R^2	0.975	0.005	4	0.34	0.15	4
Background, nA	0.84	0.22	4	0.92	0.41	4

Figure 6.8 : The current-concentration profile comparison and comparison table for choline chloride calibrations in PBS (pH 7.4) buffer solution at 21°C using design PPD-(MMA)(CelAce)(MMA)-(ChOx)(BSA)(GA)(PEI) exposed to PEA on days 1, 3, 5, 7 and 14. CPA carried out at +700 mV *vs.* SCE. Sequential current steps for 5, 10, 20, 40, 60, 80, 100, 200, 400, 600, 800, 1000, 1500, 2000, 2500, 3000 μM choline chloride injections.

A comparison graph and data table for the PEA study are presented in Figure 6.8. In addition, a graphical representation of the kinetic parameters V_{MAX}, K_M, α and the $I_{100\ \mu M}$ current are presented illustrating the effect of PEA exposure on the sensor over a 14 day period.

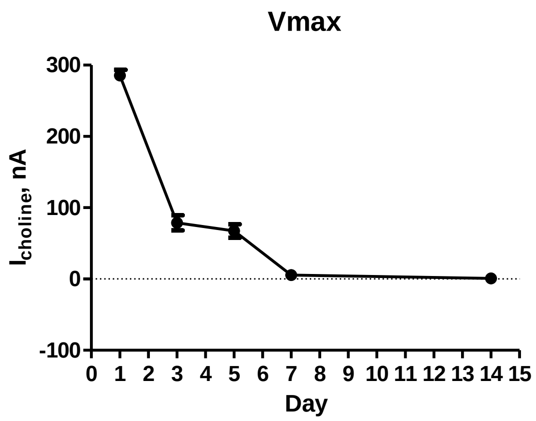

A comparison of the V_{MAX} currents illustrates a significant decrease (P = 0.0002) of 73 % in current by day 3. The current is reduced from 285.60 ± 7.88 nA, n = 4 (Day 1) to 78.82 ± 10.67 nA, n = 4 (Day 3). On day 5 the V_{MAX} current is reduced further to 67.38 ± 9.61 nA, n = 4 (Day 5) a total significant reduction (P = 0.0003) of 77 % from day 1. By day 7 the sensor was not sufficiently detecting choline and the V_{MAX} current was significantly reduced (P = 0.0001) by 98 % from 285.60 ± 7.88 nA, n = 4 (Day 1) to 5.45 ± 1.97 nA, n = 4 (Day 7). By day 14 the current was reduced by 99.75 % to 0.72 ± 1.41 nA, n = 4 (Day 14). It is clear from these results the effect that even three days of exposure to PEA has on the sensor.

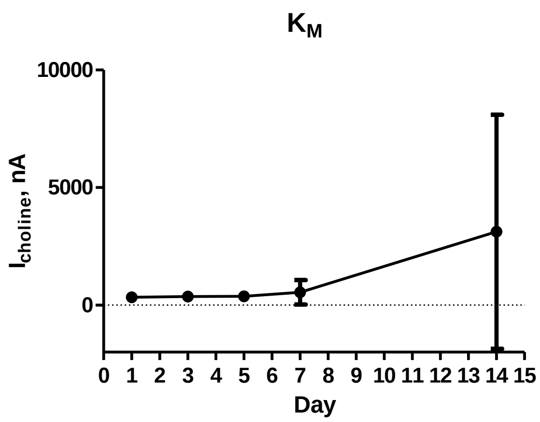

The consistency of the PEA solution has led to an increase in the K_M as the solution has coated the sensor surface blocking access of the analyte. A comparison of the K_M concentrations shows a non significant increase (P = 0.2011) by day 3 of 7 % from 339.20 ± 25.55 µM, n = 4 (Day 1) to 366.30 ± 136.30 µM, n = 4 (Day 3). The K_M was also not significantly increased (P = 0.2918) by day 5 from 339.20 ± 25.55 µM, n = 4 (Day 1) to 378.10 ± 166.00 µM, n = 4 (Day 5) an increase of 11 %. By 7 the K_M increased significantly (P = 0.0159) to 548.30 ± 520.50 µM, n = 4 (Day 7) an increase of 61 % from day 1. By day 14 the K_M concentration increased by 820 % to 3122 ± 4975 µM, n = 4. Similar to the V_{MAX} currents, by day 7 the sensor was sufficiently altered to dramatically increase the K_M concentration.

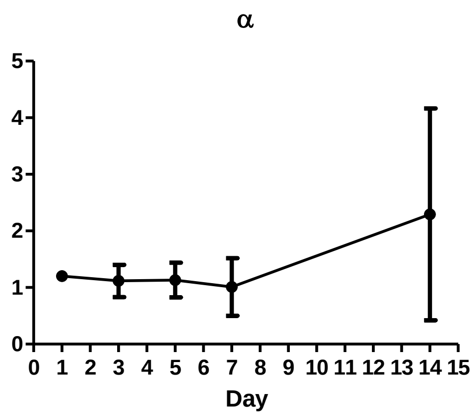

The α value was not dramatically altered within the first 5 days of exposure. By day 3 the α value was not significantly decreased (P = 0.0303) due to a 7 % drop from 1.20, n = 4 (Day 1) to 1.12, n = 4 (Day 3). By day 5 the α value had only increased to 1.13, n = 4 (P = 0.2630). However, similar to V_{MAX} and K_M the α value was dramatically altered by day 7. On day 7 the α value was significantly reduced (P = 0.0019) by 16 % from 1.20, n = 4 (Day 1) to 1.01, n = 4 (Day 7). By day 14 the α value was increased by 91 % to 2.29, n = 4 (Day 14).

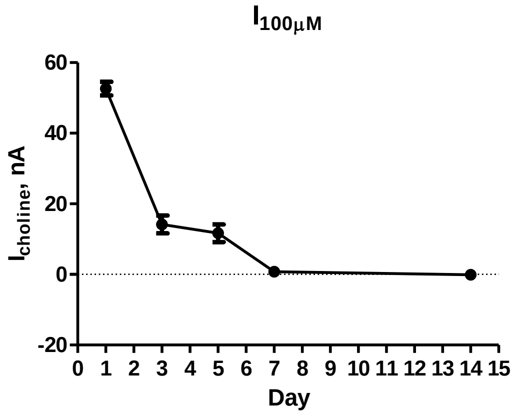

A comparison of the $I_{100\ \mu M}$ currents illustrates that the PEA has a dramatic effect on the detection of choline. By day three the current is significantly reduced (P<0.0001) by 74 % from 52.63 ± 1.94 nA, n = 4 (Day 1) to 14.17 ± 2.54 nA, n = 4 (Day 3). The current is the further reduced by day 5 to 11.68 ± 2.51 nA, n = 4 (Day 5) a total reduction in current of 78 % from day 1 (*P* = 0.0002). Similar to previous parameters, by day 7 the sensor was not adequately detecting choline. This significantly reduced (P<0.0001) the current by 98 % to 0.75 ± 0.31 nA, n = 4 (Day 7). By day 14 the current was reduced by 100 % as the current at 100 µM choline was -0.09 ± 0.05 nA, n = 4 (Day 14). This negative current is possibly as a result of background drift.

This section has illustrated the effect of exposure to PEA over a 14 day period. This test is a harsh test which utilises a very high concentration of PEA. In addition, the PEA is not a dissolved solution this in turn tends to stick onto the sensor surface. This is not an accurate representation of the effect of free lipids in the brain however, is an interesting test to gain insight into the ability of the sensor to function when fouled by proteinaceous species.

6.3.5. Brain Tissue

Although the previous sections allowed for the evaluation of the stability of the sensor while in contact with proteins and lipids, these tend to be very harsh treatments. As this is the case a more accurate measurement of the stability of the sensor in the brain is the exposure of the sensor to brain tissue *in-vitro*. This section will look at the effect of emersion of the sensors in brain tissue for 14 days. The sensors were calibrated on days 1, 3, 5, 7 and 14.

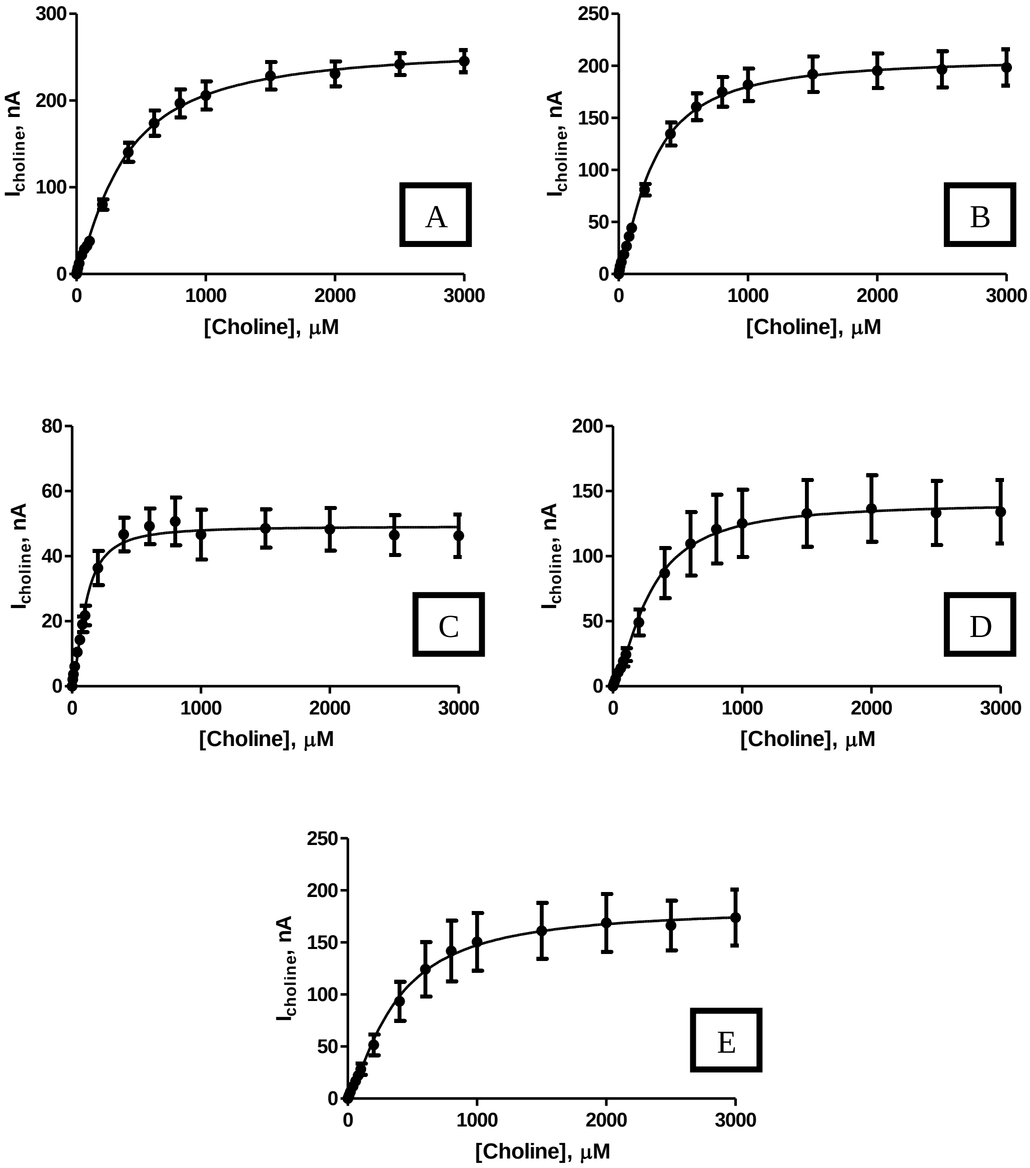

Figure 6.9 : The current-concentration profile and table (below) for choline chloride calibrations in PBS (pH 7.4) buffer solution at 21°C using design PPD-(MMA)(CelAce)(MMA)-(ChOx)(BSA)(GA)(PEI) exposed to brain tissue on days (A) 1, (B) 3, (C) 5, (D) 7 and (E) 14. CPA carried out at +700 mV *vs*. SCE. Sequential current steps for 5, 10, 20, 40, 60, 80, 100, 200, 400, 600, 800, 1000, 1500, 200, 2500, 3000 μM choline chloride injections.

	Day 1			Day 3			Day 5		
Conc, µM	**Mean, nA**	**S.E.M, nA**	**n**	**Mean, nA**	**S.E.M, nA**	**n**	**Mean, nA**	**S.E.M, nA**	**n**
0	0.00	0.00	4	0.00	0.00	4	0.00	0.00	4
5	3.62	0.20	4	3.59	0.16	4	2.10	0.25	4
10	7.13	0.42	4	7.38	0.27	4	3.70	0.39	4
20	12.33	0.72	4	11.49	0.48	4	6.12	0.70	4
40	21.82	1.31	4	18.79	0.89	4	10.48	1.23	4
60	28.50	1.68	4	26.73	1.18	4	14.28	1.43	4
80	32.25	1.97	4	36.09	1.94	4	19.02	2.39	4
100	37.87	2.47	4	44.27	2.66	4	21.78	3.02	4
200	80.05	6.01	4	81.07	5.56	4	36.37	5.27	4
400	140.38	10.98	4	134.59	11.15	4	46.67	5.16	4
600	173.98	14.70	4	160.69	12.88	4	49.20	5.52	4
800	196.79	16.15	4	174.94	14.24	4	50.71	7.34	4
1000	205.88	16.14	4	181.76	15.61	4	46.65	7.65	4
1500	228.49	15.98	4	192.05	17.07	4	48.54	5.92	4
2000	230.76	14.44	4	195.31	16.76	4	48.27	6.57	4
2500	241.91	12.63	4	196.61	17.45	4	46.49	6.13	4
3000	245.37	12.71	4	198.48	17.54	4	46.28	6.53	4

	Day 7			Day 14		
Conc, µM	Mean, nA	S.E.M, nA	n	Mean, nA	S.E.M, nA	n
0	0.00	0.00	4	0.00	0.00	4
5	1.41	0.35	4	1.63	0.32	4
10	3.16	0.73	4	3.45	0.68	4
20	5.67	1.22	4	6.47	1.28	4
40	10.61	2.16	4	11.75	2.27	4
60	13.87	2.83	4	16.76	3.22	4
80	19.19	3.90	4	22.11	4.18	4
100	24.34	4.84	4	28.25	5.37	4
200	49.07	9.98	4	51.58	10.02	4
400	87.00	19.31	4	93.34	18.75	4
600	109.51	24.47	4	124.23	26.17	4
800	120.81	26.46	4	141.78	29.07	4
1000	125.29	25.82	4	150.49	27.75	4
1500	132.94	25.71	4	161.17	26.89	4
2000	136.67	25.67	4	168.81	27.79	4
2500	133.21	24.69	4	166.31	23.85	4
3000	134.15	24.47	4	173.89	26.87	4

The data in Figure 6.9 illustrates that exposure to brain tissue gradually decreased the sensitivity of the sensor and changes the kinetic parameters.

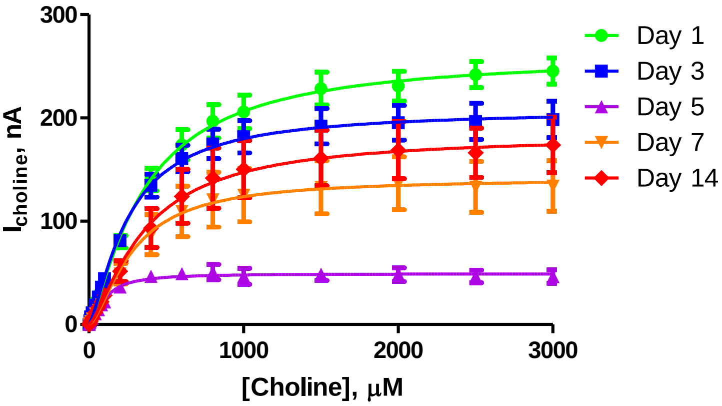

Kinetic Parameters	Day 1			Day 3			Day 5		
	Mean	S.E.M	n	Mean	S.E.M	n	Mean	S.E.M	n
V_{MAX}, nA	261.70	10.00	4	207.80	8.01	4	49.17	2.05	4
Km, µM	357.20	35.74	4	254.80	28.66	4	102.40	14.39	4
α	1.28	0.11	4	1.36	0.145	4	1.61	0.35	4
$I_{100\mu M}$, nA	37.87	2.47	4	44.27	2.66	4	21.78	3.02	4
Sensitivity, nA/µM	0.38	0.01	4	0.40	0.01	4	0.18	0.01	4
R^2	0.967	0.002	4	0.9957	0.0003	4	0.988	0.003	4
Background, nA	1.96	0.22	4	3.12	0.12	4	0.79	0.10	4

Kinetic Parameters	Day 7			Day 14		
	Mean	S.E.M	n	Mean	S.E.M	n
V_{MAX}, nA	141.20	183.30	4	183.30	16.27	4
Km, µM	279.60	360.50	4	360.50	81.31	4
α	1.54	1.38	4	1.38	0.30	4
$I_{100\mu M}$, nA	24.34	4.84	4	28.25	5.37	4
Sensitivity, nA/µM	0.242	0.003	4	0.258	0.005	4
R^2	0.9966	0.0001	4	0.9987	0.0001	4
Background, nA	0.59	0.09	4	0.69	0.08	4

Figure 6.10 : The current-concentration profile comparison and comparison table for choline chloride calibrations in PBS (pH 7.4) buffer solution at 21°C using design PPD-(MMA)(CelAce)(MMA)-(ChOx)(BSA)(GA)(PEI) exposed to brain tissue on days 1, 3, 5, 7 and 14. CPA carried out at +700 mV *vs.* SCE. Sequential current steps for 5, 10, 20, 40, 60, 80, 100, 200, 400, 600, 800, 1000, 1500, 2000, 2500, 3000 µM choline chloride injections.

A comparison graph and data table are presented in Figure 6.10. In addition, a graphical representation of the kinetic parameters V_{MAX}, K_M, α and the $I_{100\ \mu M}$ current are presented illustrating the effect of brain tissue exposure on the sensor over a 14 day period.

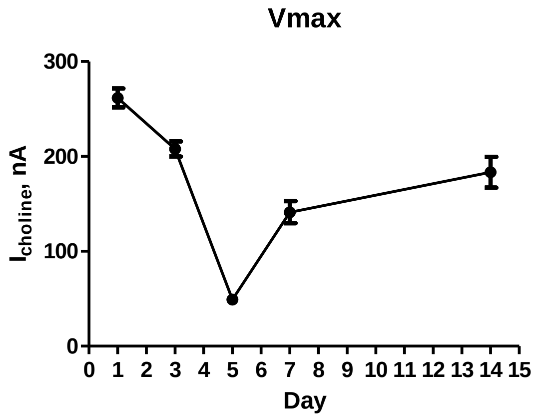

A comparison of the V_{MAX} currents illustrates that by day 3 there is a significant reduction (*P* = 0.0051) of 20 % from 261.70 ± 10.00 nA, n = 4 (Day 1) to 207.80 ± 8.01 nA, n = 4 (Day 3). Similarly to data shown in the BSA study, day 5 appears as an outlier. The V_{MAX} current is significantly reduced (*P* = 0.0007) from 261.70 ± 10.00 nA, n = 4 (Day 1) to 49.17 ± 2.05 nA, n = 4 (Day 5) a reduction of 80 %. This however increases by day 7 to 141.20 ± 183.30 nA, n = 4 (Day 7) demonstrating a 47 % reduction (*P* = 0.0209) in current compared to day 1. By day 14 the current was not significantly reduced (*P* = 0.0523) by 30 % from day 1 to 183.30 ± 16.27 nA, n = 4 (Day 14).

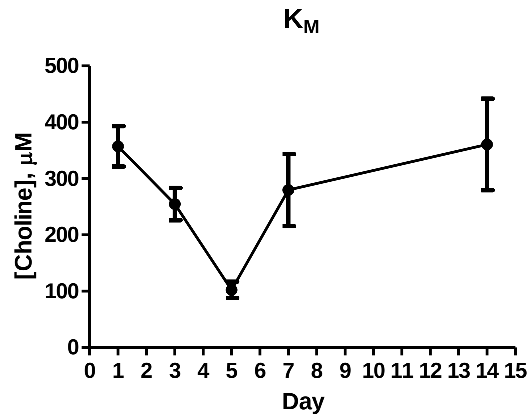

The effect of brain tissue on K_M concentration illustrates a decrease within the first 5 days. By day 3 the current is not significantly decreased (*P* = 0.0824) from 357.20 ± 35.74 µM, n = 4 (Day 1) to 254.80 ± 28.66 µM, n = 4 (Day 3) a reduction of 29 %. On day 5 the current was significantly reduced (*P* = 0.0062) by 78 % to 102.40 ± 14.39 µM, n = 4 (Day 1). This correlates with the reduction in the V_{MAX} between days 1 and 5. By day 7 the K_M concentration increases to 279.60 ± 360.50 µM, n = 4 (Day 7). This is not a significant reduction (P = 0.1017) of 22 % from day 1. By day 14 the K_M concentration had returned to 100 % with a concentration of 260.50 ± 10.00 nA, n = 4 (Day 14) not significantly different to day 1 (*P* = 0.7081).

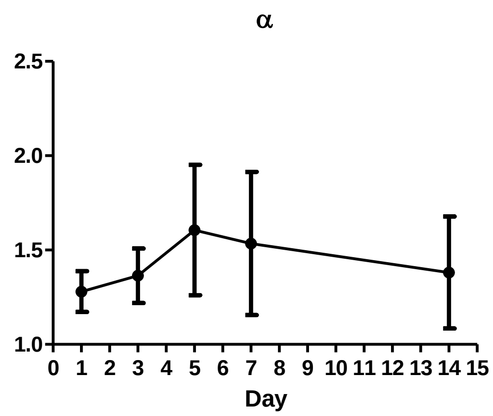

The α value increased steadily between day 1 and 5, increasing 6 % (P = 0.3396) between day 1 and 3 from 1.28, n = 4 (Day 1) to 1.36, n = 4 (Day 3). The α value significantly increased (*P* = 0.0057) by 25 % on day 5 to 1.61, n = 4 (Day 5). The α value then decreased between day 5 and day 14. An increase of 19 % (*P* = 0.0834) was observed by day 7 from the value observed on day 1. A 6 % decrease from that observed on day 5 presenting an α value of 1.54, n = 4. By day 14 the α value was not significantly increased (P = 0.4716) by 7 % from that observed on day 1 increasing the value from 1.28, n = 4 (Day 1) to 1.38, n = 4 (Day 14).

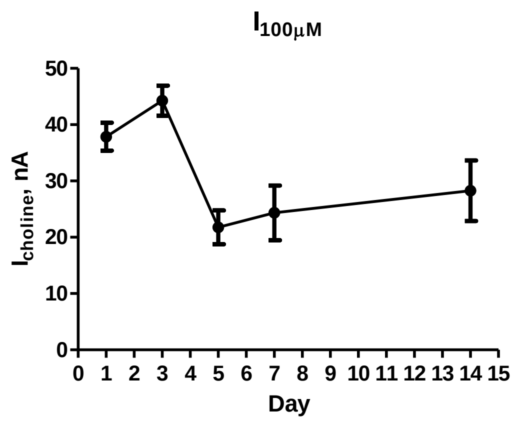

The effect of the exposure to brain tissue on the $I_{100\mu M}$ current is also illustrated above. This illustrates that the current by day 3 increased by 16 % from 37.87 ± 2.47 nA, n = 4 (Day 1) to 44.27 ± 2.66 nA, n = 4 (Day 3) this was not a significant decrease (*P* = 0.1074). By day 5 however, the current was significantly reduced (*P* = 0.0301) by 47 % to 21.78 ± 3.02 nA, n = 4 (Day 5). This possibly an outlier as the current then increased to 24.34 ± 4.84 nA, n = 4 (Day 7) a drop of 36 % from day 1 (*P* = 0.0715). By day 14 the current drop was 26 % that of day 1 a non significant decrease (*P* = 0.1778) with a current value of 28.25 ± 5.37 nA, n = 4 (Day 14).

This section has illustrated the effect of exposure to brain tissue over a 14 day period. This is a more accurate test of the stability of the sensor which resulted in a decrease in current of 100 µM choline of 26 %. Some of this decrease may be attributed to the repeated calibration test seen in Section 6.3.1. The decrease observed during repeated calibrations was 70 %, the storage of the sensor in brain tissue appears to alleviate the reduction in sensitivity observed, similar to the storage observed in BSA (see Section 6.3.3.).

6.3.6. Limit of detection

The limit of detection (LOD) of a biosensor is an additional parameter to consider which may prove crucial when monitoring neurotransmitters of low concentration. The limit of detection is determined as three times the standard deviation of the baseline (O'Neill *et al.*, 2008).

The choline biosensor demonstrates high sensitivity towards choline with a sensitivity of 0.59 ± 0.01 nA, n = 8. The limit of detection of this sensor is determined as 0.11 ± 0.02 µM, n = 8.

6.3.7. Response Times

In addition to the LOD an important parameter for consideration is the response time of the sensor. The response time is determined as the time taken for the analyte response to increase from 10 % to 90 % (O'Neill *et al.*, 2008) (Garguilo & Michael, 1995).

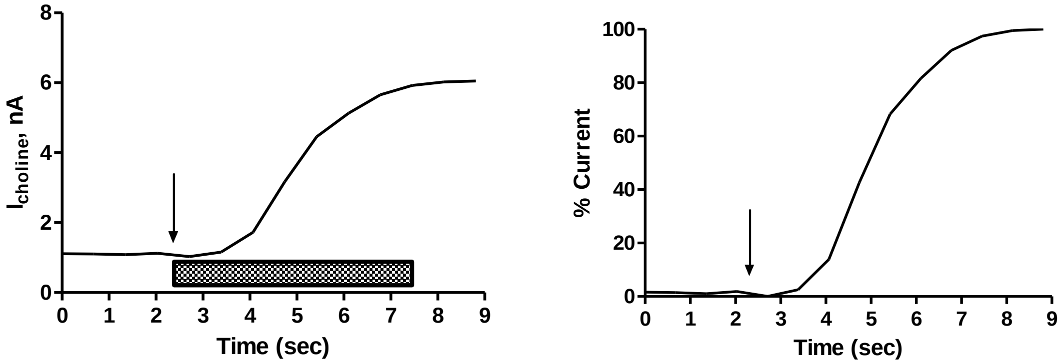

Figure 6.11 : A typical example of a response time for a choline chloride injection of 5 µM choline chloride in PBS (pH 7.4) buffer solution at 21°C for the choline biosensor. CPA carried out at +700 mV *vs.* SCE. Arrow indicates the point of injection.

The graph in Figure 6.11 illustrates a typical example of the response time of an electrode. This sensor has an average response time of 5.03 ± 0.76 sec, n = 8. The highlighted section above demonstrates the period of mixing in the solution. As the response time is less than the mixing time it suggests that the response of the sensor is subsecond recording.

6.3.8. Temperature Dependence

The temperature dependence of a biosensor is an important factor for the full characterisation. All work carried out during the development of this sensor has been at room temperature of 21°C. However, any increase in temperature to a specific limit may enhance the reaction rate of the enzyme (Tripathi, 2009). The increase in reaction rate will occur until the 'optimum temperature' is reached, after which the enzyme will begin to denature (Indira *et al.*, 2010). Therefore, it is important to investigate the effect of an increase in temperature to 37°C, a physiologically relevant temperature, to determine if there is an increase in the rate on enzyme turnover in the *in-vivo* environment.

This section looks at the calibration of the choline biosensor at 21°C and 37°C.

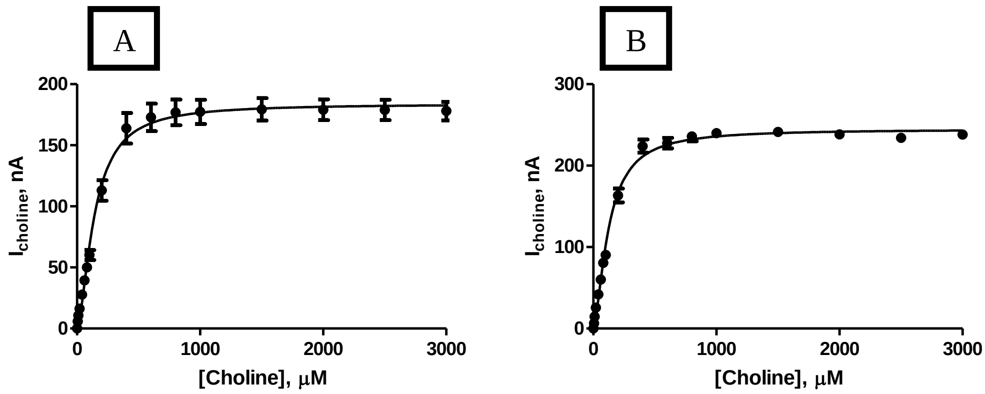

	21°C			37°C		
Conc, µM	**Mean, nA**	**S.E.M, nA**	**n**	**Mean, nA**	**S.E.M, nA**	**n**
0	0.00	0.00	3	0.00	0.00	3
5	5.89	0.39	3	6.40	0.38	3
10	10.69	0.66	3	14.73	0.96	3
20	16.32	0.96	3	25.54	1.40	3
40	27.78	1.81	3	41.85	2.88	3
60	39.36	2.78	3	60.06	4.08	3
80	50.02	3.78	3	80.74	4.46	3
100	60.19	4.09	3	90.47	5.16	3
200	113.06	8.44	3	163.34	8.46	3
400	163.94	12.45	3	223.98	8.06	3
600	172.87	11.23	3	227.63	6.40	3
800	176.87	10.51	3	235.77	5.90	3
1000	177.34	9.84	3	239.94	5.05	3
1500	179.39	9.13	3	241.27	4.37	3
2000	179.14	8.47	3	238.25	3.54	3
2500	178.85	8.34	3	234.15	3.70	3
3000	178.04	7.62	3	238.10	4.00	3

Figure 6.12 : The current-concentration profile and table for choline chloride calibrations in PBS (pH 7.4) buffer solution at (A) 21°C and (B) 37°C using design (MMA)(CelAce)(MMA)-(ChOx)(BSA)(GA)(PEI). CPA carried out at +700 mV *vs*. SCE. Sequential current steps for 5, 10, 20, 40, 60, 80, 100, 200, 400, 600, 800, 1000, 1500, 200, 2500, 3000 µM choline chloride injections.

The results obtained from the investigation into the effect of temperature on the sensitivity of the choline biosensor are presented in Figure 6.12. The calibration data and a table of results for each data point of the calibration are presented above.

This data illustrates that increasing the temperature to a more physiological one (37°C) does increase the rate of the reaction, thus increasing the current observed.

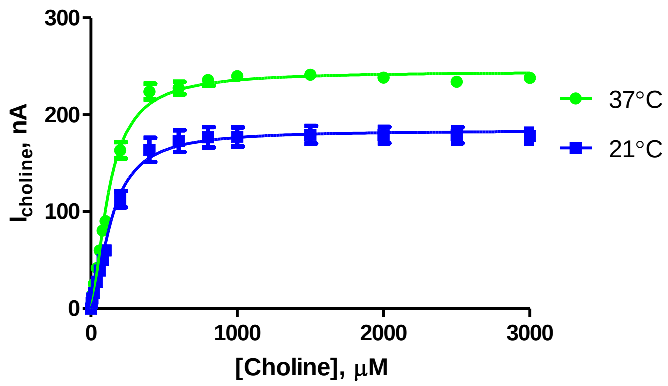

Kinetic Parameters	21°C			37°C		
	Mean	S.E.M	n	Mean	S.E.M	n
V_{MAX}, nA	183.90	3.61	3	244.80	2.94	3
Km, μM	140.70	9.27	3	124.10	5.05	3
α	1.62	0.14	3	1.57	0.09	3
$I_{100\mu M}$, nA	60.19	4.09	3	90.47	5.16	3
Sensitivity, nA/μM	0.58	0.02	3	0.91	0.04	3
R^2	0.9938	0.0002	3	0.9905	0.0018	3
Background, nA	1.42	0.52	3	1.96	0.25	3

Figure 6.13 : The current-concentration profile comparison and comparison table for choline chloride calibrations in PBS (pH 7.4) buffer solution at 21°C and 37°C using design. CPA carried out at +700 mV *vs*. SCE. Sequential current steps for 5, 10, 20, 40, 60, 80, 100, 200, 400, 600, 800, 1000, 1500, 2000, 2500, 3000 μM choline chloride injections.

A comparison graph and data table are presented in Figure 6.13. The data illustrates the effect of increasing temperature to be a more physiologically relevant value. The comparison graph above illustrates that the increase in temperature has increased the rate of the reaction, thus increasing the current value observed. A comparison of the $I_{100\mu M}$ current shows a significant increase (P = 0.0486) in current from 60.19 ± 4.09 nA, n = 3 (21°C) to 90.47 ± 5.16 nA, n = 3 (37°C). The V_{MAX} also significantly increased (P = 0.0280) from 183.90 ± 3.61 nA, n = 3 (21°C) to 244.80 ± 2.94 nA, n = 3 (37°C). The kinetics of the design was improved with the increase in temperature, decreasing the K_M concentration non significantly (P = 0.1606) from 140.70 ± 9.27 μM, n = 3 (21°C) to

124.10 ± 5.05 μM, n = 3 (37°C). The α value was not significantly (P = 0.0506) reduced from 1.62, n = 3 (21°C) to 1.57, n = 3 (37°C).

6.3.9. pH Effect

Sensors designed for use in the *in-vivo* environment are routinely tested for their response to pH changes; usually in the range 6.8 to 8 (Tian *et al.*, 2009) (Bolger *et al.*, 2011a), as pH changes may occur in physiological experiments (Zimmerman & Wightman, 1991). Choline oxidase is susceptible to activity changes as a result of pH and has been found to have an optimum pH of 8, meanwhile it is inactivated at pH ranges 3-6 and 9-11 (Hekmat *et al.*, 2008). Therefore, a range of pH's were tested to determine the pH of the sensor. pH 6.8, 7.2, 7.4, 7.6, 8 and 9 were chosen as the range of pH that was physiologically relevant.

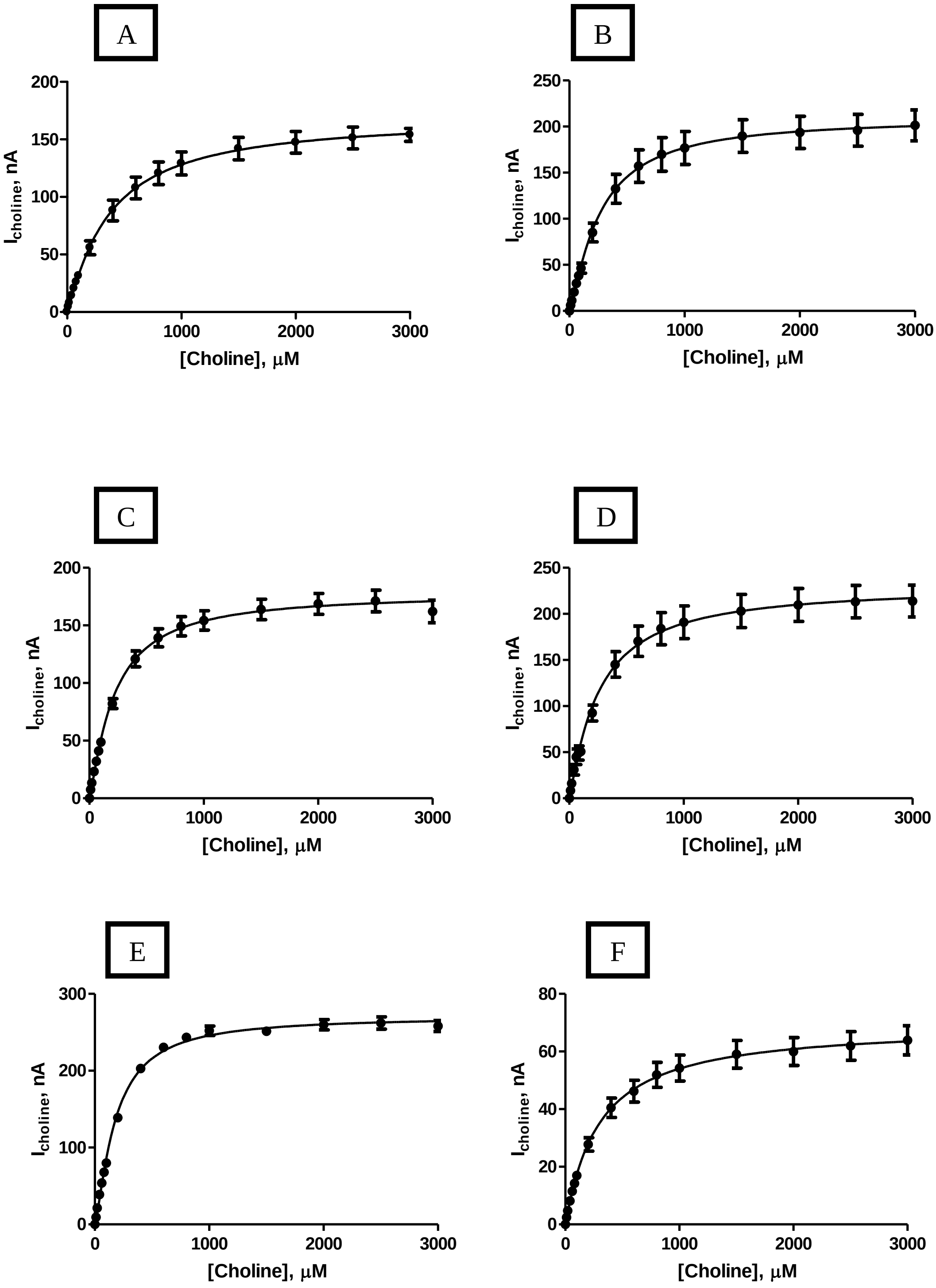

Figure 6.14 : The current-concentration profile and table (below) for choline chloride calibrations in PBS (pH 7.4) buffer solution at pH (A) 6.8, (B) 7.2, (C) 7.4, (D) 7.6, (E) 8 and (F) 9 using design (MMA)(CelAce)(MMA)-(ChOx)(BSA)(GA)(PEI). CPA carried out at +700 mV *vs*. SCE. Sequential current steps for 10, 20, 40, 60, 80, 100, 200, 400, 600, 800, 1000, 1500, 200, 2500, 3000 μM choline chloride injections.

	6.8			7.2			7.4		
Conc, µM	**Mean, nA**	**S.E.M, nA**	**n**	**Mean, nA**	**S.E.M, nA**	**n**	**Mean, nA**	**S.E.M, nA**	**n**
0	0.00	0.00	4	0.00	0.00	12	0.00	0.00	20
10	4.67	0.45	4	6.12	0.78	12	7.54	0.57	20
20	7.95	0.84	4	11.32	1.38	12	13.46	0.80	20
40	14.27	1.44	4	20.51	2.38	12	23.19	1.24	20
60	20.54	2.06	4	29.94	3.54	12	32.07	1.65	20
80	26.11	2.60	4	38.24	4.44	12	41.14	2.18	20
100	31.43	3.18	4	46.41	5.46	12	48.80	2.55	20
200	55.86	6.12	4	85.04	10.23	12	82.10	4.24	20
400	88.30	9.03	4	132.53	15.73	12	120.94	6.93	20
600	107.85	9.38	4	157.12	17.55	12	139.29	7.84	20
800	120.61	9.81	4	169.81	18.17	12	149.25	8.34	20
1000	129.07	9.94	4	176.85	17.90	12	154.32	8.36	20
1500	141.99	9.72	4	189.61	17.71	12	163.87	8.90	20
2000	147.47	9.45	4	193.69	17.50	12	168.74	9.08	20
2500	151.29	9.50	4	195.97	17.24	12	171.24	9.42	20
3000	153.97	5.65	4	201.30	16.78	12	162.09	9.77	16

	7.6			8			9		
Conc, µM	**Mean, nA**	**S.E.M, nA**	**n**	**Mean, nA**	**S.E.M, nA**	**n**	**Mean, nA**	**S.E.M, nA**	**n**
0	0.00	0.00	12	0.00	0.00	4	0.00	0.00	4
10	8.35	1.48	12	9.30	1.72	4	2.45	0.19	4
20	16.21	2.92	12	21.33	0.89	4	4.76	0.35	4
40	30.96	5.67	12	38.78	1.10	4	8.14	0.63	4
60	44.92	8.44	12	53.99	1.44	4	11.49	0.90	4
80	49.13	7.71	12	67.91	1.88	4	14.21	1.11	4
100	50.68	4.57	12	79.98	1.89	4	16.95	1.34	4
200	92.51	8.60	12	138.86	3.28	4	27.77	2.31	4
400	145.15	13.83	12	202.98	4.51	4	40.48	3.36	4
600	170.31	16.41	12	230.27	5.18	4	46.24	3.78	4
800	184.01	17.41	12	243.38	5.67	4	51.91	4.31	4
1000	190.98	17.76	12	252.04	6.13	4	54.26	4.49	4
1500	203.11	18.07	12	251.30	5.55	4	59.04	4.81	4
2000	209.72	17.92	12	259.92	6.70	4	59.99	4.85	4
2500	213.26	17.63	12	262.18	7.99	4	61.94	4.99	4
3000	213.83	17.23	12	258.25	7.16	4	63.90	5.09	4

The results obtained from the investigation into the effect of pH on the sensor are presented in Figure 6.14. The calibration data and a table of results for each data point of the calibration are presented above. The data illustrates a sensitivity change corresponding to the activity response as a result of the optimum pH for choline oxidase.

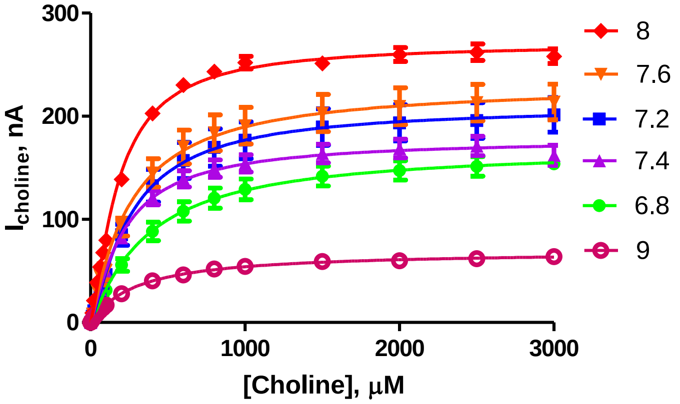

Kinetic Parameters	6.8			7.2			7.4		
	Mean	S.E.M	n	Mean	S.E.M	n	Mean	S.E.M	n
V_{MAX}, nA	169.60	8.163	4	210.00	11.54	12	178.20	5.60	20
Km, μM	365.40	48.30	4	261.50	42.16	12	215.60	20.87	20
α	1.12	0.10	4	1.25	0.17	12	1.20	0.10	20
$I_{100\mu M}$, nA	31.43	3.18	4	46.41	5.46	12	48.80	2.55	20
Sensitivity, nA/μM	0.31	0.01	4	0.46	0.01	12	0.48	0.02	20
R^2	0.996	0.001	4	0.997	0.001	12	0.990	0.002	20
Background, nA	13.22	0.77	4	13.27	2.15	12	3.69	1.08	20

Kinetic Parameters	7.6			8			9		
	Mean	S.E.M	n	Mean	S.E.M	n	Mean	S.E.M	n
V_{MAX}, nA	230.90	13.40	12	270.70	3.38	4	69.26	3.87	4
Km, µM	256.60	45.05	12	178.80	7.20	4	291.60	49.22	4
α	1.12	0.15	12	1.33	0.05	4	1.03	0.11	4
$I_{100\mu M}$, nA	50.68	4.57	12	79.98	1.89	4	16.95	1.34	4
Sensitivity, nA/µM	0.53	0.065	12	0.80	0.03	4	0.32	0.01	4
R^2	0.89	0.07	12	0.990	0.003	4	0.9965	0.0004	4
Background, nA	21.50	5.63	12	5.68	1.05	4	33.33	1.88	4

Figure 6.15 : The current-concentration profile comparison and comparison table for choline chloride calibrations in PBS (pH 7.4) buffer solution at 21°C using design (MMA)(CelAce)(MMA)-(ChOx)(BSA)(GA)(PEI) at pH 6.8, 7.2, 7.4, 7.6, 8 and 9. CPA carried out at +700 mV *vs*. SCE. Sequential current steps for 5, 10, 20, 40, 60, 80, 100, 200, 400, 600, 800, 1000, 1500, 2000, 2500, 3000 µM choline chloride injections.

A comparison graph and data table are presented in Figure 6.15. In addition, a graphical representation of the kinetic parameters V_{MAX}, K_M, α and the $I_{100\ \mu M}$ current are presented illustrating the effect of pH on the sensor.

The data has illustrated a correlation between the pH and sensitivity. As stated previously the optimum pH for the activity of choline oxidase is 8 and activity loss occurs close to pH 6 and 8. A comparison of the kinetic parameters does demonstrate that the sensor is susceptible to extreme pH's.

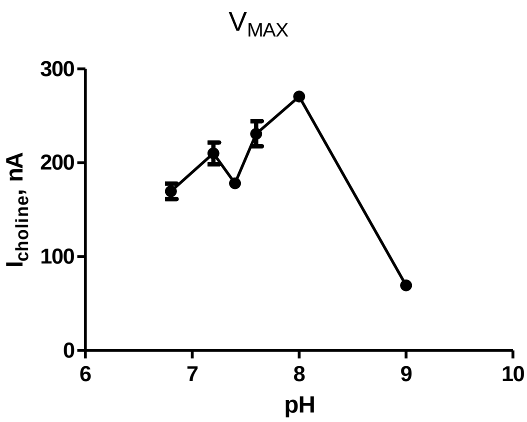

A comparison of the V_{MAX} current demonstrate a gradual increase from 169.60 ± 8.16 nA, n = 4 at pH 6.8 to 210.00 ± 11.54 nA, n = 12 at pH 7.2, this increases to 230.90 ± 13.40 nA, n = 12 at pH 7.8 and the highest V_{MAX} is demonstrated at the optimum pH of 8. The V_{MAX} is greatly reduced to 69.26 ± 3.87 nA, n = 4 at pH 9. pH 7.4 had a slightly reduced V_{MAX} of 178.20 ± 5.60 nA, n = 20 compared to the trend.

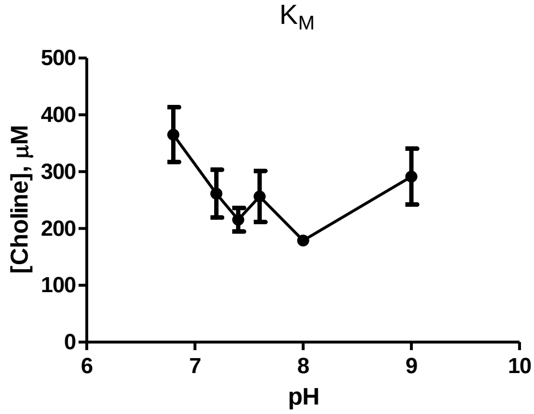

A comparison of the K_M concentrations illustrates a trend whereby the K_M decreased with increasing pH, suggesting an increase in the efficiency of the enzyme. At pH 6.8 the K_M concentration was 365.40 ± 48.30 µM, n = 4 as the pH increased to 7.2 the K_M decreased to 261.50 ± 42.16 µM, n = 12 the K_M decreased further at 7.4 to 215.60 ± 20.87 µM, n = 20. The lowest K_M of 261.50 ± 42.16 µM, n = 12 was observed at pH 8. At pH 9 the K_M was increased to 291.60 ± 20.87 µM.

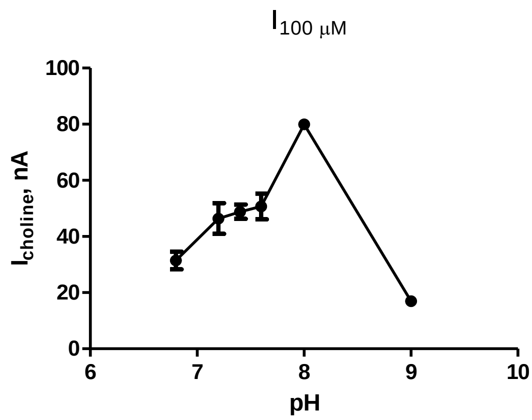

A comparison of the $I_{100\ \mu M}$ current demonstrates an increase which correlates with the increase in the pH as it approaches the optimum pH 8. The lowest current value was observed at pH 6.8 of 31.43 ± 3.18 nA, n = 4 increasing to 46.41 ± 5.46 nA, n = 12 at pH 7.2. There is little difference in the current between 7.2 and 7.4 with a minor increase in current to 48.80 ± 2.55 nA, n = 20. There is a marginal increase in the current from pH 7.4 to 7.6 increasing the current to 50.68 ± 4.57 nA, n = 12. As expected the highest current was observed at pH 8 with 79.98 ± 1.89 nA, n = 4 and is dramatically decreased at pH 9 to 16.95 ± 1.34 nA, n = 4.

This data demonstrates that over a larger pH range the sensor is susceptible to pH interference as choline oxidase is optimal at pH 8. However, the fluctuations of pH *in-vivo* are thought to be minimal, therefore, based on the current fluctuations observed between pH 7.2 and 7.6 the sensor will not be susceptible to pH interference.

6.3.10. Interference

Detailed characterisation of selectivity is another parameter which must be investigated *in-vitro*. The specificity of the biosensor can be undermined by interference from electroactive species present in the brain. For example, ascorbic acid (AA) has been shown to be detected at +700mV on the Pt surface just as H_2O_2 is, which can be detrimental to the sensitivity of the biosensor (Lowry & O'Neill, 1994). As the AA concentration has been reported to be as high as 400 µM (Miele & Fillenz, 1996), the electrodeposition of poly(*o*-phenylenediamine) (PPD) for the rejection of interference species has been utilised regularly in sensor design (Lowry & O'Neill, 1994) (Bolger *et al.*, 2011a) (O'Brien *et al.*, 2007). PPD demonstrates permeability to H_2O_2 but efficient elimination of AA due to a 'self blocking' phenomenon whereby at high concentrations of AA, the polymer becomes clogged, decreasing the sensitivity towards AA (Lowry & O'Neill, 1994) (Craig & O'Neill, 2003). In addition, PPD demonstrates more effective AA rejection when electropolymerised on a cylinder surface due to an 'edge effect' on the permselectivity of the polymer (Rothwell *et al.*, 2009). Initial experiments were undertaken to determine the detection of AA on a bare Pt cylinder electrode and a cylinder electrode (see Section 3.4.1) which incorporates a layer of PPD.

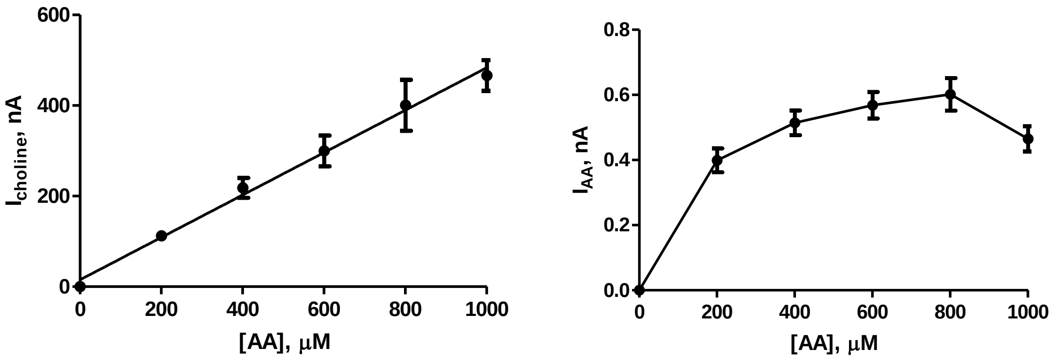

AA, μM	Pt cylinder			Pt cylinder PPD		
	Mean	S.E.M	n	Mean	S.E.M	n
0	0.00	0.00	4	0.00	0.00	8
200	112.05	11.26	4	0.40	0.04	8
400	218.39	21.90	4	0.52	0.04	8
600	299.87	34.01	4	0.57	0.04	8
800	400.51	56.45	4	0.60	0.05	8
1000	466.34	34.03	4	0.47	0.04	8

Figure 6.16 : The current-concentration profile for AA calibrations in N_2 saturated PBS (pH 7.4) buffer solution using design (A) Pt cylinder and (B) Pt cylinder PPD. CPA carried out at +700 mV *vs*. SCE. Sequential current steps 200, 400, 600, 800 and 1000 μM injections.

The results obtained from the investigation into AA rejection using PPD on cylinder electrodes are presented in Figure 6.16. The comparison of the AA response on a bare Pt cylinder electrode and a cylinder electrode with PPD is presented. The electropolymerisation of PPD onto the cylinder surface has significantly reduced the AA sensitivity. The $I_{400\ \mu M}$ current was significantly reduced ($P < 0.0001$) from 218.39 ± 21.90 nA, n = 4 to 0.52 ± 0.04 nA, n = 8. As a result of the 'self blocking' phenomenon this was reduced further as the $I_{1000\ \mu M}$ current was significantly reduced ($P < 0.0001$) from 466.34 ± 34.03 nA, n = 4 to 0.47 ± 0.04 nA, n = 8.

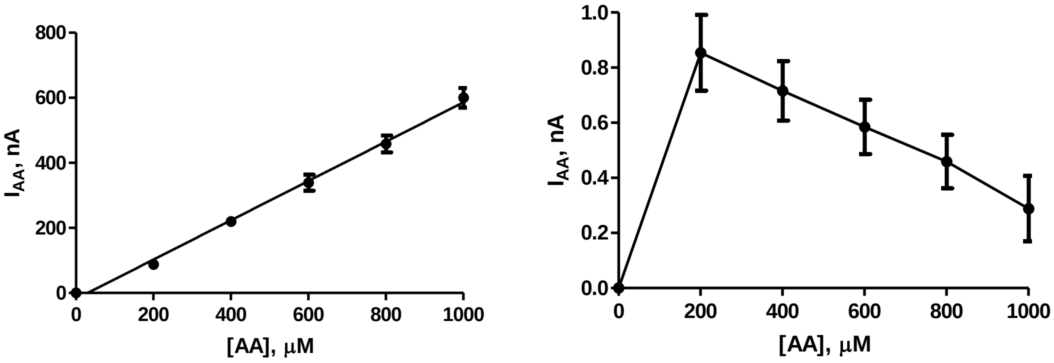

AA, µM	choline biosensor			PPD choline biosensor		
	Mean	S.E.M	n	Mean	S.E.M	n
0	0.00	0.00	4	0.00	0.00	6
200	87.90	6.29	4	0.85	0.14	6
400	219.60	14.89	4	0.72	0.11	6
600	339.00	24.35	4	0.59	0.10	6
800	458.54	25.97	4	0.46	0.10	6
1000	600.06	30.41	4	0.29	0.12	6

Figure 6.17 : The current-concentration profile for AA calibrations in N_2 saturated PBS (pH 7.4) buffer solution using design (A) Choline biosensor and (B) PPD choline biosensor. CPA carried out at +700 mV *vs.* SCE. Sequential current steps 200, 400, 600, 800 and 1000 µM injections.

The results obtained from the investigation into AA rejection using PPD on the choline biosensor are presented in Figure 6.17. The comparison of the AA response on a bare Pt cylinder choline biosensor and a cylinder with PPD choline biosensor is presented. The electropolymerisation of PPD onto the sensor surface has significantly reduced the AA sensitivity. The $I_{400\ \mu M}$ current was significantly reduced (P <0.0001) from 219.60 ± 14.89 nA, n = 4 to 0.72 ± 0.11 nA, n = 6. As a result of the ‘self blocking’ phenomenon this was further reduced as the $I_{1000\ \mu M}$ current was significantly reduced (P < 0.0001) from 600.06 ± 30.41 nA, n = 4 to 0.29 ± 0.12 nA, n = 8. This data illustrates that the additional layers of enzyme immobilisation which are incorporated for the design of the choline biosensor do not have a detrimental effect on the AA rejection of the PPD layer.

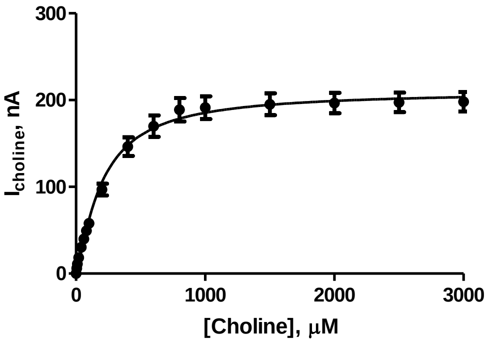

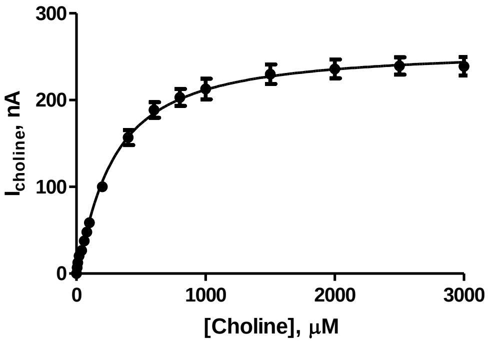

	Choline biosensor			PPD Choline biosensor		
Conc, µM	**Mean, nA**	**S.E.M, nA**	**n**	**Mean, nA**	**S.E.M, nA**	**n**
0	0.00	0.00	4	0.00	0.00	4
5	6.09	0.37	4	6.98	0.32	4
10	11.14	0.67	4	12.75	0.70	4
20	18.40	1.09	4	20.42	0.98	4
40	30.50	1.91	4	26.60	1.38	4
60	39.97	2.54	4	37.60	2.09	4
80	49.44	3.29	4	47.87	2.62	4
100	57.95	3.84	4	58.61	3.37	4
200	96.89	6.80	4	100.21	5.41	4
400	146.37	10.83	4	156.76	8.66	4
600	169.90	12.38	4	188.62	9.05	4
800	188.85	13.43	4	203.13	9.64	4
1000	191.26	13.17	4	212.76	11.95	4
1500	195.23	12.61	4	229.88	11.20	4
2000	196.68	11.79	4	235.95	10.84	4
2500	197.30	11.21	4	239.40	9.91	4
3000	198.08	11.24	4	238.97	10.70	4

Figure 6.18 : The current-concentration profile for choline calibrations in PBS (pH 7.4) buffer solution using design (A) Choline biosensor and (B) PPD choline biosensor. CPA carried out at +700 mV *vs*. SCE. Sequential current steps 200, 400, 600, 800 and 1000 µM injections.

The results obtained from the investigation into the effect of the PPD layer on the choline biosensor sensitivity are presented in Figure 6.18. It is evident that PPD does not have an effect on the sensitivity of the biosensor to choline.

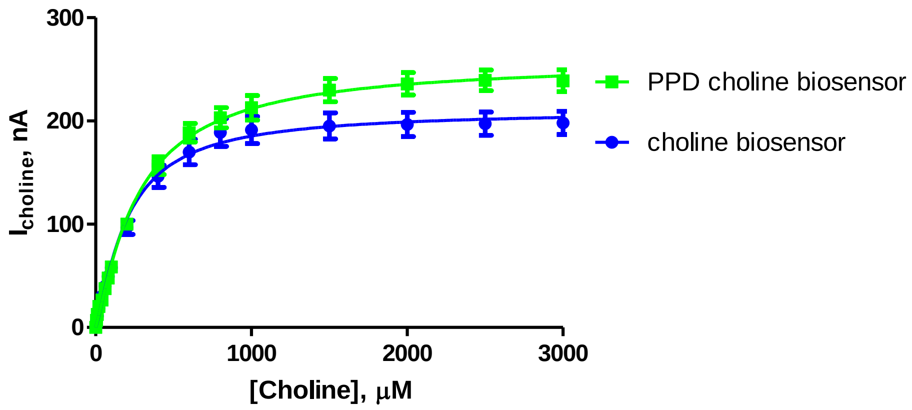

Kinetic Parameters	Choline biosensor			PPD Choline biosensor		
	Mean	S.E.M	n	Mean	S.E.M	n
V_{MAX}, nA	210.30	6.61	4	258.50	7.15	4
Km, μM	201.00	19.95	4	274.30	22.30	4
α	1.25	0.11	4	1.17	0.07	4
$I_{100\mu M}$, nA	57.95	3.84	4	58.61	3.37	4
Sensitivity, nA/μM	0.56	0.03	4	0.54	0.03	4
R^2	0.983	0.001	4	0.982	0.001	4
Background, nA	0.49	0.03	4	0.32	0.02	4

Figure 6.19 : The current-concentration profile comparison and comparison table for choline chloride calibrations in PBS (pH 7.4) buffer solution at 21°C using design (A) choline biosensor and (B) PPD choline biosensor. CPA carried out at +700 mV *vs.* SCE. Sequential current steps for 5, 10, 20, 40, 60, 80, 100, 200, 400, 600, 800, 1000, 1500, 2000, 2500, 3000 μM choline chloride injections.

A comparison graph and data table are presented in Figure 6.19 to demonstrate the effect of the PPD interference rejection layer on the choline sensitivity. A comparison of the $I_{100\ \mu M}$ current demonstrates a non-significant difference (*P* = 0.9027) in the current from 57.95 ± 3.84 nA, n=4 (choline biosensor) to 58.61 ± 3.37 nA, n=4 (PPD choline biosensor). The V_{MAX} current was significantly increased (*P* = 0.0236) from 210.30 ±

6.61 nA, n=4 (choline biosensor) to 258.50 ± 7.15 nA, n=4 (PPD choline biosensor). In addition, the K_M was significantly increased (P = 0.0089) from 201.00 ± 19.95 µM, n=4 (choline biosensor) 274.30 ± 22.30 µM, n=4 (PPD choline biosensor). The α value was not significantly altered from 1.25, n=4 (choline biosensor) to 1.17, n=4 (PPD choline biosensor).

6.3.10.1. Extensive interference calibration

In addition to the rejection of ascorbic acid, the selectivity of the sensor to a wider range of potential interferents present in the brain ECF must be determined. The compounds tested were neurotransmitters dopamine (DA) and 5-hydroxytryptomine (5-HT), their metabolites 3,4-dihydroxyphenylacetic acid (DOPAC), homovanillic acid (HVA) and 5-hydroxyindoleacetic acid (5-HIAA) and other electroactive species such as AA, L-tyrosine, L-cysteine, L-tryptophan, L-glutathione, dehydroascorbic acid (DHAA) and the purine metabolite uric acid (UA) (Bolger *et al.*, 2011b).

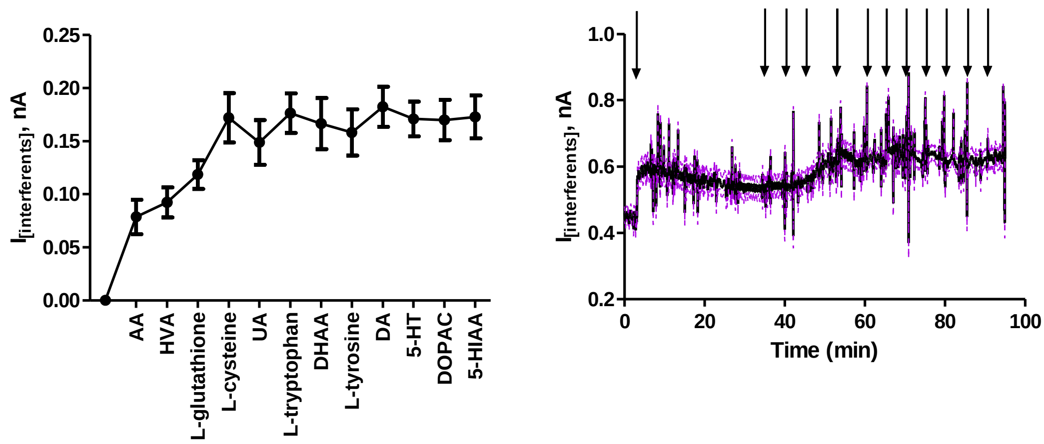

	Response from baseline			Response from interferent		
Interferent	Mean, nA	S.E.M, nA	n	Mean, nA	S.E.M, nA	n
Baseline	0.000	0.000	4	0.000	0.000	4
AA (500 µM)	0.079	0.016	4	0.079	0.016	4
HVA (10 µM)	0.092	0.014	4	0.013	0.002	4
L-glutathione (50 µM)	0.119	0.014	4	0.026	0.001	4
L-cysteine (50 µM)	0.172	0.023	4	0.053	0.010	4
UA (50 µM)	0.149	0.021	4	-0.023	0.010	4
L-tryptophan (100 µM)	0.176	0.019	4	0.028	0.010	4
DHAA (100 µM)	0.167	0.024	4	-0.009	0.010	4
L-tyrosine (100 µM)	0.158	0.022	4	-0.008	0.003	4
DA (0.05 µM)	0.182	0.019	4	0.024	0.004	4
5-HT (0.01 µM)	0.171	0.016	4	-0.011	0.003	4
DOPAC (20 µM)	0.170	0.019	4	-0.001	0.005	4
5-HIAA (50 µM)	0.173	0.020	4	0.003	0.001	4

Figure 6.20 : The current-concentration profile and results table for an interferent calibration in N_2 saturated PBS (pH 7.4) buffer solution using PPD Choline biosensor. CPA carried out at +700 mV *vs*. SCE.

The results obtained from the investigation into the rejection of a range of interferents present in the brain ECF are presented in Figure 6.20. The results table illustrates the cumulative current obtained from the addition of interferent aliquots and the individual current change from each interferent aliquot addition. The concentration of aliquots were brain extracellular fluid concentration if known, however, in the case of unknown ECF concentrations 100 µM was used (Bolger *et al.*, 2011b) .

An I_{MAX} was observed of 0.182 ± 0.019 nA, n=4. The single largest current increase was obtained from the addition of AA with a current response of 0.078 ± 0.016 nA, n=4. Negative values were observed if there was no detection of the interferent, therefore the reduction of the current can be attributed to baseline drift. The overall current response attributed to the twelve interferent species was 0.173 ± 0.020 nA, n=4. This data demonstrates that the choline biosensor is selective towards choline *in-vivo* with the incorporation of the PPD layer.

6.4. Discussion

The aim of this chapter was to fully characterise the choline biosensor *in-vitro* to determine the effect of biological factors on the sensor. Initially, stability of the sensor was determined over a 14 day period, which demonstrated that the sensor could be stored for 14 days with only a 10 % reduction in sensitivity. This time line was then used to determine the effect of biological components (lipids and proteins) on the senor to mimic the effect of *in-vivo* implantation. For accuracy, the sensor was implanted in brain tissue for 14 days and was subject to a 26 % reduction in sensitivity. The effect of physiological temperature was investigated demonstrating an increase in current at 37°C. The effect of pH was also evaluated and demonstrated that minor fluctuation would be possible between pH 7.2 and 7.6. The interference by endogenous electroactive species was also determined and demonstrated that the incorporation of PPD onto the sensor surface is efficient at blocking these electroactive species. Also the limit of detection was determined as 0.11 ± 0.02 μM with sub second response time.

A. Kane D & D. O'Neill R. (1998). Major differences in the behaviour of carbon paste and carbon fibre electrodes in a protein-lipid matrix: implications for voltammetry *In-Vivo*. *Analyst* **123,** 2899-2903.

Bolger FB, Bennett R & Lowry JP. (2011a). An *In-Vitro* characterisation comparing carbon paste and Pt microelectrodes for real-time detection of brain tissue oxygen. *Analyst* **136,** 4028-4035.

Bolger FB, McHugh SB, Bennett R, Li J, Ishiwari K, Francois J, Conway MW, Gilmour G, Bannerman DM, Fillenz M, Tricklebank M & Lowry JP. (2011b). Characterisation of carbon paste electrodes for real-time amperometric monitoring of brain tissue oxygen. *Journal of Neuroscience Methods* **195,** 135-142.

Brown FO, Finnerty NJ & Lowry JP. (2009). Nitric oxide monitoring in brain extracellular fluid: characterisation of Nafion-modified Pt electrodes *In-Vitro* and *In-Vivo*. *Analyst* **134,** 2012-2020.

Craig JD & O'Neill RD. (2003). Electrosynthesis and permselective characterisation of phenol-based polymers for biosensor applications. *Analytica Chimica Acta* **495,** 33-43.

Garguilo MG & Michael AC. (1994). Quantitation of Choline in the Extracellular Fluid of Brain Tissue with Amperometric Microsensors. *Analytical Chemistry* **66,** 2621-2629.

Garguilo MG & Michael AC. (1995). Optimization of amperometric microsensors for monitoring choline in the extracellular fluid of brain tissue. *Analytica Chimica Acta* **307,** 291-299.

Hekmat A, Saboury AA, Moosavi-Movahedi AA, Ghourchian H & Ahmad F. (2008). Effects of pH on the activity and structure of choline oxidase from Alcaligenes species. *Acta Biochimica Polonica* **55,** 549-557.

Indira L, Nagaraju K & K ZA. (2010). *College Biochemistry-II*. Global Media, India.

Lowry JP & O'Neill RD. (1994). Partial Characterization *In-Vitro* of Glucose Oxidase-Modified Poly(phenylenediamine)-coated electrodes for neurochemical analysis *In-Vivo*. *Electroanalysis* **6,** 369-379.

Lyne PD & O'Neill RD. (1990). Stearate-modified carbon paste electrodes for detecting dopamine *In-Vivo*: decrease in selectivity caused by lipids and other surface-active agents. *Analytical Chemistry* **62,** 2347-2351.

Miele M & Fillenz M. (1996). *In-Vivo* determination of extracellular brain ascorbate. *Journal of Neuroscience Methods* **70,** 15-19.

O'Neill RD. (1993). Sensor-tissue interactions in neurochemical analysis with carbon paste electrodes *In-Vivo*. *Analyst* **118,** 433-438.

O'Brien KB, Killoran SJ, O'Neill RD & Lowry JP. (2007). Development and characterization *In-Vitro* of a catalase-based biosensor for hydrogen peroxide monitoring. *Biosensors and Bioelectronics* **22,** 2994-3000.

O'Neill RD, Rocchitta G, McMahon CP, Serra PA & Lowry JP. (2008). Designing sensitive and selective polymer/enzyme composite biosensors for brain monitoring in vivo. *TrAC Trends in Analytical Chemistry* **27,** 78-88.

Ormonde DE & O'Neill RD. (1990). The oxidation of ascorbic acid at carbon paste electrodes: Modified response following contact with surfactant, lipid and brain tissue. *Journal of Electroanalytical Chemistry and Interfacial Electrochemistry* **279,** 109-121.

Rothwell SA, Kinsella ME, Zain ZM, Serra PA, Rocchitta G, Lowry JP & O'Neill RD. (2009). Contributions by a Novel Edge Effect to the Permselectivity of an Electrosynthesized Polymer for Microbiosensor Applications. *Analytical Chemistry* **81,** 3911-3918.

Tian F, Gourine AV, Huckstepp RTR & Dale N. (2009). A microelectrode biosensor for real time monitoring of l-glutamate release. *Analytica Chimica Acta* **645,** 86-91.

Tripathi G. (2009). *Enzyme Biotechnology*. ABD Publishers, Jaipur, India

Zimmerman JB & Wightman RM. (1991). Simultaneous electrochemical measurements of oxygen and dopamine *In-Vivo*. *Analytical Chemistry* **63,** 24-28.

7. *In-Vivo* Characterisation

7.1. Introduction

The *in-vitro* characterisation of the sensor has determined that the sensor is suitably sensitive toward choline. The potential O_2 sensitivities of the sensor have been determined and minimised to eliminate interference within the physiological range of both choline and O_2. Exposure to brain tissue has demonstrated that the sensor maintains sensitivity in this medium. Finally, the sensor has proven to be selective over endogenous electroactive species. Despite the *in-vitro* characterisation suggesting that the sensor is capable of detecting choline changes in the brain there are many factors *in-vivo* which cannot be accounted for in the *in-vitro* environment. There remain differences between *ex-vivo* brain tissue and the effect of this complex environment on the sensor when implanted in a freely moving rat. The complex chemical environment which includes proteins and lipids, have been simulated using high concentrations of each *in-vitro* to determine their effect. However, it is the effect of a tissue matrix which restricts mass transport to the sensor surface that cannot be accurately simulated *in-vitro* (O'Neill, 1993) (Nicholson & Syková, 1998). In addition, the immune response and the local host response mounted by the body to the foreign object also affect the sensors performance. In the initial stages of implantation, an acute inflammatory response causes the migration of immune cells to the site of the foreign body which surround the sensor. After this acute response, chronic inflammation may set in leading to the formation of an encapsulation layer known as a 'glial scar'. The formation of a 'glial scar' surrounds and isolates the sensor hindering diffusion (Polikov *et al.*, 2005; Wilson & Gifford, 2005) (Wisniewski *et al.*, 2000).

As the brain has little ability to synthesise choline *de novo*, the brain is dependent on the uptake of choline from the blood mainly through dietary sources (Tuček, 1993) (Babb *et al.*, 2004). Dietary restriction of choline has demonstrated a reduction in cerebrospinal fluid choline concentration by 33.1% reducing hippocampal acetylcholine release. This however, is not the case for the striatum (Nakamura *et al.*, 2001). This is due to the low affinity choline uptake (LACU) process which guarantees choline availability for phospholipid synthesis (Hartmann *et al.*, 2008). After cellular uptake the choline is phosphorylated and incorporated into phospholipids (Zeisel *et al.*, 1991). This bound choline can be released by phospholipases in times of low choline availability (Löffelholz, 1998). In addition to low affinity choline uptake, there is the high affinity choline uptake (HACU), which is regarded as the regulatory step in the synthesis of acetylcholine (Kuhar & Murrin, 1978). If there is excess choline not taken up into cells it is quickly removed by circulation and glial cells (Cuello, 1993). Once acetylcholine is released it is quickly hydrolysed back to choline by acetylcholine esterase (Lawler, 1961). This choline is the recycled via the HACU for further synthesis of acetylcholine. Acetylcholine exerts it affects through both the nicotinic (nAchR) and muscarinic acetylcholine receptors (mAchR) (Wevers, 2011). The striatum contains the highest concentration of muscarinic acetylcholine receptors of the CNS (Weiner *et al.*, 1990). The presynatic mAchR acts as a negative feed-back mechanism for the regulation of the HACU in the control of choline uptake and acetylcholine synthesis (Antonelli *et al.*, 1981). The deregulation of acetylcholine synthesis has been demonstrated in many movement disorders such as Parkinson's disease. This is as a result of the loss of dopaminergic nerve terminals which exert an inhibitory effect on the release of acetylcholine within the striatum leading to hyperactivity in the cholinergic system (Calabresi *et al.*, 2000).

Sensors have been designed for the detection of choline and implanted into the striatum. Garguilo *et al*. used carbon fibre microcylinder electrodes with a cross-linked redox-active gel containing horseradish peroxidase and choline oxidase. This sensor was implanted into the striatum of an anaesthetised rat alongside a micropipette. The sensor was characterised with microinjections of choline (100 mM), acetylcholine (10 mM) and acetylcholine alongside the acetylcholine esterase inhibitor neostigmine. This work demonstrated that the sensor detected changes from injected choline and the choline liberated from acetylcholine endogenously (Garguilo & Michael, 1996). In another study to monitor pharmacological changes, tetrodotoxin and neostigmine were injected, however, neither drug had any effect on choline sensitivity (Cui *et al.*, 2001). Burmeister *et al.* have also implanted their ceramic based multisite microelectrode array in the striatum of an anaesthetised rat alongside a micropipette. The sensor was characterised with ejections of choline, KCl and a choline-hemicholinium-3 (HC-3) solution. The sensor was sensitive to ejections of choline which was attenuated by the addition of HC-3. The ejections of KCl were however subject to H_2O_2 cross-talk at the recording sites (Burmeister *et al.*, 2003).

Previous sensors have been developed and their ability to detect choline in the brain has been verified. This section details the *in-vivo* characterisation performed using the choline biosensor.

7.2. Experimental

The instrumentation and software used for all experiments in this section are described in Section 3.2 . All chemicals and solutions are described in detail in Section 3.3.2.2. Solutions for perfusion during microdialysis experiments were prepared in aCSF and intraperitoneal administrations were prepared in normal saline, or a saline DMSO solution if required. All *in-vivo* experiments were carried out as described in Section 3.5.2.

The electrodes used for these experiments were PPD-(MMA)(CelAce2%)(MMA)-(ChOx)(BSA1%)(GA0.5%)(PEI2%) electrodes as characterised in Chapter 6. O_2 electrodes were bare platinum disk electrodes prepared as in Section 3.4.2.3. An applied potential of +700 mV *vs* SCE was applied to all choline electrodes and -650 mV *vs.* SCE was used for the O_2 electrodes. All experiments were carried out in freely moving animals. All data is reported as mean ± S.E.M. The significance of difference was estimated using two-tailed *t*-tests. Paired tests were used for comparing signals recorded at the same electrode, unpaired tests were used for comparing data from different electrodes. n = the number of electrodes. An denotes animal number and Ad denotes administrations.

7.3. Results and discussion

This results section comprises data from the experiments undertaken to characterise the choline biosensor *in-vivo.* All data shown is from the implantation of the choline biosensor either unilaterally or bilaterally in the left or right striatum following the procedure detailed in Section 3.5.2.2. The choline biosensors for the microdialysis experiments were implanted in the right striatum adjacent to the microdialysis probe. All O_2 electrodes were implanted in the left striatum.

7.3.1. Microdialysis

In order to determine the choline biosensors ability to detect choline in the *in-vivo* environment, a sensor and adjacent microdialysis (MD) probe were implanted in the striatum of freely-moving rats. It has been previously demonstrated with the *in-vivo* characterisation of a glucose biosensor, that the perfusion of glucose through a MD probe to increase the extracellular fluid (ECF) concentration in the local environment of the sensor, provides evidence of the ability of the glucose biosensor to respond to changes in the glucose levels in the ECF (Lowry *et al.*, 1998a). This process is termed retrodialysis (Huynh *et al.*, 2007). This method of *in-vivo* characterisation was followed with the choline biosensor.

7.3.1.1. Local aCSF Administration

Initial experiments were undertaken in order to examine the effect the perfusion of artificial cerebrospinal fluid (aCSF) on the choline biosensor response. This is a control experiment, which efficiently demonstrates the removal of choline from the ECF surrounding the sensor into the dialysate, this is as a result of the perfusate equilibration with the ECF which drives diffusion through the probe. The arrows indicate the start and endpoint of the perfusion.

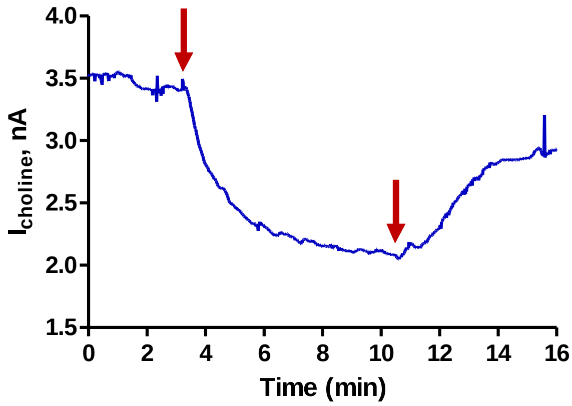

Figure 7.1 : A typical example of the perfusion of aCSF through a microdialysis probe on the current recorded at the adjacent choline biosensor. The combined probe and sensor were implanted in the right striatum of a freely-moving rat. The arrows indicate the start and end point of the perfusion.

The data in Figure 7.1 illustrates the decrease in ECF choline surrounding the sensor. The combined choline biosensor and MD probe was implanted in the right striatum. A perfusion of aCSF through the MD probe at a flow rate of 2 µL/min was monitored at the adjacent biosensor. A mean baseline of 3.45 ± 0.46 nA, n = 5 (5 an, 15 ad) was recorded prior to the perfusion. Upon perfusion of the aCSF, a decrease in current was observed of 0.93 ± 0.23 nA, n = 5 (5 an, 15 ad) until a plateau was reached at a mean current value of 2.53 ± 0.27 nA, n = 5 (5 an, 15 ad). Cessation of the perfusion demonstrated a gradual return to a mean baseline of 3.33 ± 0.40 nA, n = 5 (5 an, 15 ad). The decrease in current represents a significant decrease (*P* = 0.0013) of 23.03 ± 3.21 % from the pre-perfusion baseline. The post-perfusion baseline was not significantly different (*P* = 0.5822) from the pre perfusion baseline.

7.3.2. Local Choline Adminstration from aCSF Baseline

The previous section determined that a decrease in choline current is observed at the choline biosensor upon perfusion of aCSF, which causes the removal of endogenous species in the ECF; including choline, by way of diffusion into the perfusion medium.

In order to determine if the sensor can detect an increase in choline concentration in the local environment of the sensor, preliminary studies were undertaken where choline chloride (ChCl) of different concentrations was perfused through the MD probe. The perfusions of ChCl were started immediately after a perfusion of aCSF which can remove all local substrates from around the biosensor. During these experiments the MD tubing was connected using a uniswitch connector (see Section 3.5.2.5). This accommodated the alternation of solutions through the MD probe which did not require stopping the perfusion. There was 5 minutes dead volume when the solutions were switched. These experiments required the perfusion of aCSF into the MD probe in order to obtain an aCSF baseline whereby the choline concentration in the ECF surrounding the sensor was zero. Using the uniswitch connector, ChCl was perfused through the MD tubing until a plateau was observed. This was then switched back to the aCSF perfusion in order to return the local concentration of choline to zero. This method of ChCl perfusion into the local environment of the sensor guarantees the detection of the ChCl at the sensor as other potential interferents have been removed by the aCSF. This ensures that we can directly determine if the sensor is detecting the ChCl solution from the MD probe.

7.3.2.1. 250 μM ChCl

The initial concentration chosen for the perfusion into the MD probe was 250 μM ChCl. This concentration is substantially higher than the estimated *in-vivo* concentration of 6 μM (Garguilo & Michael, 1996). A high choline concentration is used because the microdialysis method of substrate delivery to the sensor has been shown previously to be subject to limitations by recovery. Recovery is defined as the percentage of the concentration of analyte in the dialysate with respect to the concentration in the interstitial fluid. Recovery can be ideally close to 100 %, however, the conditions during use of microdialysis in the brain as performed using long dialysis membranes and a low perfusion flow mean that recovery is estimated at approximately 70 % (Ungerstedt & Rostami, 2004). In addition to low recovery rates, microdialysis can be invasive, resulting in traumatic injury to the surrounding tissue. This can lead to alterations in the tissue adjacent to the probe compared to that undisturbed by the probe implantation (Khan & Michael, 2003). As both injury and recovery may not allow diffusion of the full concentration of substrate to the sensor, a high concentration of ChCl was chosen for the preliminary investigation to determine if the choline biosensor can detect increases in choline concentration in the local environment of the sensor.

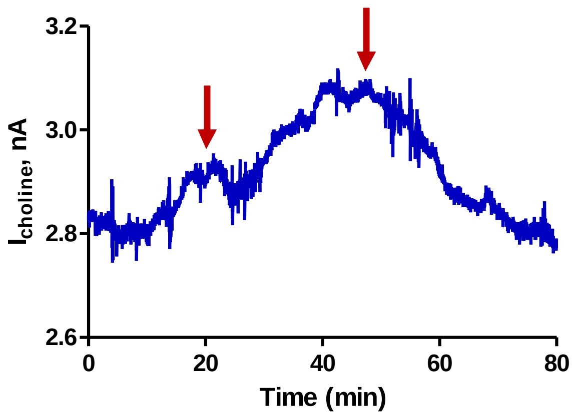

Figure 7.2 : A typical example of the perfusion of 250 µM choline chloride from an aCSF baseline followed by a perfusion of aCSF through a microdialysis probe on the current recorded at the adjacent choline biosensor. The combined probe and sensor were implanted in the right striatum of a freely-moving rat. The arrows indicate the start and end point of the choline perfusion.

The data in Figure 7.2 illustrates the increase in choline current detecting the increase in choline concentration surrounding the sensor diffused from the perfusate. The combined choline biosensor and MD probe was implanted in the right striatum. A perfusion of aCSF and ChCl through the MD probe at a flow rate of 2 µL/min was monitored at the adjacent biosensor. The initial perfusion of aCSF gave a baseline current of 2.81 nA, n = 1 (1 an, 1 ad), which increased by 0.25 nA, n = 1 (1 an, 1 ad) to 3.07 nA, n = 1 (1 an, 1 ad) upon perfusion of ChCl. A perfusion of aCSF with which to return an aCSF baseline similar to that observed prior to the perfusion of ChCl yielded a current of 2.77 nA, n = 1 (1 an, 1 ad). The current change demonstrated a 9.17 % increase from the aCSF baseline. The time taken for the ChCl to reach the MD probe is approximately five minutes from the point of switching indicated by the arrow. This data has demonstrated that the choline sensor has the capability of detecting choline perfused through the MD probe in the absence of endogenous substrates including choline.

7.3.2.2. 500 µM ChCl

The previous section has demonstrated the ability of the sensor to detect 250 µM choline perfused through a MD probe from an aCSF baseline. This yielded approximately a 9 % increase in current. The choline concentration was increased to 500 µM in order to determine the effect on the current response of the sensor.

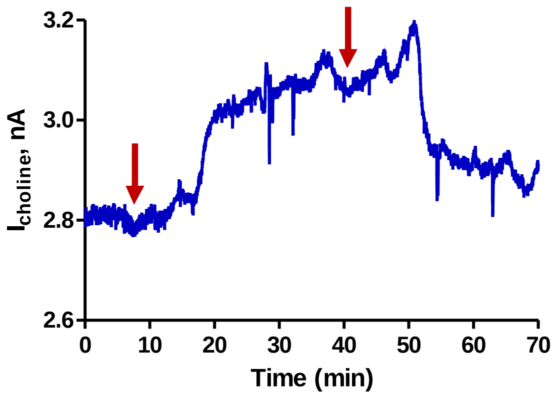

Figure 7.3 : A typical example of the perfusion of 500 µM choline chloride from an aCSF baseline followed by a perfusion of aCSF through a microdialysis probe on the current recorded at the adjacent choline biosensor. The combined probe and sensor were implanted in the right striatum of a freely-moving rat. The arrows indicate the start and end point of the perfusion.

The data in Figure 7.3 illustrates the increase in choline current detecting the increase in choline concentration surrounding the sensor diffused from the dialysate. The combined choline biosensor and MD probe was implanted in the right striatum. A perfusion of aCSF and ChCl through the MD probe at a flow rate of 2 µL/min was monitored at the adjacent biosensor. The perfusion of aCSF yielded a baseline of 2.80 nA, n = 1 (1 an, 1 ad), this was increased by 0.28 nA, n = 1 (1 an, 1 ad) to 3.08 nA upon perfusion of 500 µM ChCl. Once the plateau was achieved aCSF was perfused through the probe to return a post perfusion aCSF baseline of 2.92 nA, n = 1 (1 an, 1 ad). The arrows represent the switch from aCSF to ChCl and the clearance by aCSF, the aCSF must be cleared from the tubing before the ChCl can reach the MD probe. This current change represents a 10.02 % increase in current, a marginal increase to that observed with the perfusion of 250 µM ChCl.

7.3.2.3. 1 mM ChCl

The ChCl concentration was subsequently increased from 500 µM to 1 mM in this section to determine the effect on the current response of the choline biosensor.

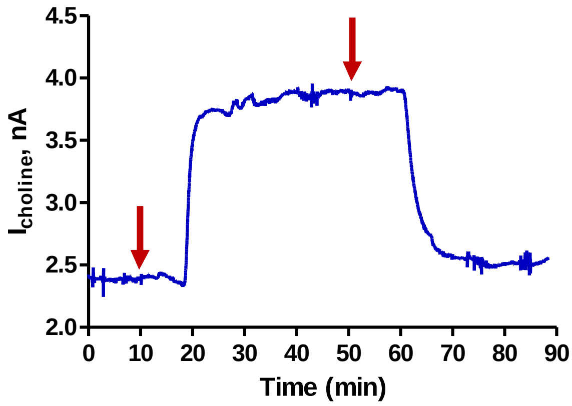

Figure 7.4 : A typical example of the perfusion of 1 mM choline chloride from an aCSF baseline followed by a perfusion of aCSF through a microdialysis probe on the current recorded at the adjacent choline biosensor. The combined probe and sensor were implanted in the right striatum of a freely-moving rat. The arrows indicate the start and end point of the perfusion.

The data in Figure 7.4 illustrates the increase in choline current detecting the increase in choline concentration surrounding the sensor diffused from the dialysate. The combined choline biosensor and MD probe was implanted in the right striatum. A perfusion of aCSF and ChCl through the MD probe at a flow rate of 2 µL/min was monitored at the adjacent biosensor. The perfusion of aCSF obtained a pre perfusion baseline of 2.59 ± 0.16 nA, n = 1 (1 an, 3 ad). Upon perfusion of 1 mM ChCl the current was increased to by 1.40 ± 0.11 nA, n = 1 (1 an, 3 ad) 3.99 ± 0.06 nA, n = 1 (1 an, 3 ad) and returned to a post perfusion aCSF baseline of 2.74 ± 0.14 nA, n = 1 (1 an, 3 ad). This represents a significant increase (*P* = 0.0065) of 54.99 ± 7.19 %, n = 1 (1 an, 3 ad). The post perfusion baseline was not significantly different (*P* = 0.0665) to that of the pre perfusion baseline. The arrows represent the switch from aCSF to ChCl and the clearance by aCSF, however the switch does not take place in the microdialysis probe and the remaining solution must be cleared before the next solution arrives to have an effect. This section has determined that the sensor can respond to both the removal and the introduction of choline in the ECF surrounding the sensor surface. This section has verified that the choline biosensor is viable for use in the *in-vivo* environment and can detect choline perfused through a MD probe.

7.3.3. Local Choline Administration

The previous section determined the capability of the choline biosensor to detect local administrations of choline chloride through the microdialysis probe. This demonstrates that the sensor can be used in conjunction with the microdialysis technique and can detect choline chloride introduced into the ECF surrounding the sensor by diffusion of the perfusate. Microdialysis has been demonstrated as a method of obtaining extracellular concentrations of neurotransmitters using the Lonnroth zero net flux (ZNF) (Lonnroth *et al.*, 1987). This method of extracellular concentration determination has been used for ascorbate (Miele & Fillenz, 1996) and glucose in the striatum (Lowry *et al.*, 1998b) and glucose in the hippocampus (Krebs-Kraft *et al.*, 2009). This method of neurotransmitter concentration determination relies on the concentration gradient between the perfusate and the ECF. The perfusion of a concentration lower than that of the ECF will decrease the current at the biosensor and a concentration higher than the ECF will increase the current at the biosensor. Regression analysis can then be used to determine the point at which the concentration is at equilibrium with the surrounding fluid (Lonnroth *et al.*, 1987; Miele & Fillenz, 1996). In this section, different concentrations of choline chloride were perfused through the MD probe from baseline in order to observe a reduction in current or increase in current to determine if a ZNF is viable for choline.

7.3.3.1. 20 µM ChCl

Initially, 20 µM choline was perfused through the MD probe. This concentration is higher than the estimated *in-vivo* concentration of 6 µM.

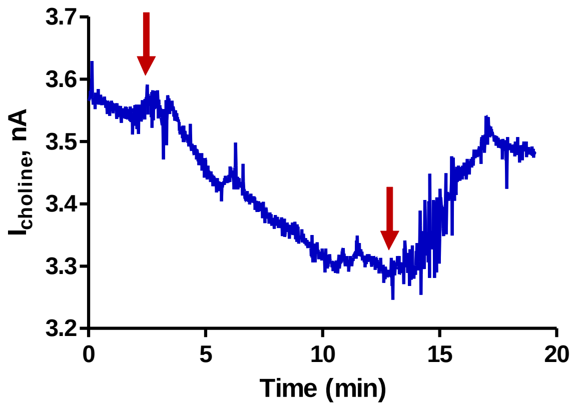

Figure 7.5 : A typical example of the perfusion of 20 µM choline chloride through a microdialysis probe on the current recorded at the adjacent choline biosensor. The combined probe and sensor were implanted in the right striatum of a freely-moving rat. The arrows indicate the start and end point of the perfusion.

The data in Figure 7.5 illustrates the decrease in ECF choline surrounding the sensor. The combined choline biosensor and MD probe was implanted in the right striatum. A perfusion of ChCl through the MD probe at a flow rate of 2 µL/min was monitored at the adjacent biosensor. The pre perfusion baseline obtained was 4.30 ± 0.52 nA, n = 4 (4 an, 5 ad) which reduced by 1.11 ± 0.34 nA, n = 4 (4 an, 5 ad) to 3.19 ± 0.54 nA, n = 4 (4 an, 5 ad) upon perfusion of 20 µM ChCl. Post perfusion the baseline returned to 4.60 ± 0.73 nA, n = 4 (4 an, 5 ad). This represents a significant decrease in current (*P* = 0.0297) of 26.15 ± 8.56 %. The post perfusion baseline was not significantly different (*P* = 0.3968) from that prior to the perfusion.

7.3.3.2. 40 µM ChCl

The concentration of ChCl was increased from 20 µM to 40 µM to determine the effect on the current response.

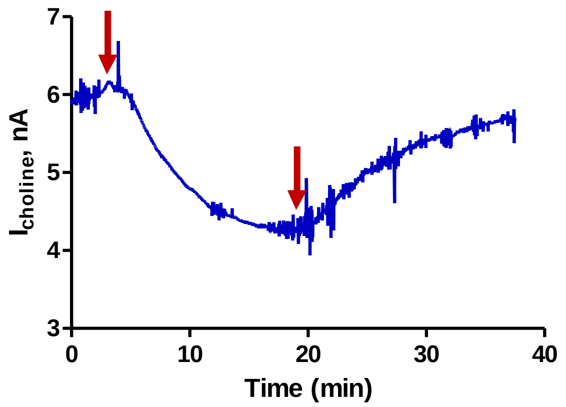

Figure 7.6 : A typical example of the perfusion of 40 µM choline chloride through a microdialysis probe on the current recorded at the adjacent choline biosensor. The combined probe and sensor were implanted in the right striatum of a freely-moving rat. The arrows indicate the start and end point of the perfusion.

The data in Figure 7.6 illustrates the decrease in ECF choline surrounding the sensor. The combined choline biosensor and MD probe was implanted in the right striatum. A perfusion of ChCl through the MD probe at a flow rate of 2 µL/min was monitored at the adjacent biosensor. The baseline current observed prior to the perfusion was 5.84 ± 1.13 nA, n = 2 (2 an, 3 ad) which was reduced by 2.02 ± 0.28 nA, n = 2 (2 an, 3 ad) to 3.83 ± 0.88 nA, n = 2 (2 an, 3 ad). Cessation of the ChCl perfusion returned the current to a post perfusion baseline of 5.73 ± 1.36 nA, n = 2 (2 an, 3 ad). The reduction in current represented a significant decrease ($P = 0.0188$) of 35.75 ± 4.06 %. The post perfusion baseline was not significantly different ($P = 0.7352$) to the baseline prior to the perfusion.

7.3.3.3. 60 µM ChCl

The concentration of the ChCl perfused through the MD probe was increased from 40 µM to 60 µM.

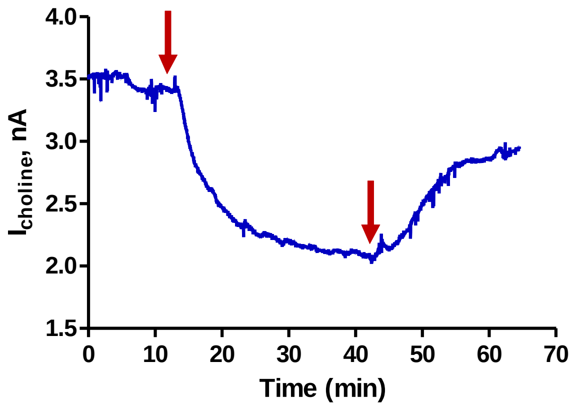

Figure 7.7 : A typical example of the perfusion of 60 µM choline chloride through a microdialysis probe on the current recorded at the adjacent choline biosensor. The combined probe and sensor were implanted in the right striatum of a freely-moving rat. The arrows indicate the start and end point of the perfusion.

The data in Figure 7.7 illustrates the decrease in ECF choline surrounding the sensor. The combined choline biosensor and MD probe was implanted in the right striatum. A perfusion of ChCl through the MD probe at a flow rate of 2 µL/min was monitored at the adjacent biosensor. Prior to the perfusion of ChCl a mean baseline current of 3.57 ± 0.42 nA, n = 2 (2 an, 3 ad) was observed, this was decreased by 1.03 ± 0.25 nA, n = 2 (2 an, 3 ad) to 2.54 ± 0.31 nA, n = 2 (2 an, 3 ad) upon perfusion of the ChCl. This returned to a baseline of 3.57 ± 0.33 nA, n = 2 (2 an, 3 ad). The current decreased non significantly ($P = 0.0529$) by 23.38 ± 5.87 %. The post perfusion baseline was not significantly different ($P = 0.9941$) to that observed prior to the perfusion.

7.3.3.4. 100 µM ChCl

The ChCl concentration was increased from 60 µM to 100 µM in order to determine the effect on the current response observed.

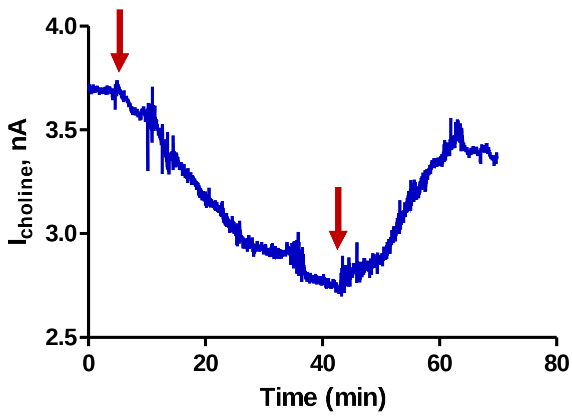

Figure 7.8 : A typical example of the perfusion of 100 µM choline chloride through a microdialysis probe on the current recorded at the adjacent choline biosensor. The combined probe and sensor were implanted in the right striatum of a freely-moving rat. The arrows indicate the start and end point of the perfusion.

The data in Figure 7.8 illustrates the decrease in ECF choline surrounding the sensor. The combined choline biosensor and MD probe was implanted in the right striatum. A perfusion of ChCl through the MD probe at a flow rate of 2 µL/min was monitored at the adjacent biosensor. Prior to the perfusion of ChCl a mean baseline current of 3.08 ± 0.32 nA, n = 3 (3 an, 5 ad) was observed, this was decreased by 0.66 ± 0.13 nA, n = 3 (3 an, 5 ad) to 2.42 ± 0.22 nA upon perfusion of the ChCl. A mean post perfusion baseline current of 3.00 ± 0.26 nA, n = 3 (3 an, 3 ad) was observed. The decrease in current represents a significant decrease (P = 0.0067) of 20.63 ± 2.55 % from baseline. The post perfusion baseline was not significantly different (P = 0.5815) from that prior to the perfusion.

7.3.3.5. 200 µM ChCl

The concentration of the ChCl perfused through the MD probe was increased to 200 µM.

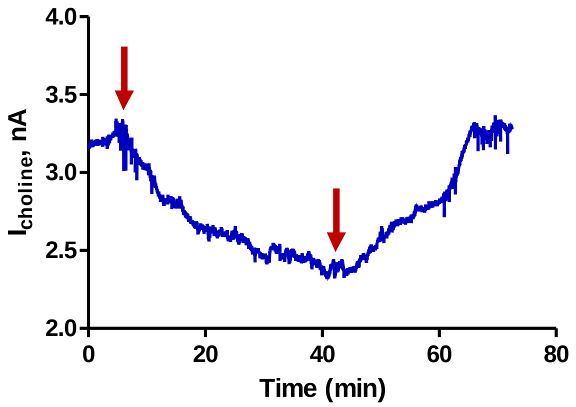

Figure 7.9 : A typical example of the perfusion of 200 µM choline chloride through a microdialysis probe on the current recorded at the adjacent choline biosensor. The combined probe and sensor were implanted in the right striatum of a freely-moving rat. The arrows indicate the start and end point of the perfusion.

The data in Figure 7.9 illustrates the decrease in ECF choline surrounding the sensor. The combined choline biosensor and MD probe was implanted in the right striatum. A perfusion of ChCl through the MD probe at a flow rate of 2 µL/min was monitored at the adjacent biosensor. The baseline current observed was 3.19 nA, n = 1 (1 an, 1 ad) which was reduced by 0.79 nA to 2.40 nA, n = 1 (1 an, 1 ad) upon perfusion of ChCl. This returned to a baseline of 3.29 nA, n = 1 (1 an, 1 ad). The reduction in the current represents a 24.87 % decrease in current.

7.3.3.6. 500 µM ChCl

The concentration of the ChCl perfused through the MD probe was increased to 500 µM.

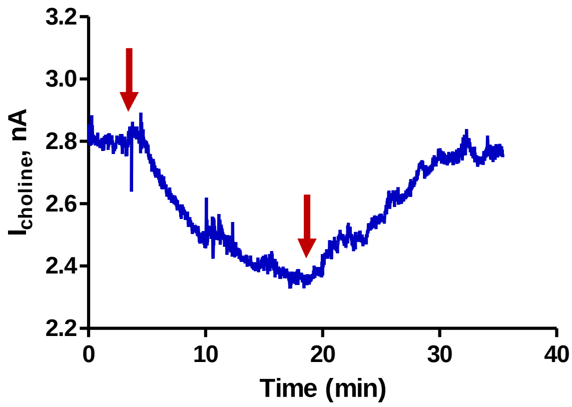

Figure 7.10: A typical example of the perfusion of 500 µM choline chloride through a microdialysis probe on the current recorded at the adjacent choline biosensor. The combined probe and sensor were implanted in the right striatum of a freely-moving rat. The arrows indicate the start and end point of the perfusion.

The data in Figure 7.10 illustrates the decrease in ECF choline surrounding the sensor. The combined choline biosensor and MD probe was implanted in the right striatum. A perfusion of ChCl through the MD probe at a flow rate of 2 µL/min was monitored at the adjacent biosensor. The mean baseline current observed was 2.96 ± 0.22 nA, n = 3 (3 an, 4 ad) which was reduced by 0.51 ± 0.19 nA, n = 3 (3 an, 4 ad) to 2.45 nA, n = 3 (3 an, 4 ad) upon perfusion of ChCl. This returned to a baseline of 2.87 ± 0.18 nA, n = 3 (3 an, 4 ad). This represents a non significant reduction (P = 0.0699) in the current of 16.53 ± 5.20 %. The post perfusion baseline was not significantly different (P = 0.7805) to that prior to the perfusion.

7.3.3.7. 800 µM ChCl

The concentration of the ChCl perfused through the MD probe was increased to 800 µM.

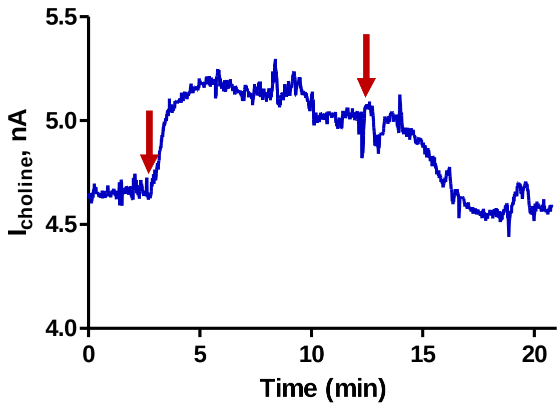

Figure 7.11 : A typical example of the perfusion of 800 µM choline chloride through a microdialysis probe on the current recorded at the adjacent choline biosensor. The combined probe and sensor were implanted in the right striatum of a freely-moving rat. The arrows indicate the start and end point of the perfusion.

The data in Figure 7.11 illustrates the increase in ECF choline surrounding the sensor. The combined choline biosensor and MD probe was implanted in the right striatum. A perfusion of aCSF and ChCl through the MD probe at a flow rate of 2 µL/min was monitored at the adjacent biosensor. The mean baseline current observed was 3.43 ± 1.22 nA, n = 2 (2 an, 2 ad) which was increased by 0.33 ± 0.16 nA, n = 2 (2 an, 2 ad) to 3.75 nA, n = 2 (2 an, 2 ad) upon perfusion of ChCl. This returned to a baseline of 3.44 ± 1.15 nA, n = 2 (2 an, 2 ad). This represents an increase in the current of 9.12 ± 1.30 %.

7.3.3.8. 1 mM ChCl

The concentration of the ChCl perfused through the MD probe was increased to 1 mM.

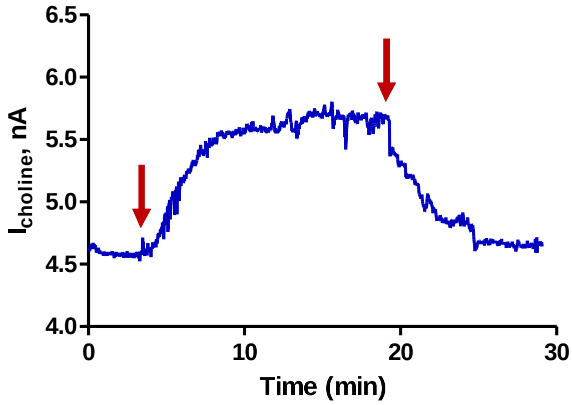

Figure 7.12 : A typical example of the perfusion of 1 mM choline chloride through a microdialysis probe on the current recorded at the adjacent choline biosensor. The combined probe and sensor were implanted in the right striatum of a freely-moving rat. The arrows indicate the start and end point of the perfusion.

The data in Figure 7.12 illustrates the increase in ECF choline surrounding the sensor. The combined choline biosensor and MD probe was implanted in the right striatum. A perfusion of aCSF and ChCl through the MD probe at a flow rate of 2 µL/min was monitored at the adjacent biosensor. The baseline current observed was 4.57 nA, n = 1 (1 an, 1 ad) which was increased by 1.13 nA to 5.70 nA, n = 1 (1 an, 1 ad) upon perfusion of ChCl. This returned to a baseline of 4.64 nA, n = 1 (1 an, 1 ad). This represents an increase in the current of 24.76 %.

7.3.4. Zero Net Flux

The Zero Net Flux (ZNF) method of ECF concentration determination has been used previously and successfully for analytes present in the ECF (Miele & Fillenz, 1996). This method requires the perfusion of analyte concentrations above and below the point of ZNF to produce a net loss or gain from the tissue into the dialysis probe and regression analysis in order to determine the concentration which produced no current change. This data represents the current change observed by the local choline perfusions of 20, 40, 60, 100, 200, 500, 800 and 1000 µM from baseline.

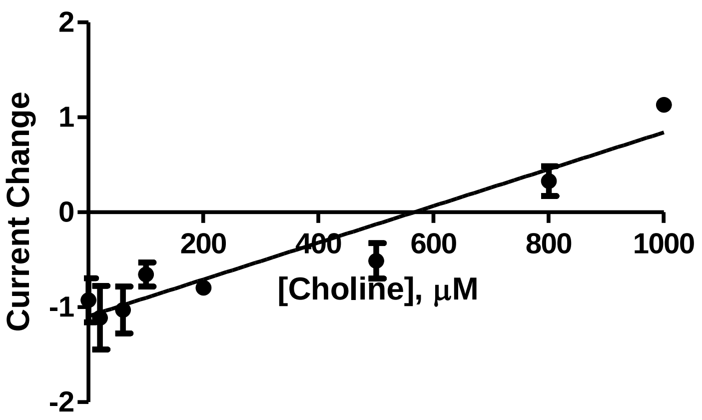

	Current change		
ChCl Perfusion Concentration	MEAN, nA	SEM, nA	Perfusions
0 µM	-0.93	0.23	15
20 µM	-1.11	0.34	5
60 µM	-1.03	0.25	3
100 µM	-0.66	0.13	5
200 µM	-0.79	0.00	1
500 µM	-0.51	0.19	4
800 µM	0.33	0.16	2
1000 µM	1.13	0.00	1

Figure 7.13 : The ZNF plot and current change table for choline chloride perfusions in a freely moving animal using a combined MD probe and choline biosensor for the perfusion of 20, 40, 60, 100, 200, 500, 800, 1000 µM ChCl.

The data presented in Figure 7.13 demonstrates the effect of perfusions of ChCl into the local environment of the choline biosensor. Concentrations of ChCl which were lower than the ECF concentration resulted in a reduction in the current observed as it lead to diffusion of choline into the dialysis probe. Concentrations of ChCl which were higher than the ECF concentration resulted in diffusion into the ECF and an increase in the observed current. Linear regression analysis (R^2 = 0.9181) was used in order to determine the point of ZNF which was determined as approximately 565 µM. This value is considerably larger than the estimated concentration of 6 µM. This demonstrates the inaccuracy of the zero net flux method for some analytes due to damage and recovery. However, this section has demonstrated that the choline biosensor is sensitive to exogenous choline in a linear fashion.

7.3.5. Controls

Prior to pharmacological testing, the effect of control experiments was examined. As all systemic injections were administered by interperitoneal (i.p.) injection, normal saline was used to determine the effect of the injection stress. Also, normal saline is the vehicle of choice for all i.p. injections with the exception of Diamox which was administered using a 2:1 saline:DMSO. The effect of this vehicle is also examined.

7.3.5.1. Saline

The effect of an i.p. injection of normal saline (NaCl, 0.9%) on the choline current observed was investigated as this was the route of administration for the drugs used.

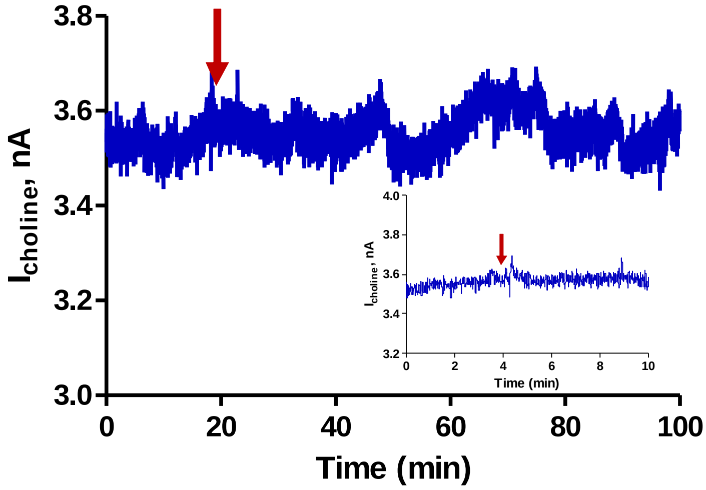

Figure 7.14 : A typical example of the effect of saline on the observed current recorded at the choline biosensor. Inset: 6 minutes post injection. The sensor was implanted in the striatum of a freely-moving rat.

The data in Figure 7.14 illustrates the effect of an i.p. injection of saline on the choline concentration observed by the biosensor. The choline sensor was implanted in the striatum. The baseline current observed at the choline biosensor prior to the injection was 3.99 ± 0.48 nA, n = 9 (5 an, 5 ad). Upon administration of saline the choline current was not significantly increased (*P* = 0.1817) to 4.66 ± 0.77 nA, n = 9 (5 an, 5 ad). This returned to a baseline not significantly different (*P* = 0.1966) to that observed prior to the injection with a current value of 3.94 ± 0.49 nA, n = 9 (5 an, 5 ad) after approximately 27 ± 4 minutes. This is an average timescale which varied between 10 and 30 minutes as a result of the activity of the animal post injection.

7.3.5.2. Saline:DMSO

The vehicle used for Diamox administrations requires the use of dimethyl sulfoxide (DMSO) in addition to saline. The effect of an intraperitoneal (i.p.) injection of saline:DMSO on the choline current observed was investigated as this was the route of administration for Diamox.

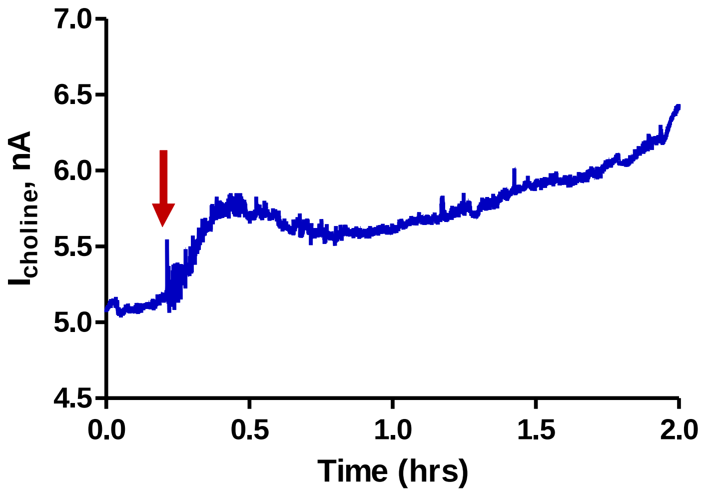

Figure 7.15 : A typical example of the effect of saline:DMSO on the observed current recorded at the choline biosensor. The sensor was implanted in the striatum of a freely-moving rat.

The data in Figure 7.15 illustrates the effect of an i.p. injection of saline:DMSO on the choline concentration observed by the biosensor. The choline sensor was implanted in the striatum. The baseline current observed at the choline biosensor prior to the injection was 5.45 ± 0.35 nA, n = 1 (1 an, 2 ad). Upon administration of saline:DMSO the choline current increased to 6.15 ± 0.40 nA, n = 1 (1 an, 2 ad). This continued to increase to a current value of 6.48 ± 0.56 nA, n = 1 (1 an, 2 ad). The current does not return to a baseline similar to that observed prior to the injection. The sample taken is a relevant period of time relative to an O_2 change using Diamox.

7.3.6. Interferents

7.3.6.1. Sodium Ascorbate

As demonstrated in Chapter 6 extensive work is undertaken *in-vitro* to ensure that the sensor has the ability to reject potential electroactive interferents with the incorporation of the permselective membrane polyphenylenediamine (PPD). The main interferent present in the brain is ascorbic acid (AA) which has been shown to be as high as 400 μM (Miele & Fillenz, 1996). It is important to determine the effect of systemic injections of ascorbate on the current *in-vivo*.

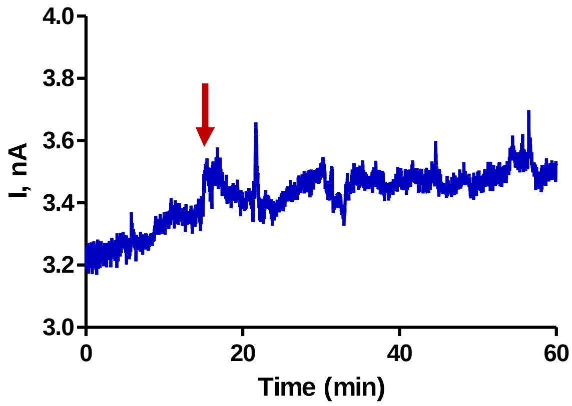

Figure 7.16 : A typical example of the effect of ascorbate (0.5g/kg) on the observed current recorded at the choline biosensor. The sensor was implanted in the striatum of a freely-moving rat.

The data in Figure 7.16 illustrates the effect of an i.p. injection of ascorbate on the current observed by the choline biosensor. The choline sensor was implanted in the striatum. The current is monitored over 60 minutes which is an ideal timeframe to determine if there is a response at the sensor (Lowry *et al.*, 1996). Prior to the administration of ascorbate the baseline observed was 3.09 ± 0.28 nA, n = 4 (1 an, 1 ad). This was not significantly increased (P = 0.3505) after the administration of ascorbate to a current value of 3.12 ± 0.26 nA, n = 4. This demonstrates that the integrity of the PPD layer is sustained *in-vivo* illustrating that the sensor does not detect interfering species as demonstrated by *in-vitro* data in Section 6.3.10 and 6.3.11.

7.3.7. Stability

7.3.7.1. Baseline

As demonstrated in Chapter 6 the exposure of the biosensor to a biological environment and its constituents can be detrimental to the performance of the sensor. This has been demonstrated previously in response to brain tissue (Garguilo & Michael, 1994) (Hu *et al.*, 1994). As this is the case the baseline current of the sensor was monitored over 14 days in order to determine the stability of the sensor *in-vivo*. Day 1 is determined as 24 hours after the application of the potential.

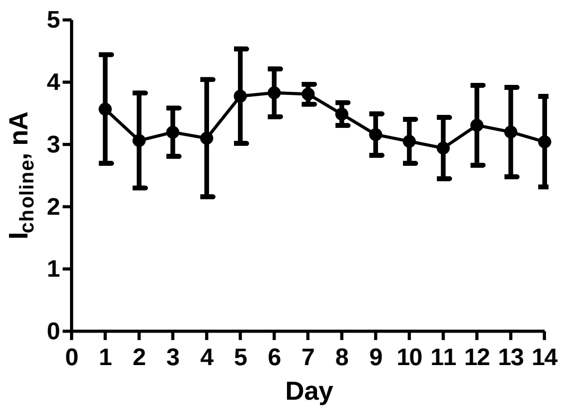

Day	**Mean, nA**	**S.E.M, nA**	**n**
1	3.57	0.87	11
2	3.07	0.76	6
3	3.20	0.39	6
4	3.10	0.94	2
5	3.78	0.76	3
6	3.83	0.38	3
7	3.81	0.16	4
8	3.49	0.18	4
9	3.16	0.33	4
10	3.05	0.35	4
11	2.95	0.49	4
12	3.31	0.64	4
13	3.20	0.72	4
14	3.05	0.73	4

Figure 7.17 : The baseline current and table of baseline currents of the choline biosensor recorded over a 14 day period. The sensor was implanted in the right striatum of a freely-moving rat.

The decay in the baseline current observed by the choline biosensor over a 14 day period is demonstrated in Figure 7.17. The 14 day period coincides with the 14 day exposure to brain tissue observed during the *in-vitro* characterisation of the sensor (see Section 6.3.5). The current observed on day 1 was 3.57 ± 0.87 nA, n = 11 this was not significantly reduced (P = 0.7376) to 3.05 ± 0.73 nA, n = 4 by day 14. This reduction in current observed corresponds to a reduction of 14 % over the 14 days. This is comparable to the *in-vitro* reduction observed of 24 % upon exposure to brain tissue. The zero net flux method of ECF concentration estimation suggested that the ECF concentration was 565 µM. An alternative approach to determine the ECF concentration, is from baseline currents from *in-vivo* data and *in-vitro* calibration data and compare this with the ZNF. The slope obtained from the choline biosensors used in the baseline experiments was 0.56 ± 0.07 nA/µM. The 24% reduction in current was taken into account for the sensitivity of these electrodes. The average baseline current was determined over the 14 days and the value calculated for the ECF concentration was 7.93 µM. The is more in line with the 6 µM suggested by Garguilo *et al.* (Garguilo & Michael, 1996)

7.3.8. Oxygen Dependence

Extensive *in-vitro* studies were undertaken to determine the O_2 dependence of the choline biosensor and strategies were developed to decrease the O_2 sensitivity. However, in order to determine if the sensor was O_2 independent in the *in-vivo* environment pharmacological manipulations were performed to alter the O_2 concentration surrounding the sensor and to investigate any simultaneous alterations in the choline current as a result.

7.3.8.1. Chloral Hydrate

Chloral hydrate has been used previously to increase the levels of striatal O_2 (Fillenz & Lowry, 1998; Lowry & Fillenz, 2001) and is a common anaesthetic agent causing general CNS depression (Bolger & Lowry, 2005). The effect of chloral hydrate on choline concentration has previously been determined using MD, demonstrating an initial twenty minute decrease followed by an increase in the levels of choline as a result of administration (Damsma & Fibiger, 1991). This section looks at the effect of chloral hydrate simultaneously on both a choline and O_2 sensor in order to determine if the increase on O_2 concurrently increases choline.

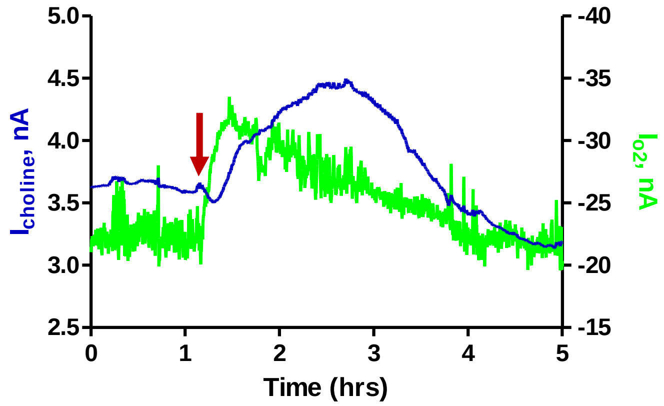

Figure 7.18 : A typical example of the effect of chloral hydrate (350mg/kg, i.p.) on the observed current recorded at the choline and O_2 sensors. The sensors were implanted in the striatum of a freely-moving rat.

The data in Figure 7.18 illustrates the effect of an i.p. injection of chloral hydrate (350 mg/kg) on the choline and O_2 response of the sensors. The choline and O_2 sensors were implanted in the striatum. The choline current observed prior to injection was 3.48 ± 0.46 nA, n = 4 (3 an, 4 ad) this was observed alongside an O_2 current of -45.26 ± 14.41 nA, n = 3 (3 an, 4 ad). Upon administration of chloral hydrate, as expected the O_2 current increased, the I_{MAX} observed was -81.93 ± 28.84 nA after approximately 19 ± 6 minutes, n = 3 (3 an, 4 ad). The choline current observed at the highest levels of oxygen was increased to 3.67 ± 0.48 nA, n = 4 (3 an, 4 ad). This demonstrates a significant increase (P = 0.0303) of approximately 5 % which corresponds to an increase in current of 0.19 ± 0.07 nA, n = 4 (3 an, 4 ad). This is a concentration increase of approximately 0.42 µM, n = 4 (3 an, 4 ad) choline. An oxygen current of -44.97 ± 11.92 nA, n = 3 (3 an, 4 ad) was observed upon return to baseline. The choline current observed as the O_2 current returned to baseline was not significantly increased (P = 0.1725) to 4.43 ± 1.02 nA, n = 4 (3 an, 4 ad) from pre injection baseline. As the oxygen levels were returning to baseline, all choline currents continued to increase reaching I_{MAX} approximately 35 ± 7 minutes, n = 4 (3 an, 4 ad) from the injection of the chloral hydrate. As demonstrated in the typical example above, the administration of chloral hydrate increases both the O_2 levels and the choline levels although in different time courses. The increase in the choline detection after the O_2 begins to return to baseline suggests that the choline is not detecting O_2 dependent choline changes, however rather the chloral hydrate has itself increased the endogenous levels of choline. The initial decrease in the choline current at the point of injection further supports the O_2 independence of this sensor in conjunction with further experiments carried out in this section.

7.3.8.2. Diamox

Acetazolamide (Diamox) has been demonstrated to increase striatal O_2 by the dilation of cerebral blood vessels (Bolger & Lowry, 2005) (Dixon *et al.*, 2002). This section was undertaken to determine the effect of increasing the O_2 concentration on the choline biosensor.

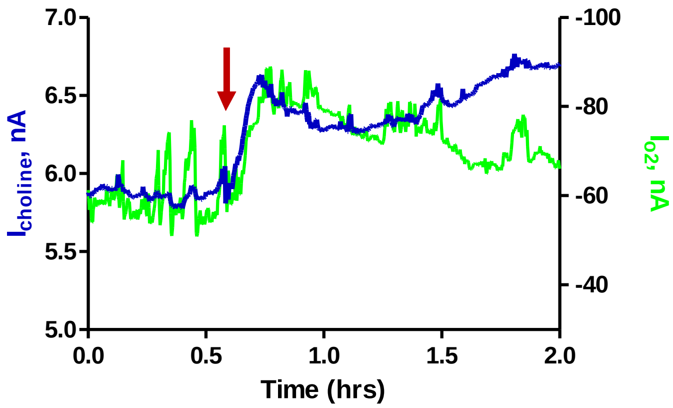

Figure 7.19 : A typical example of the effect of Diamox (50mg/kg, i.p.) on the observed current recorded at the choline and O_2 sensors. The sensors were implanted in the striatum of a freely-moving rat.

The data in Figure 7.19 illustrates the effect of an i.p. injection of Diamox (50 mg/kg) on the choline and O_2 responses of the sensors. The choline and O_2 sensors were implanted in the striatum. The baseline current recorded at the choline biosensor prior to the injection was 3.56 ± 0.42 nA, n = 5 (4 an, 7 ad). The pre-injection baseline observed at the O_2 sensor was -44.19 ± 5.93 nA, n = 4 (4 an, 7 ad). Upon administration of Diamox, the O_2 current increased to -62.14 ± 9.65 nA, n = 4 (4 an, 7 ad) after approximately 92 ± 45 minutes, n = 4 (4 an, 7 ad). At the I_{MAX} of the O_2 current the choline current increased to 3.75 ± 0.48 nA, n = 5 (4 an, 7 ad). This is a non significant increase (P = 0.0652) of approximately 5 % which corresponds to a current increase of 0.19 ± 0.64 nA, n = 5 (4 an, 7 ad). This is a concentration increase of approximately 1.13 ± 0.41 μM, n = 5 (4 an, 7 ad). The O_2 current returned to a baseline of -48.33 ± 6.97 nA, n = 4 (4 an, 7 ad). The choline current observed as the O_2 returned to baseline was 4.04 ± 0.53 nA, n = 4 (4 an, 7 ad), a significant increase (*P* = 0.0201) from the pre injection baseline. The choline current continues to increase and peaks approximately 240 ± 52 minutes after administration of Diamox whereby the O_2 levels have long since returned to baseline. This data suggests that Diamox has an independent effect on the choline levels around the sensor, increasing these levels endogenously, not increasing the detection levels as a result of increased levels of O_2. The uncorrelated responses which demonstrate an increase in the levels of choline after the O_2 levels have returned to baseline further demonstrate that the sensor is not subject to O_2 dependence.

7.3.8.3. L-NAME

N (G)-nitro-L-arginine methyl ester (L-NAME) has previously been shown to decrease cerebral blood flow via vasoconstriction (Wei *et al.*, 1994). As blood flow and O_2 are closely correlated the vasoconstriction will decrease the concentration of O_2 around the sensor (Lowry *et al.*, 1997). This section looks at the effect of a decrease in O_2 concentration on the choline current observed at the biosensor.

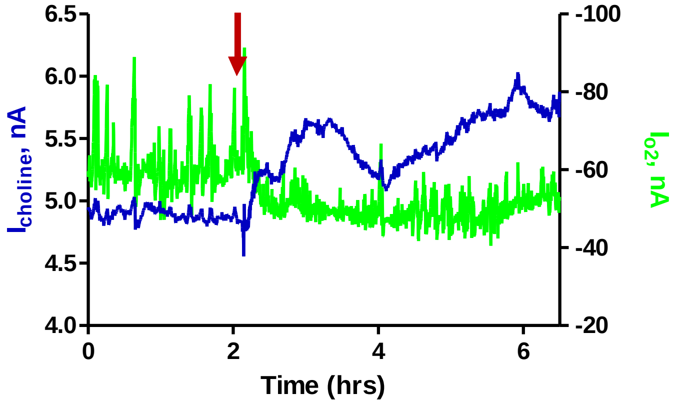

Figure 7.19 : A typical example of the effect of L-NAME (30mg/kg, i.p.) on the observed current recorded at the choline and O_2 sensors. The sensors were implanted in the striatum of a freely-moving rat.

The data in Figure 7.19 illustrates the effect of an i.p. injection of L-NAME (30 mg/kg) on the choline and O_2 response of the sensors. The choline and O_2 sensors were implanted in the striatum. The baseline current observed at the choline biosensor prior to the injection was 4.46 ± 0.24 nA, n = 2 (2 an, 3 ad). The pre injection baseline observed at the O_2 sensor was -72.31 ± 14.54 nA, n = 2 (2 an, 3 ad). Upon administration of L-NAME the O_2 current decreased to -61.39 ± 12.93 nA, n = 2 (2 an, 3 ad) a maximum decrease was observed after approximately 41 ± 10 minutes. The decrease in O_2 current did not cause a decrease in the choline current, rather at the maximum decrease observed at the O_2 sensor an increase in the choline current was observed with a current of 4.76 ± 0.34 nA, n = 3. This corresponds to an increase in current of 0.30 ± 0.11 nA, n = 2 (2 an, 3 ad), a non significant (P = 0.1113) increase of approximately 6 %. This is a concentration increase of approximately 0.78 ± 0.56 μM, n = 2 (2 an, 3 ad) choline. The decrease in the oxygen current did not correlate to a decrease in the current observed at the choline biosensor as expected if the sensor was O_2 sensitive. Alternatively the choline response increased in line with the decrease in the O_2 concentration. This result clearly demonstrates that the choline biosensor is not subject to O_2 interference issues.

7.3.9. Pharmacological manipulations

The sensors ability to detect changes in choline concentration surrounding the sensor has been validated in Section 7.3.3. This section determines if the sensor has the ability to detect changes in choline as a result of pharmacological manipulations.

7.3.9.1. Atropine

Atropine is widely used as a muscarinic acetylcholine receptor (mAChR) antagonist (Zwart & Vijverberg, 1997). Atropine is largely used in the determination of its effect on acetylcholine release. Previous studies have demonstrated an increase in the release in acetylcholine in different brain regions as a result of atropine administration (Buyukuysal *et al.*, 1995) (Koppen *et al.*, 1997). Very few however, focus on the changes in the extracellular concentration of choline. The changes in extracellular concentrations of both choline and acetylcholine have been monitored in the striatum by microdialysis in response to atropine. This study demonstrated that alongside an increase in acetylcholine release, atropine decreased the extracellular concentration of choline (Ikarashi *et al.*, 1997). The reduction in choline concentration upon administration of atropine correlates with findings that atropine increases the rate of choline uptake via the high affinity choline uptake (HACU) system; thereby increasing the rate of acetylcholine production and release (Antonelli *et al.*, 1981). This section determines the effect of atropine on the extracellular choline concentration monitored by the choline biosensor.

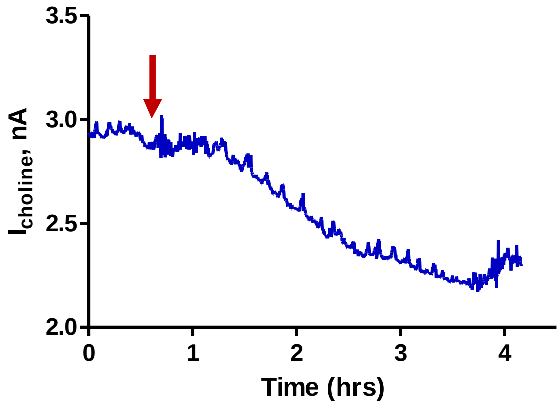

Figure 7.20 : A typical example of the effect of Atropine (5mg/kg, i.p.) on the observed current recorded at the choline biosensor. The sensor was implanted in the striatum of a freely-moving rat.

The data in Figure 7.20 illustrates the effect of an i.p. injection of atropine on the choline concentration observed by the biosensor. The choline sensor was implanted in the striatum. The baseline current observed at the choline biosensor prior to the injection was 5.39 ± 1.75 nA, n = 5 (3 an, 3 ad). Upon administration of atropine the choline current was significantly decreased (P = 0.0020) to 4.45 ± 1.64 nA, n = 5 (3 an, 3 ad) after approximately 103 ± 14 minutes. This is a current decrease of 0.94 ± 0.13 nA, which corresponds to a concentration decrease of 2.13 ± 0.28 μM. This returned to a baseline not significantly different (P = 0.1507) to that observed prior to the injection with a current value of 5.18 ± 1.85 nA, n = 5 (3 an, 3 ad) after approximately 130 ± 11 minutes. This data demonstrates that the biosensor is capable of detecting the decrease in choline caused by atropine. The decrease in the concentration of choline in the ECF as a result of increased uptake by the HACU is monitored in real-time by the biosensor.

7.3.9.2. HC-3

The HACU system has long been demonstrated as the rate limiting step in acetylcholine synthesis. Hemicholinium-3 (HC-3) is a well known inhibitor of this uptake system (Kuhar & Murrin, 1978). HC-3 has been verified using microdialysis and microelectrode arrays, to increase choline concentrations in the striatum as a result of inhibiting this regulatory uptake system and subsequently decreases acetylcholine synthesis (Ikarashi *et al.*, 1997) (Burmeister *et al.*, 2003). However, HC-3 does not cross the blood brain barrier. This section determines the effect of a local perfusion of HC-3 through a microdialysis probe from an aCSF baseline on the extracellular choline concentration monitored by the adjacent choline biosensor.

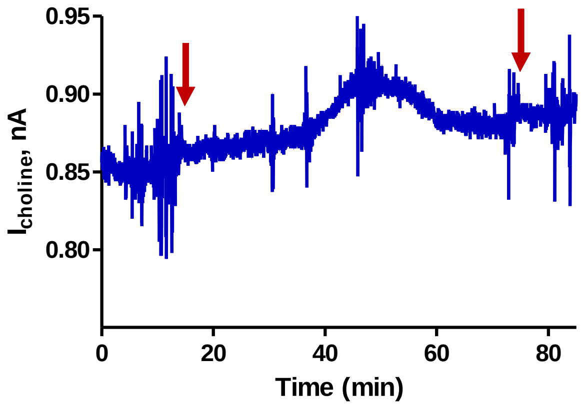

Figure 7.21 : A typical example of the perfusion of HC-3 (200 µM) from an aCSF baseline followed by a perfusion of aCSF through a microdialysis probe on the current recorded at the adjacent choline biosensor. The combined probe and sensor were implanted in the right striatum of a freely-moving rat. The arrows indicate the start and end point of the perfusion.

The data in Figure 7.21 illustrates the increase in ECF choline surrounding the sensor as a result of a HC-3 perfusion. aCSF was perfused prior to and post perfusion of HC-3 in order to obtain a background concentration of zero. The combined choline biosensor and MD probe was implanted in the right striatum. A perfusion of aCSF and HC-3 through the MD probe at a flow rate of 2 µL/min was monitored at the adjacent biosensor. The initial perfusion of aCSF gave a baseline current of 3.64 ± 1.55 nA, n = 2 (2 an, 4 ad), which increased to 3.77 ± 1.62 nA, n = 2 (2 an, 4 ad) upon perfusion of HC-3 after approximately 10 ± 4 minutes. This is a current increase of 0.13 ± 0.10 nA which corresponds to a concentration increase of 0.32 ± 0.16 µM choline. A perfusion of aCSF with which to return an aCSF baseline similar to that observed prior to the perfusion of HC-3 yielded a current of 3.64 ± 1.56 nA, n = 2 (2 an, 4 ad). The increase in current demonstrated which is then removed while still perfusing HC-3 was seen in each experiment. The time taken for the HC-3 to reach the MD probe is approximately five minutes from the point of switching indicated by the arrow. This data demonstrates the sensors ability to detect the increase in choline caused by HC-3. The increase in the level of choline in ECF as a result of the inhibition of the HACU is monitored in real time by the choline biosensor.

7.3.9.3. Neostigmine

The hydrolysis of acetylcholine (Ach) by acetylcholinesterase (AchE) is a rapid and efficient process whereby one molecule of AchE can hydrolyse 5000 molecules of Ach per second (Lawler, 1961). As this is the case, in many microdialysis studies acetylcholinesterase inhibitors are frequently used to increase dialysate concentrations of Ach (Chang *et al.*, 2006). Neostigmine, an AchE inhibitor, has been used in microdialysis to determine its effect on acetylcholine concentration (Vinson & Justice Jr, 1997). In addition, neostigmine has previously been used in conjunction with microsensors to demonstrate the contribution of Ach hydrolysis to the choline signal (Garguilo & Michael, 1996). This section determines the effect of neostigmine on the choline current observed at the choline biosensor.

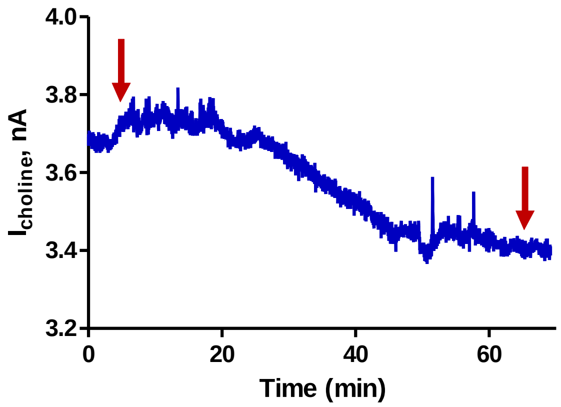

Figure 7.22 : A typical example of the perfusion of neostigmine (100 mM) from an aCSF baseline followed by a perfusion of aCSF through a microdialysis probe on the current recorded at the adjacent choline biosensor. The combined probe and sensor were implanted in the right striatum of a freely-moving rat. The arrows indicate the start and end point of the perfusion.

The data in Figure 7.22 illustrates the increase in ECF choline surrounding the sensor. The combined choline biosensor and MD probe was implanted in the right striatum. A perfusion of aCSF and neostigmine through the MD probe at a flow rate of 2 µL/min was monitored at the adjacent biosensor. The initial perfusion of aCSF gave a baseline current of 8.68 ± 2.97 nA, n = 2 (2 an, 3 ad), which decreased to 8.19 ± 2.83 nA, n = 2 (2 an, 3 ad) upon perfusion of neostigmine after approximately 34 ± 5 minutes. This is a current decrease of 0.48 ± 0.15 nA which corresponds to a concentration decrease of 1.41 ± 0.58 µM. A perfusion of aCSF with which to return an aCSF baseline similar to that observed prior to the perfusion of neostigmine yielded a current of 8.84 ± 3.17 nA, n = 2 (2 an, 3 ad). The time taken for the neostigmine to reach the MD probe is approximately five minutes from the point of switching indicated by the arrow. This data demonstrates the sensors ability to detect the decrease in choline caused by neostigmine. The decrease in the level of choline in ECF as a result of the inhibition of AchE is monitored in real time by the choline biosensor. This indicates that the choline liberated from the Ach contributes to the choline signal observed.

7.3.9.4. Systemic Choline Administration

Dietary restriction of choline in rats has been demonstrated to affect acetylcholine release in the brain (Nakamura *et al.*, 2001). This is due to the brains inability to synthesise choline, therefore choline used for the synthesis of acetylcholine, is sourced from the extracellular fluid which enters the brain from systemic circulation (Michel *et al.*, 2006). It has been noted that systemic choline administration increased the acetylcholine levels in the striatum, however, the administration of choline did not increase striatal choline levels (Buyukuysal *et al.*, 1995). This section investigates the effect of choline chloride administration on the striatal choline concentration.

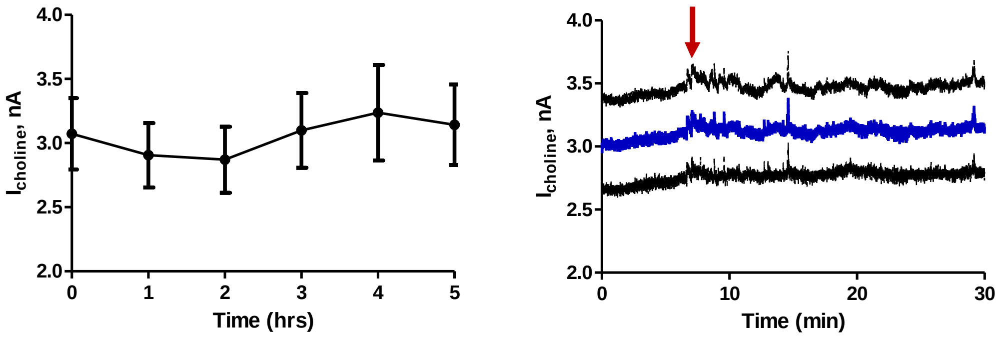

Figure 7.23 : Average response and raw data of choline chloride injection (60mg/kg, i.p.) on striatal choline and the observed current recorded at the choline biosensor. The sensor was implanted in the striatum of a freely-moving rat.

The data in Figure 7.23 illustrates the effect of an i.p. injection of choline chloride (60mg/kg) on the choline response of the sensors. The current response prior to injection was 3.07 ± 0.27 nA, n = 12. The current decreased over the subsequent two hour to 2.91 ± 0.25 nA, n = 12 (1 hr) and 2.87 ± 0.25 nA, n = 12 (2 hr). The current then increased to 3.10 ± 0.29 nA, n = 12 (3 hr), 3.24 ± 0.37 nA, n = 12 (4 hr) and 3.14 ± 0.31 nA, n = 12. The current response after the subsequent 5 hour period post injection did not show significant variation from the point of injection (*P* = 0.3281). This demonstrates that the systemic injection of choline chloride does not increase ECF choline levels. This may be due to quick uptake and removal processes which can account for increases in striatal acetylcholine levels. These results are consistent with previous findings by other research groups (Buyukuysal *et al.*, 1995). It has been demonstrated in the hippocampus, an elevation in the concentration of choline 15 minutes after an i.p of 20 mg/kg choline chloride (Koppen *et al.*, 1997). The raw data of 20 minutes post injection is demonstrated in Figure 7.23 demonstrating that this is not observed in the striatum. The raw data is an i.p injection in one animal recorded on four electrodes.

7.3.10. Physiological fluctuations

7.3.10.1. Movement

The basal ganglia, which in part consists of the striatum, plays a role in motor function (Hauber, 1998). The striatum consist of spiny projection neurons which constitute 95% of the cell type and the remaining striatal neurons are interneurons (Kemp & Powell, 1971). There are four subtypes of interneuron, one of which is cholinergic (Zhou *et al.*, 2002). Acetylcholine (Ach) mediated neurotransmission has a pivotal role in the control of voluntary movement exerted by the striatum, hence, this region has the highest levels of Ach muscarinic receptors and other cholinergic markers in the CNS (Weiner *et al.*, 1990). The disruption of the cholinergic system has been implicated in movement disorders such as Parkinson's disease (PD) and Dystonia (Pisani *et al.*, 2007). In PD, a disruption of the Dopamine (DA) –Ach balance, whereby DA exerts an inhibitory effect on Ach release in the striatum from its most prominent dopaminergic imput; the substantia nigra pars compacta, leads to the appearance of motor symptoms (DeBoer *et al.*, 1996; Calabresi *et al.*, 2000). Microdialysis has previously demonstrated the correlation between Ach and movement in the striatum (Day *et al.*, 1991). Over 12 hours, the correlation between movement and the levels of choline in the striatum were monitored.

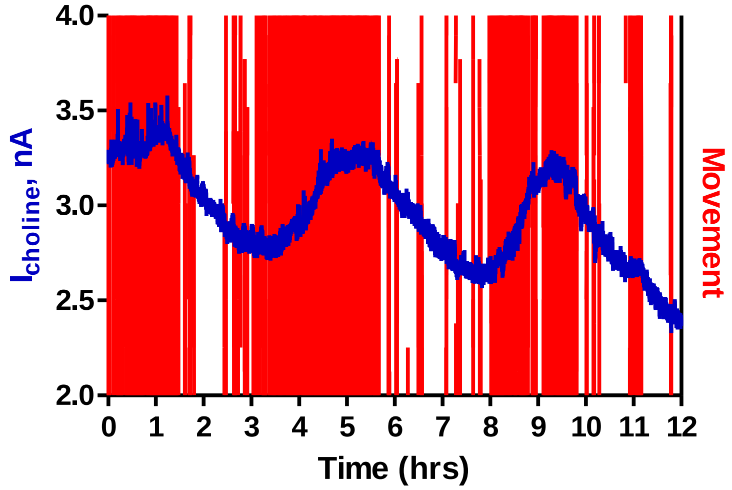

Figure 7.24 : A typical example of the fluctuation of choline and the observed current recorded at the choline biosensor coupled with motor activity. The sensor was implanted in the right striatum of a freely-moving rat.

The effect of activity on the recorded choline current is shown in Figure 7.24. The choline current is coupled with a movement meter as described in Section 3.2.3. The correlation between activity and an increase in choline current can be observed in Figure 7.24. The periods of high activity increase the choline current which then decreases upon cessation of the activity. This demonstrates the ability of the choline biosensor to monitor physiological changes in choline concentration in the striatum which is noted for the high levels of cholinergic activity due to movement.

7.3.10.2. Movement and Rest

The previous section has illustrated the effect of movement on the choline response at the biosensor. This section looks at the effect of neuronal activation as a result of movement on the choline current followed by a period of rest.

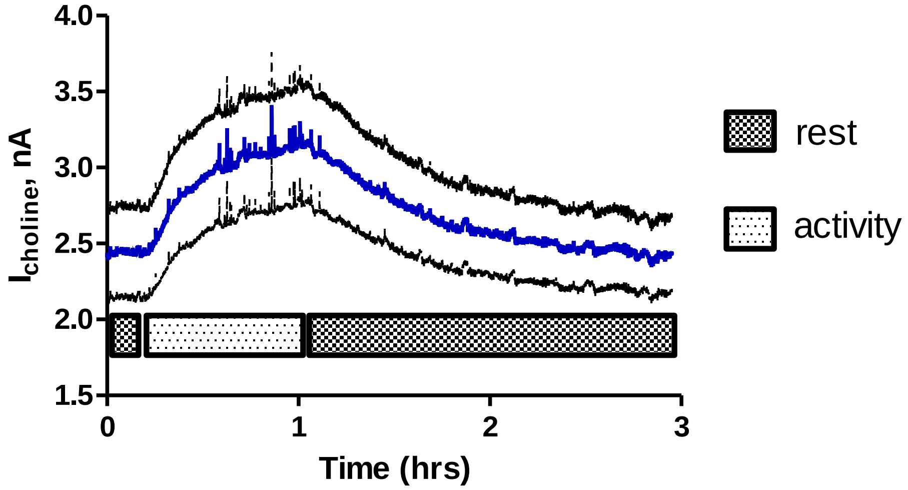

Figure 7.25 : Average response (n = 4) of the fluctuation of choline observed current recorded at the choline sensors coupled with motor activity. The sensors were implanted in the striatum of a freely-moving rat.

The effect of activity and rest on the recorded choline current is shown in Figure 7.25. The baseline current observed at the choline biosensor prior to the period of activity; during rest, was 2.45 ± 0.30 nA, n = 4. Upon commencement of activity the choline current was significantly increased (*P* = 0.0044) to 3.12 ± 0.38 nA, n = 4. This returned to a baseline not significantly different (*P* = 0.6248) to that observed prior to activity with a current value of 2.42 ± 0.25 nA, n = 4. The period of activity constituted eating, drinking, grooming and running. Upon cessation of the activity, and the commencement of sleep, the increased choline current gradually returned to baseline. This data illustrates the increase in choline current as a result of movement and neuronal activation and the subsequent return to baseline in the absence of these.

7.3.10.3. Movement and Oxygen

As demonstrated in Section 7.3.10.1 the choline biosensor can detect changes in the choline concentration as a result of movement. However, it is important to determine that the changes which are observed are not as a result of increases in the levels in O_2

due to increased blood flow, thus changing the current observed at the sensor due to O_2 dependence. As shown in Chapter 5 the level of O_2 dependence observed *in-vitro* is minimal. As the approximate concentration of choline in the striatum of only 6 μM, similarly demonstrated here as approximately 7μM, *in-vitro* O_2 dependence studies suggest that this concentration is low enough that it should not demonstrate O_2 dependence. In addition, the *in-vivo* studies to elucidate the effect of O_2 changes on the choline biosensor have demonstrated that the sensor does not respond directly to changes in O_2 concentration as a result of O_2 dependence (see Section 7.3.8).

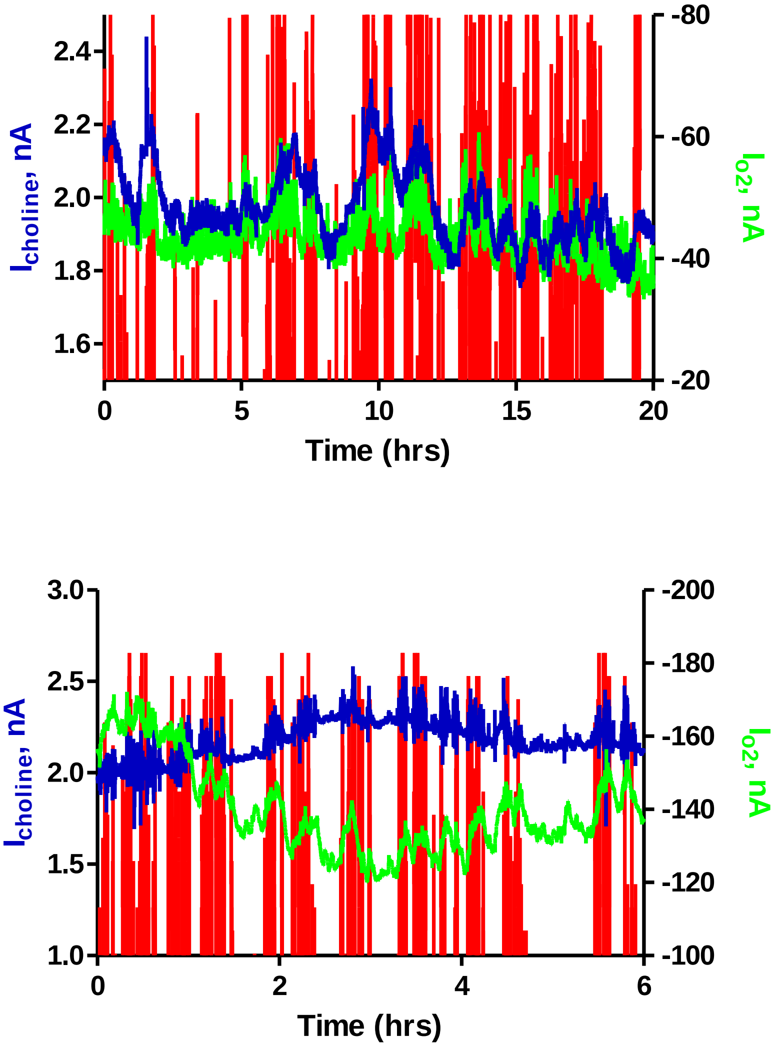

Figure 7.26 : Typical examples of the fluctuation of choline and O_2 and the observed current recorded at the choline and O_2 sensors coupled with motor activity. The sensors were implanted in the striatum of a freely-moving rat.

The effect of activity on the recorded choline and O_2 currents is shown in Figure 7.26. The choline and O_2 current is coupled with a movement meter as described in Section 3.2.3. The correlation between activity and an increase in choline and O_2 currents can be observed in Figure 7.26 (top). As mentioned previously, the effect due to O_2 dependence is likely to be very minimal as demonstrated by the various methods of O_2 dependence characterisation performed both *in-vitro* and *in-vivo*. The changes in choline current may potentially be due to changes in blood flow. Demonstrated previously, an O_2 sensor implanted in the striatum can be used as an indicator of blood flow. This was shown using both a carbon paste electrode to monitor O_2 changes and the H_2 clearance technique to monitor blood flow. It was demonstrated that O_2 and blood flow both increased as a result of activity and the O_2 can be the index of blood flow (Lowry *et al.*, 1997). Figure 7.26 (Bottom) clearly demonstrates the correlation between movement choline and O_2, however, the reduction in the O_2 concentration corresponds to an increase in choline current. This data demonstrates the link between motor activity, choline and O_2, although it also demonstrates a disparity in the choline and O_2 trends further illustrating that the choline fluctuations observed alongside the O_2 fluctuations are not as a result of O_2 interference of the sensor.

7.3.10.4. Circadian Rhythm

The cholinergic system has been shown to be influenced by circadian rhythmicity due to circadian fluctuations in cholinergic synthesis and degradation (Hut & Van der Zee, 2011). The fluctuations in acetylcholine due to circadian rhythmicity have been demonstrated to differ between brain regions. The motor cortex has been shown to not be under the influence of circadian fluctuations (Jiménez-Capdeville & Dykes, 1996). However, this section was undertaken to investigate if the choline biosensor could detect any circadian rhythmicity. This section is an example of 4 light and 5 dark phases of continuous monitoring of the choline response in order to determine if cholinergic circadian fluctuations were present.

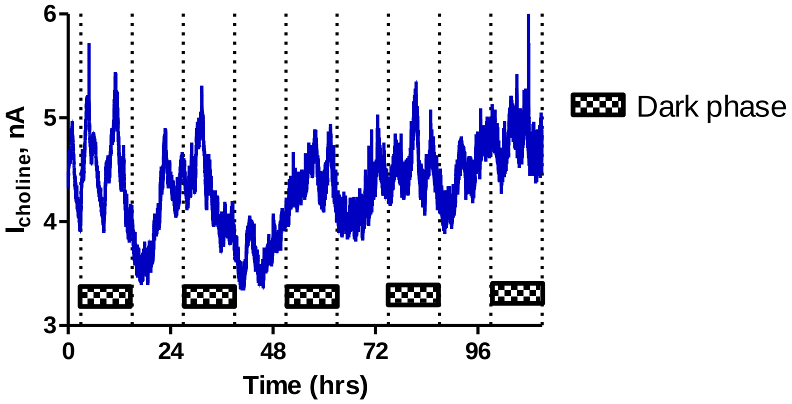

Figure 7.27 : An example of the fluctuation of choline and the observed current recorded at the choline biosensor. The sensor was implanted in the right striatum of a freely-moving rat.

The effects of the light dark cycle on the fluctuations in choline current are presented in Figure 7.27. There does not appear to be a clear trend indicating that striatal choline is influenced by the circadian cycle. However, as demonstrated in Section 7.3.10.1 there is a clear coupling of choline concentration increases and movement. The increases in choline concentration during the dark phase are likely due to an increase in the activity levels of the rat rather than circadian fluctuations.

7.4. Conclusion

Initial experiments were carried out in order to determine if the choline biosensor was capable of detecting exogenously administered choline. These experiments were performed from an aCSF baseline and demonstrated that the MD method could be used in conjunction with the biosensor, detecting increases in choline concentrations. Experiments were then performed in order to determine if using the MD technique a ZNF could be performed in order to estimate the *in-vivo* concentration of choline. The ZNF did not produce results which were consistent with the estimated choline concentration value and differed from the value estimated from baseline. These results demonstrated that although the choline biosensor was capable of detecting changes in the choline concentration surrounding the sensor the ZNF method of concentration determination is not suitable for this analyte.

The i.p. administration of sodium ascorbate was performed to determine the effect on the observed choline response. This study was important with respect to determining the effect of interferents on the sensor. It was demonstrated that ascorbate did not affect the choline current observed at the biosensor.

The stability of the biosensor was determined over a 14 day period. This correlated with the brain tissue studies performed *in-vitro* (see Section 6.3.5). Similar results were seen *in-vivo* as were demonstrated *in-vitro.* These results demonstrated that the sensor was stable over a 14 day period.

Determination of the O_2 sensitivity of the sensor was undertaken. This included pharmacological manipulations of O_2 levels. Using chloral hydrate and Diamox to increase the levels of O_2 both increased the choline current observed, although on different timescales to the O_2. The control studies demonstrated that the saline:DMSO affects the choline current, therefore, this potentially has a role in the fluctuation of the choline current and the O_2 fluctuations are not influencing the signal. In addition, L-NAME was used to decrease the O_2 concentration. This coincided with an increase in the choline current supporting the view that the sensor is not subject to O_2 interference. The level of O_2 at baseline is sufficient for the detection of baseline choline and can adequately detect increases in choline concentration.

In order to determine if the sensor was capable of detecting pharmacological changes in the choline concentration, aspects of the cholinergic system were targeted. Atropine a muscarinic acetylcholine receptor (mAChR) antagonist was used in order to increase the rate of choline uptake via the high affinity choline uptake (HACU) system. A decrease in the choline concentration is clearly detected at the choline biosensor. HC-3 was used to inhibit the HACU and increase the extracelluar concentration of choline. This was detected at the choline biosensor. In addition to this, neostigmine was used to inhibit AchE activity. This would decrease the choline concentration as the choline contribution from the Ach would be eliminated. A decrease in current was observed at the choline biosensor.

The correlation between fluctuations in choline and movement were also demonstrated. A clear correlation between the activity level of the animal and the choline current was observed. It was important however to determine if this was as a result of O_2 fluctuations for the same reason. It was demonstrated that although fluctuations in choline current alongside O_2 and movement are observed, a disparity between the long term fluctuations suggest that the choline is fluctuating in response to neuronal activation and an increase in blood flow rather than O_2 sensitivity. Circadian rhythms were examined under a 12 h light dark cycle. Although increases in choline current could be observed during the dark phase this is potentially more likely from an increase in activity during the dark phase than circadian fluctuations.

This section has demonstrated that the choline biosensor is capable of detecting exogenous choline through MD, changes in striatal choline concentration through pharmacological manipulations, physiological changes and is not sensitive to local O_2 fluctuations.

Antonelli T, Beani L, Bianchi C, Pedata F & Pepeu G. (1981). Changes in synaptosomal high affinity choline uptake following electrical stimulation of guinea-pig cortical slices: effect of atropine and physostigmine. *British Journal of Pharmacology* **74,** 525-531.

Babb SM, Ke Y, Lange N, Kaufman MJ, Renshaw PF & Cohen BM. (2004). Oral choline increases choline metabolites in human brain. *Psychiatry Research: Neuroimaging* **130,** 1-9.

Bolger FB & Lowry JP. (2005). Brain tissue oxygen: *In-Vivo* monitoring with carbon paste electrodes. *Sensors* **5,** 473-487.

Burmeister JJ, Palmer M & Gerhardt GA. (2003). Ceramic-based multisite microelectrode array for rapid choline measures in brain tissue. *Analytica Chimica Acta* **481,** 65-74.

Buyukuysal RL, Ulus IH, Aydin S & Kiran BK. (1995). 3,4-Diaminopyridine and choline increase in vivo acetylcholine release in rat striatum. *European Journal of Pharmacology* **281,** 179-185.

Calabresi P, Centonze D, Gubellini P, Pisani A & Bernardi G. (2000). Acetylcholine-mediated modulation of striatal function. *Trends in Neurosciences* **23,** 120-126.

Chang Q, Savage LM & Gold PE. (2006). Microdialysis measures of functional increases in ACh release in the hippocampus with and without inclusion of acetylcholinesterase inhibitors in the perfusate. *Journal of Neurochemistry* **97,** 697-706.

Cuello AAC. (1993). *Cholinergic Function and Disfunction*. Elsevier Science.

Cui J, Kulagina NV & Michael AC. (2001). Pharmacological evidence for the selectivity of in vivo signals obtained with enzyme-based electrochemical sensors. *Journal of Neuroscience Methods* **104,** 183-189.

Damsma G & Fibiger HC. (1991). The effects of anaesthesia and hypothermia on interstitial concentrations of acetylcholine and choline in rat striatum. *Life Sciences* **48,** 2469-2474.

Day J, Damsma G & Fibiger HC. (1991). Cholinergic activity in the rat hippocampus, cortex and striatum correlates with locomotor activity: An in vivo microdialysis study. *Pharmacology Biochemistry and Behavior* **38,** 723-729.

DeBoer P, Heeringa MJ & Abercrombie ED. (1996). Spontaneous release of acetylcholine in striatum is preferentially regulated by inhibitory dopamine D2 receptors. *European Journal of Pharmacology* **317,** 257-262.

Dixon BM, Lowry JP & O'Neill RD. (2002). Characterization *In-Vitro* and *In-Vivo* of the oxygen dependence of an enzyme/polymer biosensor for monitoring brain glucose. *Journal of Neuroscience Methods* **119,** 135-142.

Fillenz M & Lowry JP. (1998). The relation between local cerebral blood flow and extracellular glucose concentration in rat striatum. *Experimental Physiology* **83,** 233-238.

Garguilo MG & Michael AC. (1994). Quantitation of Choline in the Extracellular Fluid of Brain Tissue with Amperometric Microsensors. *Analytical Chemistry* **66,** 2621-2629.

Garguilo MG & Michael AC. (1996). Amperometric microsensors for monitoring choline in the extracellular fluid of brain. *Journal of Neuroscience Methods* **70,** 73-82.

Hartmann J, Kiewert C, Duysen EG, Lockridge O & Klein J. (2008). Choline availability and acetylcholine synthesis in the hippocampus of acetylcholinesterase-deficient mice. *Neurochemistry International* **52,** 972-978.

Hauber W. (1998). Involvement of basal ganglia transmitter systems in movement initiation. *Progress in Neurobiology* **56,** 507-540.

Hu Y, Mitchell KM, Albahadily FN, Michaelis EK & Wilson GS. (1994). Direct measurement of glutamate release in the brain using a dual enzyme-based electrochemical sensor. *Brain Research* **659,** 117-125.

Hut RA & Van der Zee EA. (2011). The cholinergic system, circadian rhythmicity, and time memory. *Behavioural Brain Research* **221,** 466-480.

Huynh GH, Ozawa T, Deen DF, Tihan T & Szoka Jr FC. (2007). Retro-convection enhanced delivery to increase blood to brain transfer of macromolecules. *Brain Research* **1128,** 181-190.

Ikarashi Y, Takahashi A, Ishimaru H, Arai T & Maruyama Y. (1997). Relations between the extracellular concentrations of choline and acetylcholine in rat striatum. *Journal of Neurochemistry* **69,** 1246-1251.

Jiménez-Capdeville ME & Dykes RW. (1996). Changes in cortical acetylcholine release in the rat during day and night: differences between motor and sensory areas. *Neuroscience* **71,** 567-579.

Kemp JM & Powell TPS. (1971). The Structure of the Caudate Nucleus of the Cat: Light and Electron Microscopy. *Philosophical Transactions of the Royal Society of London Series B, Biological Sciences* **262,** 383-401.

Khan AS & Michael AC. (2003). Invasive consequences of using micro-electrodes and microdialysis probes in the brain. *TrAC Trends in Analytical Chemistry* **22,** 503-508.

Koppen A, Klein J, Erb C & Loffelholz K. (1997). Acetylcholine release and choline availability in rat hippocampus: effects of exogenous choline and nicotinamide. *Journal of Pharmacology and Experimental Therapeutics* **282,** 1139-1145.

Krebs-Kraft DL, Rauw G, Baker GB & Parent MB. (2009). Zero net flux estimates of septal extracellular glucose levels and the effects of glucose on septal extracellular GABA levels. *European Journal of Pharmacology* **611,** 44-52.

Kuhar MJ & Murrin LC. (1978). Sodium-Dependent, High Affinity Choline Uptake. *Journal of Neurochemistry* **30,** 15-21.

Lawler HC. (1961). Turnover time of acetylcholinesterase. *Journal of Biological Chemistry* **236,** 2296-2301.

Löffelholz K. (1998). Brain choline has a typical precursor profile. *Journal of Physiology-Paris* **92,** 235-239.

Lonnroth P, Jansson PA & Smith U. (1987). A microdialysis method allowing characterization of intercellular water space in humans. *American Journal of Physiology* **253,** E228-E231.

Lowry JP, Boutelle MG & Fillenz M. (1997). Measurement of brain tissue oxygen at a carbon paste electrode can serve as an index of increases in regional cerebral blood flow. *Journal of Neuroscience Methods* **71,** 177-182.

Lowry JP, Boutelle MG, O'Neill RD & Fillenz M. (1996). Characterization of carbon paste electrodes *In-Vitro* for simultaneous amperometric measurement of changes in oxygen and ascorbic acid concentrations *In-Vivo*. *Analyst* **121,** 761-766.

Lowry JP & Fillenz M. (2001). Real-time monitoring of brain energy metabolism *In-Vivo* using microelectrochemical sensors: the effects of anesthesia. *Bioelectrochemistry* **54,** 39-47.

Lowry JP, Miele M, O'Neill RD, Boutelle MG & Fillenz M. (1998a). An amperometric glucose-oxidase/poly(o-phenylenediamine) biosensor for monitoring brain extracellular glucose: *In-Vivo* characterisation in the striatum of freely-moving rats. *Journal of Neuroscience Methods* **79,** 65-74.

Lowry JP, O'Neill RD, Boutelle MG & Fillenz M. (1998b). Continuous Monitoring of Extracellular Glucose Concentrations in the Striatum of Freely Moving Rats with an Implanted Glucose Biosensor. *Journal of Neurochemistry* **70,** 391-396.

Michel V, Yuan Z, Ramsubir S & Bakovic M. (2006). Choline transport for phospholipid synthesis. *Experimental Biology and Medicine* **231,** 490-504.

Miele M & Fillenz M. (1996). *In-Vivo* determination of extracellular brain ascorbate. *Journal of Neuroscience Methods* **70,** 15-19.

Nakamura A, Suzuki Y, Umegaki H, Ikari H, Tajima T, Endo H & Iguchi A. (2001). Dietary restriction of choline reduces hippocampal acetylcholine release in rats: *In-Vivo* microdialysis study. *Brain Research Bulletin* **56,** 593-597.

Nicholson C & Syková E. (1998). Extracellular space structure revealed by diffusion analysis. *Trends in Neurosciences* **21,** 207-215.

O'Neill RD. (1993). Sensor-tissue interactions in neurochemical analysis with carbon paste electrodes *In-Vivo*. *Analyst* **118,** 433-438.

Pisani A, Bernardi G, Ding J & Surmeier DJ. (2007). Re-emergence of striatal cholinergic interneurons in movement disorders. *Trends in Neuroscience* **30,** 545-553.

Polikov VS, Tresco PA & Reichert WM. (2005). Response of brain tissue to chronically implanted neural electrodes. *Journal of Neuroscience Methods* **148,** 1-18.

Tuček S. (1993). Short-term control of the synthesis of acetylcholine. *Progress in Biophysics and Molecular Biology* **60,** 59-69.

Ungerstedt U & Rostami E. (2004). Microdialysis in neurointensive care. *Current Pharmaceutical Design* **10,** 2145-2152.

Vinson PN & Justice Jr JB. (1997). Effect of neostigmine on concentration and extraction fraction of acetylcholine using quantitative microdialysis. *Journal of Neuroscience Methods* **73,** 61-67.

Wei HM, Chi OZ, Liu X, Sinha AK & Weiss HR. (1994). Nitric oxide synthase inhibition alters cerebral blood flow and oxygen balance in focal cerebral ischemia in rats. *Stroke* **25,** 445-449.

Weiner DM, Levey AI & Brann MR. (1990). Expression of Muscarinic Acetylcholine and Dopamine Receptor mRNAs in Rat Basal Ganglia. *Proceedings of the National Academy of Sciences of the United States of America* **87,** 7050-7054.

Wevers A. (2011). Localisation of pre- and postsynaptic cholinergic markers in the human brain. *Behavioural Brain Research* **221,** 341-355.

Wilson GS & Gifford R. (2005). Biosensors for real-time *In-Vivo* measurements. *Biosensors and Bioelectronics* **20,** 2388-2403.

Wisniewski N, Moussy F & Reichert WM. (2000). Characterization of implantable biosensor membrane biofouling. *Fresenius' Journal of Analytical Chemistry* **366,** 611-621.

Zeisel SH, Da Costa KA, Franklin PD, Alexander EA, Lamont JT, Sheard NF & Beiser A. (1991). Choline, an essential nutrient for humans. *Federation of American Societies for Experimental Biology Journal* **5,** 2093-2098.

Zhou F-M, Wilson CJ & Dani JA. (2002). Cholinergic interneuron characteristics and nicotinic properties in the striatum. *Journal of Neurobiology* **53,** 590-605.

Zwart R & Vijverberg HP. (1997). Potentiation and inhibition of neuronal nicotinic receptors by atropine: competitive and noncompetitive effects. *Molecular Pharmacology* **52,** 886-895.

8. Acetylcholine

8.1. Introduction

The monitoring of extracellular choline has been suggested as indirect monitoring of acetylcholine (Burmeister *et al.*, 2003; Giuliano *et al.*, 2008). This is suggested as choline is the precursor to acetylcholine synthesis (Löffelholz, 1998). Upon acetylcholine synthesis it is rapidly hydrolysed to choline by acetylcholinesterase (AchE). This choline is then taken back up into the cell by the high affinity uptake system. It is this step that is deemed the rate determining step in acetylcholine synthesis (Antonelli *et al.*, 1981; Vinson & Justice Jr, 1997). Although, the suggestion that monitoring choline is an indirect measurement of acetylcholine, modifications to choline sensors have been undertaken in order to monitor acetylcholine directly (Garguilo *et al.*, 1993; Burmeister *et al.*, 2008). In order to monitor acetylcholine, a choline biosensor must incorporate acetylcholinesterase which can convert acetylcholine to choline, which can then be converted to H_2O_2 and detected at the platinum surface (see Section 2.6.3 and Section 2.6.4) (Burmeister *et al.*, 2008). Previous sensors have included the immobilisation of horse radish peroxidase (HRP), choline oxidase and acetylcholinesterase in a cross linked redox polymer on glassy carbon macroelectrodes which has successfully demonstrated the detection of acetylcholine (Garguilo *et al.*, 1993; Garguilo & Michael, 1995)). Alternatively, microelectrode arrays have been modified with AchE on two of the four recording sites for the simultaneous recording of choline and acetylcholine. This sensor has been used to detect theses analytes in the pre frontal cortex (Burmeister *et al.*, 2008) (Bruno *et al.*, 2006). As the choline biosensor has been characterised *in-vitro* and *in-vivo*, this section determines if the modification of the choline biosensor with AchE can be used for the detection of acetylcholine *in-vitro*.

8.2. Experimental

The instrumentation used in this section is described in Section 3.2. All chemicals and solutions are described in detail in Section 3.3. The electrodes were constructed from the 1 mm cylinder choline biosensor design with additional acetylcholinesterase layers.

All data was recorded in PBS at an applied potential of +700 mV *vs* SCE for working electrodes involving constant potential amperometry (CPA) as this is the value used for monitoring H_2O_2 (Lowry & O'Neill, 1994). Initially a choline calibration was performed with aliquots of choline chloride injected (see Section 3.5.1.3) into PBS to compare the choline response of the sensors. The choline calibration was followed with an acetylcholine calibration with aliquots of acetylcholine chloride (see Section 3.5.1.4).

The data is reported as mean ± SEM, n = number of electrodes, unless otherwise stated. The SEM is given as three significant figures and the number of significant figures for the mean is determined by the size of the SEM. The significant differences observed were estimated using a two-tailed *t*-test. Paired tests were used for comparing signals recorded with the same electrodes, unpaired tests were carried out on data from different electrodes.

Choline calibration data in this section represented the linear region of the enzyme kinetics therefore linear regression analysis was performed. The acetylcholine data obeyed Michaelis-Menten Hill-type enzyme kinetics (see Section 2.6.2).

The initial choline calibration was used to determine the effect on choline sensitivity which is carried on as an acetylcholine calibration.

8.3. Results and discussion

The results section comprises the data from the development experiments for the acetylcholine sensor. Data is shown comparing the layering effect of acetylcholinesterase on both the choline sensitivity and the acetylcholine sensitivity.

8.3.1. AchE x1

Acetylcholine cannot be directly measured with a one enzyme biosensor as the hydrolysis of Ach by AchE generates choline. This liberated choline however can be measured with the choline biosensor where the development and characterisation has been described in this thesis. The choline biosensor requires the addition of AchE to convert acetylcholine to choline, this choline will then generate H_2O_2 through enzymatic turnover by choline oxidase. Monitoring the H_2O_2 is a direct measurement of the Ach. Initial experiments were undertaken in order to determine if one layer of AchE can be used for the detection of Ach.

8.3.1.1. Choline

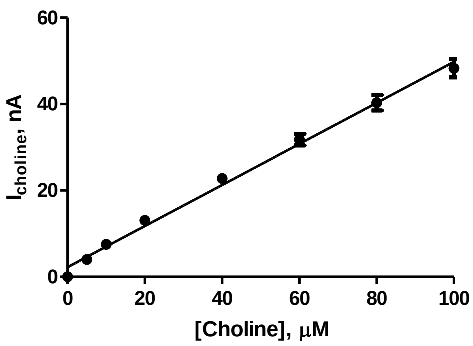

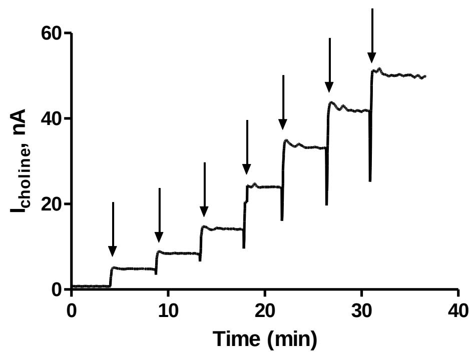

Conc, μM	Mean, nA	S.E.M, nA	n
0	0.00	0.00	4
5	4.01	0.17	4
10	7.55	0.31	4
20	13.06	0.55	4
40	22.77	0.98	4
60	31.77	1.36	4
80	40.32	1.79	4
100	48.30	2.15	4

Figure 8.1 : The current-concentration profile and table for choline chloride calibration in PBS (pH 7.4) buffer solution at 21°C using design (MMA)(CelAce)(MMA)-(ChOx)(BSA)(GA)(PEI)$_{10}$)(AchEx1). CPA carried out at +700 mV *vs.* SCE. Sequential current steps for 5, 10, 20, 40, 60, 80, 100 µM choline chloride injections.

Demonstrated in Section 5.3.4.1 the $I_{100\ \mu M}$ current observed at the choline biosensor is 61.19 ± 10.06 nA, n = 3. The data in Figure 8.1 demonstrates that the choline current of the acetylcholine sensor which incorporates 1 layer of AchE is not significantly reduced (P = 0.2026) to 48.30 ± 2.15 nA, n = 4.

8.3.1.2. Acetylcholine

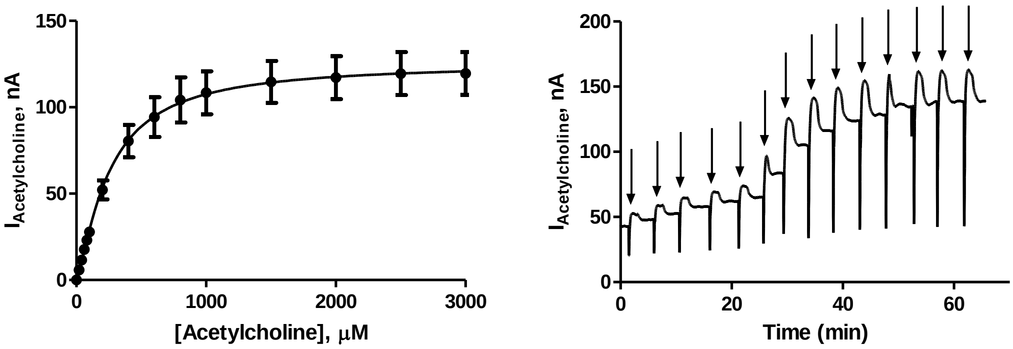

Conc, µM	Mean, nA	S.E.M, nA	n
0	0.00	0.00	4
20	5.85	0.54	4
40	11.50	1.02	4
60	17.70	1.45	4
80	23.02	1.96	4
100	27.82	2.67	4
200	52.17	5.45	4
400	80.43	9.40	4
600	94.33	11.53	4
800	104.22	13.04	4
1000	108.42	12.44	4
1500	114.68	12.17	4
2000	117.18	12.44	4
2500	119.46	12.43	4
3000	119.61	12.38	4

Figure 8.2 : The current-concentration profile and table for acetylcholine chloride calibration in PBS (pH 7.4) buffer solution at 21°C using design (MMA)(CelAce)(MMA)-

(ChOx)(BSA)(GA)(PEI)$_{10}$)(AchEx1). CPA carried out at +700 mV *vs*. SCE. Sequential current steps for 20, 40, 60, 80, 100, 200, 400, 600, 800, 1000, 1500, 2000, 2500 and 3000 μM acetylcholine chloride injections.

The data presented in Figure 8.2 demonstrates that one layer of AchE is sufficient to hydrolyse the acetylcholine to choline. This is understandable as the one molecule of AchE can hydrolyse 5000 molecules of Ach per second (Lawler, 1961). In addition, the choline sensitivity has remained intact which has allowed for detection of the liberated choline to generate the signal. The $I_{20\mu M}$ Ach current obtained with this design is 5.85 ± 0.54 nA, n = 4. The 20 μM value chosen as the comparison value as an arbitrary calibration concentration to compare as the basal acetylcholine concentration is unknown.

8.3.2. AchE x3

One layer of AchE has demonstrated a non significant decrease in the choline current also demonstrating detecting Ach. This section determines the effect of three layers of AchE on both the choline sensitivity; which is required for detection of the liberated choline and the Ach sensitivity, which will increase if the AchE loading is increased, however not obstructing access to the choline oxidase in the lower layers.

8.3.2.1. Choline

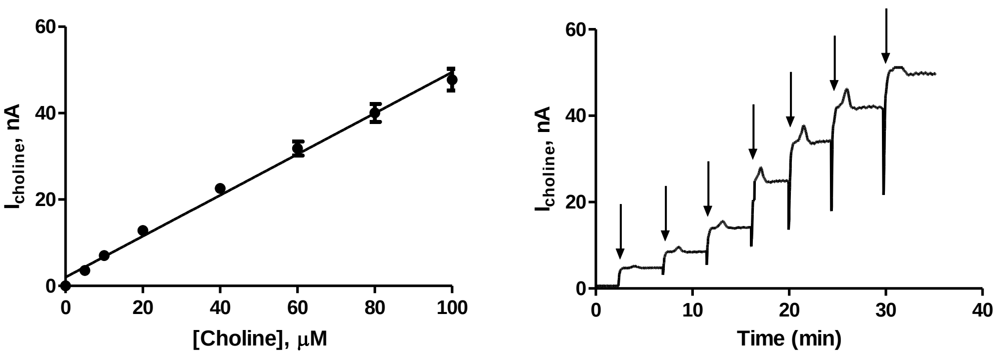

Conc, µM	Mean, nA	S.E.M, nA	n
0	0.00	0.00	16
5	3.56	0.20	12
10	7.02	0.33	16
20	12.84	0.58	16
40	22.58	1.06	16
60	31.80	1.64	16
80	40.07	2.08	16
100	47.75	2.54	16

Figure 8.3 : The current-concentration profile and table for choline chloride calibration in PBS (pH 7.4) buffer solution at 21°C using design (MMA)(CelAce)(MMA)-(ChOx)(BSA)(GA)(PEI)$_{10}$)(AchEx3). CPA carried out at +700 mV *vs.* SCE. Sequential current steps for 5, 10, 20, 40, 60, 80, 100 µM choline chloride injections.

The data in Figure 8.3 demonstrates that the $I_{100\ \mu M}$ choline current at the acetylcholine sensor which incorporates 3 layers of AchE is not significantly reduced (P = 0.9181) to 47.75 ± 2.54 nA, n = 16 (3 layers) from 48.30 ± 2.15 nA, n = 4 (1 layer). This current is also not a significant reduction (P = 0.0749) from the $I_{100\ \mu M}$ current observed at the unmodified choline biosensor (61.19 ± 10.06 nA, n = 3).

8.3.2.2. Acetylcholine

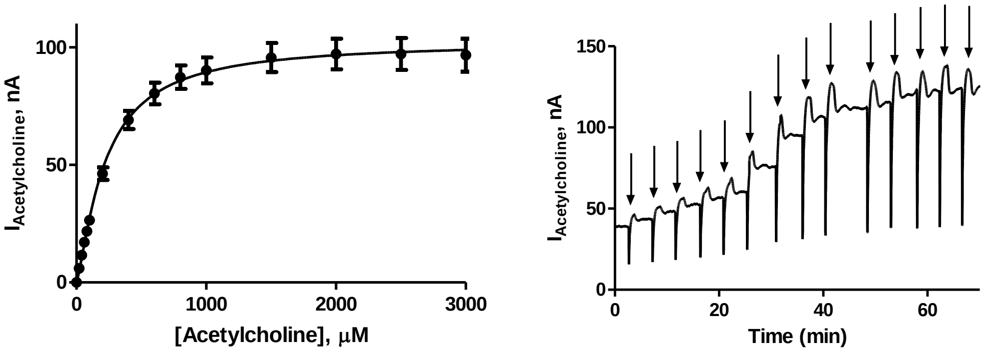

Conc, µM	Mean, nA	S.E.M, nA	n
0	0.00	0.00	16
20	6.05	0.38	16
40	11.64	0.72	16
60	17.14	1.14	16
80	21.74	1.42	16
100	26.44	1.71	16
200	46.28	2.67	16
400	69.08	3.86	16
600	80.31	4.59	16
800	87.26	5.03	16
1000	90.17	5.47	16
1500	95.60	6.17	16
2000	97.09	6.52	16
2500	97.12	6.82	16
3000	96.62	7.00	16

Figure 8.4: The current-concentration profile and table for acetylcholine chloride calibration in PBS (pH 7.4) buffer solution at 21°C using design (MMA)(CelAce)(MMA)-(ChOx)(BSA)(GA)(PEI)$_{10}$)(AchEx3). CPA carried out at +700 mV vs. SCE. Sequential current steps for 20, 40, 60, 80, 100, 200, 400, 600, 800, 1000, 1500, 2000, 2500 and 3000 µM acetylcholine chloride injections.

The data presented in Figure 8.4 demonstrated that one layer of AchE is sufficient to hydrolyse the acetylcholine to choline. Increasing the AchE layers from 1 to 3 has not significantly increased (P = 0.5708) the $I_{20\mu M}$ Ach current from 5.85 ± 0.54 nA, n = 4 (1 layer) to 6.05 ± 0.38 nA, n = 16 (3 layers). The increase in AchE layers has allowed for increased detection of Ach meanwhile not having a detrimental effect on the efficiency of the choline biosensor to detect the liberated choline.

8.3.3. AchE x 5

As increasing the AchE layers from 1 to 3 increased the Ach detection meanwhile not significantly decreasing the choline sensitivity, the number of layers of AchE were increased to 5.

8.3.3.1. Choline

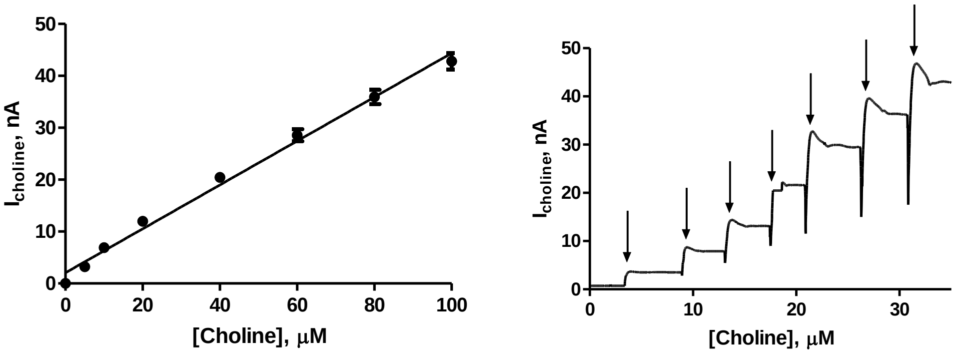

Conc, µM	**Mean, nA**	**S.E.M, nA**	**n**
0	0.00	0.00	8
5	3.21	0.13	8
10	6.89	0.34	8
20	11.96	0.60	8
40	20.43	0.86	8
60	28.57	1.17	8
80	35.93	1.38	8
100	42.82	1.58	8

Figure 8.5 : The current-concentration profile and table for choline chloride calibration in PBS (pH 7.4) buffer solution at 21°C using design (MMA)(CelAce)(MMA)-(ChOx)(BSA)(GA)(PEI)$_{10}$)(AchEx5). CPA carried out at +700 mV *vs*. SCE. Sequential current steps for 5, 10, 20, 40, 60, 80, 100 µM choline chloride injections.

The data in Figure 8.5 demonstrates that the $I_{100\ \mu M}$ choline current at the acetylcholine sensor which incorporates 5 layers of AchE is not significantly reduced (*P* = 0.2072) to 42.82 ± 1.58 nA, n = 8 (5 layers) from 47.75 ± 2.54 nA, n = 16 (3 layers). This current is a significant reduction (*P* = 0.0155) from the $I_{100\ \mu M}$ current observed at the unmodified choline biosensor (61.19 ± 10.06 nA, n = 3).

8.3.3.2. Acetylcholine

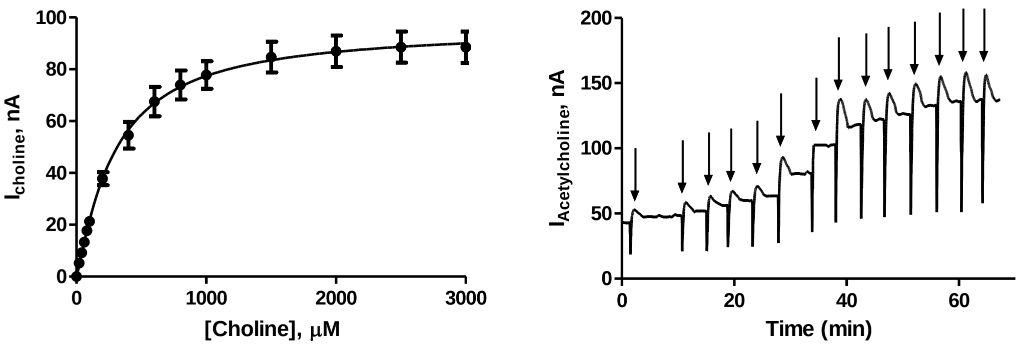

Conc, μM	**Mean, nA**	**S.E.M, nA**	**n**
0	0.00	0.00	8
20	5.20	0.37	8
40	9.21	0.63	8
60	13.27	0.89	8
80	17.68	0.99	8
100	21.30	1.15	8
200	37.79	2.49	8
400	54.57	5.17	8
600	67.53	5.64	8
800	73.97	5.57	8
1000	77.77	5.33	8
1500	84.71	5.94	8
2000	86.98	6.10	8
2500	88.52	6.00	8
3000	88.53	6.04	8

Figure 8.6 : The current-concentration profile and table for acetylcholine chloride calibration in PBS (pH 7.4) buffer solution at 21°C using design (MMA)(CelAce)(MMA)-(ChOx)(BSA)(GA)(PEI)$_{10}$)(AchEx5). CPA carried out at +700 mV *vs*. SCE. Sequential current steps for 20, 40, 60, 80, 100, 200, 400, 600, 800, 1000, 1500, 2000, 2500 and 3000 μM acetylcholine chloride injections.

The data presented in Figure 8.6 demonstrates increasing the AchE layers from 3 to 5 has not significantly decreased (P = 0.1710) the $I_{20\mu M}$ Ach current from 6.05 ± 0.38 nA, n = 16 (3 layers) to 5.20 ± 0.37 nA, n = 8 (5 layers). The increase in AchE layers has reduced the detection choline and Ach. The Ach current has reduced as a result of increasing the AchE, this may be as a result of the decrease in the choline sensitivity observed. The AchE may have blocked the access of the liberated choline thereby decreasing the current observed.

8.3.4. AchE x 10

The number of AchE layers was increased to 10 in order to determine if this could increase the Ach current observed and if the increased layering would further decrease the choline current observed.

8.3.4.1. Choline

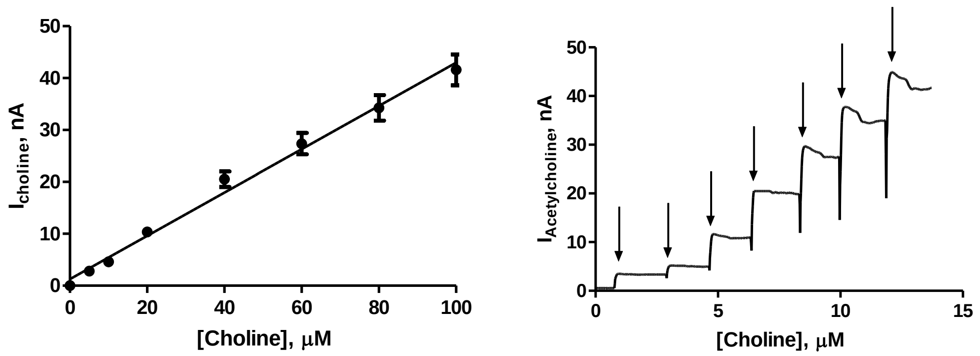

Conc, µM	**Mean, nA**	**S.E.M, nA**	**n**
0	0.00	0.00	4
5	2.83	0.19	4
10	4.59	0.31	4
20	10.36	0.72	4
40	20.52	1.51	4
60	27.36	2.06	4
80	34.27	2.45	4
100	41.60	2.97	4

Figure 8.7 : The current-concentration profile and table for choline chloride calibration in PBS (pH 7.4) buffer solution at 21°C using design (MMA)(CelAce)(MMA)-(ChOx)(BSA)(GA)(PEI)$_{10}$)(AchEx10). CPA carried out at +700 mV *vs.* SCE. Sequential current steps for 5, 10, 20, 40, 60, 80, 100 µM choline chloride injections.

The data in Figure 8.7 demonstrates that the $I_{100\ \mu M}$ choline current at the acetylcholine sensor which incorporates 10 layers of AchE is not significantly reduced (*P* = 0.6962) to 41.60 ± 2.97 nA, n = 4 (10 layers) from 42.82 ± 1.58 nA, n = 8 (5 layers). This current is not a significant reduction (*P* = 0.0845) from the $I_{100\ \mu M}$ current observed at the unmodified choline biosensor (61.19 ± 10.06 nA, n = 3). The additional 5 layers did not demonstrate a significant reduction in the choline sensitivity.

8.3.4.2. Acetylcholine

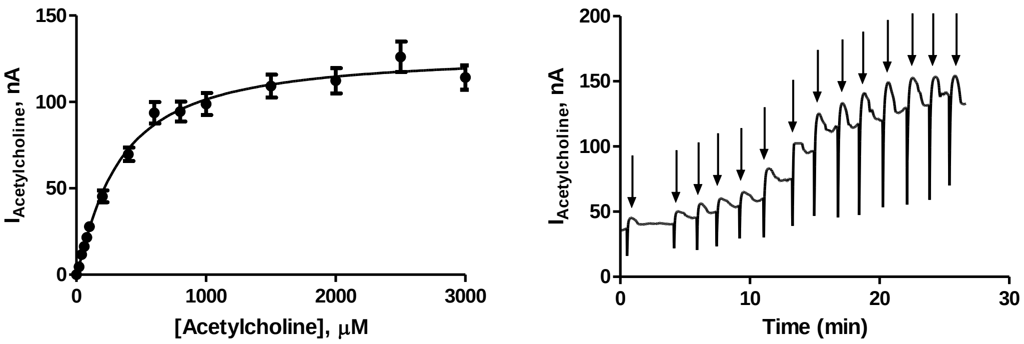

Conc, µM	Mean, nA	S.E.M, nA	n
0	0.00	0.00	4
20	4.54	0.31	4
40	11.64	1.03	4
60	16.34	1.63	4
80	21.58	1.86	4
100	27.76	2.45	4
200	45.34	3.42	4
400	69.71	3.85	4
600	93.73	6.22	4
800	94.43	5.73	4
1000	98.82	6.42	4
1500	109.17	6.64	4
2000	112.27	7.35	4
2500	126.12	8.80	4
3000	114.13	7.11	4

Figure 8.8 : The current-concentration profile and table for acetylcholine chloride calibration in PBS (pH 7.4) buffer solution at 21°C using design (MMA)(CelAce)(MMA)-(ChOx)(BSA)(GA)(PEI)$_{10}$)(AchEx10). CPA carried out at +700 mV *vs*. SCE. Sequential current steps for 20, 40, 60, 80, 100, 200, 400, 600, 800, 1000, 1500, 2000, 2500 and 3000 µM acetylcholine chloride injections.

Increasing the AchE layers from 5 to 10 demonstrated in Figure 8.8 has not significantly decreased (P = 0.2778) the $I_{20\mu M}$ Ach current from 5.20 ± 0.37 nA, n = 8 (5 layers) to 4.54 ± 0.31 nA, n = 4 (10 layers). The increase in AchE layers although not decreasing the choline current significantly, has had a larger effect on Ach sensitivity. It is possible that the additional AchE layers are hindering access of the Ach to the enzyme which is having a larger contribution on the Ach sensitivity than the choline sensitivity.

8.3.5. Comparison

8.3.5.1. Choline

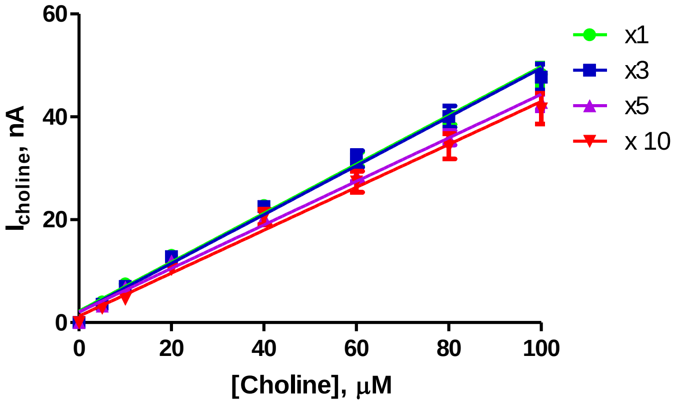

Kinetic Parameters	X1			X3			X5			X10		
	Mean	S.E.M	n	Mean	S.E.M	n	Mean	S.E.M	n	Mean	S.E.M	n
$I_{100\mu M}$, nA	48.30	2.15	4	47.75	2.54	16	42.82	1.58	8	41.59	2.97	4
Sensitivity, nA/µM	0.48	0.02	4	0.48	0.02	16	0.42	0.02	8	0.42	0.02	4
R^2	0.994	0.001	4	0.993	0.001	16	0.992	0.002	8	0.992	0.002	4
Background, nA	0.77	0.10	4	1.68	0.47	16	0.73	0.02	8	0.59	0.04	4

Figure 8.9 : The current-concentration profile comparison and comparison table for acetylcholine chloride calibration in PBS (pH 7.4) buffer solution at 21°C using designs (A) (MMA)(CelAce)(MMA)-(ChOx)(BSA)(GA)(PEI)$_{10}$)(AchEx1), (B) (MMA)(CelAce)(MMA)-(ChOx)(BSA)(GA)(PEI)$_{10}$)(AchEx3), (C) (MMA)(CelAce)(MMA)-(ChOx)(BSA)(GA)(PEI)$_{10}$)(AchEx5) and (D) (MMA)(CelAce)(MMA)-(ChOx)(BSA)(GA)(PEI)$_{10}$)(AchEx10). CPA carried out at +700 mV *vs*. SCE. Sequential current steps for 5, 10, 20, 40, 60, 80, 100 µM choline chloride injections.

Figure 8.9 is a comparison of the choline calibrations performed on the acetylcholine sensor which demonstrates the effect of the AchE layers on the choline sensitivity. As the acetylcholine detection requires the underlying choline oxidase, it is important that the additional layers of AchE are not having a detrimental effect on the choline detection. A choline calibration from 0 – 100 µM was performed to compare the choline sensitivities of the electrodes with the AchE layers. The individual results are presented throughout this section and compared in Figure 8.9. The data demonstrates that increasing the AchE layers from 1 layer to 3 layers is not detrimental to sensitivity as the sensitivity does not change from 0.48 ± 0.02 nA n = 4 (1 layer) to 0.48 ± 0.02 nA n = 16 (3 layers). However, 5 and 10 layers of AchE do decrease the sensitivity although the sensitivities between the two designs are similar. The sensitivity is reduced to 0.42 ± 0.02 nA n = 8 for 5 layers but remains 0.42 ± 0.02 nA n = 4 using 10 layers. The linearity of the trace is reduced by increasing the number of AchE layer of the sensor. The R^2 value was reduced from 0.994 ± 0.001 n = 4 (1 layer) to 0.993 ± 0.001 n = 16 (3 layers). This was reduced to 0.992 ± 0.002 n = 8 (5 layers) which remained the same when incorporating 10 layers (0.992 ± 0.002 n = 4). This data must be interpreted in conjunction with the Ach sensitivities obtained as the optimum Ach detection will ultimately be a fine balance between AchE loading which is sufficient meanwhile not undermining the ChOx sensitivity.

8.3.5.2. Acetylcholine

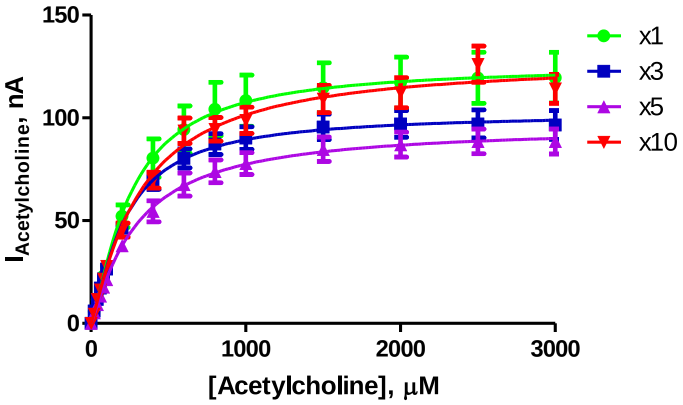

Kinetic Parameters	X1			X3			X5			X10		
	Mean	S.E.M	n	Mean	S.E.M	n	Mean	S.E.M	n	Mean	S.E.M	n
Vmax, nA	125.70	7.05	4	102.40	3.56	16	96.13	4.58	8	128.20	5.67	4
Km, μM	254.00	41.83	4	221.60	23.60	16	293.00	40.22	8	317.70	39.54	4
α	1.30	0.19	4	1.28	0.12	16	1.16	0.12	8	1.16	0.11	4
$I_{20\mu M}$, nA	5.85	0.54	4	6.05	0.38	16	5.20	0.37	8	4.54	0.30	4
Sensitivity, nA/μM	0.28	0.01	4	0.26	0.01	16	0.21	0.01	8	0.28	0.01	4
R^2	0.998	0.001	4	0.996	0.001	16	0.993	0.002	8	0.994	0.004	4

Figure 8.10 : The current-concentration profile comparison and comparison table for acetylcholine chloride calibration in PBS (pH 7.4) buffer solution at 21°C using designs (A) (MMA)(CelAce)(MMA)-(ChOx)(BSA)(GA)(PEI)$_{10}$)(AchEx1), (B) (MMA)(CelAce)(MMA)-(ChOx)(BSA)(GA)(PEI)$_{10}$)(AchEx3), (C) (MMA)(CelAce)(MMA)-(ChOx)(BSA)(GA)(PEI)$_{10}$)(AchEx5) and (D) (MMA)(CelAce)(MMA)-(ChOx)(BSA)(GA)(PEI)$_{10}$)(AchEx10). CPA carried out at +700 mV *vs.* SCE. Sequential current steps for 20, 40, 60, 80, 100, 200, 400, 600, 800, 1000, 1500, 2000, 2500 and 3000 μM acetylcholine chloride injections.

Figure 8.10 is a comparison of the acetylcholine calibrations performed on the acetylcholine sensor which demonstrates the effect of the AchE layers on the acetylcholine sensitivity. The individual calibrations throughout the chapter have demonstrated the effect of the AchE layers on the $I_{20\mu M}$ current value. Increasing the AchE layers from 1 to 3, increased the Ach current accordingly this then decreased with increasing AchE layers. Additional parameters to consider include the V_{MAX}, K_M and α value. The V_{MAX} Ach current was significantly decreased (P = 0.0090) from 125.70 ± 7.05 nA, n=4 (1 layer) to 102.40 ± 3.56 nA, n=16 (3 layers) with increased AchE layers. This was further decreased significantly (P = 0.0046) to 96.13 ± 4.58 nA, n=8 with 5 layers. However the addition of 10 layers increased the V_{MAX} current to 128.20 ± 5.67 nA, n=4 a non significant increase (P = 0.7917) from 1 layer. The increase in the V_{MAX} observed using 10 layers is possibly due to the change in enzyme kinetics observed which can be demonstrated with the extended K_M of this design of 317.70 ± 39.54 µM, n=4. This is not significantly increased (P = 0.3108) from 254.00 ± 41.83 µM, n = 4 using 1 layer. This decreased non significantly (P = 0.5397) using 3 layers to 221.60 ± 23.60 µM, n = 16. This increased non significantly (P = 0.5600) to 293.00 ± 40.22 µM, n=8 using 5 layers. The high K_M concentrations are representative of the increased diffusion constraints caused by additional layering. In addition to the V_{MAX} current and the K_M concentration the α value also demonstrates the effect of the additional layers on the kinetics of the enzyme. Ideal Michaelis-Menten kinetics have an α value of 1. The additional layer of AchE enzyme had an α value of 1.30 (1 layer) this remained similar with 3 layers of AchE (1.28). The incorporation of more layers decreased the α values to 1.16 (5 layers) and 1.16 (10 layers). This data suggests that the incorporation of 3 AchE is the best design for the detection of Ach. Three layers of AchE has high sensitivity to Ach and maintains the choline sensitivity.

8.4. Conclusions

This chapter was undertaken in order to investigate if the choline biosensor could be modified for the detection of acetylcholine. The detection of acetylcholine requires the incorporation of AchE which liberates choline, this choline is then turned over by the ChOx underneath to generate the H_2O_2 which is then detected at the active surface of the electrode. As two enzymes are required for the detection of Ach, a balance must be maintained between optimal AchE loading to sufficiently detect the Ach present, and not over loading the AchE which blocks access for the choline to the underneath ChOx. In order to determine the optimal amount of enzyme loading a comparison was undertaken between 1, 3, 5 and 10 layer of AchE. In order to monitor the balance between Ach and choline sensitivities each design underwent an initial choline calibration followed by an acetylcholine calibration. The choline calibrations for each design were compared demonstrating that the addition of 1 and 3 layer do not differ significantly. There is however a reduction in the sensitivity when compared to the unmodified choline biosensor in Section 5.3.4.1. The Ach calibrations were then compared to determine if additional AchE layers increases Ach detection in spite of a decreasing choline current. The results demonstrate that an excess of AchE on the sensor surface does not increase the Ach detection, however, lower AchE loading, increasing access to the ChOx, is far more beneficial in the detection of Ach. This section has verified that the choline biosensor can be modified to detect Ach and that 3 layers of AchE is optimal for this.

Antonelli T, Beani L, Bianchi C, Pedata F & Pepeu G. (1981). Changes in synaptosomal high affinity choline uptake following electrical stimulation of guinea-pig cortical slices: effect of atropine and physostigmine. *British Journal of Pharmacology* **74,** 525-531.

Bruno JP, Gash C, Martin B, Zmarowski A, Pomerleau F, Burmeister J, Huettl P & Gerhardt GA. (2006). Second-by-second measurement of acetylcholine release in prefrontal cortex. *European Journal of Neuroscience* **24,** 2749-2757.

Burmeister JJ, Palmer M & Gerhardt GA. (2003). Ceramic-based multisite microelectrode array for rapid choline measures in brain tissue. *Analytica Chimica Acta* **481,** 65-74.

Burmeister JJ, Pomerleau F, Huettl P, Gash CR, Werner CE, Bruno JP & Gerhardt GA. (2008). Ceramic-based multisite microelectrode arrays for simultaneous measures of choline and acetylcholine in CNS. *Biosensors and Bioelectronics* **23,** 1382-1389.

Garguilo MG & Michael AC. (1995). Enzyme-modified electrodes for peroxide, choline, and acetylcholine. *TrAC Trends in Analytical Chemistry* **14,** 164-169.

Garguilo MG, Nhan H, Proctor A & Michael AC. (1993). Amperometric sensors for peroxide, choline, and acetylcholine based on electron transfer between horseradish peroxidase and a redox polymer. *Analytical Chemistry* **65,** 523-528.

Giuliano C, Parikh V, Ward JR, Chiamulera C & Sarter M. (2008). Increases in cholinergic neurotransmission measured by using choline-sensitive microelectrodes: enhanced detection by hydrolysis of acetylcholine on recording sites? *Neurochemistry International* **52,** 1343-1350.

Lawler HC. (1961). Turnover time of acetylcholinesterase. *Journal of Biological Chemistry* **236,** 2296-2301.

Löffelholz K. (1998). Brain choline has a typical precursor profile. *Journal of Physiology-Paris* **92,** 235-239.

Lowry JP & O'Neill RD. (1994). Partial Characterization *In-Vitro* of Glucose Oxidase-Modified Poly(phenylenediamine)-coated electrodes for neurochemical analysis *In-Vivo*. *Electroanalysis* **6,** 369-379.

Vinson PN & Justice Jr JB. (1997). Effect of neostigmine on concentration and extraction fraction of acetylcholine using quantitative microdialysis. *Journal of Neuroscience Methods* **73,** 61-67.

9. General Conclusions

Clinical intervention in neurological disorders, which usually act on neuromediator related sites, has demonstrated the importance of understanding intercellular signalling in the brain to understand neuronal networks. The study of neurochemical phenomena in the intact brain has been successful with the utilisation of Long Term *In-Vivo* Electrochemistry (LIVE). This technique allows for *in-situ* detection of substances in the extracellular fluid (ECF). The implantation of electrodes into specific brain regions, application of a suitable potential and recording of the resulting Faradaic current can monitor changes in the concentration of a variety of substance in the ECF with a high temporal resolution over extended periods. This allows for the monitoring of neurochemicals in neuronal signalling, drug actions and behaviours.

The detection of neurochemicals using the LIVE technique is subject to drawbacks. The main limitation is the number of electroactive species in the ECF. The detection of analytes which are not electroactive has been addressed by the development of biosensors. The incorporation of a biological recognition unit for the detection of electroinactive compounds has widened the pool of species which are detectable by the LIVE technique (Garguilo *et al.*, 1993) (Lowry *et al.*, 1994) (McMahon & O'Neill, 2005). In addition, the electroactive compounds present in the ECF, which tend to oxidise at similar potentials, can prove a challenge in resolving the signal for the detection of the desired analyte. The incorporation of permselective membranes has improved the selectivity by blocking interferents when using LIVE (Lowry & O'Neill, 1994) (McAteer & O'Neill, 1996). The use of this technique in intact brain also imposes problems. The composition of the brain tissue; mainly lipids and proteins, can decrease the sensitivity of the sensor once implanted as a result of fouling (Garguilo & Michael, 1994), the natural response of the body to a foreign object can also affect the sensor (Wisniewski *et al.*, 2000). In addition, brain tissue demonstrates restricted mass transport compared to that observed in the *in-vitro* environment (O'Neill, 1993) (Nicholson & Syková, 1998). The aim of this thesis was the development of a choline biosensor. The detection of choline was verified in the *in-vitro* environment and the detection of choline was also demonstrated in the ECF of the brain. This sensor was subsequently modified for the detection of acetylcholine in the *in-vitro* environment.

The development of choline biosensors have been demonstrated previously. Garguilo *et al.* developed an amperometric sensor for the detection of choline by immobilising horse radish peroxidase and choline oxidase onto carbon fibre microcylinder electrodes with a cross-linkable redox polymer (Garguilo & Michael, 1994). This sensor is based on a carbon fibre microcylinder electrode with dimensions of 7 or 10 µm in diameter and 200-400 µm in length. These sensors have considerably smaller dimensions than the 1 mm cylinder electrodes (with a diameter of 125 µm) used in this thesis. They overcome potential interference by operating at an applied potential of -0.1 V (*vs.* SCE) and utilising a Nafion® layer. However, the sensor incorporates a redox mediator which may be prone to leaching. The limit of detection of this sensor is 5 µM choline calibrated at 37 °C with a response time of 15 seconds. Also, exposure of the sensor to brain tissue for several hours results in a 25 % loss in sensitivity to choline. Alternatively, within the Gerhardt research group, Burmeister *et al*. developed a ceramic based multisite microelectrode array for the detection of choline (Burmeister *et al.*, 2003). The dimensions of the array consist of four serial 50 µm x 100 µm recording sites in a row. Two are modified for the detection of choline and two are reference sites. The sensitivity of this array is -13.2 ± 1.7 pA/µM, with a detection limit of 0.4 µM and a response time of 1.4 seconds. The selectivity of the sensor was aided with the incorporation of a layer of Nafion® and the selectivity toward ascorbic acid, uric acid and DOPAC was determined as >300:1. The array was calibrated for O_2 interference and determined that the response of the array *in-vivo* would be 85 % of that *in-vitro* and subject to fluctuations of 15 % over the physiological O_2 concentration range. The sensor was calibrated after *in-vivo* recording and demonstrated a 16 % reduction in the sensitivity. Also within this research group, an alternative choline biosensor was used by Parikh *et al. in-vivo* (Parikh *et al.*, 2004). This sensor used four 15 x 333 µm recording sites that were arranged side by side. The sensor utilised four layers of Nafion® and was subsequently coated with ChOx for choline detection. The sensitivity of this design was increased to 18.7 ± 1.7 pA/µM, the limit of detection was 333 ± 30 nM and the selectivity was reduced to >100:1.

This thesis details the development and characterisation of a new choline biosensor in the *in-vitro* environment. Chapter 4 outlines the work undertaken in order to optimise the sensitivity of the sensor towards choline. This chapter outlined two designs; Sty-

(ChOx)(BSA)(GA)(PEI) and MMA-(ChOx)(BSA)(GA)(PEI) which were continued with for further characterisation. As the sensor design utilises an oxidase enzyme, the determination of the level of oxygen dependence of the sensor was undertaken. The incorporation of perfluorocarbons had proven successful in overcoming O_2 dependence in the development of a glucose biosensor (Wang & Lu, 1998). The perfluorinated polymer Nafion® was previously successful in the development of a lactate biosensor in limiting O_2 interference (Bolger, 2007). This process was mimicked here in an attempt to both replicate the results and determine its mode of action. Chapter 5 demonstrates that the incorporation of Nafion® was not providing an internal O_2 supply as demonstrated by Wang *et al.* using other perfluorocarbons. Rather the Nafion® was increasing the diffusion barrier of the electrode aiding the O_2 dependence. This chapter presented the final modifications of the sensor, a 1 mm cylinder electrode of design (MMA)(CelAce)(MMA)-(ChOx)(BSA)(GA)(PEI) with a sensitivity of 0.58 nA/µM. The O_2 dependence of this sensor was determined at three choline concentrations; 20, 40 and 100 µM choline. The level of O_2 dependence of the sensor was determined with regard to the fluctuation in current observed between the physiologically relevant O_2 concentration of 30, 50 and 80 µM O_2. 20 µM choline was subject to a fluctuation of 3 %, 40 µM choline was subject to a 7 % fluctuation in current and 100 µM choline was subject to an 18 % fluctuation. The fluctuations in current observed with 100 µM choline are comparable to that observed at the microelectrode array, however, the lower concentration of choline far surpasses the level of O_2 interference of the array. Burmeister *et al.* did not observe fluctuations in the level of O_2 interference subject to increasing the choline concentrations, demonstrating a 15 % fluctuation at both 25 and 50 µM choline. This is greatly reduced on the biosensor designed here, ultimately, demonstrating no likely O_2 interference for low choline concentrations suggested by Garguilo *et al.* to be as low as 6 µM (Garguilo & Michael, 1996) *in-vivo* and estimated as 7 µM in chapter 7.

Chapter 6 determined the shelf-life of the biosensor. This sensor was subject to a 10 % drop in sensitivity over a 14 day period at 4°C. The sensor was exposed to brain tissue and demonstrated a 26 % drop in sensitivity over a 14 day period of exposure to brain tissue calibrated on days 1, 3, 5, 7, and 14. The repeated calibrations were investigated and proved to have a negative effect on the sensitivity of the sensor suggesting that the loss in sensitivity may be less than that demonstrated when implanted in the brain as it is not subjected to repeated drying and recalibrating. Other choline sensors were not investigated for their degradation over long periods, however the reduction in sensitivity is in line with Garguilo's reduction of 25 % over several hours and Burmeister's 16 % reductions after acute experiments.

Chapter 6 also outlines the response time of the sensor. This was determined as subsecond recording with a limit of detection of 0.11 µM. This is a reduction from 5 µM experienced with the carbon fibre electrode and 0.4 µM with the Burmeister array and 0.33 µM on the Parikh array. In addition, this chapter discussed other physiologically relevant parameters which can affect analyte detection. The effect of temperature demonstrated that at physiological temperature the sensitivity of the electrode was significantly increased (P = 0.0425) from 0.58 nA/µM to 0.91 nA/µM. Also, the effect of physiological pH, was investigated. Although, ChOx is subject to fluctuation as a result of pH the fluctuations within the physiologically relevant range were minimal. The rejection of endogenous electroactive species was also investigated in this section. The advantage of Garguilo's sensor is that the mediator allows for the application of a potential which does not oxidise these species. In our sensor the electropolymerisation of *o*-phenylenediamine was utilised to form a permselective layer for the rejection of electroactive interference. The sensor was calibrated against twelve relevant species with a detection of 0.182 ± 0.019 nA, and a selectivity ratio of >300:1, a value in line with the selectivity of the Burmeister microarray and improved upon the array utilised by Parikh. These sensors however also use self-referencing in order to further reduce interference. During the *in-vivo* characterisation of the Burmeister array, the self referencing technique was utilised for the removal of potassium-evoked dopamine signals. Dopamine was included in the interference rejection studies of this biosensor and is included in the selectivity value demonstrated.

Both the carbon fibre microelectrode presented by Garguilo *et al*. and the microelectrode array presented by Burmeister *et al.* have undergone *in-vivo* characterisation in the striatum of anaesthetised rats (Garguilo & Michael, 1996) (Cui *et al.*, 2001) (Burmeister *et al.*, 2003) (Burmeister *et al.*, 2008).

The Garguilo carbon fibre microelectrode was initially characterised in the *in-vivo* environment using injections of choline into the tissue with a micropipette mounted adjacent to the sensor (Garguilo & Michael, 1995). Further characterisation was carried out by injections of choline, acetylcholine and a combined solution of acetylcholine and neostigmine (Garguilo & Michael, 1996). In addition, experiments were performed using tetrodotoxin (TTX) and neostigmine (Cui *et al.*, 2001). These experiments demonstrated the detection of choline and the liberated choline from the hydrolysis of acetylcholine in acute experiments by the carbon fibre microelectrode.

The Burmeister microelectrode array was also characterised by the ejection of choline into the tissue using a micropipette attached to the array. This presented problems when utilising the self-referencing technique as the recording sites were not in contact with the same area of brain tissue and H_2O_2 cross-talk at the recording sites. This was followed by ejections of KCl which also demonstrated H_2O_2 cross-talk and interference from dopamine. The latter was subsequently removed when utilising the self-referencing technique, however as the response times of the sensors were not the same due to different thickness of the layers, the self referencing technique was not completely accurate. The uptake of choline was also inhibited with hemicholinium-3 (HC-3). HC-3 was added to the choline solution to accentuate the response to choline however, its addition to the KCl solution did not increase the amplitude of the response. The array utilised by Parikh *et al.* was implanted into the frontoparietal cortex alongside a micropipette. This sensor was characterised by ejections of choline and acetylcholine. The acetylcholine signal was also investigated alongside a co-injection of neostigmine. The effects of nerve terminal depolarisation was investigated by ejection of KCl and the pre-synaptic muscarinic receptor blocker Scopolamine was also used in both the presence and absence of neostigmine. This demonstrated that the choline signal detected was as a result of the direct hydrolysis of Ach.

In chapter 7 the characterisation of the presented choline biosensor was undertaken in the *in-vivo* environment in the striatum of a freely moving rat. Initial experiments were performed to determine that the choline biosensor was capable of responding to perfusions of choline through a microdialysis probe attached to the choline biosensor. This was achieved by perfusing the choline solution from an aCSF baseline, demonstrating the capability of detection, and the local perfusion from baseline. The perfusion of choline from baseline demonstrated linear detection of the analyte with increasing choline concentrations which resulted in a ZNF value of 565 µM. This value is largely different to the ECF concentration value proposed by Garguilo *et al.* of 6 µM (Garguilo & Michael, 1996). An estimation of the ECF concentration from baseline data however, yielded a concentration of 7.93 µM, a value more in-line with previous findings. The baseline data was also used to demonstrate a 14 % decrease in current over the 14 days of implantation, a value comparable with *in-vitro* data. The level of O_2 interference of the sensor was extensively characterised in the *in-vitro* environment. The importance of the test *in-vivo* was examined. The sensor was characterised using chloral hydrate, Diamox and L-NAME in order to increase and decrease the levels of O_2 surrounding the sensor. In combination, these experiments determined that the sensor is not subject to O_2 interference *in-vitro* or *in-vivo*. Pharmacological studies were carried out on the biosensor in order to manipulate aspects of the cholinergic system to determine if the sensor was capable of detecting them. Initially, atropine was administered in order to increase the rate of uptake of choline via the high affinity choline uptake system (HACU). This was demonstrated with a decrease in current observed at the sensor of approximately 2.13 ± 0.28 µM. HC-3 was then perfused through a MD probe in order to inhibit the uptake of choline which was observed with an increase in concentration of approximately 0.32 ± 0.16 µM. Another aspect of the cholinergic system which was manipulated was the hydrolysis of acetylcholine to choline by AchE. This process was inhibited by the perfusion of neostigmine through a MD probe which decreased the current observed at the adjacent sensor. This was a calculated decrease of approximately 1.41 ± 0.58 µM choline, which demonstrates a choline response monitored directly as a result of acetylcholine hydrolysis. Monitoring choline in a freely-moving animal illustrated the effect of movement on the choline response, and its correlation with O_2 changes determined. The results show that although the choline response is subject to fluctuations as a result of movement and neuronal activation similar to the O_2 response, the sensor is not subject to O_2 interference.

Chapter 8 demonstrates the modification of the choline biosensor with AchE for the detection of acetylcholine. The sensor design incorporated three layers of AchE giving a final design of (MMA)(CelAce)(MMA)-(ChOx)(BSA)(GA)(PEI)(AchE) with a sensitivity of 0.26 ± 0.01 nA/μM. Previous acetylcholine sensors have been reported by Garguilo *et al.* - this prototype sensor was a macro glassy carbon electrode which successfully detected acetylcholine *in-vitro* (Garguilo & Michael, 1995). In addition, Burmeister *et al.* have developed an acetylcholine microelectrode array (Burmeister *et al.*, 2008). The sensitivity of this electrode was found to be 0.0047 nA/μM. This sensor was shown to be capable of functioning in the *in-vivo* environment responding to Ach and KCl applications in the striatum of anaesthetised rats. Additionally, the sensors were investigated for their response to Ach and KCl in the pre-frontal cortex of anaesthetised rats (Bruno *et al.*, 2006).

Progression of this body of work will include the *in-vitro* and *in-vivo* characterisation of the acetylcholine sensor. In addition to this, the choline biosensor will be used in an animal model for delirium. Delirium is an acute and transient cognitive impairment with particular disruption of attention. It is highly prevalent in the aged and demented population (Fong *et al.*, 2009). It is widely accepted that an acute cholinergic insufficiency is a key feature of delirium (Trzepacz, 2000). In collaboration with Dr. Colm Cunningham (Trinity College Dublin) who has developed an animal model of delirium during dementia; by inducing systemic inflammation, the choline biosensor will be used to characterise the impact of this inflammation on the release and metabolism of acetylcholine in the hippocampus and frontal cortex during behavioural testing.

Bolger FB. (2007). The *In-Vitro* and *In-Vivo* Characterisation and Application of Real-Time Sensors and Biosensors for Neurochemical Studies of Brain Energy Metabolism. National University of Ireland, Maynooth, Maynooth.

Bruno JP, Gash C, Martin B, Zmarowski A, Pomerleau F, Burmeister J, Huettl P & Gerhardt GA. (2006). Second-by-second measurement of acetylcholine release in prefrontal cortex. *European Journal of Neuroscience* **24,** 2749-2757.

Burmeister JJ, Palmer M & Gerhardt GA. (2003). Ceramic-based multisite microelectrode array for rapid choline measures in brain tissue. *Analytica Chimica Acta* **481,** 65-74.

Burmeister JJ, Pomerleau F, Huettl P, Gash CR, Werner CE, Bruno JP & Gerhardt GA. (2008). Ceramic-based multisite microelectrode arrays for simultaneous measures of choline and acetylcholine in CNS. *Biosensors and Bioelectronics* **23,** 1382-1389.

Cui J, Kulagina NV & Michael AC. (2001). Pharmacological evidence for the selectivity of in vivo signals obtained with enzyme-based electrochemical sensors. *Journal of Neuroscience Methods* **104,** 183-189.

Fong TG, Jones RN, Shi P, Marcantonio ER, Yap L, Rudolph JL, Yang FM, Kiely DK & Inouye SK. (2009). Delirium accelerates cognitive decline in Alzheimer disease. *Neurology* **72,** 1570-1575.

Garguilo MG & Michael AC. (1994). Quantitation of Choline in the Extracellular Fluid of Brain Tissue with Amperometric Microsensors. *Analytical Chemistry* **66,** 2621-2629.

Garguilo MG & Michael AC. (1995). Enzyme-modified electrodes for peroxide, choline, and acetylcholine. *TrAC Trends in Analytical Chemistry* **14,** 164-169.

Garguilo MG & Michael AC. (1996). Amperometric microsensors for monitoring choline in the extracellular fluid of brain. *Journal of Neuroscience Methods* **70,** 73-82.

Garguilo MG, Nhan H, Proctor A & Michael AC. (1993). Amperometric sensors for peroxide, choline, and acetylcholine based on electron transfer between horseradish peroxidase and a redox polymer. *Analytical Chemistry* **65,** 523-528.

Lowry JP, McAteer K, El Atrash SS, Duff A & O'Neill RD. (1994). Characterization of Glucose Oxidase-Modified Poly(phenylenediamine)-Coated Electrodes *In-Vitro* and *In-Vivo*: Homogeneous Interference by Ascorbic Acid in Hydrogen Peroxide Detection. *Analytical Chemistry* **66,** 1754-1761.

Lowry JP & O'Neill RD. (1994). Partial Characterization *In-Vitro* of Glucose Oxidase-Modified Poly(phenylenediamine)-coated electrodes for neurochemical analysis *In-Vivo*. *Electroanalysis* **6,** 369-379.

McAteer K & O'Neill RD. (1996). Strategies for decreasing ascorbate interference at glucose oxidase-modified poly(o-phenylenediamine)-coated electrodes. *Analyst* **121,** 773-777.

McMahon CP & O'Neill RD. (2005). Polymer−Enzyme Composite Biosensor with High Glutamate Sensitivity and Low Oxygen Dependence. *Analytical Chemistry* **77,** 1196-1199.

Nicholson C & Syková E. (1998). Extracellular space structure revealed by diffusion analysis. *Trends in Neurosciences* **21,** 207-215.

O'Neill RD. (1993). Sensor-tissue interactions in neurochemical analysis with carbon paste electrodes *In-Vivo*. *Analyst* **118,** 433-438.

Parikh V, Pomerleau F, Huettl P, Gerhardt GA, Sarter M & Bruno JP. (2004). Rapid assessment of *In-Vivo* cholinergic transmission by amperometric detection of changes in extracellular choline levels. *European Journal of Neuroscience* **20,** 1545-1554.

Trzepacz PT. (2000). Is there a final common neural pathway in delirium? Focus on acetylcholine and dopamine. *Seminars in Clinical Neuropsychiatry* **5,** 132-148.

Wang J & Lu F. (1998). Oxygen-Rich Oxidase Enzyme Electrodes for Operation in Oxygen-Free Solutions. *Journal of the American Chemical Society* **120,** 1048-1050.

Wisniewski N, Moussy F & Reichert WM. (2000). Characterization of implantable biosensor membrane biofouling. *Fresenius' Journal of Analytical Chemistry* **366,** 611-621.

Appendix 1
Development

4.3.5. Units increase

A

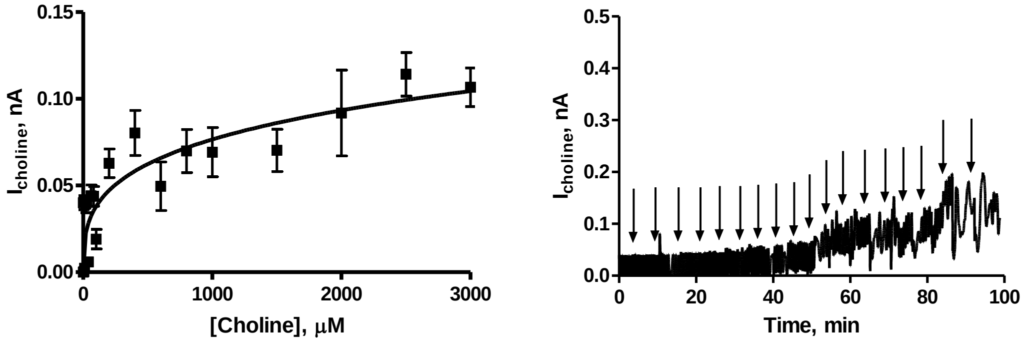

B

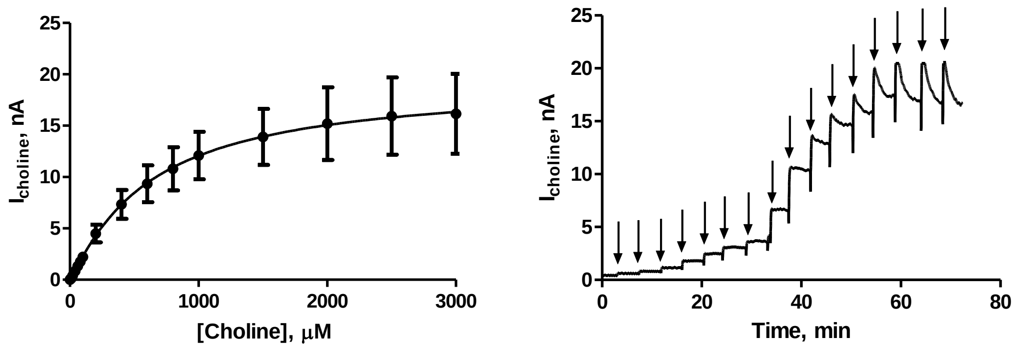

Figure 1 : The current-concentration profiles and raw data traces for choline chloride calibrations in PBS (pH 7.4) buffer solution at 21°C using designs (A) Sty-$(ChOx)_{10}$-GA (50U) and (B) Sty-$(ChOx)_{10}$-GA 500U. CPA carried out at +700 mV *vs*. SCE. Sequential current steps for 5, 10, 20, 40, 60, 80, 100, 200, 400, 600, 800, 1000, 1500, 2000, 2500 and 3000 μM choline chloride injections.

	Sty-(ChOx)$_{10}$-GA 50U			Sty-(ChOx)$_{10}$-GA 500U		
Conc, µM	**Mean, nA**	**S.E.M, nA**	**n**	**Mean, nA**	**S.E.M, nA**	**n**
0	0.00	0.00	4	0.00	0.00	4
5	0.0004	0.002	4	0.10	0.04	4
10	0.002	0.001	4	0.14	0.13	4
20	0.04	0.01	4	0.39	0.17	4
40	0.01	0.01	4	0.84	0.25	4
60	0.04	0.01	4	1.32	0.34	4
80	0.04	0.01	4	1.76	0.41	4
100	0.02	0.01	4	2.21	0.48	4
200	0.06	0.01	4	4.49	0.87	4
400	0.08	0.01	4	7.34	1.41	4
600	0.05	0.01	4	9.35	1.79	4
800	0.07	0.01	4	10.80	2.11	4
1000	0.07	0.01	4	12.10	2.31	4
1500	0.07	0.01	4	13.91	2.73	4
2000	0.09	0.03	4	15.19	3.54	4
2500	0.11	0.01	4	15.93	3.76	4
3000	0.11	0.01	4	16.16	3.90	4

Table 1 : Comparison table of mean current values for designs; (A) Sty-(ChOx)$_{10}$-GA 50U and (B) Sty-(ChOx)$_{10}$-GA 500U. Choline chloride calibrations carried out in PBS (pH 7.4) buffer solution at 21°C. CPA carried out at +700 mV *vs*. SCE. All currents are background subtracted.

4.3.6. GA Layering

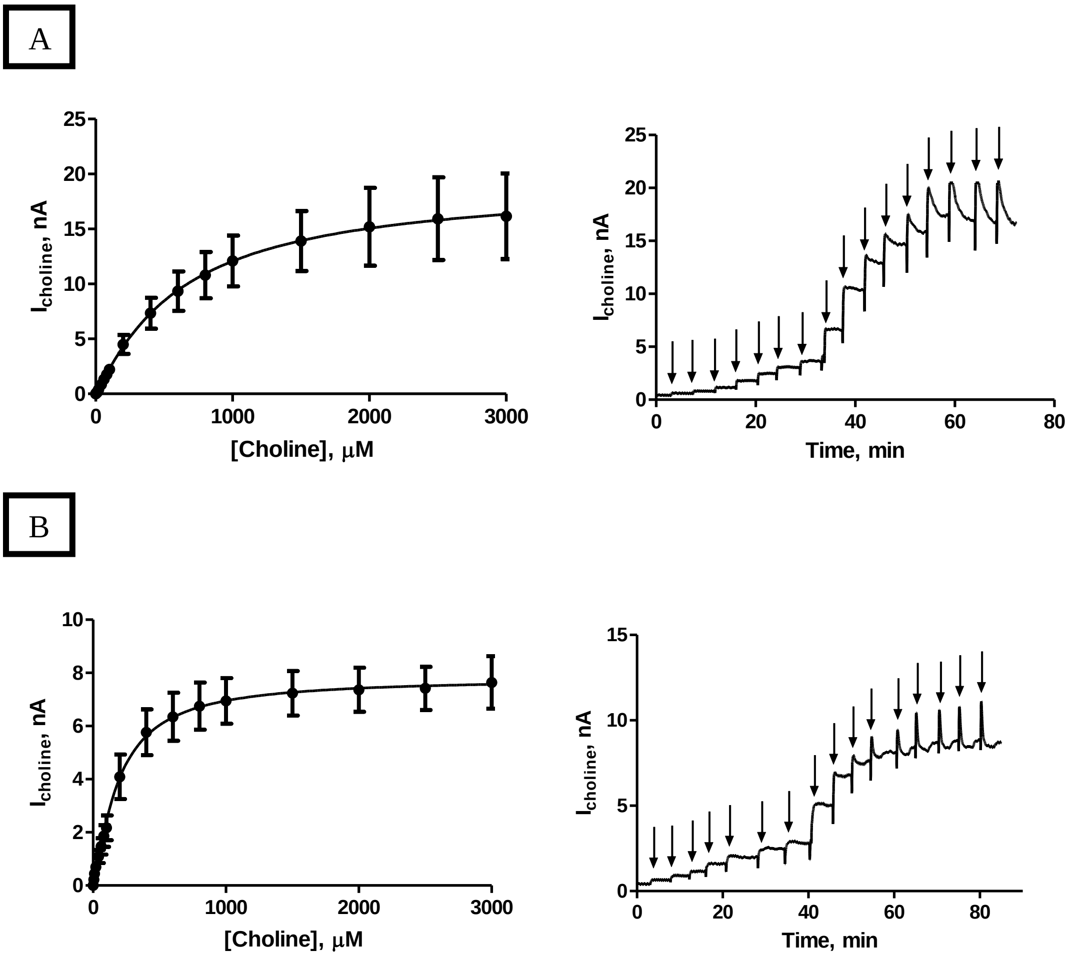

Figure 2 : The current-concentration profiles and raw data traces for choline chloride calibrations in PBS (pH 7.4) buffer solution at 21°C using designs (A) Sty-$(ChOx)_{10}$-GA and (B) Sty-$(ChOx)(GA)_{10}$. CPA carried out at +700 mV *vs*. SCE. Sequential current steps for 5, 10, 20, 40, 60, 80, 100, 200, 400, 600, 800, 1000, 1500, 2000, 2500 and 3000 µM choline chloride injections.

	Sty-(ChOx)$_{10}$-GA			Sty-(ChOx)(GA)$_{10}$		
Conc, μM	**Mean, nA**	**S.E.M, nA**	**n**	**Mean, nA**	**S.E.M, nA**	**n**
0	0.00	0.00	4	0.00	0.00	4
5	0.10	0.04	4	0.22	0.05	4
10	0.14	0.13	4	0.44	0.08	4
20	0.39	0.17	4	0.70	0.14	4
40	0.84	0.25	4	1.10	0.25	4
60	1.32	0.34	4	1.47	0.31	4
80	1.76	0.41	4	1.86	0.41	4
100	2.21	0.48	4	2.17	0.46	4
200	4.49	0.87	4	4.10	0.84	4
400	7.34	1.41	4	5.77	0.86	4
600	9.35	1.79	4	6.35	0.90	4
800	10.80	2.11	4	6.75	0.89	4
1000	12.10	2.31	4	6.95	0.86	4
1500	13.91	2.73	4	7.24	0.84	4
2000	15.19	3.54	4	7.37	0.83	4
2500	15.93	3.76	4	7.42	0.81	4
3000	16.16	3.90	4	7.64	0.99	4

Table 2 : Comparison table of mean current values for designs; (A) Sty-(ChOx)$_{10}$-GA and (B) Sty-(ChOx)(GA)$_{10}$. Choline chloride calibrations carried out in PBS (pH 7.4) buffer solution at 21°C. CPA carried out at +700 mV *vs*. SCE. All currents are background subtracted.

4.3.7. BSA Layering

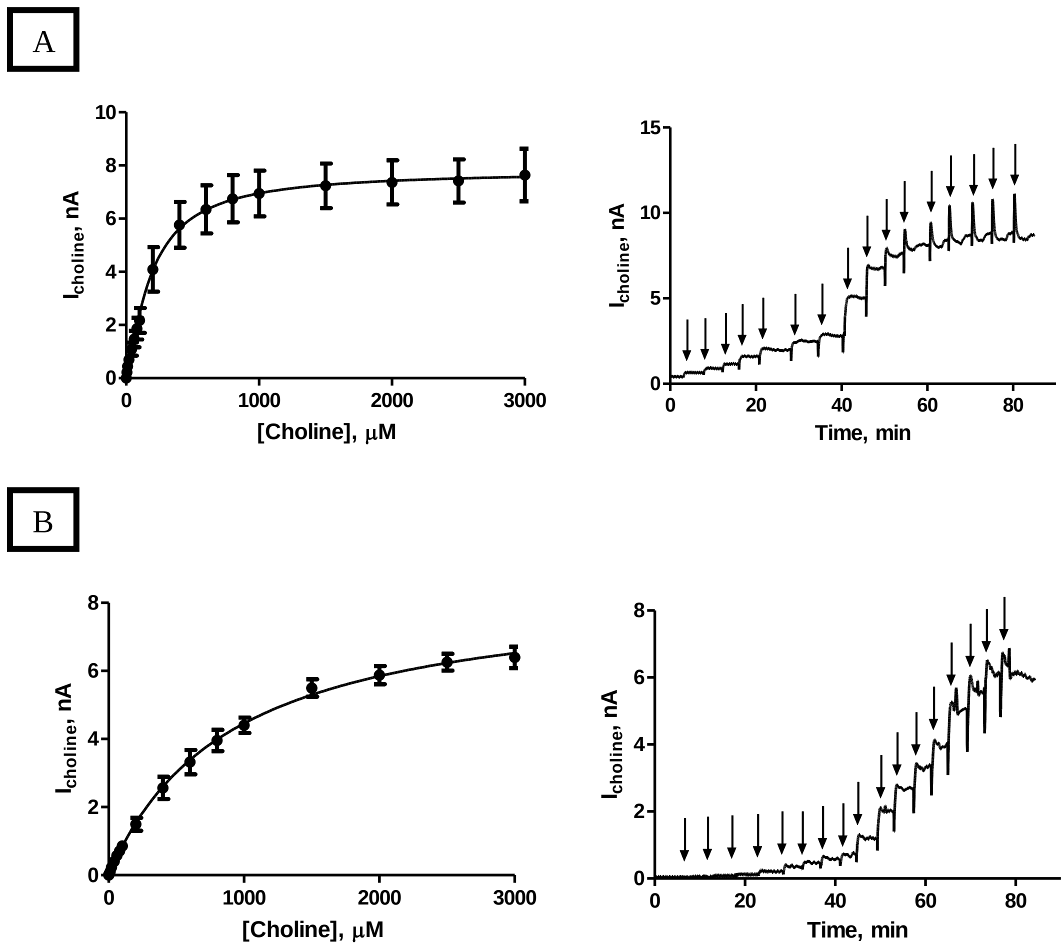

Figure 3 : The current-concentration profiles and raw data traces for choline chloride calibrations in PBS (pH 7.4) buffer solution at 21°C using designs (A) Sty-(ChOx)$(GA)_{10}$ and (B) Sty-(ChOx)(BSA)$(GA)_{10}$. CPA carried out at +700 mV *vs*. SCE. Sequential current steps for 5, 10, 20, 40, 60, 80, 100, 200, 400, 600, 800, 1000, 1500, 2000, 2500 and 3000 μM choline chloride injections.

	Sty-(ChOx)(GA)$_{10}$			Sty-(ChOx)(BSA)(GA)$_{10}$		
Conc, µM	**Mean, nA**	**S.E.M, nA**	**n**	**Mean, nA**	**S.E.M, nA**	**n**
0	0.00	0.00	4	0.00	0.00	3
5	0.22	0.05	4	0.05	0.01	3
10	0.44	0.08	4	0.11	0.01	3
20	0.70	0.14	4	0.23	0.03	3
40	1.10	0.25	4	0.40	0.05	3
60	1.47	0.31	4	0.58	0.08	3
80	1.86	0.41	4	0.71	0.09	3
100	2.17	0.46	4	0.86	0.10	3
200	4.10	0.84	4	1.49	0.19	3
400	5.77	0.86	4	2.56	0.33	3
600	6.35	0.90	4	3.32	0.35	3
800	6.75	0.89	4	3.96	0.31	3
1000	6.95	0.86	4	4.40	0.22	3
1500	7.24	0.84	4	5.50	0.26	3
2000	7.37	0.83	4	5.88	0.27	3
2500	7.42	0.81	4	6.26	0.24	3
3000	7.64	0.99	4	6.40	0.31	3

Table 3 : Comparison table of mean current values for designs; (A) Sty-(ChOx)(GA)$_{10}$ and (B) Sty-(ChOx)(BSA)(GA)$_{10}$. Choline chloride calibrations carried out in PBS (pH 7.4) buffer solution at 21°C. CPA carried out at +700 mV *vs.* SCE. All currents are background subtracted.

4.3.8. PEI Layering

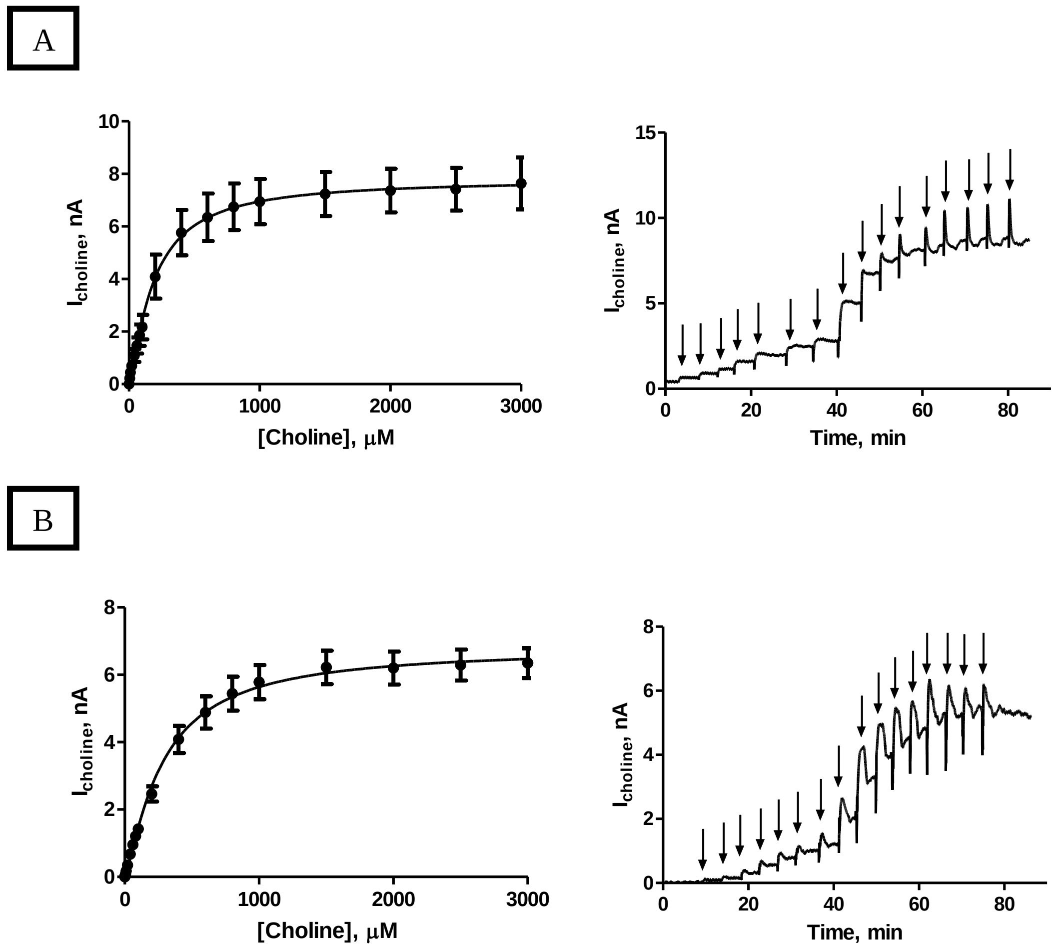

Figure 4 : The current-concentration profiles and raw data traces for choline chloride calibrations in PBS (pH 7.4) buffer solution at 21°C using designs (A) Sty-(ChOx)(GA)$_{10}$ and (B) Sty-(ChOx)(PEI)(GA)$_{10}$. CPA carried out at +700 mV *vs*. SCE. Sequential current steps for 5, 10, 20, 40, 60, 80, 100, 200, 400, 600, 800, 1000, 1500, 2000, 2500 and 3000 µM choline chloride injections.

	Sty-(ChOx)(GA)$_{10}$			Sty-(ChOx)(PEI)(GA)$_{10}$		
Conc, µM	**Mean, nA**	**S.E.M, nA**	**n**	**Mean, nA**	**S.E.M, nA**	**n**
0	0.00	0.00	4	0.00	0.00	3
5	0.22	0.05	4	0.08	0.01	3
10	0.44	0.08	4	0.17	0.02	3
20	0.70	0.14	4	0.35	0.04	3
40	1.10	0.25	4	0.68	0.07	3
60	1.47	0.31	4	0.96	0.10	3
80	1.86	0.41	4	1.21	0.13	3
100	2.17	0.46	4	1.43	0.14	3
200	4.10	0.84	4	2.46	0.23	3
400	5.77	0.86	4	4.08	0.40	3
600	6.35	0.90	4	4.88	0.48	3
800	6.75	0.89	4	5.44	0.50	3
1000	6.95	0.86	4	5.78	0.51	3
1500	7.24	0.84	4	6.22	0.50	3
2000	7.37	0.83	4	6.20	0.49	3
2500	7.42	0.81	4	6.29	0.46	3
3000	7.64	0.99	4	6.35	0.44	3

Table 4 : Comparison table of mean current values for designs; (A) Sty-(ChOx)(GA)$_{10}$ and (B) Sty-(ChOx)(PEI)(GA)$_{10}$. Choline chloride calibrations carried out in PBS (pH 7.4) buffer solution at 21°C. CPA carried out at +700 mV *vs*. SCE. All currents are background subtracted.

4.3.8.1. PEI Layering Position

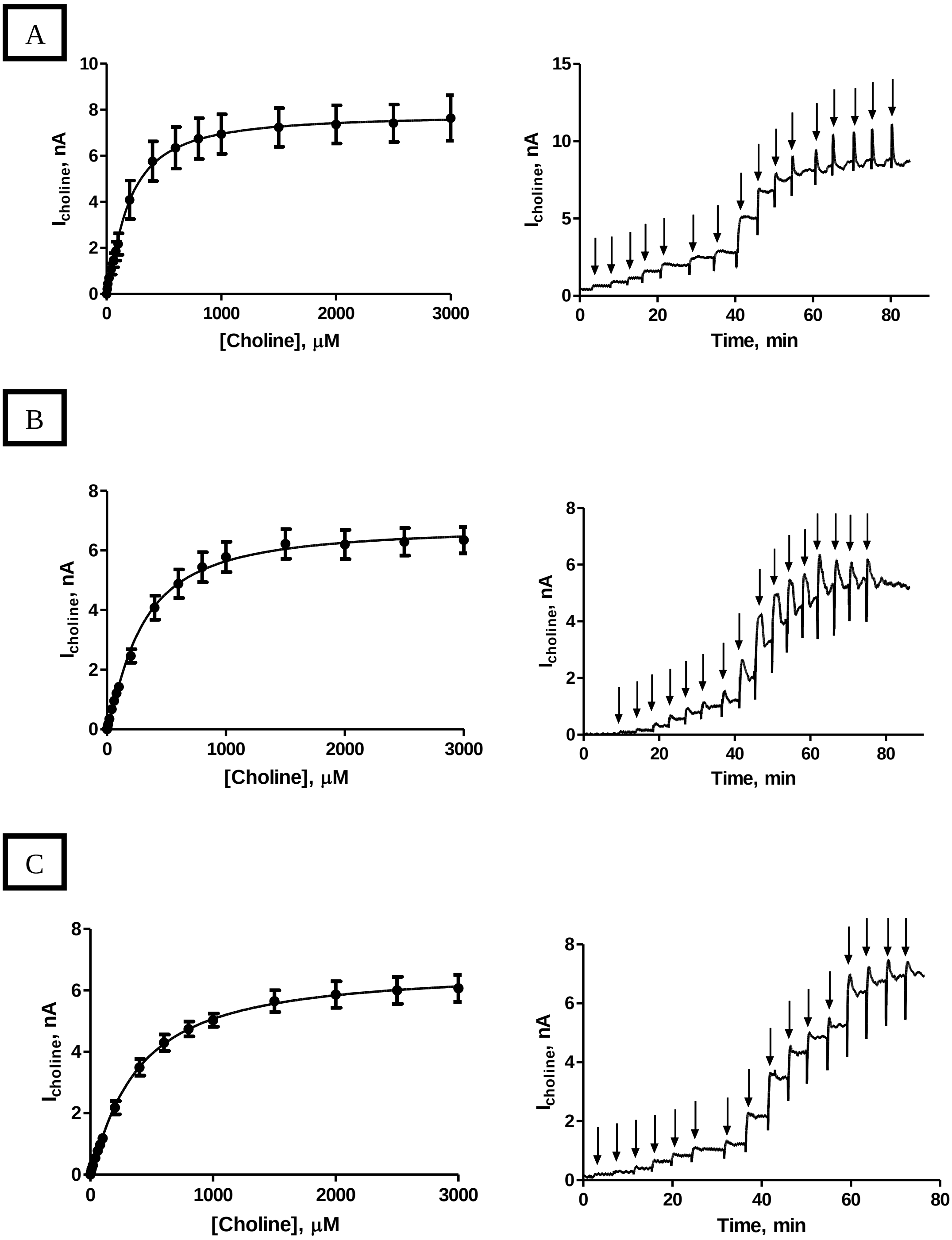

Figure 5 : The current-concentration profiles and raw data traces for choline chloride calibrations in PBS (pH 7.4) buffer solution at 21°C using designs (A) Sty-(ChOx)(GA)$_{10}$, (B) Sty-(ChOx)(PEI)(GA)$_{10}$ and (C) Sty-(ChOx)(GA)(PEI)$_{10}$. CPA carried out at +700 mV *vs.* SCE. Sequential current steps for 5, 10, 20, 40, 60, 80, 100, 200, 400, 600, 800, 1000, 1500, 2000, 2500 and 3000 μM choline chloride injections.

	Sty-(ChOx)(GA)$_{10}$			Sty-(ChOx)(PEI)(GA)$_{10}$			Sty-(ChOx)(GA)(PEI)$_{10}$		
Conc, µM	**Mean, nA**	**S.E.M, nA**	**n**	**Mean, nA**	**S.E.M, nA**	**n**	**Mean, nA**	**S.E.M, nA**	**n**
0	0.00	0.00	4	0.00	0.00	3	0.00	0.00	3
5	0.22	0.05	4	0.08	0.01	3	0.08	0.01	3
10	0.44	0.08	4	0.17	0.02	3	0.18	0.02	3
20	0.70	0.14	4	0.35	0.04	3	0.30	0.04	3
40	1.10	0.25	4	0.68	0.07	3	0.54	0.06	3
60	1.47	0.31	4	0.96	0.10	3	0.78	0.08	3
80	1.86	0.41	4	1.21	0.13	3	0.98	0.11	3
100	2.17	0.46	4	1.43	0.14	3	1.18	0.14	3
200	4.10	0.84	4	2.46	0.23	3	2.18	0.22	3
400	5.77	0.86	4	4.08	0.40	3	3.49	0.27	3
600	6.35	0.90	4	4.88	0.48	3	4.30	0.27	3
800	6.75	0.89	4	5.44	0.50	3	4.74	0.24	3
1000	6.95	0.86	4	5.78	0.51	3	5.03	0.22	3
1500	7.24	0.84	4	6.22	0.50	3	5.65	0.35	3
2000	7.37	0.83	4	6.20	0.49	3	5.87	0.43	3
2500	7.42	0.81	4	6.29	0.46	3	6.00	0.44	3
3000	7.64	0.99	4	6.35	0.44	3	6.07	0.44	3

Table 5 : Comparison table of mean current values for designs; (A) Sty-(ChOx)(GA)$_{10}$ and (B) Sty-(ChOx)(PEI)(GA)$_{10}$ and (C) Sty-(ChOx)(GA)(PEI)$_{10}$. Choline chloride calibrations carried out in PBS (pH 7.4) buffer solution at 21°C. CPA carried out at +700 mV *vs.* SCE. All currents are background subtracted.

4.3.8.2. BSA Layering

A

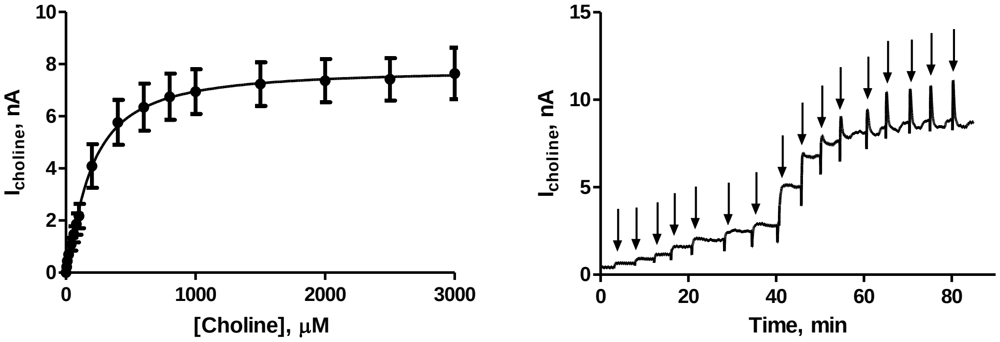

B

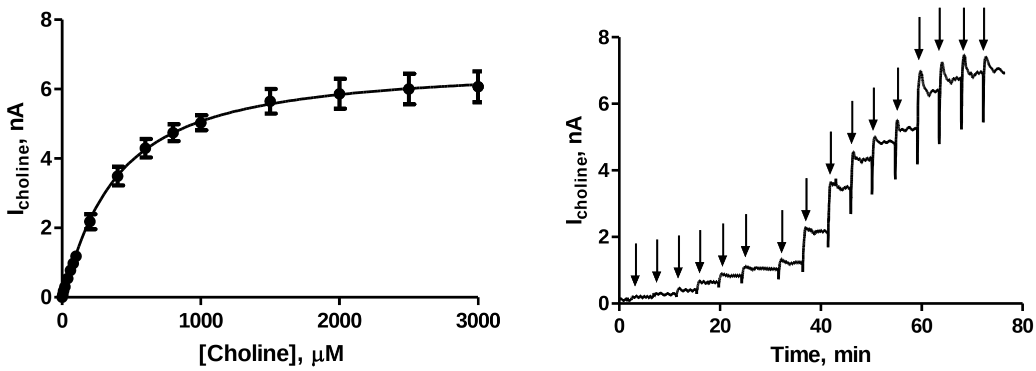

C

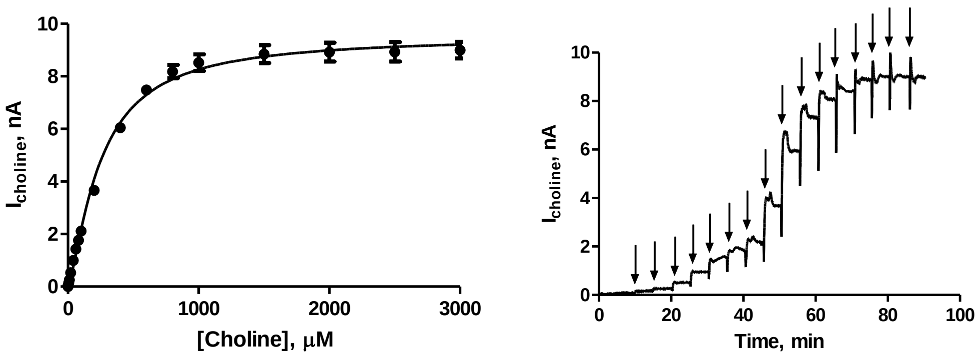

Figure 6 : The current-concentration profiles and raw data traces for choline chloride calibrations in PBS (pH 7.4) buffer solution at 21°C using designs (A) Sty-(ChOx)(GA)$_{10,}$ (B) Sty-(ChOx)(GA)(PEI)$_{10}$ and (C) Sty-(ChOx)(BSA)(GA)(PEI)$_{10}$. CPA carried out at +700 mV *vs.* SCE. Sequential current steps for 5, 10, 20, 40, 60, 80, 100, 200, 400, 600, 800, 1000, 1500, 2000, 2500 and 3000 μM choline chloride injections.

	Sty-(ChOx)(GA)$_{10}$			Sty-(ChOx)(GA)(PEI)$_{10}$			Sty-(ChOx)(BSA)(GA)(PEI)$_{10}$		
Conc, µM	**Mean, nA**	**S.E.M, nA**	**n**	**Mean, nA**	**S.E.M, nA**	**n**	**Mean, nA**	**S.E.M, nA**	**n**
0	0.00	0.00	4	0.00	0.00	3	0.00	0.00	4
5	0.22	0.05	4	0.08	0.01	3	0.14	0.01	4
10	0.44	0.08	4	0.18	0.02	3	0.25	0.01	4
20	0.70	0.14	4	0.30	0.04	3	0.53	0.02	4
40	1.10	0.25	4	0.54	0.06	3	0.99	0.03	4
60	1.47	0.31	4	0.78	0.08	3	1.43	0.04	4
80	1.86	0.41	4	0.98	0.11	3	1.76	0.03	4
100	2.17	0.46	4	1.18	0.14	3	2.11	0.04	4
200	4.10	0.84	4	2.18	0.22	3	3.66	0.07	4
400	5.77	0.86	4	3.49	0.27	3	6.10	0.12	4
600	6.35	0.9	4	4.30	0.27	3	7.48	0.19	4
800	6.75	0.89	4	4.74	0.24	3	8.18	0.26	4
1000	6.95	0.86	4	5.03	0.22	3	8.52	0.32	4
1500	7.24	0.84	4	5.65	0.35	3	8.85	0.34	4
2000	7.37	0.83	4	5.87	0.43	3	8.92	0.36	4
2500	7.42	0.81	4	6.00	0.44	3	8.93	0.37	4
3000	7.64	0.99	4	6.07	0.44	3	8.99	0.32	4

Table 6 : Comparison table of mean current values for designs; (A) Sty-(ChOx)(GA)$_{10}$ and (B) Sty-(ChOx)(PEI)(GA)$_{10}$ (C) Sty-(ChOx)(GA)(PEI)$_{10}$. Choline chloride calibrations carried out in PBS (pH 7.4) buffer solution at 21°C. CPA carried out at +700 mV *vs*. SCE. All currents are background subtracted.

4.3.9.1. PEI Concentration

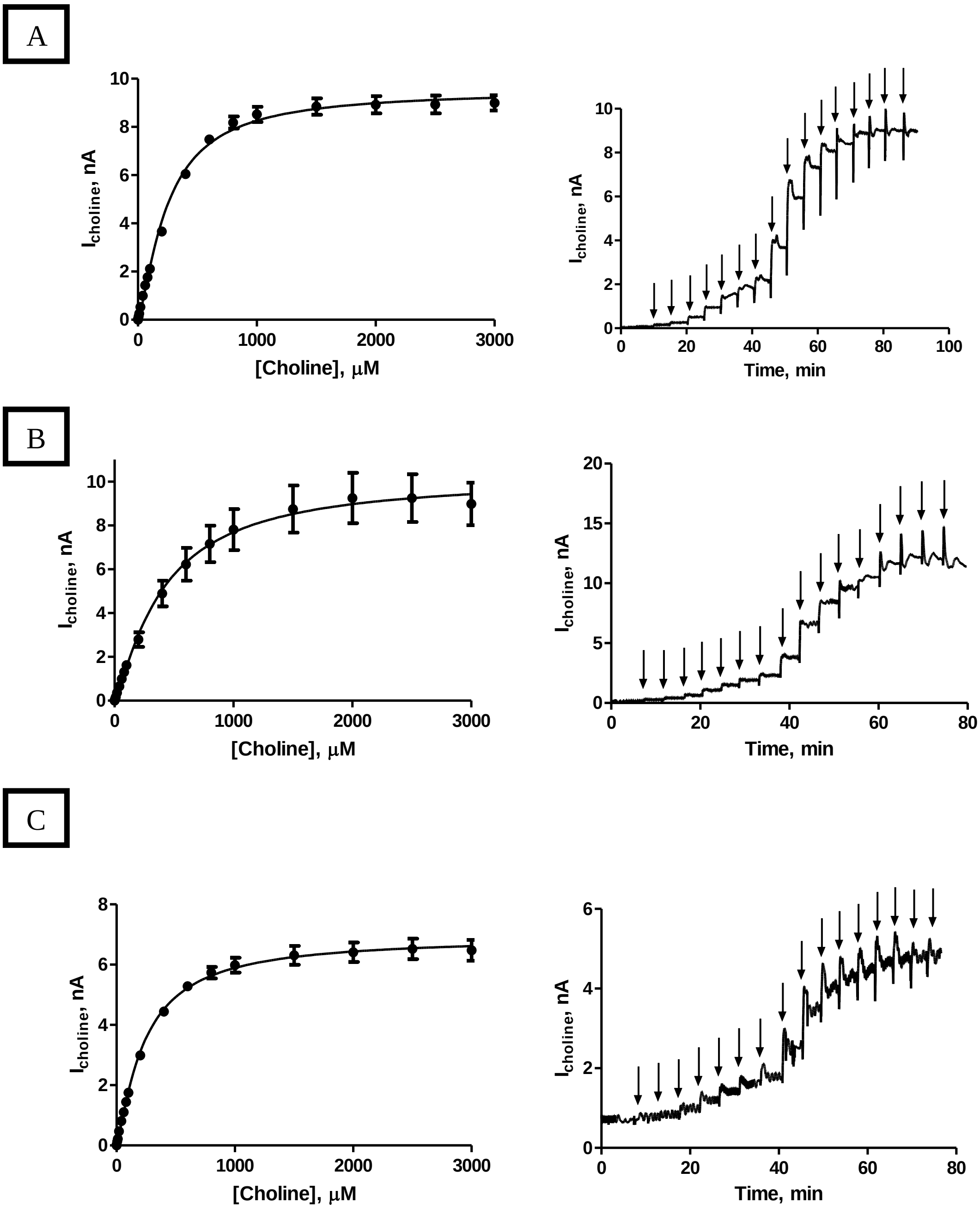

Figure 7 : The current-concentration profiles and raw data traces for choline chloride calibrations in PBS (pH 7.4) buffer solution at 21°C using designs (A) Sty-(ChOx)(BSA)(GA)(PEI1%)$_{10}$, (B) Sty-(ChOx)(BSA)(GA)(PEI0.75%)$_{10}$ and (C) Sty-(ChOx)(BSA)(GA)(PEI2%)$_{10}$. CPA carried out at +700 mV *vs*. SCE. Sequential current steps for 5, 10, 20, 40, 60, 80, 100, 200, 400, 600, 800, 1000, 1500, 2000, 2500 and 3000 μM choline chloride injections.

	Sty-(ChOx)(BSA)(GA)(PEI 1%)$_{10}$			Sty-(ChOx)(BSA)(GA)(PEI 0.75%)$_{10}$			Sty-(ChOx)(BSA)(GA)(PEI 2%)$_{10}$		
Conc, µM	**Mean, nA**	**S.E.M, nA**	**n**	**Mean, nA**	**S.E.M, nA**	**n**	**Mean, nA**	**S.E.M, nA**	**n**
0	0.00	0.00	4	0.00	0.00	4	0.00	0.00	3
5	0.14	0.01	4	0.09	0.01	4	0.13	0.01	3
10	0.25	0.01	4	0.17	0.03	4	0.22	0.01	3
20	0.53	0.02	4	0.36	0.04	4	0.47	0.02	3
40	0.99	0.03	4	0.65	0.08	4	0.81	0.03	3
60	1.43	0.04	4	0.99	0.12	4	1.10	0.03	3
80	1.76	0.03	4	1.31	0.16	4	1.44	0.04	3
100	2.11	0.04	4	1.62	0.19	4	1.75	0.04	3
200	3.66	0.07	4	2.79	0.33	4	2.99	0.11	3
400	6.10	0.12	4	4.89	0.59	4	4.44	0.07	3
600	7.48	0.19	4	6.22	0.74	4	5.29	0.11	3
800	8.18	0.26	4	7.16	0.83	4	5.74	0.19	3
1000	8.52	0.32	4	7.81	0.94	4	5.98	0.25	3
1500	8.85	0.34	4	8.74	1.08	4	6.31	0.31	3
2000	8.92	0.36	4	9.25	1.15	4	6.41	0.33	3
2500	8.93	0.37	4	9.24	1.09	4	6.52	0.34	3
3000	8.99	0.32	4	8.98	0.97	4	6.48	0.35	3

Table 7 : Comparison table of mean current values for designs; (A) Sty-(ChOx)(BSA)(GA)(PEI 1%)$_{10}$, (B) Sty-(ChOx)(BSA)(GA)(PEI0.75%)$_{10}$ and (C) Sty-(ChOx)(BSA)(GA)(PEI2%)$_{10}$. Choline chloride calibrations carried out in PBS (pH 7.4) buffer solution at 21°C. CPA carried out at +700 mV *vs*. SCE. All currents are background subtracted.

4.3.9.2. GA Concentration

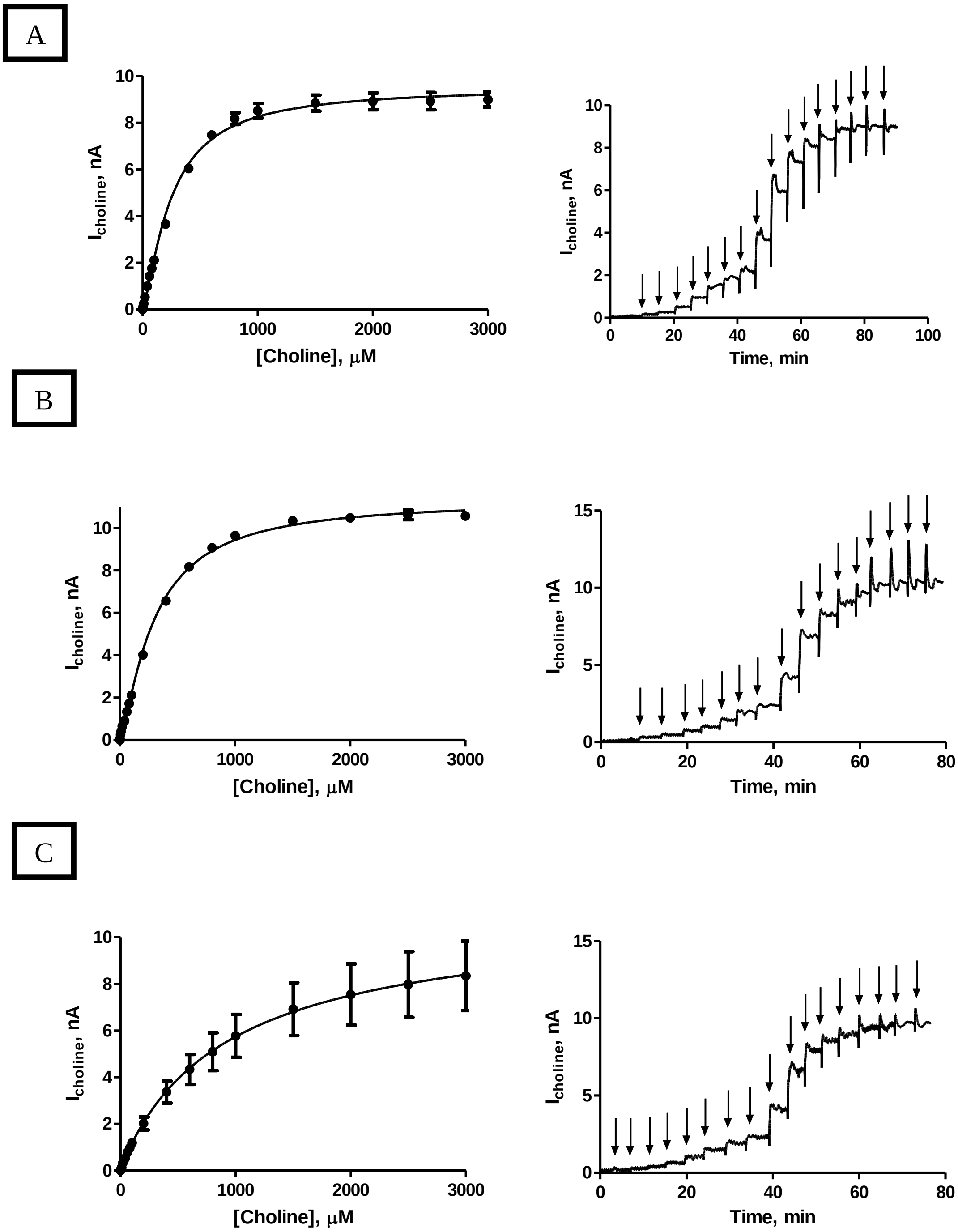

Figure 8 : The current-concentration profiles and raw data traces for choline chloride calibrations in PBS (pH 7.4) buffer solution at 21°C using designs (A) Sty-(ChOx)(BSA)(GA1%)(PEI)$_{10}$ and (B) Sty-(ChOx)(BSA)(GA0.5%)(PEI)$_{10}$ and (C) Sty-(ChOx)(BSA)(GA1.5%)(PEI)$_{10}$. CPA carried out at +700 mV *vs.* SCE. Sequential current steps for 5, 10, 20, 40, 60, 80, 100, 200, 400, 600, 800, 1000, 1500, 2000, 2500 and 3000 μM choline chloride injections.

	Sty-(ChOx)(BSA)(GA 1%)(PEI)$_{10}$			Sty-(ChOx)(BSA)(GA 0.5%)(PEI)$_{10}$			Sty-(ChOx)(BSA)(GA 1.5%)(PEI)$_{10}$		
Conc, µM	**MEAN, nA**	**S.E.M, nA**	**n**	**MEAN, nA**	**S.E.M, nA**	**n**	**MEAN, nA**	**S.E.M, n**	**n**
0	0.00	0.00	4	0.00	0.00	4	0.00	0.00	11
5	0.14	0.01	4	0.25	0.01	4	0.08	0.03	11
10	0.25	0.01	4	0.41	0.01	4	0.13	0.03	11
20	0.53	0.02	4	0.65	0.02	4	0.33	0.04	11
40	0.99	0.03	4	0.9	0.02	4	0.53	0.07	11
60	1.43	0.04	4	1.33	0.03	4	0.78	0.1	11
80	1.76	0.03	4	1.72	0.04	4	0.98	0.14	11
100	2.11	0.04	4	2.12	0.05	4	1.18	0.15	11
200	3.66	0.07	4	4.02	0.09	4	2.02	0.28	11
400	6.1	0.12	4	6.56	0.11	4	3.37	0.47	11
600	7.48	0.19	4	8.17	0.06	4	4.34	0.64	11
800	8.18	0.26	4	9.06	0.05	4	5.10	0.81	11
1000	8.52	0.32	4	9.64	0.09	4	5.77	0.92	11
1500	8.85	0.34	4	10.34	0.13	4	6.92	1.13	11
2000	8.92	0.36	4	10.47	0.18	4	7.55	1.31	11
2500	8.93	0.37	4	10.61	0.22	4	7.98	1.41	11
3000	8.99	0.32	4	10.56	0.19	4	8.35	1.49	11

Table 8 : Comparison table of mean current values for designs; (A) Sty-(ChOx)(BSA)(GA)(PEI 1%)$_{10}$, (B) Sty-(ChOx)(BSA)(GA)(PEI0.75%)$_{10}$ and (C) Sty-(ChOx)(BSA)(GA)(PEI2%)$_{10}$. Choline chloride calibrations carried out in PBS (pH 7.4) buffer solution at 21°C. CPA carried out at +700 mV *vs*. SCE. All currents are background subtracted.

4.3.9.3. 0.5% GA / PEI

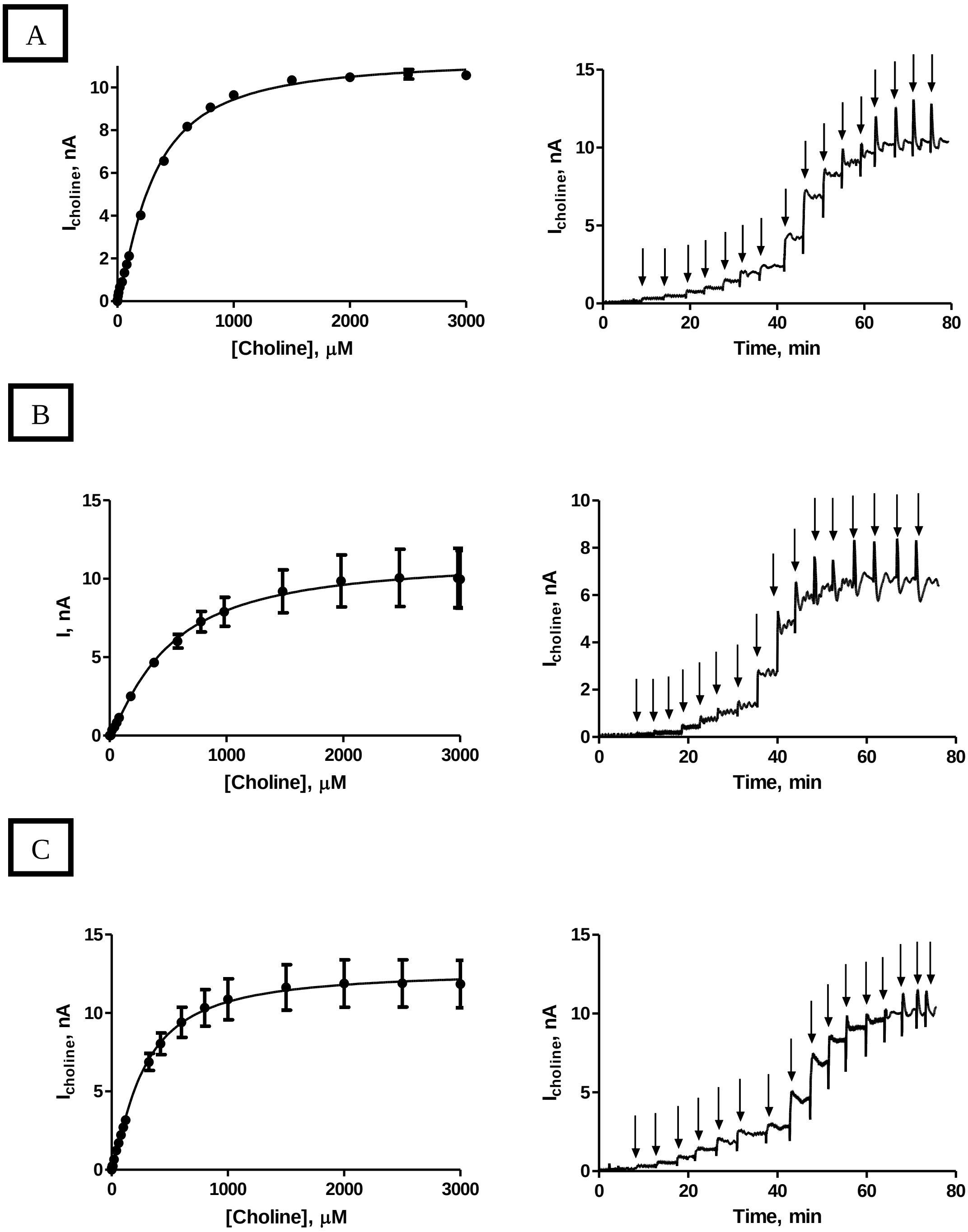

Figure 9 : The current-concentration profiles and raw data traces for choline chloride calibrations in PBS (pH 7.4) buffer solution at 21°C using designs (A) Sty-(ChOx)(BSA)(GA0.5%)(PEI1%)$_{10}$, (B) Sty-(ChOx)(BSA)(GA 0.5%)(PEI0.75%)$_{10}$ and (C) Sty-(ChOx)(BSA)(GA 0.5%)(PEI2%)$_{10}$. CPA carried out at +700 mV *vs*. SCE. Sequential current steps for 5, 10, 20, 40, 60, 80, 100, 200, 400, 600, 800, 1000, 1500, 2000, 2500 and 3000 μM choline chloride injections.

	Sty-(ChOx)(BSA)(GA 0.5%)(PEI 1%)$_{10}$			Sty-(ChOx)(BSA)(GA 0.5%)(PEI 0.75%)$_{10}$			Sty-(ChOx)(BSA)(GA 0.5%)(PEI 2%)$_{10}$		
Conc, µM	**MEAN, nA**	**S.E.M, nA**	**n**	**MEAN, nA**	**S.E.M, nA**	**n**	**MEAN, nA**	**S.E.M, nA**	**n**
0	0.00	0.00	4	0.00	0.00	4	0.00	0.00	3
5	0.25	0.01	4	0.001	0.010	4	0.24	0.01	3
10	0.41	0.01	4	0.04	0.02	4	0.23	0.02	3
20	0.65	0.02	4	0.35	0.02	4	0.66	0.03	3
40	0.90	0.02	4	0.55	0.04	4	1.23	0.06	3
60	1.33	0.03	4	0.83	0.06	4	1.71	0.09	3
80	1.72	0.04	4	1.15	0.07	4	2.22	0.13	3
100	2.12	0.05	4	1.42	0.08	4	2.71	0.16	3
200	4.02	0.09	4	2.72	0.15	4	5.13	0.29	3
400	6.56	0.11	4	4.79	0.29	4	7.38	0.067	3
600	8.17	0.06	4	6.14	0.46	4	9.41	0.97	3
800	9.06	0.05	4	7.33	0.68	4	10.33	1.17	3
1000	9.64	0.09	4	7.95	0.94	4	10.87	1.3	3
1500	10.34	0.13	4	9.22	1.38	4	11.64	1.45	3
2000	10.47	0.18	4	9.87	1.67	4	11.88	1.51	3
2500	10.61	0.22	4	10.06	1.83	4	11.89	1.51	3
3000	10.56	0.19	4	10.04	1.89	4	11.84	1.51	3

Table 9 : Comparison table of mean current values for designs; (A) Sty-(ChOx)(BSA)(GA0.5%)(PEI 1%)$_{10}$, (B) Sty-(ChOx)(BSA)(GA0.5%)(PEI0.75%)$_{10}$ and (C) Sty-(ChOx)(BSA)(GA0.5%)(PEI2%)$_{10}$. Choline chloride calibrations carried out in PBS (pH 7.4) buffer solution at 21°C. CPA carried out at +700 mV *vs*. SCE. All currents are background subtracted.

4.3.9.4. 1.5% GA / PEI

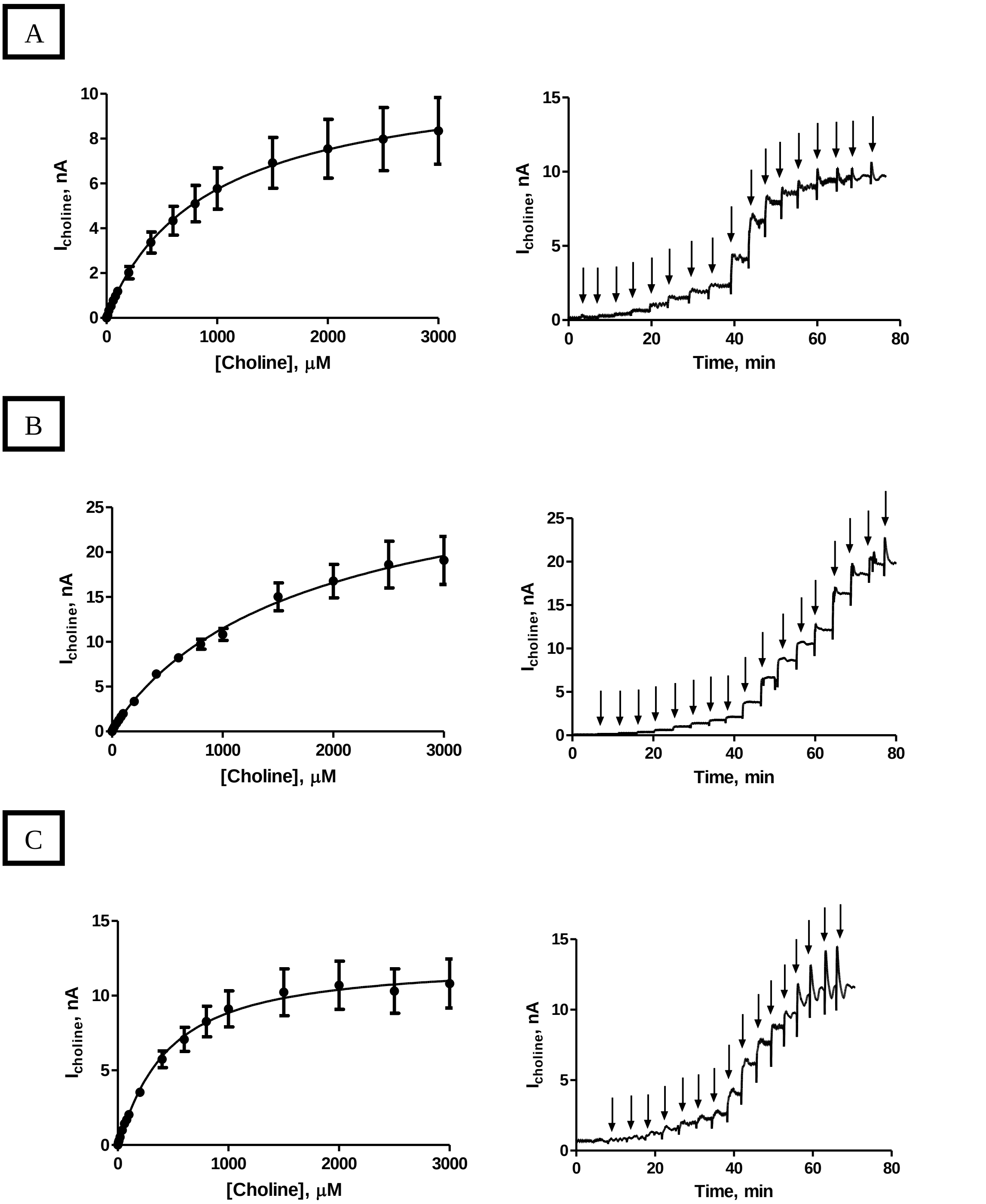

Figure 10 : The current-concentration profiles and raw data traces for choline chloride calibrations in PBS (pH 7.4) buffer solution at 21°C using designs (A) Sty-(ChOx)(BSA)(GA1.5%)(PEI1%)$_{10}$ (B) Sty-(ChOx)(BSA)(GA1.5%)(PEI0.75%)$_{10}$ and (C) Sty-(ChOx)(BSA)(GA1.5%)(PEI2%)$_{10}$. CPA carried out at +700 mV *vs.* SCE. Sequential current steps for 5, 10, 20, 40, 60, 80, 100, 200, 400, 600, 800, 1000, 1500, 2000, 2500 and 3000 μM choline chloride injections.

	Sty-(ChOx)(BSA) (GA 1.5%)(PEI 1%)$_{10}$			Sty-(ChOx)(BSA) (GA 1.5%)(PEI 0.75%)$_{10}$			Sty-(ChOx)(BSA) (GA 1.5%)(PEI 2%)$_{10}$		
Conc, µM	**Mean, nA**	**S.E.M, nA**	**n**	**Mean, nA**	**S.E.M, nA**	**n**	**Mean, nA**	**S.E.M, nA**	**n**
0	0.00	0.00	11	0.00	0.00	3	0.00	0.00	3
5	0.08	0.03	11	0.162	0.003	3	0.18	0.01	3
10	0.13	0.03	11	0.29	0.01	3	0.29	0.01	3
20	0.33	0.04	11	0.53	0.01	3	0.54	0.03	3
40	0.53	0.07	11	0.92	0.01	3	0.99	0.05	3
60	0.78	0.1	11	1.26	0.02	3	1.43	0.09	3
80	0.98	0.14	11	1.63	0.02	3	1.69	0.10	3
100	1.18	0.15	11	1.99	0.03	3	2.03	0.14	3
200	2.02	0.28	11	3.35	0.15	3	3.53	0.28	3
400	3.37	0.47	11	6.41	0.30	3	5.74	0.56	3
600	4.34	0.64	11	8.22	0.37	3	7.07	0.80	3
800	5.1	0.81	11	9.74	0.55	3	8.27	1.03	3
1000	5.77	0.92	11	10.82	0.67	3	9.11	1.21	3
1500	6.92	1.13	11	15.03	1.55	3	10.23	1.57	3
2000	7.55	1.31	11	16.77	1.87	3	10.70	1.62	3
2500	7.98	1.41	11	18.61	2.61	3	10.30	1.49	3
3000	8.35	1.49	11	19.09	2.68	3	10.81	1.64	3

Table 10 : Comparison table of mean current values for designs; (A) Sty-(ChOx)(BSA)(GA1.5%)(PEI 1%)$_{10}$, (B) Sty-(ChOx)(BSA)(GA1.5%)(PEI0.75%)$_{10}$ and (C) Sty-(ChOx)(BSA)(GA1.5%)(PEI2%)$_{10}$. Choline chloride calibrations carried out in PBS (pH 7.4) buffer solution at 21°C. CPA carried out at +700 mV *vs*. SCE. All currents are background subtracted.

4.3.10. Enzyme Medium

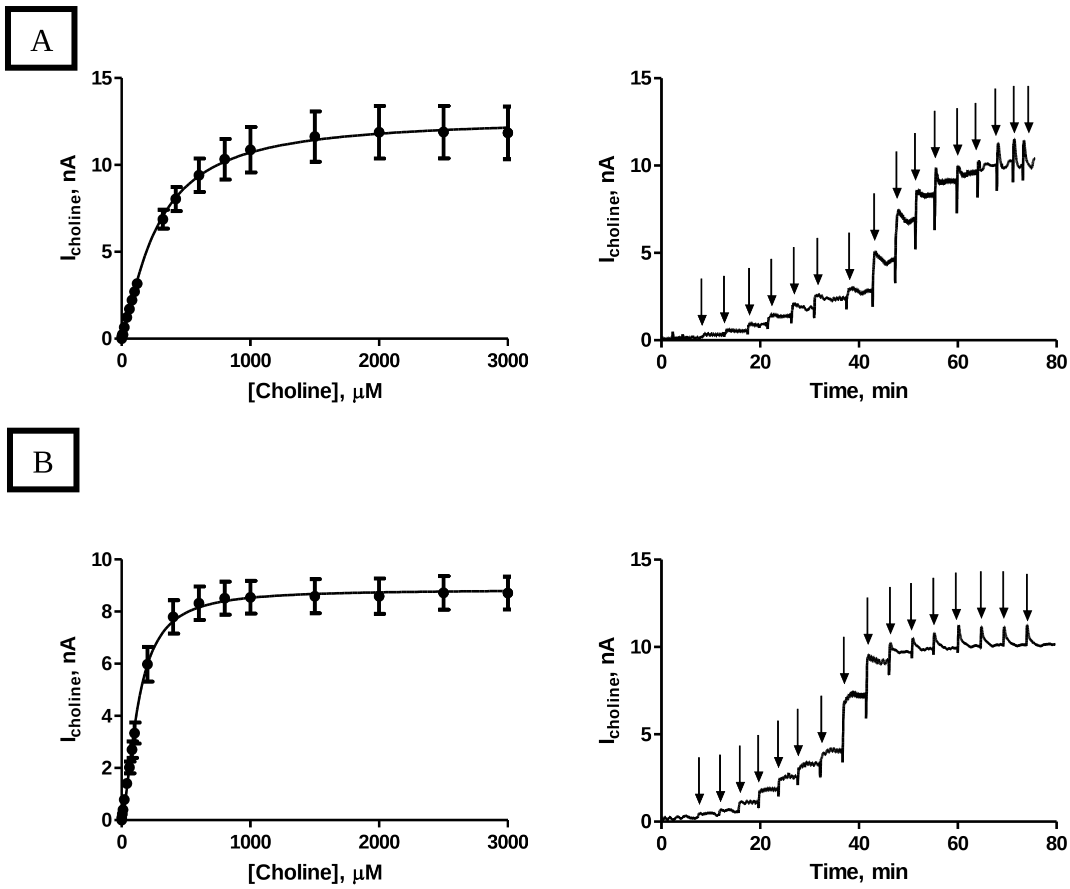

Figure 11 : The current-concentration profiles and raw data traces for choline chloride calibrations in PBS (pH 7.4) buffer solution at 21°C using designs (A) Sty-(ChOx:PBS)(BSA)(GA)(PEI)$_{10}$ and (B) Sty-(ChOx:H$_2$0)(BSA)(GA)(PEI)$_{10}$. CPA carried out at +700 mV *vs*. SCE. Sequential current steps for 5, 10, 20, 40, 60, 80, 100, 200, 400, 600, 800, 1000, 1500, 2000, 2500 and 3000 µM choline chloride injections.

	Sty-(ChOx:PBS)(BSA)(GA)(PEI)$_{10}$			Sty-(ChOx:H_2O)(BSA)(GA)(PEI)$_{10}$		
Conc, µM	**Mean, nA**	**S.E.M, nA**	**n**	**Mean, nA**	**S.E.M, nA**	**n**
0	0.00	0.00	3	0.00	0.00	3
5	0.24	0.01	3	0.23	0.03	3
10	0.23	0.02	3	0.40	0.05	3
20	0.66	0.03	3	0.79	0.086	3
40	1.23	0.06	3	1.40	0.16	3
60	1.71	0.09	3	2.02	0.22	3
80	2.22	0.13	3	2.70	0.32	3
100	2.71	0.16	3	3.34	0.41	3
200	5.13	0.29	3	5.98	0.66	3
400	7.38	0.067	3	7.80	0.64	3
600	9.41	0.97	3	8.32	0.64	3
800	10.33	1.17	3	8.51	0.63	3
1000	10.87	1.3	3	8.55	0.63	3
1500	11.64	1.45	3	8.59	0.65	3
2000	11.88	1.51	3	8.59	0.68	3
2500	11.89	1.51	3	8.72	0.65	3
3000	11.84	1.51	3	8.71	0.63	3

Table 11 : Comparison table of mean current values for designs; (A) Sty-(ChOx:PBS)(BSA)(GA)(PEI)$_{10}$ and (B) Sty-(ChOx:H_20)(BSA)(GA)(PEI)$_{10}$. Choline chloride calibrations carried out in PBS (pH 7.4) buffer solution at 21°C. CPA carried out at +700 mV *vs*. SCE. All currents are background subtracted.

4.3.11. Styrene Double Layer

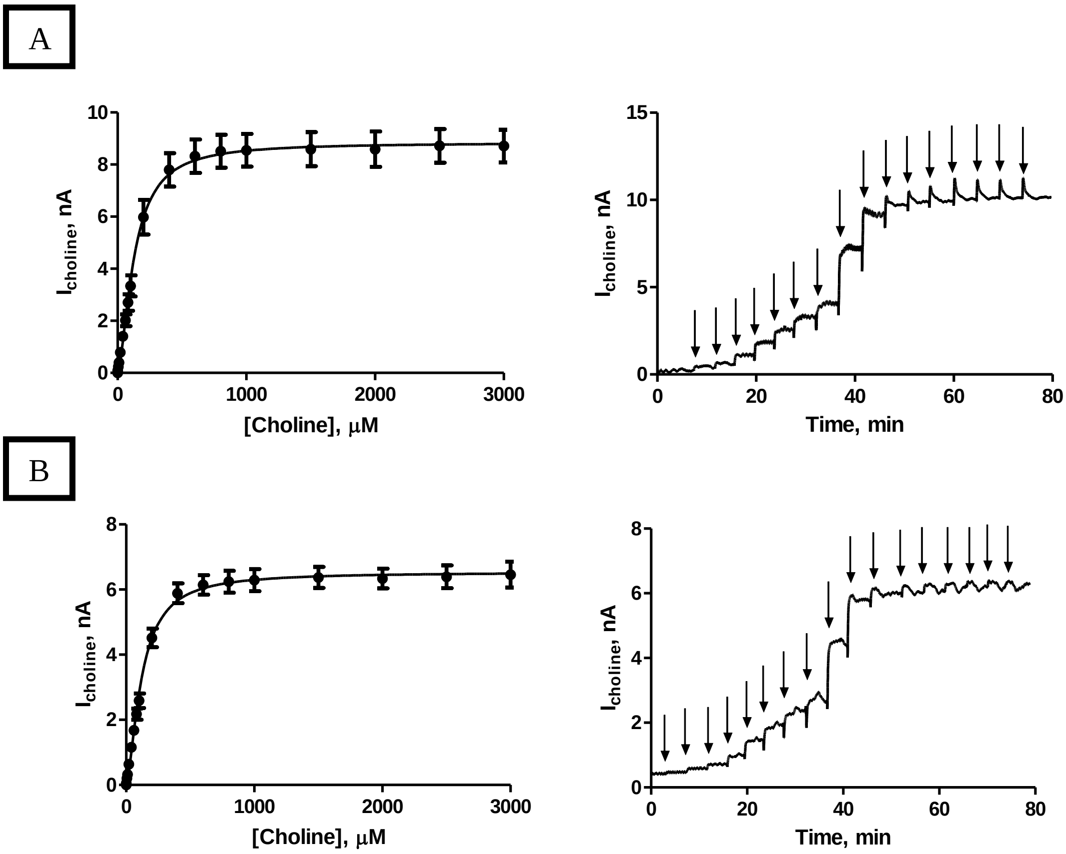

Figure 15 : The current-concentration profiles and raw data traces for choline chloride calibrations in PBS (pH 7.4) buffer solution at 21°C using designs (A) Sty-(ChOx:H_2O)(BSA)(GA)$(PEI)_{10}$ and (B) (Sty-(ChOx:PBS)(BSA)(GA)$(PEI)_{10}$)x2. CPA carried out at +700 mV *vs*. SCE. Sequential current steps for 5, 10, 20, 40, 60, 80, 100, 200, 400, 600, 800, 1000, 1500, 2000, 2500 and 3000 µM choline chloride injections.

	Sty-(ChOx.H_2O)(BSA)(GA)$(PEI)_{10}$			Pt-(Sty-(ChOx.H_2O)(BSA)(GA)$(PEI)_{10}$)x2		
Conc, µM	**MEAN, nA**	**S.E.M, nA**	**n**	**MEAN, nA**	**S.E.M, nA**	**n**
0	0.00	0.00	3	0.00	0.00	3
5	0.23	0.03	3	0.13	0.01	3
10	0.4	0.05	3	0.25	0.02	3
20	0.79	0.086	3	0.65	0.06	3
40	1.4	0.16	3	1.25	0.06	3
60	2.02	0.22	3	1.77	0.1	3
80	2.7	0.32	3	2.3	0.11	3
100	3.34	0.41	3	2.78	0.14	3
200	5.98	0.66	3	6.17	0.17	3
400	7.8	0.64	3	6.84	0.15	3
600	8.32	0.64	3	7.38	0.12	3
800	8.51	0.63	3	7.62	0.12	3
1000	8.55	0.63	3	7.74	0.12	3
1500	8.59	0.65	3	7.9	0.13	3
2000	8.59	0.68	3	7.97	0.14	3
2500	8.72	0.65	3	8.02	0.14	3
3000	8.71	0.63	3	8.05	0.14	3

Table 15 : Comparison table of mean current values for designs; (A) Sty-(ChOx:H_2O)(BSA)(GA)$(PEI)_{10}$ and (B) Sty-(ChOx:H_2O)(BSA)(GA)$(PEI)_{10}$. Choline chloride calibrations carried out in PBS (pH 7.4) buffer solution at 21°C. CPA carried out at +700 mV *vs*. SCE. All currents are background subtracted.

4.3.12. MMA Modifications

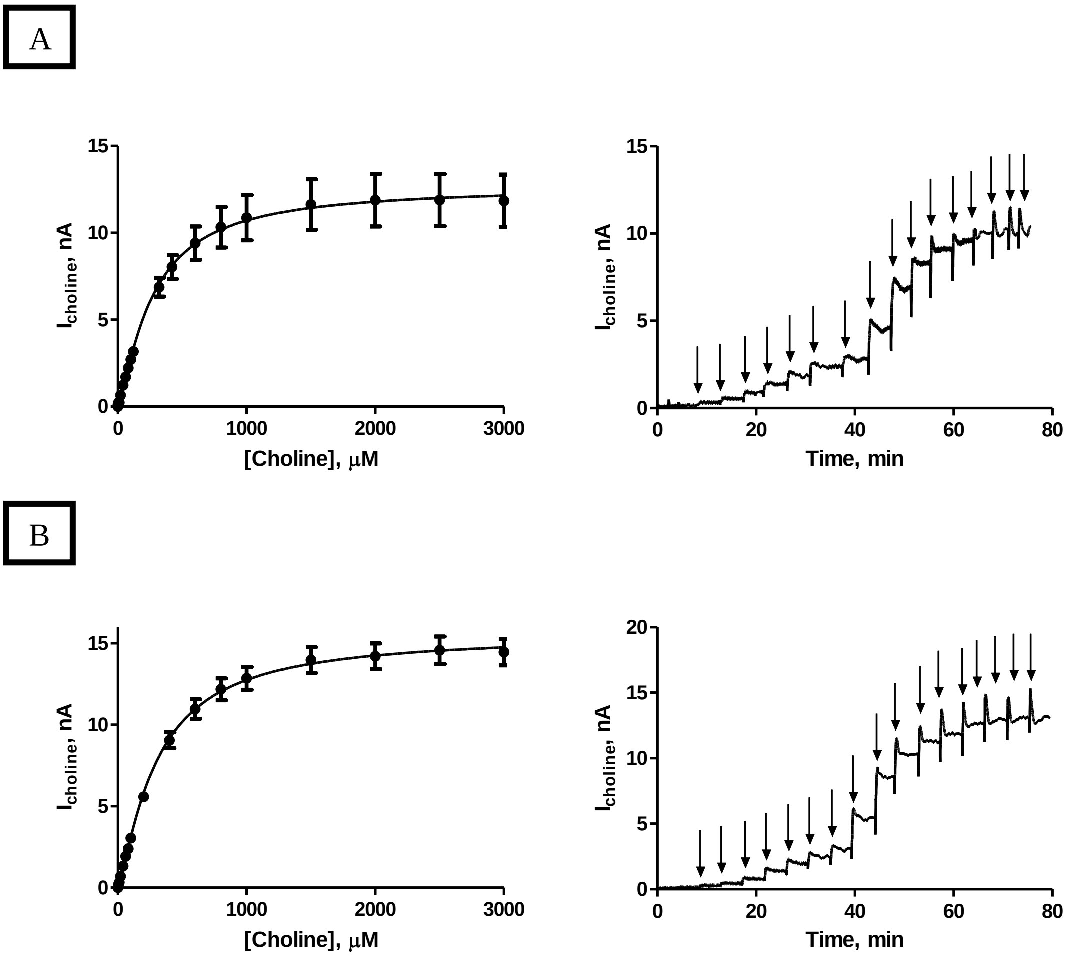

Figure 12 : The current-concentration profiles and raw data traces for choline chloride calibrations in PBS (pH 7.4) buffer solution at 21°C using designs (A) Sty-(ChOx)(BSA)(GA)(PEI)$_{10}$ and (B) MMA-(ChOx)(BSA)(GA)(PEI)$_{10}$. CPA carried out at +700 mV *vs.* SCE. Sequential current steps for 5, 10, 20, 40, 60, 80, 100, 200, 400, 600, 800, 1000, 1500, 2000, 2500 and 3000 μM choline chloride injections

	Sty-(ChOx)(BSA)(GA)(PEI)$_{10}$			MMA-(ChOx)(BSA)(GA)(PEI)$_{10}$		
Conc, µM	**MEAN, nA**	**S.E.M, nA**	**n**	**MEAN, nA**	**S.E.M, nA**	**n**
0	0.00	0.00	3	0.00	0.00	4
5	0.24	0.01	3	0.21	0.01	4
10	0.23	0.02	3	0.32	0.02	4
20	0.66	0.03	3	0.71	0.03	4
40	1.23	0.06	3	1.33	0.06	4
60	1.71	0.09	3	1.92	0.09	4
80	2.22	0.13	3	2.39	0.13	4
100	2.71	0.16	3	3.04	0.14	4
200	5.13	0.29	3	5.57	0.28	4
400	7.38	0.07	3	9.05	0.49	4
600	9.41	0.97	3	10.96	0.6	4
800	10.33	1.17	3	12.17	0.68	4
1000	10.87	1.30	3	12.86	0.7	4
1500	11.64	1.45	3	13.97	0.8	4
2000	11.88	1.51	3	14.20	0.79	4
2500	11.89	1.51	3	14.58	0.85	4
3000	11.84	1.51	3	14.46	0.82	4

Table 12 : Comparison table of mean current values for designs; (A) Sty-(ChOx)(BSA)(GA)(PEI)$_{10}$ and (B) MMA-(ChOx)(BSA)(GA)(PEI)$_{10}$. Choline chloride calibrations carried out in PBS (pH 7.4) buffer solution at 21°C. CPA carried out at +700 mV *vs*. SCE. All currents are background subtracted.

4.3.12.1. Enzyme Medium

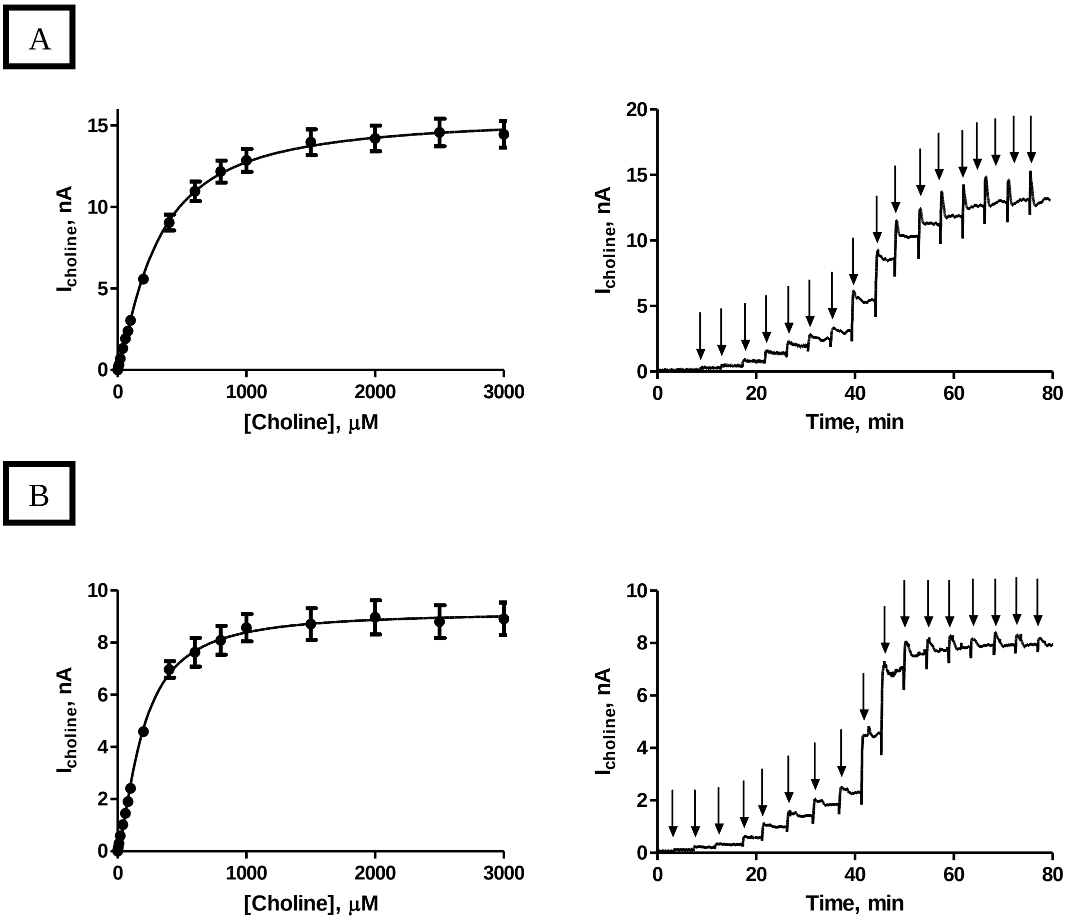

Figure 13 : The current-concentration profiles and raw data traces for choline chloride calibrations in PBS (pH 7.4) buffer solution at 21°C using designs (A) MMA-(ChOx:PBS)(BSA)(GA)$(PEI)_{10}$ and (B) MMA-(ChOx:H_2O)(BSA)(GA)$(PEI)_{10}$. CPA carried out at +700 mV *vs*. SCE. Sequential current steps for 5, 10, 20, 40, 60, 80, 100, 200, 400, 600, 800, 1000, 1500, 2000, 2500 and 3000 μM choline chloride injections.

	MMA-(ChOx:PBS)(BSA)(GA)$(PEI)_{10}$			MMA-(ChOx:H_2O)(BSA)(GA)$(PEI)_{10}$		
Conc, µM	**Mean, nA**	**S.E.M, nA**	**n**	**Mean, nA**	**S.E.M, nA**	**n**
0	0.00	0.00	3	0.00	0.00	4
5	0.24	0.01	3	0.15	0.01	4
10	0.23	0.02	3	0.30	0.01	4
20	0.66	0.03	3	0.60	0.03	4
40	1.23	0.06	3	1.02	0.05	4
60	1.71	0.09	3	1.45	0.08	4
80	2.22	0.13	3	1.91	0.1	4
100	2.71	0.16	3	2.41	0.12	4
200	5.13	0.29	3	4.58	0.15	4
400	7.38	0.07	3	6.97	0.32	4
600	9.41	0.97	3	7.63	0.55	4
800	10.33	1.17	3	8.09	0.55	4
1000	10.87	1.3	3	8.57	0.53	4
1500	11.64	1.45	3	8.71	0.61	4
2000	11.88	1.51	3	8.97	0.66	4
2500	11.89	1.51	3	8.81	0.63	4
3000	11.84	1.51	3	8.91	0.62	4

Table 13 : Comparison table of mean current values for designs; (A) MMA-(ChOx:PBS)(BSA)(GA)$(PEI)_{10}$ and (B) MMA-(ChOx:H_2O)(BSA)(GA)$(PEI)_{10}$. Choline chloride calibrations carried out in PBS (pH 7.4) buffer solution at 21°C. CPA carried out at +700 mV *vs.* SCE. All currents are background subtracted.

4.3.12.2. MMA Double Layer

A

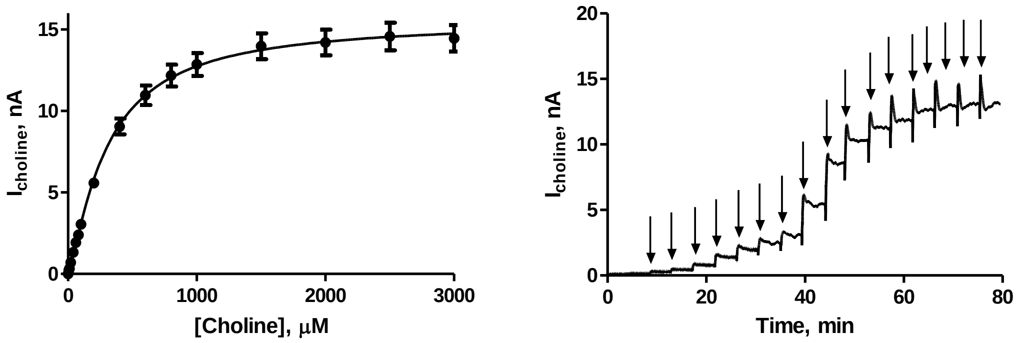

B

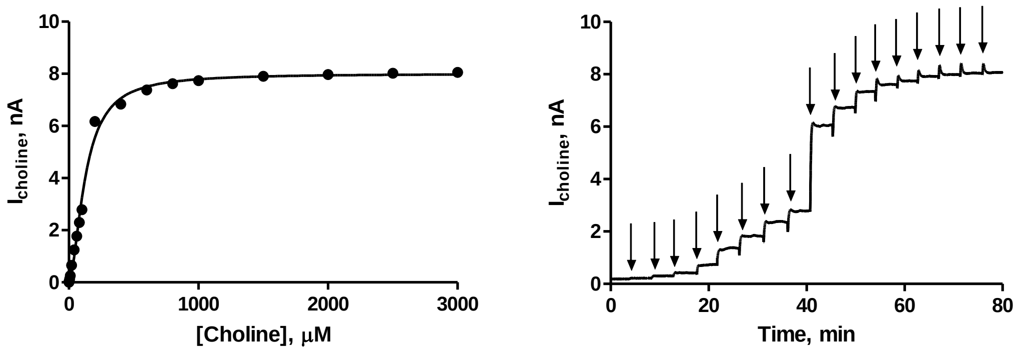

Figure 16 : The current-concentration profiles and raw data traces for choline chloride calibrations in PBS (pH 7.4) buffer solution at 21°C using designs (A) MMA-(ChOx:PBS)(BSA)(GA)$(PEI)_{10}$ and (B) (MMA-(ChOx:PBS)(BSA)(GA)$(PEI)_{10}$)x2. CPA carried out at +700 mV *vs*. SCE. Sequential current steps for 5, 10, 20, 40, 60, 80, 100, 200, 400, 600, 800, 1000, 1500, 2000, 2500 and 3000 μM choline chloride injections.

	(MMA-(ChOx.PBS)(BSA)(GA)(PEI)$_{10}$			MMA-(ChOx.PBS)(BSA)(GA)(PEI)$_{10}$)x2		
Conc, µM	**Mean, nA**	**S.E.M, nA**	**n**	**Mean, nA**	**S.E.M, nA**	**n**
0	0.00	0.00	3	0.00	0.00	4
5	0.24	0.01	3	0.21	0.01	4
10	0.23	0.02	3	0.32	0.02	4
20	0.66	0.03	3	0.71	0.03	4
40	1.23	0.06	3	1.33	0.06	4
60	1.71	0.09	3	1.92	0.09	4
80	2.22	0.13	3	2.39	0.13	4
100	2.71	0.16	3	3.04	0.14	4
200	5.13	0.29	3	5.57	0.28	4
400	7.38	0.07	3	9.05	0.49	4
600	9.41	0.97	3	10.96	0.6	4
800	10.33	1.17	3	12.17	0.68	4
1000	10.87	1.3	3	12.86	0.7	4
1500	11.64	1.45	3	13.97	0.8	4
2000	11.88	1.51	3	14.2	0.79	4
2500	11.89	1.51	3	14.58	0.85	4
3000	11.84	1.51	3	14.46	0.82	4

Table 16 : Comparison table of mean current values for designs; (A) MMA-(ChOx:H_2O)(BSA)(GA)(PEI)$_{10}$ and (B) (MMA-(ChOx:H_2O)(BSA)(GA)(PEI)$_{10}$)x2. Choline chloride calibrations carried out in PBS (pH 7.4) buffer solution at 21°C. CPA carried out at +700 mV *vs.* SCE. All currents are background subtracted.

4.3.13. Best Design

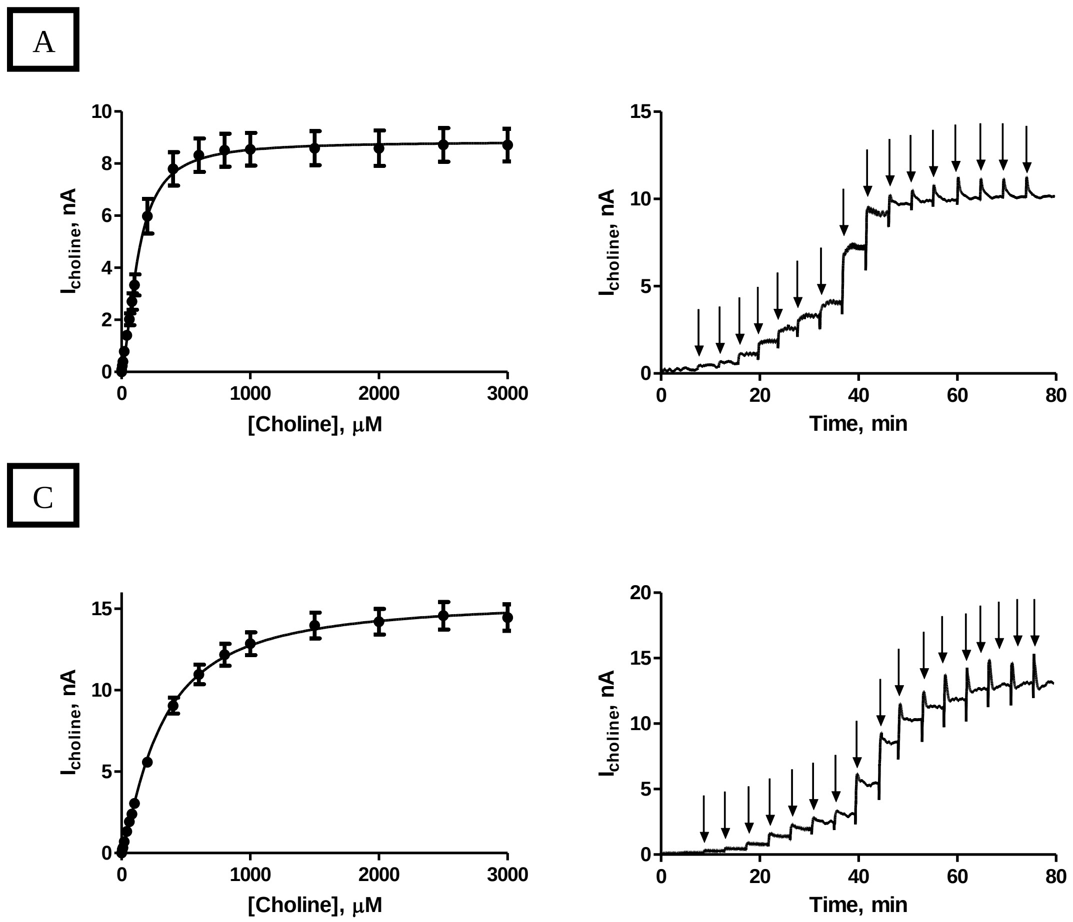

Figure 14 : The current-concentration profiles and raw data traces for choline chloride calibrations in PBS (pH 7.4) buffer solution at 21°C using designs (A) Sty-(ChOx:H_2O)(BSA)(GA)(PEI)$_{10}$ and (B) MMA-(ChOx:PBS)(BSA)(GA)(PEI)$_{10}$. CPA carried out at +700 mV *vs*. SCE. Sequential current steps for 5, 10, 20, 40, 60, 80, 100, 200, 400, 600, 800, 1000, 1500, 2000, 2500 and 3000 µM choline chloride injections.

	Sty-(ChOx:H_2O)(BSA)(GA)$(PEI)_{10}$			MMA-(ChOx:PBS)(BSA)(GA)$(PEI)_{10}$		
Conc, µM	**Mean, nA**	**S.E.M, nA**	**n**	**Mean, nA**	**S.E.M, nA**	**n**
0	0.00	0.00	3	0.00	0.00	3
5	0.23	0.03	3	0.24	0.01	3
10	0.40	0.05	3	0.23	0.02	3
20	0.79	0.086	3	0.66	0.03	3
40	1.4	0.16	3	1.23	0.06	3
60	2.02	0.22	3	1.71	0.09	3
80	2.70	0.32	3	2.22	0.13	3
100	3.34	0.41	3	2.71	0.16	3
200	5.98	0.66	3	5.13	0.29	3
400	7.80	0.64	3	7.38	0.07	3
600	8.32	0.64	3	9.41	0.97	3
800	8.51	0.63	3	10.33	1.17	3
1000	8.55	0.63	3	10.87	1.3	3
1500	8.59	0.65	3	11.64	1.45	3
2000	8.59	0.68	3	11.88	1.51	3
2500	8.72	0.65	3	11.89	1.51	3
3000	8.71	0.63	3	11.84	1.51	3

Table 14 : Comparison table of mean current values for designs; (A) Sty-(ChOx:H_2O)(BSA)(GA)$(PEI)_{10}$ and (B) MMA-(ChOx:PBS)(BSA)(GA)$(PEI)_{10}$. Choline chloride calibrations carried out in PBS (pH 7.4) buffer solution at 21°C. CPA carried out at +700 mV *vs.* SCE. All currents are background subtracted.

Appendix 2
Oxygen Dependence

5.3.1. Oxygen Dependence

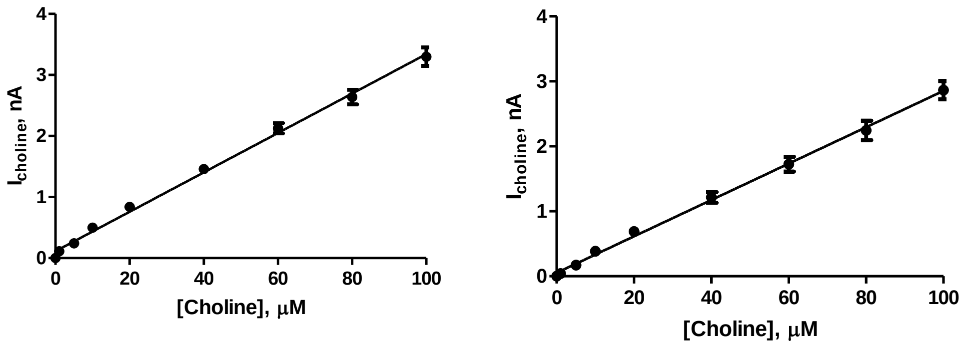

Figure : The current-concentration profile for choline chloride in PBS (pH 7.4) buffer solution at 21°C using design (A) Sty-(ChOx)(BSA)(GA)(PEI)$_{10}$ and (B) MMA-(ChOx)(BSA)(GA)(PEI)$_{10}$. CPA carried out at +700 mV *vs*. SCE for choline electrodes. Sequential current steps for 5, 10, 20, 40, 60, 80, 100 µM choline chloride injections.

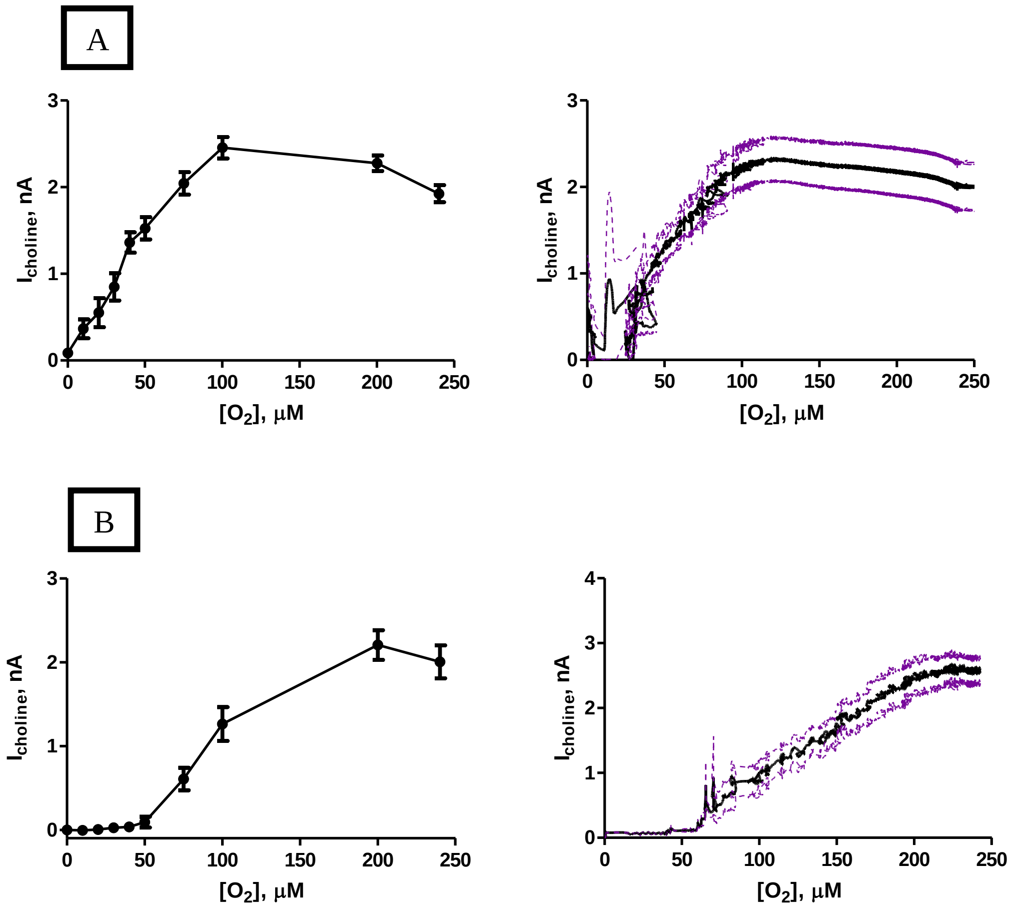

Figure : The choline current-oxygen concentration profile and raw data trace for choline chloride in PBS (pH 7.4) buffer solution at 21°C using design (A) Sty-(ChOx)(BSA)(GA) $(PEI)_{10}$ and (B) MMA-(ChOx)(BSA)(GA)$(PEI)_{10}$. CPA carried out at +700 mV *vs*. SCE for choline electrodes. CPA carried out at -650 mV *vs*. SCE for O_2 electrodes. Sequential current steps for 100 µM choline chloride injection at 10, 20, 30, 40, 50, 75, 100, 200, 240 µM O_2 concentrations.

5.3.2.1. Styrene

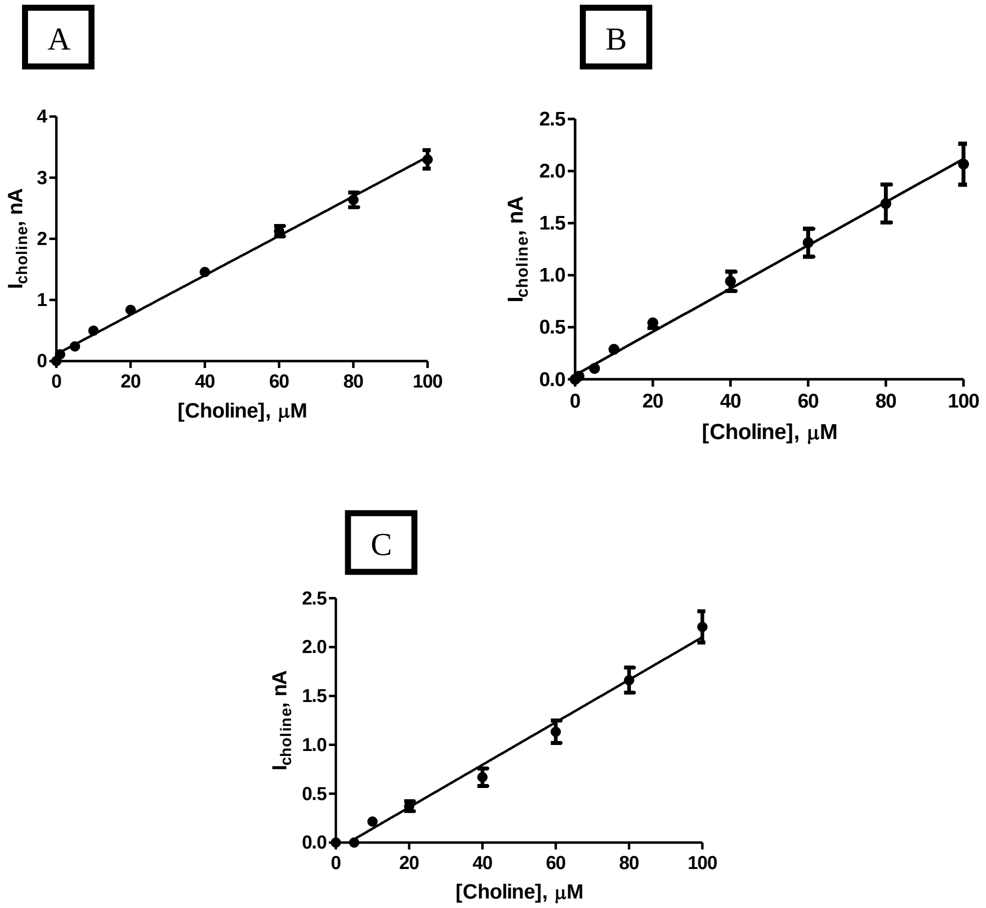

Figure : The current-concentration profile for choline chloride in PBS (pH 7.4) buffer solution at 21°C using design (A) 0 % Nafion®, (B) 0.5 % Nafion® and (C) 1 % Nafion®. CPA carried out at +700 mV *vs*. SCE for choline electrodes. Sequential current steps for 5, 10, 20, 40, 60, 80, 100 μM choline chloride injections.

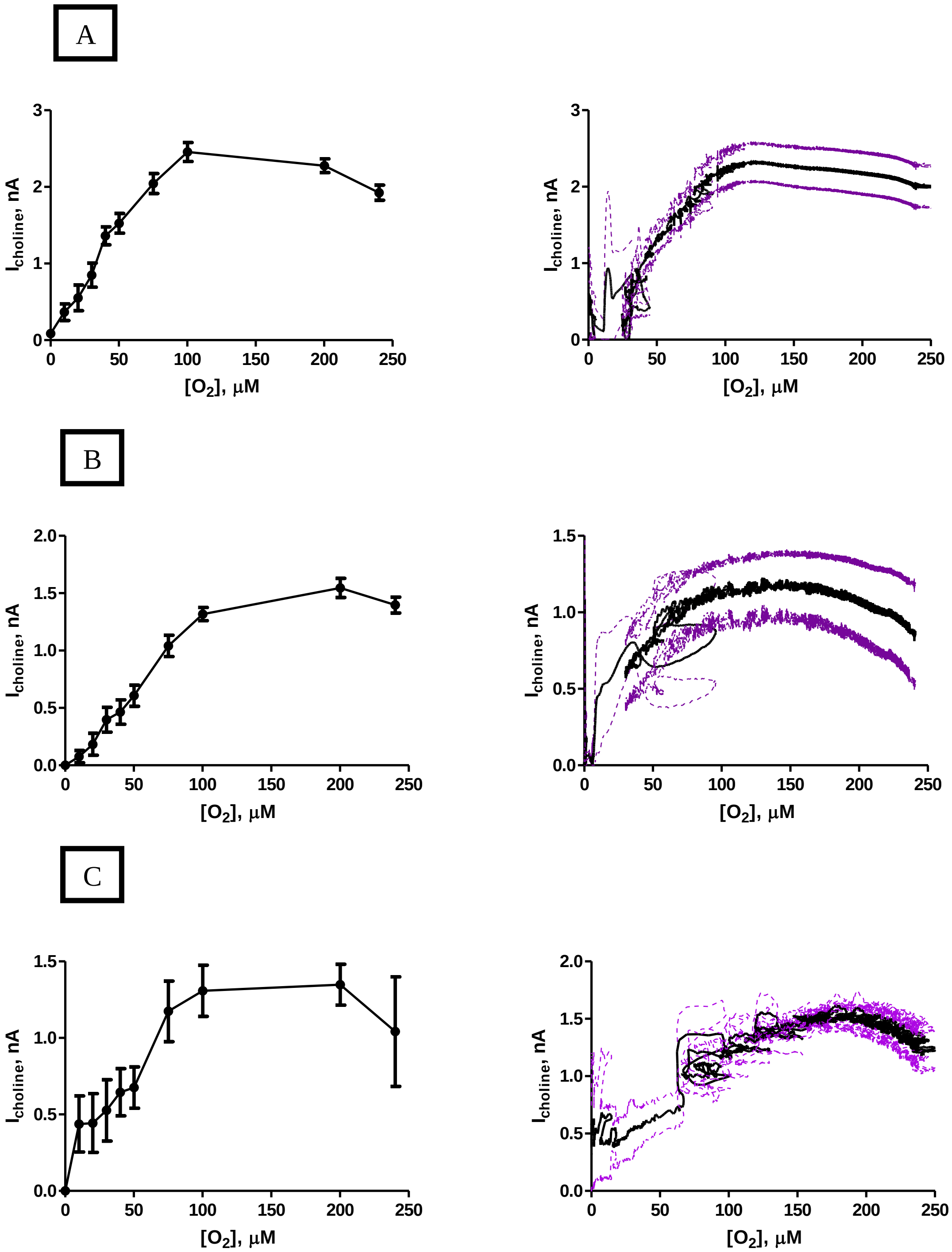

Figure : The choline current-oxygen concentration profile for choline chloride in PBS (pH 7.4) buffer solution at 21°C using design (A) 0 % Nafion®, (B) 0.5 % Nafion® and (C) 1 % Nafion®. CPA carried out at +700 mV *vs.* SCE for choline electrodes. CPA carried out at -650 mV *vs.* SCE for O_2 electrodes. Sequential current steps for 100 µM choline chloride injection at 10, 20, 30, 40, 50, 75, 100, 200, 240 µM O_2 concentrations.

5.3.2.2. MMA

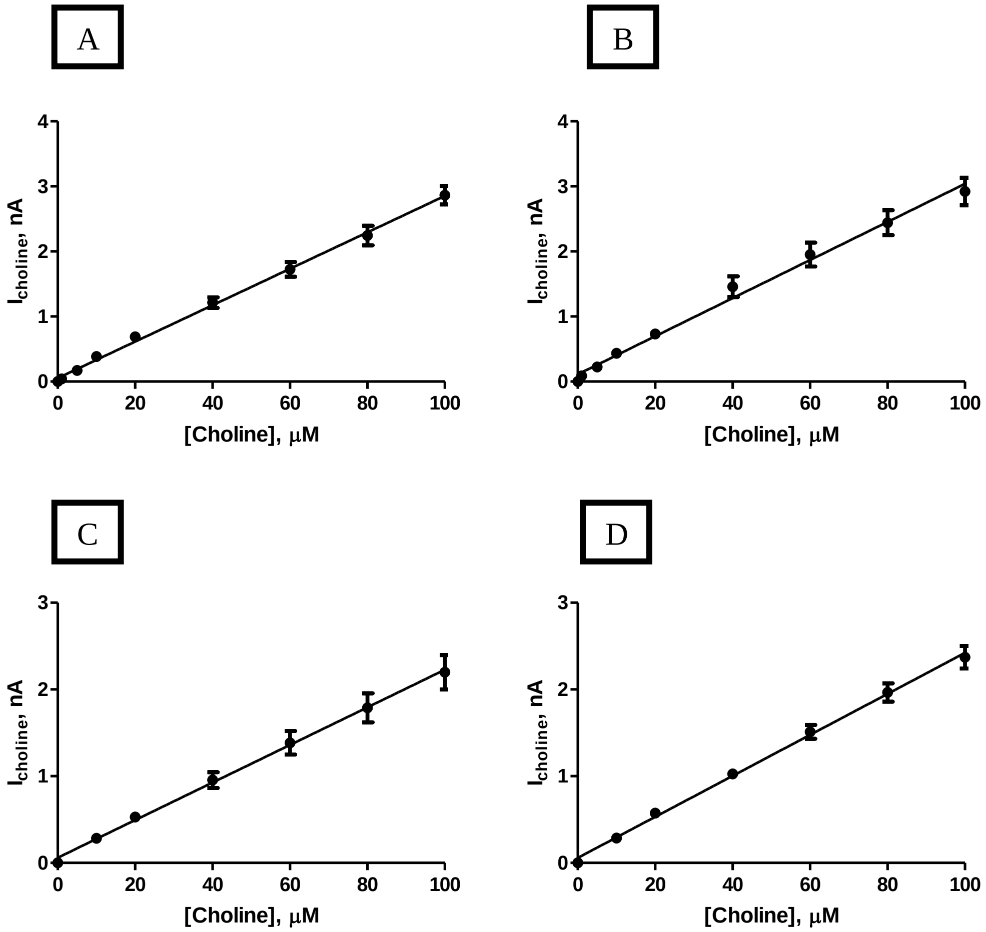

Figure : The current-concentration profile for choline chloride in PBS (pH 7.4) buffer solution at 21°C using design (A) 0 % Nafion®, (B) 0.5 % Nafion®, (C) 1 % Nafion® and (D) 1.5 % Nafion®. CPA carried out at +700 mV *vs.* SCE for choline electrodes. Sequential current steps for 5, 10, 20, 40, 60, 80, 100 μM choline chloride injections.

A

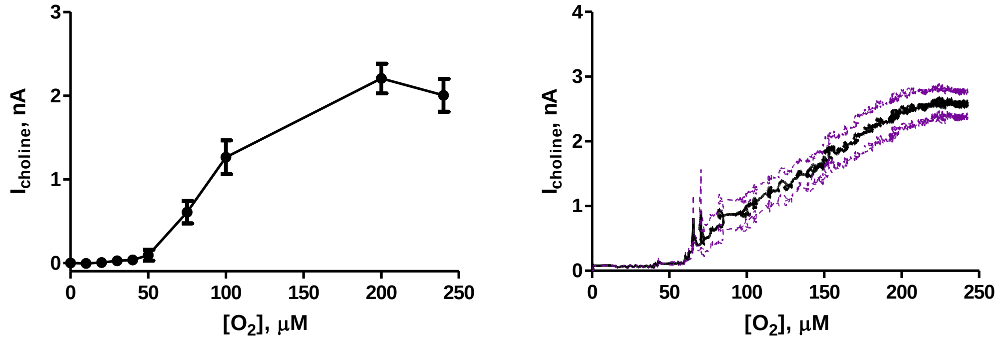

$I_{choline}$, nA
$[O_2]$, μM
$I_{choline}$, nA
$[O_2]$, μM

B

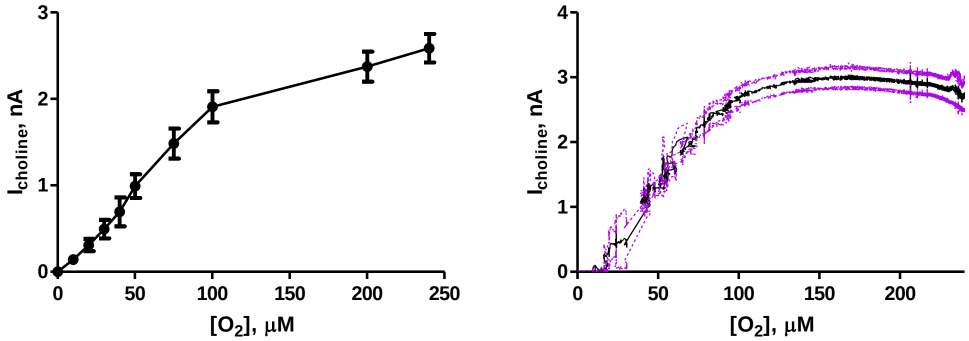

$I_{choline}$, nA
$[O_2]$, μM
$I_{choline}$, nA
$[O_2]$, μM

C

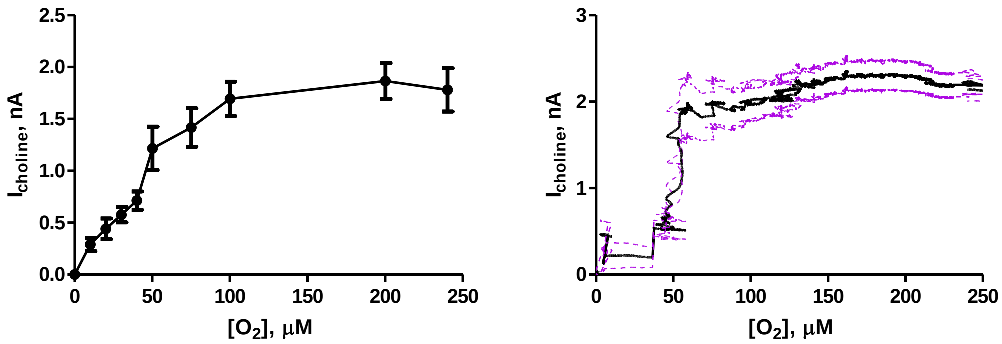

$I_{choline}$, nA
$[O_2]$, μM
$I_{choline}$, nA
$[O_2]$, μM

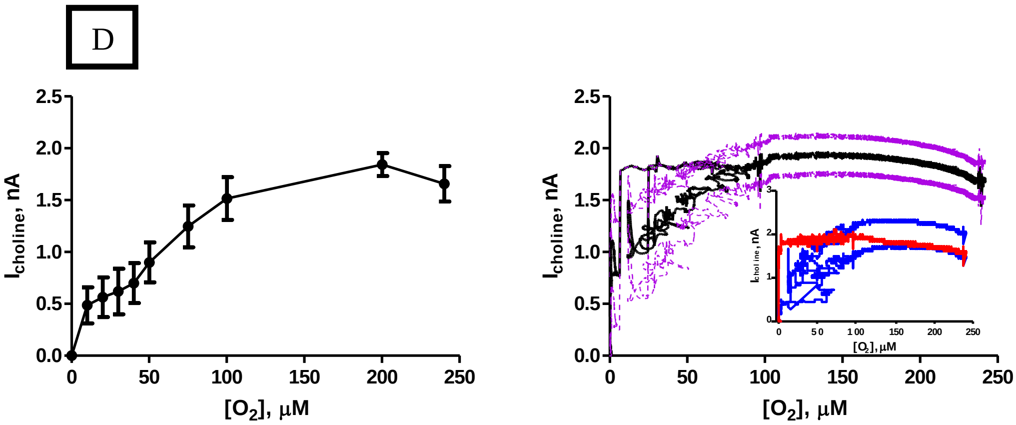

Figure : The choline current-oxygen concentration profile and raw data trace for choline chloride in PBS (pH 7.4) buffer solution at 21°C using design (A) 0 % Nafion®, (B) 0.5 % Nafion®, (C) 1 % Nafion® and (D) 1.5 % Nafion®. CPA carried out at +700 mV *vs.* SCE for choline electrodes. Sequential current steps for 5, 10, 20, 40, 60, 80, 100 µM choline chloride injections. CPA carried out at -650 mV *vs.* SCE for O_2 electrodes. Sequential current steps for 100 µM choline chloride injection at 10, 20, 30, 40, 50, 75, 100, 200, 240 µM O_2 concentrations. Inset: Figure D also illustrates the O_2 dependence observed on the three individual electrodes.

5.3.2.3. 1.5 % Nafion®

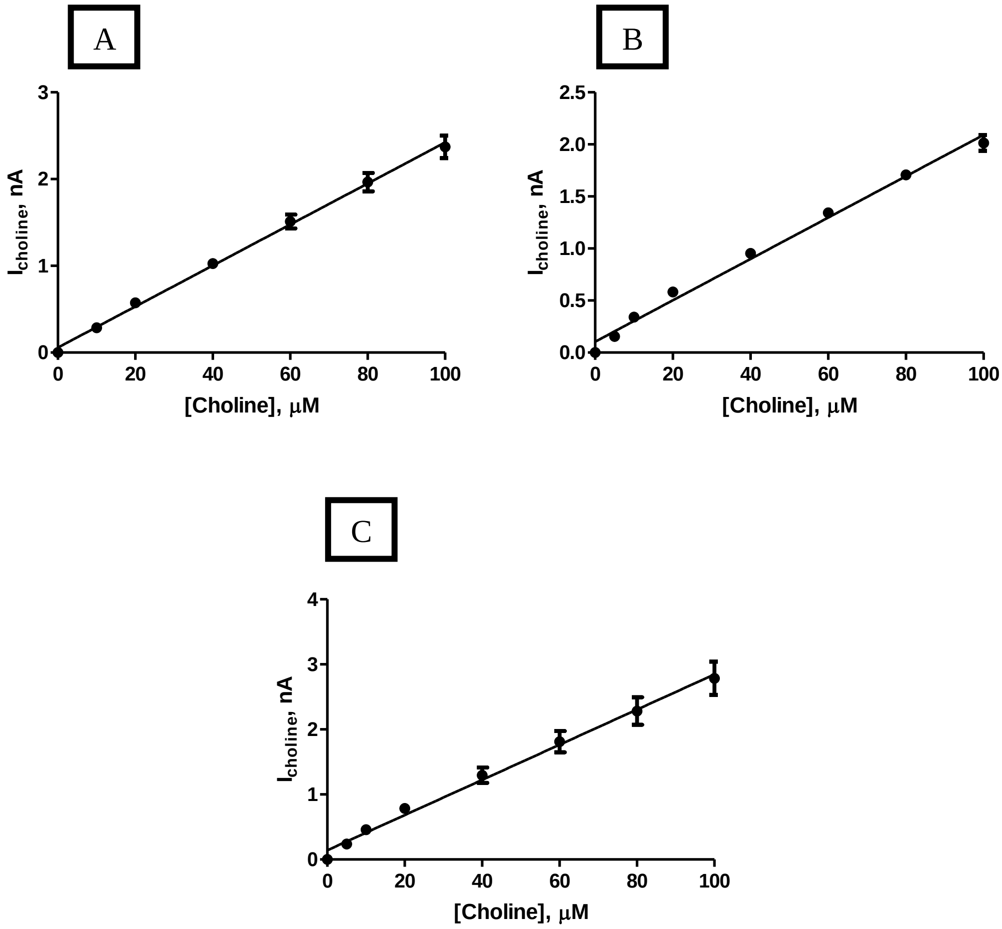

Figure : The current-concentration profile for choline chloride in PBS (pH 7.4) buffer solution at 21°C using design (A) 1.5 % Nafion®, (B) 1.5 % Nafion® (Vortexed) and (C) (1.5 % Nafion®)$_3$. CPA carried out at +700 mV *vs*. SCE for choline electrodes. Sequential current steps for 5, 10, 20, 40, 60, 80, 100 µM choline chloride injections.

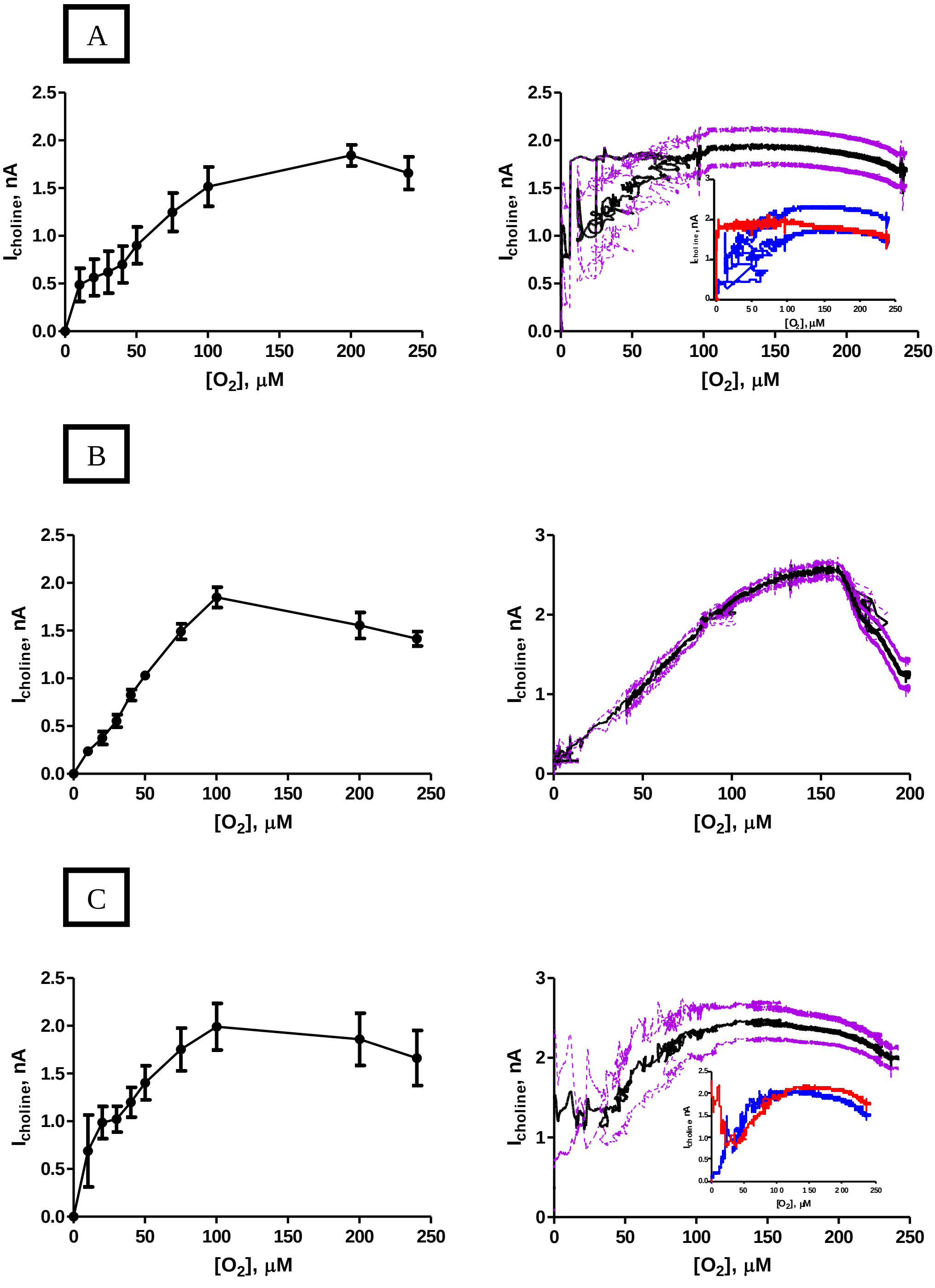

Figure : The choline current-oxygen concentration profile and raw data trace for choline chloride in PBS (pH 7.4) buffer solution at 21°C using design (A) 0 % Nafion®, (B) 0.5 % Nafion®, (C) 1 % Nafion® and (D) 1.5 % Nafion®. CPA carried out at +700 mV *vs.* SCE for choline electrodes. Sequential current steps for 5, 10, 20, 40, 60, 80, 100 µM choline chloride injections. CPA carried out at -650 mV *vs.* SCE for O_2 electrodes. Sequential current steps for 100 µM choline chloride injection at 10, 20, 30, 40, 50, 75, 100, 200, 240 µM O_2 concentrations. Inset: Figure A illustrates the O_2 dependence observed at the three individual electrodes. Figure C illustrates the O_2 dependence observed at the two individual electrodes.

5.3.2.4. Nafion® Position

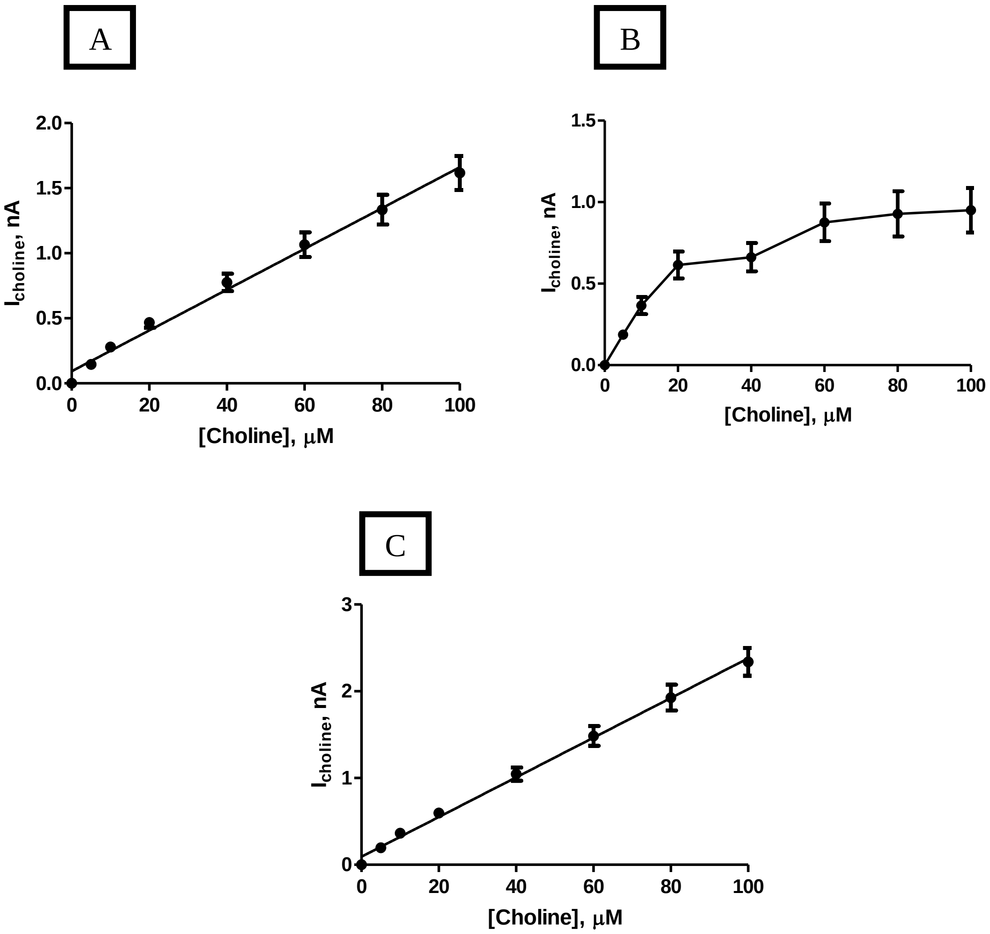

Figure : The current-concentration profile for choline chloride in PBS (pH 7.4) buffer solution at 21°C using design (A) (MMA)(5%Nafion®), (B) (5%Nafion®)(MMA) and (C) (MMA)(5%Nafion®)(MMA). CPA carried out at +700 mV *vs*. SCE for choline electrodes. Sequential current steps for 5, 10, 20, 40, 60, 80, 100 μM choline chloride injections.

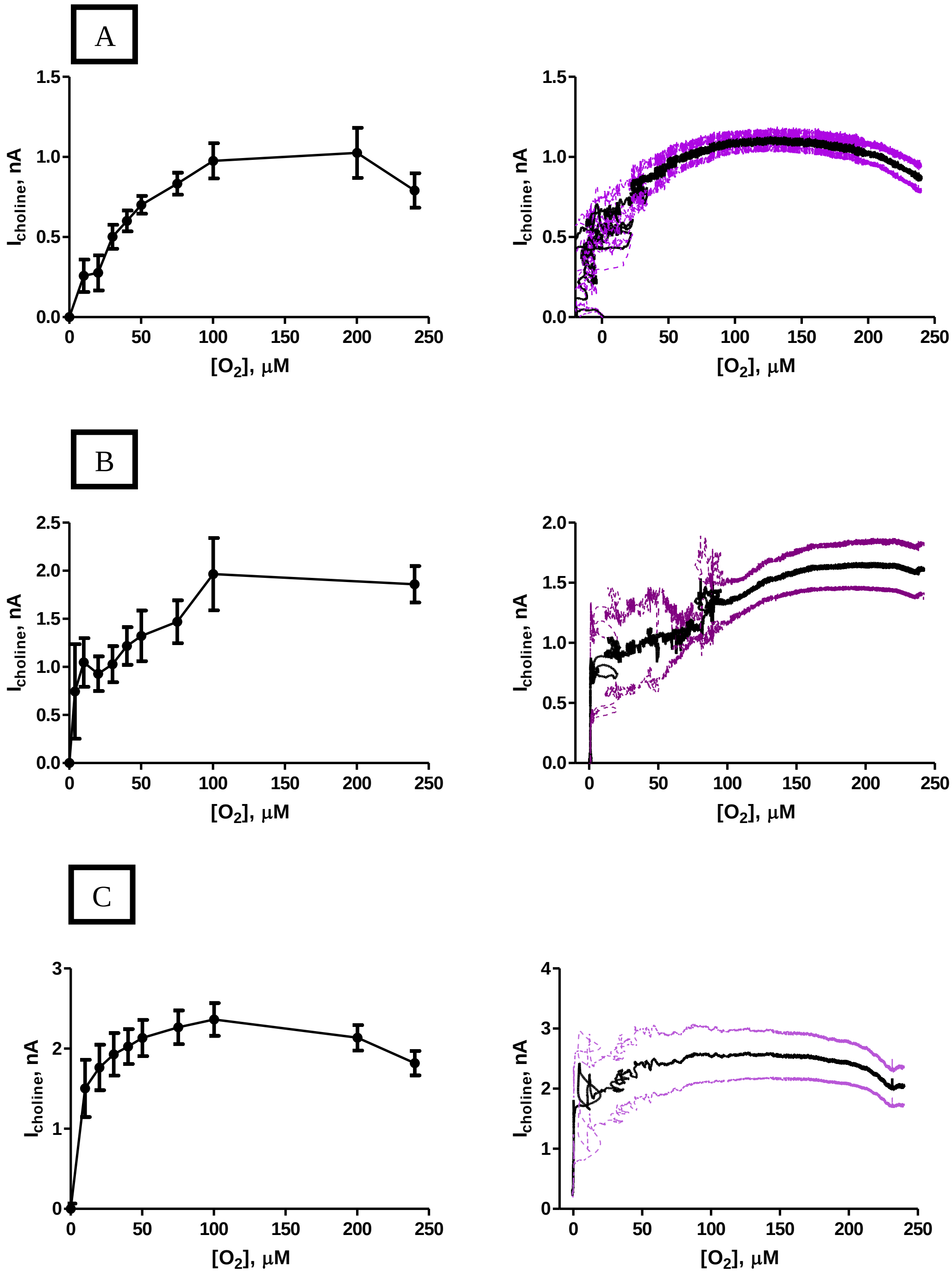

Figure : The choline current-oxygen concentration profile and raw data trace for choline chloride in PBS (pH 7.4) buffer solution at 21°C using design (A) (MMA)(5%Nafion®), (B) (5%Nafion®)(MMA) and (C) (MMA)(5%Nafion®)(MMA). CPA carried out at +700 mV *vs.* SCE for choline electrodes. Sequential current steps for 5, 10, 20, 40, 60, 80, 100 µM choline chloride injections. CPA carried out at -650 mV *vs.* SCE for O_2 electrodes. Sequential current steps for 100 µM choline chloride injection at 10, 20, 30, 40, 50, 75, 100, 200, 240 µM O_2 concentrations.

5.3.2.5. Nafion® Concentration Comparison

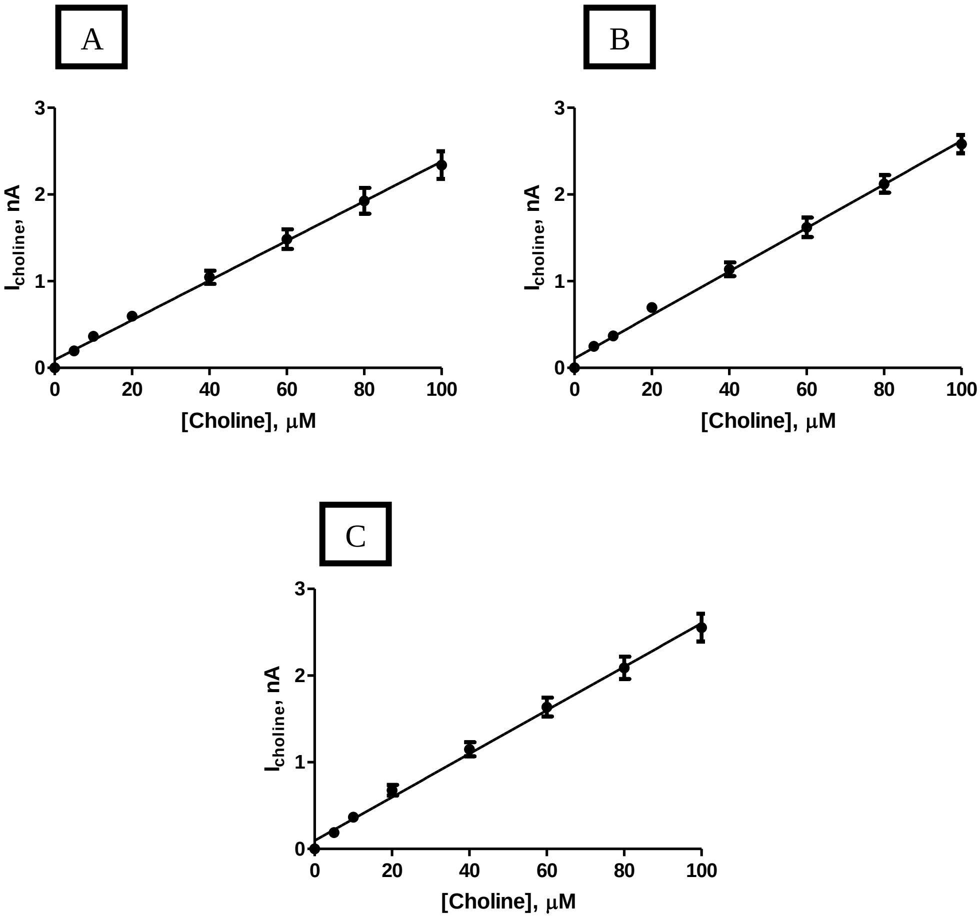

Figure : The current-concentration profile for choline chloride in PBS (pH 7.4) buffer solution at 21°C using design (A) (MMA)(5%Nafion®)(MMA), (B) (MMA)(2.5%Nafion®)(MMA) and (C) (MMA)(1.25%Nafion®)(MMA). CPA carried out at +700 mV *vs*. SCE for choline electrodes. Sequential current steps for 5, 10, 20, 40, 60, 80, 100 µM choline chloride injections.

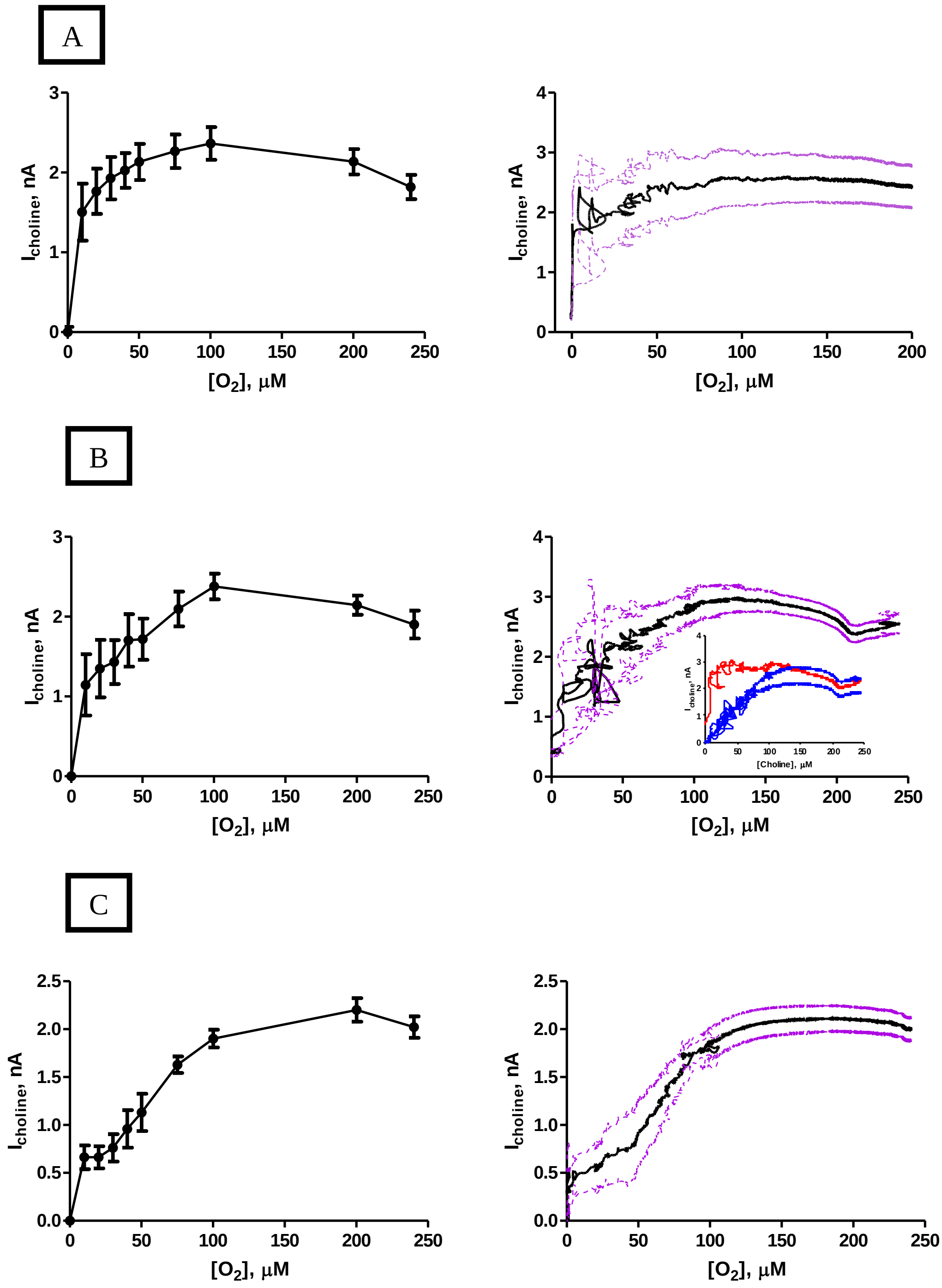

Figure : The choline current-oxygen concentration profile and raw data trace for choline chloride in PBS (pH 7.4) buffer solution at 21°C using design (A) (MMA)(5%Nafion®)(MMA), (B) (MMA)(2.5%Nafion®)(MMA) and (C) (MMA)(1.25%Nafion®)(MMA). CPA carried out at +700 mV *vs.* SCE for choline electrodes. Sequential current steps for 5, 10, 20, 40, 60, 80, 100 µM choline chloride injections. CPA carried out at -650 mV *vs.* SCE for O_2 electrodes. Sequential current steps for 100 µM choline chloride injection at 10, 20, 30, 40, 50, 75, 100, 200, 240 µM O_2

concentrations. Inset Figure D also illustrates the O_2 dependence observed on the three individual electrodes.

5.3.4. Effect of Diffusion

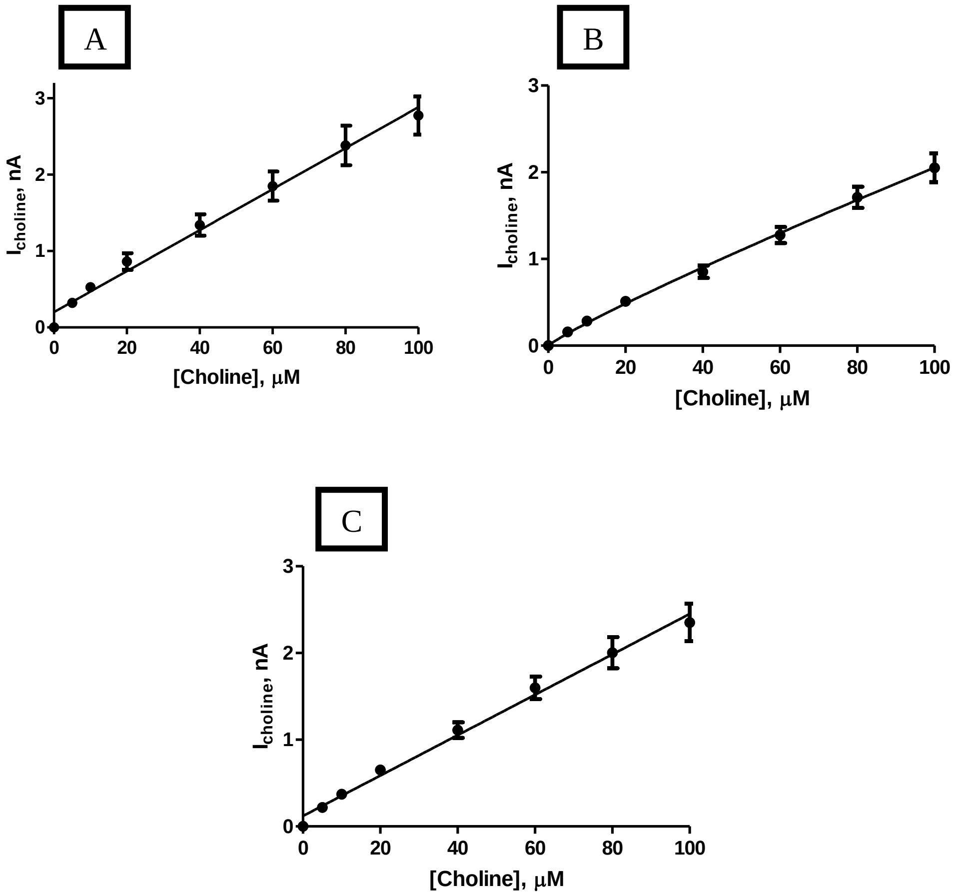

Figure : The current-concentration profile comparison and comparison table for choline chloride calibration in PBS (pH 7.4) buffer solution at 21°C using designs (A) 1%CelAce, (B) 2%CelAce and (C) 3%CelAce. CPA carried out at +700 mV *vs*. SCE. Sequential current steps for 5, 10, 20, 40, 60, 80, 100 µM choline chloride injections.

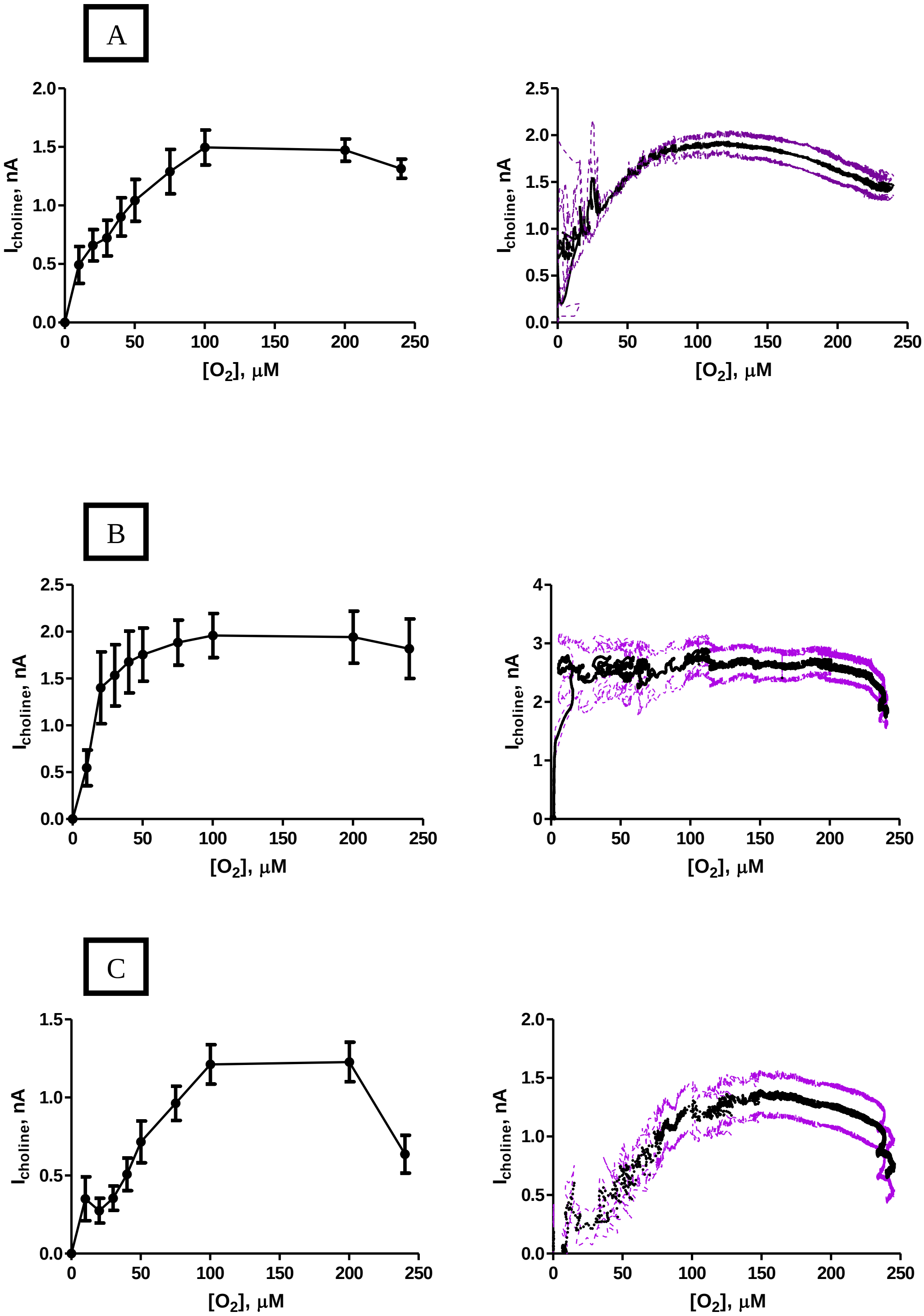

Figure : The choline current-oxygen concentration profile and raw data trace for choline chloride in PBS (pH 7.4) buffer solution at 21°C using design (A) 1%CelAce, (B) 2%CelAce and (C) 3%CelAce. CPA carried out at +700 mV *vs*. SCE for choline electrodes. Sequential current steps for 5, 10, 20, 40, 60, 80, 100 μM choline chloride injections. CPA carried out at -650 mV *vs*. SCE for O_2 electrodes. Sequential current steps for 100 μM choline chloride injection at 10, 20, 30, 40, 50, 75, 100, 200, 240 μM O_2 concentrations.

Conferences

1. *The development of a choline biosensor for the real time monitoring of brain extracellular choline*. **Poster presentation** at the 63rd Irish Universities Chemistry Research Colloquium (2011).
2. *Development of an MMA based choline biosensor for the in-vivo detection of choline in the brain*. **Poster presentation** at the 6th Annual Meeting of Neuroscience Ireland (2011).
3. *Development of a styrene based biosensor for the detection of choline*. **Poster presentation** at the 6th Conference on Analytical sciences Ireland (CASi) (2011).
4. *Development of a biosensor for the in-vivo detection of choline*. **Poster presentation** at the 13th International Conference on *In-vivo* Methods. Monitoring Molecules in Neuroscience (2010).